



UNIVERSIDAD DE BURGOS
DEPARTAMENTO DE QUÍMICA
ÁREA DE QUÍMICA INORGÁNICA

**SYNTHESIS AND CHARACTERIZATION OF Ru(II),
Rh(III) AND Ir(III) COMPLEXES BEARING
ARYLAZOLE LIGANDS. APPLICATIONS IN
ANTICANCER CHEMOTHERAPY, LEC DEVICES AND
PHOTOCATALYSIS**

Marta Martínez Alonso
PhD Thesis
Burgos, February 2017



UNIVERSIDAD DE BURGOS

DEPARTAMENTO DE QUÍMICA

ÁREA DE QUÍMICA INORGÁNICA

DR. GUSTAVO ESPINO ORDÓÑEZ PROFESOR DEL ÁREA DE QUÍMICA INORGÁNICA DE LA
UNIVERSIDAD DE BURGOS

CERTIFICA:

Que la licenciada Dña. Marta Martínez Alonso ha realizado bajo su dirección el trabajo titulado “Synthesis and characterization of Ru(II), Rh(III) and Ir(III) complexes bearing arylazole ligands. Applications in anticancer chemotherapy, LEC devices and photocatalysis”.

Considerando que dicho trabajo reúne los requisitos exigidos para ser presentado como Tesis Doctoral, expresa su conformidad con dicha presentación.

Y para que conste, firma el presente certificado en Burgos a veinticinco de noviembre de dos mil dieciseis.

Burgos, a 25 de noviembre de 2016

Fdo. Gustavo Espino Ordóñez

*“Research is to see what everybody else has seen,
and to think what nobody has thought”*

Albert Szent-Györgyi

Agradecimientos

Es difícil resumir en tan pocas líneas los sentimientos, recuerdos y momentos que llevan a expresar mi agradecimiento a la gente que ha estado presente a lo largo de estos años. Por eso pido perdón de antemano, si me dejo a alguien en el tintero.

Para comenzar, me gustaría agradecer al Dr. Gustavo Espino, el director de esta tesis, por darme la gran oportunidad de formar parte del mundo de la química organometálica. Gracias de corazón por tu esfuerzo y dedicación, y por creer y confiar en mí en todo momento.

A la Dra. Begoña García, por hacer posible la realización de este trabajo y facilitar e impulsar mi crecimiento científico mediante la asistencia a distintos congresos y reuniones científicas. Al grupo de química-física, y en especial a Natalia, por hacer más fácil la unión de la química con la biología, y por esas ganas de aprender y crear cosas nuevas.

A las instituciones financieras, las cuales han hecho posible llevar a cabo esta investigación. En particular, a la Obra Social “la Caixa” (Proyecto OSLC-2012-007), cuyo programa de investigación me ha permitido disfrutar de un contrato para la realización de mi tesis doctoral. También, a la Junta de Castilla y León (Fondo Social Europeo, Proyecto BU-299A12-1) y a la financiación estatal, MICINN (Proyectos CTQ2009-13051/BQU CTQ, 2011-24434, y CTQ2014-58812-C2-1-R).

Al Pr. Dr. Eric Meggers y su grupo, por recibirmelos con los brazos abiertos en la Universidad de Marburg, Alemania y enseñarme otras formas y técnicas de trabajo.

Al Dr. José Vicente Cuevas y al Dr. Enrique Ortí, por adentrarme en el complicado mundo de la química computacional. Al Dr. Henk Bolink y, por supuesto, al Dr. Antonio Pertegás, por enseñarme los secretos de los LECs, y por tu amabilidad y cercanía. Al Dr. Félix Jalón y a la Dra. Blanca Manzano, por apoyar y colaborar en la investigación que hacemos en Burgos, y también a ellos y a todo su grupo por los buenos e inolvidables momentos compartidos en los congresos del GEQO. A la Dra. Ana M^a Rodríguez Fernández-Pacheco, por su colaboración en la resolución de todas las estructuras cristalográficas de esta tesis. Al Dr. Álvaro Colina y a la Dra. Arancha Heras, por dedicar parte de su tiempo en enseñarme las técnicas espectroelectroquímicas. Al Dr. Fernando Domínguez y Mabel, por su colaboración en los estudios biológicos y médicos. Al grupo de la Dra. Mairena, por la realización de parte de los ensayos biológicos presentados en este trabajo.

A Félix, nuestro técnico, por su inestimable ayuda en los problemas surgidos en el laboratorio. Siempre dispuesto a ayudar sin recibir nada a cambio. A los profesores del área de química inorgánica, por los cafés con ciencia, tertulia y risas y por su completa disponibilidad para ayudar y resolver cualquier asunto.

A Jacinto, Marta y Pilar del I+D+i, por su plena disponibilidad, dedicación y ayuda para llevar a cabo este trabajo y por enseñarme las distintas técnicas de las que son responsables. Gran parte de esta tesis os pertenece.

A los compañeros y amigos del laboratorio Cristina, Jesús, Héctor, Larry, Jairo, Leticia, Natalia, Igor, Matteo, Mónica, Alba, Iván. Todos me habéis ayudado en este trabajo.

A los “químicos inorgánicos” (Cristina, Victoria, Fuen, Isa, Mª Luz, Víctor), por hacer que mis primeros años y mi contacto con la investigación fueran especiales y divertidos, y porque siempre recordaré los buenos momentos que pasamos. A Blanca, Vero y Erica, porque la ciencia, de una u otra forma unió nuestros caminos.

Al resto de químicos que, aún sin decir nombres (puesto que sería muy largo y no quiero dejarme a nadie), han estado ahí, compartiendo horas de laboratorio, cafés y confidencias desde mis comienzos en la química.

A Alex y Silvia, por hacer de mi estancia en Alemania una experiencia inolvidable. Sin vosotras no hubiese sido igual (y por supuesto sin los “auflauf” y sin el encanto de Marburg tampoco).

A mis amigos. A Marta, por estar siempre ahí, a pesar de la distancia y por esas confidencias sin las cuales nuestra amistad no sería tan intensa. A Victoria, mi “hermanita mayor”, por apoyarme siempre y aconsejarme con sinceridad. A las “cabuérnigas” (Raquel, Noe, Eva, Mary, Lourdes, Silvia), por hacer de cada “reunión”, un motivo para sonreír. A mis valdorranos (Raquel, Cristina, César, Sara, Paula, Fer, Javi), por esos veranos de desconexión, esas caminatas y meriendas, y las acampadas a la intemperie para ver estrellas o saltar arroyos. A mi compi de idiomas, Álvaro, por sacarme una sonrisa en cualquier momento.

A mis padres, Javier y Begoña, por brindarme la oportunidad de estudiar una carrera, por valorarme y quererme. Por respetar mis decisiones, acertadas o no, y no cortar mis alas. Gracias a vosotros soy lo que soy. También a mi hermana, Silvia, por tu paciencia y comprensión. Siempre consigues dar color a la vida. En cualquier caso, todos me habéis apoyado y habéis aguantado mis enfados y desplantes. A mi abuelo, Ángel, que, aunque ya no está entre nosotros, siempre le llevaré en mi corazón. A mis tíos, Pilar y Patri, y a mi abuela, Paquita, por intentar comprender lo que no siempre es fácil.

Y por supuesto, a Roberto, mi compañero de viaje, por apoyarme incondicionalmente, creer en mí y evitar que me derrumbara en los momentos más arduos y complicados. Siempre consigues dibujar una sonrisa en mi cara.

A todos los que en algún momento habéis formado parte de mi vida u os habéis cruzado en ella, porque de todos y cada uno de vosotros he aprendido algo. Gracias.

Acknowledgements

It's difficult to sum up in so few lines the feelings and memories that lead to express my thankful to everyone who has stayed with me throughout these years. Thus, I apologize in advance, just in case I forget someone.

To begin with, I would like to thank to Dr. Gustavo Espino, my thesis supervisor, for giving me the chance to be part of the organometallic chemistry world. Grateful thanks for your effort and dedication, and for believing in me at every time.

To Dra. Begoña García, for making this work possible and for facilitating and motivating my scientific growth by attending some symposia and conferences. To the physicochemical group, and specially Natalia, to make easy the chemistry-biology joint, and for the continuous learning and setting up of new things.

To the funding institutions, which have made possible the research for this work. In particular, to Obra Social "la Caixa" (Project OSLC-2012-007), whose researching program has afforded a contract to carry out my PhD. Also, to Junta de Castilla y León (Fondo Social Europeo, Project BU-299A12-1) and to the Spanish government, MICINN (Projects CTQ2009-13051/BQU CTQ, 2011-24434, and CTQ2014-58812-C2-1-R).

To Pr. Dr. Eric Meggers and his research group, for their warm welcome in the University of Marburg, Germany, and for teaching me other methods and working techniques.

To Dr. José Vicente Cuevas and Dr. Enrique Ortí, for getting me into the tough world of computational chemistry. To Dr. Henk Bolink and, of course, Dr. Antonio Pertegás, for showing me the secrets of the LEC devices, and for your kindness and closeness. To Dr. Félix Jalón and Dra. Blanca Manzano, for collaborating in the research we make in Burgos, and also to them and to all their group, for the good and amazing moments in GEQO Congresses. To Dra. Ana M^a Rodríguez Fernández-Pacheco, for her collaboration in the resolution of the crystallographic structures of this thesis. To Dr. Álvaro Colina and Dra. Arancha Heras, for spending some time teaching me the spectroelectrochemistry techniques. To Dr. Fernando Domínguez and Mabel, for your collaboration in the biological and medical studies. To the group of Dra. Mairena, for the realization of some of the biological assays presented in this work.

To Félix, our lab technician, for his invaluable help in the different issues that come up in the lab. Always prepared to help, receiving nothing in return. To the professors of the inorganic chemistry area, for the coffees with science, talks and laughs, and for your complete availability to help and solve any issue.

To Jacinto, Marta and Pilar, from the I+D+I, for their full availability, dedication and help to carry out this work and for teaching me the different techniques they are responsible for. A great part of this thesis belongs to you.

To the lab mates and friends: Cristina, Jesús, Héctor, Larry, Jairo, Leticia, Natalia, Igor, Matteo, Mónica, Alba, Iván. All of you have contributed to my work.

To the “químicos inorgánicos” (Cristina, Victoria, Fuen, Isa, Mª Luz, Víctor), for making special and fun my first years and my approach to research, and because I am sure I will always remember the good time we spent together. To Blanca, Vero and Erica, because science joined our lives.

To the rest of my chemists’ friends, that even saying no names (as it would be too long and I don’t want to forget anyone), have been there, sharing laboratory hours, coffees and confidences from my beginnings in chemistry.

To Alex and Silvia for turning my stay in Germany into an unforgettable experience. I think it wouldn’t have been the same without you, and of course without the “auflauf” and without Marburg’s charm.

To my friends. Marta, for being always on the lookout and for these confidences, without which our friendship wouldn’t be so strong and lively. Victoria, my “little elder sister”, for supporting me and giving me advice sincerely. To the “Cabuérnigas” (Raquel, Noe, Eva, Mary, Lourdes, Silvia), for turning out every “get-together” in a reason to smile and laugh. To my “Valdorranos” (Raquel, Cristina, César, Sara, Paula, Fer, Javi), for those summertimes to unwind, the walks and meals, and the outings in the middle of the night to watch the sky full of stars or to cross streams. To my language mate, Álvaro, for making me smile at any time.

To my parents, Javier and Begoña, for giving me the chance of studying a degree and a Master, for relying on me and appreciating my work. For respecting my decisions, either the right or the wrong ones, and for not clipping my wings. Thanks to them I’m what I am. Also to my sister, Silvia, for your patience and comprehension. You always give colour to life. Anyway, all of you have unconditionally relied on me and have put up with my anger and when I’ve felt blue. To my grandpa, Ángel, who despite not being between us, he’ll always stay in my heart. To my aunts, Pilar and Patri, and my grandma, Paquita, for trying to understand what isn’t always easy.

And finally, to the most important person in my life, Roberto, my traveler’s mate, for relying on me, believing in me, cheering me up and avoiding my falls in the hardest and most difficult moments. You always manage to draw a smile on my face.

To all of you, who have been taken part in any stage of my life, because I’ve learnt something from all of you.

THANK YOU ALL

The thesis in statistic figures

Number of...	Total	Ru(II)	Rh(III)	Ir(III)	Ir(III)
		Half-sandwich	Half-sandwich	Half-sandwich	Biscyclometallated
Ligands used	11	10	1	10	5
Synthesised or modified ligands	4	-	-	-	-
Synthesised starting dimers	5	4	1	1	1
Synthesised complexes	83	51	2	17	13
Crystal structures	31 (4 non-publishable)	25	-	4	2
DNA interaction studies	19	10	1	8	-
Cytotoxicity assays	45 in 9 different cell lines*	32	2	11	-
Complexes tested with animals (in vivo assays)	3	1	1	1	-
LEC devices developed from complexes of this thesis	7	-	-	-	7
Published papers in this thesis	2	2 +1 written	-	-	1 submitted + 1 written
Papers	3	-	-	-	-

List of published papers and times cited

1. *Anticancer Activity and DNA Binding of a Bifunctional Ru(II) Arene Aqua-Complex with the 2,4-Diamino-6-(2-pyridyl)-1,3,5-triazine Ligand.* Bustos, N.; Valladolid, J.; Martínez-Alonso, M.; Lozano, H. J.; Jalón, F. A.; Manzano, B. R.; Rodríguez, A. M.; Carrión, M. C.; Biver, T.; Leal, J. M.; Espino, G.; García, B. *Inorg. Chem.* **2013**, 52, 9962–9974. Times cited: 25
2. *Derivation of Structure–Activity Relationships from the Anticancer Properties of Ruthenium(II) Arene Complexes with 2-Aryldiazole Ligands.* Martínez-Alonso, M.; Bustos, N.; Jalón, F. A.; Manzano, B. R.; Leal, J. M.; Rodríguez, A. M.; García, B.; Espino, G. *Inorg. Chem.* **2014**, 53, 11274–11288. Times cited: 19
3. *Monomer–Dimer Divergent Behavior toward DNA in a Half-Sandwich Ruthenium(II) Aqua Complex. Antiproliferative Biphasic Activity.* Bustos, N.; Martínez-Alonso, M.; Leal, J. M.; Rodríguez, A. M.; Domínguez, F.; Acuña, M. I.; Espino, G.; García, B. *Organometallics* **2015**, 34, 319–327. Times cited: 5
4. *Highly Stable and Efficient Light-Emitting Electrochemical Cells Based on Cationic Iridium Complexes Bearing Arylazole Ancillary Ligands.* Martínez-Alonso, M.; Cerdá, J.; Momblona, C.; Pertegás, A.; Junquera-Hernández, J. M.; Heras, A.; Rodríguez, A. M.; Espino, G.; Bolink, H.; Ortí, E. Submitted to Chem. Mater.

* A2780, A2780cis, MCF-7, A549, HeLa, HCT-116, HCT-116p53- (as cancer cell lines) and MRC-5 and IMR-90 (as healthy cell lines).

ABBREVIATIONS

General abbreviations

9MeG	9-Methylguanine	ITO	Indium Tin Oxide
acac	acetylacetone	J	Current density
ATR	Attenuated Total Reflectance	L	Luminance
Bmim	1-butyl-3- methylimidazolium	LC	Ligand Centred
bz	benzene	LEC	Light-Emitting Electrochemical Cell
CD	Circular Dichroism	LED	Light-Emitting Diode
CHN	Elemental Analysis	LFSE	Ligand-Field Splitting Energy
DDQ	2,3-Dichloro-5,6-dicyano- 1,4-benzoquinone	LLCT	Ligand to Ligand Charge Transfer
dmnp	2,6-dimethyl-4-nitro- pyridine	LMCT	Ligand to Metal Charge Transfer
DNA	Deoxyribonucleic Acid	lp	lone pair
ECD	Electrochemical doping	LSIMS	Liquid Secondary Ion Mass Spectroscopy
ED	Electrodynamical doping	LUMO	Lowest Unoccupied Molecular Orbital
EI	Electronic Impact	MC	Metal Centred
EQE	External Quantum Efficiency	MLCT	Metal to Ligand Charge Transfer
ESI	Electrospray ionization	MO	Molecular Orbital
FAB	Fast Atom Bombardment	MS	Mass Spectrometry
GMP	5'-deoxyguanosine monophosphate	MS	Molecular Sieve
GSH	Glutathione	NaCaC	Sodium Cacodylate, $(\text{CH}_3)_2\text{AsO}_2\text{Na}$
GSSG	Oxidized Glutathione	NADH	Nicotinamide adenine dinucleotide
Hb	Haemoglobin	NCI	National Cancer Institute
HOMO	Highest Occupied Molecular Orbital	NHE	Normal Hydrogen Electrode
HSA	Human Serum Albumin	NMR	Nuclear Magnetic Resonance
IBX	o-iodoxybenzoic acid	NP-TLC	Normal Phase Thin Layer Chromatography
IC₅₀	Inhibitory Concentration- 50	NSCLC	Non-Small-Cell Lung Carcinoma
IL	Inter- or Intraligand		
IL	Ionic Liquid		
IR	Infrared Spectroscopy		
iTMC-LEC	ionic Transition-Metal Complex LEC		

OLED	Organic Light-Emitting Diode	NMR abbreviations	
ORTEP	Oak Ridge Thermal Ellipsoid Plot	{¹H}	Decoupled Hydrogen
OTf	Triflate - Trifluoromethanesulfonate	br	broad
OTs	Tosylate - <i>p</i> -toluensulfonate	COSY	Correlation Spectroscopy
PCE	Power efficiency	d	doublet
<i>p</i>-cym	<i>p</i> -cymene	HdP	Hydrogen decoupled Phosphorous
PDT	Photodynamic Therapy	HETCOR	Heteronuclear Correlation
phoxet	phenoxyethanol	HMBC	Heteronuclear Multiple Bond Correlation
PLEC	Polymer LEC	HSQC	Heteronuclear Single Quantum Correlation
PLQY	Photoluminescent Quantum yield	NOESY	Nuclear Overhauser Effect Spectroscopy
PS	Photosensitizer	q	quadruplet
R_f	Retardation factor	ROESY	Rotating-frame Overhauser Effect Spectroscopy
RF	Resistance Factor	s	singlet
ROS	Reactive Oxygen Species	sept	septuplet
RP-TLC	Reversed Phase Thin Layer Chromatography	t	triplet
RT	Room Temperature	TOCSY	Total Correlation Spectroscopy
SF	Selectivity Factor	IR abbreviations	
SOC	Spin-Orbit Coupling	as	asymmetric
SOD	Superoxide dismutase	br	broad
SSL	Solid-state Lighting	ip	in plane
Tf	Transferrin	m	medium
TLC	Thin Layer Chromatography	oop	out of plane
Trx	Thioredoxin	s	strong
u	unified atomic mass unit	sym	symmetric
UV	Ultraviolet	vs	very strong
Λ_m	Molar Conductivity	w	weak
		δ	bending vibrational mode
		v	stretching vibrational mode

INDEX

Agradecimientos	7
Acknowledgements	9
The thesis in statistic figures.....	11
Abbreviations	13
Researching objectives	21
EXPERIMENTAL AND CHARACTERIZATION TECHNIQUES.....	23
1. EXPERIMENTAL TECHNIQUES	25
2. CHARACTERIZATION TECHNIQUES	26
3. OTHER TECHNIQUES	28
4. BIBLIOGRAPHY	30
GENERAL INTRODUCTION.....	31
1. ABOUT THE METALS.....	33
1.1. Ruthenium	33
1.2. Rhodium.....	34
1.3. Iridium.....	34
2. ABOUT THE CHELATING LIGANDS.....	35
2.1. Arylbenzazoles	35
3. BIBLIOGRAPHY	40
PART I. Ru(II), Rh(III) and Ir(III) HALF-SANDWICH COMPLEXES WITH ANTICANCER PROPERTIES	43
CANCER: A BRIEF STORY OF ORGANOMETALLIC DRUGS AND MECHANISMS OF ACTION	45
1. CANCER	47
1.1. Early history of anticancer drugs: cisplatin.....	47
1.1.1. Cisplatin: Mechanism of Action	50
1.2. Other platinum group metals	54
1.2.1. Palladium.....	54
1.2.2. Ruthenium.....	56
1.2.3. Osmium	59
1.2.4. Rhodium	61
1.2.5. Iridium	62
1.3. Other transition metals.....	63
1.3.1. Titanium	63
1.3.2. Gold	64

2. MECHANISM OF ACTION OF ORGANOMETALLIC DRUGS.....	65
2.1. DNA	65
2.2. Generation of ROS	67
2.3. Other targets.....	68
2.3.1. Glutathione. Cell Detoxification.....	68
2.3.2. NAD ⁺ /NADP ⁺	70
2.4. Crossing the cell membrane: Lipophilicity.....	70
3. MECHANISM OF ACTION OF ORGANOMETALLIC DRUGS.....	72
3.1. Ruthenium arene complexes	72
3.2. Iridium and Rhodium pentamethylcyclopentadienyl complexes.....	73
4. LIGANDS	73
5. BIBLIOGRAPHY	75

CHAPTER 1. Ru(II) HALF-SANDWICH COMPLEXES BEARING PYRIDYLIAZOLE ANCILLARY LIGANDS: SYNTHESIS, CHARACTERIZATION AND ANTICANCER PROPERTIES..... 79

1. RESULTS AND DISCUSSION	82
1.1. Synthesis	82
1.2. Characterization.....	84
1.3. Aqueous Solubility	102
1.4. Aquation-Anation Equilibria	103
1.5. Deprotonation of [4a](BF ₄) ₂	103
1.6. Interaction with nucleobases and nucleotides.....	104
1.7. Cytotoxic Activity	105
1.8. SAR	106
2. CONCLUDING REMARKS	107
3. EXPERIMENTAL SECTION	108
4. BIBLIOGRAPHY	121

CHAPTER 2. Ru(II), Ir(III) AND Rh(III) HALF-SANDWICH COMPLEXES BEARING 2-PHENYLBENZIMIDAZOLE ANCILLARY LIGANDS: SYNTHESIS, CHARACTERIZATION AND ANTICANCER PROPERTIES..... 123

1. RESULTS AND DISCUSSION	126
1.1. Synthesis	126
1.2. Characterization.....	128
1.3. Cl ⁻ /DMSO Substitution	135
1.4. Aqueous Solubility	137
1.5. Aquation.....	137

1.6. Lipophilicity	138
1.7. Reactivity against Nucleobases and Nucleotides	140
1.8. Reactivity against Glutathione	141
1.9. Peroxide formation by Metal-Catalysed Transfer-Hydrogenation	143
1.10. Cytotoxic Activity	144
2. CONCLUDING REMARKS	146
3. EXPERIMENTAL SECTION	148
4. BIBLIOGRAPHY	156

**CHAPTER 3. Ru(II) HALF-SANDWICH COMPLEXES BEARING
HYDROXYPHENYLBENZAZOLE ANCILLARY LIGANDS: SYNTHESIS, CHARACTERIZATION
AND ANTICANCER PROPERTIES 159**

1. RESULTS AND DISCUSSION	162
1.1. Synthesis	162
1.2. Characterization.....	163
1.3. Thiocyanate Coordination Mode	176
1.4. Stability of complex [18a] and arene loss.....	177
1.5. Aqueous Solubility	179
1.6. Aquation-Anation Equilibria	180
1.7. Reactivity against Nucleobases and Nucleotides	180
1.8. Cytotoxic Activity	182
1.9. DNA interaction	183
2. CONCLUDING REMARKS	187
3. EXPERIMENTAL SECTION	188
4. BIBLIOGRAPHY	197

**CHAPTER 4. Ru(II) HALF-SANDWICH COMPLEXES BEARING AMINOPHENYLBENZAZOLE
ANCILLARY LIGANDS: SYNTHESIS, CHARACTERIZATION AND ANTICANCER
PROPERTIES 199**

1. RESULTS AND DISCUSSION	202
1.1. Synthesis	202
1.2. Characterization.....	203
1.3. Aqueous Solubility	215
1.4. Aquation-Anation Equilibria	215
1.5. Cytotoxic Activity	216
2. CONCLUDING REMARKS	217
3. EXPERIMENTAL SECTION	218
4. BIBLIOGRAPHY	228

CHAPTER 5. Ru(II) HALF-SANDWICH COMPLEXES BEARING PYRIDYL BENZOAZOLE AND THIABENDAZOLE: SYNTHESIS, CHARACTERIZATION AND ANTICANCER PROPERTIES	229
1. RESULTS AND DISCUSSION	232
1.1. Synthesis	232
1.2. Characterization.....	233
1.3. Aqueous Solubility	238
1.4. Aquation-Anation Equilibria	238
1.5. Hydration Energy	239
1.6. Cytotoxic Activity	239
2. CONCLUDING REMARKS	240
3. EXPERIMENTAL SECTION	241
4. BIBLIOGRAPHY	246
CHAPTER 6. Ir(III) HALF-SANDWICH COMPLEXES BEARING ARYL BENZAZOLE ANCILLARY LIGANDS: SYNTHESIS, CHARACTERIZATION AND ANTICANCER PROPERTIES	247
1. RESULTS AND DISCUSSION	250
1.1. Synthesis	250
1.2. Characterization.....	251
1.3. Aquation-Anation Equilibria	258
1.4. Reactivity against Nucleobases, Nucleotides and DNA: A Deep ¹ H NMR Study	260
1.5. Cytotoxic Activity	264
2. CONCLUDING REMARKS	265
3. EXPERIMENTAL SECTION	266
4. BIBLIOGRAPHY	274
ANNEX i.....	275
PART II. Ir(III) BISCYCLOMETALATED COMPLEXES WITH LUMINESCENT PROPERTIES	287
LUMINESCENCE IN ORGANOMETALLIC COMPOUNDS: A BRIEF REVIEW OF PROCESSES, FEATURES, PROPERTIES AND APPLICATIONS.....	289
1. LUMINESCENCE.....	291
1.1. Process of Luminescence	291
1.2 d-Block Metal Complexes	294
1.3. Cyclometalated Ir(III) and Rh(III) complexes	295
1.3.1. Synthesis	296

1.4. Stereoisomerism	297
1.4.1. Diastereoisomerism: <i>cis</i> - and <i>trans</i> - and <i>fac</i> - and <i>mer</i> - isomers	297
1.4.2. Enantiomerism derived from helicoidal chirality.....	298
1.5. Intrinsic Properties.....	299
1.6. Properties according to External Features	304
1.7. Applications	305
2. BIBLIOGRAPHY	308

**CHAPTER 7. Ir(III) BISCYCLOMETALATED COMPLEXES BEARING ARYLIAZOLE
ANCILLARY LIGANDS: SYNTHESIS, CHARACTERIZATION AND LUMINESCENT
PROPERTIES. APPLICATION IN LEC DEVICES..... 311**

1. RESULTS AND DISCUSSION	314
1.1. Synthesis	314
1.2. Characterization.....	315
1.3. Photophysical Properties.....	325
1.4. Electrochemistry	327
1.5. Theoretical Calculations.....	328
2. APPLICATIONS: LEC DEVICES.....	332
2.1. Fabrication of LEC devices	333
2.2. PL in thin films.....	334
2.3. Electroluminescent properties of the LECs.....	335
3. CONCLUDING REMARKS	339
4. EXPERIMENTAL SECTION	341
5. BIBLIOGRAPHY	351

**CHAPTER 8. Ir(III) BISCYCLOMETALATED COMPLEXES BEARING
HYDROXIPHENYL BENZAZOLE ANCILLARY LIGANDS: SYNTHESIS, CHARACTERIZATION
AND LUMINESCENT PROPERTIES. PHOTOCATALYSIS 353**

1. RESULTS AND DISCUSSION	356
1.1. Synthesis	356
1.2. Characterization.....	357
1.3. Photophysical Properties.....	359
1.4. Theoretical Calculations.....	362
1.5. Oxygen-Sensitive Photoluminescence.....	366
1.6. Photocatalysis	368
1.6.1. Oxidation of thioanisole	368
1.7. pH-dependent Photoluminescence and Reactivity of [48a].....	371
2. CONCLUDING REMARKS	372

3. EXPERIMENTAL SECTION	373
4. BIBLIOGRAPHY	375
ANNEX ii.....	377
Glossary.....	381

RESEARCHING OBJECTIVES

- ✓ To design and synthesize new families of organometallic half-sandwich complexes with potential anticancer activity and organometallic tris-chelate complexes with suitable luminescent properties.
- ✓ To characterise the new complexes by NMR spectroscopy, infrared spectroscopy, mass spectrometry, elemental analysis and molar conductivity.
- ✓ To obtain quality single crystals to solve the crystal structure of the complexes by X-ray diffraction.
- ✓ To study the reactivity of the complexes against biomolecules by NMR spectroscopy and mass spectrometry.
- ✓ To determine the cytotoxic activity of the complexes and to establish structure-activity relationships (SAR).
- ✓ To study the luminescent properties of the complexes.
- ✓ To use the complexes in LEC devices.
- ✓ To study the complexes in the photocatalysis of thioanisole from the photoactivation of molecular oxygen to singlet oxygen.

EXPERIMENTAL AND CHARACTERIZATION TECHNIQUES



**EXPERIMENTAL
TECHNIQUES**

CHARACTERIZATION TECHNIQUES	Elemental Analysis
	Infrared Spectroscopy
	Nuclear Magnetic Resonance Spectroscopy
	Molar Conductivity
	Mass Spectrometry
	X-ray Diffraction
OTHER TECHNIQUES	pH
	UV Spectroscopy
	Circular Dichroism
	Fluorescence Spectroscopy
	Spectroelectrochemistry-Cyclic Voltammetry
	LECs performance

The techniques used in this work are divided into three main groups. The “experimental techniques” describe the methods used in the synthesis of the complexes. The “characterization techniques” have been used in the complete characterization of all the complexes. Finally, “other techniques” include those techniques employed in the DNA-complex interaction or in characterization of other properties, like photoluminescence.

1. EXPERIMENTAL TECHNIQUES

Since some of the products, especially ruthenium complexes, might be oxygen-sensitive, all synthetic manipulations were carried out under N₂ atmosphere (water- and oxygen-free) using Schlenk techniques. The solvents, with the exceptions of water and ethanol, were distilled under nitrogen in the presence of the respective drying agents before its use (see Fig. 1).



Fig. 1. Distillation assembly.

2. CHARACTERIZATION TECHNIQUES

2.1.Elemental Analysis (CHN)

The elemental analyses were performed in an elemental analyzer LECO CHNS-932. Three different measurements were recorded to express the results as average values.

2.2.Infrared Spectroscopy (IR)

Medium Infrared spectra were recorded in a Nicolet Impact 410 (within the frequency range 4000 - 400 cm⁻¹), and in a Jasco FT/IR-4200 (see Fig. 2). Samples were prepared either in KBr pellets (refraction) or with an ATR accessory (reflexion) and spectra were recorded with 32 or 64 scans, respectively, and a resolution of 4.0 cm⁻¹. Data were treated with Spectra Manager v.2.10.01 (*Build 1*).



Fig. 2. Infrared Jasco FT/IR-4200 equipment.

2.3.Nuclear Magnetic Resonance (NMR)

NMR spectra were registered with a VARIAN UNITY INOVA 400 MHz spectrometer (¹H, 399.94 MHz; ³¹P, 161.9 MHz; ¹⁹F, 376.28 MHz; ¹³C, 100.6 MHz) and BRUKER ADVANCE 300 MHz. Both monodimensional (¹H, ³¹P, ¹⁹F and ¹³C) and bidimensional (¹H-¹H gCOSY, ¹H-¹H NOESY, ¹H-¹H ROESY, ¹H-¹³C gHSQC, ¹H-¹³C gHMBC and exceptionally ¹H-¹H gTOCSY and ¹H-³¹P HETCOR) experiments were recorded in common deuterated solvents (CDCl₃, CD₃OD, DMSO-d₆, D₂O, CD₃CN and THF-d₄), so as to establish a complete assignment of the signals. The spectra were usually recorded at 25 °C and with 32 scans and processed with MestReNova v10.0.2-15465. Water suppression PRESAT was occasionally used to clarify the spectra.

Deuterated solvents were deoxygenated by applying freezing-vacuum cycles and introducing a dry nitrogen atmosphere. Occasionally, some of them were also dried with molecular sieve (MS).

2.4.Molar Conductimetry (Λ_m)

Conductivity measurements were carried out with a CRISON 522 conductimeter (see Fig. 3), connected to a conductivity cell CRISON 52 92 with platinum electrodes. The commonly used solvents were water and acetonitrile, whose dielectric constants are 78.4 and 36.2 Ω⁻¹cm²mol⁻¹, respectively.¹ The solutions of the complexes (10⁻³ M) were prepared in 5 mL volumetric flasks and measured in test tubes.

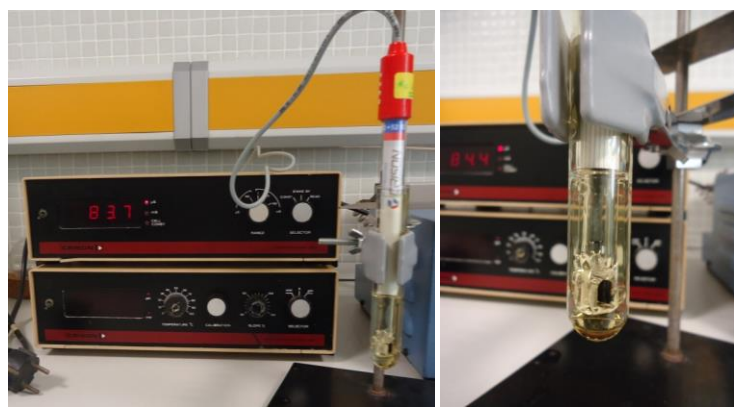


Fig. 3. (a) CRISON 522 conductimeter and (b) conductivity cell

2.5. Mass Spectrometry (FAB⁺-LSIMS and EI; ESI-MS)

Mass spectra were recorded with a Micromass AutoSpec spectrometer (FAB⁺ and EI) and with a LC-MS 6545 Q-TOF (ESI). EI was selected for organic molecules, whereas LSIMS and ESI-MS were preferred for organometallic complexes.

2.6. X-ray Diffraction

Acquisition of X-ray diffraction data of single crystal samples of some complexes was performed with a BRUKER SMART APEX CCD equipment. The structural resolution was carried out by Ana María Rodríguez- Fernández Pacheco, from the University of Castilla La Mancha (UCLM). Mercury 3.0 (Build RC5) was used to calculate the characteristic parameters of the structures, such as distances, angles, planes, etc.

Single crystals were grown by assorted methods. The most common and successful technique was slow evaporation of the solvent or of a mixture of solvents, although liquid diffusion, vapour diffusion or slow cooling of solutions were also employed (see Fig. 4 and Fig. 5).

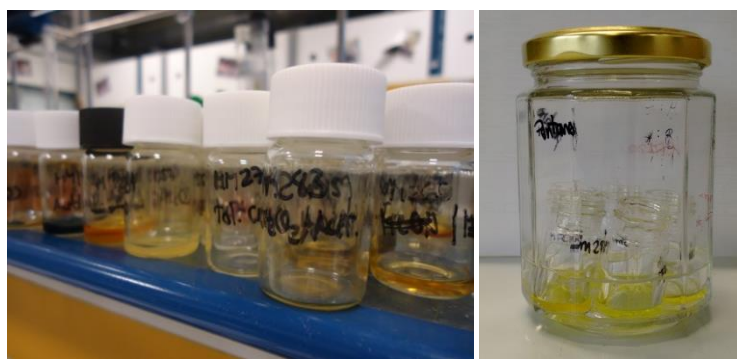


Fig. 4. Crystallizations by (a) slow evaporation and (b) vapour diffusion.

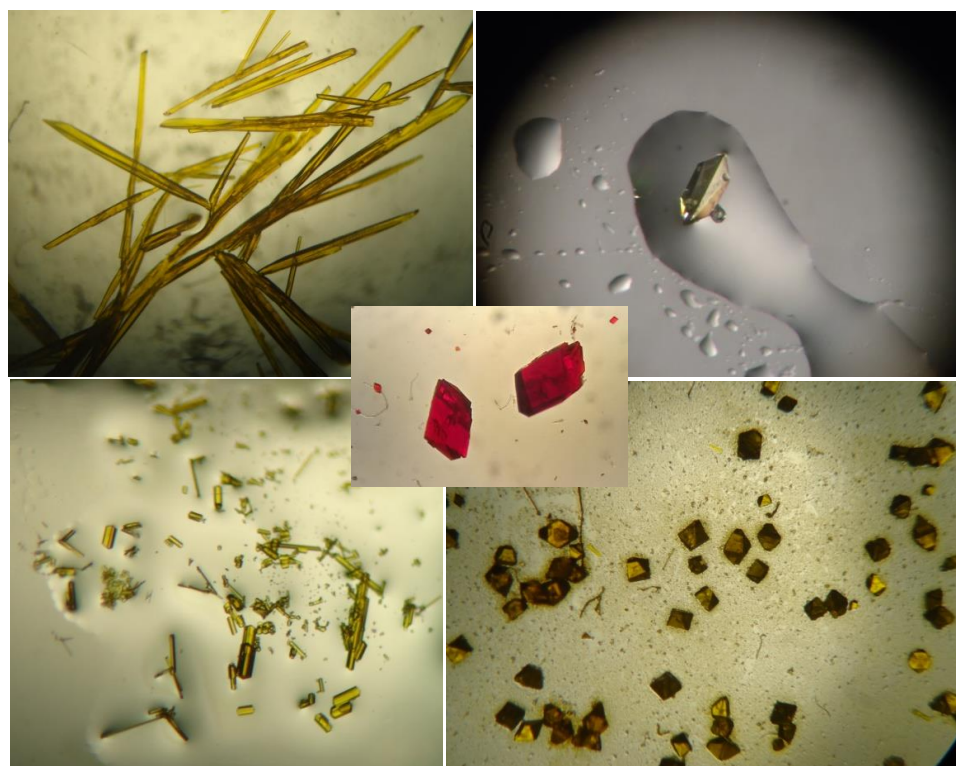


Fig. 5. Examples of crystals obtained by different techniques.

Suitable crystals were selected under a polarizing microscope, left on a slide and preserved in nujol to protect them against air or humidity (see Fig. 6).

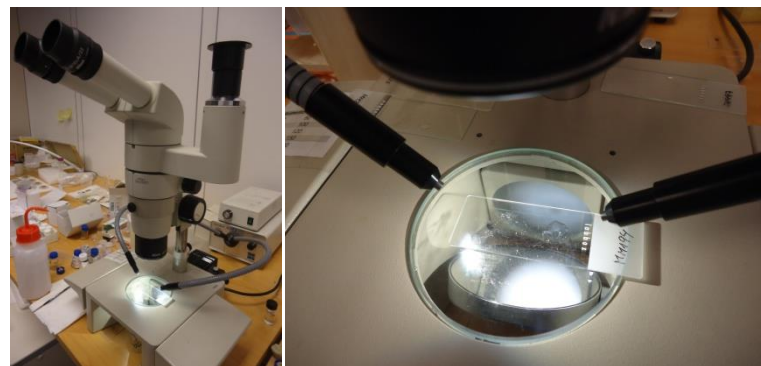


Fig. 6. Crystals selection process in the microscope.

Single crystals were mounted on a loop and the data were acquired at room or low temperature (77 K).

3. OTHER TECHNIQUES

3.1. pH

The pH values were measured at room temperature using a Metrohm 16 DMS Titrino pH meter fitted with a combined glass electrode and a 3 M KCl solution as a liquid junction, which was calibrated with Radiometer Analytical SAS buffer solutions.

3.2.UV spectroscopy

Spectrophotometric measurements of half-sandwich complexes were performed on a Hewlett-Packard 8453A spectrophotometer fitted out with diode array detection. The measurements were performed in a 1.0 cm path-length cell.

Spectrophotometric measurements of the Ir(III) biscyclometalated complexes were performed by M^a del Carmen Carrión in the group of F. A. Jalón and B. R. Manzano, from the University of Castilla La Mancha, Ciudad Real on a SECOMAM-UVIKON XS model. The measurements were also performed in a 1.0 cm path-length cell.

3.3.Circular Dichroism (CD)

CD spectra were recorded on a MOS-450 BioLogic spectrometer. The measurements were performed at 25 °C in 1.0 cm path-length cells in the physical-chemistry laboratory of Begoña García.

3.4.Fluorescence Spectroscopy

Luminescent properties of the complexes were registered by M^a del Carmen Carrión in the group of F. A. Jalón and B. R. Manzano, from the University of Castilla La Mancha, Ciudad Real, in a PTI spectrofluorometer with a Xenon arc lamp. The same equipment was used in the lifetime measurements, using a high resolution PTI N₂ laser GL-3300 model.

In addition, some measurements were carried out by the group of E. Ortí and H. Bolink, from the ICMol, University of Valencia. An integrating sphere Hamamatsu absolute quantum yield C9920 was used in the emission maxima and quantum yields measurements, using an excitation wavelength of 320 nm.

3.5.Spectroelectrochemistry - Cyclic Voltammetry (CV)



Fig. 7. Spelec equipment and electrolytic cell showing electrodes.

UV-VIS spectroelectrochemistry measurements were carried out in collaboration with the group of A. Colina and A. Heras, from the University of Burgos, with SPELEC instrument (DropSens, Spain) used in combination with a reflection probe, working in a near-normal reflection configuration in a reflection cell (DRP-REFLECELL, DropSens, Spain) (see Fig. 7).

Electrochemical measurements were performed by Dra. A. Heras, from the University of Burgos using a customized SPELEC (DropSens) equipment, a commercial fully integrated synchronized spectroelectrochemical device, that includes a bipotentiostat/galvanostat controlled by DropView (DropSens). All experiments were carried out with a three-electrode cell using a platinum-disc with a diameter of 2 mm or a carbon-disc with a diameter of 3 mm as working electrode, a platinum-wire as auxiliary electrode, and a silver-wire as pseudo-reference electrode.

3.6.LECs performance

The LEC devices were prepared by A. Pertegás and C. Momblona in the group of H. Bolink, from the ICMol, University of Valencia. The device lifetime was measured by applying a pulsed current and monitoring the voltage and the luminance versus time by a True Colour Sensor MAZeT (MTCSiCT Sensor) with a Botest OLT OLED Lifetime-Test System. The electroluminescent (EL) spectra were measured using an Avantes AvaSpec-2048 Fiber Optic Spectrometer during device lifetime measurement.

4. BIBLIOGRAPHY

- (1) Angelici, R. J. In *Técnicas y Síntesis en Química Inorgánica*; Editorial Reverté, S.A., 1979; p. 243.

GENERAL INTRODUCTION



1. ABOUT THE METALS

Three different transition metals have been selected in this work: ruthenium, rhodium and iridium. All of them are within the “platinum group” of the periodic table (see Fig. 1), even though they exhibit different chemical and physical properties. They belong to the second and third transition rows and have 4d and 5d half-filled orbitals, which confer them special properties as organometallic complexes.

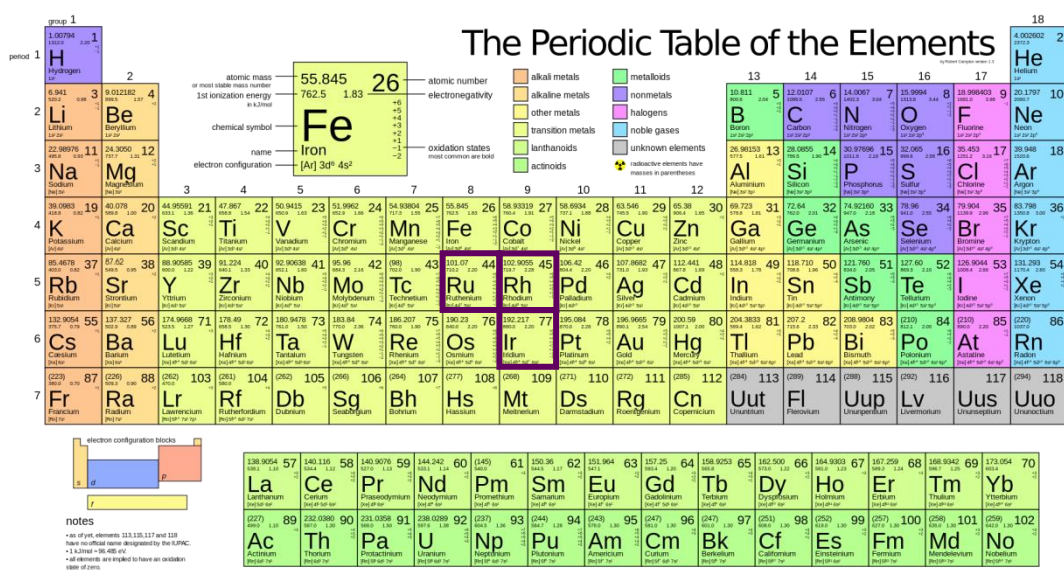


Fig. 1. Periodic Table of the elements.

1.1.Ruthenium

Ruthenium is an element of the group 8 in the second transition row of the periodic table, with an atomic number of 44, an atomic weight of 101.07 u and electronic configuration [Kr]4d⁷5s¹. Seven different naturally occurring isotopes are stable: ⁹⁶Ru(5.5%), ⁹⁸Ru(1.9%), ⁹⁹Ru(12.7%), ¹⁰⁰Ru(12.6%), ¹⁰¹Ru(17.0%), ¹⁰²Ru(31.6%) and ¹⁰⁴Ru(18.7%)¹. It shows a wide range (0 - +8) of oxidation states, being +2 and +3 the most common and relevant ones. Octahedral ruthenium(II) shows a LS d⁶ (t_{2g}⁶) electronic configuration and therefore is a diamagnetic nucleous suitable for NMR characterization. Ruthenium(III), is a LS d⁵ (t_{2g}⁵) and hence, is paramagnetic. The rest of oxidation states (+4 - +8) are less common or rare, so they are not discussed in this introduction.

We will focus on Ru(II) species because all the synthesized complexes have this oxidation state. The most characteristic geometries for ruthenium(II) compounds are octahedral and pseudo-octahedral and the uses of these type of complexes are very diverse.²

1.2.Rhodium

Rhodium is an element of the group 9 and belongs to the second transition row of the periodic table, with an atomic number of 45, an atomic weight of 102.9055 u and electronic configuration [Kr]4d⁸5s¹. Only one naturally occurring isotope is stable: ¹⁰³Rh(100%)¹, yet it is active in NMR. Octahedral rhodium(III) shows a LS d⁶ (t_{2g}⁶) electronic configuration and therefore is a diamagnetic nucleous suitable for NMR characterization. Rhodium(I), is a d⁸ and also diamagnetic.²

1.3.Iridium

Iridium is an element of the group 9 and belongs to the third transition row of the periodic table, with an atomic number of 77, an atomic weight of 192.217 u and electronic configuration [Xe]4f¹⁴5d⁷6s². Two different naturally occurring isotopes are stable: ¹⁹¹Ir(37.3%) and ¹⁹³Ir(62.7%).¹ Octahedral iridium(III) shows a LS d⁶ (t_{2g}⁶) electronic configuration and therefore a diamagnetic nucleous suitable for NMR characterization. Iridium(I), is a d⁸ and also diamagnetic.²

Rhodium and Iridium exhibit also a wide range of oxidation states, from -3 to +6. Although the most common one is +3, the +1 oxidation state is usually well stabilized and favoured with π -acceptor ligands. The oxidation state +4 marks a difference between rhodium and iridium, as it occurs in iridium but not in rhodium.³

As far as the features of the elements are concerned, Table 1 shows some differences among them. These differences are essential, so as to understand and interpret the behaviour of each metal in coordination chemistry.

Table 1. Properties of the elements.³

	Ru	Rh	Ir
Atomic number (Z)	44	45	77
Natural Isotopes	7	1	2
Atomic Weight /gmol⁻¹	101.07	102.9055	192.217
Electronic configuration	[Kr]4d ⁷ 5s ¹	[Kr]4d ⁸ 5s ¹	[Xe]4f ¹⁴ 5d ⁷ 6s ²
Electronegativity	2.2	2.2	2.2
Metallic radius (12-coordinate)/ pm	134	134	135.5
Ionic radius (6-coordinate)/ pm			
Oxidation state IV	62	60	62.5
Oxidation state III	68	66.5	68
Oxidation state II	-	-	-
Density (20 °C)/g cm⁻³	7.847	12.39	22.56

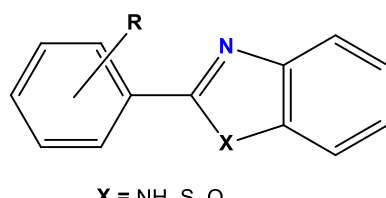
It is noteworthy that the three element have similar metal radius, even though iridium belongs to a different row from that of ruthenium and rhodium. This is due to

the lanthanide contraction. Likewise, the same effect occurs with the ionic radius. Nevertheless, the densities of the three metals are very different. In the case of iridium, the presence of a much higher Z number (more number of protons and neutrons) makes the density increase.

2. ABOUT THE CHELATING LIGANDS

2.1. Arylbenzazoles

Arylbenzazole (see Fig. 2) is the general name used to describe 2-substituted derivatives of benzazoles. These structures contain a benzene ring fused to an 1,3-azole ring,⁴ which can be an imidazole, an oxazole or a thiazole. Aryl moieties can be pyridyl, phenyl or phenyl derivatives, the latter of which undergo cyclometallation easily with Ru(II), Rh(III) and Ir(III). They display luminescence, owing to the excited-state intramolecular electron transfer.⁵ In addition, these **pharmacophores** are part of different natural products (*e.g.* vitamine B12, see Fig. 3) as well as relevant drugs (*e.g.* omeprazole, see Fig. 3).^{6,7,8,9}



$X = \text{NH, S, O}$

Fig. 2. General structure of arylbenzazole group.

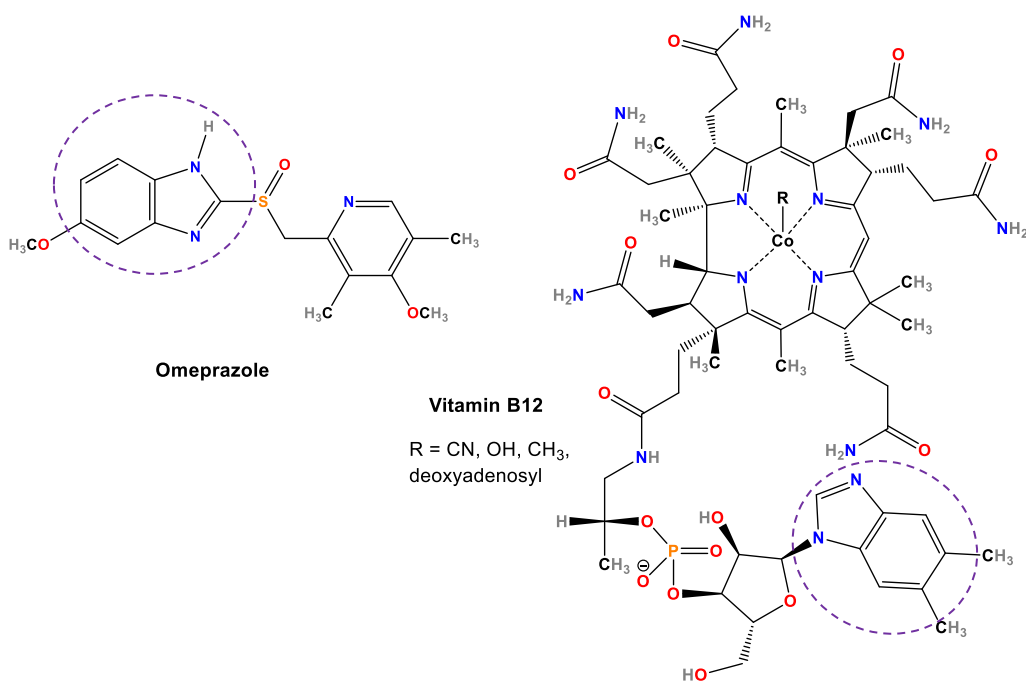


Fig. 3. Chemical structures of Omeprazole and Vitamin B12. The dashed purple circles highlight the benzimidazole moieties of the corresponding molecules.

As far as benzimidazoles are concerned, the first benzimidazole was synthesised in 1872 by Hoebrecker. They were called “anhydrobases”, as they are formed by the loss of water.⁴ These compounds exhibit tautomerism in solution⁴, as a result of which, the

NH proton exchanges rapidly between both N atoms, making them equivalent in the NMR time scale at room temperature (see Fig. 4).

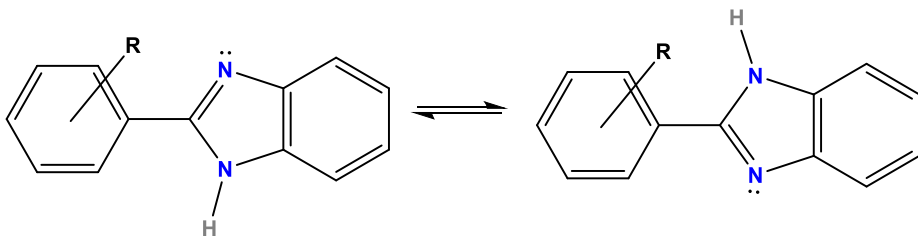


Fig. 4. Tautomeric exchange of benzimidazoles.

Imidazole, oxazole and thiazole five-membered rings

Five-membered rings with two heteroatoms (1,3-azoles) are composed of a sp^2 -hybridized azomethine nitrogen atom (pyridine-type or imine-type nitrogen) and another heteroatom ($X = \text{NH}, \text{O}, \text{S}$). Thus, the basicity of the ring depends on the latter. In addition, the heteroatom X exerts two opposite effects: (i) mesomerically electron-donor effect (base-strengthening effect) and (ii) inductively electron-withdrawal effect (base-weakening effect). When both heteroatoms are nitrogen, the mesomeric effect predominates and consequently its basicity increases. On the contrary, when the heteroatom is oxygen or sulphur, the inductive effect is higher and as a result, their basicity decreases. Thus, the tendency of the basicity of the azoles are: imidazole ($\text{pK}_a = 7.0$) > thiazole ($\text{pK}_a = 2.5$) > oxazole ($\text{pK}_a = 0.8$).¹⁰ These features can modify the properties of the corresponding metal complexes.

Metal complexes with arylbenzazoles have been widely synthesised^{11,12,13,14} and used as catalysts^{15,16,17,18,19,20}, drugs (**anthelmintic**, anticancer, Alzheimer disease)^{21,22,23,24,25,26,27,28} or as solar cells²⁹, but also in cells staining³⁰ and lighting devices,³¹ owing to their excellent luminescent properties^{32,33,34,35}. They adopt a bidentate chelate coordination mode when they bind to a metal, so they behave as N,N-, O,N- and C,N-donors. The azole ring always coordinates through the nitrogen atom, since it exhibits a lone pair in an sp^2 hybrid orbital in the plane of the ring available to form σ -covalent bonds with metals and one electron in a pure p_z orbital, delocalized in the aromatic π -system (aromatic sextet). This p_z orbital is half-filled, so that the orbital can accept one electron from a d orbital of a metal and consequently, the bond is reinforced (π -backbonding). However, both oxygen and sulphur ($X = \text{O}, \text{S}$, in benzoxazole and benzothiazole, respectively) have a lone pair as part of the aromatic sextet, apart from the lone pair in an sp^2 hybrid orbital in the plane of the ring. Since the p_z orbital of the heteroatom is full, the π -backbonding is blocked. Thus, they are less prone than nitrogen to binding to a metal (see Fig. 5).^{10,36}

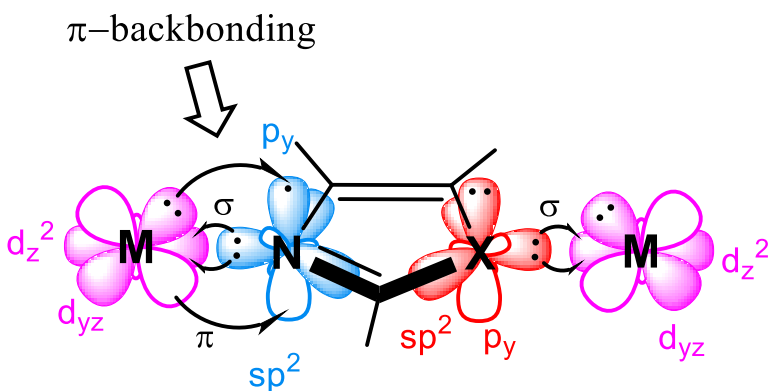


Fig. 5. Hypothetical M-N and M-X coordination modes for the azole ring (X = O, S).

2.1.1. Pyridylbenzazoles

Among pyridylbenzazoles, 2-(2'-pyridyl)benzimidazole (pybim) and 2-(2'-pyridyl)benzoxazole (pybox) have been selected for this work (see Fig. 10).

Moreover, the secondary amine group of the imidazole allows the alkylation of the nitrogen through deprotonation with a strong base (*e.g.* potassium or cesium carbonate) followed by the insertion of the alkyl group from the respective halide derivative (see Fig. 6).¹⁷

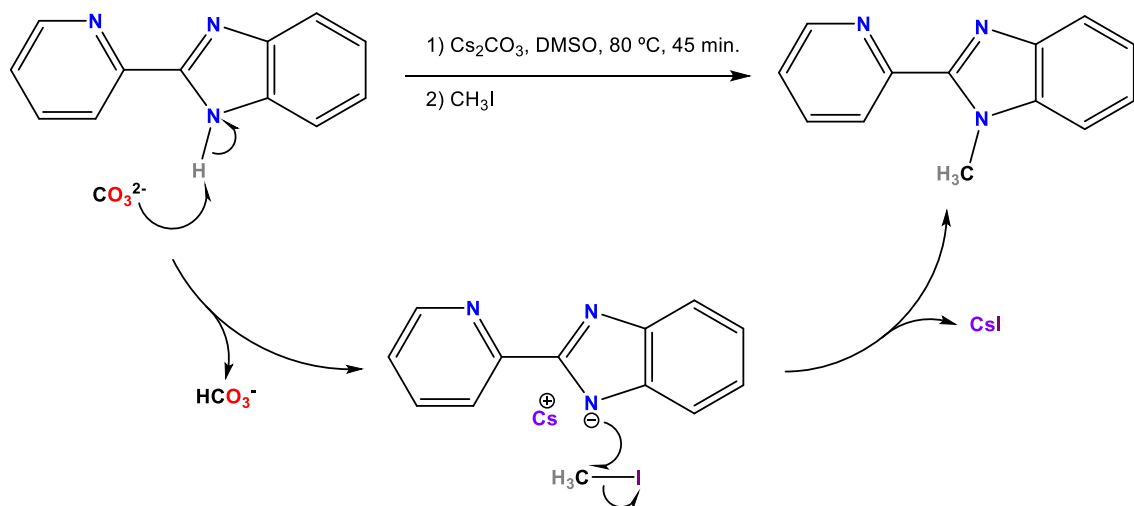


Fig. 6. Synthesis of 2-(2-pyridyl)-N-methylbenzimidazole.

The 2-(2'-pyridylbenzoxazole) ligand (see Fig. 10) can be synthesised from 2-aminophenol and 2-pyridinecarboxaldehyde as the starting products by using different oxidants, for instance, silver oxide³⁷, oxygen with activated carbon (Shirasagi reaction)^{38,39}, DDQ⁴⁰ or IBX⁴¹. The pathway of the reaction involves the formation of a Schiff's base and its subsequent oxidation. However, the latter oxidant (IBX) was selected, due to the easiness of the synthesis and the good yields (see Fig. 7).

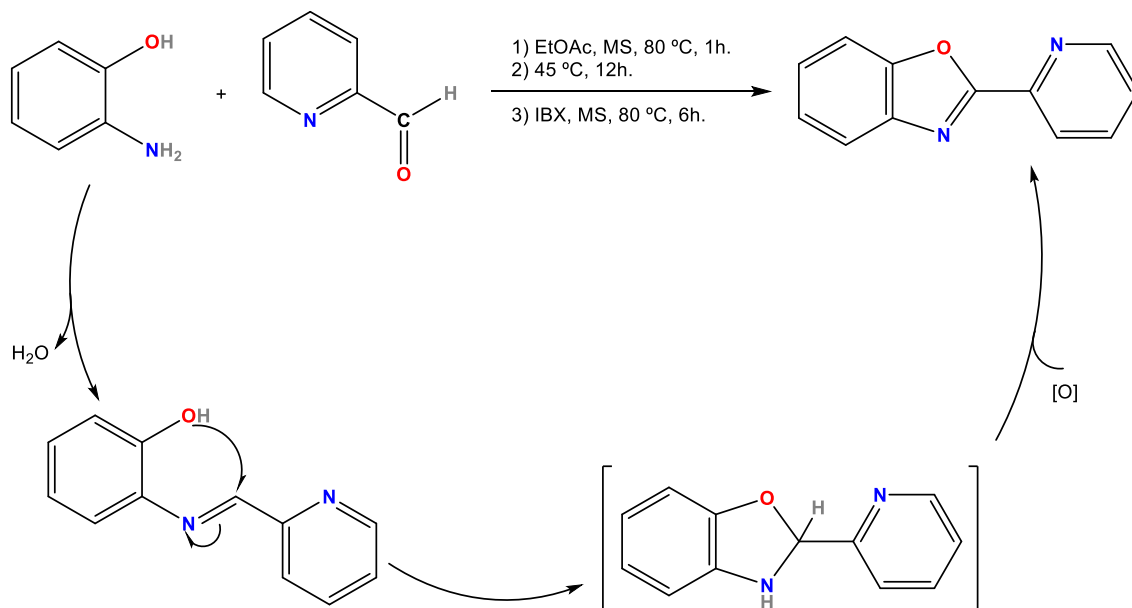


Fig. 7. Synthesis of 2-(2-pyridyl)benzoxazole.

2.1.2. Pyridylimidazole

The 2-(2'-pyridyl)imidazole (pyim) ligand was synthesised (see Fig. 8) from the cold mixture of 2-pyridinecarboxaldehyde, glyoxal and aqueous ammonia.^{42,43}

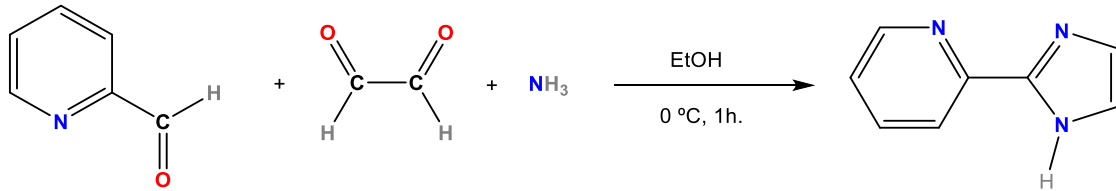


Fig. 8. Synthesis of 2-(2-pyridyl)imidazole.

2.1.3. Phenylbenzimidazoles

The 2-phenylbenzimidazole (pbim) ligand (see Fig. 10) is a promising alternative to the cyclometalating phenylpyridine C,N-ligand, which acts as an anionic ligand after C-H bond activation in the presence of a weak base (*e.g.* sodium acetate) favoured by the presence of a metal ion.⁴⁴ After deprotonation, the anionic sp^2 carbon atom stabilizes the electronic charge of the metal cation and reinforces the M-C bond.

2.1.4. Hydroxyphenylbenzazoles

The hydroxyphenylbenzazoles (see Fig. 10) selected for this work are 2-(2'-hydroxyphenyl)benzimidazole (hpbitm) and 2-(2'-hydroxyphenyl)benzothiazole (hpbtz). They both need deprotonation of the hydroxyl group with a strong base (*e.g.* triethylamine), so as to coordinate to a metal.²⁷ The formation of a six-membered chelate ring with the metal bends and twists the ligands, resulting in the lack of coplanarity between the two aromatic rings that form the ligand.

2.1.5. Aminophenylbenzazoles

The aminophenylbenzazoles (see Fig. 10) behave as N,N-chelate ligands and they do not need deprotonation of the amino group to coordinate to the metal. 2-(2'-aminophenyl)benzimidazole (apbim) and 2-(2'-aminophenyl)benzothiazole (apbtz) were chosen for this work.^{27,45} As well as in the case of hydroxiphenylbenzoazoles, the formation of a six-membered chelate ring causes the lack of coplanarity between the two moieties of the ligands.

2.1.6. Thiabendazoles

Thiabendazole (2-(4-thiazolyl)benzimidazole or tbz – see Fig. 10) is one of the best-known benzimidazoles and has been widely used as an anthelmintic and an antifungal agent.^{7,9} It is also an arylbenzazole and its structure is similar to the pyridylbenzimidazole. The difference is basically focused on the 2-substituted ring of the benzimidazole. Thiabendazole has a thiazolyl ring, instead of a pyridine, yet the thiazolyl ring also displays aromaticity. The benzimidazole moiety can also be N-alkylated as for pyridylbenzimidazole (see Fig. 9 for conditions).¹⁷

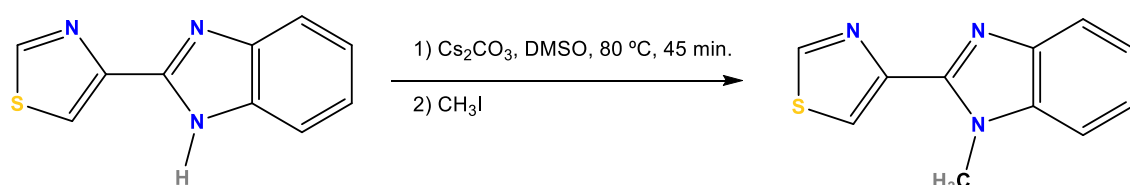


Fig. 9. Synthesis of N-Methylthiabendazole.

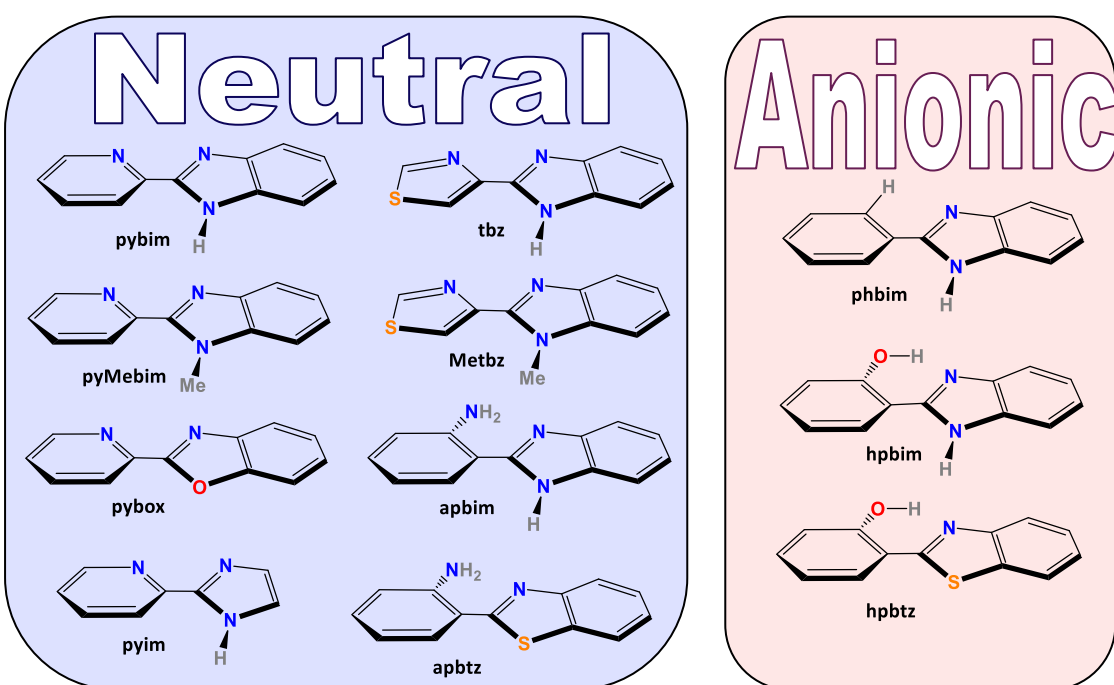


Fig. 10. Ligands used in this work, the neutral N,N-ligands (left-blue) and the proligands used as precursors of anionic C,N- and O,N-ligands (right-pink).

3. BIBLIOGRAPHY

- (1) Housecroft, C. E.; Sharpe, A. E. *Inorganic Chemistry*; Fourth edition; Pearson, **2012**.
- (2) *Comprehensive Coordination Chemistry: The Synthesis, Reactions, Properties & Applications of Coordination Compounds*; Wilkinson, G.; Gillard, R. D.; McCleverty, J. A., Eds.; Pergamon, **1987**.
- (3) Greenwood, N. N.; Earnshaw, A. *Chemistry of the Elements*; Second Edition; Butterworth Heinemann, **1997**.
- (4) Wright, J. B. *Chem. Rev.* **1951**, *48*, 397–541.
- (5) Fahrni, C. J.; Henary, M. M.; Vanderveer, D. G. *J. Phys. Chem. A* **2002**, *106*, 7655–7663.
- (6) Taylor, P.; Roopashree, B.; Gayathri, V. *J. Coord. Chem.* **2012**, *65*, 1354–1370.
- (7) Khokra, S. L.; Choudhary, D. *Asian J. Biochem. Pharm. Res.* **2011**, *1*, 476–486.
- (8) R.G., I.; D.D., M. *Int. J. Drug Res. Technol.* **2011**, *1*, 26–32.
- (9) Gurvinder, S.; Maninderjit, K.; Mohan, C. *Int. Res. J. Pharm.* **2013**, *4*, 82–87.
- (10) Gupta, R. R.; Kumar, M.; Gupta, V. *Heterocyclic Chemistry II*; Springer Berlin Heidelberg: Berlin, Heidelberg, **1999**.
- (11) Machura, B.; Wolff, M.; Kusz, J.; Kruszynski, R. *Polyhedron* **2009**, *28*, 2949–2964.
- (12) Esparza-Ruiz, A.; González-Gómez, G.; Mijangos, E.; Peña-Hueso, A.; López-Sandoval, H.; Flores-Parra, A.; Contreras, R.; Barba-Behrens, N. *Dalt. Trans.* **2010**, *39*, 6302–6309.
- (13) Chanda, N.; Sarkar, B.; Kar, S.; Fiedler, J.; Kaim, W.; Lahiri, G. K. *Inorg. Chem.* **2004**, *43*, 5128–5133.
- (14) Thakur, P.; Chakravortty, V.; Dash, K. C. *Indian J. Chem.* **1999**, *38A*, 1223–1227.
- (15) Ogweno, A. O.; Ojwach, S. O.; Akerman, M. P. *Appl. Catal. A Gen.* **2014**, *486*, 250–258.
- (16) Sun, W.-H.; Hao, P.; Zhang, S.; Shi, Q.; Zuo, W.; Tang, X.; Lu, X. *Organometallics* **2007**, *26*, 2720–2734.
- (17) Zeng, F.; Yu, Z. *Organometallics* **2008**, *27*, 2898–2901.
- (18) Gao, R.; Xiao, L.; Hao, X.; Sun, W.-H.; Wang, F. *Dalt. Trans.* **2008**, 5645–5651.
- (19) Ojwach, S. O.; Westman, G.; Darkwa, J. *Polyhedron* **2007**, *26*, 5544–5552.
- (20) Ogweno, A. O.; Ojwach, S. O.; Akerman, M. P. *Dalt. Trans.* **2014**, *43*, 1228–1237.
- (21) He, X.-F.; Vogels, C. M.; Decken, A.; Westcott, S. A. *Polyhedron* **2004**, *23*, 155–160.
- (22) Taylor, P.; Roopashree, B.; Gayathri, V.; Gopi, A.; Devaraju, K. S. *J. Coord. Chem.* **2012**, *65*, 4023–4040.
- (23) Bharti, N.; Shailendra; Garza, M. T. G.; Cruz-Vega, D. E.; J. Castro-Garza, b K. S.; Naqvi, F.; Maurya, M. R.; Azam, A. *Bioorganic Med. Chem. Lett.* **2002**, *12*, 869–871.
- (24) Stepanenko, I. N.; Novak, M. S.; Gerhard, M.; Roller, A.; Hejl, M.; Arion, V. B.; Jakupec, M. A.; Keppler, B. K. *Inorg. Chem.* **2011**, *50*, 11715–11728.
- (25) Ginzinger, W.; Mu, G.; Arion, V. B.; Jakupec, M. A.; Roller, A.; Galanski, M.; Reithofer, M.; Berger, W.; Keppler, B. K. *J. Med. Chem.* **2012**, *55*, 3398–3413.
- (26) Yellol, G. S.; Yellol, J. G.; Kenche, V. B.; Liu, X. M.; Barnham, K. J.; Donaire, A.; Janiak, C.; Ruiz, J. *Inorg. Chem.* **2015**, *54*, 470–475.
- (27) Rodri, C.; Ventura, S. *J. Am. Chem. Soc.* **2009**, *131*, 1436–1451.
- (28) Shi, D.-F.; Bradshaw, T. D.; Wrigley, S.; McCall, C. J.; Lelieveld, P.; Fichtner, I.; Stevens, M. F. G. *J. Med. Chem.* **1996**, *39*, 3375–3384.

- (29) Huang, W.-K.; Cheng, C.-W.; Chang, S.-M.; Lee, Y.-P.; Diau, E. W.-G. *Chem. Commun.* **2010**, *46*, 8992–8994.
- (30) Baggaley, E.; Weinstein, J. a.; Williams, J. a G. *Coord. Chem. Rev.* **2012**, *256*, 1762–1785.
- (31) Jia, W.-L.; Hu, Y.-F.; Gao, J.; Wang, S. *Dalton Trans.* **2006**, 1721–1728.
- (32) Tong, Y.-P.; Lin, Y.-W. *J. Chem. Crystallogr.* **2008**, *38*, 613–617.
- (33) Liu, Q. De; Jia, W. L.; Wang, S. *Inorg. Chem.* **2005**, *44*, 1332–1343.
- (34) Shankar, B.; Sahu, S.; Deibel, N.; Schweinfurth, D.; Sarkar, B.; Elumalai, P.; Gupta, D.; Hussain, F.; Krishnamoorthy, G.; Sathyendiran, M. *Inorg. Chem.* **2014**, *53*, 922–930.
- (35) Tong, Y.; Zheng, S.; Chen, X. *Inorg. Chem.* **2005**, *44*, 4270–4275.
- (36) Joule, J. A.; Mills, K. *Heterocyclic Chemistry*; Fifth Edition; John Wiley & Sons, Inc, **2010**.
- (37) Yoshifuji, M.; Nagase, R.; Kawashima, T.; Inamoto, N. *Heterocycles* **1978**, *10*, 57–60.
- (38) Hayashi, M. *Chem. Rec.* **2008**, *8*, 252–267.
- (39) Kawashita, Y.; Nakamichi, N.; Kawabata, H.; Hayashi, M. *Org. Lett.* **2003**, *5*, 3713–3715.
- (40) Chang, J.; Zhaob, K.; Pan, S. *Tetrahedron Lett.* **2002**, *43*, 951–954.
- (41) Chen, F.; Shen, C.; Yang, D. *Tetrahedron Lett.* **2011**, *52*, 2128–2131.
- (42) CHISWELL, B.; LIOSS, Fr.; MORRIS, B. S. *Inorg. Chem.* **1964**, *3*, 110–113.
- (43) Stupka, G.; Gremaud, L.; F. Williams, A. *Helv. Chim. Acta* **2005**, *88*, 487–495.
- (44) Boutadla, Y.; Davies, D. L.; Jones, R. C.; Singh, K. *Chem. - A Eur. J.* **2011**, *17*, 3438–3448.
- (45) Małecki, J. G. *Struct. Chem.* **2011**, *23*, 461–472.

PART I. Ru(II), Rh(III) and Ir(III) HALF-SANDWICH COMPLEXES WITH ANTICANCER PROPERTIES



CANCER: A BRIEF STORY OF ORGANOMETALLIC DRUGS AND MECHANISMS OF ACTION



1. CANCER

What is it?

Cancer is one of the most malignant diseases in the world. It is produced by the uncontrolled growth and spread of cells and it can affect almost any part of the body.¹ The WHO (World Health Organization) has determined in 8.2 million the number of deaths caused by cancer in the year 2012 worldwide with 14.1 million new cases detected in the same year. The most malignant cancers are lung, liver, stomach, colorectal and breast. There are five behavioural and dietary risks we should control, in order to avoid the development of the diseases: (i) high blood mass index, (ii) low fruit and vegetable intake, (iii) lack of physical activity, (iv) tobacco and (v) alcohol, being the last one the most relevant risk. In addition, there are other risk factors such as chronic infections (Hepatitis B and Hepatitis C virus), some types of Human Papilloma Virus (HPV), air pollution and indoor smoke from household use of solid fuels.²

How is it produced?

Cancer arises when one single cell turns from a normal cell into a tumour cell. This change is the result of the interaction between a person's genetic factors and three kind of external agents:²

- Physical carcinogens: UV and ionizing radiation.
- Chemical carcinogens: asbestos, components of tobacco smoke, aflatoxin (a food contaminant) and arsenic (a drinking water contaminant).
- Biological carcinogens: infections with certain viruses, bacteria or parasites.

Which are the treatments?

There are three main strategies to cure cancer: surgery, chemotherapy and radiotherapy. Nevertheless, nowadays another treatment is growing: immunotherapy. Furthermore, when the disease has no cure, there are some palliative cares to relieve symptoms and to make people live more comfortably.²

In this work, we will focus on chemotherapy. To begin with, we will discuss and comment the beginnings of anticancer agents, as well as the most relevant metal compounds used as chemotherapeutic agents.

1.1. Early history of anticancer drugs: cisplatin

Due to the big amount of deaths caused by cancer, the development of new anticancer drugs is the main aim of research in this field. As far as chemotherapy is concerned, transition metal complexes are promising drugs for cancer treatment. Cisplatin was the first metal anticancer drug serendipitously discovered by Barnett Rosenberg. In 1961 he realized that cells behaved as dipoles in cell division, so he decided to apply an electromagnetic radiation to cells to mimic the process. Barnett

Rosenberg and L. VanCamp set the device to carry out the experiment with platinum electrodes and exposed *Escherichia Coli* to an electric field, before testing the same experiment in mammalian cells. When they examined the bacterial cells after the experiment, they discovered that the bacterial rods had grown, which meant that the cell division was inhibited, but not the growth. However, they immediately realized that it was not due to the action of the electric field but due to the action of electrolysis products from the platinum electrodes. T. Krigas, a chemist, identified the product responsible for the above-mentioned effect as probably $[\text{NH}_4]_2[\text{PtCl}_6]$. Nevertheless, when they added the synthesised compound to the bacterial cells, they found a bactericidal activity instead of the growth of rods.^{3,4} After some experiments they found out that light was essential to produce the neutral platinum(IV) complex $[\text{Pt}(\text{NH}_3)_2\text{Cl}_4]$ with two isomers: *cis*- and *trans*- . The latter was the more thermodynamically stable and the one they first prepared. They also synthesized the corresponding *cis*-platinum(IV) complex and the platinum(II) derivatives and found both the complexes of Pt(II) and Pt(IV) in the *cis*- conformation were active against cell division, whereas the *trans*- conformations were inactive. In 1968 they tested the complexes in cancer cells and found that the same effect with the *cis*- isomer as in bacterial cells³ and in 1969 a paper was published with some interesting results of the anticancer activity against sarcoma and leukaemia cancers of these platinum complexes.⁵

Since that moment cisplatin, as it was called, became the most important drug to treat almost every kind of cancer worldwide and nowadays it is still used. This serendipitous discovery encouraged the search of new platinum compounds and gave rise to a series of empirical rules that active platinum compounds (either square-planar or octahedral) should have. The conclusion was that these complexes ought to^{6,7}:

- 1) be neutral to facilitate passive diffusion into cells.
- 2) contain two *cis* leaving groups.
- 3) have relatively inert ligands working as nonleaving groups. Ammines seem to be preferred.
- 4) have leaving groups with a “window of lability” centered on chloride. This is, the nature of the leaving group modifies the reactivity of the complex, and chloride ions are preferred, as they have an intermediate leaving ability.

However, cisplatin has severe side effects, such as nausea, vomiting, nephrotoxicity and loss of sensation in the extremities, and some drawbacks like non-specificity of the drug or platination of the sulphur residues on proteins.⁸ For these reasons and taking into account the previous statements, some new platinum-based complexes were synthesized and screened, with the aim of improving toxicity and specificity (see Fig. 1). As less labile leaving groups were thought to improve toxicity, carboplatin (diammine[1,1-cyclobutanedicarboxylato(2-)O,O']platinum(II)) was tested (see Fig. 1). The substitution of the leaving group did improve nephrotoxicity.⁹ Carboplatin was the first platinum derivative clinically used after cisplatin. It reduces the side effects due to the aquation rate constant, which is lower than for cisplatin and thus, administration

doses can be higher and can last longer. Nevertheless, it did not overcome platinum resistance. Oxaliplatin (see Fig. 1) was the first drug able to overcome this resistance through the inhibition of DNA synthesis and also reduces the side effects of cisplatin. Both carboplatin and oxaliplatin have been approved for world-wide use (Carboplatin: 1989. Oxaliplatin: France, 1996; USA, 2002 and Japan, 2005).^{10,11} Picoplatin (see Fig. 1), a cisplatin derivative, was shown to overcome resistance to cisplatin, carboplatin and oxaliplatin. The methyl group of the pyridine ring is placed nearly over the metal centre, what provides steric hindrance to the attack by nucleophiles, especially thiols. Thus, it prevents glutathione-mediated drug resistance. It entered clinical trials in 1997.^{10,11}

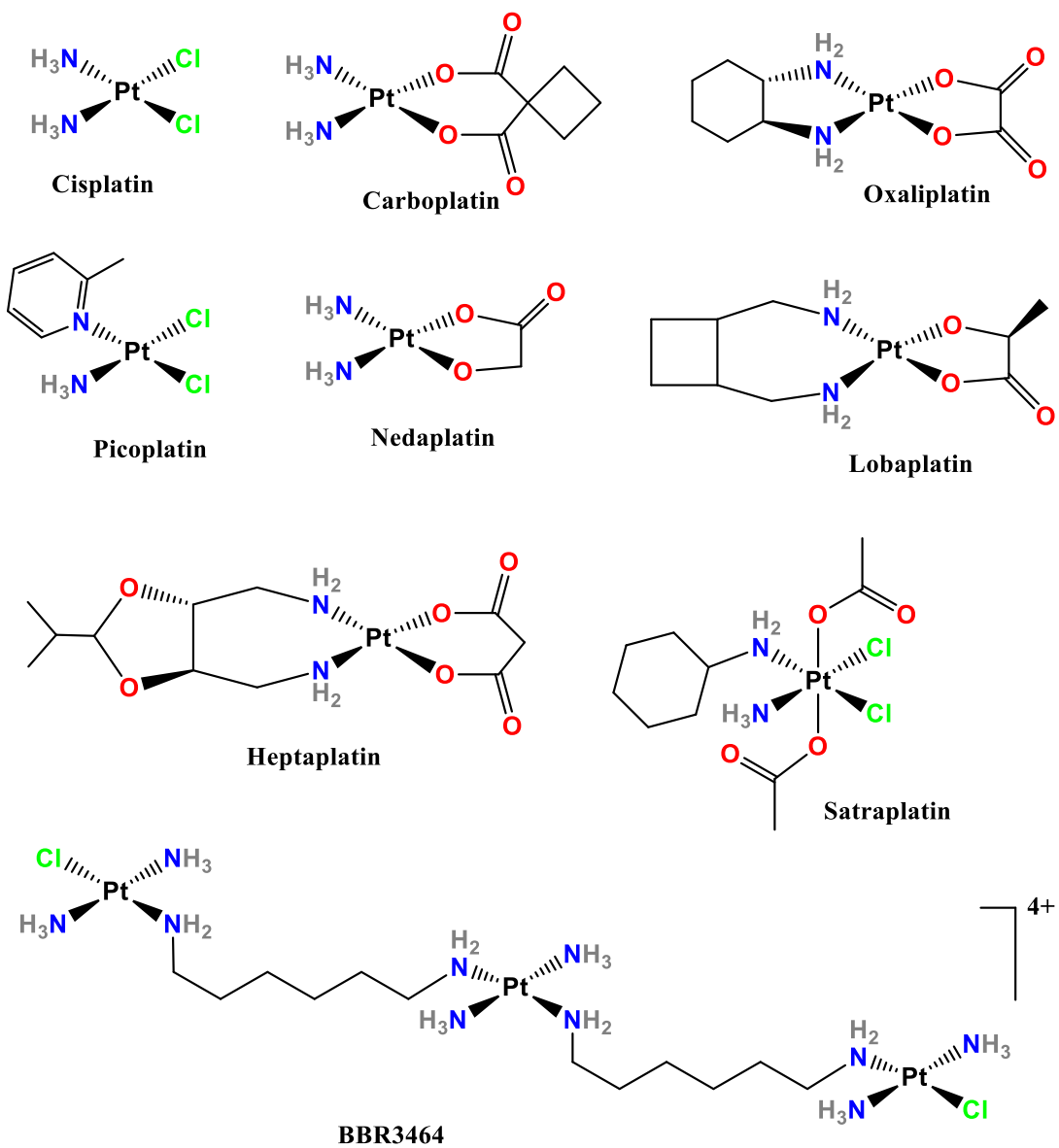


Fig. 1. Platinum-based anticancer drugs.^{12,13,10,14}

Nedaplatin, lobaplatin and heptaplatin are based in the latter platinum complexes, even though they have been only approved for its use in Japan (1995), China (2003) and South Korea (1999), respectively. Nedaplatin (see Fig. 1) is a second generation cisplatin analogue much more soluble (*ca.* 10 times) and with lower nephrotoxicity than cisplatin. Phase I and II clinical trials are ongoing in combined therapies with other drugs for the

treatment of different types of cancers, showing promising results. Lobaplatin (see Fig. 1) is a third generation platinum anticancer drug used in a type of leukaemia and exhibit important activity against cisplatin and carboplatin cross-resistance. It has entered phase III clinical trials in combination with other drugs.^{10,11,15} Heptaplatin (see Fig. 1) was successfully designed to have higher antitumour activity and lower toxicity than cisplatin. It exhibits high stability in solution and is active against cisplatin-resistant cancer cells through deactivation of metallothioneins. It has reached phase II clinical trials in combination with other drugs and has currently entered phase III, where has demonstrated activities similar to cisplatin.^{10,11,15}

Satraplatin (2007, see Fig. 1) is a Pt(IV) complex, which can be administrated as an oral drug. The two acetate ligands increase its lipophilicity and it is reduced in the bloodstream, the same as most Pt(IV) derivatives, with the consequent loss of the acetates. DNA is also the main target for this drug, although, unlike other platinum drugs, the mechanism involves the block of the DNA repair, as the DNA mismatch repair proteins do not recognize the adducts formed. Phase I, II and III clinical trials have been carried out and are still in process either alone or in combination with other drugs.^{10,11,15}

Finally, among multinuclear platinum complexes, BBR3464 (see Fig. 1) has relevant activity, since it is the first compound not showing covalent interaction with DNA with activity similar to cisplatin. Its mechanism of action implies the formation of intrastrand and interstrand crosslinks (*via* hydrogen bonding to the oxygen atoms of the phosphate groups) that cannot be repaired. Different phase I, II and III clinical trials have been reported with good results but some important side effects.^{10,11}

1.1.1. Cisplatin: Mechanism of Action

Cisplatin as well as other platinum-based drugs have DNA as the main target¹⁶, and are used either alone or in combination with other drugs. Direct intravenous administration is usually the best option for cisplatin, due to the low stability and low water-solubility of the complex. When it is in the bloodstream, cisplatin interacts with plasma proteins such as human serum albumin (HSA), haemoglobin (Hb) or transferring (Tf), which transport the drug to the different tissues. The complex enters the cells by passive diffusion or by active protein-mediated transport systems, for instance human organic cation transporter (hOCT2) and the copper transport protein (Ctr1).¹¹ Within the cell, cisplatin (Fig. 2-a) is hydrolyzed (Fig. 2-b) and therefore, the neutral complex converts into a cationic aquo-derivative. Hydrolysis only occurs in the cytoplasm, where chloride concentration is 5-20 mM; whereas in the bloodstream this concentration increases up to 100 mM, so this process is inhibited.¹⁷ The lability of water allows platinum to bind DNA bases (Fig. 2-d), specially N7 of guanine (G) and adenine (A) and N3 of cytosine (C). The second chloride can also be displaced by a water molecule (Fig. 2-c) and by DNA in a second step (Fig. 2-e) to form a bifunctional adduct between two adjacent bases on the same strand.

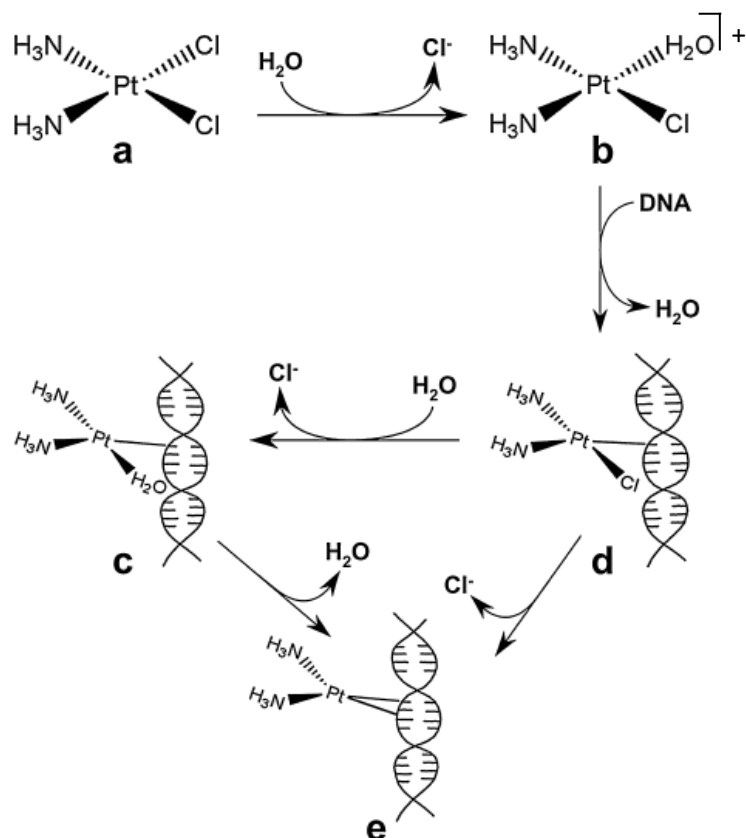


Fig. 2. Mechanism pathway of cisplatin-DNA interaction modes. Scheme extracted from Trudu, F.; Amato, F.; Vaňhara, P.; Pivetta, T.; Peña-Méndez, E. M.; Havel, J. *J. Appl. Biomed.* 2015, 13, p 81.¹¹

Thus, there are many possibilities for cisplatin to bind DNA (see Fig. 3): 1,2-intrastrand GG cross-link (50%-60%), 1,2-intrastrand AG cross-link (20%-30%), 1,3-intrastrand GXG cross-link (10%), interstrand GG adduct (<1%) and DNA-protein cross-links (<1%)^{8,11,18} (see [DNA interactions](#), page 65). The coordination to two adjacent bases together with the fact that the platinum centre is located in the major groove lead to a bend of DNA of *ca.* 45° towards the site of platination and consequently, the opening of the minor groove. All these conformational changes inhibit the molecular recognition processes, such as transcription and replication and finally lead to cell death.^{8,16}

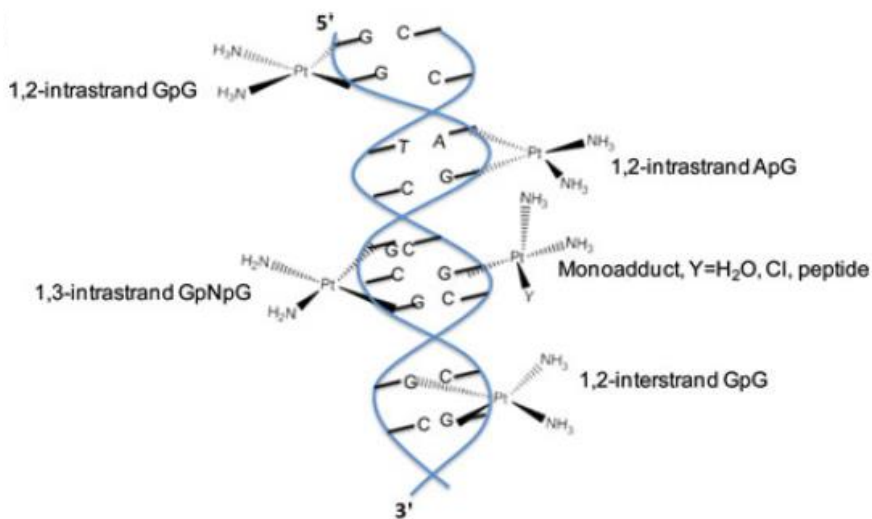


Fig. 3. Types of DNA-cisplatin crosslinks. Figure extracted from Shamsi, M. H.; Kraatz, H.-B. *J. Inorg. Organomet. Polym. Mater.* 2012, 23, p 19.¹⁹

Nevertheless, platinum-based drugs are still very toxic and consequently have acute side effects. This reason promoted the development of anticancer drugs based in other transition metal complexes, such as palladium, ruthenium, gold, silver, copper, rhodium, iridium, osmium or rhenium.¹² A search of the published papers from 1980 to 2015, with the term “metal anticancer” (*e.g.* platinum anticancer or gold anticancer) in the Web of Science gives an idea of the quick increase and interest in organometallic or metallo-organic anticancer drugs, with quasi exponential increment (see Fig. 4). It is remarkable that platinum is far more used as anticancer drug than any other metal. On the other hand, rhodium and iridium have been hardly studied. A brief review of some of these metal complexes will be shown in the next pages.

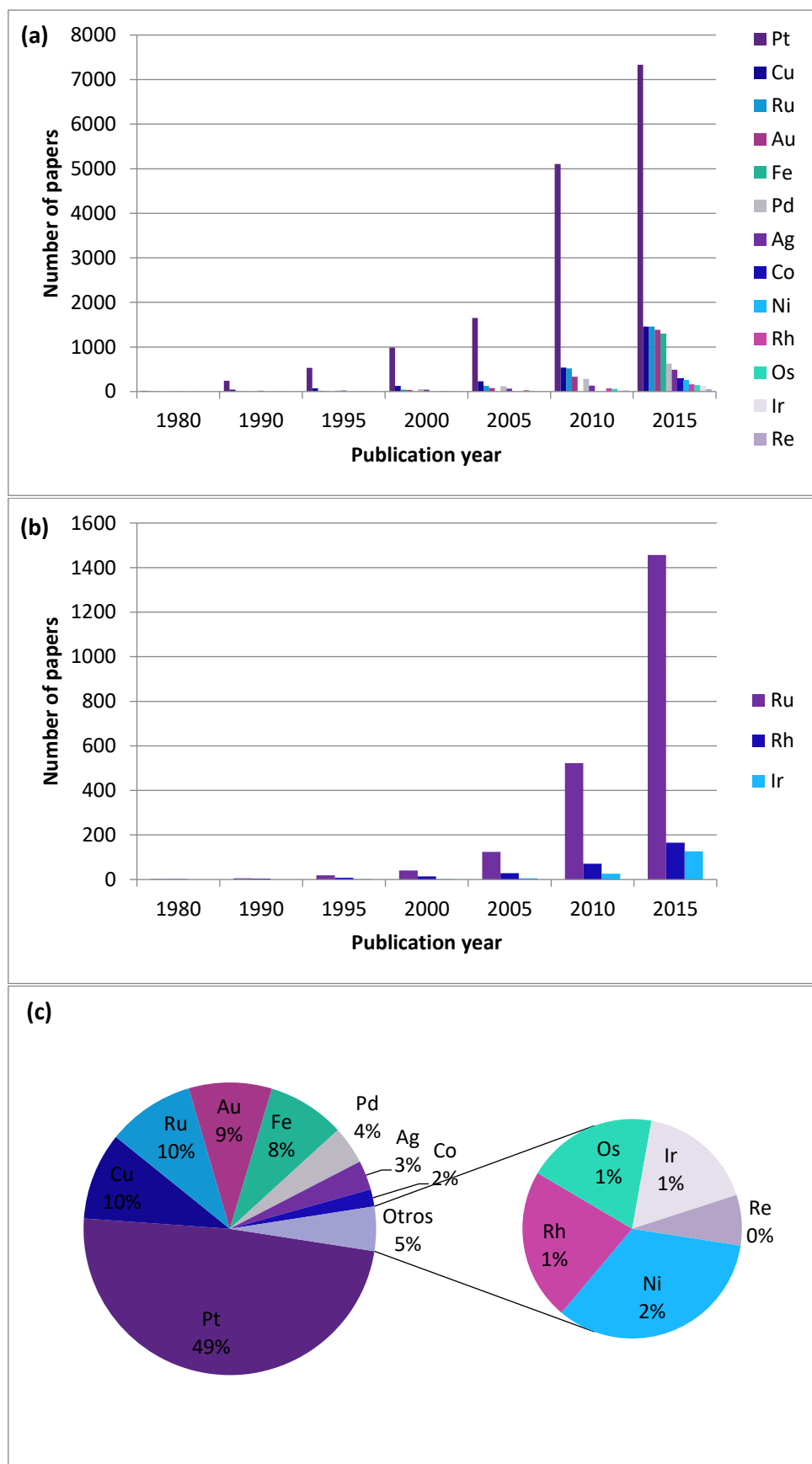
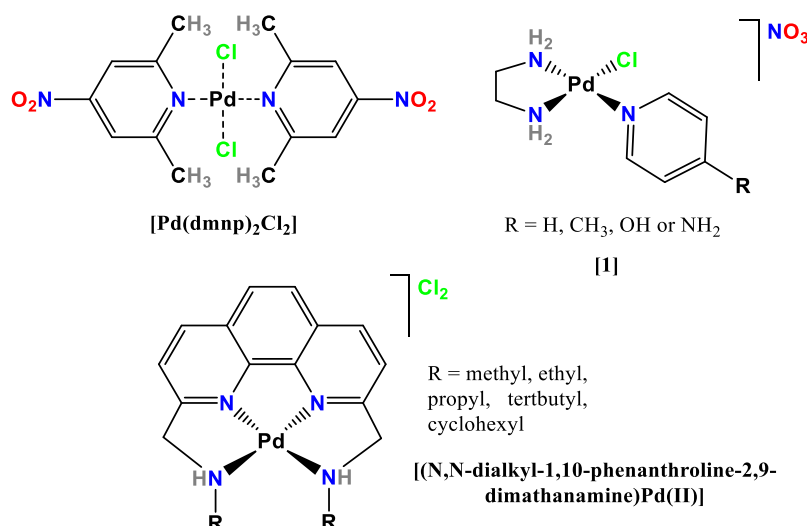
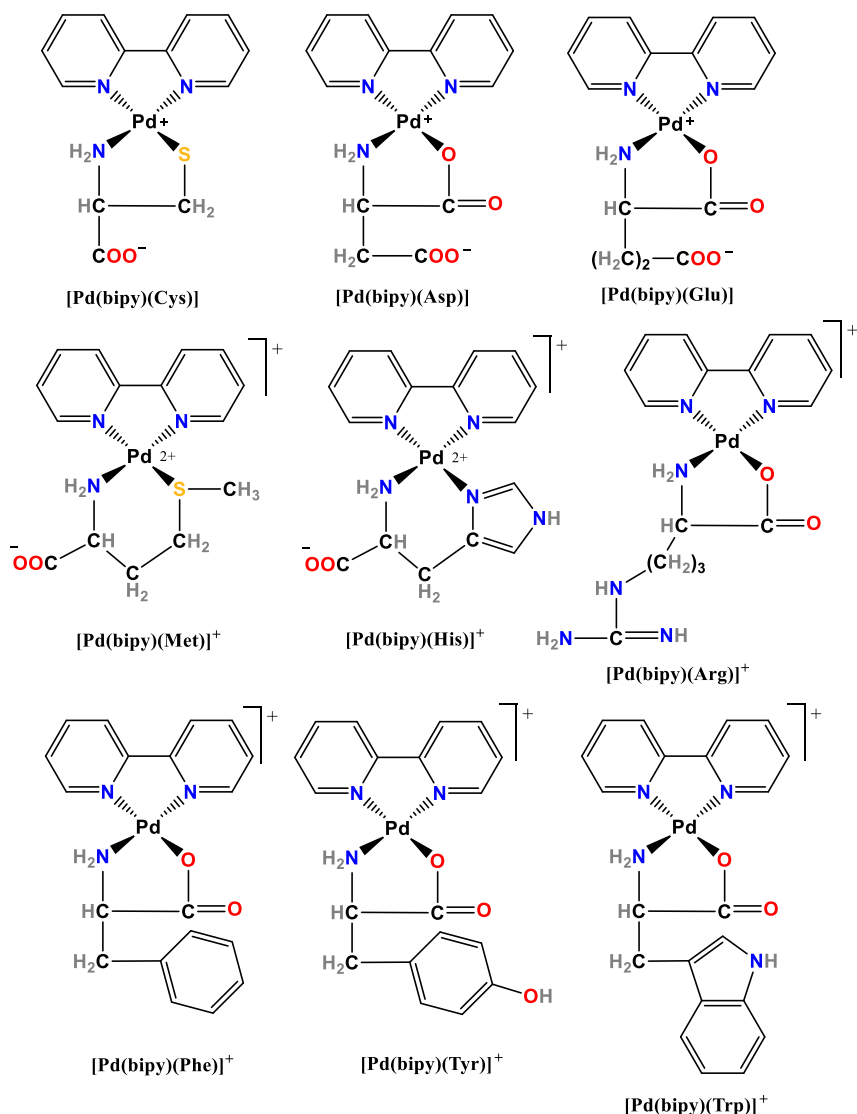


Fig. 4. Bar codes and pie chart for published papers from 1980 to 2015 about the use of metal complexes as anticancer drugs. (a) Evolution of different transition metals, (b) evolution of the metals used in this work and (c) relative abundance of papers with the use of different metal complexes in the year 2015.

1.2. Other platinum group metals

1.2.1. Palladium

Palladium is an element of the group 10 and belongs to the second transition row and to the “platinum group”, with an electronic configuration [Kr]4d¹⁰.²⁰ Palladium has been widely used in catalysis chemistry for years. Nevertheless, the similar coordination chemistry to Pt(II) turned Pd(II) into a new anticancer metal to search for. However, the ligand exchange process (*e.g.* hydrolysis) for Pd(II) compounds is about 10⁵ times faster than that for Pt(II). This ligand dissociation generates very active species able to bind different macromolecules even in the bloodstream, avoiding the drug to reach its target (*e.g.* DNA). Initially, palladium-based complexes turned to be inactive, toxic and useless as therapeutic drugs, even though bulky chelating ligands can stabilise the complex. In addition, whereas *cis*- configuration complexes are more active in Pt(II), *trans*-configuration is predominant in Pd(II) and some *cis*- isomers transform into inactive *trans*- derivatives.^{12,21} Among these trans-derivatives the complex [Pd(dmnp)₂Cl₂] was synthesised (see Fig. 5) and tested in some cell lines. It was much more active than either the free ligand or cisplatin even against some resistant cell lines.²² In addition, some complexes with ethylenediamine as chelating ligand, chloride and a monodentate N-donor ligand were reported ([1], see Fig. 5). They presented interesting cytotoxicity against a human leukaemia cell line. The increase of the electron donor properties of the R substituents led to an increase of the donor strength of the coordinated pyridines, which implied an increase in the cytotoxic activity of these kind of complexes.^{22,23} Another group of bulky and planar chelating ligands (phenanthrolines) with different R substituents were studied $\left[\left(\text{N,N-dialkyl-1,10-phenanthroline-2,9-dimethanamine}\right)\text{Pd(II)}\right]$, see Fig. 5). These complexes showed that an increase of the lipophilicity of the complexes, directly led to an increase of the cytotoxicity. As a result, the complexes with propyl, tertbutyl and cyclohexyl substituents exhibited better activities than cisplatin. Furthermore, these compounds do not interact with chloride anions and therefore, they are expected to be active against gastrointestinal tumours, since in the intestines the chloride concentration is so high that chloride ions can inhibit the activation of drugs like cisplatin.²² In order to avoid this process and owing to the stability of metal complexes with amino acids (aa), some palladium complexes with bipyridine as chelating ligand and different amino acids were synthesised (see Fig. 6). Among all the L-amino acids, only nine of them (cysteine, aspartic acid, glutamic acid, methionine, histidine, arginine, phenylalanine, tyrosine and tryptophan) improved cisplatin cytotoxicity. The platinum analogues showed a general tendency for biological activity: nonpolar > polar uncharged > charged side groups, which is not observed for palladium complexes. However, Pd(II) amino acid derivatives possess much more inhibitory activity for nuclear transcription than their Pt(II) analogues.²² In addition, the chelating coordination mode of most of them occurs through the amine group and the side chain of the amino acid, which allows the carboxylate function to bind other amino acids or peptides.^{21,23}

Fig. 5. Palladium complexes with anticancer properties.^{21,22,23}Fig. 6. Palladium complexes with L-amino acids ligands.²²

Recently, two palladium(II) porphyrin compounds TOOKAD® and TOOKAD® Soluble (see Fig. 7) are in phase III clinical trials as sensitizers in PDT.²⁴ They are Pd-

bacteriochlorophyll derivatives developed as a second generation photosensitizers and used for the treatment of bulky solid tumours, like prostate carcinoma. They do not act directly in the tumour cells, but induce damage to the tumour vascular system. Furthermore, they easily eliminate and show a selective action as a result of PDT treatment.²⁵

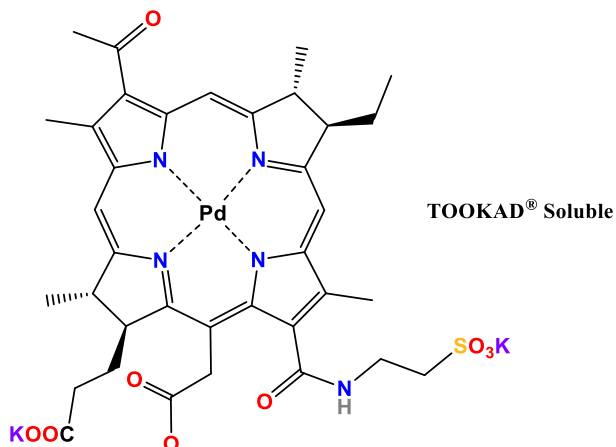


Fig. 7. TOOKAD® soluble.²⁶

A great deal of palladium complexes has been synthesised in the last years, even though their biological activities are moderate and only TOOKAD® has entered clinical trials, so far.

1.2.2. Ruthenium

The use of ruthenium complexes as anticancer agents is the result of the search of new non-platinum drugs, since the latter exhibit serious drawbacks in cancer chemotherapy. As a consequence, ruthenium complexes have become the most promising alternative to platinum drugs. They are less toxic and many of them are effective in platinum resistant cancers.²⁷ There are also some characteristics that make ruthenium complexes suitable for medicinal applications²⁸:

- Multiple oxidation states (+2, +3 and +4) accessible in the presence of biological reductants (*e.g.* ascorbate and glutathione) or oxidants (O_2 or H_2O_2) in physiological conditions.^{29,30}
- High reactivity or ligand-exchange kinetics with low toxicity.
- Selective antitumour activity in both *in vivo* and *in vitro* studies.
- Different membrane transport mechanisms: active transport, passive diffusion or a mixture of both processes.
- Different molecular action mechanisms: intercalation and covalent binding with DNA and binding to extracellular sites inducing conformational modifications that can have an **antineoplastic** effect.
- The ability to exchange ligands with O- and N-donor biomolecules similarly to platinum drugs.
- Octahedral geometry that provides numerous synthetic opportunities for tuning the biological activities.

Both Ru(III) and Ru(II) compounds form hexa-coordinated complexes, even though Ru(III) acts as prodrug, since it is usually reduced in physiological media. This reduction process is even faster in hypoxic tumour tissues, where the oxygen content is lower, and can be reverted with molecular oxygen.¹¹ Clarke and co-workers proposed this reduction process for the first time with an octahedral chloride and ammonia complex [RuCl₃(NH₃)₃] (see Fig. 8). However, it was too insoluble for clinical uses.³¹ Another two octahedral Ru(III) complexes, NAMI-A and KP1039 (see Fig. 8), have entered phase II clinical trials.²⁸ Despite their structural similarities, they exhibit substantially different anticancer properties.²⁹ KP1019 shows cytotoxic activity against some primary cancers, whereas NAMI-A is non-toxic and has antimetastatic activity against solid tumours.^{29,31}

NAMI-A was the first ruthenium compound to enter clinical trials. In the related derivative NAMI (see Fig. 8), ruthenium is coordinated to one imidazole ligand, one DMSO molecule and four chloride anions and the charge is stabilized with a sodium cation as counterion. It has good water solubility, a high Ru(III/II) reduction potential and inertness in aqueous solution due to the π -acceptor effect of the S-bound DMSO. It is noticeable that its activity, which does not involve DNA binding, is independent of its concentration, although only small amounts of NAMI reach the tumour target. Notwithstanding, the cation seems to be important, as the sodium salt was unstable to enter clinical trials. The replacement of sodium by imidazolium in NAMI-A allowed more stability of the complex keeping the same biological effects. The mechanism of action is still unknown, even though DNA is not the primary target.²⁸ An *in vitro* anticancer drug screening in the 60-cell line NCI panel shows no activity and it is 1000-times less cytotoxic than cisplatin.¹⁷ However, NAMI-A inhibits and influences the main steps in the dissemination process (metastasis inhibition), such as re-adhesion, mobility and invasion of tumour cells, affecting only tumour cells endowed with metastatic ability.²⁸ Phase I clinical trials began in 1999 and were reported in 2004. The study allowed to determine the administration dose of the drug after it was tested in 24 patients with different kind of tumours, with lung cancer patients providing the more promising result (specially NSCLC = non-small-cell lung carcinoma). Finally, the optimal treatment was fixed in a daily intravenous infusion (300 mg/m²/day) for 5 days every 3 weeks.^{29,32} A phase I/II study with NAMI-A and gemcitabine, a potent anticancer drug, in NSCLC cancer patients has been recently developed. The results do not show an improvement in relation to the use of gemcitabine alone, although more studies are needed to establish definitive conclusions.³³ In addition, some more studies are being performed with NAMI-A, for instance, a combinatorial therapy of the drug with doxorubicin for mammary cancer is ongoing.³⁴

Another ruthenium(III) complex which is currently in phase II clinical trials is KP1019 (see Fig. 8). Ruthenium is coordinated to two identical axial indazole heterocycles (*trans*- disposition) via nitrogen atoms and four chloride groups.²⁹ It has shown activity both *in vitro* (it induces **apoptosis** in colorectal cancer cell lines) and *in vivo* (on chemo-resistant colon carcinoma). DNA synthesis inhibition is suggested to be the mechanism of action, although mitochondrial DNA is preferred rather than nuclear.^{29,28} Initial testing were performed in 1998 with promising results³⁵ and phase I

clinical trials were published in 2009. The pharmacokinetic study showed higher ruthenium concentration in the plasma than in the ultrafiltrate of blood, which means that KP1019 in the bloodstream is bound preferably to proteins (HSA and Tf). The results of the trials were promising, as only mild cytotoxicities were detected and the optimal dose was fixed in 400 mg for more than three weeks of treatment.³⁶

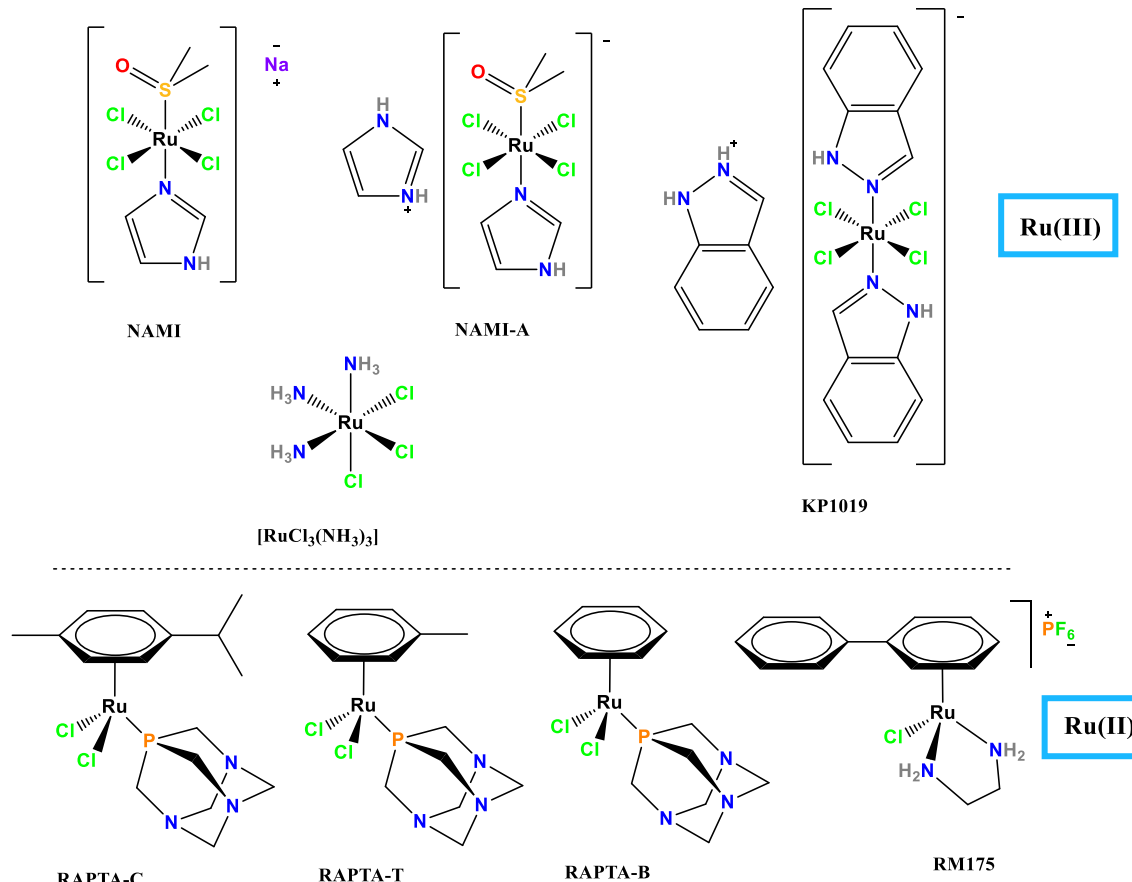


Fig. 8. Ruthenium based anticancer drugs. Ru(III) above and Ru(II)-arene below.^{31,37,38}

As said before, both NAMI-A and KP1019 undergo reduction of the oxidation state of ruthenium, in order to be activated. These redox potentials ($E_{1/2} = 0.03$ V and 0.25 V versus NHE, respectively) are pH independent around neutral pH values and achievable by some physiological reductants such as glutathione ($E^0 = -0.25$ V) or ascorbic acid ($E^0 = +0.06$ V).³⁹ The reduction of these complexes causes the fill of the t_{2g} orbitals and thus, π -donating ligands bind less strongly and it is especially effective in tumour hypoxic issues. Once the reduction has occurred, ruthenium complexes are more reactive and can interact either with water (aquation) or with proteins or DNA.²⁸

As far as ruthenium(II) complexes are concerned, arene complexes are the most studied in relation with their anticancer properties. They adopt a pseudo-octahedral coordination mode and are also called half-sandwich or piano-stool complexes, due to their similarity with these objects. Moreover, since Ru(III) complexes are proposed to be reduced in physiologic media, Ru(II) compounds have received a growing interest in the last years. The arene stabilises the ruthenium(II) centre and increases hydrophobicity, which facilitates the transport through cell membranes. In addition, modifications of the three ligand positions allow the fine-tuning of their characteristics and reactivity^{40,41} (see

[Ruthenium arene complexes](#) in page 72). Among this kind of complexes some ethylenediamine and RAPTA types have also entered clinical trials. RM175 (ONCO4417), prepared and studied by Sadler and co-workers⁴¹ (see Fig. 8), shows strong cytotoxicity and even overcomes resistance to cisplatin. This piano stool complex is formed by an arene (biphenyl), a diamine chelate ligand and one chloride anion. The ethylenediamine, a bidentate N-donor ligand reduces the lability of the chloride leaving group, which slows down the hydrolysis process. The cytotoxicity of the complex is related to a dual DNA interaction mode. Apart from the typical guanine covalent coordination via hydrolysis of chloride, RM175 is able to intercalate into DNA base pairs through the biphenyl ligand. This fact enhances DNA damage at levels similar to those of cisplatin.^{28,42}

Dyson and co-workers synthesised and tested the RAPTA complexes. These compounds are composed of an arene, two chloride ligands and a PTA ligand (1,3,5-triaza-7-phosphatricyclo-[3.3.1.1]-decane or 1,3,5-triaza-7-phosphaadamantane, (see CHAPTER 2), which provides solubility both in aqueous and organic media (amphiphilic nature). The change of the arene has led to different complexes, for instance, RAPTA-C with *p*-cymene, RAPTA-T with toluene and RAPTA-B with benzene (see Fig. 8). All of them undergo aquation due to the lability of one chloride, although a high chloride concentration suppresses this process.^{27,43,44} RAPTA-T has shown antimetastatic properties *in vitro* and *in vivo*, being extracellular matrix components (extracellular proteins) and the cell surface the observed targets, instead of DNA and cell nucleus.²⁸ RAPTA-C induces apoptosis through different pathways, which implies that the complex is unlikely to suffer from acquired resistance.⁴⁵ It is also pH sensitive, which involves that at pH < 7 (hypoxic cells) DNA is damaged, whereas at pH > 7 (normal cells) DNA is not affected.⁴⁶ In all these compounds, PTA seems to be a key factor in the toxic mechanism of RAPTA complexes, as well as the active agent responsible for the antimetastatic properties. The protonated form of PTA is considered the active structure able to either facilitate the cross of the cell membrane or improve solubility.²⁸

1.2.3. Osmium

Osmium, the heavier ruthenium congener, is an element of the group 8 and belongs to the third transition row and to the “platinum group”, with an electronic configuration [Xe]4f¹⁴5d⁶s².²⁰ Therefore, +2 and +3 are the most common oxidation states, as for ruthenium, although +4 is also accessible. Despite the similarity between ruthenium and osmium complexes, there are quite a few differences, for instance in the chemical and physical properties as well as in the biological activity. Osmium compounds are relatively inert, since they exhibit lower kinetic rates than the ruthenium derivatives.^{47,48} In addition, other features such as the preference for higher oxidation states, slower ligand exchange, stronger π-backdonation from lower oxidation states and markedly stronger spin-orbit coupling, make osmium an interesting alternative to ruthenium.⁴⁹ Notwithstanding, it is possible to change the reactivity modifying their structural elements, specifically the chelating ligand in osmium arene complexes.¹² The first strategies for the development of osmium anticancer drugs lead to the metal substitution of the well-established ruthenium compounds (NAMI-A, KP1019, RAPTA-C and RM175), due to their successful biological activities (see Fig. 9: osmium derivatives

from NAMI-A - [2], KP1019- [3], [4], [5] and [6], RAPTA-C – [7] and RM175 - [8]). Surprisingly, the coordination mode for ruthenium(III) in KP1019 differs from that of osmium(III) analogues. Indazole is bonded to Ru(III) only through *N*2, whereas in Os(III) and Os(IV) complexes it is coordinated through both *N*1 and *N*2 (see Fig. 9, [3], [4] and [5]). This tautomerization process has relevant consequences in their biological behaviour. The complex with ruthenium inhibits the tumour growth, whereas the one with osmium reduces **necrosis**.⁴⁹ Moreover, two osmium oxidation states are possible for the compound with two indazole ligands. The Os(III) complex is accessible via chemical or electrochemical reduction of the Os(IV) compound without changes in the coordination mode and scarce variations in the cytotoxic activity.⁵⁰ As far as the osmium arene complexes are concerned, they are less active than the ruthenium analogues. In addition, hydrolysis processes are far slower (*ca.* 40 times), which could be the reason of their low cytotoxicity.⁴⁷

Sadler and co-workers reported some osmium *N,N*-azopyridine derivatives (see Fig. 9, [9]) with noteworthy anticancer activity against a variety of cancer cell lines both *in vivo* and *in vitro*.⁴⁹

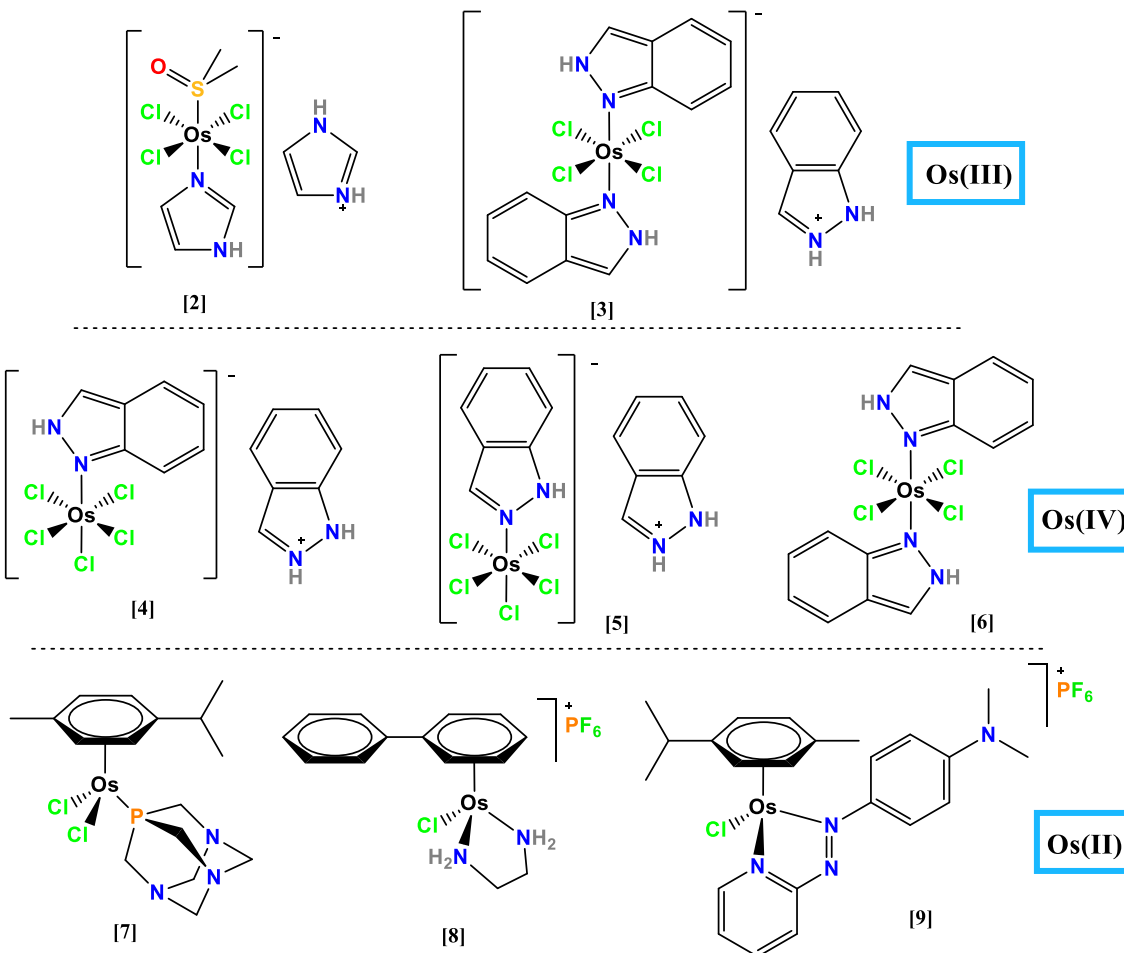


Fig. 9. Osmium anticancer complexes in different oxidation states (III) upper, (IV) middle, (II) down.^{49,47}

In order to make a SAR study on osmium arene complexes, replacements in the chelate ligand were performed. As said before, hydrolysis was slow with neutral *N,N*-ligands. However, when these ligands were substituted by anionic *O,O*-ligands, like acetylacetone (acac⁻), the rate of hydrolysis was increased, giving rise to a new dimer

compound $[(\eta^6\text{-arene})\text{Os}(\mu\text{-OH})_3\text{Os}(\eta^6\text{-arene})]^+$. This complex was the result of the loss of the acac^- ligand. These dimers were inert and inactive *in vivo*. Afterwards, a new change of the chelate ligand was made with anionic N,O -ligands (picolimates). This replacement led to more stable complexes with slower hydrolysis rates and promising activity. Moreover, they were found to bind DNA through guanine and adenine.⁴⁰ To conclude, these changes showed different behaviour in physiological media for each chelate ligand (see Fig. 10).⁴⁹

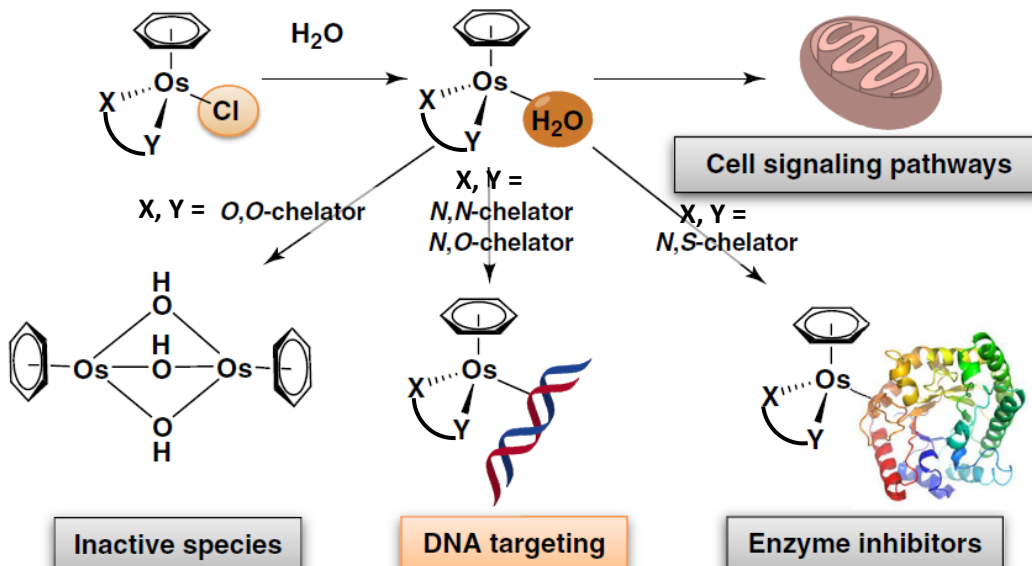


Fig. 10. Schematic representation of the mechanisms of action of osmium-arene complexes. Figure extracted from Hanif, M.; Babak, M. V.; Hartinger, C. G. *Drug Discov. Today* 2014, 19, p 1645.⁴⁹

1.2.4. Rhodium

Rhodium complexes have not been studied as widely as complexes of other late-transition metals, even though rhodium compounds with anticancer properties were known since 1953 when RhCl_3 was studied along with other metal chloride salts.⁵¹ This work showed different behaviour among metals, and some of them were a bit cytotoxic when administrated to mice in drinking water.⁵² A later study (in 2012) revealed a slight effect of low concentration of rhodium tri-chloride salt (RhCl_3) on cells.⁵³ Furthermore, the Rh(III) complexes of type *mer*- $[\text{RhCl}_3(\text{NH}_3)_3]$ and *mer,cis*- $[\text{RhCl}_3(\text{DMSO})_2(\text{NH}_3)]$ were reported to display significant antineoplastic activity.⁵¹ In the 1970s dirhodium(II) complexes caught the attention of researchers, especially carboxylate-bridged compounds (see Fig. 11, [10]), owing to their **carcinostatic** activity.¹² This kind of complexes with general formula $[\text{Rh}_2(\text{RCOO})_4(\text{solvent})_2]$ possess a Rh(II)-Rh(II) bond, four equatorial ligands and two axial ligands, which usually are solvent molecules. Rh(II) is a d^7 paramagnetic metal ion, but when coordinated to another Rh(II) metal centre the complex becomes diamagnetic. Nevertheless, they exhibited such a high toxicity, that their use was avoided.¹² Regarding the R group, the cytotoxic activity increases with the size of the alkyl group, showing activity against Ehrlich ascites (a type of breast cancer) tumour cells in mice.⁵⁴ When the R group is a butyl group (the carboxylate group becomes a butyrate), the subsequent complex inhibits the ubiquitin-proteasome pathway, which is closely related to cytotoxicity.^{55,56} Within this group a wide variety of complexes have been reported like a rhodium sulfosalicylate complex, which improves

the solubility with regard to the common dirhodium carboxylates.⁵⁷ Rh(III) polypyridyl complexes with facial ligands like 1,4,7-trithiacyclonane ([9]aneS₃) (see Fig. 11) can slow down the ligand substitution, and consequently, improve cytotoxicity.⁵¹ Some complexes with promising results and even better than those for cisplatin were reported.⁵⁸

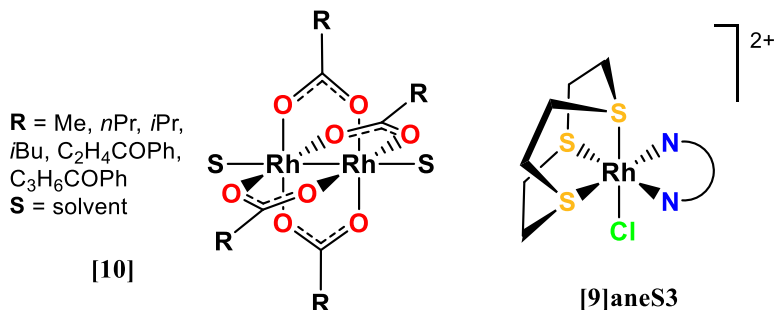


Fig. 11. Most relevant rhodium complexes: dirhodium(II/II) carboxylates and Rh(III) trithiacyclononane.^{51,54,58}

1.2.5. Iridium

The use of iridium complexes as anticancer drugs has been spread very recently. Moreover, there are not complexes in clinical trials so far, what makes difficult to review this metal. In the 1970s and 1980s iridium(I) complexes with square-planar geometry (see Fig. 12) caught the attention of researchers, due to the similarity to cisplatin. [Ir(acac)(cod)] was extremely active against Ehrlich ascites in mice and Lewis lung carcinoma, whereas [IrCl(cod)]₂ showed activity in the Lewis lung model, but no inhibition of primary tumours.^{12,59} More recently iridium chloride salt (IrCl₃) was tested in rat fibroblasts and was found to be able to inhibit cell growth.⁵³ Then, the attention was focused on Ir(III) complexes, especially with the pentamethylcyclopentadienyl ligand. Sadler and co-workers have deeply studied these iridium complexes with bipyridine and phenylpyridine type ligands^{60,61} as well as with N,N-ligands (en, phen, etc.).^{62,63} Sheldrick and co-workers have also reviewed iridium and rhodium complexes with different oxidation states. Concerning the half-sandwich compounds, promising cytotoxicity values in three different cancer cell lines were obtained with polypyridyl ligands. In most cases DNA is again the main target.⁵¹

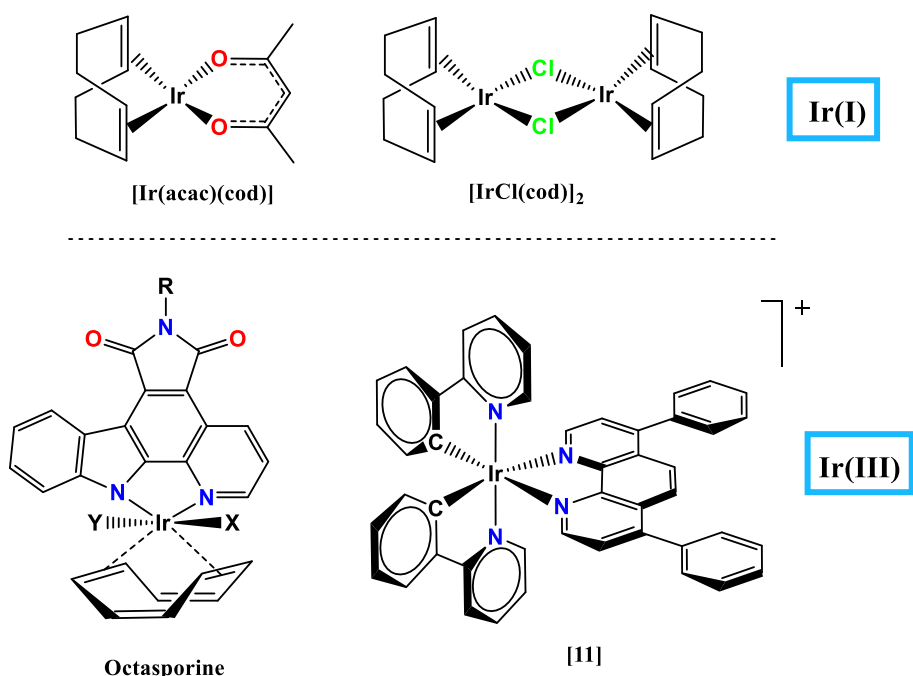


Fig. 12. Iridium(I) (above) and Iridium(III) (below) complexes with significant cytotoxic activity.^{59,64,65}

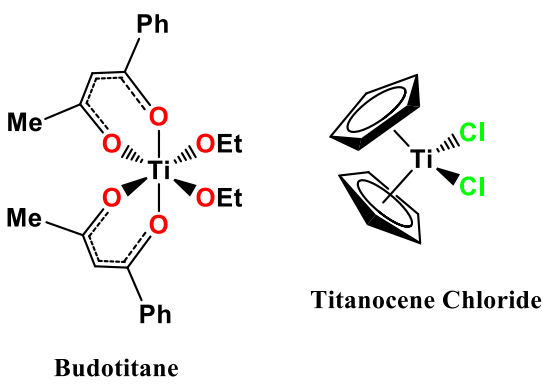
Meggers and co-workers designed iridium(III) staurosporine derivatives, generally called octasperines (see Fig. 12), which show a very specific activity as kinase inhibitors.^{51,56,64,66}

Iridium(III) complexes have been also used with orthometalated ligands, showing luminescent properties. Owing to this feature, they often act as bioimaging agents, although there are still some of them which target, for instance, mitochondria (see Fig. 12, [11]).⁶⁵

1.3. Other transition metals

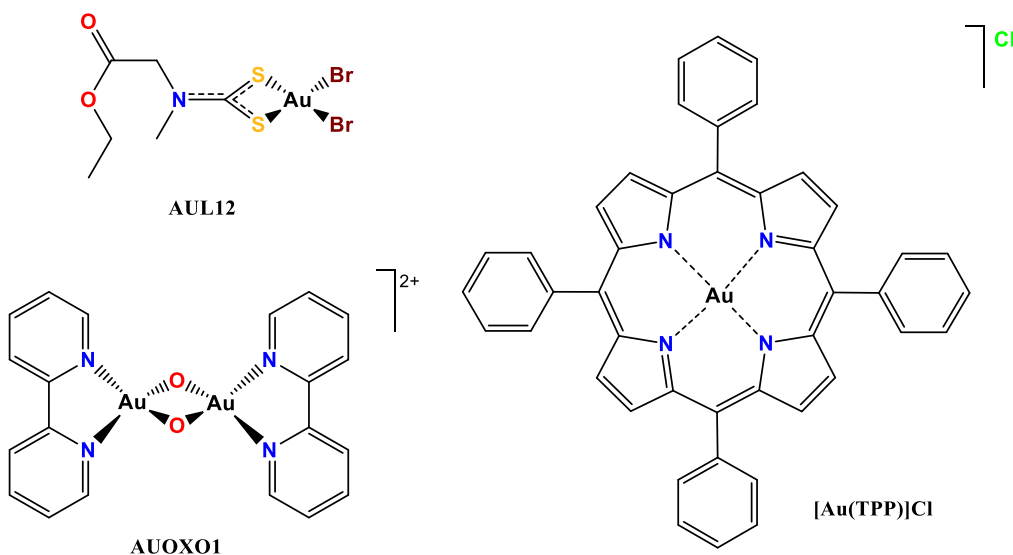
1.3.1. Titanium

Titanium is an element of the group 4 and the first transition row (an early transition metal), with an electronic configuration $[Ar]3d^24s^2$.²⁰ The most important oxidation state is +4 (d^0). Two families of titanium(IV) complexes have been used for biological applications. Budotitane (see Fig. 13) was the first nonplatinum drug to enter clinical trials, although it was not cytotoxic. The comparison with some analogues showed a dependence on the planarity of the ligands, suggesting DNA as the target.^{11,37,67} Titanocene dichloride (see Fig. 13) instead exhibited promising results in both phase I (1993) and phase II clinical trials. It is known that the mechanism of action involves DNA binding, behaving like cisplatin. Nevertheless, these compounds have poor solubility in water and undergo fast hydrolysis of chloride under physiological conditions. They can even lose the Cp. This lead to a mixture of species and it is still unclear which the active species is. In order to overcome this issue, titanocene chloride was modified. These kind of complexes bind also to human serum transferring, which could favour the transport to the cancer tissue.^{37,44,67,68}

Fig. 13. Most important titanium(IV) complexes with anticancer properties.³⁷

1.3.2. Gold

Gold is an element of the group 11 and belongs to the third transition row, with an electronic configuration $[Xe]4f^{14}5d^{10}6s^1$ and with +1 and +3 as the most important oxidation states.²⁰ As Au(III) (d^8) and Pt(II) are isoelectronic and isostructural (square-planar four-coordinate complexes), it was thought that both could have a similar behaviour as antitumour complexes. There are some promising gold(III) complexes such as AUL12, $[\text{Au}(\text{TPP})]\text{Cl}$ and AUOXO1 (see Fig. 14) active in different tumour tissues. This activity is often linked to the generation of ROS, to the changes in mitochondrial potential and ultimately to the inhibition of the thioredoxin reductase (TR) enzyme.⁶⁹ However, Au(III) complexes easily undergo reduction to Au(I) or Au(0) under physiological conditions and are sensitive to light, which have slowed down their development as useful drugs.

Fig. 14. Promising gold(III) complexes with anticancer properties.⁶⁹

On the other hand, Au(I) complexes, which are usually linear, are thought to have better properties as antitumour pro-drugs, since they quickly exchange their ligands. Au(I) is a soft acid metal and therefore it prefers soft ligands such as thiolates, cyanides, phosphines and soft halides. Thus, sulphur-containing proteins and biomolecules are likely to coordinate to the metal. Main gold(I) complexes with anticancer activity are aurothiomalate, aurothioglucose, auro(bis)thiosulfate and auranofin (see Fig. 15). Most

of them, with the exception of the latter, polymerise through thiolate sulphur bridges.^{14,44} Auranofin is a gold(I) phosphine complex traditionally used for the treatment of rheumatoid arthritis, which also acts as a thioredoxin reductase (TR) inhibitor.¹¹ In the 1970s and 1980s the complex was tested against the growth of tumour cells. Both auranofin and other gold phosphine complexes inhibited DNA, RNA and protein synthesis, without direct DNA interaction, but with good cytotoxic activity.³⁷ Moreover, thiosemicarbazone derivatives, like $[\text{Au}(\text{N}-4\text{-methyl-2-acetylpyridine})\text{Cl}]$ (see Fig. 15), has also relevance as TR inhibitor and is active against a leukaemia cancer.⁶⁹

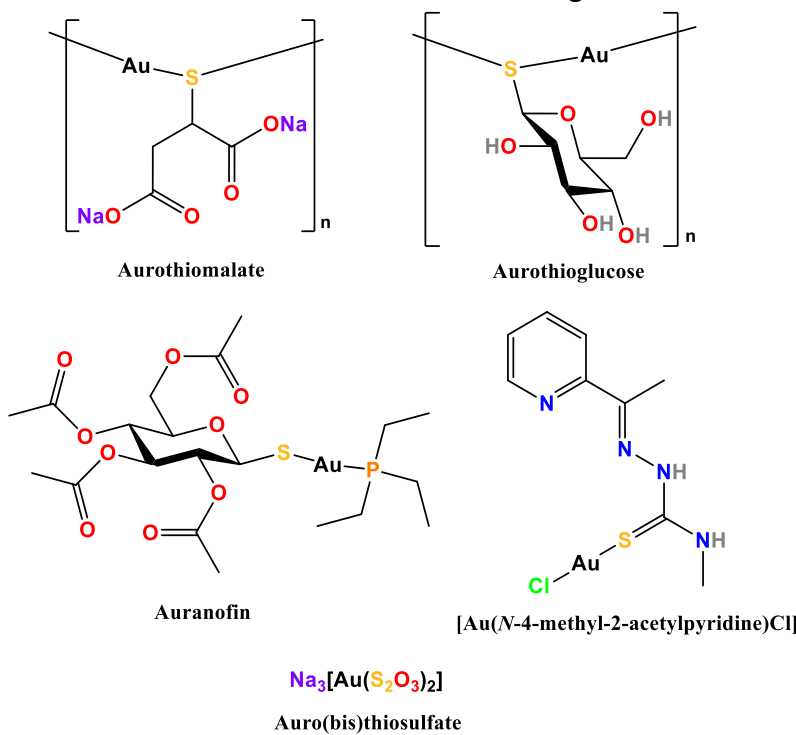


Fig. 15. Most relevant gold(I) complexes with anticancer properties.¹⁴

2. MECHANISM OF ACTION OF ORGANOMETALLIC DRUGS

There are thousands of mechanisms to induce cell death, although we will focus on the two most relevant mechanisms for metal complexes. The first one implies *DNA-drug interaction*, and the second one involves the *generation of ROS*. Furthermore, there are some other mechanisms of either activation or deactivation of drugs, for instance, through proteins.

2.1.DNA

DNA is the most common and widely studied biological target for metal complexes, since the mechanism of action of cisplatin is based on DNA binding. Thus, both DNA and its binding sites are perfectly determined and well-studied. There are two main coordination modes (see Fig. 16): (i) irreversible (covalent or coordination binding) and (ii) reversible (intermolecular association: electrostatic interactions, groove binding and intercalation).⁷⁰

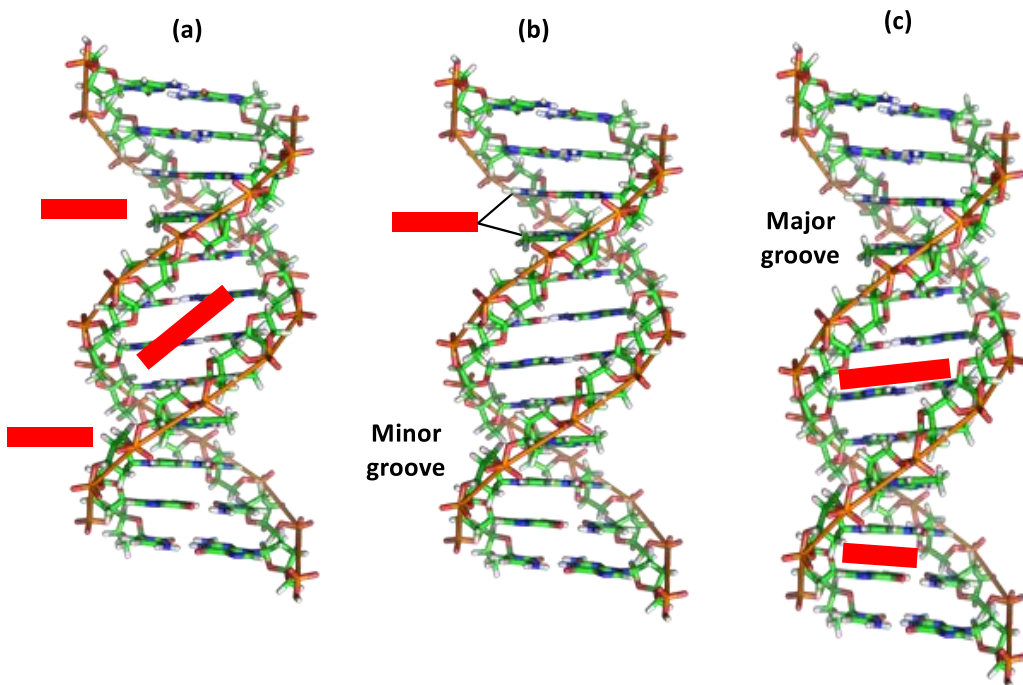


Fig. 16. Graphical illustration of DNA binding modes. (a) Groove binding, (b) covalent binding and (c) intercalation.

- *Covalent binding:* it is usually formed by an intrastrand cross-link between the nucleobases, generally through direct binding of the metal ion to the N7 of two consecutive guanine residues⁷¹, although there are other possible covalent binding atoms. For instance, some metal complexes bind oxygen atoms of the phosphate group (hard metals) and even bind hydroxyl groups of ribonucleotides, even though it is less frequent.⁷²
- *Groove binding:* metal complexes interact with DNA through one of the grooves, either major or minor (see Fig. 17), taking into account different features such as shape, size, hydrogen-bonding potential, polarizability of ligands and charge.⁷⁰

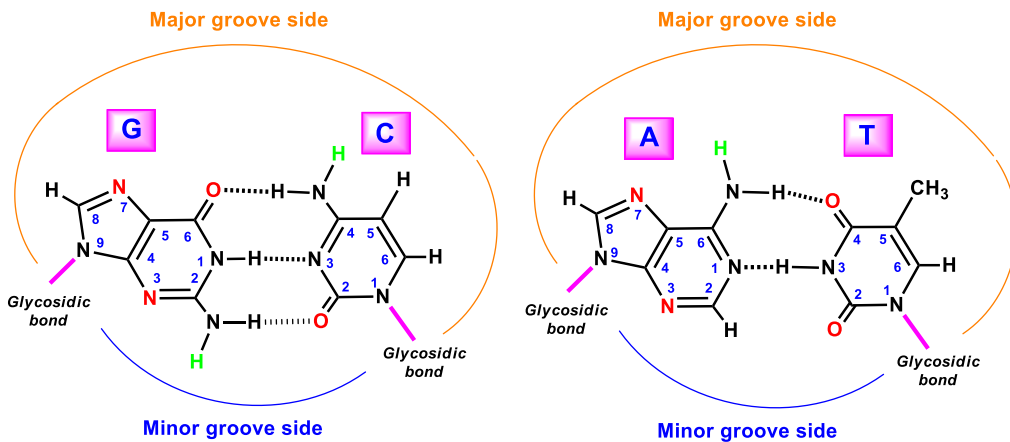


Fig. 17. Base pairing in DNA G≡C and A=T through their respective hydrogen bonds and the resulting major and minor grooves.

- *Intercalation:* this mechanism implies the insertion of planar aromatic systems between base pairs of DNA. The interaction is stabilized by π-π stacking and

causes a separation of adjacent base pairs and, consequently, distorts the helix. This effect finally turns into the unwinding of the duplex.^{70,71} There are also two main modes of intercalation: classical intercalation and threading intercalation. The former implies direct insertion of the aromatic system of the intercalator between guanine base pairs of DNA duplex. The latter involves, along with the insertion, a simultaneous interaction through both the major and minor grooves. Furthermore, this kind of intercalating modes greatly depend on the geometry of the complex. Square-planar and octahedral complexes usually intercalate through aromatic ligands, whereas metal complexes containing σ-bonded ligands with side arms as intercalators, and organometallic complexes with arenes as intercalators adopt a dual binding mode: arenes and side arms can intercalate between DNA bases and the metal can coordinate directly to a DNA base.⁷³

2.2. Generation of ROS

This is a common process occurring in normal cells, specifically in the mitochondria, although reactive oxygen species (ROS) levels are higher in tumour cells.⁶⁹ There are many processes involved in the generation of ROS: irradiation with UV light, X-rays and gamma-rays; products of metal-catalyzed reactions; pollutants in the atmosphere; neutrophiles and macrofagues during inflammation.⁷⁴

The redox balance is regulated by enzymatic and non-enzymatic reactions. The enzymatic reactions involve reductases (glutathione reductases, thioredoxin reductases), oxidases (catalase) and peroxidases (superoxide dismutase, glutathione peroxidases), whereas the non-enzymatic processes imply glutathione, thioredoxin and some vitamins.^{14,69} When the **homeostatic** balance is displaced and the amount of ROS increases, the cell is led to apoptosis⁷⁴ (see Fig. 18). The most important ROS (see Table 1) are superoxide ($O_2^{\bullet-}$), hydrogen peroxide (H_2O_2) and hydroxyl radical (OH^{\bullet}).¹⁴

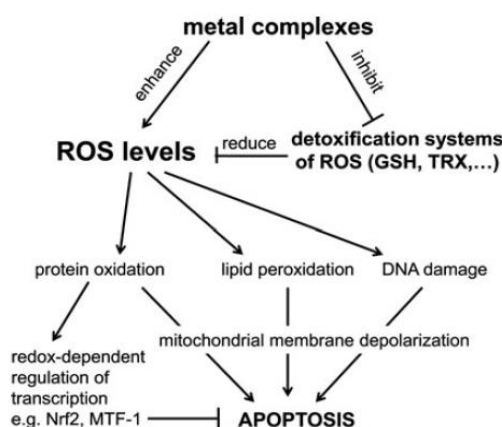


Fig. 18. The role of ROS in the anticancer activity of metal drugs. Figure extracted from Jungwirth, U.; Kowol, C. R.; Keppler, B. K.; Hartinger, C. G.; Berger, W.; Heffeter, P. *Antioxid. Redox Signal.* 2011, 15, p. 1086.¹⁴

Table 1. Most relevant ROS species and their physicochemical and biological properties. Extracted from Jungwirth, U.; Kowol, C. R.; Keppler, B. K.; Hartinger, C. G.; Berger, W.; Heffeter, P. *Antioxid. Redox Signal.* 2011, **15**, p. 1087.^{14,74}

	Reactivity	Reactions in cells	$E^{\circ'} [V]$	Antioxidative defense
OH^{\bullet}	Most reactive oxygen radical, which reacts immediately after its generation	Reacts immediately with almost every molecule found in living cells, including sugars, amino acids, phospholipids and DNA bases	+2.31 $[\text{OH}^{\bullet} + \text{e}^- + \text{H}^+ \leftrightarrow \text{H}_2\text{O}]$	Glutathione
$\text{O}_2^{\bullet-}$	Low reactivity in aqueous solution at pH 7.4. Damage is based on reactions with other radicals or metal ions. Membrane is impermeable but can cross cell membranes via anion channels	Reaction with [4Fe-4S] clusters and radicals such as NO^{\bullet} generating peroxynitrit (ONOO^{\bullet})	+0.94 $[\text{O}_2^{\bullet-} + \text{e}^- + 2\text{H}^+ \leftrightarrow \text{H}_2\text{O}_2]$ -0.16 $[\text{O}_2^{\bullet-} + \text{e}^- \leftrightarrow \text{O}_2^{\bullet-}]$	Superoxide dismutase; glutathione; non-enzymatic dismutation
H_2O_2	Weak oxidizing and reducing agent; generally poorly reactive; very diffusible between cells	Oxidation of cysteine and methionine; can be reduced to OH^{\bullet} and water by transition metals like Fe^{II} (Fenton reaction)	+0.32 $[\text{H}_2\text{O}_2 + \text{e}^- + \text{H}^+ \leftrightarrow \text{H}_2\text{O} + \text{OH}^{\bullet}]$	Catalase; peroxidases; peroxiredoxins

2.3. Other targets

2.3.1. Glutathione. Cell Detoxification

Reduced glutathione (GSH – see Fig. 19) is an intracellular low-molecular-weight antioxidant with a tripeptide composition (γ -L-Glu-L-Cys-Gly). It acts as a redox buffer to the cell, where GSH is highly abundant: cytosol (1-11 mM), mitochondria (5-10 mM) and

nucleus (3–15 mM).^{74,75} Nevertheless, the concentration in the blood plasma is in the μM range.¹⁴ GSH participates in many different processes with the aim of maintaining the redox balance, such as the detoxification of enzymes against oxidative stress, the regulation of protein sulphhydryl groups necessary for DNA repair and the regeneration of some antioxidants (*e.g.* vitamins C and E).⁷⁴ Furthermore, GSH is involved in cell death regulation and in the detoxification of heavy metal complexes.¹⁴

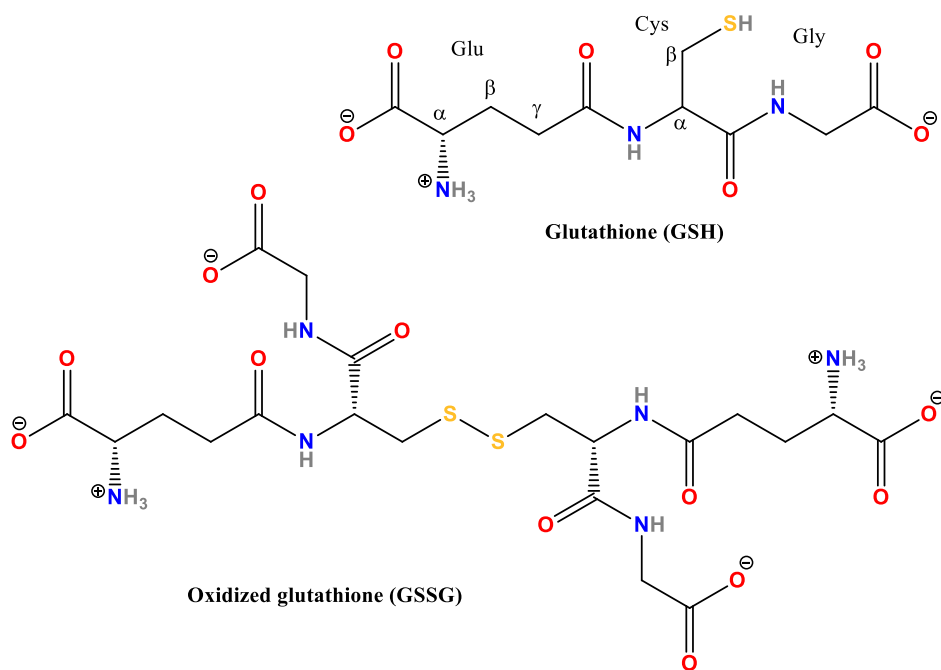


Fig. 19. Structures of GSH and GSSG at pH(5–7).^{75,76,77}

Owing to the high diversity of its chemical functions (ten donor atoms), GSH can form metal complexes in three different binding sites: (i) the glutamic set of amine and carboxylate, (ii) the thiol and (iii) the peptide O=C-NH units, depending on the metal identity and the solvent. Hard metals would rather interact with the glutamic moiety, whereas the soft ones prefer the thiol.⁷⁵ The resistance of cells to metal complexes is usually the result of high cellular GSH levels.¹⁴ In solution, the behaviour of GSH modifies when the solvent is changed. For instance, in aqueous solutions the tripeptide possesses both “extended” and “folded” conformations, while in DMSO, the “folded” conformation is blocked and the main functional groups are involved in strong hydrogen bonding with a DMSO molecule, avoiding GSH to bind other molecules.⁷⁸

Oxidation of GSH is possible in two main ways. The most important one implied in the redox balance is the formation of oxidized glutathione (GSSG – see Fig. 19), a dimeric product derived from two glutathione molecules bonded through a disulphide bond. GSSG accumulates inside the cell, but at low concentrations, as it is removed through the cell membrane and reduced by glutathione reductase.⁷⁵ Elevated concentrations of GSSG may oxidize some sulphhydryl groups of proteins, causing disulphides with longer half-lives (protein-SSG). For this reason, the ratio GSH/GSSG is

an excellent measure of oxidative stress in cells.⁷⁴

- *L*-*Buthionine sulfoxime (L-BSO)*:

L-BSO is an inhibitor of the γ -glutamylcysteine synthetase, which is implied in the rate-limiting step in the synthesis of GSH, so that GSH levels decrease (by 40%). It is usually co-administrated with metal complexes in order to potentiate its cytotoxic activity. When it is used as a single drug, it is able to increase ROS levels and thus, cause cell apoptosis. Likewise, low concentrations of L-BSO are employed to enhance the sensitivity of cell lines.^{69,79,80,81}

2.3.2. NAD⁺/NADP⁺

NAD⁺ (nicotinamide adenine dinucleotide) and NADP⁺ (nicotinamide adenine dinucleotide phosphate) are coenzymes synthesised from the vitamin nicotinic acid (B3) that participate in redox-type reactions (see Fig. 20).⁸² They are considered as electron carriers.⁸³ NADH (the reduced form of NAD⁺) is a cofactor of L-lactate dehydrogenase, acting as a reducing agent of pyruvate to L-lactate in the anaerobic glycolysis.⁸⁴ NADPH is known to be relevant in the cellular oxidative defence systems and seems to have a critical influence on the cellular survival.⁸³ Both oxidised (NAD⁺, NADP⁺) and reduced (NADH, NADPH) forms are in equilibrium inside the cell, although the oxidised form is rather predominant (i.e. NAD⁺/NADH ratio \approx 3-10). NADPH (the reduced form of NADP⁺) intracellular concentration is lower than that for NADH, falling in the submillimolar range. In any case, they are not free in the cell but protein bound.⁸³

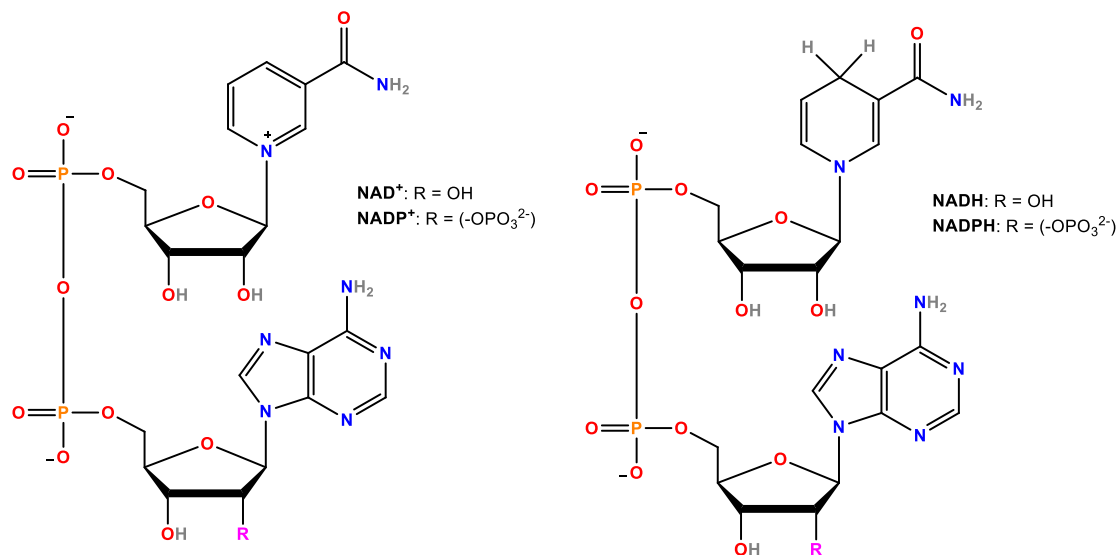


Fig. 20. Structures of the coenzymes NAD⁺ and NADP⁺.

2.4. Crossing the cell membrane: Lipophilicity

The aim when using these kind of metal complexes is to control the activation of the drugs by ligand exchange or redox processes.⁶⁹ Notwithstanding, for these interactions to successfully happen the complex must enter the cell. There are different pathways

such as passive diffusion, facilitated diffusion, active protein transport and endocytosis (see Fig. 21).⁷¹

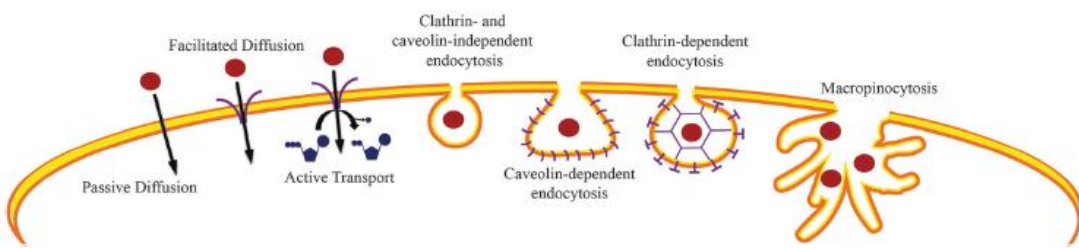


Fig. 21. Schematic diagram of the different possible transport routes of entry into the cell taken by small complexes. Figure extracted from Komor, A. C.; Barton, J. K. *Chem. Commun. (Camb)*. 2013, **49**, p. 3624.⁷¹

Thus, lipophilicity plays an important role so that the complexes can cross the phospholipid bilayer. The more lipophilic a complex is, the better its ability is to cross the cell membrane. This feature is expressed by the partition coefficient (P), which represents the octanol-water coefficient (see Eq. 1).⁸⁵

$$P_{ow} = C_o/C_w \quad (1)$$

This parameter is frequently expressed as the $\log P$, since it can range over many orders of magnitude. The P parameter was selected as a measurement of hydrophobicity, since it is related to the free-energy from the Van't Hoff isotherm (see Eq. 2):

$$\Delta G = -RT \ln P \quad (2)$$

which represents the free energy change during the transfer of the solute from water to a non-aqueous phase. This transfer is affected by lipophilic, polar, electronic and steric factors.⁸⁶ There are several techniques to determine this value, represented as $\log P$. Unlike classical methods such as "shake-flask" or "HPLC", reversed-phase thin layer chromatography (RP-TLC) is a simple and fast method to test lipophilicity. Nevertheless, its use has been limited in organometallic compounds and only in the last years it has been used for vanadium and ruthenium complexes.^{87,88} The RP-TLC method provides the retardation factor (R_f) calculated as the ratio of distances between the spotted compound and the solvent front in a given time. The parameter R_m was determined from the R_f value, as the correlation measurement of $\log P$ (see Eq. 3).⁸⁶

$$R_m = \log \left(\frac{1}{R_f} - 1 \right) \quad (3)$$

R_m values are linearly dependent on the concentration of organic modifier (φ) in the mobile phase (see Eq. 4).

$$R_m = R_m^o + b\varphi \quad (4)$$

where b and R_m^o are the slope and intercept of the equation, respectively. R_m^o represents the extrapolated R_m value at 0% organic solvent. This equation is different for each compound.⁸⁹ Parameter C^o , calculated as the ratio between R_m^o and b ($C^o = -R_m^o/b$), indicates the concentration of organic modifier in the mobile phase for which the distribution of the solute between the two phases becomes equal.⁸⁸

3. FEATURES OF THE METAL COMPLEXES

3.1. Ruthenium arene complexes

They belong to the group of the so-called half-sandwich or “piano-stool” complexes, showing a pseudo-octahedral geometry. Two main elements define their general structure with the general formula $[\text{Ru}(\eta^6\text{-arene})(\text{X})(\text{YZ})]^{0/n+}$ (see Fig. 22a): (i) an arene (the seat of the piano stool) and (ii) either three monodentate ligands or a bidentate and a monodentate ligands (the three legs of the stool). Their structural elements can be modulated in order to tune the reactivity of the complexes.^{12,24,31,40,68,90}

- **Metal centre, Ru(II).** Ruthenium is found in its lowest oxidation state and exhibit hydrophilic character.
- **Arene.** The arene stabilizes the low oxidation state through the η^6 -coordination mode, which exhibits π -acceptor character. It also provides a hydrophobic face to the molecule, which can help the complex to cross the lipophilic cell membrane and thus, to reach with the intracellular targets. Cytotoxicity is thought to be associated with lipophilicity. The arene is relatively inert towards displacement in physiological conditions.
- **Chelating ligand (YZ).** The chelating or ancillary ligand provides additional stability to the complex and its variation can modify the electronic density of the metal centre depending on the donor character of the atoms, typically, N,N -, N,O -, O,O - and C,N - polypyridyl ligands are commonly used, due to their intercalating and photoluminescent properties.
- **Monodentate ligand or leaving group (X).** The monodentate ligand can be replaced by other molecules and targets (water, proteins, DNA...) when the Ru-X bond is labile enough. It is usually a halide (chloride) easy to displace, but it can also be a non-labile ligand, like PTA.
- **Charge (0/n+).** The overall charge of the complex is defined by both the ancillary and the monodentate ligands. On the one hand, positively charged complexes attract the negatively charged DNA. On the other hand, neutral complexes cross membranes more readily and usually become positive charged after activation by replacement.

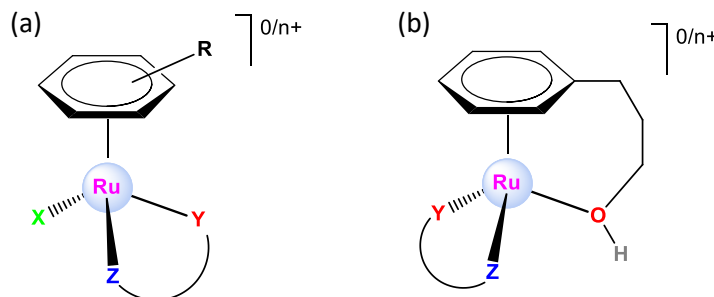


Fig. 22. (a) General structure for Ru(II)-arene complexes and (b) example structure of tethered compounds.

With all these features a wide variety of complexes can be synthesized, from neutral to dicationic. As far as the arene is concerned, the more π -extended they are, the better intercalate DNA.^{31,40} Furthermore, both the arene and the ancillary ligand can introduce a functional group in order to be specific for different targets, for instance, active sites in enzymes and proteins.^{91,92} Besides the functional group, a side chain in arenes often improves solubility or even their activity. When the side chain is also bonded to the metal centre, tethered complexes are formed (see Fig. 22b).^{93,94} In this case, the arene acts as a hemilabile ligand, even though only a few examples with alcohol and amines functions are reported.⁹⁴ Owing to the poorly coordination of these groups the process is reversible, it means, the functional group can coordinate or uncoordinate depending on the physiological conditions.⁹³ With regard to the leaving group (usually Cl^-), the hydrolysis rate depends on both the ligand and the chloride concentration in physiological conditions. The intracellular Cl^- concentration is lower than the extracellular concentration: 4 mM in nucleus, 23 mM in cytoplasm and 103 mM outside the cell. When the chloride concentration is high, the hydrolysis is suppressed.⁶⁸

3.2. Iridium and Rhodium pentamethylcyclopentadienyl complexes

Like in the case of ruthenium, iridium and rhodium pentamethylcyclopentadienyl (Cp^*) complexes are also half-sandwich and “piano-stool” complexes. Although unlike arene congeners, the “seat” of the stool is an anionic ligand, which stabilizes the metal ions Rh(III) and Ir(III) owing to the steric and electron-donating effect of the five methyl groups and the negative charge (see Fig. 23).⁹⁵ The structural elements of this kind of compounds can be modulated in the same way that ruthenium-arene complexes. Regarding the leaving group, the lability of M-Cl bonds depends on the strong *trans* effect of Cp^* .⁹⁶ Thus, substitution rates are much higher than those for ruthenium-arene complexes,⁵¹ in spite of the fact that substitution reaction rates for Ir(III) complexes without Cp^* are very low in general.

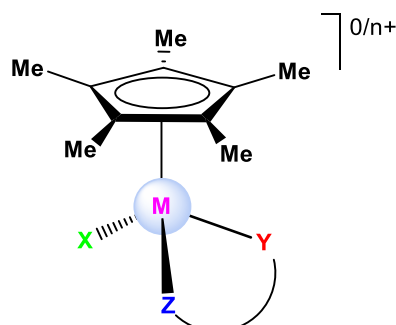


Fig. 23. General structure for Rh(III) and Ir(III) half-sandwich complexes with Cp^* .

4. LIGANDS

The [chelating ligands](#) used in the half-sandwich complexes were arylbenzoazoles with diverse 2-arylsubstituted groups, such as hydroxyl or amino moieties, which has been already reviewed in pages 35-39.

The leaving groups selected for these complexes were halides or pseudohalides (Cl^- , I^- and SCN^-), but also N-donor (N-methylimidazole), P-donor (PTA) or water molecules.

As regards the halides, chloride has been widely used due to the good properties as leaving group. The iodide, however, is not such a good leaving group, which is explained by its lower hydration energy compared to Cl^- (see CHAPTER 5).

5. BIBLIOGRAPHY

- (1) WHO <http://www.who.int/topics/cancer/en/>.
- (2) WHO <http://www.who.int/mediacentre/factsheets/fs297/en/>.
- (3) Rosenberg, B. In *Cisplatin Chemistry and Biochemistry of a Leading Anticancer Drug*; Lippert, B., Ed.; Verlag Helvetica Chimica Acta: Zürich, **1999**; pp. 1–27.
- (4) Rosenberg, B.; Vancamp, L.; Krigas, T. *Nature* **1965**, *205*, 698–699.
- (5) Rosenberg, B.; VanCamp, L.; Trosko, J. E.; Mansour, V. H. *Nature* **1969**, *222*, 385–386.
- (6) Cleare, M. J.; Hoeschele, J. D. *Bioinorg. Chem.* **1973**, *2*, 187–210.
- (7) Lippard, S. J. In *Bioinorganic Chemistry*; **1994**; pp. 505–583.
- (8) Hannon, M. J. *Pure Appl. Chem.* **2007**, *79*, 2243–2261.
- (9) O'Dwyer, P. J.; Stevenson, J. P.; Johnson, S. W. In *Clinical Status of Cisplatin, Carboplatin, and Other Platinum-Based Antitumor Drugs*; Lippert, B., Ed.; Verlag Helvetica Chimica Acta: Zürich, **1999**; pp. 29–69.
- (10) Wheate, N. J.; Walker, S.; Craig, G. E.; Oun, R. *Dalton Trans.* **2010**, *39*, 8113–27.
- (11) Trudu, F.; Amato, F.; Vaňhara, P.; Pivetta, T.; Peña-Méndez, E. M.; Havel, J. J. *Appl. Biomed.* **2015**, *13*, 79–103.
- (12) Medici, S.; Peana, M.; Nurchi, V. M.; Lachowicz, J. I.; Crisponi, G.; Zoroddu, M. A. *Coord. Chem. Rev.* **2015**, *284*, 329–350.
- (13) Ostrowski, A. D.; Ford, P. C. *Dalton Trans.* **2009**, *10660*–9.
- (14) Jungwirth, U.; Kowol, C. R.; Keppler, B. K.; Hartinger, C. G.; Berger, W.; Heffeter, P. *Antioxid. Redox Signal.* **2011**, *15*, 1085–1127.
- (15) Ali, I.; A. Wani, W.; Saleem, K.; Haque, A. *Anticancer. Agents Med. Chem.* **2013**, *13*, 296–306.
- (16) M. Takahara, P.; C. Rosenzweig, A.; A. Frederick, C.; J. Lippard, S. Crystal structure of double-stranded DNA containing the major adduct of the anticancer drug cisplatin. *Nature* **1995**, *377*, 649–652.
- (17) Bergamo, A.; Sava, G. *Chem. Soc. Rev.* **2015**, *44*, 8818–8835.
- (18) Zangrandi, E.; Pichierri, F.; Randaccio, L.; Lippert, B. *Coord. Chem. Rev.* **1996**, *156*, 275–332.
- (19) Shamsi, M. H.; Kraatz, H.-B. *J. Inorg. Organomet. Polym. Mater.* **2012**, *23*, 4–23.
- (20) Greenwood, N. N.; Earnshaw, A. *Chemistry of the Elements*; Second.; Butterworth Heinemann, **1997**.
- (21) Abu-surrah, A. S.; Al-sa, H. H.; Abdalla, M. Y. *Cancer Ther.* **2008**, *6*, 1–10.
- (22) Gao, E.; Liu, C.; Zhu, M.; Lin, H.; Wu, Q.; Liu, L. *Anticancer. Agents Med. Chem.* **2009**, *9*, 356–368.
- (23) Abu-Surrah, A. S.; Kettunen, M. *Curr. Med. Chem.* **2006**, *13*, 1337–1357.
- (24) Nazarov, A. a.; Hartinger, C. G.; Dyson, P. J. *J. Organomet. Chem.* **2014**, *751*, 251–260.
- (25) Koudinova, N. V; Pinthus, J. H.; Brandis, A.; Brenner, O.; Bendel, P.; Ramon, J.; Eshhar, Z.; Scherz, A.; Salomon, Y. *Int. J. Cancer* **2003**, *104*, 782–789.
- (26) Allardyce, C. S.; Dyson, P. J. *Dalt. Trans.* **2016**, *45*, 3201–3209.
- (27) Scolaro, C.; Chaplin, A. B.; Hartinger, C. G.; Bergamo, A.; Cocchietto, M.; Keppler, B. K.; Sava, G.; Dyson, P. J. *Dalton Trans.* **2007**, *2*, 5065–5072.
- (28) Blunden, B. M.; Stenzel, M. H. *J. Chem. Technol. Biotechnol.* **2014**, *90*, 1177–1195.
- (29) Antonarakis, E. S.; Emadi, A. *Cancer Chemother. Pharmacol.* **2010**, *66*, 1–9.
- (30) Levina, A.; Mitra, A.; Lay, P. *a Metallomics* **2009**, *1*, 458–470.

- (31) Yan, Y. K.; Melchart, M.; Habtemariam, A.; Sadler, P. J. *Chem. Commun.* **2005**, 4764–4776.
- (32) Rademaker-Lakhai, J. M. *Clin. Cancer Res.* **2004**, *10*, 3717–3727.
- (33) Leijen, S.; Burgers, S. A.; Baas, P.; Pluim, D.; Tibben, M.; van Werkhoven, E.; Alessio, E.; Sava, G.; Beijnen, J. H.; Schellens, J. H. M. *Invest. New Drugs* **2015**, *33*, 201–214.
- (34) Bergamo, A.; Riedel, T.; Dyson, P. J.; Sava, G. *Invest. New Drugs* **2015**, *33*, 53–63.
- (35) Kersten, L.; Bräunlich, H.; Keppler, B. K.; Gliesing, C.; Wendelin, M.; Westphal, J. J. *Appl. Toxicol.* **1998**, *18*, 93–101.
- (36) Hartinger, C. G.; Jakupc, M. A.; Zorbas-Seifried, S.; Groessl, M.; Egger, A.; Berger, W.; Zorbas, H.; Dyson, P. J.; Keppler, B. K. *Chem. Biodivers.* **2008**, *5*, 2140–2155.
- (37) Ott, I.; Gust, R. *Arch. Pharm. (Weinheim)*. **2007**, *340*, 117–126.
- (38) Bergamo, A.; Sava, G. *Dalt. Trans.* **2007**, 1267–1272.
- (39) Reisner, E.; Arion, V. B.; Keppler, B. K.; Pombeiro, A. J. L. *Inorganica Chim. Acta* **2008**, *361*, 1569–1583.
- (40) Peacock, A. F. A.; Sadler, P. J. *Chem. An Asian J.* **2008**, *3*, 1890–1899.
- (41) Morris, R. E.; Aird, R. E.; del Socorro Murdoch, P.; Chen, H.; Cummings, J.; Hughes, N. D.; Parsons, S.; Parkin, A.; Boyd, G.; Jodrell, D. I.; Sadler, P. J. *J. Med. Chem.* **2001**, *44*, 3616–3621.
- (42) Bergamo, A.; Gaiddon, C.; Schellens, J. H. M.; Beijnen, J. H.; Sava, G. *J. Inorg. Biochem.* **2012**, *106*, 90–99.
- (43) Kilpin, K. J.; Cammack, S. M.; Clavel, C. M.; Dyson, P. J. *Dalt. Trans.* **2013**, *42*, 2008–2014.
- (44) Hartinger, C. G.; Dyson, P. J. *Chem. Soc. Rev.* **2009**, *38*, 391–401.
- (45) Chatterjee, S.; Kundu, S.; Bhattacharyya, A.; Hartinger, C. G.; Dyson, P. J. *JBIC J. Biol. Inorg. Chem.* **2008**, *13*, 1149–1155.
- (46) Vock, C. a; Scolaro, C.; Phillips, A. D.; Scopelliti, R.; Sava, G.; Dyson, P. J. *J. Med. Chem.* **2006**, *49*, 5552–5561.
- (47) Păunescu, E.; Nowak-Sliwinska, P.; Clavel, C. M.; Scopelliti, R.; Griffioen, A. W.; Dyson, P. J. *ChemMedChem* **2015**, *10*, 1539–1547.
- (48) Pizarro, A. M.; Sadler, P. J. *Biochimie* **2009**, *91*, 1198–211.
- (49) Hanif, M.; Babak, M. V.; Hartinger, C. G. *Drug Discov. Today* **2014**, *19*, 1640–1648.
- (50) Kuhn, P.-S.; Büchel, G. E.; Jovanović, K. K.; Filipović, L.; Radulović, S.; Rapta, P.; Arion, V. B. *Inorg. Chem.* **2014**, *53*, 11130–11139.
- (51) Geldmacher, Y.; Oleszak, M.; Sheldrick, W. S. *Inorganica Chim. Acta* **2012**, *393*, 84–102.
- (52) Taylor, A.; Charmichael, N. *Cancer Stud. II* **1953**, 36–79.
- (53) Iavicoli, I.; Cufino, V.; Corbi, M.; Goracci, M.; Caredda, E.; Cittadini, A.; Bergamaschi, A.; Sgambato, A. *Toxicol. Vitr.* **2012**, *26*, 963–969.
- (54) Katsaros, N.; Anagnostopoulou, A. *Crit. Rev. Oncol. Hematol.* **2002**, *42*, 297–308.
- (55) Siu, F.-M.; Lin, I. W.-S.; Yan, K.; Lok, C.-N.; Low, K.-H.; Leung, T. Y.-C.; Lam, T.-L.; Che, C.-M. *Chem. Sci.* **2012**, *3*, 1785.
- (56) Leung, C.-H.; Zhong, H.-J.; Chan, D. S.-H.; Ma, D.-L. *Coord. Chem. Rev.* **2013**, *257*, 1764–1776.
- (57) Nothenberg, M. S.; de Souza, A. R.; Matos, J. do R. *Polyhedron* **2000**, *19*, 1305–1309.
- (58) Bieda, R.; Ott, I.; Dobroschke, M.; Prokop, A.; Gust, R.; Sheldrick, W. S. *J. Inorg.*

- Biochem.* **2009**, *103*, 698–708.
- (59) Liu, Z.; Sadler, P. J. *Acc. Chem. Res.* **2014**, *47*, 1174–1185.
- (60) Liu, Z.; Salassa, L.; Habtemariam, A.; Pizarro, A. M.; Clarkson, G. J.; Sadler, P. J. *Inorg. Chem.* **2011**, *50*, 5777–5783.
- (61) Liu, Z.; Habtemariam, A.; Pizarro, A. M.; Clarkson, G. J.; Sadler, P. J. *Organometallics* **2011**, *30*, 4702–4710.
- (62) Liu, Z.; Habtemariam, A.; Pizarro, A. M.; Fletcher, S. A.; Kisova, A.; Vrana, O.; Salassa, L.; Bruijnincx, P. C. A.; Clarkson, G. J.; Brabec, V.; Sadler, P. J. *J. Med. Chem.* **2011**, *54*, 3011–3026.
- (63) Novohradsky, V.; Liu, Z.; Vojtiskova, M.; Sadler, P. J.; Brabec, V.; Kasparkova, J. *Metalloomics* **2014**, *6*, 682–690.
- (64) Ma, D.-L.; Chan, D. S.-H.; Leung, C. *Acc. Chem. Res.* **2014**, *47*, 3614–3631.
- (65) Cao, R.; Jia, J.; Ma, X.; Zhou, M.; Fei, H. *J. Med. Chem.* **2013**, *56*, 3636–3644.
- (66) Feng, L.; Geisselbrecht, Y.; Blanck, S.; Wilbuer, A.; Atilla-gokcumen, G. E.; Filippakopoulos, P.; Kr, K.; Celik, M. A.; Harms, K.; Maksimoska, J.; Marmorstein, R.; Frenking, G.; Knapp, S.; Essen, L.; Meggers, E. *J. Am. Chem. Soc.* **2011**, *133*, 5976–5986.
- (67) N. Kaluderovic, G.; Paschke, R. *Curr. Med. Chem.* **2011**, *18*, 4738–4752.
- (68) Pizarro, A. M.; Habtemariam, A.; Sadler, P. J. *Top Organomet. Chem.* **2010**, *32*, 21–56.
- (69) Romero-Canelón, I.; Sadler, P. J. *Inorg. Chem.* **2013**, *52*, 12276–12291.
- (70) García-ramos, J. C.; Galindo-murillo, R.; Cortés-guzmán, F.; Ruiz-azuara, L.; Conjunto, C.; Investigación, D.; Sustentable, Q. *J. Mex. Chem. Soc.* **2013**, *57*, 245–259.
- (71) Komor, A. C.; Barton, J. K. *Chem. Commun. (Camb.)* **2013**, *49*, 3617–3630.
- (72) Lippert, B. *Coord. Chem. Rev.* **2000**, *200*–*202*, 487–516.
- (73) Liu, H.-K.; Sadler, P. J. *Acc. Chem. Res.* **2011**, *44*, 349–359.
- (74) Valko, M.; Rhodes, C. J.; Moncol, J.; Izakovic, M.; Mazur, M. *Chem. Biol. Interact.* **2006**, *160*, 1–40.
- (75) Kręzel, A.; Bal, W. Coordination chemistry of glutathione. *Acta Biochim. Pol.* **1999**, *46*, 567–580.
- (76) Shoeib, T.; Sharp, B. L. *Inorganica Chim. Acta* **2013**, *405*, 258–264.
- (77) Mokdsi, G.; Harding, M. M. *J. Inorg. Biochem.* **2001**, *86*, 611–616.
- (78) Zhang, R.; Wu, W.; Luo, S. *J. Solution Chem.* **2011**, *40*, 1784–1795.
- (79) Hearn, J. M.; Romero-Canelón, I.; Qamar, B.; Liu, Z.; Hands-Portman, I.; Sadler, P. J. *ACS Chem. Biol.* **2013**, *8*, 1335–1343.
- (80) Liu, Z.; Romero-Canelón, I.; Qamar, B.; Hearn, J. M.; Habtemariam, A.; Barry, N. P. E.; Pizarro, A. M.; Clarkson, G. J.; Sadler, P. J. *Angew. Chemie Int. Ed.* **2014**, *53*, 3941–3946.
- (81) Romero-Canelón, I.; Salassa, L.; Sadler, P. J. *J. Med. Chem.* **2013**, *56*, 1291–300.
- (82) Fromm, H. J.; Hargrove, M. *Essentials of Biochemistry*; Springer Berlin Heidelberg: Berlin, Heidelberg, **2012**.
- (83) Pollak, N.; Dölle, C.; Ziegler, M. *Biochem. J.* **2007**, *402*, 205–218.
- (84) Kanomata, N.; Nakata, T. *J. Am. Chem. Soc.* **2000**, *122*, 4563–4568.
- (85) Sangster, J. *J. Phys. Chem. Ref. Data.* **1989**, *18*, 1111–1227.
- (86) Dearden, J. C. *Environ. Health Perspect.* **1985**, *61*, 203–228.
- (87) Fernández, M.; Becco, L.; Correia, I.; Benítez, J.; Piro, O. E.; Echeverria, G. A.;

- Medeiros, A.; Comini, M.; Laura, M.; González, M.; Cerecetto, H.; Moreno, V.; Costa, J.; Garat, B.; Gambino, D. *J. Inorg. Biochem.* **2013**, *127*, 150–160.
- (88) Shweshein, K. S. A. M.; T, F. A.; T, A. R. I.; Zlatar, M.; T, M. G.; Teši, C. T.; T, D. M. *Sci. World J.* **2014**, *2014*, 1–10.
- (89) Wang, Q. S.; Zhang, L. *J. Liq. Chromatogr. Relat. Technol.* **1999**, *22*, 1–14.
- (90) Bruijnincx, P. C. A.; Sadler, P. J. In *Advances in Inorganic Chemistry*; Elsevier, **2009**; Vol. 61, pp. 1–62.
- (91) Ong, J. X.; Yap, C. W.; Ang, W. H. *Inorg. Chem.* **2012**, *51*, 12483–12492.
- (92) Dörr, M.; Meggers, E. *Curr. Opin. Chem. Biol.* **2014**, *19*, 76–81.
- (93) Lastra-Barreira, B.; Díez, J.; Crochet, P.; Fernández, I. *Dalt. Trans.* **2013**, *42*, 5412–5420.
- (94) Therrien, B. *Coord. Chem. Rev.* **2009**, *253*, 493–519.
- (95) White, C.; Yates, A.; Maitlis, P. M.; Heinekey, D. M. In *Inorg. Synth.*; **1992**; Vol. 29, pp. 228–234.
- (96) Lo, K. K.-W.; Zhang, K. Y. *RSC Adv.* **2012**, *12069*–12083.

CHAPTER 1.

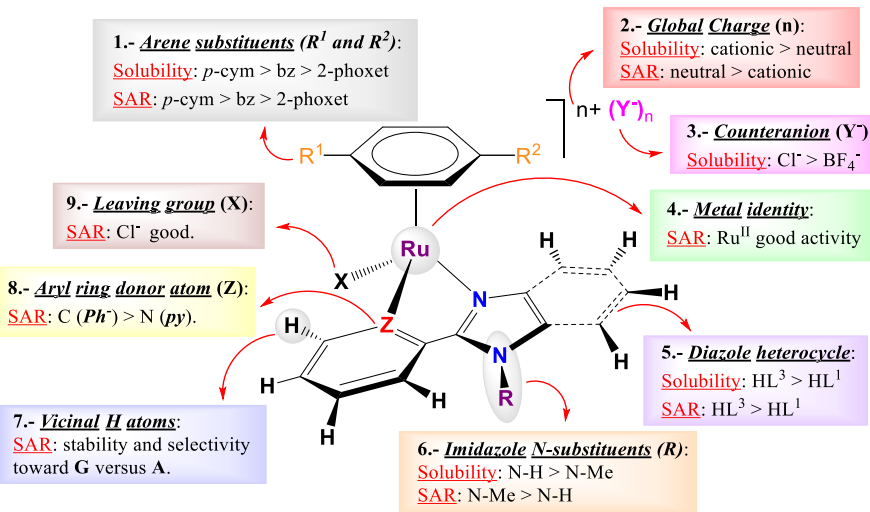
Ru(II) HALF-SANDWICH COMPLEXES BEARING PYRIDYLIAZOLE ANCILLARY LIGANDS: SYNTHESIS, CHARACTERIZATION AND ANTICANCER PROPERTIES



CHAPTER 1. Ru(II) HALF-SANDWICH COMPLEXES BEARING PYRIDYLIAZOLE ANCILLARY LIGANDS: SYNTHESIS, CHARACTERIZATION AND ANTICANCER PROPERTIES

ABSTRACT: In this chapter a family of 18 new ruthenium arene complexes of general formulae $[\text{Ru}(\eta^6\text{-arene})(\kappa^2\text{-}N,N\text{-HL})X]Y$ or $[\text{Ru}(\eta^6\text{-arene})(\kappa^2\text{-}N,N\text{-L})X]$ (X = leaving group; Y = counterion)

bearing 2-(2'-pyridyl)benzimidazole (pybim), 2-(2'-pyridyl)-N-methylbenzimidazole (pyMebim) or 2-(2'-pyridyl)imidazole (pyim) as ancillary ligands was prepared and their cytotoxic activity was determined so as to establish some structure-activity relationships (SAR). The reactivity of these complexes against DNA and their modes of interaction with this biomolecule were studied in collaboration with the group of Begoña García, from the University of Burgos.^{1,2}



CONTEXT: Half-sandwich ruthenium(II) arene complexes have been identified as an alternative class of potential anticancer drugs that could complement the medicines nowadays in clinical use,^{3,4,5} such as cisplatin and congeners.^{6,7} Benzimidazoles and, in particular, aryl-substituted benzimidazole derivatives exhibit a wide slate of potential pharmaceutical applications, as previously discussed. Some examples of palladium(II) and platinum(II) complexes with 2-(2'-pyridyl)benzimidazole have been studied in relation to their cytotoxicity.^{8,9} In addition, novel families of ruthenium(II) complexes bearing benzimidazole scaffolds in the ancillary ligands have been reported as potential anticancer drugs.^{10,11,12}

1. RESULTS AND DISCUSSION

1.1. Synthesis

The new complexes were synthesised from the ruthenium chloro-bridged dimers $[\text{Ru}(\eta^6\text{-arene})(\mu\text{-Cl})\text{Cl}]_2$, which in turn were prepared by reacting $\text{RuCl}_3 \cdot n\text{H}_2\text{O}$ with the corresponding cyclohexadiene in ethanol or ethylene glycol, as shown in Fig. 1.^{13,14}

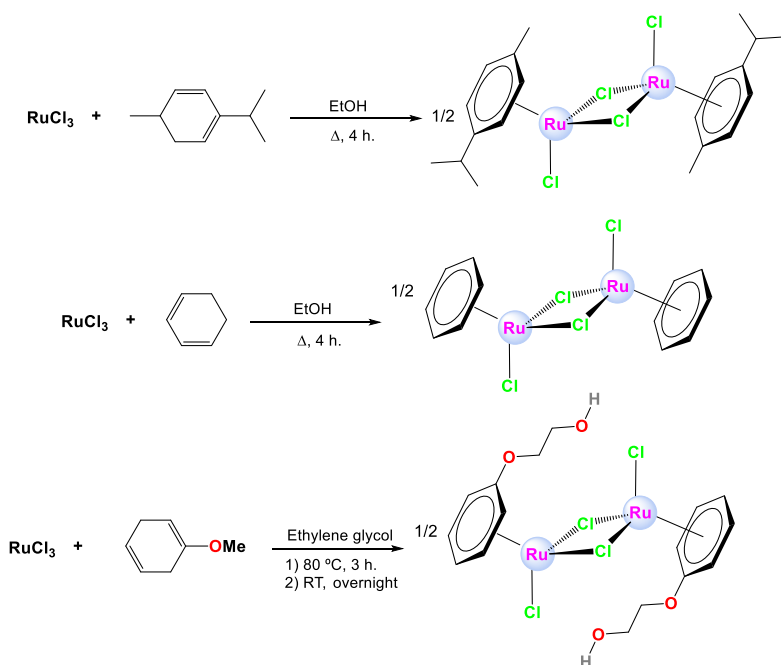


Fig. 1. Synthesis of chloro-bridged ruthenium arene complexes.

The complexes can be divided in two groups: cationic and neutral and their schematic synthesis is shown in Fig. 2.

Cationic complexes

The reaction between the arene ruthenium(II) starting dimers and the ligands (pybim, pyMebim and pyim) at room temperature and using methanol as the solvent yielded monocationic compounds of general formulae $[(\eta^6\text{-arene})\text{RuCl}(\kappa^2\text{-}N,N\text{-HL})]\text{Cl}$ (**[1a]Cl**, **[1b]Cl**, **[1c]Cl**, **[2a]Cl**, **[3a]Cl**), where HL is the ligand and the arene corresponds to: **a** = *p*-cymene (*p*-cym); **b** = benzene (bz) and **c** = 2-phenoxyethanol (phoxet). The respective BF_4^- salts of general formulae $[(\eta^6\text{-arene})\text{RuCl}(\kappa^2\text{-}N,N\text{-pybim})]\text{BF}_4$ (**[1a](BF₄)**, **[1b](BF₄)**, **[1c](BF₄)**) were synthesised by a related protocol in the presence of AgBF_4 and using dichloromethane as the solvent.

The dicationic aqua derivatives of general formula $[(\eta^6\text{-arene})\text{Ru}(\text{H}_2\text{O})(\kappa^2\text{-}N,N\text{-pybim})](\text{Y})_2$ (**[4a]**(BF₄)₂, **[4b]**(BF₄)₂, **[4c]**(BF₄)₂, **[4a]**(OTf)₂, **[4b]**(OTf)₂, **[4c]**(OTf)₂), where Y = BF₄⁻ or OTf⁻, were prepared by the reaction of the monocationic complexes **[1a]Cl**, **[1b]Cl** and **[1c]Cl** with an excess of the corresponding silver salts (AgBF₄ and AgOTf) in distilled water or in a mixture of water and ethanol. The reaction of complex **[1c]Cl** with

an excess of AgBF_4 in methanol was expected to yield the tethered derivative $[(\eta^6\text{-C}_6\text{H}_5\text{O}(\text{CH}_2)_2\text{OH})\text{Ru}(\kappa^2\text{-}N,N\text{-pybim})](\text{BF}_4)_2$. Nonetheless, in a methanolic solution, the NOESY spectrum showed evidence of the formation of the methanol derivative $[(\eta^6\text{-phoxet})\text{Ru}(\text{CH}_3\text{OH})(\kappa^2\text{-}N,N\text{-pybim})](\text{BF}_4)_2$ or the fast coordination-decoordination process of the sidearm (**[5c](BF₄)₂**). The nucleobase derivative $[(\eta^6\text{-}p\text{-cym})\text{Ru}(9\text{-MeG})(\kappa^2\text{-}N,N\text{-pybim})](\text{PF}_6)_2$ (**[6a](PF₆)₂**), was prepared by reacting **[1a](BF₄)** with 9-methylguanine (9-MeG) at 37 °C in distilled water and isolated as a PF₆⁻ salt by adding an excess of (NH₄)PF₆.

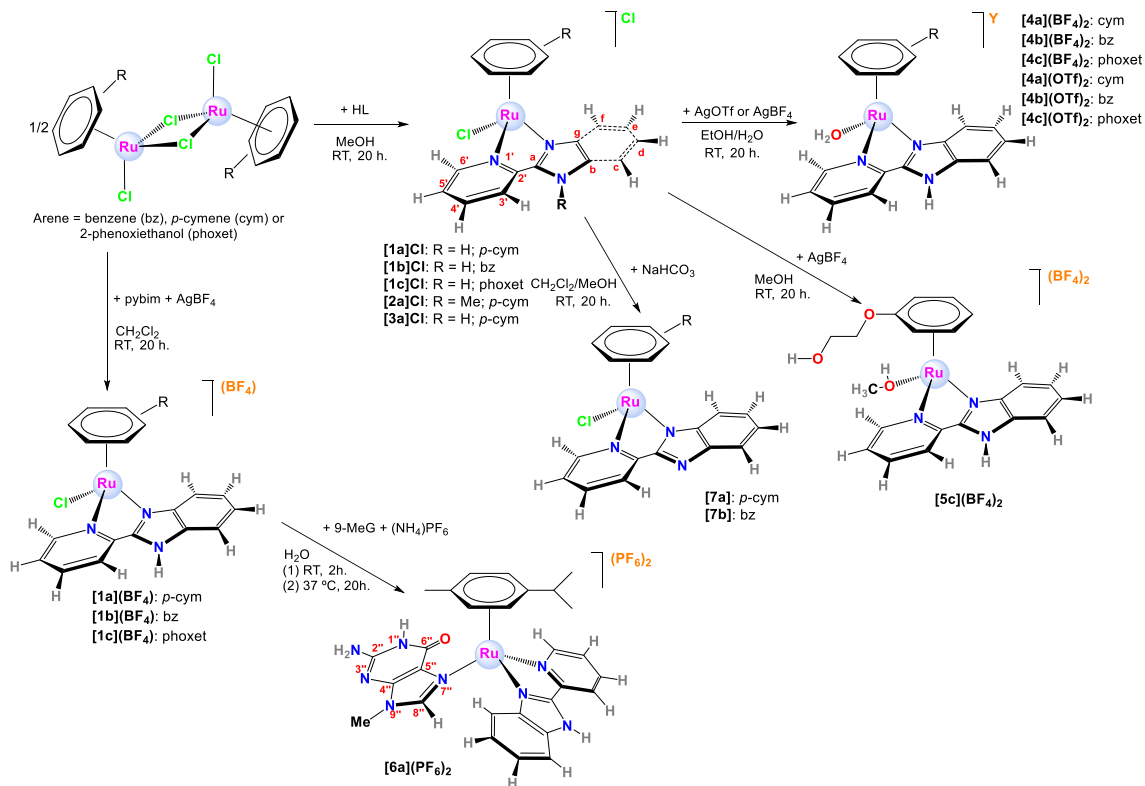


Fig. 2. Schematic synthesis of the new Ruthenium(II) complexes.

Neutral complexes

Complexes **[1a]Cl** and **[1b]Cl** were reacted with NaHCO₃ in a mixture of dichloromethane/methanol or acetone/methanol (to favour the solubility of **[1b]Cl**), respectively, at room temperature¹⁵ to yield neutral complexes $[(\eta^6\text{-arene})\text{RuCl}(\kappa^2\text{-}N,N\text{-pybim}')](\text{[7a]}, \text{[7b]})$, where pybim' = deprotonated pybim.

All the complexes were isolated in moderate to good yields (from 43% to 85%) as the corresponding racemates (R_{Ru} or S_{Ru}) in the form of yellow, orange or brown solids.

1.2. Characterization

All the complexes have been fully characterised by NMR spectroscopy, IR spectroscopy, positive fast atom bombardment (FAB⁺) mass spectrometry, molar conductivity and elemental analysis.

1.2.1. NMR

The ^1H NMR spectra of the monocationic complexes were recorded in DMSO-d₆, CDCl₃ and CD₃OD at 25 °C. The coordination of the corresponding *N,N*-ligands to the metallic centres was proved, since some signals of the ligands were downfield-shifted with regard to those of the free ligands (see Fig. 3). Specially, one of the signals H^{6'}(py) showed the strongest shift with $\Delta\delta = 0.68\text{-}0.99$ ppm. In addition, complexes with pybim and pyim showed a broad resonance assigned to the N-H group, at 15 and 16 ppm, respectively. All the spectra display some characteristic areas (see Fig. 3) for this kind of complexes: the amino/N-H area, very downfield-shifted; the aromatic area (5-9 ppm), which includes both the ligand (7-9 ppm) and the arene (5-7 ppm) signals; and the aliphatic area (0.5-4.5 ppm). Both the aromatic and the aliphatic areas of the *p*-cym and phoxet derivatives confirmed the asymmetric nature of the complexes. The *p*-cym derivatives showed an ABCD spin system for the aromatic resonances and two doublets for the diastereotopic methyls of *iPr*, whereas the phoxet derivatives showed an ABCDE pattern for the aromatic protons and four multiplets for the two diastereotopic methylene groups. The bz derivatives only exhibited a singlet at 6.30 ppm. In every case, the signals of the coordinated arenes were upfield-shifted with regard to those of the free ones, but downfield-shifted with respect to arenes in the starting dimers. It is remarkable, that the anion has no significant influence over chemical shifts in monocationic complexes in DMSO-d₆ (see Fig. 4). Bidimensional ^1H - ^1H NOESY spectrum of **[1a](BF₄)** showed NOE cross peaks between residual water and H^c and H^{3'}, suggesting a hydrogen-bonding interaction of the H₂O molecule (from residual water in DMSO-d₆) with the N-H group of the ligand. In addition, the NOESY exhibited some exchange peaks between the H₂O and the N-H group, suggesting an interchange process between these protons (see Fig. 5). These facts explain the deshielding effect on the hydrogen signal in the N-H group in the ^1H NMR spectra.

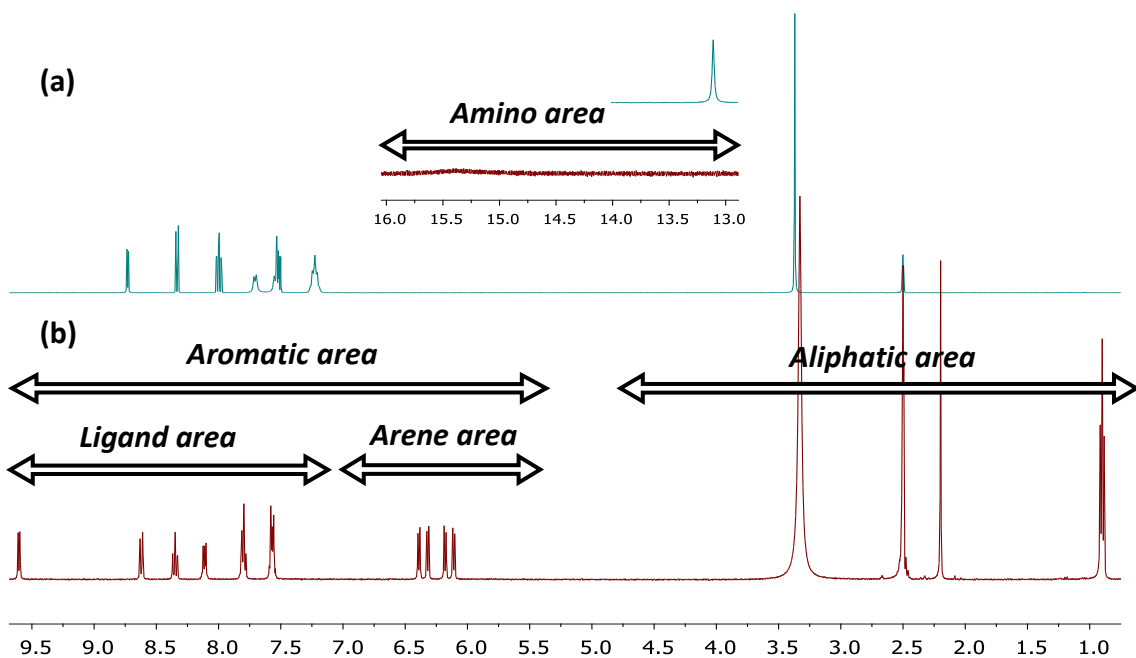


Fig. 3. Comparison of ^1H NMR spectra between (a) the free ligand pybim and (b) the complex [1a]Cl in DMSO-d_6 at 25°C , and illustration of the characteristic areas of aromatic and aliphatic protons.

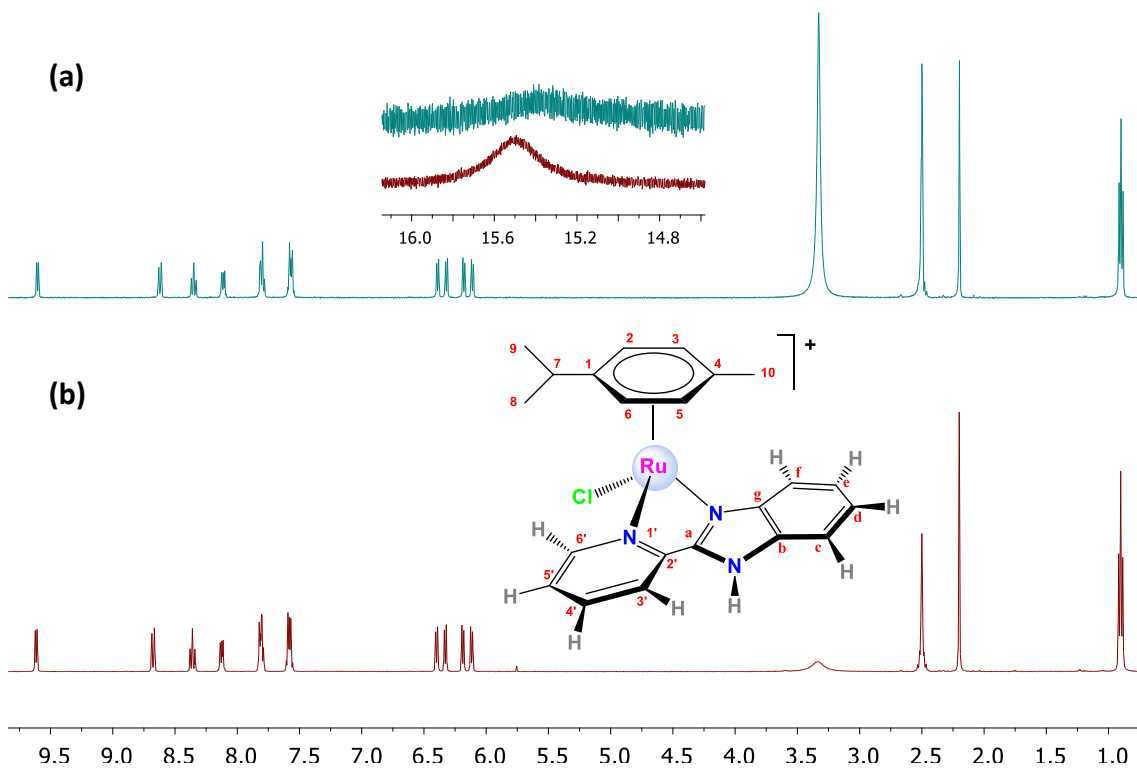


Fig. 4. Comparison of ^1H NMR spectra of complexes [1a]Cl (a) and [1a]BF₄ (b) in DMSO-d_6 at 25°C .

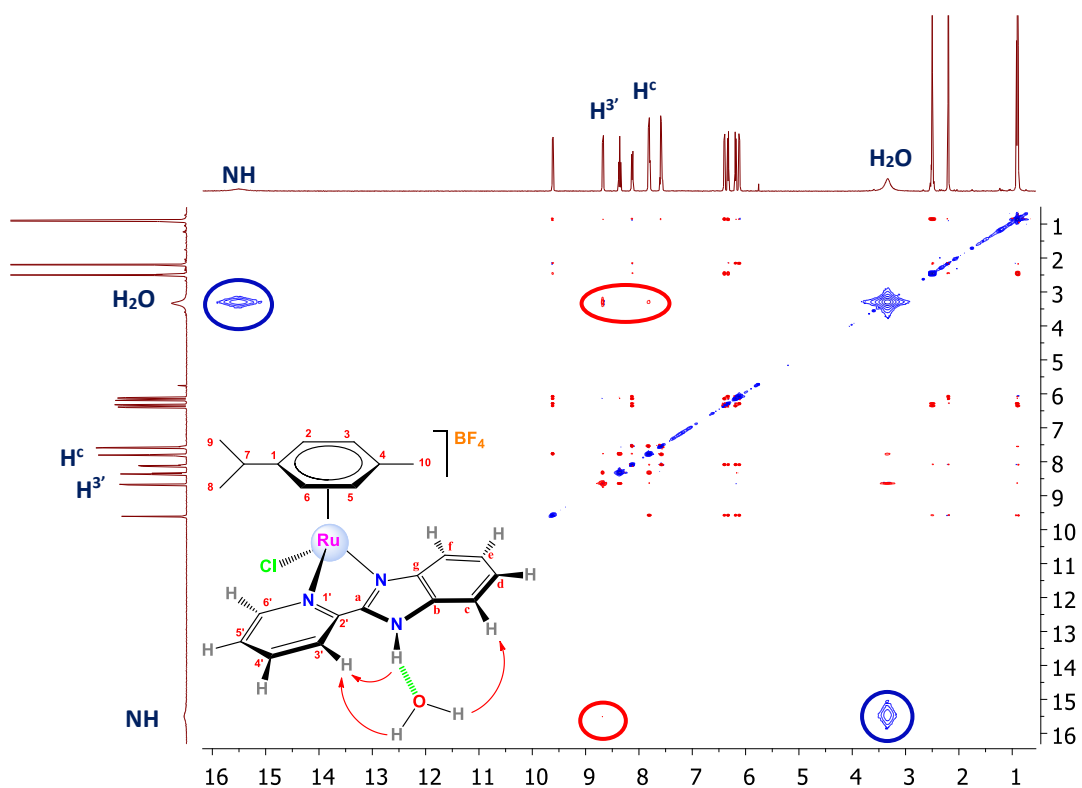


Fig. 5. 2D ^1H - ^1H NOESY spectrum for [1a](BF₄) in DMSO-d₆ at 25 °C.

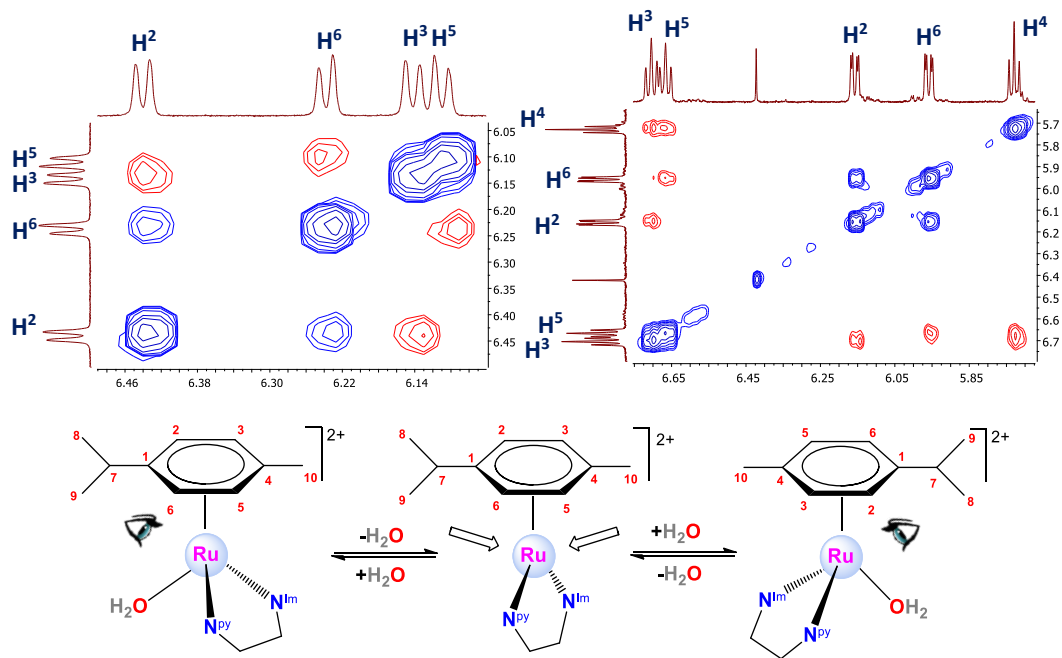


Fig. 6. (a) Arene aromatic protons area (*p*-cym and phoxet) in NOESY spectra of complexes [4a](BF₄)₂ (D₂O at 25 °C) and [4c](BF₄)₂ (CD₃OD at 25 °C). (b) Proposed mechanism for the interconversion process between enantiomers of [4a]²⁺. For instance, H⁶ in the first structure and H² in the last one ‘see’ the same atoms. An analogous mechanism was proposed for [4c]²⁺.

The ^1H NMR spectra of the aqua derivatives $[\mathbf{4x}]^{2+}$ were registered in D_2O at 25°C and were similar to those of the monocationic derivatives $[\mathbf{1x}]^+$. In this case, the signals of the aromatic protons are downfield-shifted, whereas those of the aliphatic ones are

upfield-shifted with respect to the corresponding resonances of the monocationic complexes. Regarding ^1H - ^1H NOESY or ^1H - ^1H ROESY spectra, the aqua derivatives with *p*-cym and phoxet show an interesting feature. There are exchange peaks between H^2 and H^6 , and H^3 and H^5 , although the latter are overlapped with diagonal cross-peaks. This fact made us propose an interconversion process between the two possible enantiomers (R_{Ru} or S_{Ru}), in which the water molecule is implied. The high lability of the water molecule favours its dissociation and the subsequent coordination of another water molecule from the opposite side. This process is slow enough to be detected by NMR (see Fig. 6).

The ^1H NMR of complex $[\text{5c}](\text{BF}_4)_2$ was registered in CD_3OD at 25 °C. The ^1H - ^1H NOESY spectrum of $[\text{5c}](\text{BF}_4)_2$ showed a NOE cross-peak between the methylene hydrogen H^7 and $\text{H}^{6'}$. This is bound to occur only in a free η^6 -coordination mode of phoxet. These evidences suggest two possible structures (see Fig. 7). Supposing a huge lability of the Ru-O bond, a rapidly coordination-decoordination process of the sidearm could take place, allowing the binding of solvent molecules such as water or methanol. This process could favour a better stability of the methanol derivative or other solvent derivatives. Some theoretical calculations by P. Crochet and I. Fernández support the idea of the easiness to break the Ru-O bond, which could provide unsaturated species (see Fig. 7a). Furthermore, both their calculations and experimental facts prove that the oxygen ($\text{C}_{\text{ipso}}\text{-O}$) lone pairs in phoxet participate in the electronic delocalization of the arene, stabilizing it. Thus, the rotation of the sidearm gets restricted, avoiding the approach of the OH group to the ruthenium centre.¹⁶ Since the rotation of the sidearm is impeded, the structure with coordinate methanol is likely to form in methanolic solution, although we cannot be sure about the structure in solid state (see Fig. 7b).

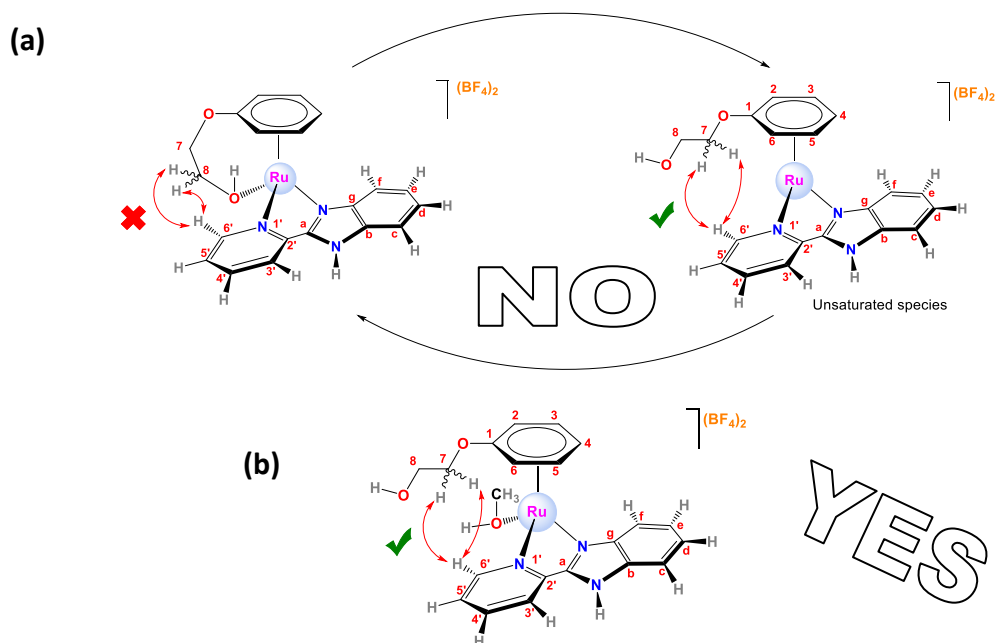


Fig. 7. Proposed structures for complex $[\text{5a}](\text{BF}_4)_2$. (a) Coordination-decoordination of the sidearm, leading to unsaturated species and (b) methanol derivative.

The ^1H NMR of the derivative with 9MeG (**[6a](PF₆)₂**) in DMSO-d₆ shows clearly evidences of the coordination of 9MeG to the metallic centre when compared to the spectrum of free 9MeG. The ^1H - ^1H ROESY was recorded so as to assign all the signals and it shows noteworthy NOE cross-peaks between residual water and H^c and H^{3'}, suggesting a hydrogen-bonding interaction between the H₂O molecule and the N-H group of the ligand. In fact, an exchange peak was detected between the NH group and the water molecule. Likewise, the expected NOE interactions between protons of guanine were observed, for instance, between NH₂ and H^{1''}, and between H^{Me} and H^{8''} (see Fig. 8).

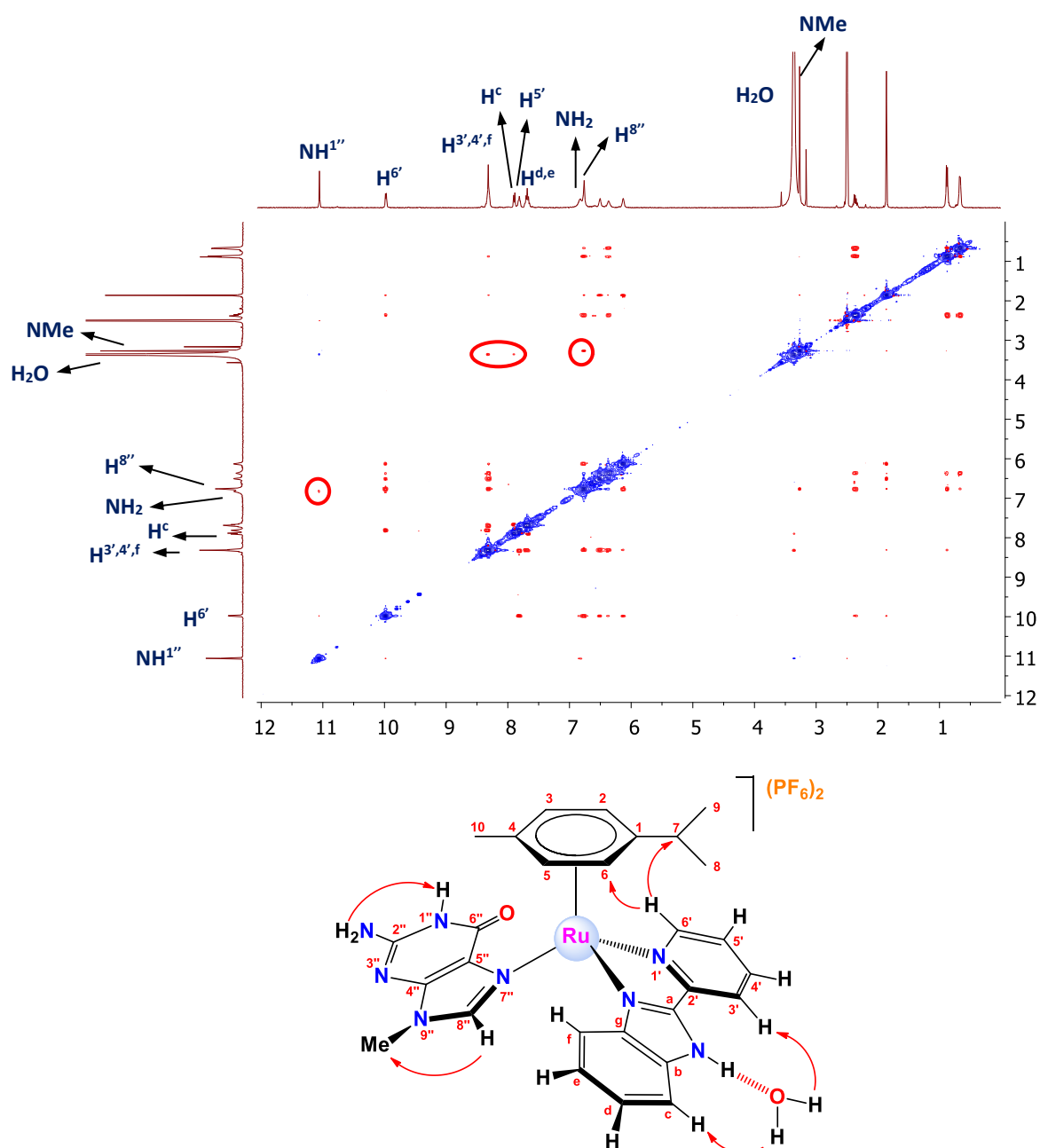


Fig. 8. Significant NOE contacts for **[6a](PF₆)₂** with a hydrogen-bonded H₂O molecule in the second coordination sphere, as observed by 2D ^1H - ^1H ROESY in DMSO-d₆ at 25 °C.

The ^1H NMR spectra of the neutral complexes (**[7a]**, **[7b]**) in DMSO-d₆ show the lack of signals in the low-field region when compared to the monocationic derivatives, owing to the deprotonation of the N-H group. Furthermore, the anionic nature of the ligand and consequently its higher electron density, shield the signals of both the ligand and the arene with regard to those of their respective precursors.

As far as $^{13}\text{C}\{^1\text{H}\}$ NMR is concerned, it shows the characteristic pattern with two different areas for the complexes: the aromatic area (70-160 ppm), including both the ligand (90-160 ppm) and the arene (70-90 ppm) signals; and the aliphatic area (15-60 ppm). It is noteworthy the shift observed for the signals of neutral complexes **[7a]** and **[7b]** in comparison to those of their cationic precursors **[1a]Cl** and **[1b]Cl** (see Fig. 9). The arene signals hardly move, whereas the peaks of quaternary carbons of the pybim ligand are deshielded (especially C^g in the imidazole entity, $\Delta\delta = 10.6$ ppm) and the rest of the resonances are shielded. The $^{13}\text{C}\{^1\text{H}\}$ NMR in D₂O for cationic complexes with the anion triflate show a quartet corresponding to the C-F coupling at 120.2 ppm with $^1J_{\text{C}-\text{F}} = 317$ Hz.

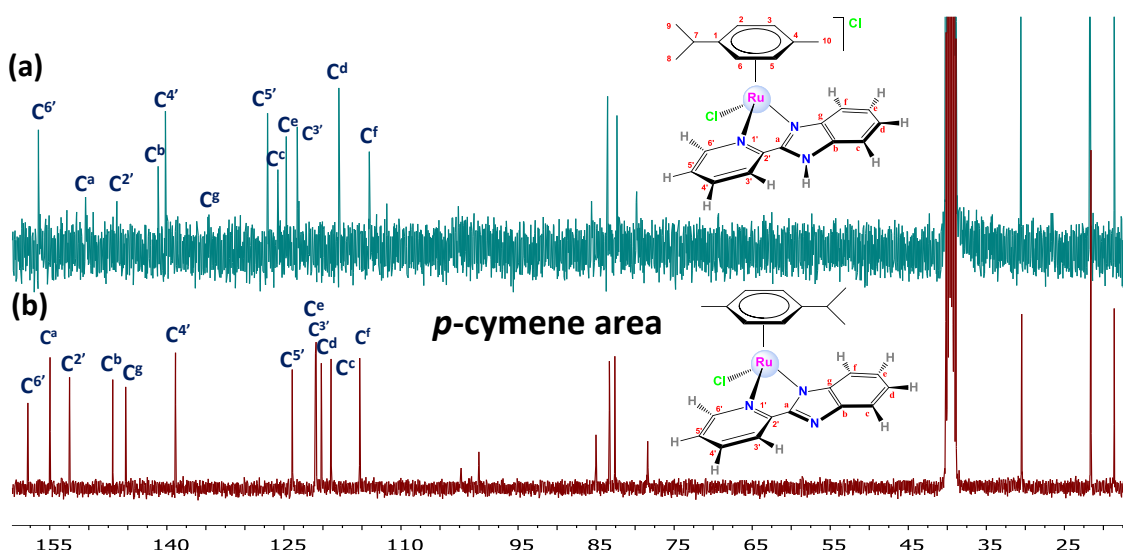


Fig. 9. Comparison of $^{13}\text{C}\{^1\text{H}\}$ NMR spectra for **[1a]Cl** (a) and **[7a]** (b) in DMSO-d₆ at 25 °C.

$^{19}\text{F}\{^1\text{H}\}$ NMR spectra were recorded for monocationic and dicationic complexes with BF₄⁻, PF₆⁻ and OTf⁻ as counterions. The expected doublet was observed for PF₆⁻ at -70.5 ppm in DMSO-d₆, as a result of the P-F coupling ($^1J_{\text{P}-\text{F}} = 713$ Hz). On the other side, a singlet at -79.3 ppm was observed for triflate. However, tetrafluoroborate exhibits two singlets with an integration ratio (1:4) according to the isotopic distribution for ¹⁰B/¹¹B. Furthermore, these spectra showed evidence of slow hydrolysis of the BF₄⁻ counterions even at 5 °C (kept in the fridge), as two more signals (A and B) appear in the spectra of aqua complexes **[4a](BF₄)₂**, **[4b](BF₄)₂** and **[4c](BF₄)₂** (see Fig. 10). For instance, the molar ratios (A:B:BF₄⁻) for **[4b](BF₄)₂** were 4:1:95 after 15 days and 24:17:59 after 60 days. The signal B at -144.1 ppm [1:1:1:1 quartet, $^1J(^{11}\text{B}-^{19}\text{F}) = 14.7$ Hz], was attributed to BF₃(OD)⁻. The signal A at -130.45 ppm (s) was assigned to SiF₆²⁻, which is likely formed

from the reaction between DF (HF) and the borosilicate glass of the NMR tube (see equations in Fig. 10).¹⁷

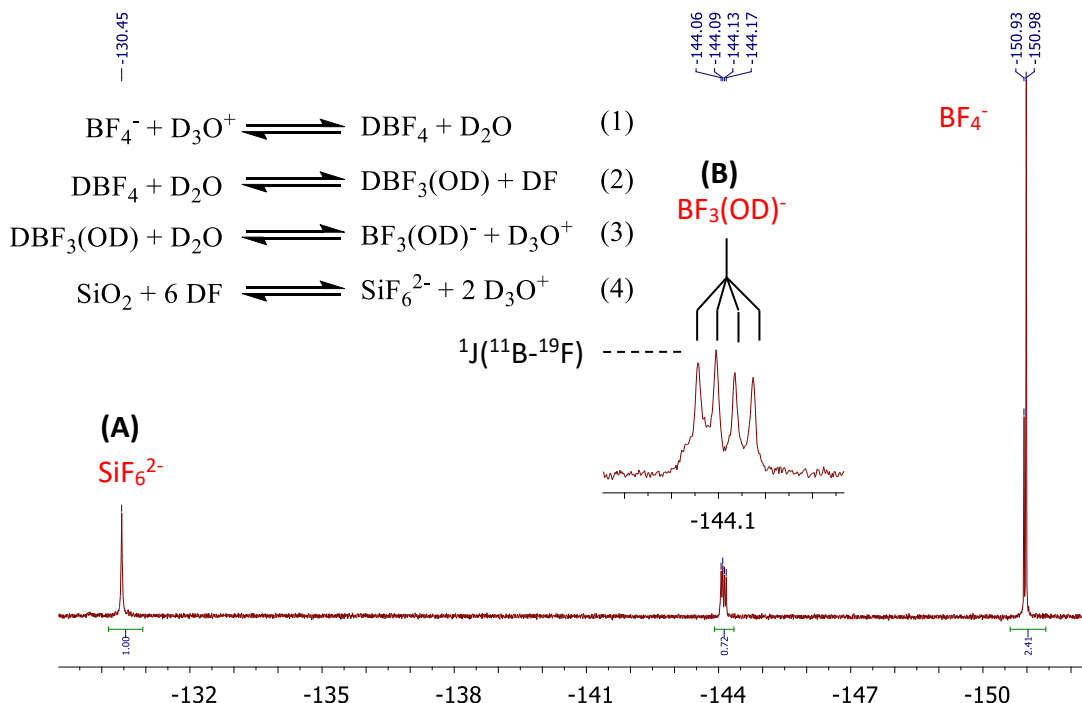


Fig. 10. $^{19}\text{F}\{^1\text{H}\}$ NMR spectrum of [4b](BF₄)₂ in D₂O at 25 °C after 60 days, showing signals for BF₄⁻, BF₃(OD)⁻ and SiF₆²⁻. Hydrolysis and acid-base equilibria explaining the formation of BF₃(OD)⁻ and SiF₆²⁻ are also shown. A four-lines multiplet is observed for BF₃(OD)⁻ due to the spin-spin coupling between ¹¹B (I = 3/2) and ¹⁹F (I = 1/2). The respective multiplet due to the spin-spin coupling between ¹⁰B (I = 3) and ¹⁹F (I = 1/2) is obscured by the former.

For BF₄⁻ two singlets are recorded since no ¹¹B-¹⁹F or ¹⁰B-¹⁹F spin-spin couplings are observed.

1.2.2. Mass Spectra

The FAB⁺ mass spectra of the complexes exhibit the characteristic set of peaks for the expected isotopic distribution patterns. [M-Y]⁺ fragments were recorded for monocationic complexes, where Y is the counterion; fragments with a water molecule for the aqua derivatives; a [M-2PF₆-H]⁺ fragment for the adduct with 9MeG, and a [M]⁺ fragment for neutral complexes. The mass spectra of [5c](BF₄)₂ does not clarify the structure of the complex, as no coordination of solvent molecule was observed.

1.2.3. IR Spectra

Infrared spectra show characteristic peaks for the normal vibrational modes of the corresponding rings ($\nu_{\text{C}=\text{N}}$, $\nu_{\text{C}=\text{C}}$, δ_{CHoop}) besides the very strong peaks for the counterions, except chloride. For BF₄⁻, the characteristic peak $\nu_{\text{B}-\text{F}}$ appears at 1098-1036 cm⁻¹. For PF₆⁻ there are two strong diagnostic peaks for the symmetric and asymmetric stretching modes $\nu_{\text{P-Fsym}}$ and $\nu_{\text{P-Fas}}$ at 845 and 558 cm⁻¹ respectively. For the triflate anion there are three characteristic bands, $\nu_{\text{C}-\text{F}}$, $\nu_{\text{SO}_3-\text{as}}$, $\nu_{\text{SO}_3-\text{sym}}$ at 1292-1245, 1168-1165 and 1030 cm⁻¹ respectively.^{18,19,20}

1.2.4. Molar Conductivity

Molar conductivity (Λ_M) for the complexes was measured in aqueous solutions (10⁻³ M). The values, gathered in Table 1, confirmed the 1:1 electrolyte nature of

monocationic complexes and 1:2 for the dicationic derivatives.²¹ Nevertheless, the values are higher than expected for monocationic complexes with Cl⁻ as ligand, owing to the partial dissociation of chloride in water, involving a change in the global charge of the compounds.

Table 1. Molar conductivity values for selected complexes measured in water.

Complex	Solvent	Λ_m (S·cm ² ·mol ⁻¹)
[1a]Cl	H ₂ O	188.9
[1b]Cl	H ₂ O	191.7
[1c]Cl	H ₂ O	199.5
[1a](BF ₄)	H ₂ O	159.4
[1b](BF ₄)	H ₂ O	174.8
[1c](BF ₄)	H ₂ O	176.8
[2a]Cl	H ₂ O	137.9
[3a]Cl	H ₂ O	132.1
[4a](BF ₄) ₂	H ₂ O	224.9
[4a](OTf) ₂	H ₂ O	147.5
[6a](PF ₆) ₂	H ₂ O	243.3
[7a]	H ₂ O	103.1

1.2.5. Elemental Analysis

The aqua derivatives [4a](BF₄)₂, [4b](BF₄)₂ and [4c](BF₄)₂ along with the complex [5c](BF₄)₂ (whose structure was unclear) were ruled out for biological studies, since their elemental analysis showed possible contamination with the AgBF₄ salt, used in the synthesis. Moreover, these complexes become darker and sticky with the time, supporting this experimental fact. Elemental analysis of [5c](BF₄)₂ is compatible with the presence of a methanol molecule in the coordination sphere of the complex.

1.2.6. X Ray Diffraction

Single crystals suitable for X-ray diffraction analysis were obtained by slow evaporation of solvent or mixture of solvents for [1a](BF₄)·H₂O (H₂O), [1b](BF₄)·2H₂O (H₂O), [1c]Cl·2H₂O (Acetone/H₂O), [2a]Cl (Acetone), [4a'](BF₄) (H₂O), [4a](OTf)₂·H₂O (H₂O), {[4b](BF₄)(SiF₆)_{0.5}}·2H₂O (D₂O), [4c](SiF₆) (CD₃OD, unsuitable to publish) and [6a](PF₆)₂·H₂O (H₂O).

The ORTEP diagrams for all the complexes are represented in Fig. 11 and Fig. 12 and the unit cells show the expected pair of enantiomers (R_{Ru} and S_{Ru}) with the pseudooctahedral three-legged piano-stool geometry and the ruthenium π-bonded to a η⁶-arene.

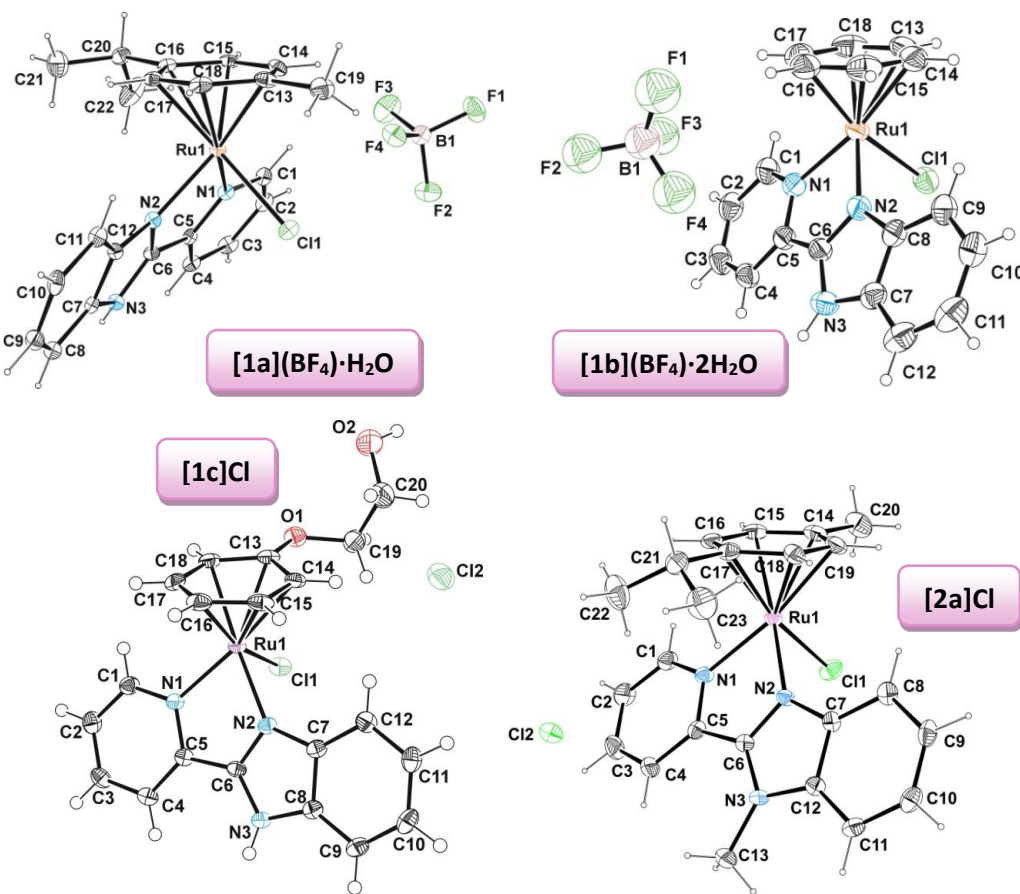


Fig. 11. ORTEP diagrams for complexes **[1a](BF₄)·H₂O**, **[1b](BF₄)·2H₂O**, **[1c]Cl·2H₂O** and **[2a]Cl**.

The Ru-centroid distances fall in a narrow range (1.668-1.692 Å). The Ru-Cl bond distances are in the usual interval and the Ru-N distances are shorter for the benzimidazole heterocycle than for the pyridyl moiety in all the cationic complexes with pybim and pyMebim (**[1x]⁺** and **[2x]⁺**). This fact is in agreement with the higher donor nature of the benzimidazole unit compared to the pyridine moiety.

Table 2. Selected bond lengths (Å) and angles (°) for complexes **[1a](BF₄)·H₂O**, **[1b](BF₄)·2H₂O**, **[1c]Cl·2H₂O** and **[2a]Cl**.

<i>Distance/angle</i>	[1a](BF₄)·H₂O	[1b](BF₄)·2H₂O	[1c]Cl·2H₂O	[2a]Cl
<i>Ru1-Cl1</i>	2.4105(12)	2.4068(16)	2.3851(8)	2.4047(12)
<i>Ru1-N1</i>	2.108(3)	2.128(5)	2.093(2)	2.104(3)
<i>Ru1-N2</i>	2.078(4)	2.078(4)	2.075(2)	2.078(3)
<i>N2-C6</i>	1.321(5)	1.316(7)	1.319(3)	1.334(5)
<i>N3-C6</i>	1.346(6)	1.361(7)	1.341(4)	1.351(5)
<i>N2-Ru1-N1</i>	76.52(13)	76.56(18)	76.64(9)	75.85(12)
<i>N1-Ru1-Cl1</i>	84.69(10)	85.55(13)	85.25(6)	85.13(9)
<i>N2-Ru1-Cl1</i>	83.24(10)	84.74(13)	85.55(6)	84.20(9)

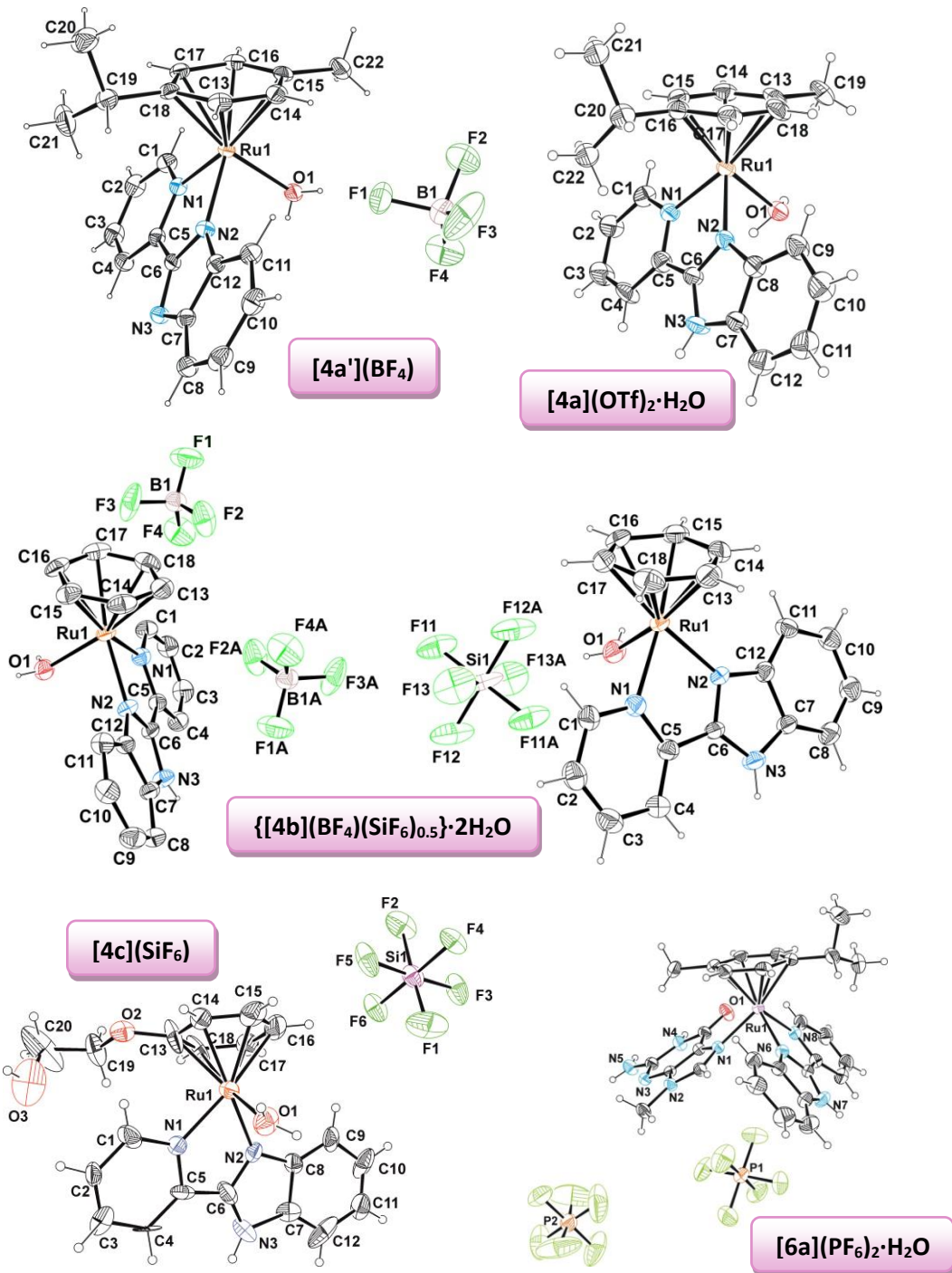


Fig. 12. ORTEP diagrams for complexes [4a'](BF₄), [4a](OTf)₂·H₂O, {[4b](BF₄)(SiF₆)_{0.5}}·2H₂O, [4c](SiF₆) and [6a](PF₆)₂·H₂O. Ellipsoids are shown at 30% probability.

The N-Ru-N angles of the chelate ligand are determined by the features of the corresponding free bidentate ligands. These angles are very similar for all of the arylbenzimidazoles with values between 72.12(13) $^{\circ}$ and 76.8(2) $^{\circ}$. Bond lengths, angles and other relevant features of the structures are gathered in Table 2, Table 3 and Table 4.

Table 3. Selected bond lengths (Å) and angles (°) for complexes [4a'](BF₄), [4a](OTf)₂·H₂O, {[4b](BF₄)(SiF₆)_{0.5}}·2H₂O and [6a](PF₆)₂·H₂O.

<i>Distance/angle</i>	[4a'](BF ₄)	[4a](OTf) ₂ ·H ₂ O	{[4b](BF ₄)(SiF ₆) _{0.5} }·2H ₂ O	<i>Distance/angle</i>	[6a](PF ₆) ₂ ·H ₂ O
Ru1-O1	2.122(3)	2.134(5)	2.124(3)	Ru1-N1(9MeG)	2.134(3)
Ru1-N1	2.114(3)	2.123(6)	2.132(4)	Ru1-N8(py)	2.135(4)
Ru1-N2	2.066(3)	2.082(6)	2.070(4)	Ru1-N6	2.077(3)
N2-C6	1.351(4)	1.319(8)	1.333(6)	N6-C7	1.328(5)
N3-C6	1.333(4)	1.351(9)	1.336(6)	N7-C7	1.341(5)
N2-Ru1-N1	76.73(10)	76.80(2)	76.79(16)	N6-Ru1-N8	76.12(13)
N1-Ru1-O1	84.72(12)	83.90(2)	82.14(16)	N1-Ru1-N8	89.07(12)
N2-Ru1-O1	85.55(11)	81.40(2)	82.61(16)	N6-Ru1-N1	85.66(12)

Table 4. Selected geometric parameters^[a] for the metal complexes of [1a](BF₄)·H₂O, [1b](BF₄)·2H₂O, [1c]Cl·2H₂O, [2a]Cl, [4a'](BF₄), [4a](OTf)₂·H₂O, {[4b](BF₄)(SiF₆)_{0.5}}·2H₂O and [6a](PF₆)₂·H₂O.

<i>Distances (Å)/ Angles(°)</i>	[1c]Cl	[1b](BF ₄) ·H ₂ O	[1a](BF ₄) ·H ₂ O	[2a]Cl	[4a](OTf) ₂ ·H ₂ O	[4a'](BF ₄)	{[4b](BF ₄) (SiF ₆) _{0.5} } ·2H ₂ O	[6a](PF ₆) ₂ ·H ₂ O
Range of Ru-C distances	2.159(3)	2.155(7)	2.175(4)	2.164(4)	2.166(7)	2.156(3)	2.149(6)	2.167(4)
Ru-centroid	-	-	-	-	-	-	-	-
α ^[b]	1.69	1.68	1.69	1.69	1.67	1.67	1.67	1.69
θ (N-C-C-X) ^[c]	2.5	6.9	11.4	8.0	4.6	3.2	2.5	-3.0
β (chelate-arene) ^[d]	1.9	-0.3	4.4	4.4	2.2	2.7	-1.2	-3.0
(C _x -C _{ipso} -Ru-Y) ^[e]	64.2	55.5	57.9	55.2	62.3	56.8	59.5	53.5
λ ^[ff]	2.9	-	-3.0	2.0	2.6	5.1	-	-4.6
	4.8	1.8	0.8	1.9	3.0	1.1	1.3	2.7

[a]Calculated with Mercury, version 3.8. [b]α = Angle between the mean planes of the two rings in the bidentate ligand, pyridyl or phenyl and diazole. [c]θ = Torsion angle formed by the atoms of the chelate ring (N-C-C-X). [d]β = Angle between the mean planes of the chelate ring (defined by the four atoms of the ligand) and the arene. [e]γ = Dihedral angle formed by the atoms: Cx-Cipso-Ru-Y (°), Cx represents the carbon atom linked to the methyl group of *p*-cym ([1a]BF₄, [4a'](BF₄), [6a](PF₆)₂), the O-MeOH group of phoxet ([1c]Cl). [f]λ = Angle between the mean planes formed by N-Ru-X and N-C-C-X (X = N or C), as a measure of the planarity of the chelate ring.

The compounds [1c]Cl, [1a]BF₄ and [1b]BF₄ exhibit a H₂O molecule in the second coordination sphere, linked to the N-H group of pybim through a strong hydrogen bond (N-H···O), as suggested by NMR spectra.

The crystal structure of [1a](BF₄)·H₂O is supported by C-H···π and hydrogen bonding interactions (see Fig. 13 and Table 5). The enantiomers are mutually connected through the C-H···π interactions between the *p*-cymene and the hydrogen of isopropyl, forming complex pairing (see Fig. 13b). There are some extra hydrogen bonding interactions involving the Cl⁻ ligand and the BF₄⁻ counterions as acceptors and C-H aromatic groups or water protons as donors. It is remarkable the bend of the hydrogen of the NH group, which is 15.05° out of the plane of imidazole.

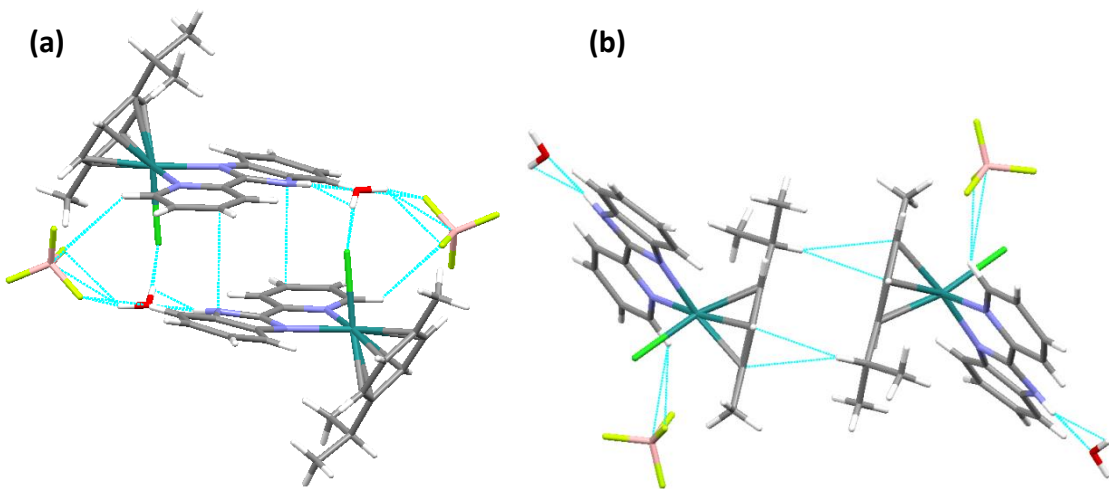


Fig. 13. Hydrogen bonding (a) and C-H···π interactions (b) building the crystal structure of $[1a](BF_4)\cdot H_2O$.

Table 5. Hydrogen bonding interactions in the crystal structure of complex $[1a](BF_4)\cdot H_2O$.

H-bonding	D···A (Å)	H···A (Å)	D···H (Å)	α (°)
N(3)-H(3A)···O(1)	2.707	1.854	0.855	175.30
C(1)-H(1)···F(4)	3.342	2.601	0.929	137.16

The crystal structure of $[1b](BF_4)\cdot H_2O$ also shows complex pairing established by mean of hydrogen bonding which connects one of the solvation water molecules to the Cl⁻ of one cation complex and the NH group of its enantiomer (see Fig. 14a). In addition, π-π stacking interactions between the benzene ring and the benzimidazole moiety link also the enantiomers (see Fig. 14b). Table 9 gathers all parameters of the π-π stacking interactions.

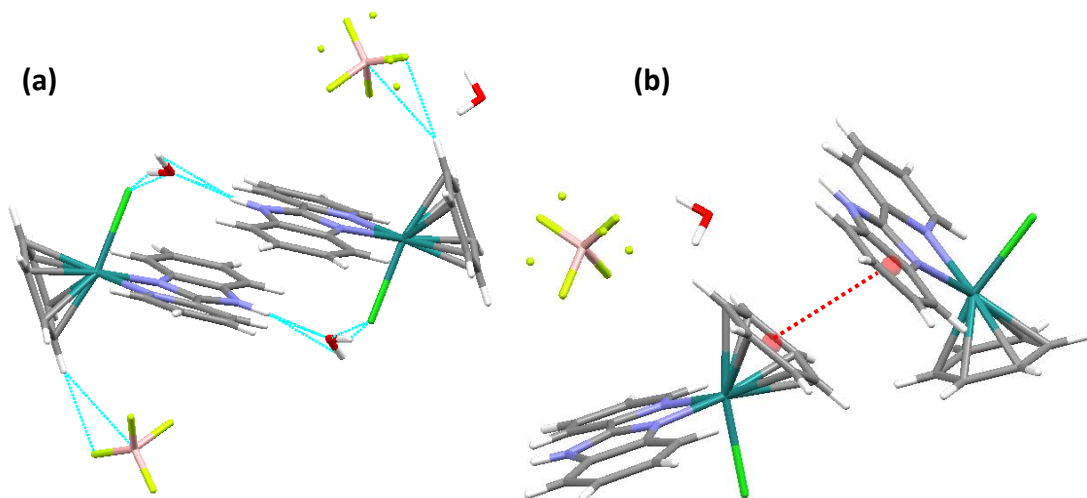


Fig. 14. 3D crystal architecture for complex $[1b](BF_4)\cdot H_2O$ through (a) hydrogen bonding and (b) π-π stacking interactions.

As for complex $[1c]Cl$, the crystal structure is mainly based on π-π stacking interactions as well as on hydrogen bonding. Fig. 15a displays the offset π-π stacking between the pyridyl moiety of the bidentate ligand and the benzimidazole unit of an

adjacent cationic complex. In addition, phoxet rings also show parallel π - π stacking (see Fig. 15b). The parameters of this kind of interactions are gathered in Table 6 and Table 9.

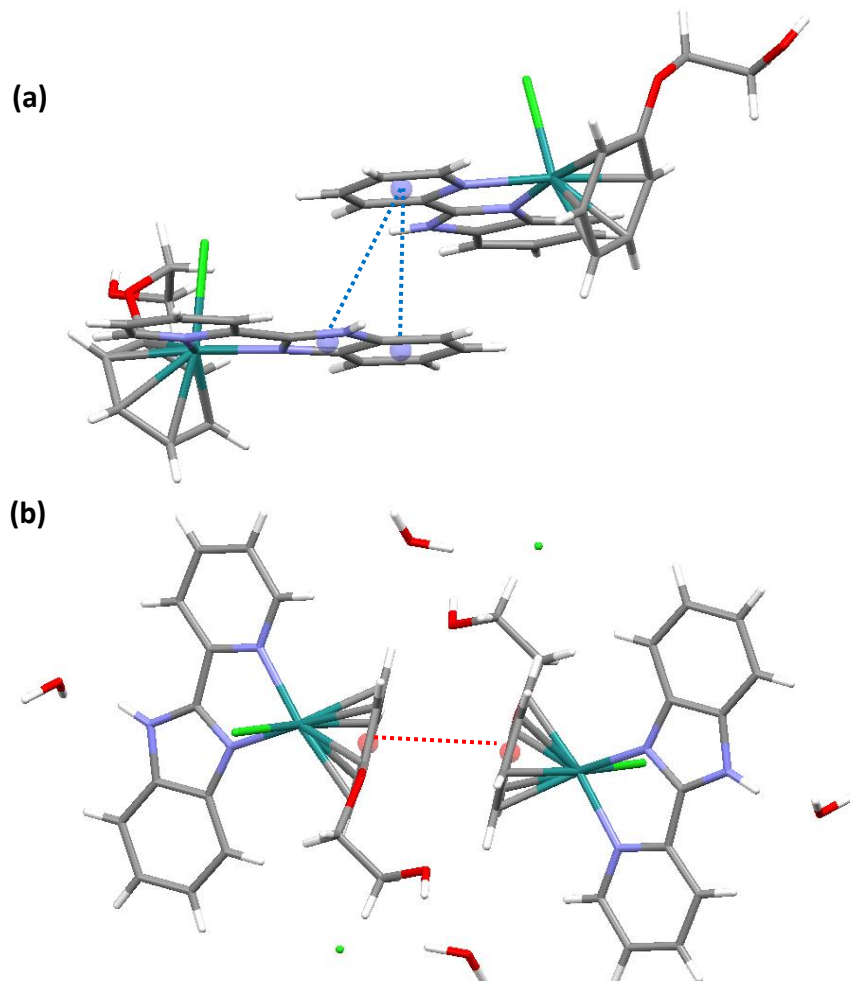


Fig. 15. π - π stacking interactions for complex [1c]Cl, showing the centroids of the rings.

Table 6. Hydrogen bonding interactions for complex [1c]Cl.

H-bonding	D…A (Å)	H…A (Å)	D…H (Å)	α (°)
N(3)-H(31)…O(3)	2.709	1.876	0.854	164.53
O(4)-H(41A)…Cl(2)	3.251	2.267	0.999	168.02
C(14)-H(14)…Cl(2)	3.653	2.835	0.931	147.37
C(12)-H(12)…Cl(2)	3.735	2.910	0.930	148.48
O(2)-H(21)…Cl(2)	3.142	2.371	0.821	156.91
O(4)-H(41B)…Cl(2)	3.160	2.225	0.941	172.08
C(18)-H(18)…O(1)	3.415	2.527	0.930	159.74

The crystal structure of [2a]Cl is built on the basis of weak hydrogen bonding of type C-H…Cl (see Fig. 16a), although C-H… π interactions (see Fig. 16b) are also observed,

connecting the C-H of the isopropyl group of *p*-cymene and the pyridyl ring of the chelating ligand. Table 7 shows the parameters of this interaction.

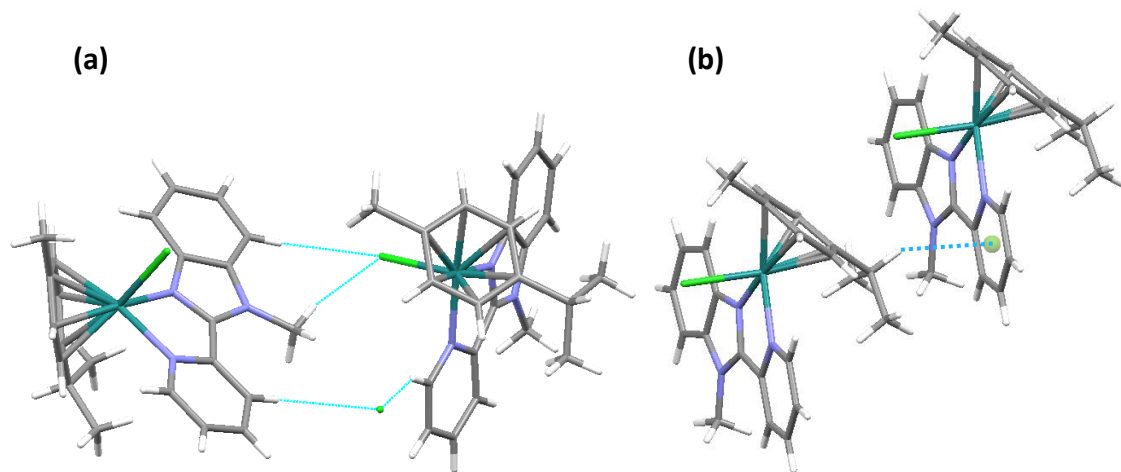


Fig. 16. (a) Weak hydrogen bonding connecting R and S enantiomers of [2a]Cl and (b) C-H...π interactions.

Table 7. Parameters of the C-H...π interaction in complex [2a]Cl.

Compound	$d_{C\text{-cent}}$ (Å)	$d_{H\text{-cent}}$ (Å)	$d_{C\text{-H}}$ (Å)	$\angle C\text{-H}\text{-cent}$ (°)	$\angle H\text{-cent-normal}$ (°)
[2a]Cl (C-H...π)	3.706	2.874	0.981	143.21	178.49

Regarding the aqua-complexes $[4a](OTf)_2\cdot H_2O$, $[4a'](BF_4)$ and $\{[4b](BF_4)(SiF_6)_{0.5}\}\cdot 2H_2O$, we assumed that the two cationic species $[4a]^{2+}$ and $[4a']^+$ are in equilibrium in aqueous media (see Fig. 17), and thus the crystallization of the monocationic specimen from a solution of $[4a']^+$ most likely occurs due to its lower polarity compared to the dicationic precursor. The 3D crystal architectures of these complexes are built on the basis of hydrogen bonds, C-H...π and π-π stacking interactions. It is worth mentioning the aqua-complex $[4a'](BF_4)$, which shows a characteristic motif in the 3D architecture, consisting on the pairing of enantiomeric isomers through both double π-π contacts between the aromatic rings of the ligand (py-bim/bim-py), on the one hand, and reciprocal strong hydrogen bonds between the coordinated water molecule of each enantiomer as the donor and the deprotonated N atom corresponding to the other complex as acceptor (O-H...N), on the other hand (see Fig. 18 and Table 9).

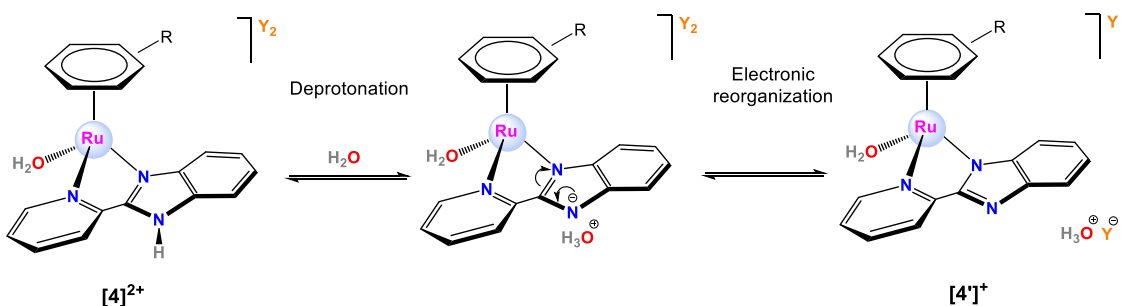


Fig. 17. Proposed equilibrium between cationic species [4]²⁺ and [4']⁺ in aqueous medium (Y = counterion).

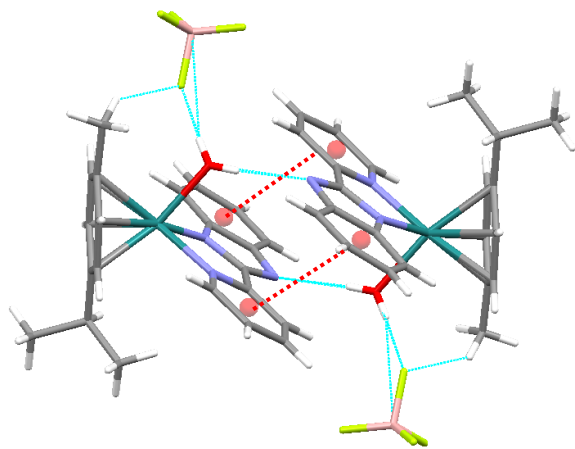


Fig. 18. Representation of complex pairing in the crystal structure of [4a'](BF₄). Both π-π contacts (red) and hydrogen bonding interactions (blue) are involved in the association.

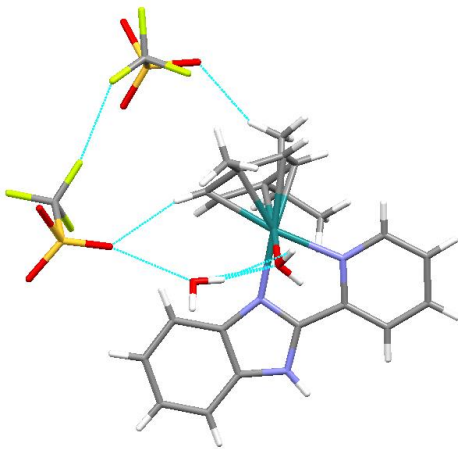


Fig. 19. Hydrogen bonding interactions in the asymmetric unit of complex [4a](OTf)₂. Some atoms on the structure present disorder and they have been removed for clarity.

The unit cell of complex **[4a](OTf)₂·H₂O** presents hydrogen bonding interactions among the metal complex, the triflate counterions and the solvation water molecule. Moreover, there are some anion-π or lone pair-π (lp-π) interactions, involving the triflate molecule (see CHAPTER 5, page 236, for further details). Thus, one of the C-F bonds shows a contact with the *p*-cymene aromatic ring (see Fig. 20a and Table 8), whereas the S=O unit is linked to the imidazole ring (see Fig. 20b and Table 8).

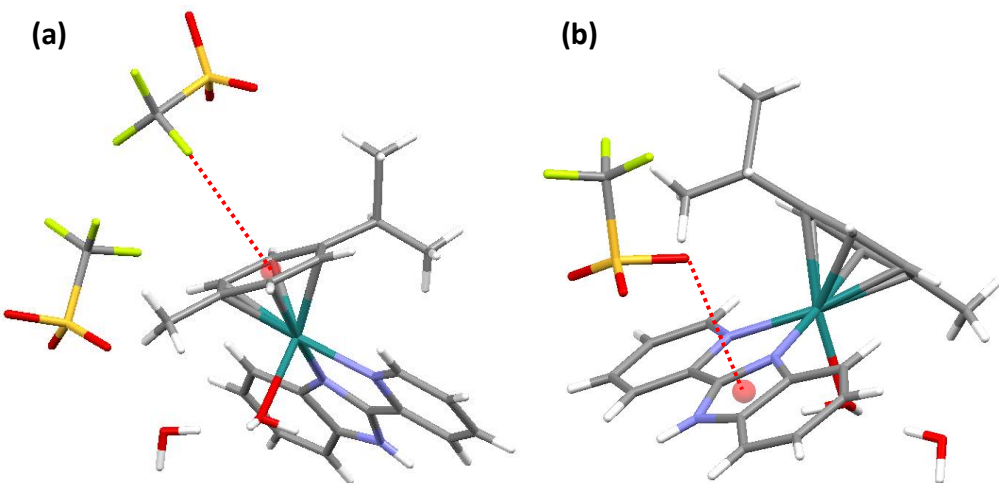


Fig. 20. Anion- π interactions in $[4a](OTf)_2 \cdot H_2O$, involving the triflate counterion: (a) C-F $\cdots\pi$ and (b) S=O $\cdots\pi$ contacts.

Table 8. Geometric parameters for the anion- π interactions (C-F $\cdots\pi$ and S=O $\cdots\pi$) for the complex $[4a](OTf)_2 \cdot H_2O$.

Compound	d _{x-cent} (Å)	d _{x-plane} (Å)	d _{offset} (Å)	α _{y-x-cent} (°)	θ (°)
[4a](OTf)₂ (S=O$\cdots\pi$)	3.325	3.312	0.294	117.51	84.93
[4a](OTf)₂ (C-F$\cdots\pi$)	3.427	3.327	0.822	139.12	76.12

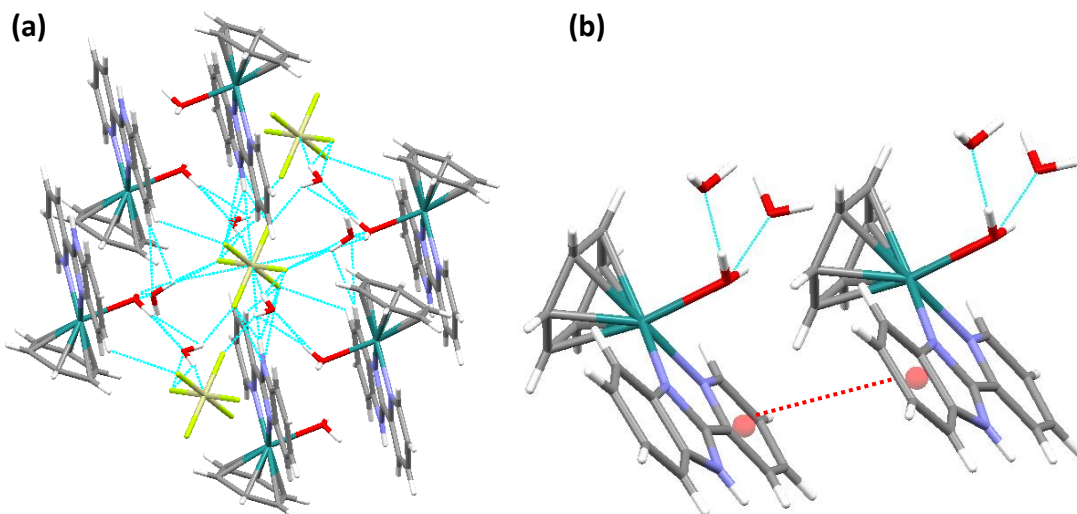


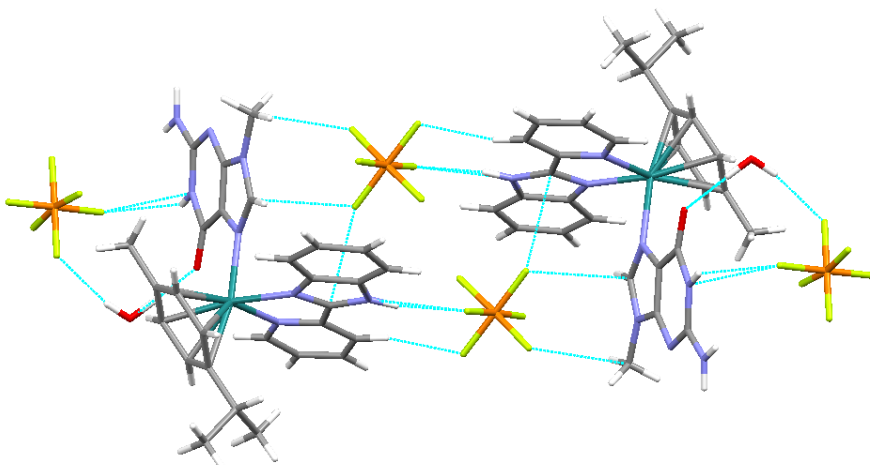
Fig. 21. (a) 3D architecture of $\{[4b](BF_4)(SiF_6)_{0.5}\} \cdot 2H_2O$ involving SiF_6^{2-} counterion and (b) $\pi\text{-}\pi$ stacking interactions.

As for the compound $\{[4b](BF_4)(SiF_6)_{0.5}\} \cdot 2H_2O$, the asymmetric unit shows a complex architecture with half an anion of SiF_6^{2-} (1 SiF_6^{2-} per unit cell). This is the result of the hydrolysis process of the BF_4^- in the glass of the NMR tube. Each SiF_6^{2-} unit connects six metallic fragments (see Fig. 21a). The structure also presents two water molecules in the second coordination sphere, connected by hydrogen bonding to the coordinated water molecule. Besides the hydrogen bonding, the crystal structure shows $\pi\text{-}\pi$ stacking interactions (py/bim) (see Fig. 21b and Table 9).

Table 9. Offset $\pi\cdots\pi$ stacking interactions of selected complexes.

Compound	$d_{cent-cent}$ (Å)	α (°)	$d_{cent-pl}$ (Å)	β (°)	d_{offset} (Å)
[1b](BF₄) (bz/bim)	3.485	3.82	3.329	17.21	1.031
			3.390	13.41	0.808
[1c]Cl·2H₂O (phoxet/phoxet)	3.412	0.00	3.311	13.98	0.824
			3.311	13.98	0.824
[1c]Cl·2H₂O (py/bim)	3.697	4.44	3.371	24.24	1.518
			3.263	28.04	1.730
[1c]Cl·2H₂O (py/im)	3.830	4.44	3.323	29.82	1.904
			3.397	27.51	1.769
[4a'](BF₄) (py/bim)	3.657	2.05	3.394	21.86	1.362
			3.439	19.88	1.244
[4a'](BF₄) (py/im)	3.800	3.24	3.373	27.42	1.750
			3.413	26.08	1.671
{[4b](BF₄)(SiF₆)_{0.5}}·2H₂O (py/bim)	3.848	2.43	3.491	24.88	1.619
			3.511	24.16	1.575

In the unit cell of **[6a](PF₆)₂·H₂O** the two possible enantiomers are connected by two PF₆⁻ counterions through hydrogen bonding (N-H···F and C-H···F) (Table 10 and Fig. 22) and anion-π interactions (see Table 11 and Fig. 23), similar to those found in the literature (see CHAPTER 5).²² In addition, adjacent complexes are linked through double hydrogen bonds between the guanine moieties (N-H···N) (see Fig. 24).

**Fig. 22.** Complex pairing in the unit cell of **[6a](PF₆)₂·H₂O**.**Table 10.** Hydrogen bonds for **[6a](PF₆)₂·H₂O**.

H-bonding	D···A (Å)	H···A (Å)	D···H (Å)	α (°)
N(5)-H(5A)···N(3)	3.049	2.233	0.860	158.25
C(15)-H(15)···F(16)	3.321	2.408	0.929	167.32
N(7)-H(7)···F(12)	2.908	2.112	0.860	153.70
C(6)-H(6B)···F(13)	3.150	2.674	0.960	111.13

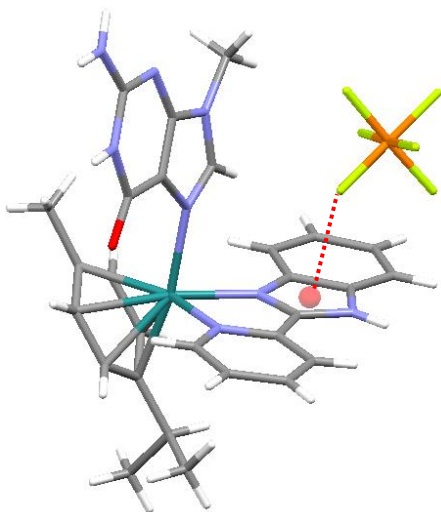


Fig. 23. Anion- π interaction for complex $[6a](\text{PF}_6)_2 \cdot \text{H}_2\text{O}$.

Table 11. Geometric parameters of anion- π interactions ($\text{P}-\text{F} \cdots \pi$) for the complex $[6a](\text{PF}_6)_2 \cdot \text{H}_2\text{O}$.

Compound	$d_{\text{F-cent}}$ (Å)	$d_{\text{F-plane}}$ (Å)	d_{offset} (Å)	$\alpha_{\text{P-F-cent}}$ (°)	θ (°)
$[6a](\text{PF}_6)_2 \cdot \text{H}_2\text{O}$	3.134	3.012	0.866	125.24	73.96

* d_{offset} has been calculated as $(d_{\text{centroid}}^2 - d_{\text{plane}}^2)^{1/2}$.²²

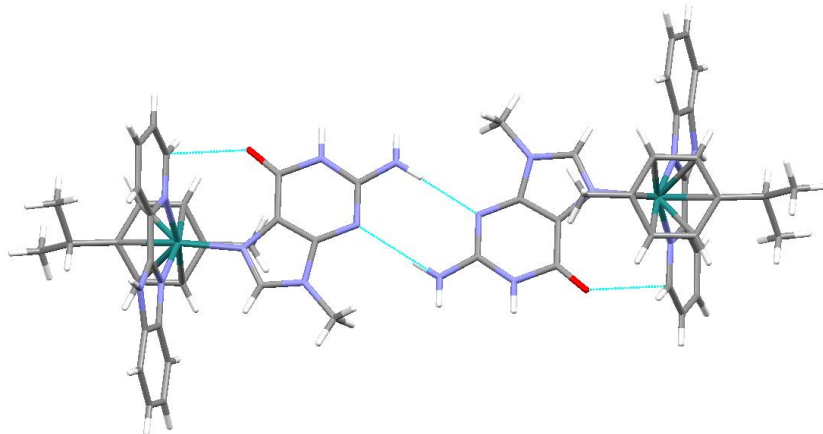


Fig. 24. Double hydrogen bonding between nucleobases of adjacent cation complex in the crystal structure of $[6a](\text{PF}_6)_2$ and intramolecular hydrogen bond C-H \cdots O.

For the complex $[6a](\text{PF}_6)_2 \cdot \text{H}_2\text{O}$, the O atom of 9MeG is oriented toward the pyridyl moiety of pybim, so that it takes part in a triple hydrogen bonding interaction as an acceptor (see Fig. 25). Two of these contacts are intramolecular: C(21)-H(21) \cdots O(1) with the *p*-cym ring and C(18)-H(18) \cdots O(1) with the pyridyl group. As a consequence, the link between the nucleobase and the fragment $[(p\text{-cym})\text{Ru}(\text{pybim})]^{2+}$ is reinforced, which makes the interaction selective vs. other nucleobases like adenine. Moreover, there is a strong intermolecular hydrogen bond with a solvation H_2O molecule, O(2)-H(1O2) \cdots O(1). Table 12 collects the parameters of some of the hydrogen bonding interactions, involving the O atom of guanine.

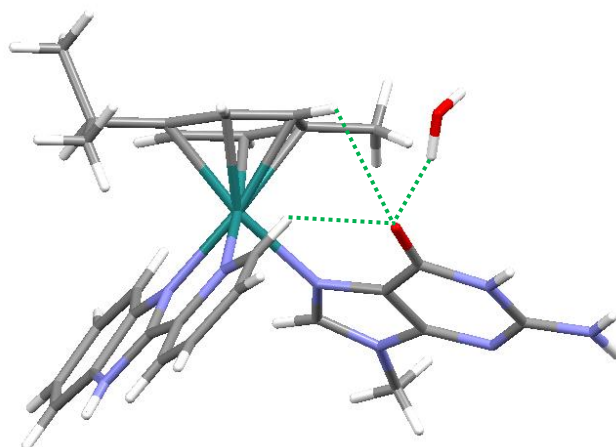


Fig. 25. Representation on intra- and intermolecular hydrogen bonds involving O(9MeG), the cationic fragment $[(p\text{-cym})\text{Ru}(\text{pybim})]^{2+}$ and a water molecule in the crystal structure of $[6\text{a}](\text{PF}_6)_2$.

Table 12. Relevant hydrogen bonding interactions for $[6\text{a}](\text{PF}_6)_2$, involving O(1) as acceptor.

H-bonding	D···A (Å)	H···A (Å)	D···H (Å)	α (°)
C(21)-H(21)···O(1)	3.221	2.715	0.930	115.03
C(18)-H(18)···O(1)	2.956	2.353	0.929	122.32
O(2)-H(1O2)···O(1)	2.801	1.995	0.865	154.63

1.3. Aqueous Solubility

The aqueous solubility of some complexes was measured at room temperature (19 – 21 °C) and the results are gathered in Table 13. All the complexes are water-soluble, whereas the free ligands are insoluble, due to strong self-association by hydrogen bonding and π-π stacking interactions. In the complexes, the coordination of the metal fragment blocks the hydrogen-bonding acceptor atoms (N atoms) and thus, the solubility is enhanced. In addition, the cation-cation repulsion and anion interposition in the cationic complexes contribute to the disruption of the intermolecular hydrogen bonds present in the crystal networks of the free ligands.²³ Likewise, the solubility depends on the counterion, the overall charge of the complex and the arene identity. The chloride salts are much more soluble in water than their BF_4^- counterparts, what is explained in the literature as a result of the high hydration energy attributed to the Cl^- anion.^{24,25} Regarding the arene, *p*-cymene derivatives give better solubilities than the benzene and 2-phenoxyethanol derivatives. Among *p*-cym derivatives, the solubility decreases according to the sequence $[3\text{a}]\text{Cl} > [1\text{a}]\text{Cl} > [2\text{a}]\text{Cl} > [4\text{a}](\text{OTf})_2 > [7\text{a}]$. Regarding the monocationic complexes, the most soluble is $[3\text{a}]\text{Cl}$ with pyim as N,N-ligand, owing to its lower hydrophobicity compared to pybim that has a benzo ring fused to the imidazole heterocycle. On the other hand, the N-Me in the benzimidazole heterocycle is less polar and less prone to hydrogen bonding than the N-H group, which explains the reduced solubility of $[2\text{a}]\text{Cl}$ vs. $[1\text{a}]\text{Cl}$. Unexpectedly, the aqua-complex $[4\text{a}](\text{OTf})_2$ exhibits low solubility, likely, due to the hydrophobicity of the triflate ion and $[7\text{a}]$ shows very poor solubility due to its neutral nature.

1.4. Aquation-Anation Equilibria

The aquation-anation equilibria were studied under pseudopharmacological conditions by recording the corresponding ^1H NMR spectra of 3 mM solutions in D_2O at 25 °C, in the absence of NaCl and then in the presence of NaCl (5 or 100 mM as model concentrations for the intracellular and blood plasma conditions, respectively)²⁶. Two sets of signals were observed, remaining constant after an hour, which suggests a fast equilibration. The two doublets appearing at the highest frequencies were assigned to H⁶ protons both of the aqua derivative (9.69–9.62 ppm) and its chloride precursor (9.56–9.48) and used as references for integration purposes. In the absence of NaCl all the monocationic complexes undergo aquation to a notable extent, from 49 to 74 %, with some differences depending on the counterion, the arene, or the bidentate pyridyliazole ligand. In the presence of NaCl, the equilibria are shifted to the chlorido side with very similar aquation values, between moderate (in 5 mM NaCl) and low (in 100 mM NaCl), showing a small dissociation of the chloride anion. In addition, aquation of the neutral complex [7a] is the highest, 85.5 % at 5 mM NaCl and even 30.6 % at 100 mM NaCl (see Table 13). This fact is likely due to the high σ-donor character of its anionic N,N-ligand, which must favour dissociation of chloride.

Table 13. Solubility Data in water and the aquation-anation ratio at different NaCl concentrations for selected compounds, expressed as a percentage of the aqua derivative in the respective equilibrium mixture of Ru-OH_2 and Ru-Cl complexes in D_2O 3 mM.

Ref.	Compound	Solubility (mM)	% aquation		
			0 mM NaCl	5 mM NaCl	100 mM NaCl
[1a](BF ₄)	[(<i>p</i> -cym)RuCl(pybim)](BF ₄)	6.5	60	41	9
[1b](BF ₄)	[(bz)RuCl(pybim)](BF ₄)	5.9	69	49	9
[1c](BF ₄)	[(phoxet)RuCl(pybim)](BF ₄)	2.9	74	50	9
[1a]Cl	[(<i>p</i> -cym)RuCl(pybim)]Cl	141.2	52	44	11
[1b]Cl	[(bz)RuCl(pybim)]Cl	10.5	54	41	14
[1c]Cl	[(phoxet)RuCl(pybim)]Cl	4.3	65	44	14
[2a]Cl	[(<i>p</i> -cym)RuCl(pyMebim)]Cl	37.0	49	35	12
[3a]Cl	[(<i>p</i> -cym)RuCl(pyim)]Cl	157.5	59	45	12
[4a](OTf) ₂	[(<i>p</i> -cym)Ru(OH ₂)(pybim)](OTf) ₂	27.5	100	65	13
[7a]	[(<i>p</i> -cym)RuCl(pybim')]Cl	3.0	94	86	31

1.5. Deprotonation of [4a](BF₄)₂

As we have seen before, the complex [4a](BF₄)₂ has crystallized in both dicationic [4a]²⁺ and monocationic [4a']⁺ forms. Therefore, a ^1H NMR experiment was performed in order to verify this proton transfer equilibrium. After recording the spectrum of [4a](BF₄)₂ (6 mM) in D_2O at 25 °C, NaHCO₃ (6 mM) was added to deprotonate the NH of the benzimidazole unit. Bubbling was observed as a symptom of CO₂ release, just after the addition of the base.

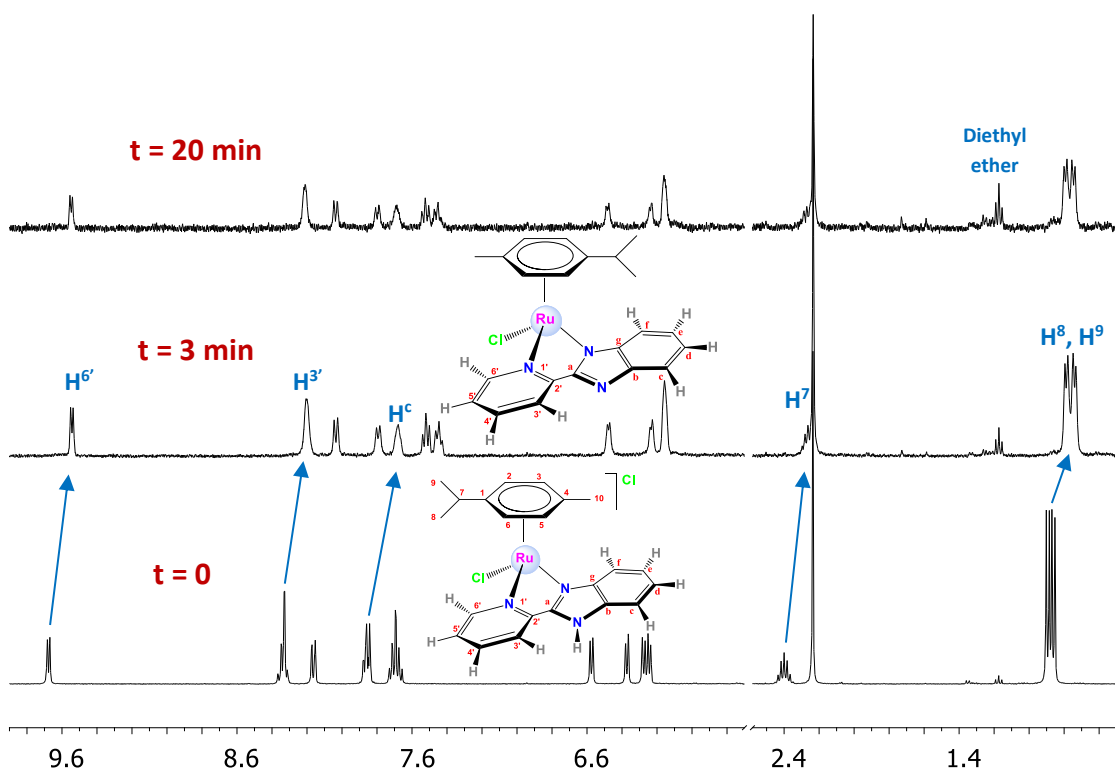


Fig. 26. ¹H NMR spectrum of [4a](BF₄)₂ in D₂O at 25 °C and after the addition of NaHCO₃.

All the signals shifted upfield and those which were nearly affected by NH NOE (*i.e.* H^{3'} and H^c) broadened (see Fig. 26). Peaks for *p*-cym protons underwent notable shifts: H⁷ ($\Delta\delta = 0.13$ ppm), H⁸ and H⁹ ($\Delta\delta = 0.11$ ppm), as well as the resonances of the chelating ligand, for instance, the most deshielded was H^{6'} ($\Delta\delta = 0.13$ ppm). The equilibrium was reached in only a few minutes (3–4 min), and it kept constant after 20 min. Partial precipitation was observed after this time.

1.6. Interaction with nucleobases and nucleotides

The reaction of [1a](BF₄) with the nucleobase 9MeG in water at 37 °C led to the formation of the guanine derivative [6a](PF₆)₂ coordinated through the N7, as it has been discussed previously in the X-ray section. In addition, the reactivity of [4a](OTf)₂ (5 mM) against the nucleotide 5'-dGMP (25 mM) was examined by ¹H NMR and ³¹P{¹H} NMR in D₂O at 25 °C and pH 5 and pH 7. When the pH was adjusted to 7 the complex [4a](OTf)₂ precipitated, so we decided to repeat the experiment at a lower pH (pH < pK_a), so as to assure the presence of [4a]²⁺. The substitution reaction was monitored by ¹H NMR at different times, although it was almost finished in 3 or 5 minutes. The NMR experiments along with the physicochemical measurements carried out by the group of Pr. Begoña García from the University of Burgos confirmed the coordination of the metallic fragment [Ru(arene)(pybim)]²⁺ to 5'-dGMP by mean of a covalent binding to N7 of guanine and DNA intercalation of the complexes [1a]Cl, [1b]Cl and [1c]Cl in aqueous media¹ (complexes [1x]⁺ undergo aquation becoming complexes [4x]²⁺).

1.7. Cytotoxic Activity

The cytotoxic activity of the ligands and selected complexes have been evaluated in a comparative in vitro MTT cell viability assay after incubation times of 96 h at 37 °C with human ovarian carcinoma cells (A2780), cisplatin-resistant human ovarian carcinoma cells (A2780cis), and the human hormone-dependent breast cancer cells (MCF-7). Moreover, MRC-5 cell line represents fibroblasts as model for health cells. The values are expressed as the inhibitory potency (IC_{50}) and cisplatin was used as the positive control in all the cell lines. Table 14 gathers the IC_{50} values in the different cell lines as well as the resistance factor (RF) and the selectivity factor (SF). The cytotoxicity of free ligands is very low ($IC_{50} > 100 \mu\text{M}$). Likewise, the dimeric starting material is inactive in these cell lines according to literature. By contrast, most of the ruthenium compounds evaluated in the cell line A2780 showed moderate or good activity. The most prominent in vitro inhibitory potency in this cell line was obtained for the monocationic derivative **[3a]Cl**. In the MCF-7 cells, the best results were achieved for **[2a]Cl** and **[3a]Cl**, which are only between 2- or 3-fold less active than cisplatin. The antiproliferative activity of compounds **[2a]Cl** and **[3a]Cl** toward the A2780cis cells is remarkable as long as the corresponding IC_{50} values are lower than those for the A2780 cells. Thus, the RF (IC_{50}) for these compounds is below unity, indicating that **[2a]Cl** and **[3a]Cl** overcome cisplatin resistance. The selectivity factors ($SF = IC_{50} \text{ for MRC-5}/IC_{50} \text{ for the respective cancer cells}$) have been determined for some compounds as a measure of the tumour-selective antiproliferative potency. The most prominent drug turned out to be **[1a]Cl** because of the low cytotoxicity of this compound toward fibroblasts. Thus, the SF values for **[1a]Cl** are higher than those of cisplatin in the three cancer cell lines – 7.5 versus 5.6 (A2780); 3.3 versus 0.4 (MCF-7) and 6.6 versus 0.9 (A2780cis) – and this compound can be postulated as a clinical alternative in the treatment of ovarian cancer on the basis of this result.

Table 14. IC_{50} (μM , 96 h, 37 °C) values for ligands and selected compounds in the cell lines A2780, A2780cis, MCF-7 and MRC-5.

Ref.	Compound	A2780	A2780 cis	RF	MCF-7	MRC-5	SF		
							A2780	A2780 cis	MCF-7
	cisplatin	0.87 ± 0.01	5.17 ± 0.11	5.94	12 ± 1	4.87 ± 0.07	5.6	0.9	0.4
	pybim	>100							
	pyMebim	>100							
	pyim	>100							
	[(<i>p</i>-cym)RuCl₂]₂	>300			>300				
[1a]Cl	[(<i>p</i>-cym)RuCl(pybim)]Cl	30 ± 1	34 ± 1	1.13	68 ± 1	224 ± 20	7.5	6.6	3.3
[1b]Cl	[(bz)RuCl(pybim)]Cl	96 ± 1			110 ± 6				
[1c]Cl	[(phoxet)RuCl(pybim)]Cl	149 ± 3			68 ± 1				
[1a](BF₄)	[(<i>p</i>-cym)RuCl(pybim)](BF₄)	29 ± 1			68 ± 3				
[2a]Cl	[(<i>p</i>-cym)RuCl(pyMebim)]Cl	35 ± 2	10 ± 2	0.29	29 ± 1	55 ± 4	1.6	5.5	1.9
[3a]Cl	[(<i>p</i>-cym)RuCl(pyim)]Cl	19 ± 1	16 ± 1	0.84	38 ± 1	25 ± 1	1.3	1.6	0.7
[7a]	[(<i>p</i>-cym)RuCl(pybim')]Cl	33 ± 2	30 ± 1	0.91			4.15	4.6	1.7

Furthermore, a comparison of the IC₅₀ values obtained for **[1a]Cl**, **[1b]Cl** and **[1c]Cl** in the A2780 and MCF-7 cells suggests that the arene ring affects the cytotoxic activity. In both cell lines, **[1a]Cl** with *p*-cym is more active than **[1b]Cl** with bz. Compound **[1c]Cl** shows erratic behavior because it is the less active compound in the A2780 cells, but exhibits an activity similar to that of **[1a]Cl** in the MCF-7 cells.

As a matter of fact, the arene group is known to have a crucial effect on the cytotoxicity.²⁷ Moreover, as P. Sadler and co-workers have shown, the arene type affects the coordination rate of the Ru center to the guanine N7 site, with complexes containing an extended arene being faster than those containing a monoarene group.²⁸ In fact, complexes endowed with an extended arene are able to interact with DNA by both covalent binding and intercalation of the arene moiety.^{29,30} Furthermore, the cytotoxic activity in A2780 cancer cells has been shown to increase with the size of the coordinated arene: bz < *p*-cym < biphenyl < dihydroanthracene < tetrahydroanthracene.³¹ Thus, our results confirm and support all these experimental facts.

1.8.SAR

The new complexes described in this work have been furnished with different motifs in order to gain a better understanding of the optimal features for antitumor activity. Thus, Fig. 27 displays the inferred global overview of the structure-properties and structure-activity relationships obtained from this work.

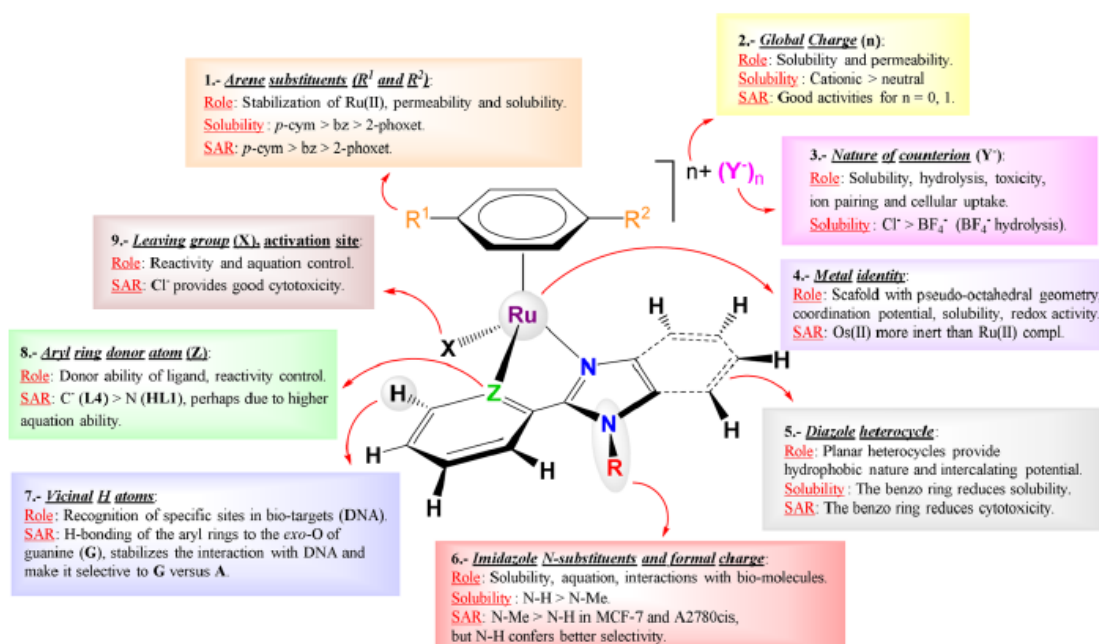


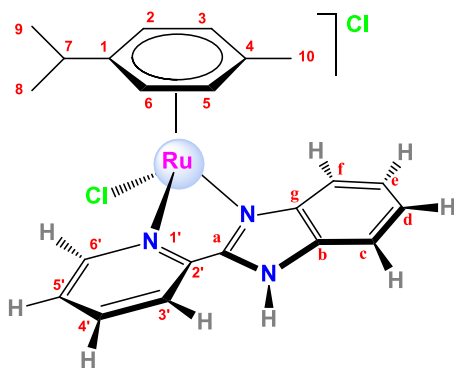
Fig. 27. Graphical scheme showing the general role/function of different structural elements, the aqueous solubility, and the SAR based on the IC₅₀ values for A2780, A2780cis, and MCF-7 for the present family of complexes.¹

2. CONCLUDING REMARKS

- A family of 18 new complexes has been synthesised and completely characterised, both in solution and some of them in solid state.
- All the complexes are water soluble, which is an essential feature from the point of view of the biological/physiological environment. Most of them undergo aquation in aqueous solution, which activates the complexes regarding their reactivity against biomolecules such as DNA.
- NMR and physicochemical experiments have demonstrated that the complexes are able to interact with DNA: covalently through the N7 of guanine and by intercalation of the chelate ligand.
- The cytotoxicity data highlight complex **[1a]Cl** as the most relevant, since its SF is higher than that for cisplatin. In addition, complexes **[2a]Cl** and **[3a]Cl** are able to overcome cisplatin resistance.
- The cytotoxic activity along with the solubility of the new complexes allowed us to establish some structure activity relationships (SAR study), to clarify the role and effect of the arene, the counterion, the global charge, the leaving group and the chelating ligand.

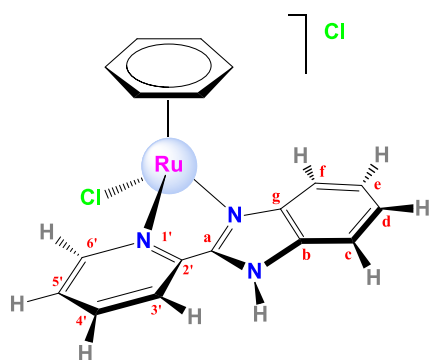
3. EXPERIMENTAL SECTION

Cationic Complexes

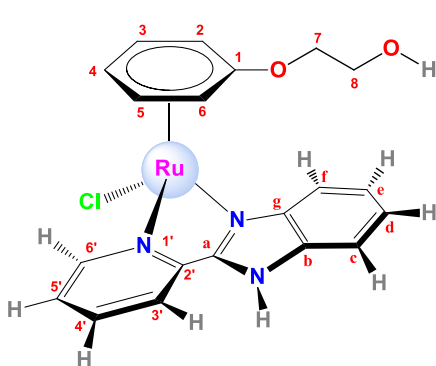


Synthesis of $[(\eta^6\text{-}p\text{-cymene})\text{RuCl}(\text{pybim})]\text{Cl}$, [1a]Cl. In a 100 mL Schlenk flask, 2-(2-pyridyl)benzimidazole (pybim) (63.9 mg, 0.327 mmol) was added under a nitrogen atmosphere to a solution of $[(\eta^6\text{-}p\text{-cymene})\text{RuCl}_2]_2$ (100 mg, 0.164 mmol) in degassed methanol (15 mL). The mixture was stirred for 20 hours at room temperature. The solvent was removed under vacuum and the solid residue was washed with *n*-hexane (3×5 mL) and dried under vacuum, to produce a yellow solid. Yield: 115 mg (0.228 mmol, 70%). **M_r** (**C₂₂H₂₃Cl₂N₃Ru**) = 501.4192 g/mol. **Anal. Calcd for C₂₂H₂₃Cl₂N₃Ru·(H₂O):** C 50.87; H 4.85; N 8.09; Found: C 50.53; H 4.85; N 8.11. **¹H NMR (400 MHz, DMSO-d₆, 25 °C)** δ 15.39 (s, 1H, H^{N-H}), 9.61 (d, *J* = 5.6 Hz, 1H, H^f), 8.63 (d, *J* = 7.9 Hz, 1H, H^{3'}), 8.35 (t, *J* = 7.8 Hz, 1H, H^{4'}), 8.15 – 8.08 (m, 1H, H^f), 7.85 – 7.77 (m, *J* = 6.6 Hz, 2H, H^{5',c}), 7.63 – 7.52 (m, 2H, H^{e,d}), 6.39 (d, *J* = 6.1 Hz, 1H, H² or H⁶), 6.32 (d, *J* = 6.2 Hz, 1H, H² or H⁶), 6.18 (d, *J* = 6.0 Hz, 1H, H³ or H⁵), 6.11 (d, *J* = 6.3 Hz, 1H, H³ or H⁵), 2.50 (sept, H⁷), 2.20 (s, 3H, H¹⁰), 0.91 (d, *J* = 6.5 Hz, 6H, H⁸), 0.89 (d, *J* = 6.5 Hz, 6H, H⁹) ppm. The resonance for H⁷ is obscured under the signal of DMSO at 2.50 ppm. **¹³C{¹H} NMR (101 MHz, DMSO-d₆, 25 °C)** δ 156.5 (s, 1C, C^{6'}), 150.4 (s, 1C, C^a), 146.4 (s, 1C, C^{2'}), 141.1 (s, 1C, C^g), 140.2 (s, 1C, C^{4'}), 134.7 (s, 1C, C^b), 127.1 (s, 1C, C^{5'}), 125.8 (s, 1C, C^d), 124.7 (s, 1C, C^e), 123.3 (s, 1C, C^{3'}), 118.0 (s, 1C, C^f), 114.1 (s, 1C, C^c), 103.4 (s, 1C, C⁴), 102.6 (s, 1C, C¹), 85.6 (s, 1C, C² or C⁶), 83.5 (s, 1C, C² or C⁶), 82.3 (s, 1C, C³ or C⁵), 79.8 (s, 1C, C³ or C⁵), 30.6 (s, 1C, C⁷), 21.7 (d, *J* = 2.5, Hz, 2C, C^{8,9}), 18.6 (s, 1C, C¹⁰) ppm. **FT-IR (KBr, cm⁻¹) selected bands:** 3063 (w, v_{C=CH, N-H}), 2964 (w, v_{-CH}), 1610, 1594 (s, v_{C=C + C-N}), 1483 (m), 1456 (s, v_{C=N}), 1447 (s), 1388 (w, δ_{CH₃}), 1325 (m), 1152 (w), 792 (w, δ_{C-C}), 761-752 (s, δ_{CHOop}). **MS (FAB+):** m/z (%) = 466 (100) ([M-Cl]⁺), 430 (80) ([M-2Cl-H]⁺). **Molar conductivity (H₂O):** 189 S·cm²·mol⁻¹.

Solubility: soluble in methanol, ethanol, water, DMSO. Partially soluble in acetone.

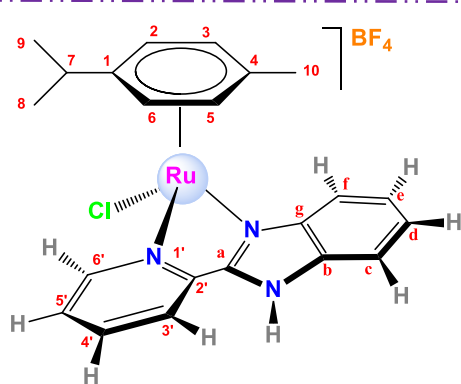


Synthesis of $[(\eta^6\text{-benzene})\text{RuCl}(\text{pybim})]\text{Cl}$, [1b]Cl. The synthesis was performed as for [1a]Cl using 2-(2-pyridyl)benzimidazole (pybim) (78.2 mg, 0.403 mmol) and $[(\eta^6\text{-benzene})\text{RuCl}_2]_2$ (100 mg, 0.200 mmol) adding some acetonitrile. Yellow-brownish solid. Yield: 139 mg (0.312 mmol, 79%). **M_r** ($\text{C}_{18}\text{H}_{15}\text{Cl}_2\text{N}_3\text{Ru}$) = 445.312 g/mol. **Anal. Calcd for** $\text{C}_{18}\text{H}_{15}\text{Cl}_2\text{N}_3\text{Ru}$ (H_2O)_{1.8}: C 45.25; H 3.92; N 8.80; **Found:** C 45.17; H 3.93; N 8.92. **$^1\text{H NMR}$ (400 MHz, DMSO-d₆, 25 °C)** δ 9.71 (d, J = 5.7 Hz, 1H, H^{6'}), 8.55 (d, J = 8.0 Hz, 1H, H^{3'}), 8.35 (t, J = 7.2 Hz, 1H, H^{4'}), 8.18 – 8.10 (m, 1H, H^f), 7.87 – 7.76 (m, 2H, H^{5',c}), 7.62 – 7.54 (m, 2H, H^{e,d}), 6.30 (s, 6H, H^{bz}) ppm. **$^{13}\text{C}\{\text{H}\}$ NMR (101 MHz, DMSO-d₆, 25 °C)** δ 156.6 (s, 1C, C^{6'}), 150.6 (s, 1C, C^a), 146.7 (s, 1C, C^{2'}), 141.3 (s, 1C, C^g), 140.2 (s, 1C, C^{4'}), 134.7 (s, 1C, C^b), 127.0 (s, 1C, C^{5'}), 125.7 (s, 1C, C^d), 124.7 (s, 1C, C^c), 123.3 (s, 1C, C^{3'}), 118.0 (s, 1C, C^f), 114.1 (s, 1C, C^c), 85.1 (s, 6C, C^{bz}). **FT-IR (KBr, cm⁻¹) selected bands:** 3063 (m, $\nu_{\text{C-H}}$, N-H), 1610 (s, $\nu_{\text{C=C+C-N}}$), 1481 (w), 1457 (s, $\nu_{\text{C=N}}$), 1445 (s), 1325 (m), 1156–1148 (m), 1007–938 (w), 849 (m), 785 (w, $\delta_{\text{C-C}}$), 745 (s, δ_{CHoop}). **MS (FAB+):** m/z (%) = 410 (51) ([M-Cl]⁺), 374 (27) ([M-2Cl-H]⁺). **Molar conductivity (H₂O):** 192 S·cm²·mol⁻¹. **Solubility:** soluble in methanol, ethanol, water, DMSO.



Synthesis of $[(\eta^6\text{-phoxet})\text{RuCl}(\text{pybim})]\text{Cl}$, [1c]Cl. The synthesis was performed as for [1a]Cl using 2-(2-pyridyl)benzimidazole (pybim) (63.3 mg, 0.324 mmol) and $[(\eta^6\text{-phoxet})\text{RuCl}_2]_2$ (100 mg, 0.162 mmol). Yellow solid. Yield: 139 mg (0.275 mmol, 85%). **M_r** ($\text{C}_{20}\text{H}_{19}\text{Cl}_2\text{N}_3\text{O}_2\text{Ru}$) = 505.3644 g/mol. **Anal. Calcd. for** $\text{C}_{20}\text{H}_{19}\text{Cl}_2\text{N}_3\text{O}_2\text{Ru} \cdot (\text{H}_2\text{O})_{2.5}$: C 43.64; H 4.40; N 7.63; **Found:** C 43.77; H 4.50; N 7.51. **$^1\text{H NMR}$ (400 MHz, DMSO-d₆, 25 °C)** δ 15.43 (s, 1H, H^{N-H}), 9.61 (d, J = 5.1 Hz, 1H, H^{6'}), 8.64 (d, J = 7.9 Hz, 1H, H^{3'}), 8.33 (td, J = 7.8, 1.4 Hz, 1H, H^{4'}), 8.17 – 8.07 (m, 1H, H^f), 7.85 – 7.75 (m, 2H, H^{5',c}), 7.65 – 7.48 (m, 2H, H^{e,d}), 6.50 (t, J = 5.9 Hz, 1H, H³ or H⁵), 6.45 (t, J = 5.9 Hz, 1H, H³ or H⁵), 6.13 (dd, J = 6.3, 1.8 Hz, 1H, H² or H⁶), 5.93 (dd, J = 6.3, 1.8 Hz, 1H, H² or H⁶), 5.55 (t, J = 5.4 Hz, 1H, H⁴), 4.98 (s, 1H, H^{O-H}), 4.19 – 4.00 (m, 2H, H⁷), 3.64 (m, 2H, H⁸) ppm. **$^1\text{H NMR}$ (400 MHz, CD₃OD, 25 °C)** δ 9.56 (d, J = 5.8 Hz, 1H, H^{6'}), 8.28 (d, J = 4.1 Hz, 2H, H^{3',4'}), 8.09 (dd, J = 6.5, 2.9 Hz, 1H, H^f), 7.77 (dd, J = 9.6, 4.2 Hz, 2H, H^{5',c}), 7.68 – 7.54 (m, 2H, H^{e,d}), 6.51 (t, J = 5.9 Hz, 1H, H³ or H⁵), 6.44 (t, J = 5.9 Hz, 1H, H³ or H⁵), 5.99 (dd, J = 6.4, 1.8 Hz, 1H, H² or H⁶), 5.83 (dd, J = 6.4, 1.7 Hz, 1H, H² or H⁶), 5.54 (t, J = 5.4 Hz, 1H, H⁴), 4.18 (m, J = 16.5, 5.1 Hz, 2H, H⁷), 3.81 (t, J = 4.7 Hz, 2H, H⁸). **$^{13}\text{C}\{\text{H}\}$ NMR (101 MHz, DMSO-d₆, 25 °C)** δ 156.1 (s, 1C, C^{6'}), 150.4 (s, 1C, C^a), 146.7 (s, 1C, C^{2'}), 141.2 (s, 1C, C^g), 139.9 (s, 1C, C^{4'}), 138.1 (s, 1C, C¹), 134.5 (s, 1C, C^b), 126.8 (s, 1C, C^{5'}), 125.7 (s, 1C, C^d), 124.5 (s, 1C, C^e), 123.1 (s, 1C, C^{3'}), 118.1 (s, 1C, C^f), 113.9 (s, 1C, C^c), 92.7 (s, 1C, C³ or C⁵), 91.0 (s, 1C, C³ or C⁵), 71.6 (s, 1C, C⁷), 71.4 (s, 1C, C⁸), 64.1 (s, 1C, C² or C⁶), 62.3 (s, 1C, C² or C⁶), 58.8 (s, 1C, C⁴) ppm. **FT-IR (KBr, cm⁻¹) selected bands:** 3388 (s, $\nu_{\text{O-H}}$), 3064 (m, $\nu_{\text{C-H}}$, N-H), 2928 (w, ν_{CH}), 1609 (s, $\nu_{\text{C=C+C-N}}$), 1526 (s), 1457 (s, $\nu_{\text{C=N}}$), 1326 (m), 1267 (s, $\nu_{\text{C-O-Cas}}$), 1153 (w), 1071 (m, $\nu_{\text{C-Osym}}$), 909 (m, $\nu_{\text{C-Oas}}$), 792 (w, $\delta_{\text{C-C}}$), 757–751 (s, δ_{CHoop}), 665 (s, $\delta_{\text{O-Hoop}}$). **MS (FAB+):** m/z (%) = 470 (100) ([M-Cl]⁺), 434 (20) ([M-2Cl-H]⁺), 390 (35) ([M-2Cl-H-(CH₂CH₂OH)+H]⁺). **Molar**

conductivity (H_2O): 200 S·cm²·mol⁻¹. **Solubility:** soluble in methanol, ethanol, water, dichloromethane and acetone. Partially soluble in DMSO.

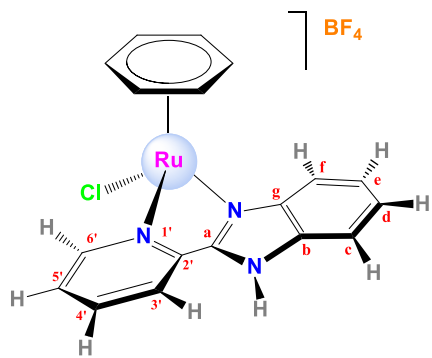


Synthesis of $[(\eta^6\text{-}p\text{-cymene})\text{RuCl}(\text{pybim})]\text{BF}_4$, [1a](BF₄). In a 100 mL Schlenk flask protected from light, AgBF₄ (0.0636 g, 0.0327 mmol) was added under a nitrogen atmosphere to a solution of $[(\eta^6\text{-}p\text{-cymene})\text{RuCl}_2]_2$ (100 mg, 0.162 mmol) in degassed dichloromethane (15 mL). The suspension was stirred for 2 hours at room temperature. The ligand 2-(2-pyridyl)benzimidazole (pybim) (63.8 mg, 0.327 mmol) was then added and the mixture stirred for 15 additional hours at room temperature. The AgCl was filtered off. The solvent was removed under vacuum and the solid residue was washed with *n*-hexane (3×5 mL) and dried under vacuum, to produce an orange-yellow solid. Yield: 94.6 mg (0.171 mmol, 52%). **M**, (C₂₂H₂₃BClF₄N₃Ru) = 552.7711 g/mol.

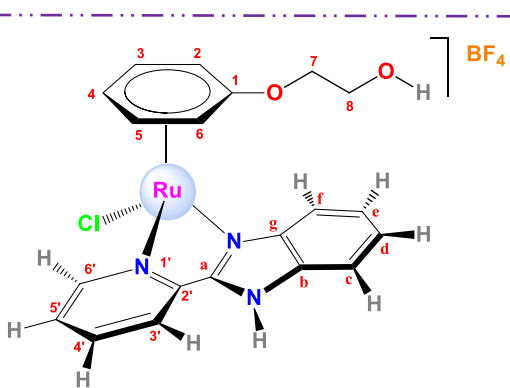
Anal. Calcd for C₂₂H₂₃BClF₄N₃Ru·(H₂O)_{0.2}: C 47.49; H 4.24; N 7.55; **Found:** C 47.53; H 4.70; N 7.85.

¹H NMR (400 MHz, DMSO-d₆, 25 °C) δ 15.49 (s, 1H, N-H), 9.62 (d, *J* = 5.4 Hz, 1H, H^{6'}), 8.68 (d, *J* = 7.9 Hz, 1H, H^{3'}), 8.36 (t, *J* = 7.8 Hz, 1H, H^{4'}), 8.12 (dd, *J* = 5.5, 3.8 Hz, 1H, H^{1'}), 7.90 – 7.71 (m, 2H, H^{5',c}), 7.71 – 7.51 (m, 2H, H^{e,d}), 6.40 (d, *J* = 6.1 Hz, 1H, H² or H⁶), 6.33 (d, *J* = 6.1 Hz, 1H, H² or H⁶), 6.19 (d, *J* = 6.1 Hz, 1H, H³ or H⁵), 6.12 (d, *J* = 5.9 Hz, 1H, H³ or H⁵), 2.50 (sept, H⁷), 2.20 (s, 3H, H¹⁰), 0.91 (d, *J* = 6.5 Hz, 3H, H⁸), 0.89 (d, *J* = 6.5 Hz, 3H, H⁹) ppm. The resonance of H⁷ is obscured under the signal of DMSO at 2.50 ppm. **¹³C{¹H} NMR (101 MHz, DMSO-d₆, 25 °C)** δ 156.5 (s, 1C, C^{6'}), 150.2 (s, 1C, C^a), 146.3 (s, 1C, C^{2'}), 141.0 (s, 1C, C^g), 140.2 (s, 1C, C^{4'}), 134.4 (s, 1C, C^b), 127.2 (s, 1C, C^{5'}), 125.9 (s, 1C, C^d), 124.8 (s, 1C, C^e), 123.4 (s, 1C, C^{3'}), 118.0 (s, 1C, C^f), 113.9 (s, 1C, C^c), 103.5 (s, 1C, C⁴), 102.7 (s, 1C, C¹), 85.6 (s, 1C, C² or C⁶), 83.5 (s, 1C, C² or C⁶), 82.3 (s, 1C, C³ or C⁵), 79.9 (s, 1C, C³ or C⁵), 30.6 (s, 1C, C⁷), 21.7 (d, *J* = 2.7 Hz, 2C, C^{8,9}), 18.6 (s, 1C, C¹⁰). **¹⁹F{¹H} NMR (376 MHz, DMSO-d₆, 25 °C)** δ -148.74 (s, ¹⁰B-F, BF₄⁻), -148.79 (s, ¹¹B-F, BF₄⁻) ppm. **FT-IR (KBr, cm⁻¹)**

selected bands: 3063 (w, ν=CH, N-H), 2964 (w, ν-CH), 1610-1594 (s, ν_{C=C + C-N}), 1483 (m), 1456 (s, ν_{C=N}), 1447 (s), 1388 (w, δ_{CH₃}), 1325 (m), 1152 (w), 1083-1058-1036 (vs, ν_{B-F}), 792 (w, δ_{C-C}), 762-752 (s, δ_{CH_{oop}}). **MS (FAB+):** m/z (%) = 466 (62) ([M-BF₄]⁺), 430 (75) ([M-BF₄-Cl-H]⁺). **Molar conductivity (H_2O):** 159 S·cm²·mol⁻¹. **Solubility:** soluble in methanol, water, DMSO, and partially soluble in acetone.

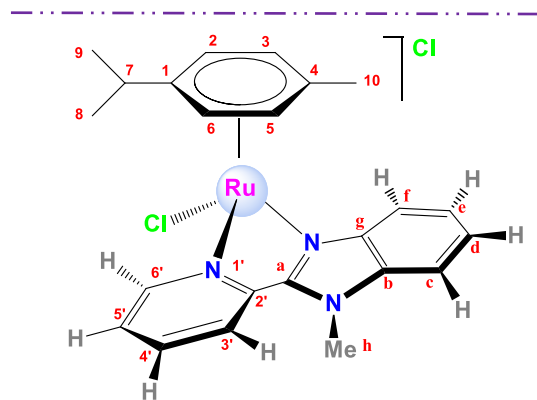


Synthesis of $[(\eta^6\text{-benzene})\text{RuCl}(\text{pybim})]\text{BF}_4$, [1b](BF₄). The synthesis was performed as for **[1a]BF₄** using AgBF₄ (0.080 g, 0.041 mmol), $[(\eta^6\text{-benzene})\text{RuCl}_2]_2$ (100 mg, 0.200 mmol) and 2-(2-pyridyl)benzimidazole (pybim) (79.1 mg, 0.405 mmol) adding some acetonitrile. Yellow solid. Yield: 99.7 mg (0.201 mmol, 50%). **M_r** (**C₁₈H₁₅BClF₄N₃Ru**) = 496.6639 g/mol. **Anal. Calcd for C₁₈H₁₅BClF₄N₃Ru·(CH₃CN)_{0.25}(H₂O)_{1.2}:** C 42.04; H 3.46; N 8.61; **Found:** C 42.03; H 3.49; N 8.64. **¹H NMR (400 MHz, DMSO-d₆, 25 °C)** δ 14.75 (s, 1H, N-H), 9.70 (d, *J* = 5.6 Hz, 1H, H^{6'}), 8.43 – 8.32 (m, 2H, H^{3',4'}), 8.18 – 8.12 (m, 1H, H^f), 7.87 – 7.78 (m, 2H, H^{5',c}), 7.65 – 7.55 (m, 2H, H^{e,d}), 6.30 (s, 6H, H^{bz}). ppm. **¹³C{¹H} NMR (101 MHz, DMSO-d₆, 25 °C)** δ 156.7 (s, 1C, C^{6'}), 150.2 (s, 1C, C^a), 146.2 (s, 1C, C^{2'}), 141.1 (s, 1C, C^g), 140.4 (s, 1C, C^{4'}), 134.0 (s, 1C, C^b), 127.2 (s, 1C, C^{5'}), 126.1 (s, 1C, C^d), 124.9 (s, 1C, C^e), 123.1 (s, 1C, C^{3'}), 118.2 (s, 1C, C^f), 113.9 (s, 1C, C^c), 85.1 (s, 6C, C^{bz}) ppm. **¹⁹F{¹H} NMR (376 MHz, DMSO-d₆, 25 °C)** δ -148.75 (s, ¹⁰B-F, BF₄⁻), -148.80 (s, ¹¹B-F, BF₄⁻) ppm. **FT-IR (KBr, cm⁻¹) selected bands:** 3065 (m, ν_{=CH, N-H}), 1611 (s, ν_{C=C + C-N}), 1484 (w), 1456 (s, ν_{C=N}), 1445 (s), 1324 (m), 1150 (m), 1082–1061 (vs, ν_{B-F}), 846 (w), 791 (w, δ_{C-C}), 751 (s, δ_{CHoop}). **MS (FAB+): m/z (%) =** 410 (51) ([M-BF₄]⁺), 374 (27) ([M-BF₄-Cl-H]⁺). **Molar conductivity (H₂O):** 175 S·cm²·mol⁻¹. **Solubility:** soluble in water, acetone and DMSO. Partially soluble in methanol, and insoluble in chloroform.



Synthesis of $[(\eta^6\text{-phoxet})\text{RuCl}(\text{pybim})](\text{BF}_4)$, [1c](BF₄). The synthesis was performed as for **[1a]BF₄** using AgBF₄ (63.4 mg, 0.041 mmol), $[(\eta^6\text{-phoxet})\text{RuCl}_2]$ (99.4 mg, 0.162 mmol) and 2-(2-pyridyl)benzimidazole (pybim) (62.5 mg, 0.324 mmol). Orange-yellow solid. Yield: 124 mg (0.223 mmol, 70%). **M_r** ($\text{C}_{20}\text{H}_{19}\text{BClF}_4\text{N}_3\text{O}_2\text{Ru}$) = 556,7163 g/mol. **Anal.** Calcd for $\text{C}_{20}\text{H}_{19}\text{BClF}_4\text{N}_3\text{O}_2\text{Ru}$: C 43.15; H 3.44; N 7.55; **Found**: C 43.46; H 3.74; N 7.50. **¹H NMR** (400 MHz, DMSO-d₆, 25 °C) δ 14.66 (s, 1H, H^{N-H}), 9.61 (d, *J* = 5.3 Hz, 1H H^{6'}), 8.39 (d, *J* = 7.5 Hz, 1H, H^{3'}), 8.34 (t, *J* = 7.7 Hz, 1H, H^{4'}), 8.14 (dd, *J* = 6.1, 2.7 Hz, 1H, H^f), 7.89 – 7.74 (m, 2H, H^{5',c}), 7.60 – 7.51 (m, 2H, H^{e,d}), 6.50 (t, *J* = 5.9 Hz, 1H, H³ or H⁵), 6.45 (t, *J* = 5.8 Hz, 1H, H⁵ or H³), 6.13 (d, *J* = 6.3 Hz, 1H, H² or H⁶), 5.92 (d, *J* = 6.4 Hz, 1H, H⁶ or H²), 5.54 (t, *J* = 5.4 Hz, 1H, H⁴), 4.95 (s, 1H, H^{O-H}), 4.22 – 4.02 (m, 2H H⁷), 3.64 (m, 2H, H⁸) ppm. **¹³C{¹H} NMR** (101 MHz, DMSO-d₆, 25 °C) δ 156.2 (s, 1C, C^{6'}), 150.2 (s, 1C, C^{3'}),

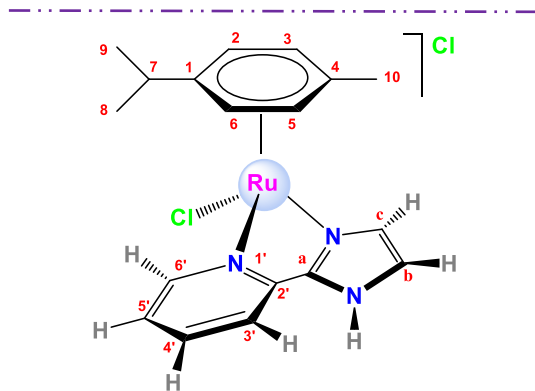
146.5 (s, 1C, C^{2'}), 141.2 (s, 1C, C^g), 140.0 (s, 1C, C^{4'}), 138.2 (s, 1C, C¹), 134.3 (s, 1C, C^b), 127.0 (s, 1C, C^{5'}), 125.9 (s, 1C, C^d), 124.7 (s, 1C, C^e), 122.9 (s, 1C, C^{3'}), 118.2 (s, 1C, C^f), 113.9 (s, 1C, C^c), 92.7 (s, 1C, C⁵ or C³), 91.0 (s, 1C, C³ or C⁵), 71.7 (s, 1C, C⁷), 71.4 (s, 1C, C⁸), 64.1 (s, 1C, C⁶ or C²), 62.3 (s, 1C, C² or C⁶), 58.9 (s, 1C, C⁴) ppm. **¹⁹F{¹H} NMR (376 MHz, DMSO-d₆, 25 °C)** δ -148.76 (s, ¹⁰B-F, BF₄⁻), -148.81 (s, ¹¹B-F, BF₄⁻) ppm. **FT-IR (KBr, cm⁻¹) selected bands:** 3385 (s, ν_{O-H}), 3060 (m, ν_{=CH}), 2924 (w, ν_{=CH}), 1610 (s, ν_{C=C+C-N}), 1526 (s), 1457 (s, ν_{C=N}), 1326 (w), 1268 (s, ν_{C-O-Cas}), 1084 (vs, ν_{B-F}), 1071 (m, ν_{C-Osym}), 910 (m, ν_{C-Oas}), 751 (s, δ_{CHoop}), 664 (s, δ_{O-Hoop}). **MS (FAB+):** m/z (%) = 470 (18) ([M-BF₄]⁺), 434 (4) ([M-BF₄-Cl-H]⁺), 390 (4) ([M-BF₄-Cl-(CH₂CH₂OH)]⁺). **Molar Conductivity (H₂O):** 176.8 S·cm²·mol⁻¹. **Solubility:** soluble in water, acetone, methanol, ethanol, dimethyl sulfoxide and slightly soluble in dichloromethane and chloroform.



*Synthesis of the ligand 1-Methyl-2-pyridin-2-yl-1H-benzimidazole, pyMebim.*¹⁵ In a 100 mL Schlenk flask, Cs₂CO₃ (3.3377 g, 10.24 mmol) was added to a solution of 2-(2'-pyridyl)benzimidazole (1.000 g, 5.12 mmol) in DMSO (25 mL). The mixture was stirred at 80 °C for 90 min. under a nitrogen atmosphere. Then methyl iodide (478 μL, 7.68 mmol) was added and the resulting mixture was stirred for 20 h at room temperature. The crude product was precipitated with water as a white solid. This solid was filtered, washed with water (2x10 mL) and dried in a desiccator until constant weigh. Yield: 0.7741 g (3.70 mmol, 72%).

Synthesis of [(η⁶-p-cymene)RuCl(pyMebim)]Cl, [2a]Cl. The synthesis was performed as for [1a]Cl using 1-Methyl-2-pyridin-2-yl-1H-benzimidazole (pyMebim) (101.7 mg, 0.486 mmol) and [(η⁶-p-cymene)RuCl₂] (129.7 mg, 0.212 mmol) and washing the solid also with THF (4×5 mL). Yellow solid. Yield: 115.6 mg (0.224 mmol, 56%). **M_r (C₂₂H₂₃Cl₂N₃Ru)** = 515.4460 g/mol. **Anal. Calcd for C₂₂H₂₃Cl₂N₃Ru·(H₂O)_{0.6}:** C 52.49; H 5.02; N 7.98; **Found:** C 52.45; H 5.02; N 8.03. **¹H NMR (400 MHz, DMSO-d₆, 25 °C)** δ 9.73 (d, J = 5.4 Hz, 1H, H^{6'}), 8.61 (d, J = 8.1 Hz, 1H, H^{3'}), 8.34 (td, J = 8.0, 1.3 Hz, 1H, H^{4'}), 8.12 (d, J = 7.4 Hz, 1H, H^f), 8.04 (d, J = 7.6 Hz, 1H, H^c), 7.84 (t, J = 6.15 Hz, 1H, H^{5'}), 7.72 – 7.59 (m, 2H, H^{d,e}), 6.39 (d, J = 6.3 Hz, 1H, H² or H⁶), 6.35 (d, J = 6.3 Hz, 1H, H⁶ or H²), 6.22 (d, J = 6.1 Hz, 1H, H³ or H⁵), 6.12 (d, J = 6.1 Hz, 1H, H⁵ or H³), 4.38 (s, 3H, H^h), 2.48 (sept, J = 6.8 Hz, 1H, H⁷), 2.20 (s, 3H, H¹⁰), 0.90 (d, J = 6.8 Hz, 3H, H⁸), 0.89 (d, J = 6.8 Hz, 3H, H⁹) ppm. The peak for H⁷ is partially overlapped with the signal of DMSO-d₆ at 2.50 ppm. **¹³C{¹H} NMR (101 MHz, DMSO-d₆, 25 °C)** δ 157.3 (s, 1C, C^{6'}), 148.9 (s, C^a), 145.6 (s, C^{2'}), 139.9 (s, 1C, C^g or C^{4'}), 139.8 (s, 1C, C^g or C^{4'}), 136.2 (s, 1C, C^b), 127.2 (s, 1C, C^{5'}), 126.0 (s, 1C, C^d), 125.3 (s, 1C, C^e or C^{3'}), 125.2 (s, 1C, C^e or C^{3'}), 118.5 (s, 1C, C^f), 112.6 (s, 1C, C^c), 104.2 (s, 1C, C⁴), 103.0 (s, 1C, C¹), 86.1 (s, 1C, C⁶ or C²), 83.8 (s, 1C, C² or C⁶), 82.7 (s, 1C, C⁵ or C³), 80.1 (s, 1C, C³ or C⁵), 33.1 (s, 1C, C^h), 30.5 (s, 1C, C⁷), 21.80 (s, 1C, C⁸ or C⁹), 21.7 (s, 1C, C⁸ or C⁹), 18.6 (s, 1C, C¹⁰) ppm. **FT-IR (KBr, cm⁻¹) selected bands:** 3572 (s, ν_{O-H}), 3388 (vs), 3048 (m, ν_{=CH}), 3013-2966 (s, ν_{C=CH}), 1603 (m, ν_{C=C+C-N}), 1528 (m,

1484 (vs, $\nu_{C=N}$), 1459-1444-1425 (s), 1350-1335 (w, δ_{CH_3}), 1223 (w), 1130-1111 (w), 1028 (w), 829 (w), 792 (m, δ_{C-C}), 772-753 (s, $\delta_{CH_{loop}}$), 506 (w), 477-439 (w). **MS (FAB+)**: m/z (%) = 480 (2) ([M-Cl]⁺). **Molar Conductivity (H_2O)**: 138 S·cm²·mol⁻¹. **Solubility**: soluble in water, methanol, ethanol, dimethyl sulfoxide, dichloromethane and partially soluble in acetone. Slightly soluble/insoluble in THF.

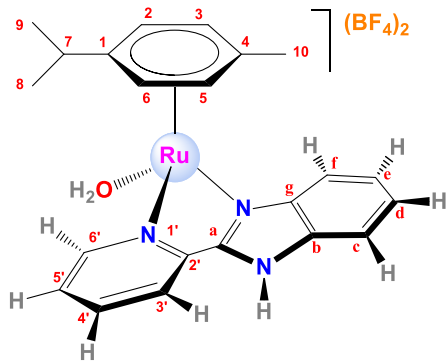


Synthesis 2-(2'-pyridyl)imidazole, pyim.^{32,33} In a 100 mL Schlenk flask, an ice-cold solution of glyoxal (2.8 mL, 24.51 mmol, 20 % ee) in ethanol (5 mL) was added to an ice-cold solution of 2-pyridylcarboxaldehyde (2.011 g, 18.68 mmol) also in ethanol (5 mL). Immediately, aqueous ammonia (7.5 mL, 114.9 mmol) was then added and the mixture was stirred at 0 °C for 1 h and then, at room temperature for 2 days. The solvent was evaporated and the residue extracted with diethyl ether (10 x 15 mL). The crude product was recrystallized from methanol to afford orange crystals. The crystals were washed with cold methanol and dried under vacuum. Yield: 0.3405 g (2.346 mmol, 13%).

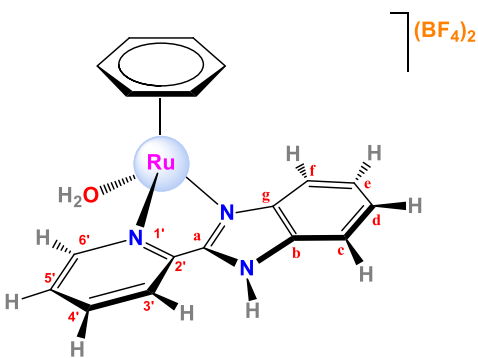
Synthesis of $[(\eta^6-p\text{-cymene})RuCl(pyim)]Cl$, [3a]Cl. In a 100 mL Schlenk flask, a solution of 2-(2'-pyridyl)imidazole (pyim) (52.5 mg, 0.362 mmol) in degassed methanol (5 mL) was added under a nitrogen atmosphere to a solution of $[(\eta^6-p\text{-cymene})RuCl_2]_2$ (100.3 mg, 0.164 mmol) in degassed methanol (5 mL). The resulting solution was stirred overnight (20 h) at room temperature. The solvent was removed under vacuum and the solid residue was washed with diethylether (5 mL) and *n*-hexane (5 mL), and then dried under vacuum. The crude product was dissolved in methanol (3 mL), and thereupon, diethylether (3 mL) was added to precipitate a solid that was filtered and washed with *n*-hexane (2×5 mL) and dried under vacuum to produce a yellow-brownish product. Yield: 96 mg (0.213 mmol, 65%). **M_r** ($C_{18}H_{21}Cl_2N_3Ru \cdot (H_2O)_{0.5}$) = 451.3594 g/mol. **Anal. Calcd for $C_{18}H_{21}Cl_2N_3Ru \cdot (H_2O)_{0.5}$** : C 46.96; H 4.82; N 9.13; **Found**: C 46.58; H 4.56; N 9.45. **¹H NMR (400 MHz, DMSO-d₆, 25 °C)** δ 14.62 (s, 1H, H^{N-H}), 9.44 (d, $J = 5.5$ Hz, 1H, H^{6'}), 8.26 (d, $J = 7.8$ Hz, 1H, H^{3'}), 8.21 (t, $J = 7.6$ Hz, 1H, H^{4'}), 8.01 (d, $J = 1.4$ Hz, 1H, H^c), 7.77 (d, $J = 1.3$ Hz, 1H, H^b), 7.63 (t, $J = 6.5$ Hz, 1H, H^{5'}), 6.19 (d, $J = 6.2$ Hz, 1H, H² or H⁶), 6.08 (d, $J = 6.2$ Hz, 1H, H² or H⁶), 5.97 (d, $J = 6.1$ Hz, 1H, H³ or H⁵), 5.85 (d, $J = 6.2$ Hz, 1H, H³ or H⁵), 2.62 (sept, $J = 6.2$ Hz, 1H, H⁷), 2.13 (s, 3H, H¹⁰), 1.02 (d, $J = 6.9$ Hz, 3H, H⁸ or H⁹), 0.96 (d, $J = 6.9$ Hz, 3H, H⁸ or H⁹) ppm. **¹H NMR (400 MHz, CDCl₃, 25 °C)** δ 15.97 (s, 1H, H^{N-H}), 9.19 (d, $J = 7.7$ Hz, 1H, H^{3'}), 9.06 (d, $J = 5.7$ Hz, 1H, H^{6'}), 7.99 (t, $J = 7.8$ Hz, 1H, H^{4'}), 7.50 (s, 1H, H^c), 7.43 (s, 1H, H^b), 7.39 (t, $J = 6.5$ Hz, 1H, H^{5'}), 5.74 (d, $J = 6.0$ Hz, 1H, H² or H⁶), 5.67 (d, $J = 6.0$ Hz, 1H, H⁶ or H²), 5.57 (d, $J = 5.9$ Hz, 1H, H⁵ or H³), 5.52 (d, $J = 6.1$ Hz, 1H, H³ or H⁵), 2.69 (sept, $J = 13.9, 6.9$ Hz, 1H, H⁷), 2.23 (s, 3H, H¹⁰), 1.12 (d, $J = 6.9$ Hz, 3H, H⁸ or H⁹), 1.08 (d, $J = 6.9$ Hz, 3H, H⁸ or H⁹) ppm. **¹³C{¹H} NMR (101 MHz, CDCl₃, 25 °C)** δ 154.0 (s, 1C, C^{6'}), 147.7 (s, 1C, C^{2'}), 145.9 (s, 1C, C^a), 140.3 (s, 1C, C^{4'}), 130.5 (s, 1C, C^c),

125.5 (s, 1C, C^{5'}), 124.3 (s, 1C, C^{3'}), 122.6 (s, 1C, C^b), 104.2 (s, 1C, C¹), 101.7 (s, 1C, C⁴), 84.9 (s, 1C, C² or C⁶), 84.1 (s, 1C, C² or C⁶), 83.5 (s, 1C, C³ or C⁵), 82.1 (s, 1C, C³ or C⁵), 31.3 (s, 1C, C⁷), 22.5 (s, 1C, C⁸ or C⁹), 22.1 (s, 1C, C⁸ or C⁹), 19.0 (s, 1C, C¹⁰) ppm. **FT-IR (KBr, cm⁻¹) selected bands:** 3425 (m, v_{O-H}), 3086 (s, v_{=CH}), 2967 (s, v_{CH}), 1617 (s, v_{C=C+C-N}), 1471 (vs, v_{C=N}), 1373 (w, δ_{CH₃}), 1160 (m), 804 (s, δ_{C-C}), 757 (m, δ_{CHOop}), 704 (m). **MS (FAB+):** m/z (%) = 416 (55) ([M-Cl]⁺), 380 (18) ([M-2Cl-H]⁺). **Molar Conductivity (H₂O):** 132 S·cm²·mol⁻¹. **Solubility:** soluble in water, methanol, acetone and chloroform.

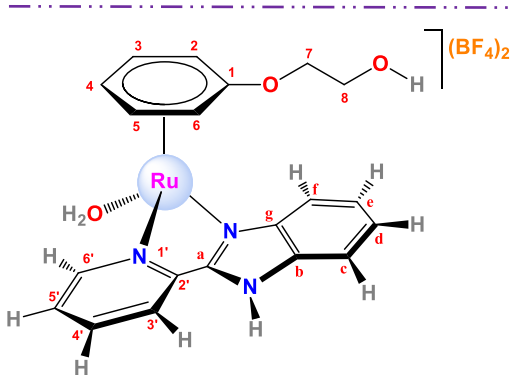
Aqua-complexes



Synthesis of [(η^6 -*p*-cymene)Ru(OH₂)(pybim)](BF₄)₂, **[4a](BF₄)₂**. In a 100 mL Schlenk flask protected from light, AgBF₄ (119.6 mg, 0.614 mmol) was added under a nitrogen atmosphere to a solution of [(η^6 -*p*-cymene)RuCl(pybim)]Cl, **[1a]Cl** (93.1 mg, 0.186 mmol) in degassed distilled water (10 mL). The suspension was stirred for 20 hours at room temperature. The AgCl was filtered off. The solvent was removed under vacuum and the solid residue was washed with diethylether (3×5 mL) and dried under vacuum, to produce a yellow solid. Yield: not calculated (impure product). **M_r (C₂₂H₂₅B₂F₈N₃ORu)** = 622.1382 g/mol. **Anal. Calcd for** C₂₂H₂₅B₂F₈N₃ORu·(AgBF₄)_{0.5}: C 38.06; H 4.79; N 6.05; **Found:** C 38.02; H 4.30; N 5.92. **¹H NMR (400 MHz, D₂O, 25 °C)** δ = 9.68 (d, J=5.7 Hz, 1H, H^{6'}), 8.33 (m, 2H, H^{4',3'}), 8.16 (d, J=7.2 Hz, 1H, H^f), 7.86 (m, 2H, H^{5',c}), 7.70 (m, 2H, H^{e,d}), 6.57 (d, J=6.0 Hz, 1H, H² or H⁶), 6.37 (d, J=6.2 Hz, 1H, H⁶ or H²), 6.28 (d, J=6.2 Hz, 1H, H³ or H⁵), 6.24 (d, J=6.1 Hz, 1H, H⁵ or H³), 2.40 (sept, J=6.9 Hz, 1H, H⁷), 2.24 (s, 3H, H¹⁰), 0.90 (d, J = 7.0 Hz, 3H, H⁸ or H⁹), 0.86 (d, J = 7.0 Hz, 3H, H⁹ or H⁸) ppm. **¹³C{¹H} NMR (101 MHz, D₂O, 25 °C)** δ = 156.7 (s, 1C, C^{5'}), 151.6 (s, 1C, C^a), 147.3 (s, 1C, C^{2'}), 142.2 (s, 1C, C^{4'}), 141.4 (s, 1C, C^g), 134.8 (s, 1C, C^b), 128.9 (s, 1C, C^{5'}), 127.5 (s, 1C, C^d), 126.4 (s, 1C, C^e), 124.5 (s, 1C, C^{3'}), 117.9 (s, 1C, C^f), 114.8 (s, 1C, C^c), 105.3 (s, 1C, C⁴), 99.6 (s, 1C, C¹), 87.6 (s, 1C, C⁶ or C²), 85.4 (s, 1C, C² or C⁶), 83.2 (s, 1C, C⁵ or C³), 79.9 (s, 1C, C³ or C⁵), 31.1 (s, 1C, C⁷), 21.7 (s, 1C, C⁸ or C⁹), 21.5 (s, 1C, C⁹ or C⁸), 18.4 (s, 1C, C¹⁰). **¹⁹F{¹H} NMR (376 MHz, D₂O, 25 °C)** δ = -150.95 (s, ¹⁰B-F, BF₄⁻), -151.00 (s, ¹¹B-F, BF₄⁻) ppm. Integration ratio (1:4) in agreement with the isotopic distribution for ¹⁰B/¹¹B. **FT-IR (KBr, cm⁻¹) selected bands:** 3417 (m, v_{O-H}), 3289 (m, v_{N-Hasociado}), 3084 (w, v_{=CH}), 2970 (w, v_{CH}), 1613-1595 (w, v_{C=C+C-N}), 1498-1485 (m), 1460 (s, v_{C=N}), 1448 (s), 1393-1382 (w, δ_{CH₃}), 1322 (w), 1306-1286 (w), 1098 (vs, v_{B-F}), 821 (w), 789 (w, δ_{C-C}), 748 (s, δ_{CHOop}), 523 (w). **FT-FIR (Nujol, cm⁻¹) selected bands:** 506 (s), 521 (w). **MS (FAB+):** m/z (%) = 450 (8) ([M+H]⁺), 430 (71) ([M-H₂O-H]⁺). **Molar Conductivity (H₂O):** 225 S·cm²·mol⁻¹.

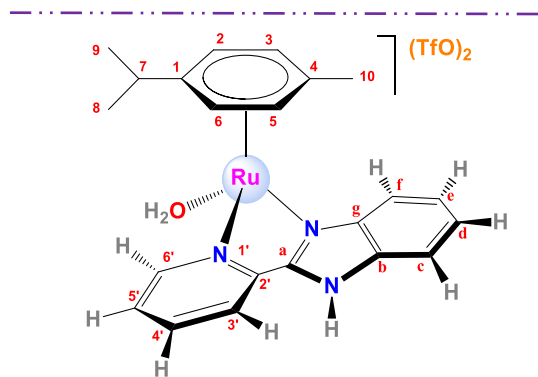


Synthesis of $[(\eta^6\text{-benzene})\text{Ru}(\text{OH}_2)(\text{pybim})](\text{BF}_4)_2$, [4b](BF₄)₂. The synthesis was performed as for **[4a](BF₄)₂** using AgBF₄ (70.2 mg, 0.361 mmol) and $[(\eta^6\text{-bz})\text{RuCl}(\text{pybim})]\text{Cl}$, **[1b]Cl** (50 mg, 0.112 mmol). Yellow solid. Yield: not calculated (impure product). **M_r (C₁₈H₁₇B₂F₈N₃ORu)** = 566.031 g/mol. **Anal. Calcd for C₁₈H₁₇B₂F₈N₃ORu·(H₂O)_{1.1}(AgBF₄)_{0.2}:** C 34.63; H 3.14; N 6.78; **Found:** C 34.60; H 3.10; N 6.73. **¹H NMR (400 MHz, D₂O, 25 °C)** δ 9.70 (d, *J* = 5.7 Hz, 1H, H^{6'}), 8.41 – 8.26 (m, 2H, H^{4',3'}), 8.15 (dd, *J* = 7.2, 1.5 Hz, 1H, H^f), 7.91 – 7.80 (m, 2H, H^{5',c}), 7.75 – 7.62 (m, 2H, H^{e,d}), 6.34 (d, *J* = 1.6 Hz, 6H, H^{bencene}) ppm. **¹³C{¹H} NMR (101 MHz, D₂O, 25 °C)** δ 156.8 (s, 1C, C^{6'}), 151.9 (s, 1C, C^a), 147.6 (s, 1C, C^{2'}), 142.2 (s, 1C, C^{4'}), 141.5 (s, 1C, C^g), 134.6 (s, 1C, C^b), 128.8 (s, 1C, C^{5'}), 127.3 (s, 1C, C^d), 126.3 (s, 1C, C^e), 124.2 (s, 1C, C^{3'}), 117.8 (s, 1C, C^f), 114.7 (s, 1C, C^c), 85.0 (s, 6C, C^{bencene}) ppm. **¹⁹F{¹H} NMR (376 MHz, D₂O, 25 °C)** δ -130.46 (s), -150.96 (s, ¹⁰B-F, BF₄⁻), -151.01 (s, ¹¹B-F, BF₄⁻) ppm. Integration ratio (1:4) in agreement with the isotopic distribution for ¹⁰B/¹¹B. **FT-IR (KBr, cm⁻¹) selected bands:** 3588 (m, ν_{O-H}), 3521 (m), 3371 (m, ν_{N-Hasociado}), 3088 (w, ν_{=CH}), 1614-1598 (w, ν_{C=C+C-N}), 1500-1487 (m), 1460 (s, ν_{C=N}), 1450 (s), 1313 (w, δ_{O-Hip}), 1067 (vs, ν_{B-F}), 847 (w), 791 (w, δ_{C-C}), 758-752 (s, δ_{CHoop}), 629 (w), 521 (w). **MS (FAB+):** m/z (%) = 394 (5) ([M-2BF₄+H]⁺), 374 (22) ([M-2BF₄-H₂O-H]⁺). **Solubility:** soluble in water, methanol and acetone.

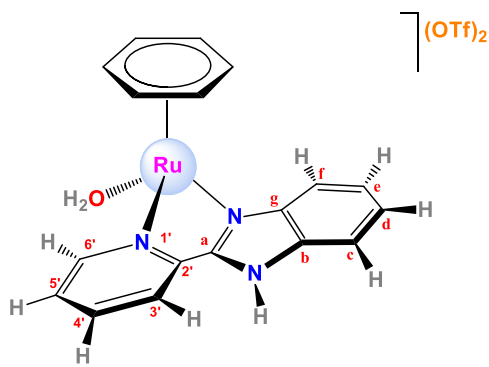


Synthesis of $[(\eta^6\text{-phenoxyethanol})\text{Ru}(\text{OH}_2)(\text{pybim})](\text{BF}_4)_2$, [4c](BF₄)₂. The synthesis was performed as for **[4a](BF₄)₂** using AgBF₄ (70 mg, 0.360 mmol) and $[(\eta^6\text{-phoxet})\text{RuCl}(\text{pybim})]\text{Cl}$, **[1c]Cl** (49.6 mg, 0.098 mmol). Yellow solid. Yield: not calculated (impure product). **M_r (C₂₀H₂₁B₂F₈N₃O₃Ru)** = 626.0834 g/mol. **Anal. Calcd for C₂₀H₂₁B₂F₈N₃O₃Ru·(H₂O)₃(AgBF₄)_{0.2}:** C 33.47; H 3.87; N 5.62; **Found:** C 33.41; H 3.78; N 5.84. **¹H NMR (400 MHz, D₂O, 25 °C)** δ 9.63 (d, *J* = 5.5 Hz, 1H, H^{6'}), 8.32 (m, 2H, H^{4',3'}), 8.15 (d, *J* = 8.4 Hz, 1H, H^f), 7.95 – 7.78 (m, 2H, H^{5',c}), 7.68 (t, *J* = 6.6 Hz, 2H, H^{e,d}), 6.62 (m, 2H, H^{3,5}), 5.94 (d, *J* = 6.6 Hz, 1H, H² or H⁶), 5.86 (d, *J* = 6.5 Hz, 1H, H² or H⁶), 5.75 (t, *J* = 5.6 Hz, 1H, H⁴), 3.99 (m, 2H, H⁷) ppm. The signal for H⁸ is into the signal of 1,4-dioxane, used as reference solvent. **¹³C{¹H} NMR (101 MHz, D₂O, 25 °C)** δ 156.3 (s, 1C, C^{6'}), 151.8 (s, 1C, C^a), 147.8 (s, 1C, C^{2'}), 142.0 (s, 1C, C^{4'}), 141.2 (s, 1C, C^g), 138.0 (s, 1C, C¹), 134.6 (s, 1C, C^b), 128.7 (s, 1C, C^{5'}), 127.3 (s, 1C, C^d), 126.2 (s, 1C, C^e), 124.0 (s, 1C, C^{3'}), 118.0 (s, 1C, C^f), 114.7 (s,

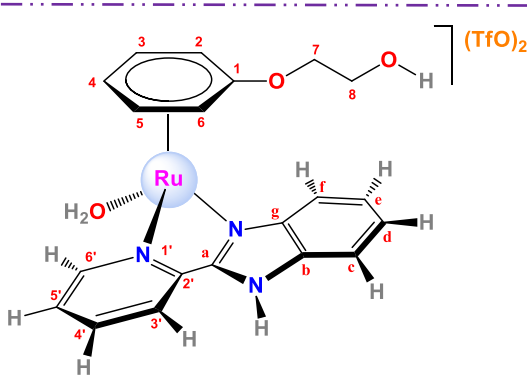
1C, C^c), 93.6 (s, 1C, C³), 93.4 (s, 1C, C⁵), 72.0 (s, 1C, C⁷ or C⁸), 70.9 (s, 1C, C⁴), 63.1 (s, 1C, C²), 62.9 (s, 1C, C⁶), 59.7 (s, 1C, C⁸ or C⁷) ppm. **¹⁹F{¹H} NMR (376 MHz, D₂O, 25 °C)** δ -150.97 (s, ¹⁰B-F, BF₄⁻), -151.03 (s, ¹¹B-F, BF₄⁻) ppm. Integration ratio (1:4) in agreement with the isotopic distribution for ¹⁰B/¹¹B. **FT-IR (KBr, cm⁻¹) selected bands:** 3097 (m, ν_{CH, N-H}), 1614 (s, ν_{C=C + C-N}), 1530 (s), 1499-1486 (w), 1462-1450 (s, ν_{C=N}), 1329 (w), 1272 (s, ν_{C-O-Cas}), 1056 (vs, ν_{B-F}), 910 (w, ν_{C-Oas}), 762-751 (s, δ_{CHOop}), 666 (s, δ_{O-Hoop}), 520 (w). **MS (FAB+):** m/z (%) = 454 (14) ([M-2BF₄+H]⁺), 434 (20) ([M-2BF₄-H₂O-H]⁺), 390 (35) ([M-2BF₄-H-(CH₂CH₂OH)+H]⁺). **Molar conductivity (H₂O):** Decomposition was observed during determination of Λ_M. **Solubility:** soluble in methanol, water, acetone and dichloromethane.



Synthesis of [(\eta⁶-p-cymene)Ru(OH₂)(pybim)](TfO)₂, [4a](TfO)₂. The synthesis was performed as for **[4a](BF₄)₂** using AgOTf (109 mg, 0.424 mmol) and **[(\eta⁶-p-cymene)RuCl(pybim)]Cl, [1a]Cl** (100.3 mg, 0.200 mmol) in a mixture of degassed water/ethanol (1:1, 6 mL). Yellow solid. Yield: not calculated. **M_r (C₂₄H₂₅F₆N₃O₇S₂Ru)** = 746.6698 g/mol. **Anal. Calcd for C₂₄H₂₅F₆N₃O₇S₂Ru (H₂O):** C 37.7; H 3.56; N 5.5; S 8.39; **Found:** C 37.29; H 3.73; N 6.00; S 7.84. **¹H NMR (400 MHz, D₂O, 25 °C)** δ 9.67 (d, J = 5.5 Hz, 1H, H^{6'}), 8.40 – 8.25 (m, 2H, H^{4',3'}), 8.16 (d, J = 8.2 Hz, 1H, H^f), 7.86 (dd, J = 9.6, 4.9 Hz, 2H, H^{5',c}), 7.80 – 7.57 (m, 2H, H^{e,d}), 6.57 (d, J = 6.2 Hz, 1H, H² o H⁶), 6.37 (d, J = 6.0 Hz, 1H, H⁶ o H²), 6.27 (d, J = 6.3 Hz, 1H, H³ o H⁵), 6.24 (d, J = 6.0 Hz, 1H, H⁵ o H³), 2.40 (sept, J = 6.9 Hz, 1H, H⁷), 2.24 (s, 3H, H¹⁰), 0.89 (d, J = 6.9 Hz, 3H, H⁸ o H⁹), 0.86 (d, J = 6.9 Hz, 3H, H⁹ o H⁸) ppm. **¹³C{¹H} NMR (101 MHz, D₂O, 25 °C)** δ 156.7 (s, 1C, C⁶), 151.6 (s, 1C, C^a), 147.3 (s, 1C, C²), 142.2 (s, 1C, C^{4'}), 141.4 (s, 1C, C^g), 134.8 (s, 1C, C^b), 128.6 (s, 1C, C⁵), 127.5 (s, 1C, C^d), 126.4 (s, 1C, C^e), 124.5 (s, 1C, C^{3'}), 120.2 (q, J = 317.0 Hz, 2C, C^{OTf}), 117.9 (s, 1C, C^f), 114.7 (s, 1C, C^c), 105.3 (s, 1C, C⁴), 99.6 (s, 1C, C¹), 87.6 (s, 1C, C⁶), 85.4 (s, 1C, C²), 83.2 (s, 1C, C⁵), 79.9 (s, 1C, C³), 31.1 (s, 1C, C⁷), 21.7 (s, 1C, C⁸), 21.5 (s, 1C, C⁹), 18.4 (s, 1C, C¹⁰) ppm. **¹⁹F{¹H} NMR (376 MHz, D₂O, 25 °C)** δ -79.2 (s, 6F, FCF₃) ppm. **FT-IR (KBr, cm⁻¹) selected bands:** 3504 (m, ν_{O-H}), 3168 (m, ν_{N-Hasociado}), 3148-3114 (w, ν_{=CH}), 2979 (w, ν_{-CH}), 1613 (w, ν_{C=C + C-N}), 1499-1485 (m), 1459 (s, ν_{C=N}), 1292-1245 (vs, ν_{C-F}), 1224-1165 (vs, ν_{SO₃-as}), 1030 (vs, ν_{SO₃-sym}), 788 (w, δ_{C-C}), 748 (s, δ_{CHOop}), 637 (vs, ν_{C-S}), 579 (w), 518 (w). **MS (FAB+):** m/z (%) = 580 (21) ([M-OTf-H₂O]⁺), 430 (58) ([M-2OTf-H₂O-H]⁺). **Molar Conductivity (H₂O):** 148 S·cm²·mol⁻¹. **Solubility:** soluble in water and acetone.

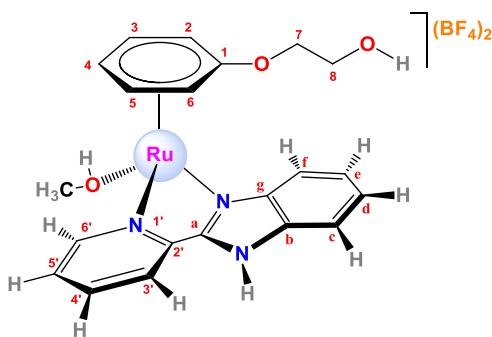


Synthesis of $[(\eta^6\text{-benzene})\text{Ru}(\text{OH}_2)(\text{pybim})](\text{TfO})_2$, [4b](TfO)₂. The synthesis was performed as for **[4a](OTf)₂** using AgOTf (36.4 mg, 0.142 mmol) and $[(\eta^6\text{-benzene})\text{RuCl}(\text{pybim})]\text{Cl}$, **[1b]Cl** (30 mg, 0.067 mmol). Orange-yellowish solid. Yield: not calculated (unstable compound). Analysis not calculated. **¹H NMR (400 MHz, D₂O, 25 °C)** δ 9.70 (d, $J = 5.6$ Hz, 1H, H^{6'}), 8.38 – 8.26 (m, 2H, H^{4',3'}), 8.15 (d, $J = 7.2$ Hz, 1H, H^f), 7.88 – 7.80 (m, 2H, H^{5',c}), 7.73 – 7.62 (m, 2H, H^{e,d}), 6.33 (s, 6H, H^{bz}) ppm. **¹³C{¹H} NMR (101 MHz, D₂O, 25 °C)** δ 156.8 (s, 1C, C^{6'}), 152.1 (s, 1C, C^a), 147.7 (s, 1C, C^{2'}), 142.2 (s, 1C, C^{4'}), 141.6 (s, 1C, C^g), 134.9 (s, 1C, C^b), 128.7 (s, 1C, C^{5'}), 127.2 (s, 1C, C^d), 126.3 (s, 1C, C^e), 124.2 (s, 1C, C^{3'}), 120.2 (q, $J = 317.4$ Hz, 2C, C^{OTf}), 117.7 (s, 1C, C^f), 114.8 (s, 1C, C^c), 85.0 (s, 6C, C^{bz}) ppm. **¹⁹F{¹H} NMR (376 MHz, D₂O, 25 °C)** δ -79.3 (s, 6F, F^{CF₃}). **FT-IR (KBr, cm⁻¹) selected bands:** 3463 (m, $\nu_{\text{O-H}}$), 3087 (m, ν_{CH}), 1613 (w, $\nu_{\text{C=C+C-N}}$), 1499–1487 (m), 1459 (m, $\nu_{\text{C=N}}$), 1448 (m), 1280–1251 (vs, $\nu_{\text{C-F}}$), 1168 (vs, $\nu_{\text{SO}_3\text{-as}}$), 1030 (vs, $\nu_{\text{SO}_3\text{-sym}}$), 842 (w), 789 (w, $\delta_{\text{C-C}}$), 761–750 (m, $\delta_{\text{CH}_{\text{loop}}}$), 639 (s), 576 (w), 518 (m). **MS (FAB+):** m/z (%) = 525 (34) ([M-OTf-H₂O+H]⁺), 391 (9) ([M-2OTf-2H]⁺), 374 (100) ([M-2OTf-H₂O-H]⁺). **Solubility:** soluble in water and acetone.



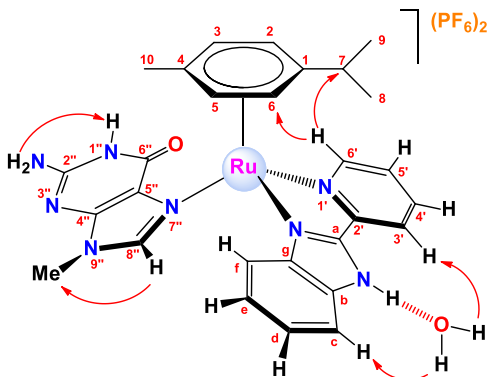
Synthesis of $[(\eta^6\text{-phoxet})\text{Ru}(\text{OH}_2)(\text{pybim})](\text{TfO})_2$, [4c](TfO)₂. The synthesis was performed as for **[4a](OTf)₂** using AgOTf (18.9 mg, 0.074 mmol) and $[(\eta^6\text{-phoxet})\text{RuCl}(\text{pybim})]\text{Cl}$, **[1c]Cl** (17.5 mg, 0.035 mmol). Orange-yellowish solid. Yield: not calculated. **M_r (C₂₂H₂₁F₆N₃O₉S₂Ru (H₂O)_{2.1}**) = 750.5664 g/mol. **Anal. Calcd for C₂₂H₂₁F₆N₃O₉S₂Ru (H₂O)_{2.1}:** C 33.51; H 3.22; N 5.33, S 8.13; **Found:** C 33.54; H 3.35; N 4.98, S 8.08. **¹H NMR (400 MHz, D₂O, 25 °C)** δ 9.62 (d, $J = 5.5$ Hz, 1H, H^{6'}), 8.37 – 8.28 (m, 2H, H^{4',3'}), 8.14 (d, $J = 8.1$ Hz, 1H, H^f), 7.89 – 7.80 (m, 2H, H^{5',c}), 7.75 – 7.60 (m, 2H, H^{e,d}), 6.65 – 6.56 (m, 2H, H^{5',3'}), 5.94 (d, $J = 6.6$ Hz, 1H, H² or H⁶), 5.85 (d, $J = 6.1$ Hz, 1H, H⁶ or H²), 5.75 (t, $J = 5.6$ Hz, 1H, H⁴), 4.01 – 3.96 (m, 2H, H⁷), 3.74 – 3.69 (m, 2H, H⁸) ppm. **¹³C{¹H} NMR (101 MHz, D₂O, 25 °C)** δ 156.3 (s, 1C, C^{6'}), 151.9 (s, 1C, C^a), 147.9 (s, 1C, C^{2'}), 142.0 (s, 1C, C^{4'}), 141.3 (s, 1C, C^g), 138.0 (s, 1C, C¹), 134.8 (s, 1C, C^b), 128.7 (s, 1C, C^{5'}), 127.2 (s, 1C, C^d), 126.1 (s, 1C, C^e), 124.0 (s, 1C, C^{3'}), 120.2 (q, $J = 317.2$ Hz, 2C, C^{OTf}), 117.9 (s, 1C, C^f), 114.8 (s, 1C, C^c), 93.6 (s, 1C, C³), 93.4 (s, 1C, C⁵), 72.0 (s, 1C, C⁷ or C⁸), 70.9 (s, 1C, C⁴), 63.1 (s, 1C, C²), 62.8 (s, 1C, C⁶), 59.7 (s, 1C, C⁸ or C⁷)

ppm. $^{19}\text{F}\{\text{H}\}$ NMR (376 MHz, D_2O , 25 °C) δ -79.3 (s, 6F, F^{CF_3}) ppm. FT-IR (KBr, cm^{-1}) selected bands: 3447 (m, $\nu_{\text{O-H}}$), 3086 (m, $\nu_{\text{C-H}}$), 1612 (w, $\nu_{\text{C=C+C-N}}$), 1527 (m), 1499-1486 (w), 1459 (m, $\nu_{\text{C=N}}$), 1448 (m), 1262 (vs, $\nu_{\text{C-F}}$), 1227-1168 (s, $\nu_{\text{SO}_3\text{-as}}$), 1031 (vs, $\nu_{\text{SO}_3\text{-sym}}$), 761-751 (m, δ_{CHoop}), 641 (s), 576 (w), 518 (m). MS (FAB+): m/z (%) = 453 (8) ($[\text{M}-2\text{OTf}]^+$), 435 (100) ($[\text{M}-2\text{OTf}-\text{H}_2\text{O}]^+$), 404 (25) ($[\text{M}-2\text{OTf}-\text{H}_2\text{O}-\text{CH}_2\text{OH}]^+$), 391 (85) ($[\text{M}-2\text{OTf}-\text{H}_2\text{O}-\text{CH}_2\text{CH}_2\text{OH}+\text{H}]^+$), 374 (17) ($[\text{M}-2\text{OTf}-\text{H}_2\text{O}-\text{OCH}_2\text{CH}_2\text{OH}]^+$), 297 (25) ($[\text{M}-2\text{OTf}-\text{H}_2\text{O}-\text{arene}]^+$). Solubility: soluble in water, acetone.



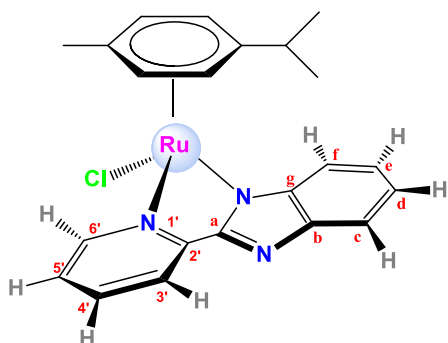
Synthesis of $[(\eta^6\text{-}\kappa^1\text{-phenoxyethanol})\text{Ru}(\text{pybim})](\text{BF}_4)_2$, [5c](BF₄)₂. In a 100 mL Schlenk flask protected from light, excess of AgBF₄ (73.9 mg, 0.380 mmol) was added under a nitrogen atmosphere to a solution of $[(\eta^6\text{-phoxet})\text{RuCl}(\text{pybim})]\text{Cl}$, [1c]Cl (50.8 mg, 0.101 mmol) in degassed methanol (10 mL). The suspension was stirred for 20 hours at room temperature. The AgCl was filtered off. The solvent was removed under vacuum and the solid residue was washed with diethylether (3×5 mL) and dried under vacuum, to produce a yellow solid. Yield: 38.1 mg (0.063 mmol, 62%). M_r (C₂₀H₁₉N₃O₂B₂F₈Ru) = 608.072 g/mol. Anal. Calcd for C₂₀H₁₉N₃O₂B₂F₈Ru·(AgBF₄)_{0.5}·(H₂O)·(CH₃OH): C 33.39; H 3.34; N 5.56; Found: C 33.51; H 3.52; N 5.80. ^1H NMR (400 MHz, CD₃OD, 25 °C) δ 9.78 (d, J = 5.6 Hz, 1H, H^{6'}), 8.40 (d, J = 4.1 Hz, 2H, H^{3',4'}), 8.25 (d, J = 8.2 Hz, 1H, H^f), 7.90 (dd, J = 9.3, 5.5 Hz, 1H, H^{5'}), 7.83 (d, J = 7.6 Hz, 1H, H^c), 7.69 (t, J = 7.1 Hz, 1H, H^e), 7.63 (t, J = 7.3 Hz, 1H, H^d), 6.72 (t, J = 6.0 Hz, 1H, H^{3 o H⁵), 6.68 (t, J = 6.0 Hz, 1H, H^{5 o H³), 6.17 (dd, J = 6.5, 1.8 Hz, 1H, H^{2 o H⁶), 5.97 (dd, J = 6.4, 1.8 Hz, 1H, H^{6 o H²), 5.75 (t, J = 5.5 Hz, 1H, H⁴), 4.10 (dd, J = 8.5, 3.8 Hz, 2H, H⁷), 3.79 – 3.73 (m, 2H, H⁸) ppm. $^{19}\text{F}\{\text{H}\}$ NMR (376 MHz, CD₃OD, 25 °C) δ -154.9 (s, ¹⁰B-F, BF₄⁻), -155.0 (s, ¹¹B-F, BF₄⁻) ppm. FT-IR (KBr, cm^{-1}) selected bands: 3097 (m, $\nu_{\text{C-H}}$), 1614 (s, $\nu_{\text{C=C+C-N}}$), 1530 (s), 1499-1486 (w), 1462-1450 (s, $\nu_{\text{C=N}}$), 1329 (w), 1272 (s, $\nu_{\text{C-O-Cas}}$), 1056 (vs, $\nu_{\text{C-F}}$), 910 (w, $\nu_{\text{C-Oas}}$), 762-751 (s, δ_{CHoop}), 666 (s, $\delta_{\text{O-Hoop}}$), 520 (w). MS (FAB+): m/z (%) = 434 (20) ($[\text{M}-2\text{BF}_4-\text{H}]^+$), 390 (35) ($[\text{M}-2\text{BF}_4-\text{H}-(\text{CH}_2\text{CH}_2\text{OH})+\text{H}]^+$). Solubility: soluble in water, methanol, dichloromethane and acetone.}}}}

Guanine-derivative



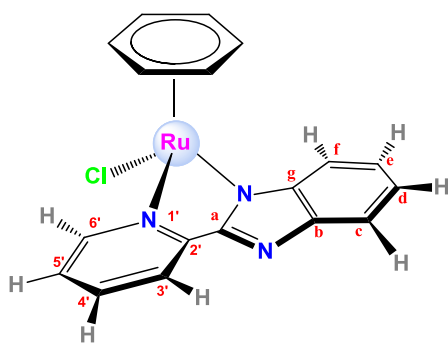
Synthesis of $[(\eta^6\text{-}p\text{-cymene})\text{Ru}(9\text{-MeG})(\text{pybim})](\text{PF}_6)_2$, [6a](PF₆)₂. In a 100 mL Schlenk flask $[(\eta^6\text{-}p\text{-cymene})\text{RuCl}(\text{pybim})]\text{BF}_4$, **[1a](BF₄)** (33.3 mg, 0.060 mmol) was dissolved in degassed water (12 mL) under a nitrogen atmosphere and the solution was stirred for 2 hours. 9-methylguanine, 9-MeG, (11.1 mg, 0.067 mmol) was then added and the mixture was heated at 37 °C with stirring for 16 hours. The mixture was filtered to remove insoluble impurities. The solution was concentrated and (NH₄)PF₆ (26 mg, 0.160 mmol) was added to precipitate a solid, which was filtered and washed with cold water (5 mL) and with diethylether (3×5 mL), and dried under vacuum to produce a yellow product. Yield: 23 mg (0.026 mmol, 43%). **M_r** ($\text{C}_{28}\text{H}_{30}\text{F}_{12}\text{N}_8\text{OP}_2\text{Ru}$) = 885.5964 g/mol. **Anal. Calcd for** $\text{C}_{28}\text{H}_{30}\text{F}_{12}\text{N}_8\text{OP}_2\text{Ru}\cdot\text{H}_2\text{O}$: C 37.22; H 3.57; N 12.4; **Found:** C 37.09; H 3.97; N 12.35. **¹H NMR (400 MHz, DMSO-d₆, 25 °C)** δ 14.98 (s, 1H, H^{N-H(Im)}), 11.05 (s, 1H, -NH, H^{1''}), 9.98 (d, *J* = 5.7 Hz, 1H, H^{6'}), 8.32 (m, *J* = 6.6 Hz, 3H, H^{3',4',f}), 7.90 (d, *J* = 7.8 Hz, 1H, H^c), 7.82 (t, *J* = 5.0 Hz, 1H, H^{5'}), 7.69 (t, *J* = 7.6 Hz, 2H, H^{d,e}), 6.83 (s, 2H, -NH₂, H^{2''}), 6.76 (s, 2H, H^{8''} and H² or H⁶), 6.51 (d, *J* = 3.6 Hz, 1H, H³ or H⁵), 6.37 (s, 1H, H⁶ or H²), 6.13 (d, *J* = 5.4 Hz, 1H, H⁵ or H³), 3.27 (s, 3H, -NMe), 2.44 – 2.30 (m, 1H, H⁷), 1.86 (s, 3H, H¹⁰), 0.88 (d, *J* = 6.9 Hz, 3H, H⁹ or H⁸), 0.67 (d, *J* = 6.4 Hz, 3H, H⁸ or H⁹). **¹⁹F{¹H} NMR (376 MHz, DMSO-d₆, 25 °C)** δ -70.5 (d, PF₆⁻, ¹J_{P-F} = 713.0 Hz) ppm. **FT-IR (KBr, cm⁻¹) selected bands:** 3630 (w, v_{NH2}), 3364 (m, v_{NH2}), 3154 (m, v_{NH}), 2965 (w, v_{-CH}), 1702–1675 (s, v_{C=O}), 1638 (s, δ_{NH}), 1608–1582 (s, v_{C=C + C-N}), 1500, 1488 (m), 1461 (s, v_{C=N}, δ_{NHip}), 1449 (w), 1177 (m), 845 (vs, v_{P-Fsym}), 779 (w, δ_{C-C}), 740 (s, δ_{CHoop}), 637 (w, δ_{NHoop}), 558 (s, v_{P-Fas}). **MS (FAB+):** m/z (%) = 595 (18) ([M-2PF₆-H]⁺), 430 (42) ([M-2PF₆-H-MeG]⁺). **Molar conductivity (H₂O):** 243 S·cm²·mol⁻¹. **Solubility:** soluble in methanol, water, acetone, DMSO, and partially soluble in dichloromethane.

Neutral derivatives



Synthesis of $[(\eta^6\text{-}p\text{-cymene})\text{RuCl}(\text{pybim}')]$, [7a]. In a 100 mL Schlenk flask, NaHCO₃ (84.6 mg, 1 mmol) was added under a nitrogen atmosphere to a solution of $[(\eta^6\text{-}p\text{-cymene})\text{RuCl}(\text{pybim})]\text{Cl}$, **[1a]Cl** (100.3 mg, 0.200 mmol) in a mixture of degassed dichloromethane/methanol (5:1, 12 mL). The suspension was stirred for 20 hours at room temperature. The NaCl formed as a byproduct was filtered off. The solvent was removed under vacuum and the resulting solid residue was washed with *n*-hexane (3×5 mL) and dried under vacuum, to produce a yellow solid. Yield: 63 mg (0.135 mmol, 68%). **M_r** ($\text{C}_{22}\text{H}_{22}\text{ClN}_3\text{Ru}\cdot(\text{H}_2\text{O})_{1.8}$) = 464.9586 g/mol. **Anal. Calcd for** $\text{C}_{22}\text{H}_{22}\text{ClN}_3\text{Ru}\cdot(\text{H}_2\text{O})_{1.8}$: C 53.13; H 5.19; N 8.45; **Found:** C 53.10; H 5.25; N 8.46. **¹H NMR (400 MHz, DMSO-d₆, 25 °C)** δ 9.37 (d, *J* = 5.2 Hz, 1H, H^{6'}), 8.10 (m, 1H, H^{3'}), 8.05 (m, 1H, H^{4'}), 7.77 (d, *J* = 7.9 Hz, 1H, H^f), 7.58 (d, *J* = 8 Hz, 1H, H^c), 7.48 (m, 1H, H^{5'}), 7.17 (m, 1H, H^e), 7.10 (m, 1H, H^d), 6.17 (d, *J* = 6.0 Hz, 1H, H² or H⁶), 6.07 (d, *J* = 6.1 Hz, 1H, H⁶ or H²), 5.96 (d, *J* = 6.0 Hz, 1H, H³ or H⁵), 5.93 (d, *J* = 6.1 Hz, 1H, H⁵ or H³), 2.34 (sept, *J* = 6.9 Hz, 1H, H⁷), 2.17 (s, 3H, H¹⁰), 0.81 (d, *J* = 6.9 Hz, 3H, H⁸ or H⁹), 0.81 (d, *J* = 6.9 Hz, 3H, H⁹ or H⁸) ppm. **¹³C{¹H} NMR (101 MHz, DMSO-d₆, 25 °C)** δ 157.81

(s, 1C, C^a), 154.97 (s, 1C, C^{6'}), 152.47 (s, 1C C^{2'}), 146.93 (s, 1C, C^b), 145.28 (s, 1C, C^g), 138.89 (s, 1C, C^{4'}), 123.94 (s, 1C, C^{5'}), 120.95 (s, 1C, C^e), 120.88 (s, 1C, C^{3'}), 120.21 (s, 1C, C^d), 118.96 (s, 1C, C^c), 115.29 (s, 1C, C^f), 102.29 (s, 1C, C⁴), 100.02 (s, 1C, C¹), 85.02 (s, 1C, C⁶ or C²), 83.30 (s, 1C, C² or C⁶), 82.60 (s, 1C, C⁵ or C³), 78.39 (s, 1C, C³ or C⁵), 30.47 (s, 1C, C⁷), 21.60 (s, 2C, C^{8,9}), 18.61 (s, 1C, C¹⁰). **FT-IR (KBr, cm⁻¹) selected bands:** 3052 (w, ν_{CH}), 2963 (w, ν_{CH}), 1611 (s, ν_{C=C + C-N}), 1517 (m), 1456-1445 (s, ν_{C=N}), 1386 (w, δ_{CH3}), 1333 (m), 1226 (m), 1155 (m), 790 (w, δ_{C-C}), 747 (s, δ_{CHoop}). **MS (FAB+):** m/z (%) = 466 (45) ([M+H]⁺), 430 (61) ([M-Cl]⁺). **Molar conductivity (H₂O):** 103 S·cm²·mol⁻¹. **Solubility:** soluble in methanol, water and DMSO. Partially soluble in acetone.



Synthesis of [(\eta⁶-benzene)RuCl(pybim')], [7b]. The synthesis was performed as for [7a] using NaHCO₃ (114.3 mg, 1.360 mmol) and [(\eta⁶-benzene)RuCl(pybim')]Cl, [1b]Cl (50.1 mg, 0.101 mmol) in a mixture of degassed acetone/methanol (4:1, 10 mL). Brown-yellowish solid. Yield: 27.5 mg (0.067 mmol, 78%). **M_r (C₁₈H₁₄ClN₃Ru)** = 408.8514 g/mol. **Anal. Calcd for C₁₈H₁₄ClN₃Ru·(NaCl)_{0.5}·(H₂O)₂:** C 45.6; H 3.83; N 8.86; **Found:** C 45.86; H 3.78; N 8.47. **¹H NMR (400 MHz, DMSO-d₆, 25 °C)** δ 9.48 (d, J = 5.6 Hz, 1H, H^{6'}), 8.11 (d, J = 7.0 Hz, 1H, H^{3'}), 8.09 – 8.02 (m, 1H, H^{4'}), 7.79 (d, J = 8.0 Hz, 1H, H^f), 7.59 (d, J = 7.9 Hz, 1H, H^c), 7.53 – 7.45 (m, 1H, H^{5'}), 7.18 (dd, J = 11.0, 4.1 Hz, 1H, H^e), 7.11 (dd, J = 11.0, 4.0 Hz, 1H, H^d), 6.12 (s, 6H, H^{bz}) ppm. **¹³C{¹H} NMR (101 MHz, DMSO-d₆, 25 °C)** δ 157.84 (s, 1C, C^a), 155.18 (s, 1C, C^{6'}), 152.55 (s, 1C C^{2'}), 146.78 (s, 1C, C^b), 145.35 (s, 1C, C^g), 139.01 (s, 1C, C^{4'}), 123.91 (s, 1C, C^{5'}), 121.05 (s, 1C, C^e), 120.99 (s, 1C, C^{3'}), 120.28 (s, 1C, C^d), 118.95 (s, 1C, C^c), 115.37 (s, 1C, C^f), 84.22 (s, C^{bz}) ppm. **FT-IR (KBr, cm⁻¹) selected bands:** 3074, 3059 (w, ν_{CH}), 2926 (w, ν_{CH}), 1615 (s, ν_{C=C + C-N}), 1564 (w), 1521 (m, ar_{C-C}), 1459 (w), 1445 (vs, ν_{C=N}), 1385 (m), 1335 (m), 1278 (m), 1024 (w), 838 (m), 822 (m, δ_{C-C}), 748 (s, δ_{CHoop}), 698 (w). **MS (FAB+):** m/z (%) = 410 (9) ([M+H]⁺), 374 (63) ([M+H-Cl]⁺). **Molar conductivity (H₂O):** Λ_M was not measured due to low solubility in water and acetonitrile. **Solubility:** soluble in methanol, acetone, chloroform and dichloromethane. Partially soluble in water and insoluble in acetonitrile.

4. BIBLIOGRAPHY

- (1) Martínez-Alonso, M.; Busto, N.; Jalón, F. A.; Manzano, B. R.; Leal, J. M.; Rodríguez, A. M.; García, B.; Espino, G. *Inorg. Chem.* **2014**, *53*, 11274–11288.
- (2) Busto, N.; Martínez-Alonso, M.; Leal, J. M.; Rodríguez, A. M.; Domínguez, F.; Acuña, M. I.; Espino, G.; García, B. *Organometallics* **2015**, *34*, 319–327.
- (3) Süss-Fink, G. *Dalt. Trans.* **2010**, *39*, 1673–1688.
- (4) Bratsos, I.; Jedner, S.; Gianferrara, T.; Alessio, E. *Chim. Int. J. Chem.* **2007**, *61*, 692–697.
- (5) Sava, G.; Bergamo, A.; Dyson, P. J. *Dalt. Trans.* **2011**, *40*, 9069–9075.
- (6) Fricker, S. P. *Dalt. Trans.* **2007**, 4903–4917.
- (7) Wheate, N. J.; Walker, S.; Craig, G. E.; Oun, R. *Dalt. Trans.* **2010**, *39*, 8113–8127.
- (8) Mock, C.; Puscasu, I.; Rauterkus, M. J.; Tallen, G.; Wolff, J. E. .; Krebs, B. *Inorganica Chim. Acta* **2001**, *319*, 109–116.
- (9) Casas, J. S.; Castiñeiras, A.; García-Martínez, E.; Parajó, Y.; Pérez-Parallé, M. L.; Sánchez-González, A.; Sordo, J. *Zeitschrift für Anorg. und Allg. Chemie* **2005**, *631*, 2258–2264.
- (10) Stepanenko, I. N.; Novak, M. S.; Gerhard, M.; Roller, A.; Hejl, M.; Arion, V. B.; Jakupc, M. A.; Keppler, B. K. *Inorg. Chem.* **2011**, *50*, 11715–11728.
- (11) Ginzinger, W.; Mu, G.; Arion, V. B.; Jakupc, M. A.; Roller, A.; Galanski, M.; Reithofer, M.; Berger, W.; Keppler, B. K. *J. Med. Chem.* **2012**, *55*, 3398–3413.
- (12) Yellol, G. S.; Donaire, A.; Yellol, J. G.; Vasylyeva, V.; Janiak, C.; Ruiz, J. *Chem. Commun.* **2013**, *49*, 11533–11535.
- (13) Bennett, M. A.; Smith, A. K. *J. Chem. Soc. Dalt. Trans.* **1974**, 233–241.
- (14) Therrien, B. *Coord. Chem. Rev.* **2009**, *293*, 493–519.
- (15) Zeng, F.; Yu, Z. *Organometallics* **2008**, *27*, 2898–2901.
- (16) Lastra-Barreira, B.; Díez, J.; Crochet, P.; Fernández, I. *Dalt. Trans.* **2013**, *42*, 5412–5420.
- (17) Musgrave, T. R.; Lin, T. S. *J. Coord. Chem.* **1973**, *2*, 323–324.
- (18) Pretsch, E.; Bühlmann, P.; Affolter, C.; Herrera, A.; Martínez, R. *Determinación estructural de compuestos orgánicos*; **2005**. Orig.; MASSON, S.A.: Barcelona, 2005.
- (19) Nakamoto, K. *Infrared and Raman Spectra of Inorganic and Coordination Compounds*; Fourth.; John Wiley and Sons, **1986**.
- (20) Heyns, A. M. *Spectrochímica Acta A* **1977**, *33*, 315–322.
- (21) Angelici, R. J. In *Técnicas y Síntesis en Química Inorgánica*; Editorial Reverté, S.A., **1979**; p. 243.
- (22) Hay, B. P.; Custelcean, R. *Cryst. Growth Des.* **2009**, *9*, 2539–2545.
- (23) Pérez, J.; Riera, L. *Chem. Commun.* **2008**, 533–543.
- (24) Veeramasuneni, S.; Hu, Y.; Miller, J. D. *Surf. Sci.* **1997**, *382*, 127–136.
- (25) Schuecker, R.; John, R. O.; Jakupc, M. A.; Arion, V. B.; Keppler, B. K. *Organometallics* **2008**, *27*, 6587–6595.

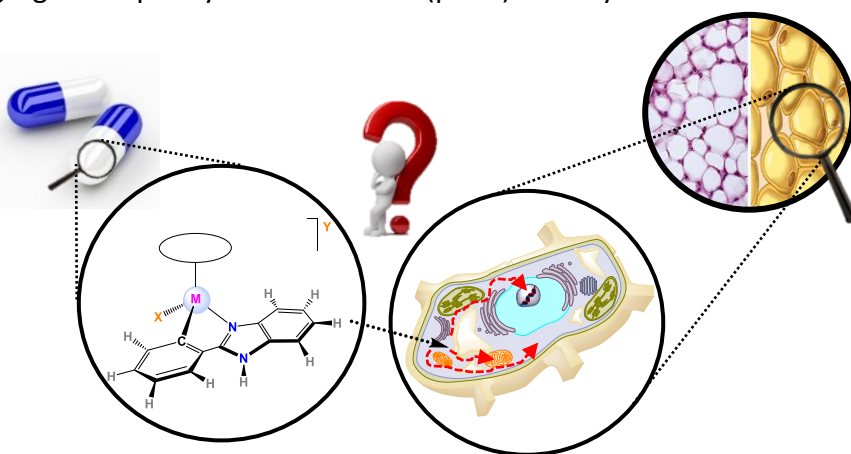
- (26) Martin, R. B. In *Cisplatin Chemistry and Biochemistry of a Leading Anticancer Drug*; Verlag Helvetica Chimica Acta: Zürich, **2006**; pp. 181–205.
- (27) Habtemariam, A.; Melchart, M.; Fernández, R.; Parsons, S.; Oswald, I. D. H.; Parkin, A.; Fabbiani, F. P. A.; Davidson, J. E.; Dawson, A.; Aird, R. E.; Jodrell, D. I.; Sadler, P. J. *J. Med. Chem.* **2006**, *49*, 6858–6868.
- (28) Peacock, A. F. A.; Sadler, P. J. *Chem. An Asian J.* **2008**, *3*, 1890–1899.
- (29) Kostrhunova, H.; Florian, J.; Novakova, O.; Peacock, A. F. A.; Sadler, P. J.; Brabec, V. *J. Med. Chem.* **2008**, *51*, 3635–3643.
- (30) Chen, H.; Parkinson, J. A.; Morris, R. E.; Sadler, P. J. *J. Am. Chem. Soc.* **2003**, *125*, 173–186.
- (31) Ronconi, L.; Sadler, P. J. *Coord. Chem. Rev.* **2007**, *251*, 1633–1648.
- (32) CHISWELL, B.; LIOSS, Fr.; MORRIS, B. S. *Inorg. Chem.* **1964**, *3*, 110–113.
- (33) Stupka, G.; Gremaud, L.; F. Williams, A. *Helv. Chim. Acta* **2005**, *88*, 487–495.

CHAPTER 2.

Ru(II), Ir(III) AND Rh(III) HALF-SANDWICH COMPLEXES BEARING 2- PHENYLBENZIMIDAZOLE ANCILLARY LIGANDS: SYNTHESIS, CHARACTERIZATION AND ANTICANCER PROPERTIES

CHAPTER 2. Ru(II), Ir(III) AND Rh(III) ORTHOMETALATED HALF-SANDWICH COMPLEXES BEARING 2-PHENYLBENZIMIDAZOLE ANCILLARY LIGANDS: SYNTHESIS, CHARACTERIZATION AND ANTICANCER PROPERTIES

ABSTRACT: In this chapter a family of 9 new complexes of general formulae $[\text{Ru}(\eta^6-p\text{-cymene})(\kappa^2\text{-C},N\text{-pbim})\text{Cl}]$, $[\text{M}(\eta^5\text{-Cp}^*)(\kappa^2\text{-C},N\text{-pbim})\text{Cl}]$, $[\text{Ru}(\eta^6\text{-arene})(\kappa^2\text{-C},N\text{-pbim})\text{X}]Y$ and $[\text{M}(\eta^5\text{-Cp}^*)(\kappa^2\text{-C},N\text{-pbim})\text{X}]Y$ ($\text{M} = \text{Ir, Rh}$; $\text{X} = \text{leaving group}$; $\text{Y} = \text{counterion}$) bearing the orthometalating ligand 2-phenylbenzimidazole (pbim) was synthesized with the main objective of testing their anticancer activity against different cancer cells. For this reason, two main key features were modified: the metal fragment (iridium



half-sandwich complexes are tested^{5,6,1} to be more effective as anticancer drugs) and the leaving group (chloride ion undergoes fast hydrolysis and it is slowed down by the substitution with other leaving groups such as pyridine⁷, PTA and Melm). The cytotoxic activity was evaluated for all the complexes, obtaining excellent results for most of them. Therefore, mechanistic studies were carried out to determine the possible pathways of cell death.

CONTEXT: Recently, several groups have studied the anticancer activity of cyclometalated Ru(II), Rh(III) and Ir(III) half-sandwich complexes. In particular, P. J. Sadler and coworkers have widely studied the cytotoxic activity of half-sandwich orthometalated complexes, bearing phenylpyridinate (ppy⁻) as the chelating ligand, both with Ru(II) and Ir(III).^{1,2} Moreover, the group of J. Ruiz has made progress in the design and study of Ru(II), Rh(III) and Ir(III) half-sandwich complexes with cyclometalated N-alkyl-benzimidazole ligands of general formula $[(\eta^5\text{-Cp}^*)\text{MCl}(\text{C}^\text{N})]$ ($\text{M} = \text{Rh, Ir}$) or $[(\eta^6\text{-p-cym})\text{RuCl}(\text{C}^\text{N})]$ to conclude that those complexes with N-butyl groups are in general more active in all the evaluated cancer cell lines than those bearing N-methyl and N-benzyl groups.³ In an additional contribution the same group has studied the effect of introducing several substituents on the phenyl unit of the C^N ligand to conclude that the new derivatives exhibit a moderate rise in their cytotoxicity in comparison to the unsubstituted compounds, and that ruthenium complexes are more potent than their iridium analogs.⁴

1. RESULTS AND DISCUSSION

1.1. Synthesis

The new complexes were synthesised from the respective metal chlorido-bridged dimers $[\text{Ru}(\eta^6\text{-}p\text{-cym})(\mu\text{-Cl})\text{Cl}]_2$, $[\text{Rh}(\eta^5\text{-Cp}^*)(\mu\text{-Cl})\text{Cl}]_2$ and $[\text{Ir}(\eta^5\text{-Cp}^*)(\mu\text{-Cl})\text{Cl}]_2$, which in turn were prepared by reaction of the metal chloride salt ($\text{MCl}_3\cdot n\text{H}_2\text{O}$) with the corresponding diene (α -phellandrene for the ruthenium dimer, and 1,2,3,4,5-pentamethylcyclopentadiene for the iridium and rhodium dimers) as illustrated in Fig. 1.^{8,9}

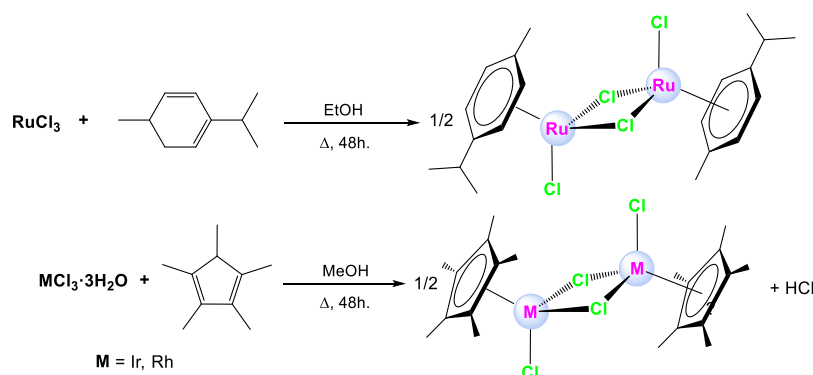


Fig. 1. Schematic synthesis of the dimers used as starting materials.

The complexes can be divided in two groups: neutral and cationic complexes.

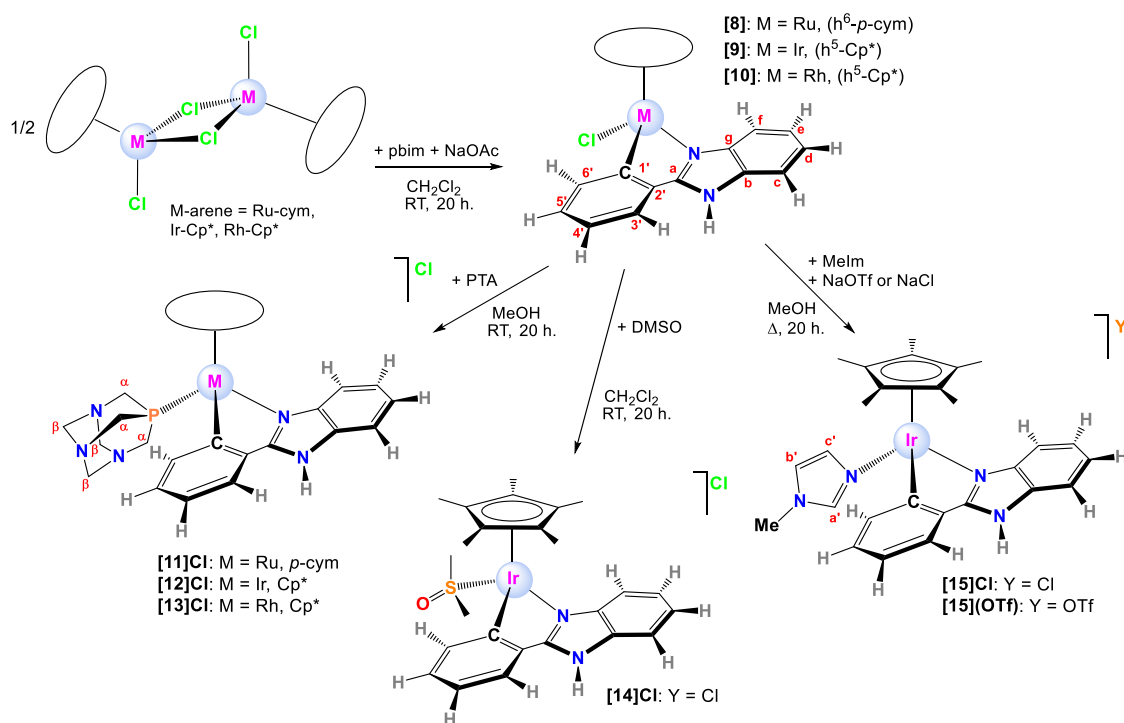


Fig. 2. Schematic synthesis of the cyclometalated complexes.

Neutral complexes

The neutral complexes of general formula $[(\eta^6-p\text{-cymene})\text{RuCl}(\kappa^2\text{-C,N-pbim})]$ (**[8]**) and $[(\eta^5\text{-Cp}^*)\text{MCl}(\kappa^2\text{-C,N-pbim})]$ (**[9]** and **[10]**) where M = Ir, Rh, were prepared at room temperature by the reaction of the starting materials with the ligand pbim in the presence of NaOAc to deprotonate or activate the C-H bond and using dichloromethane as the solvent.

Cationic complexes

The reaction between the neutral complexes **[8]**, **[9]** and **[10]** and 1,3,5-traza-7-phosphaadamantane (PTA) at room temperature and using methanol as the solvent yielded monocationic compounds of general formulae $[(\eta^6-p\text{-cymene})\text{Ru(PTA)}(\kappa^2\text{-C,N-pbim})]\text{Cl}$ (**[11]Cl**) and $[(\eta^5\text{-Cp}^*)\text{M(PTA)}(\kappa^2\text{-C,N-pbim})]\text{Cl}$ (**[12]Cl** and **[13]Cl**), where M = Ir, Rh.

The DMSO-derivative of formula $[(\eta^5\text{-Cp}^*)\text{Ir(DMSO)}(\kappa^2\text{-C,N-pbim})]\text{Cl}$ (**[14]Cl**) was prepared at room temperature by reaction of the neutral complex **[9]** with DMSO (10 eq.) and using dichloromethane as the solvent. Likewise, the reaction of **[9]** with N-methylimidazole (MeIm) in the presence of the corresponding sodium salt (NaCl or NaOTf) and using refluxing methanol yielded the MeIm-derivative complexes with formulae $[(\eta^5\text{-Cp}^*)\text{Ir(MeIm)}(\kappa^2\text{-C,N-pbim})]\text{Y}$, (**[15]Cl** and **[15]OTf**), where Y = Cl⁻ or OTf⁻.

PTA and MeIm are P- and N-donor neutral ligands extensively applied in anticancer drugs.^{10,11,12} In this work, the chloride replacement by PTA and MeIm was performed to improve the water-solubility of the parent complexes, turning them into cationic derivatives and to slow down the hydrolysis process, which is very fast for the chlorido precursors. PTA is a cage-type phosphine ligand of the adamantane type, with N atoms in positions 1, 3 and 5, and a P atom in 7 and unlike other phosphines, it is air-stable.¹³ The coordination of the monodentate ligand with the metal preferably occurs through the soft phosphorous atom instead through the hard nitrogen atoms.¹⁴ Since PTA is able to undergo protonation and deprotonation,¹⁵ DNA damage with PTA-organometallic complexes of the type $[(\eta^6-p\text{-cymene})\text{RuCl}_2(\kappa^1\text{-P-PTA})]$ has been proved to be pH-dependent. Protonated PTA seems to be the active drug in hypoxic tumour cells (typically at low pH).^{12,16} N-Methylimidazole (MeIm) is an aromatic electron-rich N-donor and strong σ-donor ligand alkylated in N1¹⁷, which mimics the histidine moiety in some macromolecules such as albumin or transferrin.¹⁸

All the complexes were isolated in moderate yields for the neutral complexes (from 42% to 65%) and in good yields for the cationic derivatives (from 68% to 83%) as the corresponding racemates (R_M or S_M) in the form of yellow, orange or white powders.

1.2. Characterization

All the complexes have been fully characterised by NMR spectroscopy, IR spectroscopy, positive fast atom bombardement (FAB⁺) mass spectrometry, molar conductivity and elemental analysis.

1.2.1. NMR

The ¹H NMR spectra of neutral complexes ([8], [9] and [10]) were recorded in CDCl₃ and DMSO-d₆ at 25 °C. The metal-ligand coordination was proved by the downfield shift of the signals of the pbim ligand. The spectra show three typical areas: the amino area (N-H signal), the aromatic area (chelating ligand and arene) and the aliphatic area (methyl groups of Cp* and *p*-cym). The hydrogen atoms of the amino group of benzimidazole are really deshielded with chemical shifts ranging from 11 to nearly 16 ppm. The *p*-cym derivatives show an ABCD spin system for the aromatic resonances and two doublets for the diastereotopic methyls of *i*Pr, whereas the Cp* derivatives display a singlet for the five equivalent methyl groups of the ring. On the other hand, due to the high coordination capacity of DMSO, the Cl⁻ ligand was replaced with DMSO-d₆ in all the chlorido complexes, when the respective NMR were performed in DMSO-d₆, being the process slow for ruthenium (days), but fairly fast (20 min) for iridium and rhodium (see [Cl⁻/DMSO SUBSTITUTION](#) below).

The ¹H NMR spectra of cationic complexes were recorded in CDCl₃, DMSO-d₆ and D₂O at 25 °C. When the spectrum of [14]Cl⁺ ([[η⁵-Cp*])Ir(DMSO)(κ²-C,N-pbim)]Cl) was recorded in D₂O, the coordination of DMSO to the metal centre was clear, since two resonances were observed for the **diastereotopic** methyls at 2.94 and 2.41 ppm. The PTA derivatives ([11]Cl, [12]Cl and [13]Cl) show a characteristic pattern of signals for the methylene groups. 2D COSY and 2D NOESY experiments allowed to recognize a multiplet around 3.50 ppm for the AB spin system of diastereotopic and geminal PCH₂N protons (H^α), and also two doublets between 4.0 and 4.3 ppm for the AX spin system formed by the intrinsically inequivalent NCH₂N protons (axial and equatorial orientations, H^{B_{ax}} and H^{B_{eq}}) (see Fig. 3). Regarding the chemical shifts, H^β hydrogens are more deshielded, since they are placed between two nitrogen atoms, whereas H^α are placed between a nitrogen atom and a phosphorous atom. The latter is less electronegative than the former and consequently, the signals are not as deshielded as those of H^β (see Table 1).

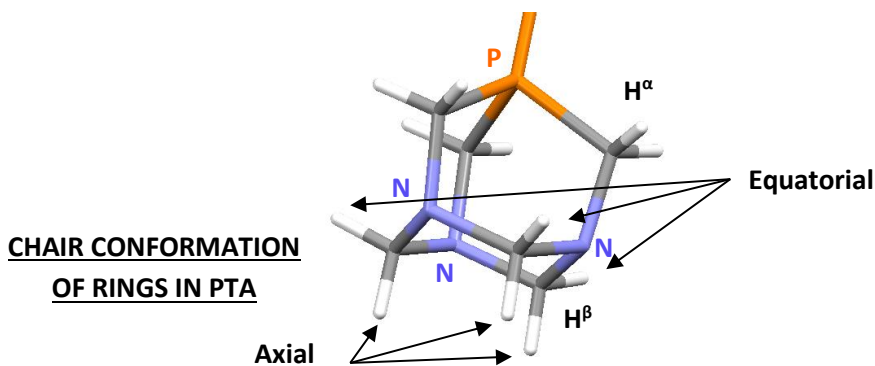


Fig. 3. PTA ligand conformation with N atoms labeled in blue and the P atom labeled in orange.

Table 1. Comparison of chemical shifts, multiplicity, integration and coupling constants for complexes [11]Cl, [12]Cl and [13]Cl in the ^1H and $^{31}\text{P}[^1\text{H}]$ NMR spectra recorded in CDCl_3 at 25 °C.

Complex	$\text{H}^{\beta\text{ax}}$	$\text{H}^{\beta\text{eq}}$	H^α	P
[11]Cl	4.20 ppm d, $J = 13.3 \text{ Hz}$, 3H	4.05 ppm d, $J = 12.9 \text{ Hz}$, 3H	3.46 ppm ABq, 6H, $\Delta\delta_{AB} = 0.03$, $J_{AB} = 15.7 \text{ Hz}$	-33.0 ppm s, 1P
[12]Cl	4.31 ppm d, $J = 12.7 \text{ Hz}$, 3H	4.02 ppm d, $J = 12.9 \text{ Hz}$, 3H	3.45 ppm ABq, 6H, $\Delta\delta_{AB} = 0.04$, $J_{AB} = 15.7 \text{ Hz}$	-71.9 ppm s, 1P
[13]Cl	4.30 ppm d, $J = 13.1 \text{ Hz}$, 3H	4.09 ppm d, $J = 13.8 \text{ Hz}$, 3H	3.52 ppm ABq, 6H, $\Delta\delta_{AB} = 0.13$, $J_{AB} = 15.5 \text{ Hz}$	-36.1 ppm d, ${}^1J_{P-\text{Rh}} = 145.5 \text{ Hz}$, 1P

The ^1H NMR spectra of the Melm derivatives ([15]Cl and [15]OTf) in CDCl_3 present, apart from the NH deshielded peak of pbim, a characteristic singlet for the N-Me of Melm, which is deshielded in relation to the free Melm (approximately $\Delta\delta = 0.4$ -0.5 ppm).

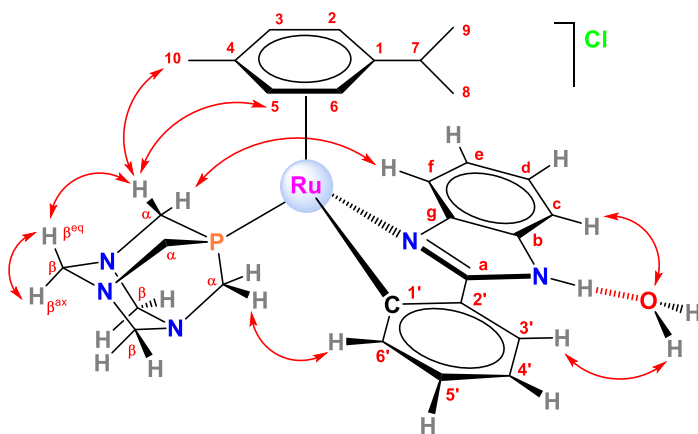


Fig. 4. NOE interactions observed in the ^1H - ^1H NOESY spectrum of [11]Cl.

Bidimensional ^1H - ^1H NOESY spectra of most of both the neutral and cationic complexes, showed NOE cross peaks between residual water and H^c and $\text{H}^{3'}$, suggesting a hydrogen-bonding interaction of the N-H group of the ligand with a water molecule. The ^1H - ^1H NOESY spectra of the PTA derivatives ([11]Cl, [12]Cl and [13]Cl) feature NOE

cross peaks between the methylenes H^α of PTA and the bidentate ligand as well as the arene (see Fig. 4).

The ¹H-¹H NOESY spectra of the Melm derivatives ([15]Cl and [15]OTf) show NOE cross-peaks between the Melm and the ancillary ligand or the Cp*.

The ¹³C{¹H} NMR spectra of all the complexes confirm the anticipated structures. The most relevant feature in every case is the presence of a highly deshielded peak for the cyclometalated carbon atom (C^{1'}) of the C≡N ligand (see Table 2). These resonances are observed as singlets for [8], [9], [12]Cl, [15]Cl and [15]OTf and as a doublet or a multiplet for the rest of the complexes due to scalar ¹³C-³¹P and ¹³C-¹⁰¹Rh couplings.

Table 2. Chemical shifts of the signal C^{1'} for the different complexes.

Comp.	δ (ppm)
	C ^{1'}
[8] ^b	177.3 (s)
[9] ^a	164.2 (s)
[10] ^a	170.5 (d, ¹ J _{C-Rh} = 31.1)
[11]Cl ^b	168.1 (d, ² J _{C-P} = 23.8 Hz)
[12]Cl ^b	146.6
[13]Cl ^b	165.1 (dd, ¹ J _{C-Rh} = 31.5 and ² J _{C-P} = 8.8 Hz)
[15]Cl ^b	158.2
[15]OTf ^b	158.6

^a Spectra recorded in DMSO-d₆.

^b Spectra recorded in CDCl₃.

The ³¹P{¹H} NMR spectra were recorded in CDCl₃ for the PTA-derivatives. Complexes [11]Cl and [12]Cl showed singlets, whereas [13]Cl showed a doublet related to the Rh-P coupling (¹J_{Rh-P} = 145.5 Hz). The resonances appear at $\delta_{[11]Cl}$ = -33.0 ppm; $\delta_{[12]Cl}$ = -71.9 ppm and $\delta_{[13]Cl}$ = -36.1 ppm (see Table 1).

The ¹⁹F{¹H} NMR spectrum of the monocationic complex [15]OTf showed a singlet for triflate at -78.3 ppm.

1.2.2. Mass Spectra

The FAB⁺ mass spectra of the complexes exhibit characteristic sets of peaks in agreement with the isotopic distribution models: [M]⁺ (only for [8]), [M-Cl]⁺ fragments for neutral complexes, [M-DMSO]⁺ for the DMSO-substituted derivatives ([14]Cl as well as the neutral complexes, since they were dissolved in DMSO), and [M-Y]⁺ fragment for the cationic complexes, where Y is the leaving group.

1.2.3. IR Spectra

The infrared spectra present characteristic peaks for the normal vibrational modes of the corresponding rings $\nu_{C=N}$, $\nu_{C=C}$ and $\delta_{CH_{oop}}$, as well as peaks for ν_{N-H} in the

benzimidazole moiety. In addition, the PTA derivatives exhibit a set of signals in the interval 1200-900 cm⁻¹ corresponding to the ν_{C-N} and ν_{P-C} vibration modes.¹⁹ The DMSO-derivative shows very strong and diagnostic peaks, $\nu_{S=O}$, ν_{C-S} at 1117 and 746 cm⁻¹ respectively.^{20,21} Moreover, three characteristic bands are detected for the OTf anion in **[15]OTf**, ν_{C-F} , ν_{SO_3-as} , ν_{SO_3-sym} at 1283-1223, 1154 and 1028 cm⁻¹ respectively.^{20,21,22}

1.2.4. Molar Conductivity

The molar conductivity (Λ_m) for the PTA and Melm derivatives (see Table 3) was measured in aqueous solutions (10⁻³ M) at room temperature (20 - 22 °C). The experimental values of complexes **[11]Cl-[13]Cl**, turned out to be lower than those expected for 1:1 electrolytes,²³ which suggest the formation of ion pairs. Complex **[15]Cl** presents, however, a higher conductivity value than its PTA counterpart **[12]Cl**, concluding that in this case, ion-pairing is not so favoured. The low water-solubility complex **[15]OTf** results in an anomalous conductivity value. Nonetheless, this fact confirms again the great solubility differences when the counterion is changed.

Table 3. Molar conductivity values for complexes measured in water.

Complex	Solvent	Λ_m (S·cm ² ·mol ⁻¹)
[11]Cl	H ₂ O	95.1
[12]Cl	H ₂ O	87.0
[13]Cl	H ₂ O	96.7
[15]Cl	H ₂ O	108.5
[15]OTf	H ₂ O	51.9*

*The complex was not completely soluble in water.

1.2.5. X Ray Diffraction

Single crystals suitable for X-ray diffraction analysis were obtained for **[8]** by slow evaporation of a solution in CH₂Cl₂, for **[9]** (unsuitable to published) by slow diffusion of toluene in DMF and for **[11](PF₆)** by slow evaporation of a solution in a mixture of MeOH and an aqueous saturated solution of (NH₄)PF₆. As far as we know, the latter is the first crystal structure reported for a Ru(II) arene complex with a cyclometallated (κ^2-C,N) ligand and a phosphine in their coordination sphere.

The ORTEP diagrams for complexes **[8]**, **[9]** and **[11](PF₆)** are represented in Fig. 5 and the unit cells show the two expected enantiomers (R_{Ru} and S_{Ru} or R_{Ir} and S_{Ir}) with the pseudooctahedral three-legged piano-stool geometry and the metal π-bonded to the η⁶-p-cymene or η⁵-Cp*. Moreover, all the complexes exhibit C₁ local symmetry. Selected bond lengths and angles with estimated standard deviations are collected only for **[8]**, and **[11](PF₆)** in Table 4, and crystallographic refinement parameters are given in Table 5 for these complexes.

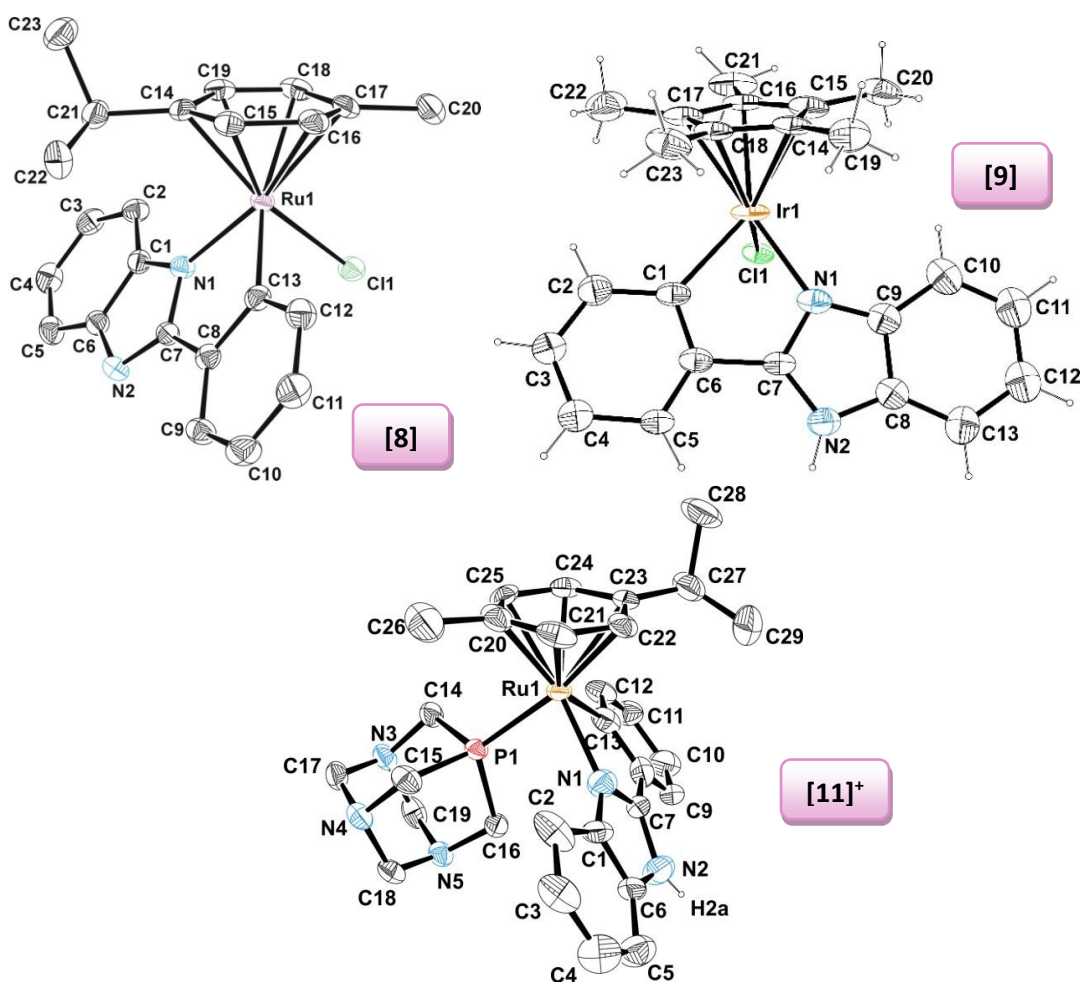


Fig. 5. ORTEP diagrams for complexes [8], [9] and [11]⁺. Thermal ellipsoids at 30% probability.

The Ru-Cl distance for [8] is in the upper limit of the range typical for similar complexes with C,N-chelating ligands.^{24,25,26} The Ru-N bond distance for [11](PF₆) is very similar to that in complex [8] (2.090(7) and 2.0957(18) Å, respectively), whereas the orthometalated Ru-C length is considerably longer than that determined for [8] (2.189(9) versus 2.072(2) Å). Moreover, the Ru-P bond distance is shorter than the equivalent distance in complex [Ru(ppy)(PTA)(MeCN)₃]PF₆ (2.2758(18) versus 2.395 Å, respectively).²⁷ The metallacycle N-Ru-C angles (77.46 ° and 75.3 °, respectively) are in the range of similar complexes depicted in the literature^{24,25,26}.

Table 4. Selected bond lengths (Å) and angles (°) for complexes [8] and [11]⁺.

<i>Distance/angle</i>	[8]	[11](PF ₆)
Ru1-Cl1/ P1	2.4251(8)	2.2758(18)
Ru1-N1	2.0957(18)	2.090(7)
Ru1-C13	2.072(2)	2.189(9)
N1-C7	1.332(3)	1.296(10)
N2-C7	1.350(3)	1.371(10)
C13-Ru1-N1	77.46(8)	75.3(3)
N1-Ru1-Cl1/P1	86.75(5)	85.67(19)
C13-Ru1-Cl1/P1	86.66(6)	81.9(2)

Table 5. Selected geometric parameters^[a] for the metal complexes of [8] and [11]⁺.

<i>Distance/angle</i>	[8]	[11](PF ₆)
<i>Range of Ru-C distances</i>	2.147(2)-2.274(2)	2.186(7)-2.310(9)
<i>Ru-centroid</i>	1.697	1.761
α	6.34	16.83
ϑ (<i>N-C-C-C</i>)	2.71	-2.23
β (<i>chelate-arene</i>)	56.88	48.45
γ (<i>Cx-C_{ipso}-Ru-Y</i>)	-18.26	25.84
λ	2.48	7.02

[a]Calculated with Mercury, version 3.8.

The unit cell of [8] shows molecular pairing for enantiomers (R_{Ru}, S_{Ru}), which is established on the basis of both double mutual π-π stacking contacts (see Table 7) between the extended planar rings of the ligand (py-bim/bim-py), and double bifurcated hydrogen bonds involving N-H and C-H groups of the chelate ligand as donors and the Cl⁻ as the acceptor (see Fig. 6 and Table 6). This motif gives rise to essentially hydrophobic channels all along the crystal network of [8] (see Fig. 7).

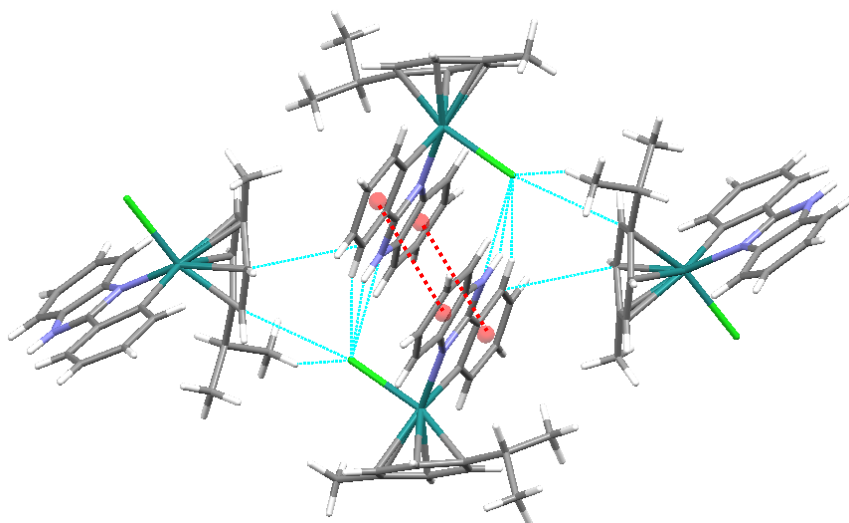


Fig. 6. Representation of hydrogen bonds and π-π stacking interactions in the crystal structure of [8].

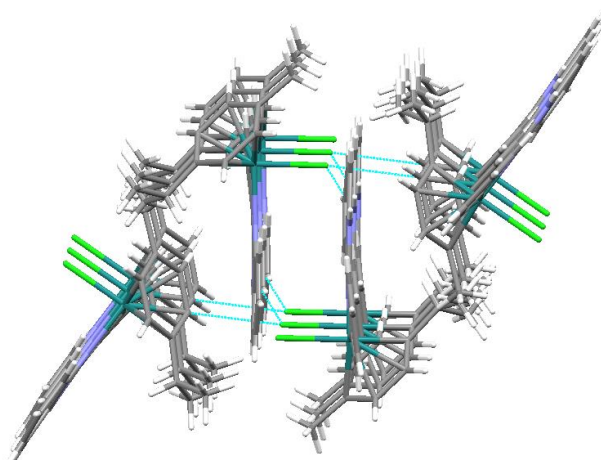


Fig. 7. Representation of hydrophobic channels in the crystal structure of [8].

Table 6. Intermolecular hydrogen bonding for complex [8].

H-bonding	D···A (Å)	X···A (Å)	D···X (Å)	α (°)
C(9)-H(9)···Cl(1)	3.717	2.829	0.930	160.20
N(2)-H(2)···Cl(1)	3.254	2.455	0.859	154.91
C(23)-H(23C)···Cl(1)	3.690	2.831	0.959	149.64

Table 7. π - π offset stacking parameters for complexes [8] and [11](PF₆).

Compound	d _{cent-cent} (Å)	α (°)	d _{cent-pl} (Å)	β (°)	d _{offset} (°)
[8]	4.059	6.34	3.478	31.03	2.093
			3.390	33.37	2.232
[11](PF ₆)	4.121	2.76	3.438	33.46	2.272
			3.347	35.69	2.404

The 3D architecture of [11](PF₆) shows H-bonding, C-H··· π and π - π stacking interactions (see Fig. 8). The counterion links three cationic moieties through weak hydrogen bonding C-H···F-P. There is also ion pairing between the benzimidazole moieties, connected through π - π stacking interactions (see Table 7). Moreover, the bulky PTA ligand seems to bend the chelate donor and intramolecular C-H(PTA)··· π (pybim) interactions are established between both ligands (see Table 8).

Table 8. Parameters of C-H··· π interactions for complex [11](PF₆).

Compound	d _{C-cent} (Å)	d _{H-cent} (Å)	d _{C-H} (Å)	<C-H-cent (°)	<H-cent-normal (°)
[11](PF ₆) (C-H··· π {ph})	3.689	2.896	0.970	139.55	155.49
[11](PF ₆) (C-H··· π {im})	3.438	2.764	0.970	127.21	167.08
[11](PF ₆) (C-H··· π {bim})	4.570	3.711	0.970	148.94	137.68

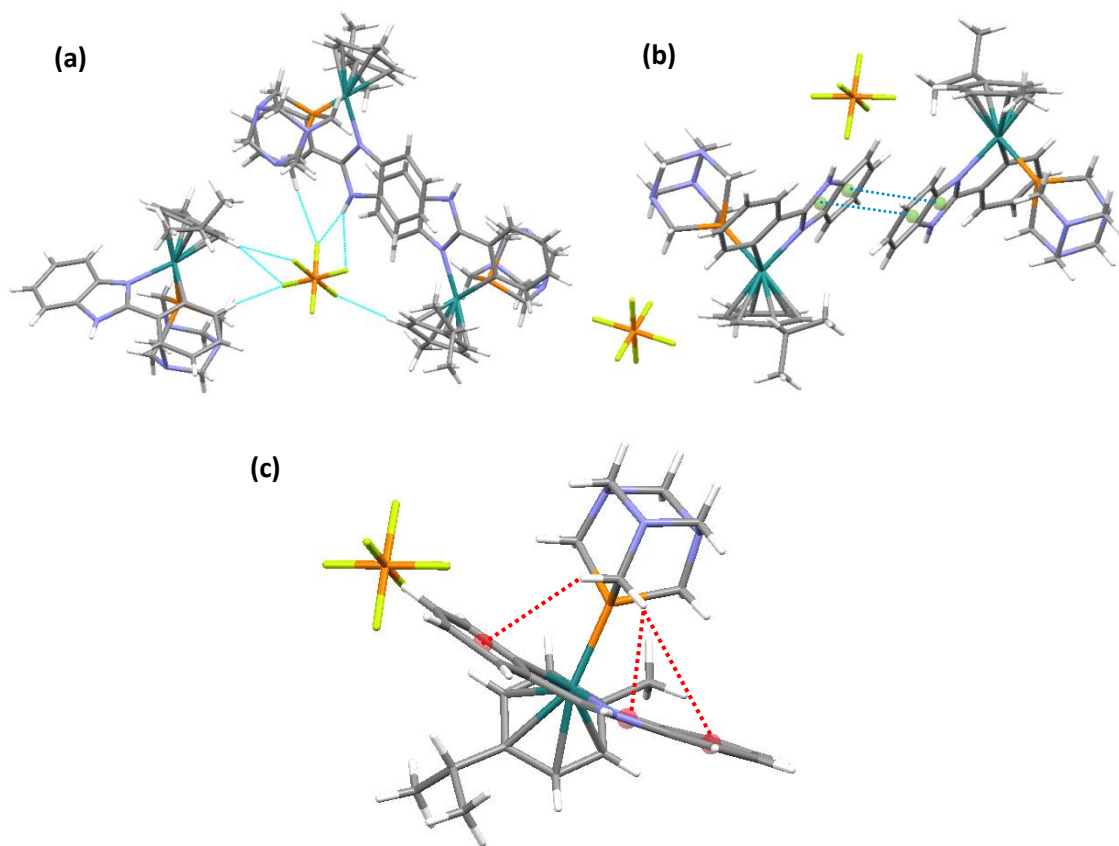


Fig. 8. Hydrogen bonding (a), π - π staking (b) and C-H \cdots π interactions (c) for complex [11](PF₆).

1.3. Cl⁻/DMSO Substitution

As previously said, the replacement of Cl⁻ ligands with DMSO was observed in all the chlorido complexes, both by ¹H NMR and by ESI-MS. The substitution was accompanied by changes in both the solubility and the colour of the resulting adducts. At the beginning, the complexes seemed to be insoluble in DMSO. Then, the corresponding suspensions turned into colourless solutions, except for the rhodium derivative, which kept yellowish. Fig. 9 shows the colour changes when DMSO is added to [9], yielding [14]Cl and Fig. 10 the reaction scheme for complexes [8], [9] and [10].

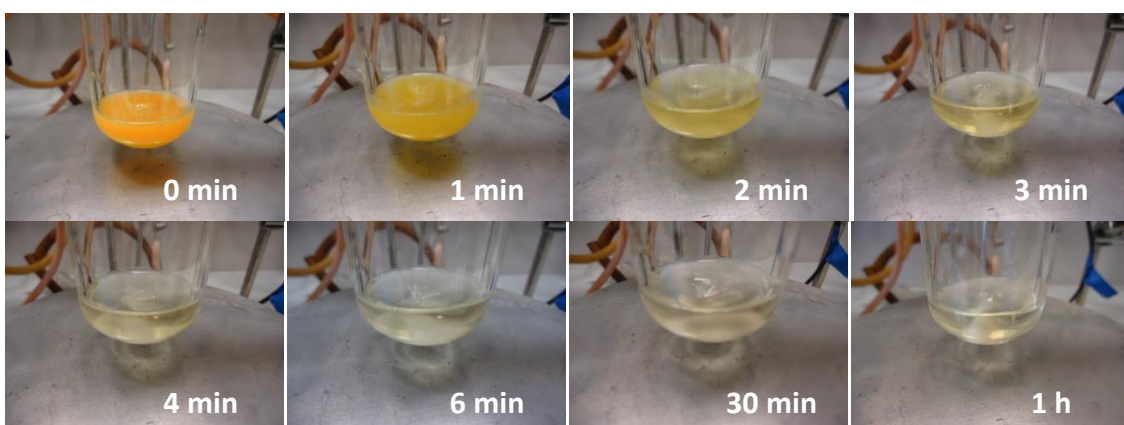
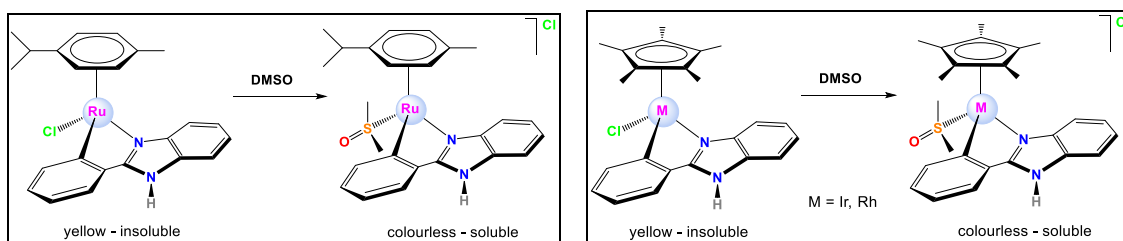
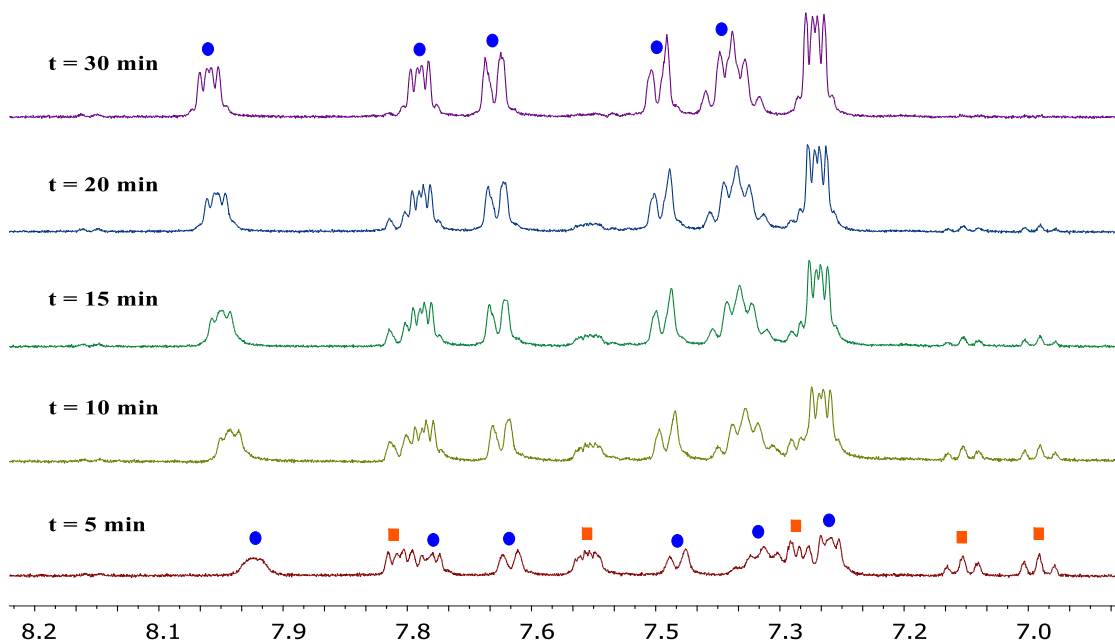


Fig. 9. Evolution of [9] in DMSO with time to yield [14]Cl. The suspension gets colourless as the reaction evolves.

Fig. 10. Cl^- displacement in DMSO for (a) [8] and for (b) [9] and [10].

The substitution reaction for [9] was followed by ^1H NMR (see Fig. 11). The spectrum clearly showed a mixture of products after 5 minutes: the chlorido complex (orange squares) and the DMSO-complex (blue spots). However, after 30 minutes, the reaction was almost finished.

Fig. 11. ^1H NMR spectra for the substitution reaction of chloride by DMSO-d_6 in complex [9].

The substitution reaction was also followed for [8] (see Fig. 12), although it was far slower than for [9]. After 3.5 days, the new set of signals of the DMSO-derivative began to grow (blue spots). Nevertheless, after 5 days, another new set of peaks appeared (green triangles and black squares). We noticed that these resonances belonged to the free p-cymene and to an unidentified Ru product. After 26 days, the spectrum showed the mixture of the three products.

The mass spectra experiments FAB^+ and ESI^+ were also consistent with the Cl^-/DMSO replacement process for these complexes over time.

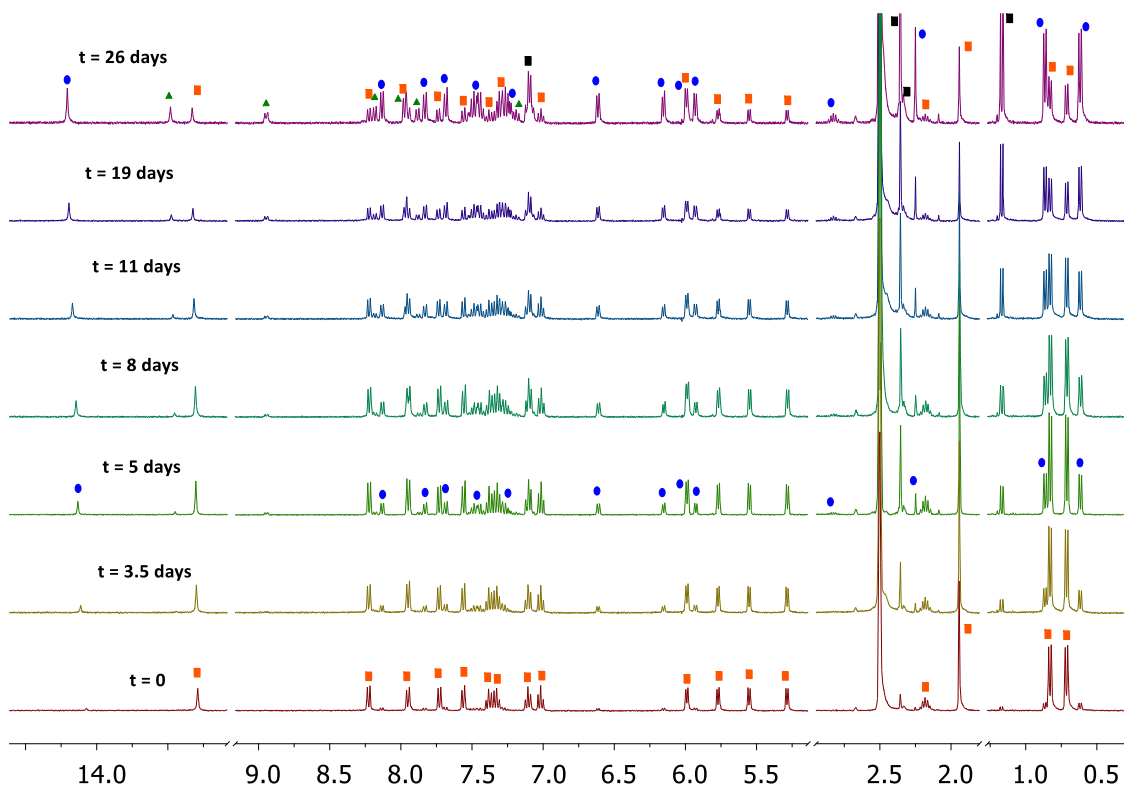


Fig. 12. ^1H NMR spectra for the evolution of [8] in DMSO-d_6 at 25°C . The orange squares correspond to the original chlorido complex, the blue spots to the resulting product of substitution of chloride by DMSO, the black squares to the free *p*-cymene and the green triangles to the unidentified Ru product without *p*-cymene.

1.4. Aqueous Solubility

The aqueous solubility of some complexes was measured at room temperature ($20 - 22^\circ\text{C}$). All the neutral complexes are not water-soluble, whereas the cationic complexes, where the Cl^- has been replaced by PTA and MeIm, exhibit enhanced water solubilities. Among the PTA-derivatives ([11]Cl, [12]Cl and [13]Cl), the rhodium derivative is about 2 times more soluble than its iridium analogue and 4 times more soluble than the ruthenium counterpart. Thus, the solubility tendency is as follows: $\text{Ru} < \text{Ir} < \text{Rh}$.

Table 9. Solubility data in water (mM) for selected compounds.

Ref.	Compound	Solubility (mM)
[11]Cl	$[(p\text{-cym})\text{Ru(pbim)}(\text{PTA})]\text{Cl}$	19.2
[12]Cl	$[(\text{Cp}^*)\text{Ir(pbim)}(\text{PTA})]\text{Cl}$	37.2
[13]Cl	$[(\text{Cp}^*)\text{Rh(pbim)}(\text{PTA})]\text{Cl}$	88.2
[15]Cl	$[(\text{Cp}^*)\text{Ir(pbim)}(\text{MeIm})]\text{Cl}$	2.9
[15]OTf	$[(\text{Cp}^*)\text{Ir(pbim)}(\text{MeIm})]\text{OTf}$	insoluble

1.5. Aquation

The stability of the cationic complexes [11]Cl, [12]Cl, [13]Cl and [15]Cl against hydrolysis was studied by monitoring the evolution with time of the corresponding solutions in D_2O by means of ^1H NMR spectroscopy (5 mM, 25°C and 3 mM for [15]Cl).

No evolution was detected for the PTA derivatives **[11]Cl**, **[12]Cl** and **[13]Cl** either after 5 minutes or after 24 hours. Nonetheless, for **[15]Cl** a new signal in the Cp* area began to grow just after 5 minutes. The evolution was followed after 21 days and a new incipient set of peaks seemed to emerge (see Fig. 13).

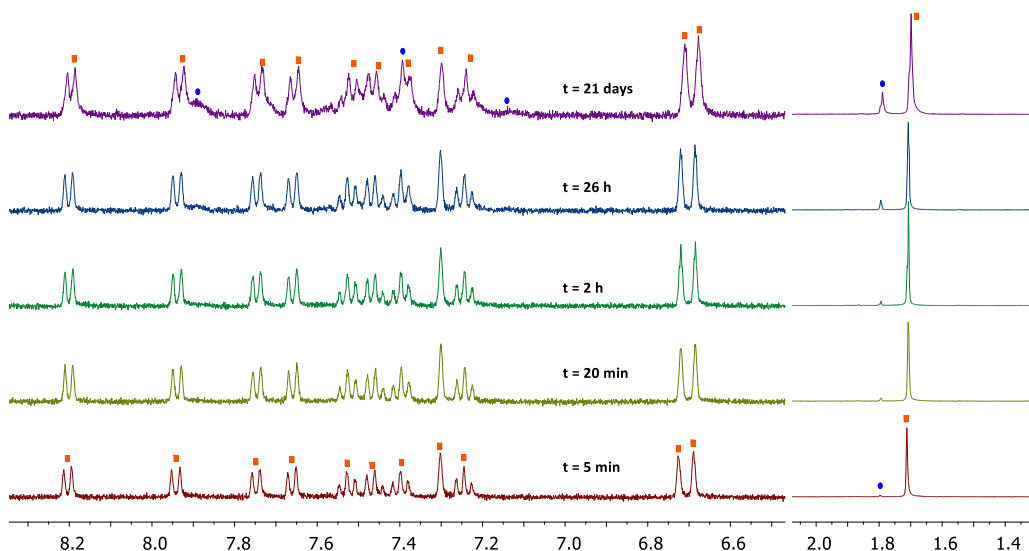


Fig. 13. Evolution of the aquation of **[15]Cl over time by ^1H NMR in D_2O at $25\text{ }^\circ\text{C}$ in the aromatic and aliphatic areas. The orange squares refer to the initial product, and the blue spots to the aquo complex.**

Furthermore, $^{31}\text{P}\{^1\text{H}\}$ NMR spectra were recorded for the PTA-derivatives after 40 minutes, but no changes were observed. This fact supports the non-aquation process of the PTA derivatives.

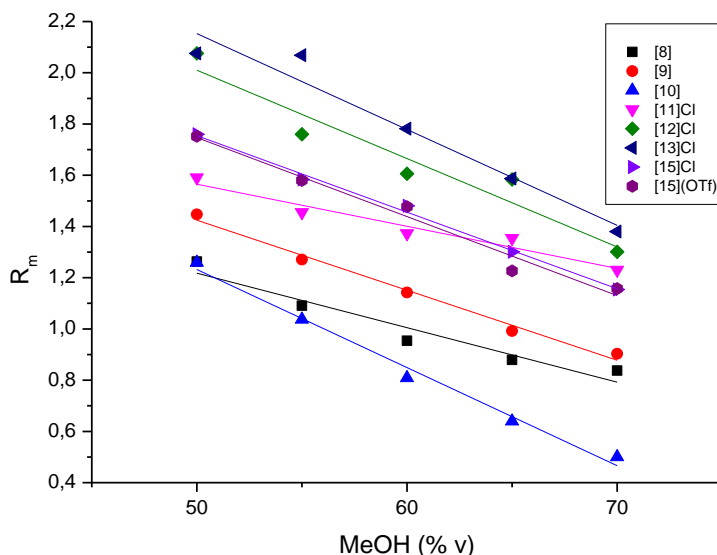
1.6. Lipophilicity

Stock solutions were prepared in two steps. *Step 1*: 1 mg of each compound was dissolved in 100 μL DMSO and left overnight to assure the substitution of chloride by DMSO. *Step 2*: 900 μL of water were added and left overnight to obtain the aqua-derivatives (1 mg/mL) (**[8']⁺**, **[9']⁺** and **[10']⁺**). Commercially available octadecyl modified silica aluminium sheets were selected as the stationary phase and they were manually spotted with the stock solutions. Different mixtures methanol-water (50 - 70% methanol) were used as mobile phase at room temperature (23 - 25 $^\circ\text{C}$). Methanol was selected since it is the most water-like organic solvent and affects less the stationary phase.²⁸ The plates were developed in a chromatographic tank, dried and the spots were revealed under UV light (254 nm).

The R_f and R_m values were calculated from equations in INTRODUCTION (see Table 10) and the R_m^0 values were determined from the extrapolation of the R_m vs. % MeOH linear regression curves (see Fig. 14 and Table 11). It is worth mentioning, that the complexes **[8]**, **[9]** and **[10]** are in fact, monocationic aquo complexes **[8']⁺**, **[9']⁺** and **[10']⁺**.

Table 10. R_f and R_m values for the selected complexes in the different MeOH/H₂O mixtures.

% MeOH	50		55		60		65		70	
	R_f	R_m								
[8'] ⁺	0.052	1.263	0.075	1.091	0.100	0.954	0.117	0.879	0.127	0.837
[9'] ⁺	0.034	1.447	0.051	1.271	0.067	1.142	0.092	0.992	0.111	0.903
[10'] ⁺	0.052	1.259	0.084	1.037	0.134	0.809	0.186	0.640	0.240	0.501
[11]Cl	0.025	1.591	0.034	1.455	0.041	1.373	0.042	1.354	0.056	1.230
[12]Cl	0.008	2.076	0.017	1.760	0.024	1.606	0.025	1.584	0.048	1.301
[13]Cl	0.008	2.076	0.008	2.068	0.016	1.782	0.025	1.587	0.040	1.380
[15]Cl	0.017	1.760	0.025	1.584	0.032	1.481	0.048	1.301	0.066	1.154
[15](OTf)	0.017	1.752	0.026	1.580	0.032	1.477	0.056	1.227	0.065	1.158

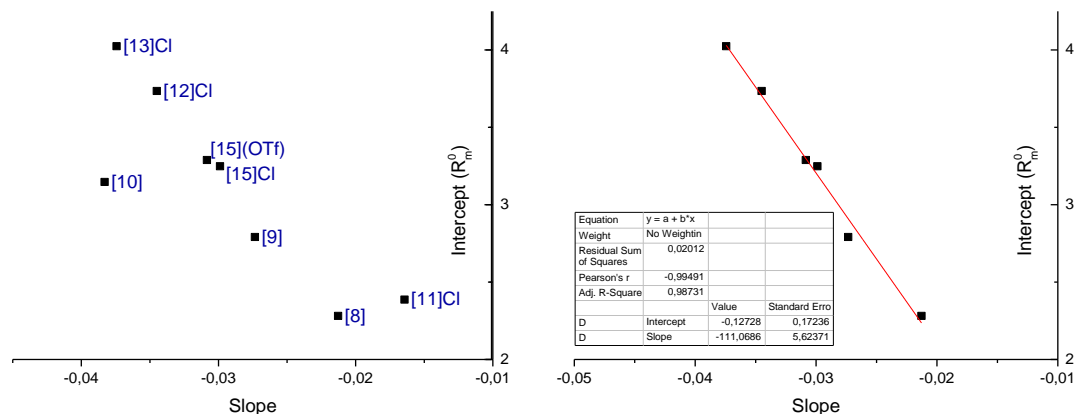
**Fig. 14.** Linear fitting for R_m^0 vs. % MeOH for the selected complexes. (Origin 8.0).

These parameters show different tendencies and relationships. The R_m^0 values are lower for complexes with chloride as the leaving group than for those with PTA or Melm, meaning that the latter are more lipophilic. Regarding the metal, the lower values are obtained for the ruthenium derivatives, followed by iridium and rhodium ($\text{Ru} < \text{Ir} < \text{Rh}$), which means that ruthenium complexes are more hydrophilic. Curiously, the water-solubility follows the same tendency. As regards the iridium complexes with Melm, **[15]Cl** and **[15]OTf**, there is no appreciable difference between them. Slopes are comparable for all iridium and rhodium complexes with the exception of the ruthenium derivatives. C° values are very similar for all complexes, although **[10]** and **[11]Cl** are a little out of the range. That is, the needed amount of organic modifier for which the distribution of the complex between the two phases becomes equal is extremely little and approximately the same for all the complexes.

Table 11. Intercept (R_m^0) and slope (b) values after the linear fitting and calculation of the C° value.

	$R_m^0 = \text{intercept}$	b=slope	$C^0 = -b/R_m^0$ (%)	R^2
[8'] ⁺	2.28 ± 0.19	-0.021 ± 0.003	9.33E-03	0.918
[9'] ⁺	2.79 ± 0.10	-0.027 ± 0.002	9.79E-03	0.986
[10'] ⁺	3.15 ± 0.14	-0.038 ± 0.002	1.22E-02	0.986
[11]Cl	2.39 ± 0.13	-0.016 ± 0.002	6.89E-03	0.934
[12]Cl	3.74 ± 0.33	-0.035 ± 0.005	9.24E-03	0.906
[13]Cl	4.02 ± 0.29	-0.037 ± 0.005	9.30E-03	0.938
[15]Cl	3.25 ± 0.07	-0.030 ± 0.001	9.20E-03	0.993
[15](OTf)	3.29 ± 0.17	-0.031 ± 0.003	9.38E-03	0.969

The relationship between the slopes (b) and intercepts (R_m^0) of the previous equations (see Fig. 15) is another feature to measure the lipophilicity of a family of congeners.²⁹ The linear fitting was performed without [10] and [11]Cl, which seem to be “anomalous” values. The rest of the values fit well to the equation presented in Fig. 15b.

**Fig. 15.** Relationship between slope and intercept of the TLC equations. (a) Data and (b) linear fitting without [10] and [11]Cl. (Origin 8.0).

To sum up, the most lipophilic complexes are [12]Cl and [13]Cl, whereas the most hydrophilic are the aqua-derivatives [8']⁺ and [9']⁺, obtained from [8] and [9], probably due to their great ability to form hydrogen bonding.

1.7. Reactivity against Nucleobases and Nucleotides

The qualitative interaction of complex [9] with 9MeG was followed by ¹H NMR in DMSO-d₆ at 25 °C. A sample of [9] in DMSO-d₆ was left to evolve overnight, to assure the complete substitution of Cl⁻ by DMSO. 9MeG was then added and some spectra were recorded over time. However, no reaction seemed to occur, since the signals of both the complex and the 9MeG did not shift or change.

In order to decipher the mechanism of action of these complexes, other biologically relevant molecules, such as glutathione (GSH) and NADH were selected for reactivity assays.

1.8. Reactivity against Glutathione

The reactivity of the neutral complexes **[8]**, **[9]** and **[10]** (5 mM), as well as the cationic complex **[14]Cl** (5 mM) against glutathione (10 mM, mimicking the cell concentrations), was tested and followed by ^1H NMR at 25 °C in DMSO-d₆ for the neutral complexes (as they are insoluble in water) and in D₂O for the monocationic one. After the DMSO-substitution reaction is complete (only for **[8]**, **[9]** and **[10]**), a spectrum was recorded and GSH was then added in a 1:2 molar ratio. The evolution was monitored over time by recording some spectra.

On the one hand, neither complex **[8]** nor complex **[9]** showed any coordination symptoms, only the signals of the oxidized glutathione emerged clearly after 17 h. Nevertheless, the literature depicts the oxidation process of GSH to GSSG with only the air as oxidant and no catalyst, which is bound to have happened in our experiments.³⁰

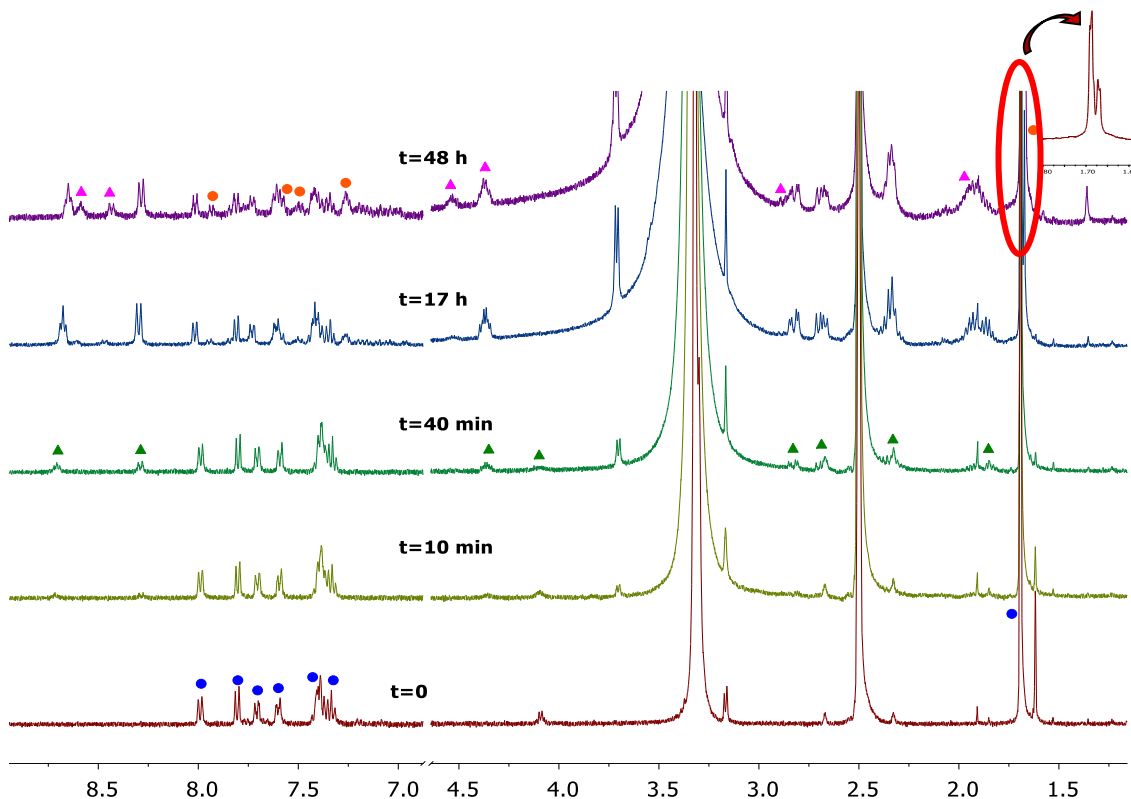


Fig. 16. Evolution of **[10]** with GSH in DMSO-d₆ at 25 °C and expansion of the Cp*. The Blue spots refer to **[10]**, the green triangles to the GSH, the pink triangles to the GSSG and the orange spots to a new complex.

On the other hand, complex **[10]** did show a change in the spectra (see Fig. 16). Apart from the set of signals of the GSSG and those of the GSH, another set of peaks both in the aromatic and aliphatic (Cp*) areas began to grow after 17 h of reaction. Although we cannot be sure about the identity of the new species, it seems that it contains the Rh-Cp* fragment.

The stability of the solutions was determined by recording new spectra for the same samples after 6 months. The complexes showed interesting features, besides the characteristic signals of oxidized glutathione (GSSG). For instance, complex [8] decomposed releasing the *p*-cymene to yield another Ru(II) compound; complex [9] only showed the original set of signals and complex [10], also exhibited the original set of signals (after 6 months), although a new product had appeared in between (after 48 h), and then disappeared.

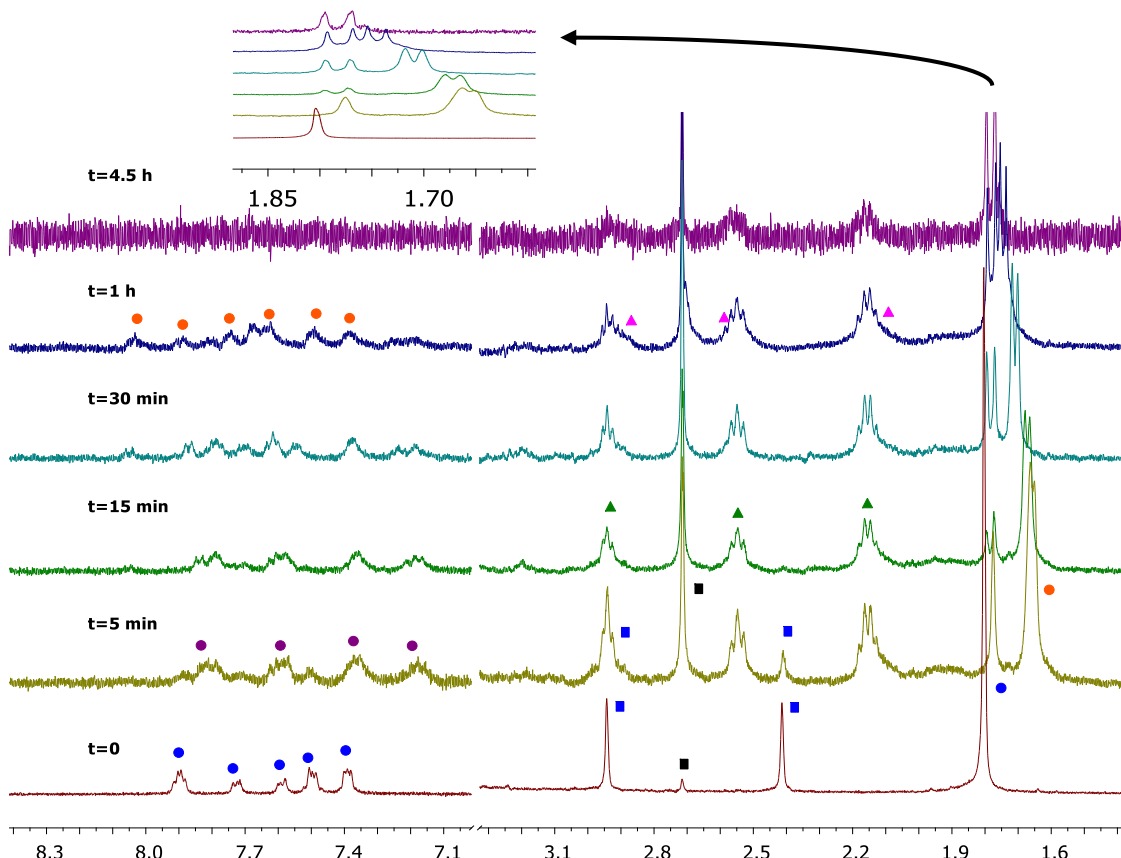


Fig. 17. Evolution of [14]Cl with GSH in D_2O at 25 °C and expansion of the Cp^* area. The Blue spots refer to the initial complex, the blue squares to the DMSO coordinated (diaestereotopic), the black squares to the free DMSO, the purple spots to the aquacomplex, the green triangles to the GSH and the pink triangles to the GSSG.

Therefore, the experiment was repeated for the complex [14]Cl in D_2O . It evolved in an interesting way (see Fig. 17). At first, the DMSO molecule was released, and after 5 minutes, the diaestereotopic methyls of coordinated DMSO became equivalent (two singlets became one; blue and black squares). At that point, the vacant coordination site seemed to be occupied by a water molecule, forming the respective aquo complex (purple spots). In addition, after 30 minutes, another different product appeared (orange spots). Finally, after 4.5 h, the signal noise relationship got worse, due to the precipitation of a solid.

On the whole, there are some conclusions or evidences we can extract from the experiments:

- Complexes [8] and [9] [Ru(II) and Ir(III)] do not interact with GSH, whereas [10] [Rh(III)] shows evidences of reaction.
- GSH oxidizes easily by the action of air in the conditions of the experiment.
- Complex [14]Cl undergoes fast aquation.
- Complex [14]Cl interacts with GSH, whereas its analogue [9] do not. This effect is probably the result of the block of the GSH folded conformation in DMSO.³¹

1.9. Peroxide formation by Metal-Catalysed Transfer Hydrogenation

NADH was selected as a possible target, since it participates in several biological reactions. In addition, coenzyme NADH can transfer hydride ions to cyclopentadienyl–Ir(III) complexes, generating iridium–hydride complexes, which are able to transfer the hydride to molecular oxygen (O_2) (see Fig. 18). Finally, ROS are formed leading to cell death through oxidative stress mechanisms. The catalytic activity of [8], [9], [10], [15]Cl and [15](OTf) in the transfer hydrogenation of O_2 from NADH was assessed by detecting the formation of H_2O_2 with colorimetric strips.^{32,2}

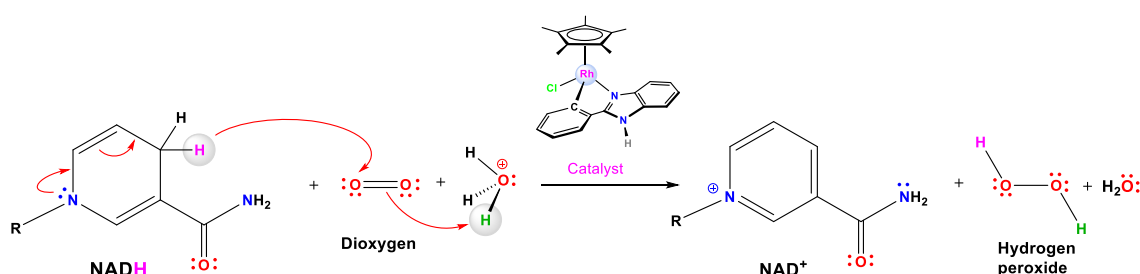


Fig. 18. Reduction of O_2 by metal-catalyzed transfer hydrogenation.

Hydrogen peroxide detection

The hydrogen peroxide formation was detected with peroxide test strips (Precision Laboratories 800-733-0266) in solutions 1 mM of complexes [8], [9], [10], [15]Cl and [15](OTf), and 3 eq. of NADH, after reacting overnight at 37 °C in the presence of air and continuous stirring. Different experiments were performed, changing the solvent system, but always in aqueous mixtures. Only the experiment performed in a mixture MeOH/H₂O (1:1) displayed approximately 10 ppm of H₂O₂ (ca. 0.26 mM) for complex [10] after 22 h (see Fig. 19). Table 12 gathers the amount of H₂O₂ detected in each experiment, although in most cases it is negligible.

Table 12. Approximate concentration of H₂O₂ detected for the selected complexes in the different solvent mixtures.

	[8]	[9]	[10]	[15]Cl	[15](OTf)
MeOH/H ₂ O	0 ppm	0 ppm	≈ 10 ppm	0 ppm	< 1 ppm
DMSO/H ₂ O	0 ppm	< 1 ppm	1 - 3 ppm	-	-
DMF/H ₂ O	< 1 ppm	0 ppm	0 ppm	-	-

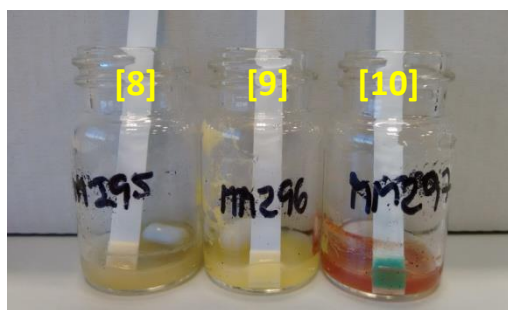


Fig. 19. Detection of hydrogen peroxide in a solution of [8], [9] and [10] (1 mM) with NADH (3 mol equiv.) in MeOH/H₂O (1:1) at 37 °C. After 22 hours, H₂O₂ (*ca.* 0.26 mM) was detected for [10].

The reactivity of [8], [9] and [10] against DNA, GSH and NADH, has been also studied by the group of Begoña García. Thus, [10] is the only complex that bind DNA, whereas [9] and [10] are reactive against GSH and again [10] reacts with NADH.

1.10. Cytotoxic Activity

The cytotoxic activity of selected complexes has been evaluated in a comparative *in vitro* MTT cell viability assay after incubation times of 24 h at 37 °C with human lung carcinoma cells (A549), human breast carcinoma cells (MCF-7), human colon carcinoma cells (HTC-116) and human colon carcinoma cells with the **tumour suppressor p53** (HTC-116p53-, p53 is inactivated). The values (see Table 13) are expressed as the inhibitory potency (IC₅₀) and cisplatin was used as the positive control in all the cell lines. The cytotoxicity of free ligands is very low (IC₅₀ > 100 µM). Likewise, the dimeric starting material is inactive in these cell lines according to the literature. The neutral complexes ([8], [9] and [10]) showed good activity, whereas the PTA derivatives ([10]Cl, [11]Cl and [13]Cl) were inactive (IC₅₀ > 200 µM in A549). The cytotoxicity of the neutral complexes, depending on the metal centre, follows the next tendency in all the cell lines, except in HCT-116p53-: *Ru*<*Rh*<*Ir*. Thus, the most relevant *in vitro* inhibitory potency was obtained for complex [9], the iridium complex.

In order to determine the target of the complexes and to understand the mechanism of action of each one, ongoing studies are being performed by the group of Dr. Fernando Domínguez from the University of Santiago de Compostela and CiMUS (Centre for Research in Molecular Medicine and Chronic Diseases). All the complexes were injected in mice. Nonetheless, the cytotoxic activity of compound [9] was so potent, that the mice's survival was dramatically affected. In this case, the target is sure to be GSH. On the other hand, complex [10] shows promising results, since its activity is related to the NADH/NAD⁺ balance and consequently it operates in the mitochondria. Thus, both mechanisms have effects over the cellular metabolism. The mechanism of action of the Ru derivative [8] is still unclear.

Table 13. IC₅₀ (μM , 24 h, 37 °C) values for selected compounds in the A549, MCF-7, HCT-116 and HTC-116p53- cell lines.

Ref.	Compound	A549	MCF-7	HCT-116	HCT-116p53-
-	Cisplatin ^d	114.2 ^c	12	-	-
-	pbim	Inactive	Inactive	Inactive	Inactive
-	$[(p\text{-cym})\text{RuCl}_2]_2^{\text{a}}$	-	184	-	-
-	$[(\text{Cp}^*)\text{IrCl}_2]_2^{\text{a}}$	-	100	-	-
-	$[(\text{Cp}^*)\text{RhCl}_2]_2^{\text{b}}$	-	11	-	-
[8]	$[(p\text{-cym})\text{RuCl}(\text{pbim})]$	50.0 ± 7.0	49.2 ± 3.7	74.2 ± 29.2	19.2 ± 3.1
[9]	$[(\text{Cp}^*)\text{IrCl}(\text{pbim})]$	15.7 ± 10.0	10.1 ± 1.4	9.7 ± 3.0	9.7 ± 1.3
[10]	$[(\text{Cp}^*)\text{RhCl}(\text{pbim})]$	43.2 ± 13.5	32.8 ± 7.3	28.9 ± 0.9	27
[11]Cl	$[(p\text{-cym})\text{Ru}(\text{pbim})(\text{PTA})]\text{Cl}$	Ambiguous results	-	-	-
[12]Cl	$[(\text{Cp}^*)\text{Ir}(\text{pbim})(\text{PTA})]\text{Cl}$	Ambiguous results	-	-	-
[13]Cl	$[(\text{Cp}^*)\text{Rh}(\text{pbim})(\text{PTA})]\text{Cl}$	220	-	-	-

^a Bibliographic data.³³

^b Bibliographic data, (cells incubated for 5 days).³⁴

^c Bibliographic data.³⁵

^d Reference dose for cisplatin = 50 μM after 24 h.

The cytotoxicity of complex [15]OTf was studied by Dra. Natalia Bustos in cancerous cells (HeLa cells) and healthy cells (IMR-90, lung fibroblasts). Table 14 shows images of the cells incubated with different doses of complex [15]OTf, whereas Fig. 20 presents the percentage of cell survival at these doses. The inhibitory potency of the compound is extremely high in the cancerous cell line HeLa (see Table 15), 8 times higher than that for cisplatin (IC₅₀ = 5.57 vs. IC₅₀ (cisplatin) = 45.44). Nonetheless, the selectivity factor (SF) of the complex is low, since the cytotoxicity is also high in the healthy cell line.

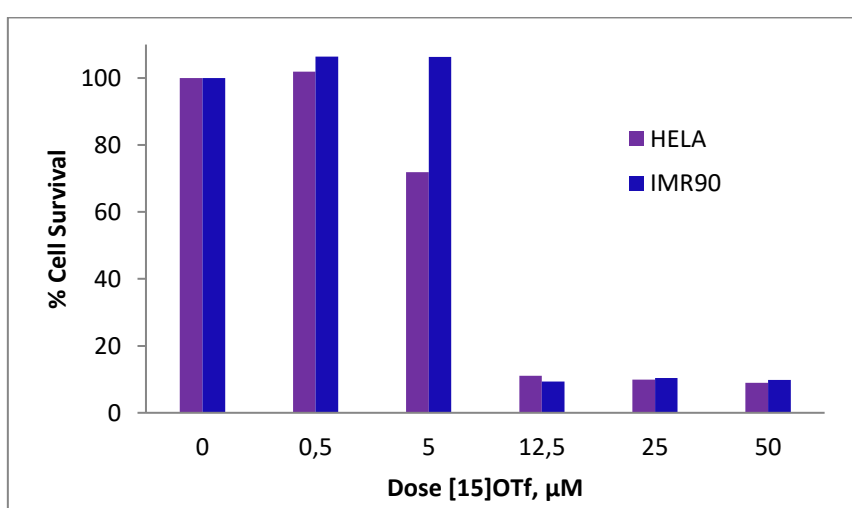


Fig. 20. Percentage of cell survival vs. dose of complex [15]OTf in HeLa and IMR-90 cells after 24 h.

Table 14. Photographs of IMR-90 and HeLa cells taken 24 h after incubation with complex [15]OTf.

[15]OTf in IMR-90	Dose	[15]OTf in HeLa	Dose
	0.5 μM		0.5 μM
	5 μM		5 μM
	12.5 μM		12.5 μM
	25 μM		25 μM
	50 μM		50 μM

Table 15. IC₅₀ (μM , 24 h, 37 °C) values for complex [15]OTf in the HeLa and IMR-90 cell lines.

Ref.	Compound	HeLa	IMR-90	SF
	cisplatin	45.44		
[15](OTf)	[(Cp*)Ir(MeIm)(pbim)](OTf)	5.57 ± 1.43	8.43 ± 1.87	1.51

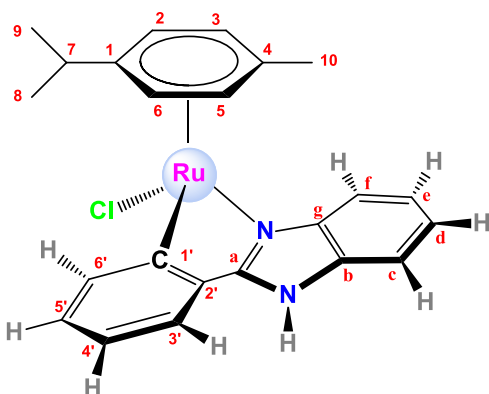
2. CONCLUDING REMARKS

- A family of 9 new complexes has been synthesised and completely characterised, both in solution and two of them in solid state.
- The cationic complexes are water soluble, whereas the neutral derivatives are insoluble in water. Moreover, solubility and lipophilicity are closely related, since both properties follow the tendency: Ru < Ir < Rh.

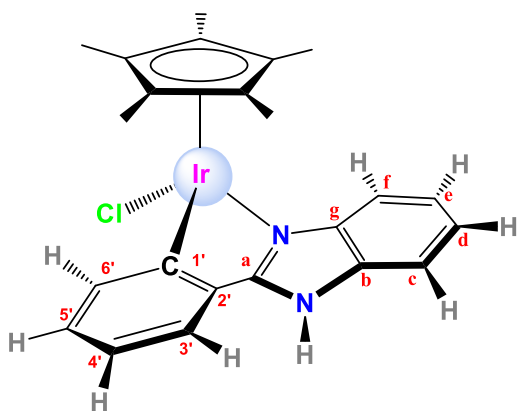
- The neutral complexes undergo chloride replacement in DMSO solution. After this, aquation is also feasible.
- The inhibitory potencies highlight the iridium complexes **[9]** $[(\eta^5\text{-Cp}^*)\text{IrCl}(\kappa^2\text{-C}, N\text{-pbim})]$ and the rhodium complex **[10]** $[(\eta^5\text{-Cp}^*)\text{RhCl}(\kappa^2\text{-C}, N\text{-pbim})]$ as promising anticancer drugs. The complex **[15]OTf** $[(\eta^5\text{-Cp}^*)\text{Ir}(\text{MeIm})(\kappa^2\text{-C}, N\text{-pbim})]\text{OTf}$ improves 8 times the cytotoxicity of cisplatin in HeLa cells.
- In general, the cytotoxicity is enhanced for those complexes with labile leaving groups.
- Experiments for detection of hydrogen peroxide, point out mitochondria as the target for complex **[10]**.

3. EXPERIMENTAL SECTION

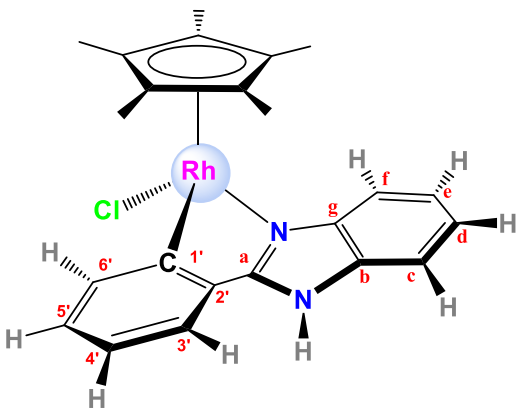
Neutral Complexes



Synthesis of $[(\eta^6\text{-}p\text{-cymene})\text{RuCl}(pbim)]$, [8]. In a 100 mL Schlenk flask, the ligand 2-phenylbenzimidazole (pbim) (63.9 mg, 0.329 mmol) was added under a nitrogen atmosphere to a solution of $[(\eta^6\text{-}p\text{-cymene})\text{RuCl}_2]_2$, (100.5 mg, 0.164 mmol) in dichloromethane (5 mL) in the presence of an excess of NaOAc (495 mg, 3.64 mmol). The suspension was stirred for 20 hours at room temperature. The NaCl formed as a byproduct was filtered off. The solution was concentrated under vacuum and *n*-hexane was added (10 mL) to precipitate a solid which was washed with *n*-hexane (3×5 mL) and dried under vacuum, to produce a dark yellow product. Yield: 100 mg (0.216 mmol, 67%). M_r ($\text{C}_{23}\text{H}_{23}\text{ClN}_2\text{Ru}$) = 463.9708 g/mol. **Anal. Calcd for** $\text{C}_{23}\text{H}_{23}\text{ClN}_2\text{Ru}\cdot(\text{CH}_2\text{Cl}_2)_{0.2}$: C 57.94; H 4.90; N 5.82; **Found:** C 57.85; H 4.90; N 5.89. **$^1\text{H NMR}$ (400 MHz, CDCl_3 , 25 °C)** δ = 11.09 (s, 1H, $\text{H}^{\text{N-H}}$), 8.15 (d, J =7.3 Hz, 1H, $\text{H}^{\text{6'}}$), 7.67 (d, J =8.0 Hz, 1H, H^{f}), 7.15 (t, J =7.2 Hz, 1H, H^{e}), 6.83 (m, 2H, $\text{H}^{\text{d},\text{5'}}$), 6.72 (d, J =7.2 Hz, 1H, $\text{H}^{\text{3'}}$), 6.65 (d, J =8.1 Hz, 1H, H^{c}), 6.14 (t, J =7.4 Hz, 1H, $\text{H}^{\text{4'}}$), 5.85 (d, J =5.8 Hz, 1H, H^{3} or H^{5}), 5.72 (d, J =5.7 Hz, 1H, H^{6} or H^{2}), 5.39 (d, J =5.8 Hz, 1H, H^{2} or H^{6}), 5.17 (d, J =5.7 Hz, 1H, H^{5} or H^{3}), 2.17 (sept, J =6.9 Hz, 1H, H^{7}), 2.06 (s, 3H, H^{10}), 0.82 (d, J =6.9 Hz, 3H, H^{8} or H^{9}), 0.68 (d, J =6.9 Hz, 3H, H^{9} or H^{8}) ppm. **$^1\text{H NMR}$ (400 MHz, DMSO-d₆, 25 °C)** δ 13.27 (s, 1H, $\text{H}^{\text{N-H}}$), 8.23 (d, J =7.5 Hz, 1H, $\text{H}^{\text{6'}}$), 7.95 (d, J =8.2 Hz, 1H, H^{f}), 7.72 (d, J =7.6 Hz, 1H, $\text{H}^{\text{3'}}$), 7.56 (d, J =7.5 Hz, 1H, H^{c}), 7.38 (t, J =7.6 Hz, 1H, H^{e}), 7.33 (t, J =7.5 Hz, 1H, H^{d}), 7.11 (t, J =7.4 Hz, 1H, $\text{H}^{\text{5'}}$), 7.02 (t, J =7.3 Hz, 1H, $\text{H}^{\text{4'}}$), 5.99 (d, J =5.6 Hz, 1H, H^{3} or H^{5}), 5.77 (d, J =5.8 Hz, 1H, H^{6} or H^{2}), 5.55 (d, J =6.0 Hz, 1H, H^{2} or H^{6}), 5.29 (d, J =5.9 Hz, 1H, H^{5} or H^{3}), 2.18 (sept, J =6.8 Hz, 1H, H^{7}), 1.94 (s, 3H, H^{10}), 0.83 (d, J =6.9 Hz, 3H, H^{8} or H^{9}), 0.71 (d, J =6.9 Hz, 3H, H^{9} or H^{8}) ppm. **$^{13}\text{C}\{^1\text{H}\}$ NMR (101 MHz, CDCl_3 , 25 °C)** δ = 177.3 (s, 1C, $\text{C}^{\text{1'}}$), 159.2 (s, 1C, $\text{C}^{\text{3'}}$), 141.5 (s, 1C, $\text{C}^{\text{8'}}$), 138.8 (s, 1C, $\text{C}^{\text{6'}}$), 133.8 (s, 1C, C^{b}), 133.5 (s, 1C, $\text{C}^{\text{2'}}$), 129.0 (s, 1C, $\text{C}^{\text{5'}}$), 123.6 (s, 1C, $\text{C}^{\text{3'}}$), 123.0 (s, 1C, $\text{C}^{\text{4'}}$), 122.8 (s, 1C, C^{d}), 122.1 (s, 1C, C^{e}), 114.9 (s, 1C, C^{f}), 113.0 (s, 1C, C^{c}), 100.7 (s, 1C, C^{4}), 97.8 (s, 1C, C^{1}), 89.7 (s, 1C, C^{6} or C^{2}), 88.2 (s, 1C, C^{3} or C^{5}), 81.8 (s, 1C, C^{2} or C^{6}), 80.4 (s, 1C, C^{5} or C^{3}), 30.9 (s, 1C, C^{7}), 22.6 (s, 1C, C^{8} or C^{9}), 21.9 (s, 1C, C^{9} or C^{8}), 19.1 (s, 1C, C^{10}) ppm. **FT-IR (KBr, cm⁻¹) selected bands:** 3160-3136-3113-3050 (m, $\nu_{\text{C-H}, \text{N-H}}$), 2953-2925 (m, v_{CH}), 1590 (s, $\nu_{\text{C=C+C-N}}$), 1533 (s), 1466 (m), 1454 (s, $\nu_{\text{C=N}}$), 1432 (s), 1373 (w, δ_{CH_3}), 1325 (m), 1276 (s), 1087 (m), 1014 (m), 826 (w, $\delta_{\text{C-C}}$), 747, 723 (vs, $\delta_{\text{CH}_\text{loop}}$), 673 (w), 458 (s). **MS (FAB+):** m/z (%) = 464 (35) ([M]⁺), 429 (100) ([M-Cl]⁺). **Molar conductivity (H₂O):** No data available due to low solubility in water or acetonitrile. **Solubility:** soluble in dichloromethane, chloroform, acetone, DMF and DMSO, partially soluble in methanol and ethanol, and insoluble in water and acetonitrile.

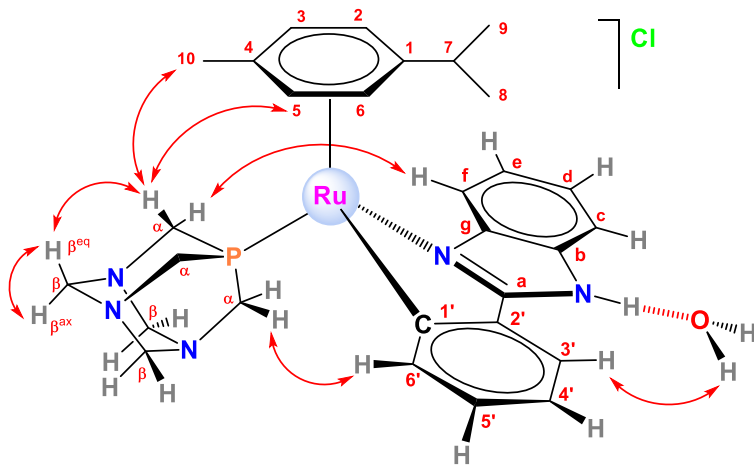


Synthesis of $[(\eta^5\text{-}C_5\text{Me}_5)\text{IrCl}(\kappa^2\text{-}N,\text{C-pbim})]$, [9]. In a 100 mL Schlenk flask, the pro-ligand 2-phenylbenzimidazole (151 mg, 0.777 mmol) was added to a solution of $[(\eta^5\text{-}C_5\text{Me}_5)\text{IrCl}_2]_2$ (300.5 mg, 0.377 mmol) and sodium acetate ($1.02 \cdot 10^3$ mg, 7.5 mmol) in degassed dichloromethane (20 mL), and the mixture was stirred at room temperature for 20 h under a nitrogen atmosphere. An orange precipitate was formed after this time. Water (3 mL) was added to extract hydrophilic compounds and the mixture was filtered to isolate the crude product. The powder was washed with dichloromethane (1×5 mL) and diethylether (1×5 mL), filtered and dried under vacuum. The orange solid was dissolved in a mixture of methanol-dichloromethane (18 mL, 2:1) with sodium chloride (6 mg, 0.103 mmol) and the mixture was stirred at room temperature overnight. The solution was concentrated to produce a precipitate. The solid was filtered and washed with dichloromethane (1×5 mL), water (1×5 mL) and diethylether (2×5 mL). The resulting orange powder was dried under vacuum. Yield: 278.9 mg (0.502 mmol, 65%). M_r ($\text{C}_{23}\text{H}_{24}\text{N}_2\text{ClIr}$) = 556.1287 g/mol. **Anal. Calcd for $\text{C}_{23}\text{H}_{24}\text{N}_2\text{ClIr} \cdot (\text{CH}_2\text{Cl}_2)_{0.4}$:** C 47.63; H 4.24; N 4.75; **Found:** C 47.58; H 4.18; N 4.37. **$^1\text{H NMR}$ (400 MHz, DMSO- d_6 , 25 °C)** δ 13.60 (s, 1H, $\text{H}^{\text{N-H}}$), 8.12 (dd, J = 5.4, 3.5 Hz, 1H, H^3), 7.80 (dd, J = 5.6, 3.0 Hz, 1H, H^6), 7.70 (dd, J = 4.7, 3.8 Hz, 1H, H^c), 7.51 (d, J = 7.3 Hz, 1H, H^f), 7.46 – 7.38 (m, 2H, H^e , H^d), 7.32 (dd, J = 5.7, 3.1 Hz, 2H, $\text{H}^{5'},\text{H}^{4'}$), 1.76 (s, 15H, $\text{H}^{\text{Cp*}(Me)}$) ppm. **$^{13}\text{C}\{^1\text{H}\}$ NMR (101 MHz, DMSO- d_6 , 25 °C)** δ 164.2 (s, 1C, C^1), 151.8 (s, 1C, C^a), 139.1 (s, 1C, C^g), 136.3 (s, 1C, C^6), 135.2 (s, 2C, C^2 , C^b), 130.9 (s, 1C, $\text{C}^{5'}$), 125.0 (s, 1C, $\text{C}^{3'}$), 124.5 (s, 1C, $\text{C}^{4'}$), 123.6 (s, 1C, C^d), 123.4 (s, 1C, C^e), 114.6 (s, 1C, C^c), 114.3 (s, 1C, C^f), 95.5 (s, 5C, $\text{C}^{\text{Cp*}}$), 8.9 (s, 5C, $\text{C}^{\text{Cp*}(Me)}$) ppm. NMR spectra were recorded in DMSO- d_6 due to the low solubility of this product in other solvents and so the resulting spectra correspond to $[(\eta^5\text{-}C_5\text{Me}_5)\text{Ir}(\text{DMSO-}d_6)(\kappa^2\text{-}N,\text{C-pbim})]\text{Cl}$. **FT-IR (ATR, cm⁻¹) selected bands:** 3423 (w, $\nu_{\text{N-H}}$), 3139–3111–3064 (m, $\nu_{\text{C-H}}$), 2962–2911 (m, $\nu_{\text{C-H}}$), 1592 (s, $\nu_{\text{C=C+C-N}}$), 1536 (s), 1469–1458 (s, $\nu_{\text{C=N}}$), 1432 (s), 1379 (w, δ_{CH_3}), 1278–1262 (s), 1095 (m), 1027 (m), 801 (w, $\delta_{\text{C-C}}$), 738–729 (vs, δ_{CHoop}), 670 (w). **MS (FAB+):** in DMSO for $[(\eta^5\text{-}C_5\text{Me}_5)\text{Ir}(\text{DMSO-}d_6)(\kappa^2\text{-}N,\text{C-Pbim})]\text{Cl}$: m/z (%) = 600 (18) ($[\text{M-Cl}+\text{H}]^+$), 522 (100) ($[\text{M-Cl-DMSO}+\text{H}]^+$). **Molar Conductivity (H₂O):** No data available due to low solubility in water or acetonitrile. **Solubility:** soluble in dimethylsulfoxide (with substitution of the Cl^-) and DMF, partially soluble in methanol and insoluble in water and dichloromethane.



Synthesis of $[(\eta^5\text{-C}_5\text{Me}_5)\text{RhCl}(\kappa^2\text{-N,C-pbim})]$, [10]. In a 100 mL Schlenk flask, the pro-ligand 2-phenylbenzimidazole (126 mg, 0.649 mmol) was added to a solution of $[(\eta^5\text{-C}_5\text{Me}_5)\text{RhCl}_2]_2$ (200 mg, 0.324 mmol) and sodium acetate (880 mg, 6.47 mmol) in degassed dichloromethane (15 mL), and the mixture was stirred at room temperature for 20 h under a nitrogen atmosphere. An orange precipitate was formed after this time. Water (6 mL) was added to extract the hydrophilic byproducts and the mixture was filtered to isolate a solid product. This powder was washed with diethylether (1×5 mL), dried under vacuum and then suspended in a mixture of methanol-dichloromethane (18 mL, 2:1) containing sodium chloride (9 mg, 0.154 mmol). The mixture was stirred at room temperature overnight. The solution was concentrated to produce a precipitate. The crude solid was filtered and washed with dichloromethane (1×5 mL), water (1×5 mL) and diethylether (2×5 mL). The resulting orange-reddish powder was dried under vacuum. Yield: 115.5 mg (0.247 mmol, 42%). **M_r** ($\text{C}_{23}\text{H}_{24}\text{N}_2\text{ClRh}$) = 466.8142 g/mol. **Anal. Calcd for** $\text{C}_{23}\text{H}_{24}\text{N}_2\text{ClRh}\cdot(\text{CH}_2\text{Cl}_2)(\text{H}_2\text{O})_{0.4}$: C 51.57; H 4.83; N 5.01; **Found:** C 51.75; H 4.87; N 5.22. **¹H NMR** (400 MHz, DMSO-d₆, 25 °C) δ 13.64 (s, 1H, H^{N-H}), 8.16 (d, *J* = 7.5 Hz, 1H, H^{3'}), 7.80 (d, *J* = 7.4 Hz, 1H, H^{6'}), 7.71 (d, *J* = 7.6 Hz, 1H, H^c), 7.60 (d, *J* = 7.8 Hz, 1H, H^f), 7.45 – 7.36 (m, 3H, H^e, H^d, H^{5'}), 7.33 (t, *J* = 7.3 Hz, 1H, H^{4'}), 1.69 (s, 15H, H^{Cp*(Me)}) ppm. **¹³C{¹H} NMR** (101 MHz, DMSO-d₆, 25 °C) δ 170.5 (d, ¹J_{C-Rh} = 31.1 Hz, 1C, C^{1'}), 160.0 (s, 1C, C^a), 139.6 (s, 1C, C^g), 136.7 (s, 1C, C^{6'}), 135.1 (s, 2C, C^{2'}, C^b), 130.8 (s, 1C, C^{5'}), 125.2 (s, 1C, C^{3'}), 125.1 (s, 1C, C^{4'}), 123.7 (s, 1C, C^d), 123.4 (s, 1C, C^e), 115.3 (s, 1C, C^c), 113.9 (s, 1C, C^f), 101.2 (d, ¹J_{C-Rh} = 5.5 Hz, 5C, C^{Cp*}), 9.1 (s, 5C, C^{Cp*(Me)}) ppm. NMR spectra were recorded in DMSO-d₆ due to the low solubility of this product in other solvents and so the resulting spectra correspond to $[(\eta^5\text{-C}_5\text{Me}_5)\text{Rh}(\text{DMSO-d}_6)(\kappa^2\text{-N,C-pbim})]\text{Cl}$. **FT-IR (ATR, cm⁻¹) selected bands:** 3094–3060 (m, ν_{CH}), 2985–2909 (m, ν_{CH}), 1589 (m, ν_{C=C + C-N}), 1534 (s), 1464–1458 (s, ν_{C=N}), 1429 (s), 1378 (w, δ_{CH3}), 1276 (s), 1020–1011 (m), 972 (m), 820 (w, δ_{C-C}), 764–745–735–725 (vs, δ_{CHoop}), 686 (m), 453 (m). **MS (FAB+)** in DMSO for $[(\eta^5\text{-C}_5\text{Me}_5)\text{Rh}(\text{DMSO-d}_6)(\kappa^2\text{-N,C-pbim})]\text{Cl}$: m/z (%) = 509 (15) ([M-Cl]⁺), 431 (100) ([M-Cl-DMSO]⁺). **Molar Conductivity (H₂O):** No data available due to low solubility in water or acetonitrile. **Solubility:** soluble in DMSO and DMF, partially soluble in methanol and insoluble in water and dichloromethane.

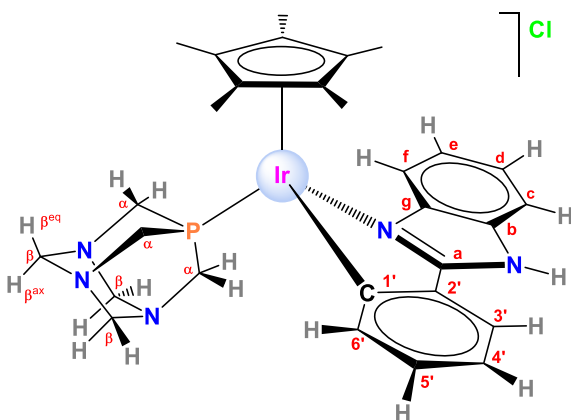
Cationic Complexes



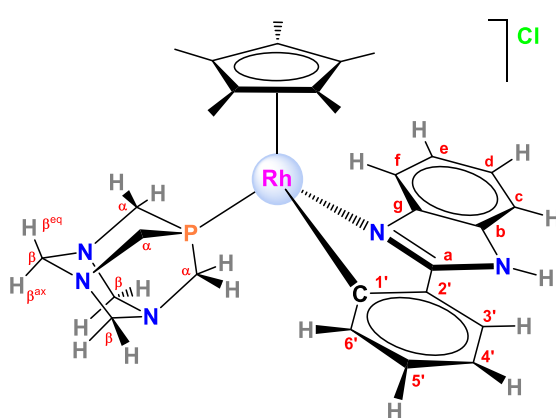
Synthesis of $[(\eta^6\text{-}p\text{-cymene})\text{Ru}(\kappa^2\text{-}N,C\text{-pbim})(\text{PTA})]\text{Cl}$, [11]Cl. In a 100 mL Schlenk flask, the ligand PTA (1,3,5-triaza-7-phosphaadamantane) (24 mg, 0.153 mmol) was added to a solution of $[(\eta^6\text{-}p\text{-cymene})\text{RuCl}(\kappa^2\text{-}N,C\text{-pbim})]$ (70.1 mg, 0.151 mmol) in methanol (11 mL), and the mixture was stirred at room temperature for 20 h and under a nitrogen atmosphere. The solution was filtered and concentrated. The product was precipitated with diethylether and isolated by filtration. The resulting white-yellowish powder was dried under vacuum. Yield: 73.7 mg (0.1187 mmol, 79%).

M_r ($\mathbf{C}_{29}\mathbf{H}_{35}\mathbf{N}_5\mathbf{P}\mathbf{Cl}\mathbf{Ru}$) = 621.1255 g/mol. **Anal. Calc.** for $\mathbf{C}_{29}\mathbf{H}_{35}\mathbf{N}_5\mathbf{P}\mathbf{Cl}\mathbf{Ru}\cdot(\mathbf{CH}_3\mathbf{OH})_{0.4}(\mathbf{H}_2\mathbf{O})_2$: C 52.71; H 6.11; N 10.45; Found: C 52.69; H 5.87; N 10.14. **¹H NMR** (400 MHz, CDCl₃, 25 °C) δ 15.23 (s, 1H, H^{N-H}), 8.67 (d, *J* = 7.5 Hz, 1H, H^{3'}), 8.00 – 7.92 (m, 1H, H^c), 7.61 (d, *J* = 7.3 Hz, 1H, H^{6'}), 7.32 (td, *J* = 5.6, 2.8 Hz, 3H, H^d, H^e, H^f), 7.20 (t, *J* = 7.5 Hz, 1H, H^{4'}), 7.14 (td, *J* = 7.3, 1.4 Hz, 1H, H^{5'}), 6.10 (d, *J* = 6.0 Hz, 1H, H³ o H⁵), 5.71 (d, *J* = 5.8 Hz, 1H, H⁵ o H³), 5.57 (d, *J* = 6.0 Hz, 1H, H⁶ o H²), 5.53 (d, *J* = 6.2 Hz, 1H, H² o H⁶), 4.20 (d, *J* = 13.3 Hz, 3H, H^{β_{ax}}), 4.05 (d, *J* = 12.9 Hz, 3H, H^{β_{eq}}), 3.46 (ABq, 6H, Δδ_{AB} = 0.03, *J_{AB}* = 15.7 Hz, H^α), 2.43 (s, 4H, H⁷, H¹⁰), 0.97 (d, *J* = 6.9 Hz, 3H, H⁸), 0.73 (d, *J* = 6.8 Hz, 3H, H⁹) ppm. **³¹P{¹H} NMR** (162 MHz, CDCl₃, 25 °C) δ -33.0 (s, 1P, P^{PTA}) ppm. **¹³C{¹H} NMR** (101 MHz, CDCl₃, 25 °C) δ 168.1 (d, ²J_{C-P} = 23.8 Hz, 1C, C^{1'}), 160.0 (s, 1C, C^a), 142.0 (s, 1C, C^g), 140.6 (s, 1C, C^{6'}), 135.2 (s, 1C, C^{2'}), 134.9 (s, 1C, C^b), 129.8 (s, 1C, C^{5'}), 127.5 (s, 1C, C^{3'}), 124.9 (s, 1C, C^{4'}), 123.9 (s, 1C, C^d), 123.4 (s, 1C, C^e), 118.6 (d, ²J_{C-P} = 5.1 Hz, 1C, C¹), 115.2 (s, 1C, C^c), 114.0 (s, 1C, C^f), 104.7 (s, 1C, C⁴), 92.18 (s, 1C, C³), 87.5 (d, ²J_{C-P} = 3.8 Hz, 1C, C²), 86.94 (s, 1C, C⁵), 86.88 (s, 1C, C⁶), 73.0 (d, ³J_{C-P} = 6.9 Hz, 3C, C^β), 52.6 (d, ¹J_{C-P} = 16.9 Hz, 1C, C^α), 31.7 (s, 1C, C⁷), 23.2 (s, 1C, C⁸), 21.7 (s, 1C, C⁹), 20.6 (s, 1C, C¹⁰) ppm. **FT-IR (ATR, cm⁻¹) selected bands:** 3356 (w, v_{N-H}), 2932-2895 (m, v_{CH}), 1591 (m, v_{C=C + C-N}), 1534 (m), 1465-1451 (m, v_{C=N}), 1379 (w, δ_{CH3}), 1280 (m), 1243 (m), 1099 (m), 1013 (s), 974-948 (vs), 898 (m), 806-787 (m, δ_{C-C}), 740 (vs, δ_{CHOop}), 578 (vs), 483 (s). **MS (FAB+):** m/z (%) = 586 (100) ([M]⁺), 429 (50) ([M-PTA]⁺). **Molar Conductivity (H₂O):** 95 S·cm²·mol⁻¹.

¹. Solubility: soluble in water, methanol, dichloromethane, chloroform and acetone.

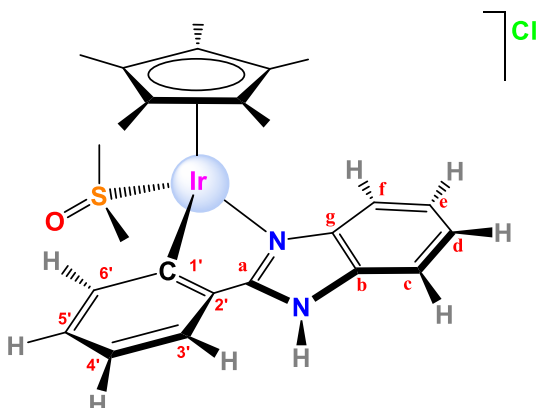


Synthesis of $[(\eta^5\text{-C}_5\text{Me}_5)\text{Ir}(\kappa^2\text{-N},\text{C-pbim})(\text{PTA})]\text{Cl}$, [12]Cl. The synthesis was performed as for [11]Cl, using (PTA) (17.1 mg, 0.109 mmol), $[(\eta^5\text{-C}_5\text{Me}_5)\text{IrCl}(\kappa^2\text{-N},\text{C-Pbim})]$ (60 mg, 0.108 mmol) in degassed methanol (11 mL). White powder. Yield: 59.6 mg (0.0836 mmol, 78%). **M_r** ($\text{C}_{29}\text{H}_{36}\text{N}_5\text{PClIr}$) = 713.2834 g/mol. **Anal. Calc.** for $\text{C}_{29}\text{H}_{36}\text{N}_5\text{PClIr} \cdot (\text{CH}_2\text{Cl}_2)_{0.75}(\text{H}_2\text{O})$: C 44.95; H 5.01; N 8.81; **Found:** C 44.91; H 5.03; N 8.53. ^1H NMR (400 MHz, CDCl_3 , 25 °C) δ 15.67 (s, 1H, $\text{H}^{\text{N-H}}$), 8.78 (d, J = 7.3 Hz, 1H, $\text{H}^{3'}$), 8.01 (d, J = 7.4 Hz, 1H, H^{c}), 7.51 (d, J = 7.5 Hz, 1H, $\text{H}^{6'}$), 7.39 – 7.29 (m, 3H, $\text{H}^{\text{d},\text{4'},\text{e}}$), 7.20 (td, J = 7.4, 1.4 Hz, 1H, $\text{H}^{5'}$), 7.15 (d, J = 7.4 Hz, 1H, H^{f}), 4.31 (d, J = 12.7 Hz, 3H, β_{ax}), 4.02 (d, J = 12.9 Hz, 3H, $\text{H}^{\beta_{\text{eq}}}$), 3.45 (ABq, 6H, $\Delta\delta_{\text{AB}} = 0.04$, $J_{\text{AB}} = 15.7$ Hz, H^{a}), 1.86 (d, J = 1.7 Hz, 15H, $\text{H}^{\text{Cp*}(\text{Me})}$) ppm. $^{31}\text{P}\{^1\text{H}\}$ NMR (162 MHz, CDCl_3 , 25 °C) δ -71.9 (s, 1P, P^{PTA}) ppm. $^{13}\text{C}\{^1\text{H}\}$ NMR (101 MHz, CDCl_3 , 25 °C) δ 146.6 (s, 1C, C^{l}), 139.9 (s, 1C, C^{a}), 139.0 (s, 1C, C^{g}), 135.8 (s, 1C, $\text{C}^{6'}$), 135.3 (s, 1C, $\text{C}^{2'}$), 135.1 (s, 1C, C^{b}), 131.0 (s, 1C, $\text{C}^{5'}$), 128.4 (s, 1C, $\text{C}^{3'}$), 125.4 (s, 1C, $\text{C}^{4'}$), 124.1 (s, 1C, C^{d}), 123.5 (s, 1C, C^{e}), 115.9 (s, 1C, C^{c}), 113.3 (s, 1C, C^{f}), 95.1 (s, 5C, $\text{C}^{\text{Cp*}}$), 73.2 (d, ${}^3J_{\text{C-P}} = 7.7$ Hz, 3C, C^{β}), 50.2 (d, ${}^1J_{\text{C-P}} = 22.4$ Hz, 3C, C^{a}), 10.3 (s, 5C, $\text{C}^{\text{Cp*}(\text{Me})}$) ppm. **FT-IR (ATR, cm⁻¹) selected bands:** 3382 (w, $\nu_{\text{N-H}}$), 2899 (m, ν_{CH}), 1591 (m, $\nu_{\text{C=C+C-N}}$), 1535 (m), 1466-1455 (m, $\nu_{\text{C=N}}$), 1382 (w, δ_{CH_3}), 1282 (m), 1242 (m), 1098 (m), 1014 (s), 971-947 (s), 897 (m), 814-803 (m, $\delta_{\text{C-C}}$), 748-740 (s, $\delta_{\text{CH}_{\text{loop}}}$), 580 (vs), 488 (m). **MS (FAB+):** m/z (%) = 1353 (3) ([2M-3H]⁺), 678 (100) ([M]⁺), 521 (42) ([M-PTA]⁺). Molar Conductivity (H_2O): 87 S·cm²·mol⁻¹. **Solubility:** soluble in dichloromethane, chloroform, methanol, water and acetone.



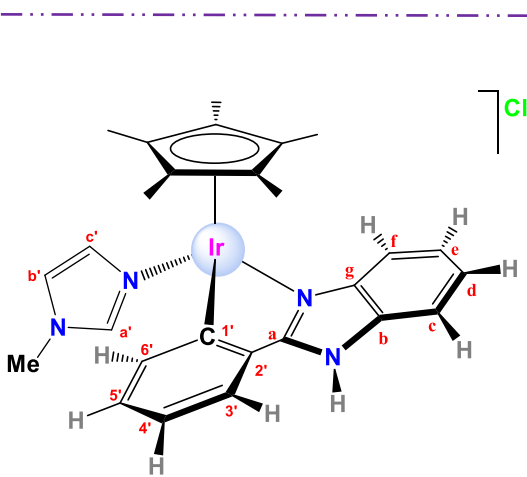
Synthesis of $[(\eta^5\text{-C}_5\text{Me}_5)\text{Rh}(\kappa^2\text{-N},\text{C-pbim})(\text{PTA})]\text{Cl}$, [13]Cl. In a 100 mL Schlenk flask 1,3,5-triaza-7-phosphoradecane (PTA) (17.1 mg, 0.109 mmol) was added to a solution of $[(\eta^5\text{-C}_5\text{Me}_5)\text{RhCl}(\kappa^2\text{-N},\text{C-pbim})]$ (50 mg, 0.107 mmol) in degassed methanol (12 mL), and the mixture

was stirred at room temperature for 20 h under a nitrogen atmosphere. The solution was filtered and concentrated under vacuum. The product was precipitated with diethylether and filtered. The resulting light yellow powder was dried under vacuum. Yield: 45.5 mg (0.0729 mmol, 68%). **M_r** ($C_{29}H_{36}N_5PClRh$) = 623.9689 g/mol. **Anal. Calc.** for $C_{29}H_{36}N_5PClRh \cdot (CH_2Cl_2)_{1.7}(H_2O)_{1.2}$: C 46.68; H 5.33; N 8.87; **Found:** C 46.64; H 5.46; N 9.29. **¹H NMR** (400 MHz, CDCl₃, 25 °C) δ 15.63 (s, 1H, H^{N-H}), 8.80 (d, *J* = 7.5 Hz, 1H, H^{3'}), 8.04 (d, *J* = 7.9 Hz, 1H, H^c), 7.44 (d, *J* = 7.5 Hz, 1H, H^{6'}), 7.37 – 7.27 (m, 4H, H^a, H^e, H^d, H^{5'}), 7.20 (d, *J* = 7.9 Hz, 1H, H^f), 4.30 (d, *J* = 13.1 Hz, 3H, H^{βax}), 4.09 (d, *J* = 13.8 Hz, 3H, H^{βeq}), 3.52 (ABq, 6H, Δδ_{AB} = 0.13, *J*_{AB} = 15.5 Hz, H^a), (d, *J* = 14.9 Hz, 3H, H^a), 3.48 (d, *J* = 14.8 Hz, 3H, H^a), 1.77 (s, 15H, H^{CP*(Me)}) ppm. **³¹P{¹H} NMR** (162 MHz, CDCl₃, 25 °C) δ -36.1 (d, *J*_{P-Rh} = 145.5 Hz, 1P, P^{PTA}) ppm. **¹³C{¹H} NMR** (101 MHz, CDCl₃, 25 °C) δ 165.1 (dd, *J*_{C-Rh} = 31.5 and *J*_{C-P} 8.8 Hz, 1C, C^{1'}), 159.6 (s, 1C, C^a), 140.4 (s, 1C, C^g), 135.8 (s, 1C, C^{6'}), 135.5 (s, 1C, C^{2'}), 135.1 (s, 1C, C^b), 130.6 (s, 1C, C^{5'}), 128.6 (s, 1C, C^{3'}), 126.0 (s, 1C, C^{4'}), 124.0 (s, 1C, C^d), 123.3 (s, 1C, C^e), 115.9 (s, 1C, C^c), 113.6 (s, 1C, C^f), 100.6 (dd, *J*_{C-Rh} = 4.8 and *J*_{C-P} = 2.2 Hz, 5C, C^{CP*}), 73.2 (d, *J*_{C-P} = 7.1 Hz, 3C, C^b), 51.1 (d, *J*_{C-P} = 15.6 Hz, 3C, C^a), 10.6 (s, 5C, C^{CP*(Me)}) ppm. **FT-IR (ATR, cm⁻¹)** selected bands: 3360 (w, v_{N-H}), 2899 (m, v_{-CH}), 1587 (m, v_{C=C + C-N}), 1533 (m), 1464–1454 (m, v_{C=N}), 1380 (w, δ_{CH₃}), 1280 (m), 1240 (m), 1096 (m), 1010 (s), 969–945 (vs), 896 (m), 800 (m, δ_{C-C}), 746 (vs, δ_{CH_{oop}}), 575 (vs), 481 (s). **MS (FAB+):** m/z (%) = 1175 (2) ([2M-H]⁺), 588 (100) ([M]⁺), 431 (45) ([M-PTA]⁺). **Molar Conductivity (H₂O):** 97 S·cm²·mol⁻¹. **Solubility:** soluble in water, methanol, dichloromethane, chloroform and acetone.

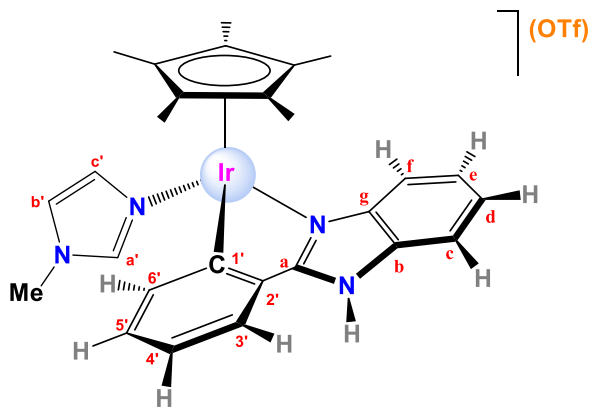


Synthesis of $[(\eta^5-C_5Me_5)Ir(DMSO)(\kappa^2-N,C-pbim)]Cl$. In a 100 mL Schlenk flask, DMSO (38 μL, 0.535 mmol) was added to a solution of $[(\eta^5-C_5Me_5)IrCl(\kappa^2-N,C-pbim)]$ (30 mg, 0.054 mmol) in degassed dichloromethane (9 mL) and the mixture was stirred at room temperature for 20 h under a nitrogen atmosphere. The solution was concentrated and diethylether was added to precipitate the product. The solvent was removed by filtration to isolate a white-yellowish powder that was washed with diethylether (2×5 mL) and dried under vacuum. Yield: 25.6 mg (0.040 mmol, 74%). **M_r** ($C_{25}H_{30}N_2SOClIr$) = 634.2635 g/mol. **Anal. Calcd** for $C_{25}H_{30}N_2SOClIr \cdot (CH_2Cl_2)_{0.6}$: C 43.89; H 4.67; N 4.16; S 4.76; **Found:** C 43.62; H 4.73; N 4.20; S 4.71. **¹H NMR** (400 MHz, DMSO-d₆, 25 °C) δ 14.29 (s, 1H, H^{N-H}), 8.00 (dd, *J* = 5.4, 3.5 Hz, 1H, H^{3'}), 7.80 (dd, *J* = 5.3, 3.2 Hz, 1H, H^{6'}), 7.71 (d, *J* = 8.2 Hz, 1H, H^c), 7.51 (d, *J* = 6.7 Hz, 1H, H^f), 7.48 – 7.40 (m, 2H, H^e, H^d), 7.32 (dd, *J* = 5.6, 3.3 Hz, 2H, H^{5'}, H^{4'}), 1.77 (s, 15H, H^{CP*(Me)}) ppm. **¹H NMR** (400 MHz, D₂O, 25 °C) δ 7.90 (dd, *J* = 8.6, 5.2 Hz, 2H), 7.76 – 7.69 (m, 1H), 7.61 – 7.56 (m, 1H), 7.52 – 7.47 (m, 2H), 7.42 – 7.36 (m, 2H), 2.94 (s, 3H, H^{CH₃(DMSO)}), 2.41 (s, 3H, H^{CH₃(DMSO)}), 1.80 (s, 15H, H^{CP*(Me)})

ppm. **FT-IR (ATR, cm⁻¹) selected bands:** 3354 (w, v_{N-H}), 2899 (m, v_{CH}), 1593 (s, v_{C=C + C-N}), 1540 (s), 1469-1455 (s, v_{C=N}), 1434 (s), 1379 (w, δ_{CH3}), 1278 (s), 1117 (vs, v_{S=O}), 1014 (vs), 746 (vs, v_{C-S}), 685 (w), 427 (vs). **MS (FAB+):** m/z (%) = 600 (4) ([M+H]⁺), 522 (10) ([M-DMSO+H]⁺). **Solubility:** soluble in dimethylsulfoxide and water, partially soluble in methanol.



Synthesis of [(\eta⁵-C₅Me₅)Ir(MeIm)(\kappa²-N,C-pbim)]Cl, [15]Cl. In a 100 mL Schlenk flask, the ligand N-methylimidazole (10 μL, 0.125 mmol) was added to a solution of [9] (0.0599 g, 0.108 mmol) and NaCl (0.0073 g, 0.125 mmol) in methanol (10 mL), and the mixture was stirred at 65 °C for 2 h and under a nitrogen atmosphere. The solvent was evaporated to dryness and the residue was solved in dichloromethane. The solution was filtered and the solid precipitated with n-hexane. The resulting white-yellowish powder was dried under vacuum. Yield: 53.8 mg (0.084 mmol, 78%). M_r (C₂₇H₃₀N₄ClIr) = 638.2335 g/mol. **Anal. Calcd for C₂₇H₃₀N₄ClIr·(H₂O)_{0.3}:** C 50.39; H 4.79; N 8.70; **Found:** C 50.38; H 4.70; N 8.57. **¹H NMR (400 MHz, CDCl₃, 25 °C)** δ 14.85 (s, 1H, H^{NH}), 8.46 (d, J = 7.6 Hz, 1H, H^{b'}), 7.89 (d, J = 7.4 Hz, 1H, H^c), 7.86 (d, J = 7.5 Hz, 1H, H^{b'}), 7.57 (d, J = 8.0 Hz, 1H, H^f), 7.30 (td, J = 7.7, 1.1 Hz, 1H, H^e), 7.27 – 7.22 (m, 1H, H^d), 7.17 (td, J = 7.4, 1.3 Hz, 1H, H^{a'}), 7.03 (t, J = 7.4 Hz, 1H, H^{d'}), 6.93 (s, 1H, H^{a'}), 6.66 (s, 1H, H^{c'}), 6.58 (s, 1H, H^{b'}), 3.46 (s, 3H, H^{N-Me}), 1.72 (s, 15H, H^{Cp*Me}) ppm. **¹³C{¹H} NMR (101 MHz, CDCl₃, 25 °C)** δ 164.7 (s, 1C, C^a), 158.2 (s, 1C, C^{1'}), 139.6 (s, 1C, C^g), 139.0 (s, 1C, C^{a'}), 135.8 (s, 1C, C^{2'}), 135.3 (s, 1C, C^b), 134.1 (s, 1C, C^{b'}), 131.5 (s, 1C, C^c), 131.2 (s, 1C, C^{5'}), 126.7 (s, 1C, C^{3'}), 124.0 (s, 1C, C^{4'}), 123.2 (s, 1C, C^d), 122.9 (s, 1C, C^e), 122.0 (s, 1C, C^{b'}), 115.1 (s, 1C, C^c), 113.4 (s, 1C, C^f), 88.5 (s, 1C, C^{CpC}), 9.9 (s, 1C, C^{Cp(Me)}). **FT-IR (ATR, cm⁻¹) selected bands:** 3410 (w, v_{N-H}), 3099 (w, v_{CH}), 1591-1537 (s, v_{C=C + C-N}), 1469-1454 (s, v_{C=N}), 1434 (m), 1384 (w, δ_{CH3}), 1277-1239 (m), 1101 (m, δ_{NHip}), 1028 (m), 821 (m, δ_{C-C}), 740 (vs, δ_{CHOop}). **MS (FAB+):** m/z (%) = 603 (35) ([M-Cl]⁺), 521 (100) ([M-Cl-MeIm]⁺). **Molar Conductivity (H₂O):** 108.5 S·cm²·mol⁻¹. **Solubility:** soluble in dichloromethane, chloroform, dimethylsulfoxide and acetone. Partially soluble in water.



Synthesis of $[(\eta^5\text{-C}_5\text{Me}_5)\text{Ir}(\text{MeIm})(\kappa^2\text{-N},\text{C}\text{-pbim})]\text{OTf}$, [15]OTf. The synthesis was performed as for **[15]Cl**, using MeIm (11.5 μl , 0.144 mmol), **[9]** (0.0704 g, 0.127 mmol) and NaOTf (0.025 g, 0.145 mmol) in degassed methanol (13 mL). White-yellowish powder. Yield: 78.8 mg (0.105 mmol, 83%). **M_r** ($\text{C}_{28}\text{H}_{30}\text{N}_4\text{F}_3\text{SO}_3\text{Ir}$) = 751.8512 g/mol. **Anal. Calcd for** $\text{C}_{28}\text{H}_{30}\text{N}_4\text{F}_3\text{SO}_3\text{Ir}\cdot(\text{C}_6\text{H}_{14})_{0.2}$: C 45.60; H 4.30; N 7.28; S 4.17; **Found:** C 45.61; H 4.36; N 6.97; S 3.66. **¹H NMR** (400 MHz, CDCl_3 , 25 °C) δ 12.75 (s, 1H, H^{NH}), 7.91 (d, J = 7.0 Hz, 1H, H^{f}), 7.85 (dd, J = 7.6, 1.0 Hz, 1H, $\text{H}^{\text{3'}}$), 7.77 (d, J = 7.7 Hz, 1H, H^{c}), 7.61 (d, J = 7.8 Hz, 1H, H^{f}), 7.33 (t, J = 7.1 Hz, 1H, H^{e}), 7.25 – 7.19 (m, 1H, H^{d}), 7.19 – 7.12 (m, 1H, $\text{H}^{\text{5'}}$), 7.06 (s, 1H, $\text{H}^{\text{a'}}$), 6.84 (td, J = 7.5, 1.1 Hz, 1H, $\text{H}^{\text{4'}}$), 6.69 (t, J = 1.4 Hz, 1H, $\text{H}^{\text{c'}}$), 6.59 (t, J = 1.6 Hz, 1H, $\text{H}^{\text{b'}}$), 3.49 (s, 3H, $\text{H}^{\text{N-Me}}$), 1.72 (s, 15H, $\text{H}^{\text{Cp*Me}}$) ppm. **¹³C{¹H} NMR** (101 MHz, CDCl_3 , 25 °C) δ 164.7 (s, 1C, C^{a}), 158.6 (s, 1C, $\text{C}^{\text{l'}}$), 139.8 (s, 1C, C^{g}), 139.4 (s, 1C, $\text{C}^{\text{d'}}$), 135.4 (s, 1C, $\text{C}^{\text{2'}}$), 135.2 (s, 1C, C^{b}), 134.6 (s, 1C, $\text{C}^{\text{6'}}$), 131.5 (s, 1C, $\text{C}^{\text{c'}}$), 131.4 (s, 1C, $\text{C}^{\text{5'}}$), 125.3 (s, 1C, $\text{C}^{\text{3'}}$), 123.9 (s, 1C, $\text{C}^{\text{4'}}$), 123.6 (s, 1C, $\text{C}^{\text{d'}}$), 123.2 (s, 1C, $\text{C}^{\text{e'}}$), 122.0 (s, 1C, $\text{C}^{\text{b'}}$), 120.9 (q, $J_{\text{C-F}} = 320.0$ Hz, 1C, C^{OTf}), 115.0 (s, 1C, C^{c}), 113.6 (s, 1C, C^{f}), 88.6 (s, 1C, C^{CpC}), 9.9 (s, 1C, $\text{C}^{\text{Cp(Me)}}$) ppm. **¹⁹F{¹H} NMR** (376 MHz, CDCl_3 , 25 °C) δ -78.3 (s, 3F, F^{OTf}) ppm. **FT-IR (ATR, cm⁻¹) selected bands:** 3130 (w, $\nu_{\text{=CH}}$), 2917 (w, $\nu_{\text{-CH}}$), 1595–1540 (m, $\nu_{\text{C=C+C-N}}$), 1470–1456 (m, $\nu_{\text{C=N}}$), 1435 (m), 1382 (w, δ_{CH_3}), 1283–1235–1223 (s, $\nu_{\text{C-F}}$), 1154 (s, $\nu_{\text{SO}_3\text{-asym}}$), 1105 (m, δ_{NHip}), 1028 (vs, $\nu_{\text{SO}_3\text{-sym}}$), 735 (s, δ_{CHoop}), 634 (vs, $\nu_{\text{C-S}}$). **MS (FAB+):** m/z (%) = 603 (63) ($[\text{M-OTf}]^+$), 521 (100) ($[\text{M-OTf-MeIm}]^+$). **Molar Conductivity (H₂O):** 51.9 S·cm²·mol⁻¹ (with solid in suspension). **Solubility:** soluble in dichloromethane, chloroform, dimethylsulfoxide. Slightly soluble in water.

4. BIBLIOGRAPHY

- (1) Liu, Z.; Sadler, P. J. *Acc. Chem. Res.* **2014**, *47*, 1174–1185.
- (2) Liu, Z.; Romero-Canelón, I.; Qamar, B.; Hearn, J. M.; Habtemariam, A.; Barry, N. P. E.; Pizarro, A. M.; Clarkson, G. J.; Sadler, P. J. *Angew. Chemie Int. Ed.* **2014**, *53*, 3941–3946.
- (3) Yellol, G. S.; Donaire, A.; Yellol, J. G.; Vasylyeva, V.; Janiak, C.; Ruiz, J. *Chem. Commun.* **2013**, *49*, 11533–11535.
- (4) Yellol, J.; Pérez, S. a.; Buceta, A.; Yellol, G.; Donaire, A.; Szumlas, P.; Bednarski, P. J.; Makhloufi, G.; Janiak, C.; Espinosa, A.; Ruiz, J. *J. Med. Chem.* **2015**, *58*, 7310–7327.
- (5) Novohradsky, V.; Liu, Z.; Vojtiskova, M.; Sadler, P. J.; Brabec, V.; Kasparkova, J. *Metallomics* **2014**, *6*, 682–690.
- (6) Liu, Z.; Habtemariam, A.; Pizarro, A. M.; Clarkson, G. J.; Sadler, P. J. *Organometallics* **2011**, *30*, 4702–4710.
- (7) Liu, Z.; Romero-Canelón, I.; Habtemariam, A.; Clarkson, G. J.; Sadler, P. J. *Organometallics* **2014**, *33*, 5324–5333.
- (8) Bennett, M. A.; Smith, A. K. *J. Chem. Soc. Dalt. Trans.* **1974**, 233–241.
- (9) White, C.; Yates, A.; Maitlis, P. M.; Heinekey, D. M. In *Inorg. Synth.*; **1992**; Vol. 29, pp. 228–234.
- (10) Kilpin, K. J.; Cammack, S. M.; Clavel, C. M.; Dyson, P. J. *Dalt. Trans.* **2013**, *42*, 2008–2014.
- (11) Vock, C. a; Scolaro, C.; Phillips, A. D.; Scopelliti, R.; Sava, G.; Dyson, P. J. *J. Med. Chem.* **2006**, *49*, 5552–5561.
- (12) Vock, C. a.; Renfrew, A. K.; Scopelliti, R.; Juillerat-Jeanneret, L.; Dyson, P. J. *Eur. J. Inorg. Chem.* **2008**, 1661–1671.
- (13) Krogstad, D. A.; Halfen, J. A.; Terry, T. J.; Young Jr., V. G. *Inorg. Chem.* **2001**, *40*, 463–471.
- (14) Scalambra, F.; Serrano-Ruiz, M.; Nahim-Granados, S.; Romerosa, A. *Eur. J. Inorg. Chem.* **2016**, *2016*, 1528–1540.
- (15) Dahrenbourg, D. J.; Robertson, J. B.; Larkins, D. L.; Reibenspies, J. H. *Inorg. Chem.* **1999**, *38*, 2473–2481.
- (16) Therrien, B. *Coord. Chem. Rev.* **2009**, *253*, 493–519.
- (17) Cardoso, C. R.; Lima, M. V. S.; Cheleski, J.; Peterson, E. J.; Venâncio, T.; Farrell, N. P.; Carlos, R. M. *J. Med. Chem.* **2014**, *57*, 4906–4915.
- (18) Bihari, Z.; Nagy, Z.; Buglyó, P. J. *Organomet. Chem.* **2015**, *782*, 82–88.
- (19) Jaros, S. W.; Guedes da Silva, M. F. C.; Florek, M.; Smoleński, P.; Pombeiro, A. J. L.; Kirillov, A. M. *Inorg. Chem.* **2016**, *55*, 5886–5894.
- (20) Pretsch, E.; Bühlmann, P.; Affolter, C.; Herrera, A.; Martínez, R. *Determinación estructural de compuestos orgánicos*; MASSON, S.A.: Barcelona, **2005**.
- (21) Nakamoto, K. *Infrared and Raman Spectra of Inorganic and Coordination Compounds*; Fourth Edition; John Wiley and Sons, **1986**.

- (22) Heyns, A. M. *Spectrochímica Acta A* **1977**, *33*, 315–322.
- (23) Angelici, R. J. In *Técnicas y Síntesis en Química Inorgánica*; Editorial Reverté, S.A., **1979**; p. 243.
- (24) Yellol, J.; Pérez, S. A.; Buceta, A.; Yellol, G.; Donaire, A.; Szumlas, P.; Bednarski, P. J.; Makhloufi, G.; Janiak, C.; Espinosa, A.; Ruiz, J. *J. Med. Chem.* **2015**, *58*, 7310–7327.
- (25) Li, B.; Roisnel, T.; Darcel, C.; Dixneuf, P. H. *Dalt. Trans.* **2012**, *41*, 10934–10937.
- (26) Zhang, L.; Li, L.; Wang, Y.; Yang, Y.; Liu, X.; Liang, Y. *Organometallics* **2014**, *33*, 1905–1908.
- (27) Leyva, L.; Sirlin, C.; Rubio, L.; Franco, C.; Le Lagadec, R.; Spencer, J.; Bischoff, P.; Gaiddon, C.; Loeffler, J. P.; Pfeffer, M. *Eur. J. Inorg. Chem.* **2007**, 3055–3066.
- (28) Lambert, W. *J. Chromatogr. A* **1993**, *656*, 469–484.
- (29) Biagi, G. L.; Barbaro, A. M.; Sapone, A.; Recanatini, M. *J. Chromatogr. A* **1994**, *662*, 341–361.
- (30) Paganelli, S.; Marchetti, M.; Bianchin, M.; Bertucci, C. *J. Mol. Catal. A Chem.* **2007**, *269*, 234–239.
- (31) Zhang, R.; Wu, W.; Luo, S. *J. Solution Chem.* **2011**, *40*, 1784–1795.
- (32) Liu, Z.; Deeth, R. J.; Butler, J. S.; Habtemariam, A.; Newton, M. E.; Sadler, P. J. *Angew. Chemie - Int. Ed.* **2013**, *52*, 4194–4197.
- (33) Lucas, S. J.; Lord, R. M.; Wilson, R. L.; Phillips, R. M.; Sridharan, V.; McGowan, P. C. *Dalt. Trans.* **2012**, *41*, 13800–13802.
- (34) Almodares, Z.; Lucas, S. J.; Crossley, B. D.; Basri, A. M.; Pask, C. M.; Hebden, A. J.; Phillips, R. M.; McGowan, P. C. *Inorg. Chem.* **2014**, *53*, 727–736.
- (35) Gutiérrez, A.; Cativiela, C.; Laguna, A.; Gimeno, M. C. *Dalt. Trans.* **2016**, *45*, 13483–13490.

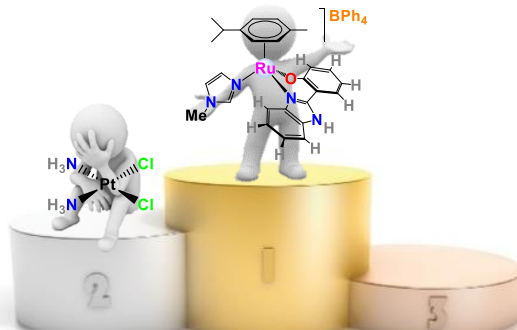
CHAPTER 3.

Ru(II) HALF-SANDWICH COMPLEXES BEARING HYDROXYPHENYL-BENZAZOLE ANCILLARY LIGANDS: SYNTHESIS, CHARACTERIZATION AND ANTICANCER PROPERTIES



CHAPTER 3. Ru(II) HALF-SANDWICH COMPLEXES BEARING HYDROXYPHENYLBENZAZOLE ANCILLARY LIGANDS: SYNTHESIS, CHARACTERIZATION AND ANTICANCER PROPERTIES

ABSTRACT: In this chapter a family of 12 new complexes of general formulae $[\text{Ru}(\eta^6\text{-arene})(\kappa^2\text{-O,N-L})\text{X}]$ and $[\text{Ru}(\eta^6\text{-arene})(\kappa^2\text{-O,N-L})\text{X}]\text{Y}$ (X = leaving group; Y = counterion) bearing 2-(2'-hydroxyphenyl)benzimidazole (hpbitz) and 2-(2'-hydroxyphenyl)benzothiazole (hpbtz) as ancillary ligands was synthesized in order to assess their anticancer properties. In particular, we aimed to analyze the effect of both the bidentate ligand and the substitution of the Cl^- leaving group by a pseudo-halide ligand or by monodentate N-donors or P-donors on the aqueous solubility and the cytotoxic activity.



CONTEXT: In the last decades organometallic complexes bearing 2-(2'-hydroxyphenyl)benzazole ligands have been reported in the literature, with transition metals such as zinc^{1,2}, iron³ or rhenium⁴, owing to the increasing interest in luminescent complexes. Nonetheless, neither ruthenium half-sandwich derivatives of 2-(2'-hydroxyphenyl)benzimidazole nor ruthenium derivatives of 2-(2'-hydroxyphenyl)benzothiazole are known so far and only a few octahedral monodentate N-coordinated and bidentate chelating complexes bearing the former have been reported with catalytic activity^{5,6,7,8} and one with cytotoxic activity.⁹ On the other hand, ruthenium(II) complexes with O,N-ancillary ligands have been commonly synthesized with picolinates. Thus, Ru(II) arene complexes bearing this kind of ligands are completely new as far as we know.

1. RESULTS AND DISCUSSION

1.1. Synthesis

The complexes were synthesised from the ruthenium chloro-bridged dimers $[\text{Ru}(\eta^6\text{-arene})(\mu\text{-Cl})\text{Cl}]_2$, already described in CHAPTER 1.^{10,11}

The complexes are divided in two groups: neutral and monocationic, whose schematic synthesis is shown in Fig. 1.

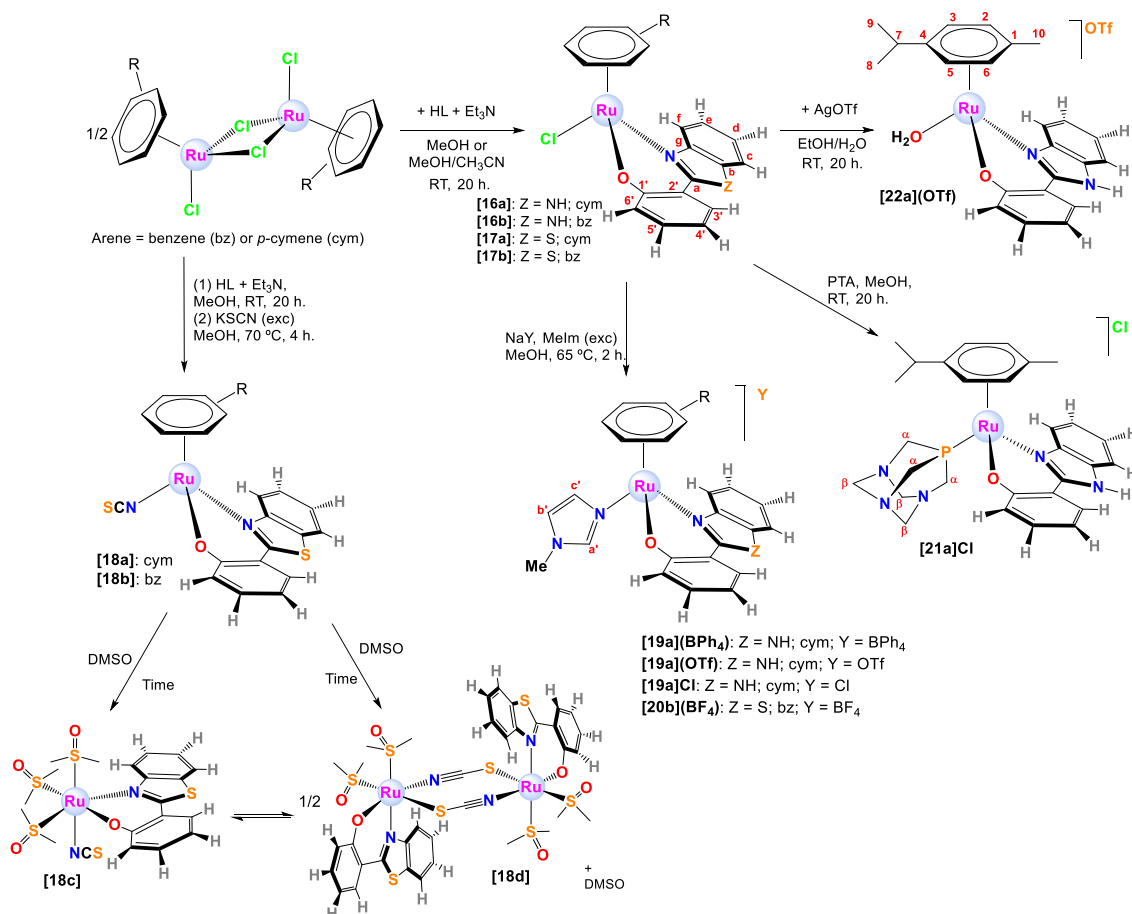


Fig. 1. Schematic synthesis of Ruthenium(II) complexes with hpbim and hpbtz.

Neutral complexes

The overnight reaction between the dimeric starting dimers with the ligands hpbim or hpbtz and triethylamine at room temperature and using methanol or a methanol/acetonitrile mixture yielded complexes of general formula $[(\eta^6\text{-arene})\text{RuCl}(\kappa^2\text{-}O,N\text{-L})]$ (**[16a]**, **[16b]**, **[17a]** and **[17b]**), where L is the deprotonated ligand and the arene = *p*-cymene (*p*-cym, series a); arene = benzene (bz, series b). The derivatives with thiocyanato of general formula $[\text{Ru}(\eta^6\text{-arene})(\text{SCN})(\kappa^2\text{-}O,N\text{-L})]$ (**[18a]** and **[18b]**) were prepared in two steps by a related protocol including a metathesis reaction, which involves stirring at 70 °C in the presence of an excess of KSCN.

Monocationic complexes

A mixture of chlorido-complexes (**[16a]**, **[16b]**, **[17a]** and **[17b]**) and methylimidazole (Melm) in the presence of a sodium salt (NaCl, NaOTf, NaBPh₄ and NaBF₄) in methanol was refluxed during two hours, yielding the complexes of general formula $[(\eta^6\text{-arene})\text{Ru}(\text{Melm})(\kappa^2\text{-}O,N\text{-L})]\text{Y}$ (**[19a](BPh₄)**, **[19a](OTf)**, **[19a]Cl** and **[20b](BF₄)**), where Y= Cl⁻, OTf⁻, BPh₄⁻ or BF₄⁻. The PTA derivative of formula $[(\eta^6\text{-}p\text{-cymene})\text{Ru}(\kappa^1\text{-}P\text{-PTA})(\kappa^2\text{-}O,N\text{-L})]\text{Cl}$ (**[21a]Cl**) was prepared likewise but at room temperature without the presence of any salt. The aquo complex of formula $[(\eta^6\text{-}p\text{-cymene})\text{Ru}(\text{OH}_2)(\kappa^2\text{-}O,N\text{-L})](\text{OTf})$ (**[22a](OTf)**), was synthesised by the reaction of the neutral complex **[16a]** with an excess of AgOTf in a mixture of distilled water and ethanol. Both PTA and Melm derivatives were prepared so as to enhance the solubility or reduce the aquation rate.

All the complexes were isolated in moderate-to-good yields (from 49% to 79% for neutral complexes and from 76% to 83% for cationic complexes) as the corresponding racemates (R_{Ru} or S_{Ru}) in the form of yellow, orange or brown powders.

1.2. Characterization

All the complexes have been fully characterised by NMR spectroscopy, IR spectroscopy, positive fast atom bombardment (FAB⁺) mass spectrometry, molar conductivity and elemental analysis.

1.2.1. NMR

The ¹H NMR spectra of neutral complexes **[16a]**, **[16b]**, **[17a]**, **[17b]**, **[18a]** and **[18b]** were recorded in CDCl₃, DMSO-d₆, CD₃CN or CD₂Cl₂ at 25 °C. As in previous complexes, the coordination of the O^N ligand to the metal deshielded the signals of the latter, especially H^f. The deshielding is enhanced in complexes with hpbtz (Z = S in Fig. 1), and especially in dimethylsulfoxide. The metal-ligand coordination is also evidenced by the absence of the resonance of the OH group. Complexes **[16a]** and **[16b]** showed a downfield-shifted signal corresponding to the NH group at δ 10.86 and 10.67 ppm respectively in CDCl₃. Moreover, some complexes like **[16b]** undergo slow solvolysis in DMSO-d₆, so that the Cl⁻ ligand is replaced by a DMSO molecule. The ¹H-¹H NOESY spectrum of **[16a]** (it cannot be observed for the benzene derivative) supported this fact, since there were some chemical exchange peaks in the *p*-cymene area, evidencing a fast process of interconversion between enantiomers (see CHAPTER 1 for further details).

The ¹H NMR spectra of monocationic complexes **[19a](BPh₄)**, **[19a](OTf)**, **[19a]Cl**, **[20b](BF₄)**, **[21a]Cl** and **[22a](OTf)** were recorded in CDCl₃, CD₃OD or DMSO-d₆ at 25 °C. The spectra of the Melm derivatives were quite complicated, especially that for the BPh₄⁻ salt, which made the signals difficult to assign. These complexes show the same pattern of peaks with some exceptions. The comparison of the three spectra for the **[19a]⁺** series in CDCl₃ allows us to extract some interesting conclusions (see Fig. 2). Thus, most of the signals for **[19a](BPh₄)** and **[19a](OTf)** are upfield shifted with regard to

those of the chloride salt. The explanation for these observations could have to do with the formation of ion pairs driven by different forces¹²:

- a) Hydrogen bonding interactions in the Cl⁻ salt (deshielding).
- b) C-H···π interactions in the BPh₄⁻ salt (shielding).

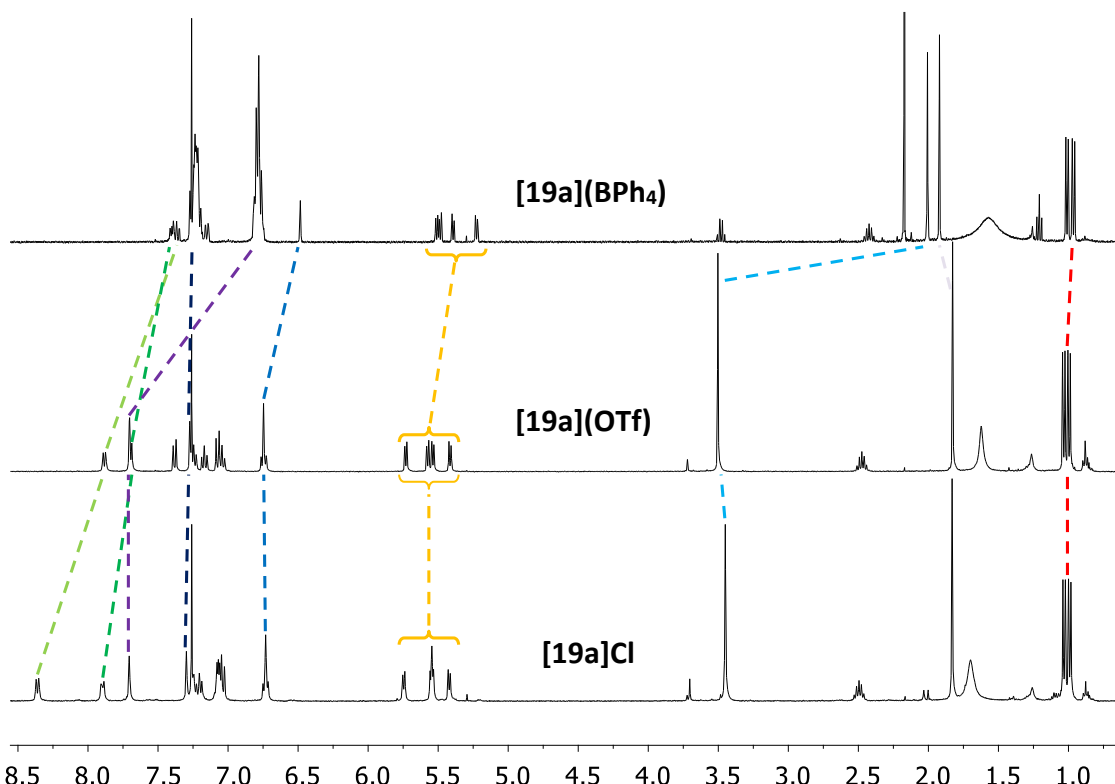


Fig. 2. Comparative spectra of [19a]Cl, [19a](OTf) and [19a](BPh₄) in CDCl₃ at 25 °C, with some characteristic highlighted signals. Melm signals are displayed in blue and purple, hpbim in green and *p*-cym in orange-coloured.

As regards the NH group in complexes with hpbim, the resonance was more deshielded (>14 ppm) than for their neutral derivatives, probably because of hydrogen bonding with the anionic counterion, especially with chloride as counterion (as the X-ray structure of [21a]Cl confirms). The ¹H NMR spectrum of [21a]Cl in CDCl₃ showed a doublet for the isopropyl group of *p*-cymene and two doublets for the hydrogens of the aromatic ring, indicating a fast dynamic process. However, no hydrolysis was observed for this complex. Moreover, a characteristic set of signals corresponding to the methylene groups of the PTA ligand was shown: a pseudo-quartet at 4.02 ppm (ABq, 6H, $\Delta\delta_{AB} = 0.07$, $J_{AB} = 14.4$ Hz, H^α) for the AB spin system of **diastereotopic** PCH₂N protons (H^α), and also another pseudo singlet (a coalesced pseudo-quartet) for the AB spin system at 4.32 ppm (ABq, 6H, $\Delta\delta_{AB} = 0.03$, $J_{AB} = 14.8$ Hz, H^β) formed by the intrinsically inequivalent NCH₂N protons (axial and equatorial orientations, H^{β_{ax}} and H^{β_{eq}}). A ¹H{³¹P} NMR was recorded so as to simplify the signals without apparent success, since the spectrum was exactly the same.

All these features suggest a fast hemilabile behaviour for the O,N-ligand, involving the dissociation of the benzimidazole moiety and its coordination after

rotation around the Ru-O bond, which allows a rapid interconversion between enantiomers (S_{Ru} , R_{Ru} ; see Fig. 3).

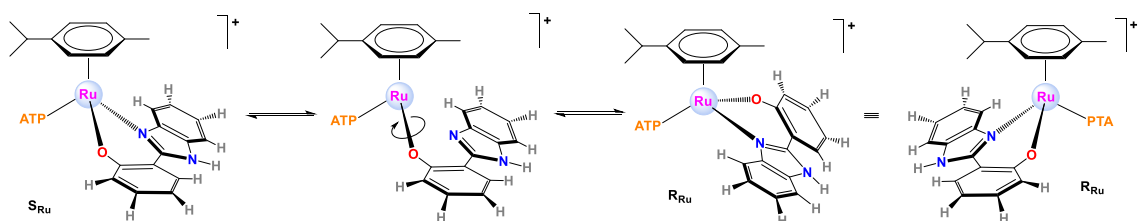


Fig. 3. Proposed mechanism for the interconversion process between enantiomers of [21a]Cl.

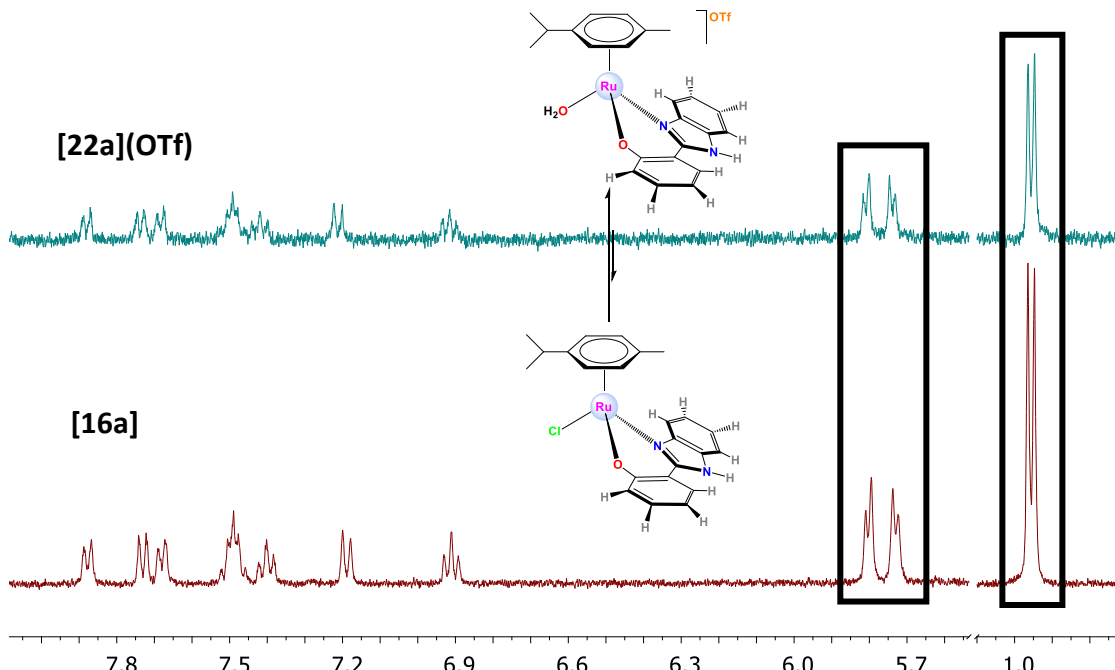


Fig. 4. ^1H -NMR comparison of [22a](OTf) with [16a] in D_2O at 25°C , showing the signals corresponding to a symmetric product.

The ^1H NMR spectrum in D_2O of the aqua-complex [22a](OTf), was coincident with that of its neutral precursor [16a] when recorded in deuterated water (see Fig. 4). In addition, *p*-cymene signals evidenced a symmetric product, as a doublet appeared for the isopropyl protons and two doublets for the aromatic ring of *p*-cymene. Thus, the aquation process for [16a] is extremely fast and we only detect the aquo complex, which is also involved in a dynamic exchange (see Fig. 5). In order to figure out this issue, different spectra of [16a] in D_2O were recorded at varying temperatures (25, 15 and 5 $^\circ\text{C}$). The spectra showed the broadening of the *p*-cymene signals, evidencing the possible division of the doublets. Nevertheless, the high melting point of water prevented us from lowering the temperature under 5 $^\circ\text{C}$.

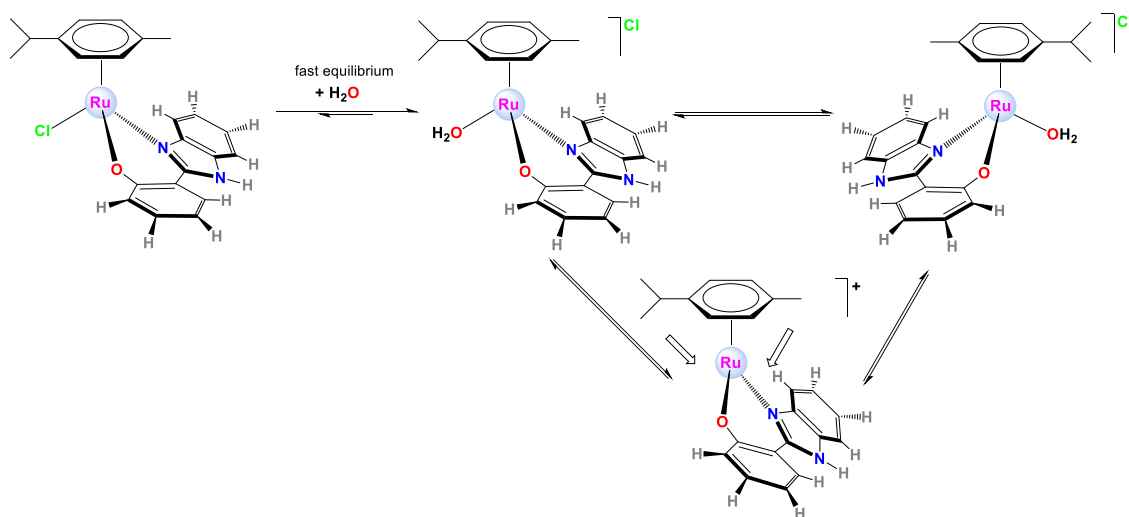


Fig. 5. Reaction schemes for the dynamic exchanges observed for [16a] in D_2O .

The $^{13}\text{C}\{^1\text{H}\}$ NMR spectra showed characteristic patterns for both the arenes and the ligands. The most downfield-shifted peak in every case was that of C^{1'} at around 167 ppm for the complexes bearing hpbim and at around 170 ppm for those with hpbtz.

Besides, the thiocyanato-complex **[18a]** showed a quaternary carbon resonance for the SCN⁻ at 135.4 ppm in DMSO-d₆. Monocationic complexes with PTA and Melm showed additional signals for their monodentate ligands.

Furthermore, complex **[21a]Cl** exhibits the C-P coupling (d , $^{1}\text{J}_{\text{C}-\text{P}} = 13.3$ Hz) for the signal of C^α of the PTA ligand. The constant coupling has similar values that other RAPTA derivatives ($^{1}\text{J}_{\text{C}-\text{P}} = 15$ Hz) depicted in the literature when coordinated to ruthenium.¹³ In addition, the coupling constant C-P increases when the PTA coordinates to a metal centre (for the free ligand: $^{1}\text{J}_{\text{C}-\text{P}} = 9$ Hz).¹⁴

$^{19}\text{F}\{^1\text{H}\}$ NMR spectra were recorded for monocationic complexes (**[19a]OTf**, **[20b]BF₄** and **[22a](OTf)**) with BF₄⁻ or OTf⁻ as counterions. A singlet was detected for triflate and two singlets were observed for tetrafluoroborate, due to the isotopic effect for ¹⁰B and ¹¹B.

The $^{31}\text{P}\{^1\text{H}\}$ NMR spectrum recorded for the complex **[21a]Cl** showed a singlet at δ -30.4 ppm, similar to other Ru-complexes reported in the literature {[Ru(*η*⁶-*p*-cymene)-(R₂acac)(PTA)]⁺, -29 to -30 ppm}.¹⁵ Moreover, the phosphorous signal shifts a lot when it coordinates to ruthenium ($Δδ = 71.2$ ppm), relative to the free ligand ($δ = -100$ ppm).

1.2.2. Mass Spectra

The FAB⁺ mass spectra of the complexes exhibit characteristic sets of peaks in agreement with the isotopic distribution patterns. [M]⁺ fragments are shown for neutral complexes and [M-Y]⁺ fragments for the monocationic ones, where Y is the counterion. Moreover, a fragment with a water molecule is featured for the aquo derivative **[22a](OTf)**.

1.2.3. IR Spectra

The infrared spectra recorded for all the complexes exhibit characteristic peaks for the normal vibrational modes of the corresponding rings $\nu_{C=N}$, $\nu_{C=C}$ and δ_{CHOop} , ν_{C-O} for hydroxyphenylbenzazole ligands. The thiocyanate derivatives show characteristic peaks at 2090-2099 cm⁻¹ (ν_{C-N}) and 750 cm⁻¹ (ν_{C-S}) and the PTA derivative presents two sets of signals at 1314-1284 and 804 cm⁻¹ corresponding to the ν_{C-N} and ν_{P-C} , respectively. The aquo complex shows very strong and diagnostic peaks for triflate, ν_{C-F} , ν_{SO_3-as} , ν_{SO_3-sym} at 1238-1225, 1170-1146 and 1029 cm⁻¹ respectively.

1.2.4. Molar Conductivity

Molar conductivity (Λ_m) values, gathered in Table 1, were measured in acetonitrile (10⁻³ M). The low values of the neutral complexes (1.9 - 13 S·cm²·mol⁻¹) confirm their nature as non-electrolytes. Moreover, molar conductivities for the cationic complexes display some anomalous values. For instance, compounds **[19a](OTf)**, **[20b](BF₄)** and **[22a](OTf)** are in the normal range for electrolytes 1:1 (142.5, 110.1 and 160.2 S·cm²·mol⁻¹, respectively), whereas **[19a]Cl**, **[19a](BPh₄)** and **[21a]Cl** are atypically below this range (67.4, 65.0 and 53.5 S·cm²·mol⁻¹, respectively).¹⁶ In light of the previous results, counterions seem to play a relevant role in molar conductivity. Chloride is able to connect to NH groups through hydrogen bonding interactions, forming ion-pairing, favoured in apolar solvents of low dielectric constant, but also in the aprotic ones like acetonitrile ($\epsilon = 37.5$ at 293K¹⁷). In addition, the tetraphenylborate counterion can form ion-pairing through π - π stacking interactions or C-H \cdots π contacts.

Table 1. Molar conductivity values for complexes measured in acetonitrile at room temperature.

Complex	Solvent	Λ_m (S·cm ² ·mol ⁻¹)
[16a]	acetonitrile	11.3
[16b]	acetonitrile	13.0
[17a]	acetonitrile	3.4
[17b]	acetonitrile	-
[18a]	acetonitrile	1.9
[18b]	acetonitrile	-
[19a]Cl	acetonitrile	67.4
[19a](OTf)	acetonitrile	142.5
[19a](BPh₄)	acetonitrile	65.0
[20b](BF₄)	acetonitrile	110.1
[21a]Cl	acetonitrile	53.5
[22a](OTf)	acetonitrile	160.2

1.2.5. X Ray Diffraction

Single crystals suitable for X-ray diffraction analysis were obtained for neutral complexes **[16b]·CH₃OH** and **[17a]** by slow evaporation of solvent (from the corresponding solution of methanol or methanol/water, respectively), **[16a]** from slow diffusion of hexane into the respective solution in dichloromethane, and **[18d]** from slow solvolysis of **[18b]** in a mixture of DMSO/acetone; and for cationic complexes **[19a](BPh₄)** (unsuitable to publish, but good enough to confirm the identity of the complex) and **[20b](BF₄)·H₂O** by slow evaporation of solvent (from the corresponding solution of methanol/acetone or water, respectively) and **[21a]Cl·CDCl₃·H₂O** by slow evaporation of CDCl₃ from an NMR sample of the complex.

The ORTEP diagrams for all the complexes are represented in Fig. 6. Bond lengths, angles and other relevant features of the structures (except **[19a](BPh₄)**) are gathered in Table 2, Table 3, Table 4 and Table 5.

In all cases, the corresponding unit cells show the two possible enantiomers (R_{Ru} and S_{Ru}) resulting from the stereogenic nature of the metal centre. The neutral and cationic complexes, with the exception of **[18d]**, adopt the expected half-sandwich pseudo-octahedral three-legged piano-stool geometry, and the arene ring displays a π -bounded η^6 -coordination mode, whereas the hydroxyphenylbenzazole ligand assumes a bidentate-chelate coordination mode (κ^2 -N,O). The third position is occupied by chloride, Melm or PTA.

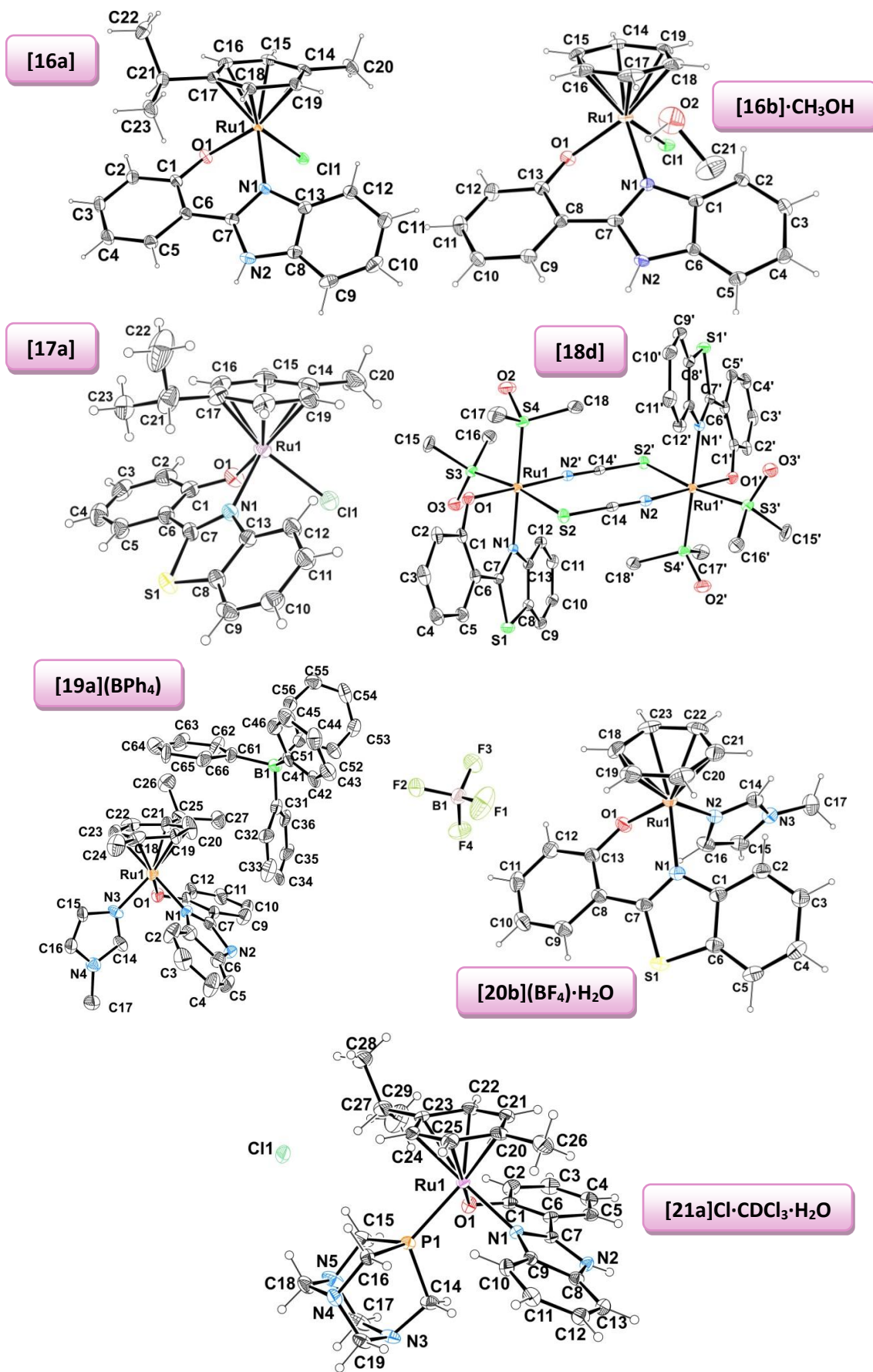


Fig. 6. ORTEP diagrams for complexes [16a], [16b]·CH₃OH, [17a], [18d], [19a](BPh₄), [20b](BF₄)·H₂O and [21a]Cl·CDCl₃·H₂O. Ellipsoids are shown at 30% probability.

Table 2. Selected bond lengths (Å) and angles (°) for complexes [16a], [16b]·CH₃OH and [17a] (S) and [17a] (R).

<i>Distance/angle</i>	[16a]	[16b]·CH ₃ OH	[17a] (S)	[17a] (R)
Ru1-Cl1	2.4312(8)	2.4289(8)	2.4069(12)	2.3992(12)
Ru1-N1	2.076(2)	2.085(2)	2.120(3)	2.112(3)
Ru1-O1	2.068(2)	2.070(2)	2.095(3)	2.075(3)
N1-C7	1.331(4)	1.339(3)	1.319(5)	1.319(5)
N2-C7	1.359(4)	1.359(4)	-	-
S1-C7	-	-	1.729(4)	1.726(4)
O1-C1	1.322(3)	1.315(3)??	1.331(5)	1.324(5)
O1-Ru1-N1	83.72(9)	82.92(9)	82.77(11)	83.29(12)
O1-Ru1-Cl1	87.15(6)	87.40(6)	84.86(9)	85.67(8)
N1-Ru1-Cl1	83.89(7)	86.01(6)	85.56(9)	87.25(9)

Table 3. Selected bond lengths (Å) and angles (°) for complexes [20b](BF₄)·H₂O and [21a]Cl·CDCl₃·H₂O.

<i>Distance/angle</i>	[20b](BF ₄)·H ₂ O	[21a]Cl·CDCl ₃ ·H ₂ O
Ru1-N2 ^a /P1 ^b	2.107(2)	2.3040(10)
Ru1-N1	2.114(2)	2.068(3)
Ru1-O1	2.0668(18)	2.069(2)
N1-C7	1.326(3)	1.339(4)
N2-C7	-	1.345(4)
S1-C7	1.737(2)	-
O1-C1/C13 ^a	1.321(3)	1.321(4)
O1-Ru1-N1	83.98(7)	82.43(10)
O1-Ru1-N2 ^a /P1 ^b	81.61(7)	80.69(7)
N1-Ru1-N2 ^a /P1 ^b	84.35(8)	88.89(8)

^a Atom numbering for [20b](BF₄)^b Atom numbering for [21a]Cl.

The chelate ring shows lack of planarity in all cases due to the oxygen atom, which adopts an sp³ hybridization. The Ru-centroid distances of the neutral derivatives fall in a narrow interval (1.660-1.669 Å). The Ru-Cl distances (2.399-2.431 Å) for neutral complexes are in the upper limit of the range, probably owing to the σ-donor nature of the bidentate anionic ligand. The Ru-O distances (2.068-2.095 Å) are slightly shorter than the Ru-N lengths (2.076-2.120 Å) in all cases. For the cationic complexes, the Ru-centroid distances (1.680-1.701 Å) are higher than those of the neutral compounds. For the PTA derivative ([21a]Cl·CDCl₃·H₂O), the Ru-N and Ru-O distances are almost the same, (2.078 Å and 2.079 Å), whereas the Ru-P distance (2.304 Å) is standard. The Melm derivative ([20b](BF₄)·H₂O) shows Ru-N and Ru-O distances of 2.114 Å and 2.067 Å, respectively, following the same tendency as in the neutral complexes. The Ru-N(Melm) distance (2.107 Å) is similar to those in related complexes reported in the literature.^{18,19} All the angles are in a similar range and are determined by the features of the ligand.

Table 4. Selected geometric parameters^[a] for the metal complexes of [16a], [16b]·CH₃OH, [17a], [20b](BF₄)·H₂O and [21a]Cl·CDCl₃·H₂O.

Distance/angle	[16a]	[16b]·CH ₃ OH	[17a] (S)	[17a] (R)	[20b](BF ₄)·H ₂ O	[21a]Cl·CDCl ₃ ·H ₂ O
Range of Ru-C distances	2.150(3)-2.202	2.123(14)-2.179(7)	2.158(4)-2.213(4)	2.140(4)-2.240(4)	2.173(3)-2.201(3)	2.202(4)-2.225(4)
Ru-centroid	1.660	1.660/ 1.647	1.666	1.669	1.680	1.701
α	18.39	17.71	20.68	16.21	19.63	17.52
ϑ (N-C-C-C)	19.88	17.07	22.48	-18.87	20.26	19.49
β (chelate-arene)	28.74	24.12	22.73	19.09	28.25	15.26
γ (C _x -C _{ipso} -Ru-Y)	-16.69	-	21.95	-13.13	-	78.57
λ	30.06	33.15	36.84	36.57	30.33	42.32

[a]Calculated with Mercury, version 3.8.

Table 5. Selected bond lengths (Å) and angles (°) for complex [18d].

Distance	[18d]	Angle	[18d]
Ru1-N2'	2.035(3)	O1-Ru1-N1	88.29(12)
Ru1-N1	2.118(3)	O1-Ru1-N2'	173.27(13)
Ru1-O1	2.047(3)	N1-Ru1-N2'	95.03(13)
Ru1-S2	2.4868(11)	N2'-Ru1-S2	90.40(10)
Ru1-S3	2.2650(11)	O1-Ru1-S2	84.02(9)
Ru1-S4	2.2579(11)	N1-Ru1-S2	85.33(9)
N1-C7	1.314(5)	S3-Ru1-S2	170.81(4)
S1-C7	1.746(4)	S4-Ru1-S2	90.91(4)
O1-C1	1.303(5)	N2'-Ru1-S3	97.39(10)
N2-C14	1.158(5)	O1-Ru1-S3	88.50(9)
S2-C14	1.654(4)	N1-Ru1-S3	89.12(9)
		S4-Ru1-S3	94.26(4)
		N2'-Ru1-S4	87.69(10)
		O1-Ru1-S4	88.63(9)
		N1-Ru1-S4	175.37(9)
		N2-C14-S2	179.6(4)

The complex [16a] presents a 3D architecture based on hydrogen bonding and π-π interactions, as shown in Fig. 7. The hydrogen bonds are built among electronegative atoms (Cl, O and N) and H atoms of aromatic rings, creating a channel (see Fig. 7a). The π-π stacking interactions, whose parameters are showed in Table 6, occur between the hydroxyphenyl ring and the benzene ring of the benzimidazole moiety, creating dimers (see Fig. 7 and Fig. 8). It is noteworthy, the bend of the H atom of the NH group, which is 13.93° out of the plane of the imidazole ring (see Fig. 7b). This curvature could be forced by the hydrogen bond N-H···Cl, with the pairing molecule.

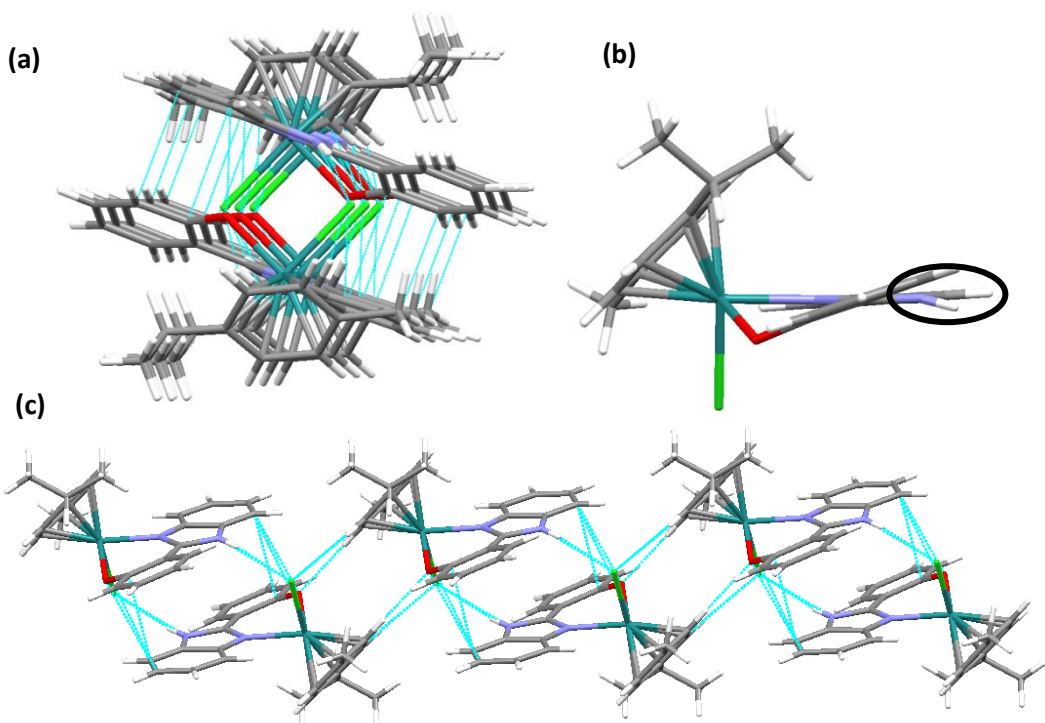


Fig. 7. 3D architecture of **[16a]** showing (a) the channel, (b) N-H bend and (c) hydrogen bonding and π - π stacking interactions.

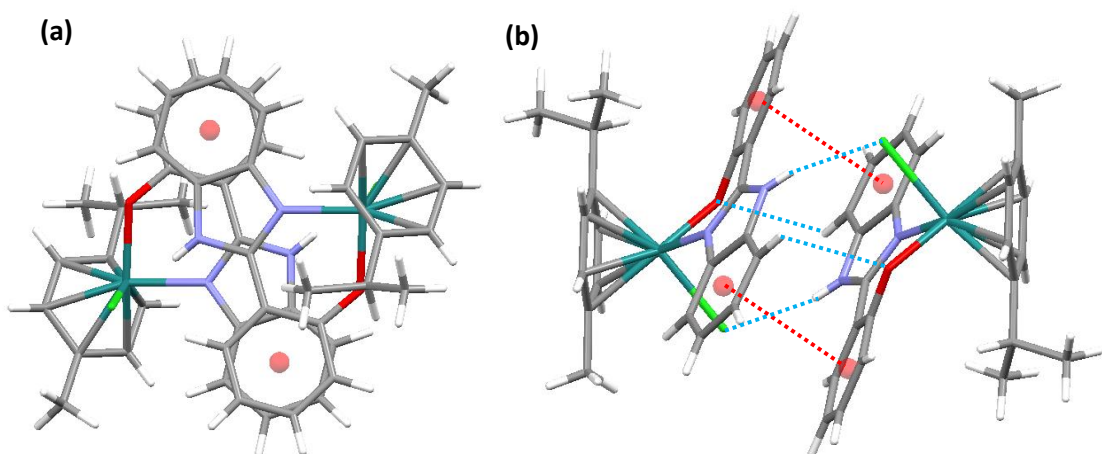


Fig. 8. π - π stacking interactions of **[16a]**. (a) An upper view with the coincident centroids of the rings (hph/bzim) and (b) complex pairing through H-bonding and π - π stacking interactions.

The asymmetric unit of **[16b]·CH₃OH** shows both enantiomers R_{Ru} and S_{Ru}. The structure exhibits a CH₃OH molecule in the second coordination sphere, which connects three different cationic units with hydrogen bonds through the chloride atom of one complex, a hydrogen atom of the arene of a second complex and a hydrogen atom of the benzimidazole moiety of a third one (see Fig. 9).

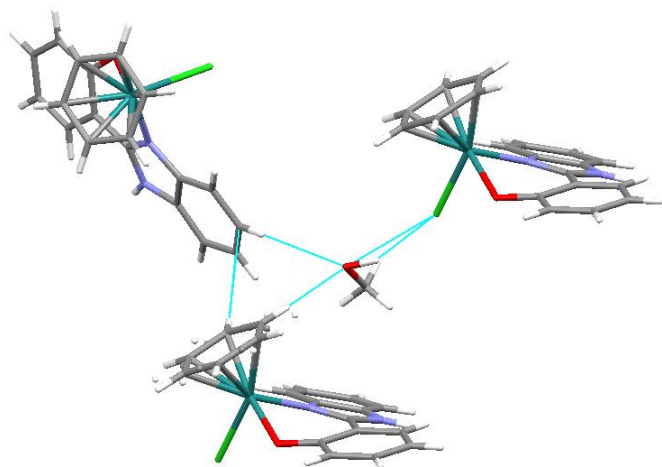


Fig. 9. Structural connection of three cationic entities through a methanol molecule for [16b]·CH₃OH.

The 3D architecture of [20b](BF₄)·H₂O exhibits the interconnection of cationic substructures through a water molecule (included in the crystalline structure) and the BF₄⁻ (see Fig. 10). The hydroxyphenyl rings of two molecules interact through an offset π-π stacking contact, whose parameters are gathered in Table 6. Furthermore, the representation of the packaging cell over the c axis shows a hole or channel, which contains the water molecules. Thus, we could say it is a hydrophilic channel.

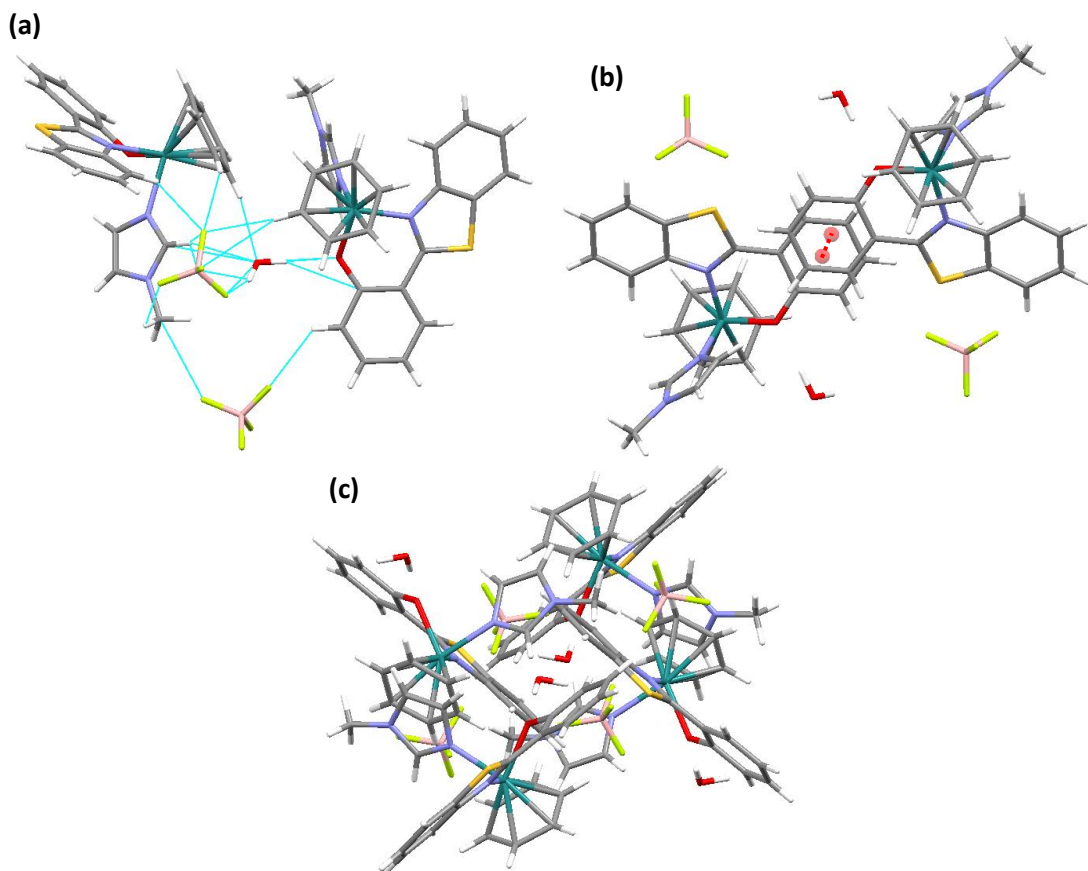


Fig. 10. Structural architecture of [20b](BF₄)·H₂O showing (a) connection between molecules, (b) offset π-π stacking interaction and (c) hydrophilic channel.

The complex **[21a]Cl·CDCl₃·H₂O** exhibits two solvent molecules in the second coordination sphere, consisting in one water molecule and one molecule of deuterated chloroform (see Fig. 11). All of them along with the chloride counterion are the assemblies that form the crystal architecture of the complex through hydrogen bonds. The phenyl rings of the benzimidazole moieties are also connected through offset π-π stacking interactions (see Table 6).

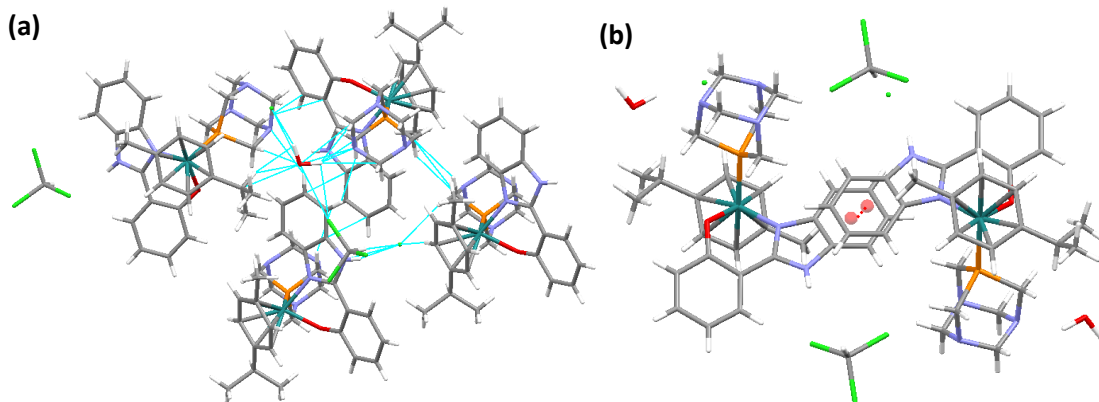


Fig. 11. Molecular assemblies of complex **[21a]Cl·CDCl₃·H₂O** showing (a) connection between molecules, (b) offset π-π stacking interaction.

Table 6. π-π offset stacking parameters for complexes **[16a]**, **[18d]**, **[20b](BF₄)·H₂O** and **[21a]Cl·CDCl₃·H₂O**.

Compound	d _{cent-cent} (Å)	α (°)	d _{cent-pl} (Å)	β (°)	d _{offset} (°)
[16a]	3.604	15.23	3.482	14.95	0.930
			3.500	13.80	0.860
[18d]	3.819	5.88	3.338	29.07	1.855
			3.323	29.53	1.882
[20b](BF₄)·H₂O	3.849	0.00	3.324	30.28	1.941
			3.324	30.28	1.941
[21a]Cl·CDCl₃·H₂O	3.794	0.00	3.340	28.32	1.800
			3.340	28.32	1.800

The structure obtained for **[18d]** from a solution of **[18b]** shows a non-expected distorted octahedral dinuclear complex, which has lost the arene and displays two thiocyanate bridges connecting both ruthenium atoms (μ -SCN). The octahedral coordination sphere for each ruthenium atom is completed with a hydroxyphenylbenzimidazole ligand adopting a bidentate-chelate coordination mode (κ^2-N,O), and two dimethylsulfoxide S-coordinated molecules in a *cis* arrangement. The resulting formula is $[\text{Ru}(\kappa^2-N,O\text{-hpbtz})\{\kappa^1\text{-S-SO}(\text{CH}_3)_2\}_2(\mu\text{-SCN})]_2$ (**[18d]**). An attempt to obtain crystals for **[18a]** in different DMSO mixtures also led to the same structure **[18d]**. A bibliographic search of related complexes with thiocyanate bridges hardly shows two results of thiocyanato-bridged ruthenium complexes.^{20,21} The Ru-S distances are slightly longer for the thiocyanate (2.4868 Å) than for the DMSO molecules (2.2579-2.2650 Å). The shortest bonds in the metal coordination sphere correspond to the Ru-O(hpbtz)

(2.047 Å) and to the Ru-N(SCN) (2.035 Å). The C-N distance is shorter than the C-S in the SCN moiety, in agreement with the triple bond nature of the C-N bond. The Ru-N-C-S units are not completely linear, due to the hybridization of N (sp) and S (sp^3) atoms. Thus, the Ru-N-C angle (164.25°) is below 180° and the Ru-S-C angle (104.46°) is slightly below 109.5°, the corresponding angles for linear sp and tetrahedral sp^3 geometries, respectively (see Fig. 13). Thus, the $\text{Ru}_2(\text{SCN})_2$ core can be described as a rhomboid. There is some weak intramolecular hydrogen bonding interactions (see Fig. 12 and Table 7), as well as a S- π interaction between the sulphur atom of the thiocyanate bridge and the hydroxyphenyl ring of the O^N ligand (see Fig. 12a and Table 8). This kind of interactions are very common among proteins (*e.g.* cysteine moieties), being the usual distance S-centroid of 3.9 Å.^{22,23} In addition, some intermolecular π - π stacking interactions were also observed between ligands (hph/btz) (see Fig. 12b and Table 6).

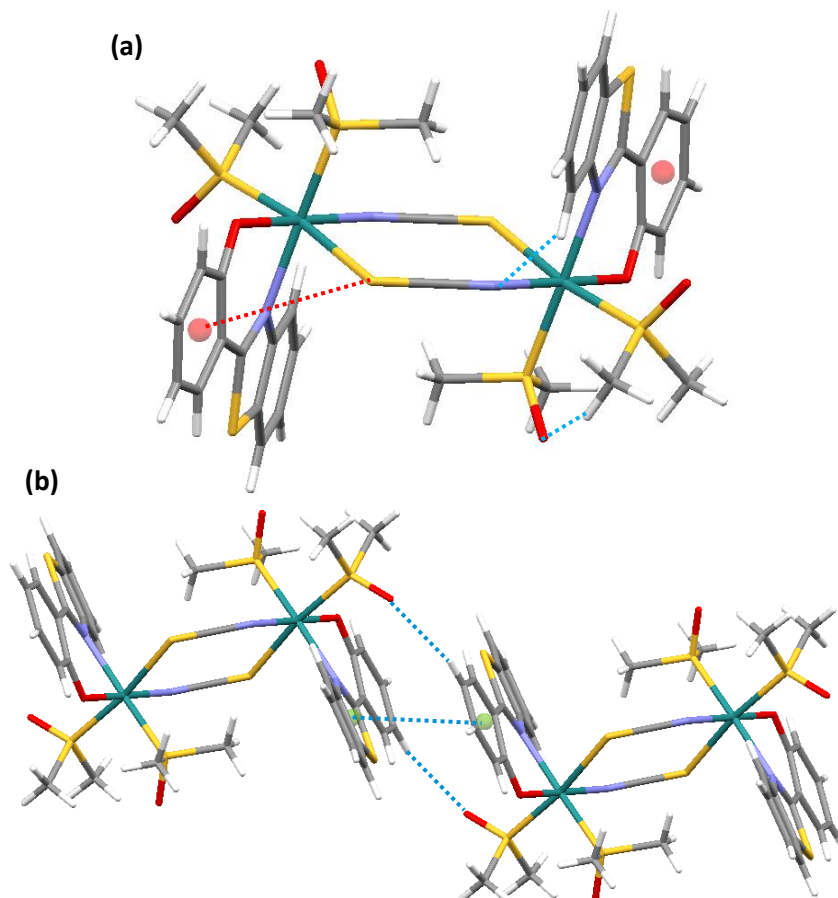


Fig. 12. X-ray structure of [18d] showing (a) the octahedral geometry of ruthenium atoms, the thiocyanate bridges, the coordination of DMSO molecules through the sulphur atom, and the hydrogen bonding (blue) and S- π interaction (red) and (b) the intermolecular π - π stacking reinforced with a C-H...O interaction.

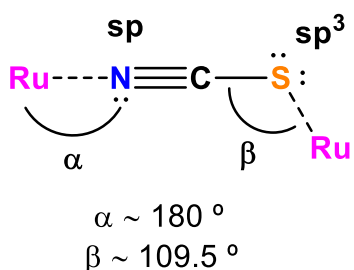


Fig. 13. Hybridization and corresponding angles for the Ru-N≡C-S-Ru unit.

Table 7. Intramolecular hydrogen bonding parameters for complex [18d].

H-bonding	D···A (Å)	X···A (Å)	D···X (Å)	α (°)
C(12)-H(12)···N(2)	3.066	2.458	0.951	121.73
C(16)-H(16B)···O(2)	3.194	2.414	0.980	136.22

Table 8. Geometric parameters of ip- π interactions (C-S··· π) for complex [18d].

Compound	$d_{S\text{-cent}}$ (Å)	$d_{S\text{-plane}}$ (Å)	d_{offset} (Å)	$\alpha_{c\text{-s-cent}}$ (°)	ϕ_1 (°)
C(14)-S(2)··· π	3.973	2.671	2.941	162.29	47.76

* d_{offset} has been calculated as $(d_{S\text{-centroid}}^2 - d_{S\text{-plane}}^2)^{1/2}$.

1.3.Thiocyanate Coordination Mode

Thiocyanato-complexes [18a] and [18b] were synthesized with the aim of exploring the cytotoxicity differences when changing the halide for a pseudo-halide as the leaving group. Thiocyanate ion is a linear ambidentate ligand able to coordinate to the metal through the hard nitrogen atom (isothiocyanato) or the soft sulphur atom (thiocyanato). Fig. 14 represents the resonance structures of the SCN⁻ anion.



Fig. 14. Resonance structures of thiocyanate anion.

In addition, a bridging coordination mode is possible when both sulfur and nitrogen coordinate to different metal centres. In order to clarify the coordination mode, a thorough characterization was performed. ¹³C{¹H} NMR and IR measurements were selected as diagnostic techniques for that purpose and both show evidences of the N-bonding in complexes [18a] and [18b] (see Fig. 15). A deep analysis of ¹³C{¹H} NMR spectra reported in the literature for different coordinated thiocyanate revealed a difference between chemical shifts depending on the bonded atom. The result leads to a sequence that could be generalized in order of increasing chemical shift: S-bound < ionic \leq N-bound.²⁴ The average chemical shift for the ionic thiocyanate is 131 ppm in DMSO-d₆ and for [18a] is downfield shifted up to 135 ppm, suggesting coordination through the nitrogen atom. Moreover, the infrared spectrum of [18a] shows a strong peak at 2090 cm⁻¹ for the C-N stretching frequency, whereas wave numbers higher than 2100 cm⁻¹ are assumed to be for S-bonded,^{25,26} evidencing the coordination through the

nitrogen atom ($\kappa^1\text{-N-SCN}$). For the complex **[18b]** a quality $^{13}\text{C}\{\text{H}\}$ NMR spectrum was impossible to record owing to the very low solubility of the complex in organic solvents. In the infrared spectrum, the C-N stretching frequency appears at 2098 cm^{-1} , which makes difficult to determine the atom bonding. Nevertheless, the C-S stretching frequency, which also acts as diagnostic peak, appears at wavenumbers above 780 cm^{-1} for N-bonded, and below 720 cm^{-1} for S-bonded complexes. Both **[18a]** and **[18b]** show the C-S band at 751 cm^{-1} and thiocyanate in **[18a]** is coordinated through the N atom. As a consequence, both ought to have the same coordination mode. The thiocyanate coordination mode also depends on the dielectric constant of the solvent as well as on the metal and ligand nature.^{27,28}

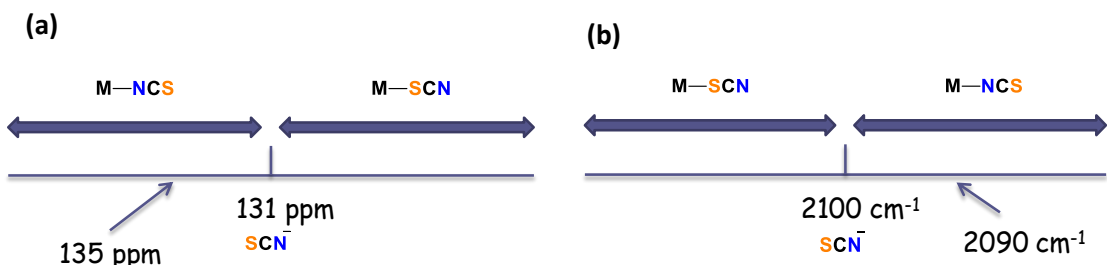


Fig. 15. Schematic drawing about typical (a) v in IR and (b) δ in ^{13}C NMR for different metal-thiocyanate coordination modes.

1.4. Stability of complex **[18a]** and arene loss

A ^1H -NMR study was carried out so as to know more about the mechanism involved in the degradation process of **[18a]** under irradiation or exposition to sunlight. The stability of **[18a]** was studied in DMSO-d₆ solution at room temperature and exposed to visible light for 3 months. Fig. 16 shows the spectra recorded at 3 minutes, and after 24 h and 3 months. After 24 h the variation in the spectrum was negligible. However, after 3 months a remarkable decomposition of the complex occurred.

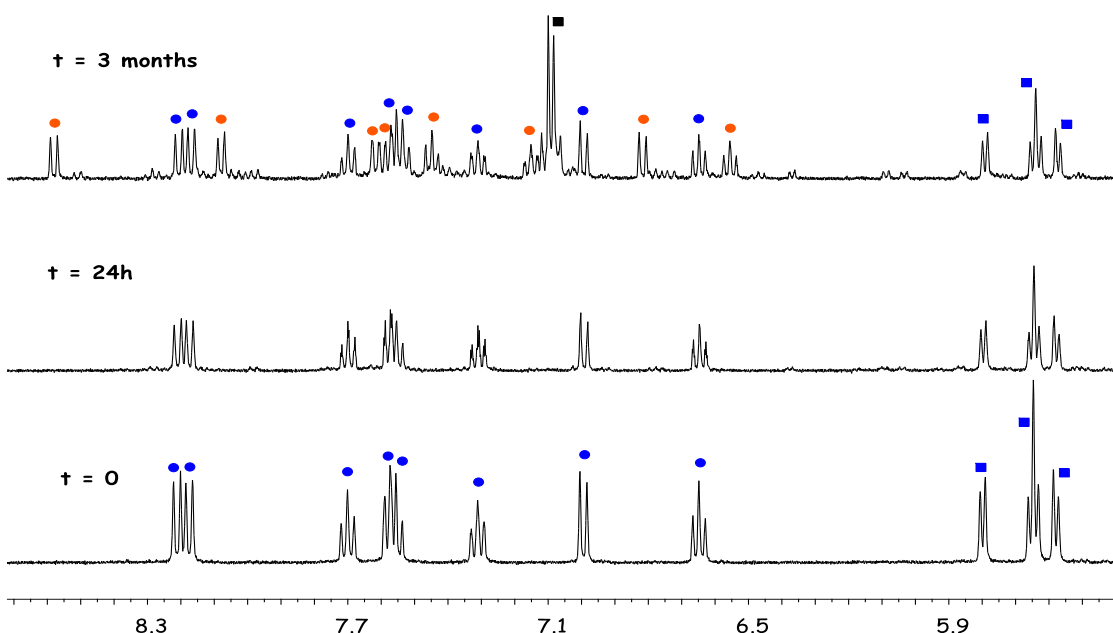


Fig. 16. ^1H -NMR study of the stability of **[18a]** in DMSO-d₆ at 25°C.

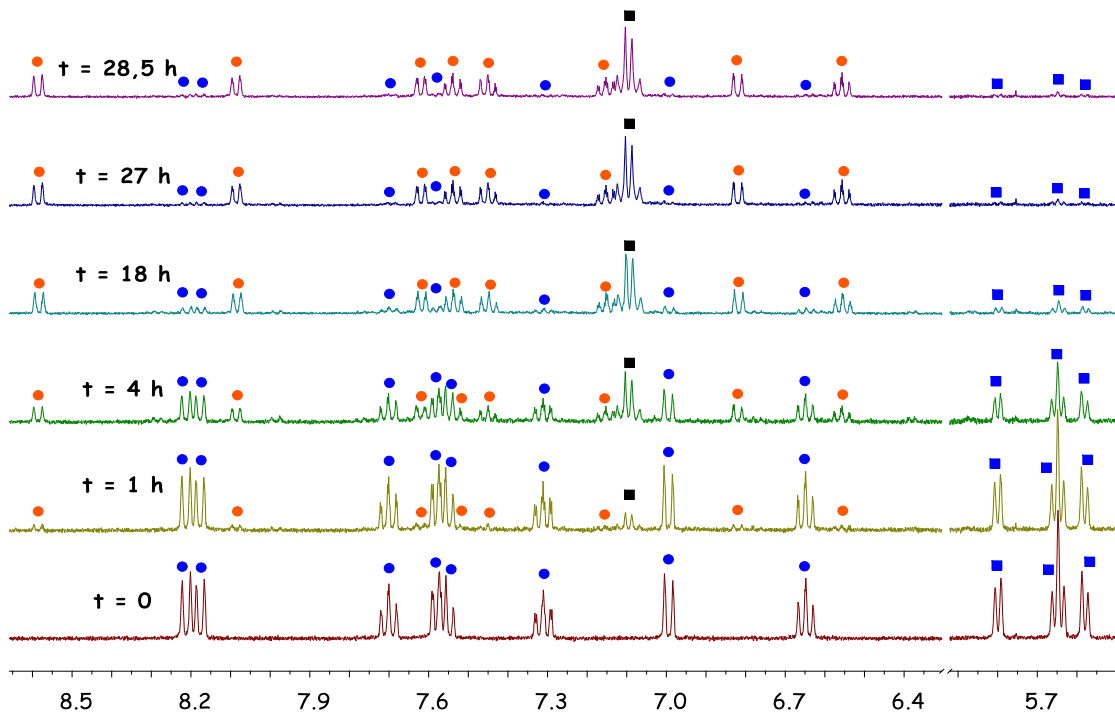


Fig. 17. ^1H -NMR spectra of the evolution of **[18a]** in DMSO-d_6 at $25\text{ }^\circ\text{C}$ after different irradiation times.

A freshly prepared DMSO-d_6 solution 1.7 mM of **[18a]** was used to evaluate the behaviour of the complex under exposure to UV-light. Some spectra were registered before irradiating the sample and after different irradiation times. The selected wavelength was 325 nm , although a potent white light also worked. Fig. 17 shows the evolution of the sample when irradiated.

The blue spots correspond to the complex **[18a]** before irradiating the sample. When it is irradiated, a new complex **[18c]** is formed (orange spots) and *p*-cymene is lost (black squares).³⁰ In addition, the corresponding signals of **[18a]** (blue squares) disappear. After approximately 29 hours, the decomposition reaction was almost finished. Fig. 18 features the reaction scheme for the arene dissociation and DMSO coordination under UV irradiation of **[18a]**. Mass spectrometry was carried out with the same NMR sample in deuterated dimethylsulfoxide after 29 h irradiation. The FAB^+ mass spectrum confirmed the hypothesis of the formation of a new octahedral complex with three DMSO-d_6 molecules coordinated to ruthenium (see Fig. 19). Furthermore, some reported works also show the loss of the arene in ruthenium complexes.^{31,30,32}

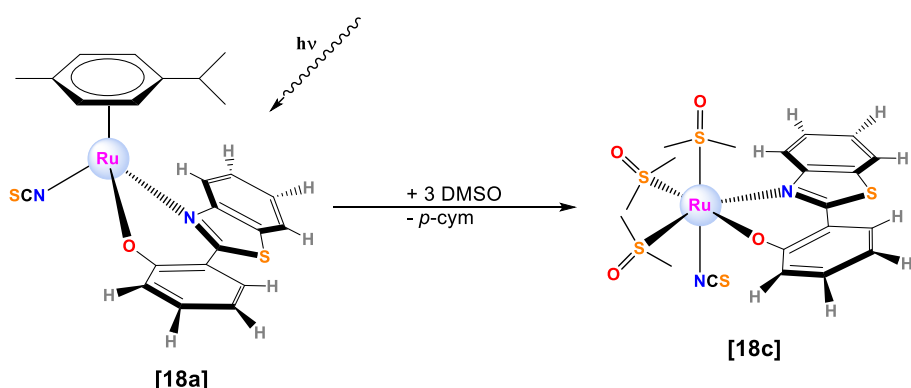


Fig. 18. Reaction scheme for the formation of **[18c]**, when a solution of **[18a]** in DMSO is irradiated.

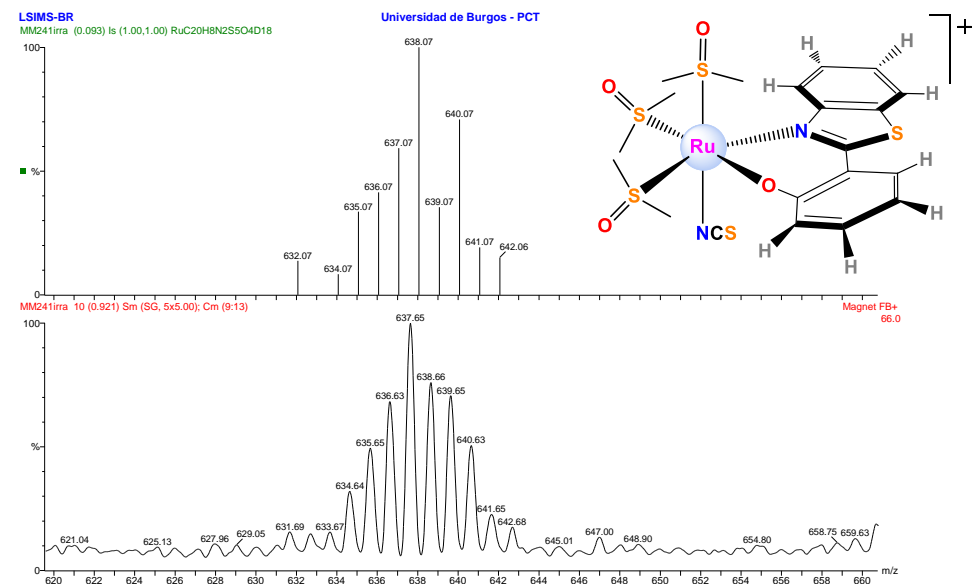


Fig. 19. FAB⁺ zoom of mass spectra of **[18c]** (**[18a]** after irradiation in DMSO-d₆) in NBA matrix (below) compared to the simulation (above). Fragmentation peak: m/z = 638 (**[18a]-p-cymene+3DMSO-d₆**)⁺ = **[18c]**⁺.

The loss of the arene was also observed for other complexes in different solvents. Complexes **[19a](BPh₄)** and **[19a](OTf)** show the same behaviour in DMSO-d₆ when they are irradiated, although in the latter the process is slower.

1.5. Aqueous Solubility

The aqueous solubility of some complexes was determined at room temperature (20 – 22 °C). All the neutral complexes with the exception of **[16a]** and **[16b]** are not water-soluble, whereas the cationic complexes are soluble in aqueous media, with the exception of **[19a]BPh₄**, due to the hydrophobicity of the tetraphenylborate anion. The comparison of the aqueous solubility of **[16a]** and **[16b]** shows the clear effect of the arene, as previously observed.^{33,34} The *p*-cymene derivative gives better solubility (*ca.* 3 times) than the benzene analogue. The effect of the counterion on the water-solubility of the series **[19a]⁺** is also clear. It decreases 10 times when the Cl⁻ is replaced by OTf, owing to the high hydration energy attributed to the Cl⁻,^{35,36} and it is completely negligible for BPh₄⁻.

Table 9. Solubility data in water (mM) for selected compounds.

Ref.	Compound	Solubility (mM)
[16a]	[(<i>p</i> -cym)RuCl(hpbim)]	3.3
[16b]	[(bz)RuCl(hpbim)]	1.2
[19a]Cl	[(<i>p</i> -cym)Ru(hpbim)(MeIm)]Cl	10.9
[19a]OTf	[(<i>p</i> -cym)Ru(hpbim)(MeIm)]OTf	1.1
[19a]BPh ₄	[(<i>p</i> -cym)Ru(hpbim)(MeIm)]BPh ₄	-
[20b]BF ₄	[(bz)RuCl(hpbtz)(MeIm)]BF ₄	2.5
[21a]Cl	[(<i>p</i> -cym)RuCl(hpbim)(PTA)]Cl	22.0

1.6. Aquation-Anation Equilibria

Hydrolysis of Ru-Cl bonds was monitored by ¹H NMR for 3 mM solutions of [16a] and [16b] in 10% MeOD-d₄/90% D₂O (v/v). Methanol was added to ensure the solubility of the complexes. Notwithstanding, it was insufficient to solubilize the complexes [17a] and [17b]. The stability of a solution of [21a]Cl in D₂O (3 mM) was monitored as well. Spectra were recorded in the absence of NaCl at different times and afterward in the presence of NaCl, mimicking the physiological conditions (5 mM and 100 mM as model concentrations for the intracellular and blood plasma conditions, respectively³⁷). Hydrolysis was complete for the neutral complexes in less than 5 minutes, but the PTA derivative [21a]Cl did not undergo aquation. However, when NaCl was added to the samples, no apparent reaction occurred, as the spectra did not show any change, in agreement with an aquation equilibrium totally shifted to the aqua derivative. A huge excess of NaCl caused the precipitation of a solid, the aquo complex, as a result of the common ion effect.

1.7. Reactivity against Nucleobases and Nucleotides

After some unsuccessful attempts to synthesise the resulting product of the reaction between 9MeG and the complex [16a] (the chlorido complex evolved to the aqua derivative, but no reaction with 9MeG was observed), the interaction of complexes [18a] and [18c] with 9MeG and 5'-GMP was followed by ¹H NMR at 25 °C in different solvent mixtures.

Reactivity against the nucleobase

The reaction of complexes [18a] and [18c] with the nucleobase 9MeG was studied by ¹H NMR in DMSO-d₆ at 25 °C. Some spectra were recorded before and after the addition of an excess of 9MG, during 24h. The spectrum of [18a] showed sets of peaks for the initial complex [18a], for the partial reaction of the complex with 9MeG [18a-G]⁺ and for [18c]. On the other hand, in the spectrum of the irradiated complex [18c] no reaction evidences were found.

Reactivity against the nucleotide

The reaction of [18a] (5 mM) and [18c] (7.93 mM) with 5'-GMP (1:1 molar ratio) was monitored with time by ¹H NMR in DMSO-d₆/D₂O (5:2).

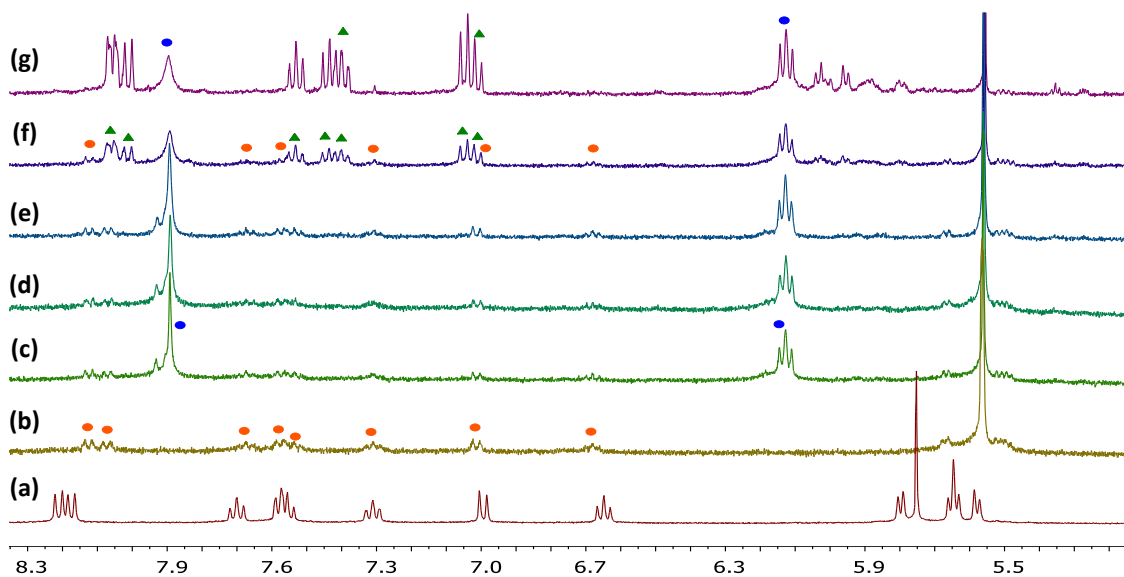


Fig. 20. Evolution of the aromatic region of **[18a]** with 5'-GMP in DMSO-d₆/D₂O (5:2) at 25 °C. The orange spots belong to the complex **[18a]**, the blue ones to the free 5'-GMP and the green triangles refer to the new product **[18a-GMP]⁺**. (a) Spectrum in DMSO-d₆, (b) after the addition of D₂O at t=0, (c) after the addition of 5'-GMP at t=5 min, (d) at t=20 min, (e) at t=55 min, (f) at t=72 h and (g) at t=1 week.

Fig. 20. show the evolution over time of **[18a]** in DMSO-d₆/D₂O with the exception of the red spectrum (a), which was only in DMSO-d₆. After 72 h (spectrum (f)) a new complex with coordinated 5'-GMP appeared **[18a-GMP]⁺**.

The ³¹P{¹H} NMR (see Fig. 21a) was recorded after a week and a new downfield-shifted signal was detected ($\delta = -0.61$ ppm; $\Delta\delta = 0.83$ ppm). In view of the previous results with 9MeG, and both the ¹H and the ³¹P{¹H} NMR experiments, we can conclude that the coordination between **[18a]** and both 9MeG and 5'-GMP occurs, yet preferably through the phosphate of the nucleotide.

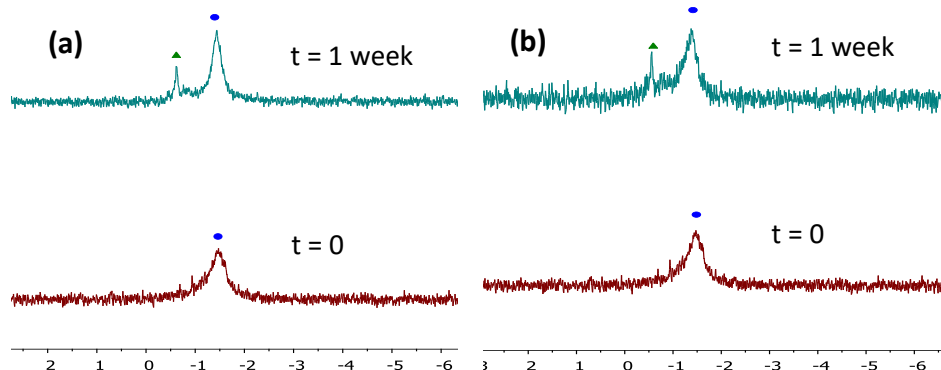


Fig. 21. ³¹P{¹H} NMR spectra for the reaction between 5'-GMP and complexes **[18a]** (a) and **[18c]** (b) recorded after a week. The blue spots show the free 5'-GMP, whereas the green triangles the coordinated complexes **[18a-GMP]⁺** and **[18c-GMP]⁺**.

Regarding the reaction between **[18c]** and 5'-GMP, the ³¹P{¹H} NMR (see Fig. 21b) was recorded in DMSO-d₆/D₂O after 6 days and again, a new downfield-shifted signal

was detected ($\delta = -0.55$ ppm; $\Delta\delta = 0.86$ ppm). These facts demonstrate the reaction between **[18c]** and 5'-GMP through the phosphate group, but not with 9MeG.

On the whole, both complexes **[18a]** and **[18c]** seem to coordinate to the phosphate group of the nucleotide, although only **[18a]** bind the nucleobase 9MeG and in a really lesser extent.

1.8. Cytotoxic Activity

The cytotoxicity of selected complexes versus three different cancer cell lines was determined by means of a MTT cell viability assay: A2780 (ovarian carcinoma cell line), A549 (lung carcinoma cell line) and HeLa (cervical carcinoma cell line), by the group of Dra. Mairena from the University of Castilla La Mancha. The values are expressed in Table 10 as the IC₅₀ in μ M units.

Table 10. Inhibition of cellular growth in different cancer cell lines by the ligands, the selected complexes and cisplatin (μ M).

Ref.	Compound	A2780 (96h)	A549 (24h)	HeLa (24h)	HeLa (48h)
	cisplatin	0.87 ± 0.01	114.2 ^b	45.44	18.96
	hpbim	8.36 ± 0.16	-	-	-
	hpbtz	>100	-	-	-
[16a]	[(<i>p</i> -cym)RuCl(hpbim)]	8.76 ± 0.43	high ^a	>1000	>1000
[16b]	[(bz)RuCl(hpbim)]	-	high ^a	>1000	739.2
[17a]	[(<i>p</i> -cym)RuCl(hpbtz)]	9.53 ± 0.23	90	465.1	206.4
[17b]	[(bz)RuCl(hpbtz)]	-	160	441.9	226.0
[18a]	[(<i>p</i> -cym)Ru(hpbtz)(SCN)]	26 ± 1	65	N/A	N/A
[18b]	[(bz)Ru(hpbtz)(SCN)]	-	-	862.5	1128
[18c]	[Ru(DMSO) ₃ (hpbtz)(SCN)]	-	37	-	-
[19a](OTf)	[(<i>p</i> -cym)Ru(hpbim)(MeIm)][OTf]	-	-	170	-
[19a](BPh₄)	[(<i>p</i> -cym)Ru(hpbim)(MeIm)][BPh ₄]	-	-	16.19	14.60
[20b](BF₄)	[(bz)Ru(hpbtz)(MeIm)][BF ₄]	-	high ^a	N/A	890
[21a]Cl	[(<i>p</i> -cym)Ru(hpbim)(PTA)]Cl	-	1000	>1000	1015

^a The cell viability percentage is very similar to the control in DMSO.

^b Bibliographic data.³⁸

N/A: Cell viability tends to infinite.

The relevant results are highlighted in red. Thus, in the cell line A2780, the ligand hpbim is cytotoxic itself. In the cell line A549, complex **[18a]** showed a relevant cytotoxicity (IC₅₀ = 65 μ M), whereas it was inactive in HeLa. Moreover, complex **[18c]** (pre-irradiation of complex **[18a]** before incubation with cells) showed an increase in the inhibitory potency of about twice with regard to its precursor **[18a]**. This results along with its behaviour after irradiation caused its selection for a deeper physicochemical study performed by the group of Begoña García. In addition, complex **[19a](BPh₄)** exhibited the best result in the HeLa cell line, even better than cisplatin (see Fig. 22) both after 24 h (IC₅₀ = 16.2 μ M) and 48 h (IC₅₀ = 14.6 μ M). Nevertheless, the substitution of the BPh₄⁻ counterion by OTf⁻ dramatically diminished the inhibitory potency; IC₅₀ **[19a](OTf)** = 170 μ M vs. IC₅₀ **[19a](BPh₄)** = 16.2 μ M after 24 h incubation (see Fig. 23). Thus, the BPh₄⁻ counterion seems to have an important influence on the cytotoxicity,

probably due to its lipophilic character. This effect has been already reported in the literature by Williams, Healy and Parsons in ruthenium³⁹ and in gold complexes⁴⁰.

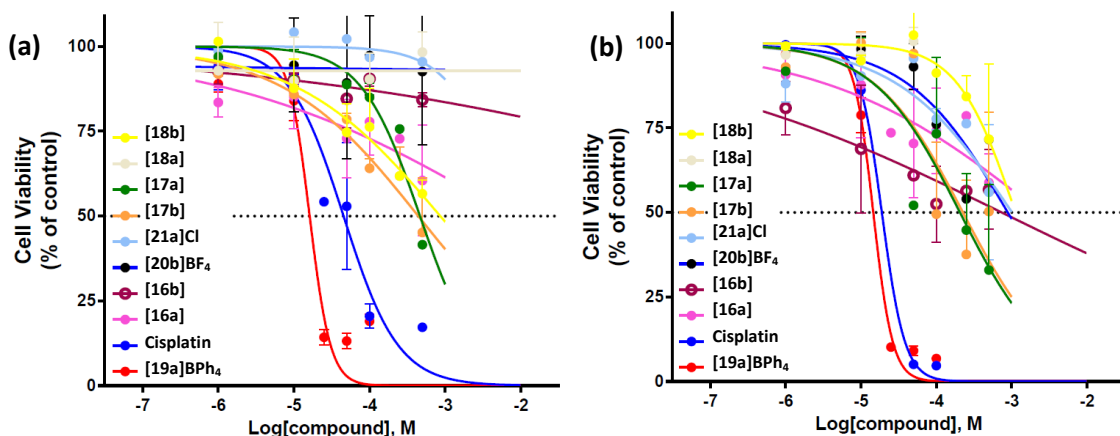


Fig. 22. Graphical curves of cell viability percentage vs. concentration for complexes in HeLa cells after (a) 24h and (b) 48h.

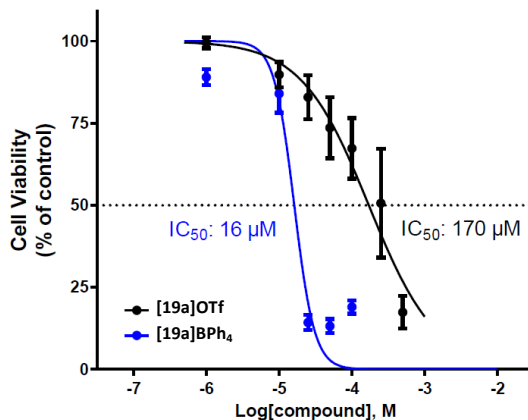


Fig. 23. Graphical curves of cell viability percentage vs. concentration for complexes [19a](BPh₄) and [19a](OTf) in HeLa cells after 24h.

1.9. DNA Interaction

Owing to the high cytotoxic activity, and the extremely low solubility of complex **[19a](BPh₄)**, the possible interaction of the complex cation with DNA was studied in the laboratory of Begoña García with a similar and more soluble complex **[19a](OTf)** by two physicochemical methods: UV-vis absorption and circular dichroism (CD). The complex was dissolved in DMSO to guarantee its complete dissolution, yet the percentage of DMSO in all the experiments did not exceed 5 % in the aqueous solutions. The pK_a was calculated by recording the absorbance spectra as a function of the pH (see Fig. 24). The absorbance at $\lambda = 324$ nm or $\lambda = 352$ was plotted vs. pH and the curve was fitted to the Henderson-Hasselbalch equation (see Fig. 25 and Eq 1), yielding the values $pK_{a1} = 6.2 \pm 0.1$, related to the deprotonation of the NH group and $pK_2 = 9.9 \pm 0.1$, related to the replacement of MeIm with OH⁻. Fig. 26 shows the proposed equilibria for the two chemical processes observed (pK_{a1} and pK_2).

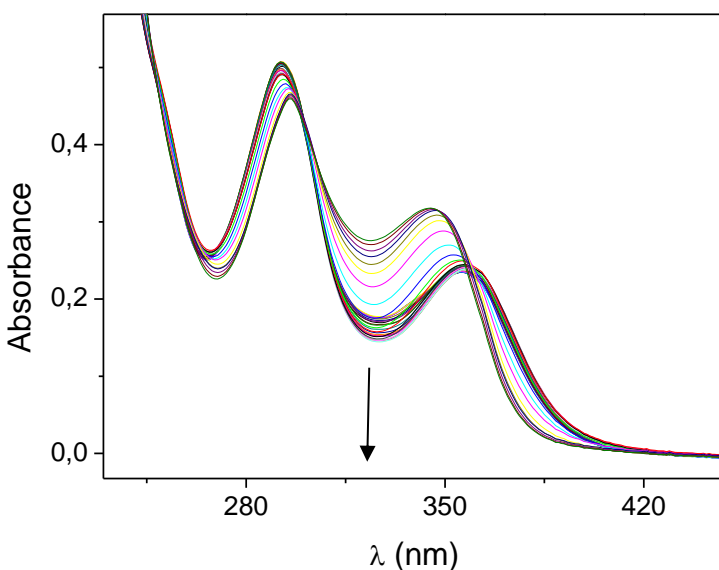


Fig. 24. Absorbance spectra of a 3.26×10^{-5} M solution of [19a](OTf), I = 0.1 M and T = 25 °C, recorded in the pH 3-12 range (arrow sense) (Origin 8.0).

$$A = \frac{A_{HB^+} - A_B}{1 + 10^{m(pK_a - pH)}} - A_{HB^+}$$

Eq 1. Modified Henderson-Hasselbalch equation for absorbance.

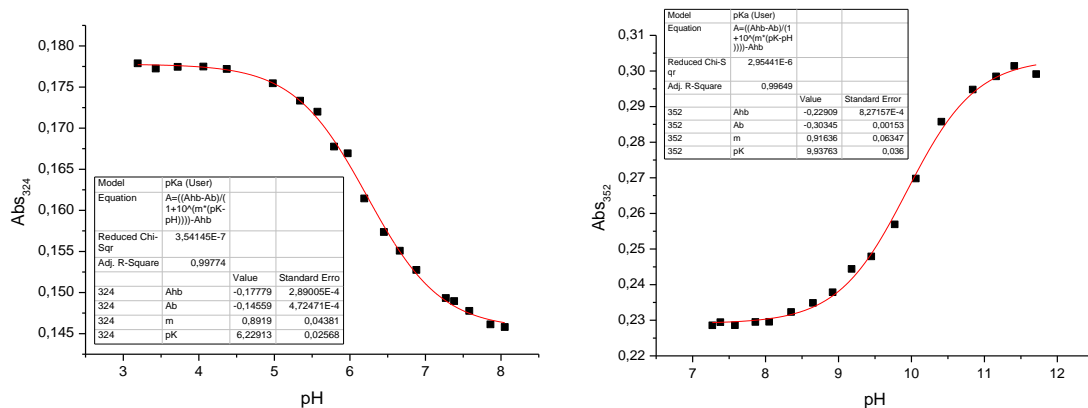


Fig. 25. Absorbance (a) at $\lambda = 324$ nm and (b) at $\lambda = 352$ nm as a function of pH (Origin 8.0).

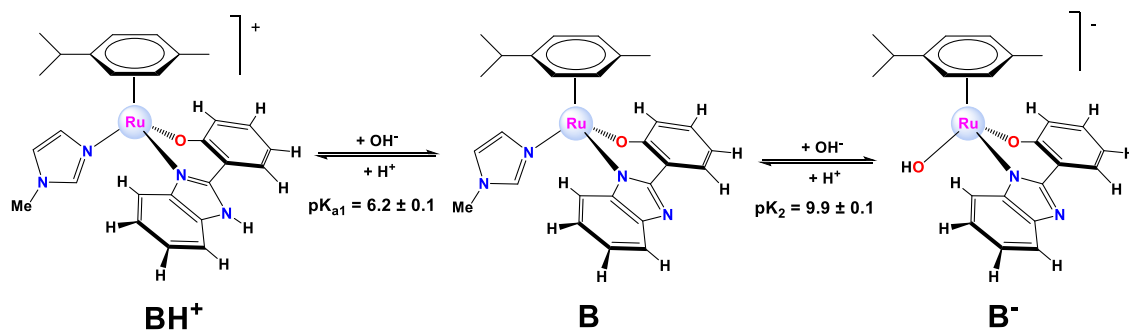


Fig. 26. Dissociation equilibria for complex [19a](OTf).

Taking into account the dissociation constants, we decided to work at physiological conditions, that is, $I = 0.1 \text{ M}$ (NaCl) and $\text{pH} = 7.5$, where **[19a](OTf)** is a neutral species (B) (see Fig. 26).

The behaviour of the complex in aqueous solution was studied by the Lambert-Beer law. The UV-vis spectra were recorded by addition of different volumes of a solution $3.03 \cdot 10^{-3} \text{ M}$ of the complex in DMSO to the buffer into the cuvette (2.5 mM NaCaC - sodium cacodylate - buffer, 0.0975 M NaCl, pH = 7.5). The representation of the absorbance vs. the concentration at $\lambda = 358 \text{ nm}$ (a relative maximum) confirmed the compliance of the law in the whole concentration range (see Fig. 27). The molar extinction coefficient was calculated from the linear fitting ($\epsilon = 7582.7 \pm 10.4 \text{ cm}^{-1} \cdot \text{M}^{-1}$ at $\lambda = 358 \text{ nm}$).

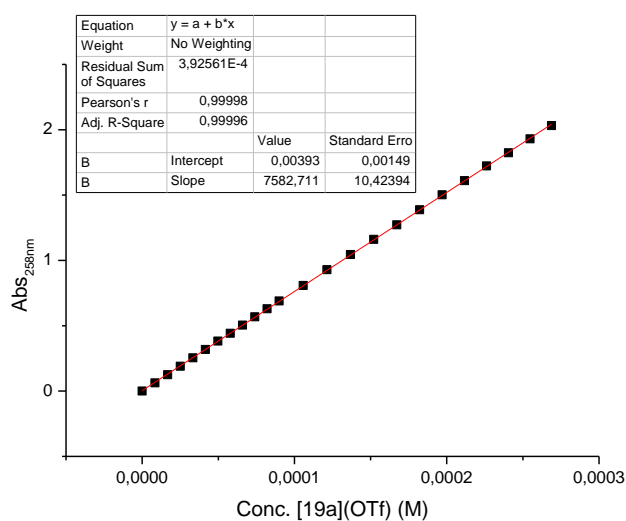


Fig. 27. Lambert-Beer law for the complex **[19a](OTf)** at $I = 0.0975 \text{ M}$ (NaCl), $\lambda = 358 \text{ nm}$, $\text{pH} = 7.5$ and $T = 25 \text{ }^{\circ}\text{C}$ (Origin 8.0).

The study in depth of the interaction of the complex with CT-DNA was performed by UV-vis absorption and CD. A stock solution of CT-DNA 2.084 mM (in 2.5 mM NaCaC buffer, 0.0975 M NaCl, pH = 7.5) was prepared for the experiments.

UV-vis experiments

The absorption spectra were recorded by the addition of increasing volumes of a CT-DNA solution 0.9 mM (in 2.5 mM NaCaC buffer, 0.0975 M NaCl, pH = 7.5), over a solution of complex **[19a](OTf)** $2.35 \cdot 10^{-5} \text{ M}$ (in 2.5 mM NaCaC buffer, 0.0975 M NaCl, pH = 7.5) at $25 \text{ }^{\circ}\text{C}$.

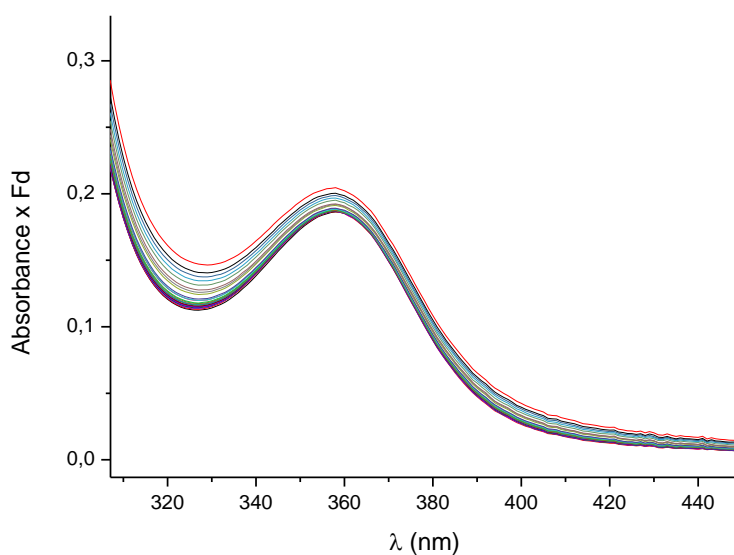


Fig. 28. Absorption spectra of the [19a](OTf)/CT-DNA at different concentration ratios, showing the relative maximum at $\lambda = 360$ nm (Origin 8.0).

Apparently, the spectra did not show any relevant change or shift (see Fig. 28). Thus, the complex seemed not to bind or interact with DNA.

CD measurements

To confirm the lack of interaction of complex **[19a](OTf)** with the CT-DNA, CD was performed by adding increasing volumes of a solution of the complex $3.03 \cdot 10^{-3}$ M in DMSO to a CT-DNA solution $5.005 \cdot 10^{-5}$ M (see Fig. 29).

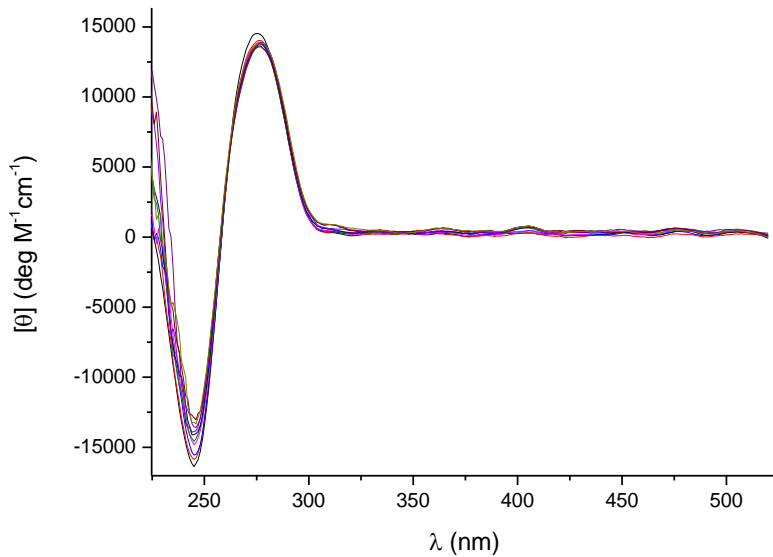


Fig. 29. CD spectra of the [19a](OTf)/CT-DNA at different concentration ratios (Origin 8.0).

DNA displays two characteristic bands, a negative band centered at 246 nm often related to helicity and a positive one centered at 275 nm related to the unwinding degree of the double helix. There were no significant changes in these DNA characteristic bands during the titration. In addition, the complex **[19a](OTf)** had no CD

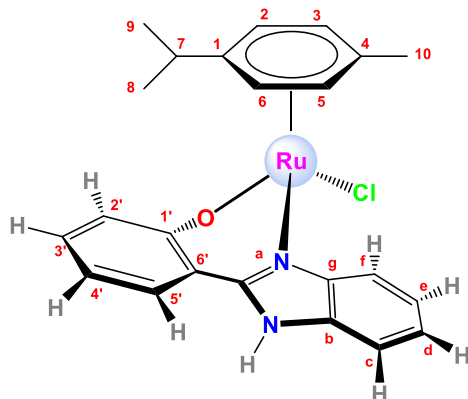
signal in solution and there were not new bands in the induced circular dichroism (ICD) region. Therefore, we can conclude that **[19a](OTf)** does not interact with DNA.

2. CONCLUDING REMARKS

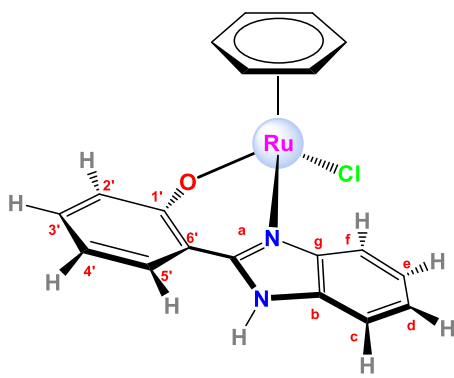
- A family of 12 new complexes has been synthesised and fully characterised, both in solution and some of them in solid state.
- The cationic complexes are water-soluble, whereas only two neutral derivatives (**[16a]** and **[16b]**) are soluble in water.
- Only complexes **[16a]** and **[16b]** undergo aquation.
- Some of the complexes (**[18a]**, **[19a](OTf)** and **[19a](BPh₄)**) lose the arene when they are exposed to light.
- In complexes **[18a]** and **[18b]**, NMR and IR have allowed us to establish that SCN⁻ adopts a $\kappa^1\text{-}N$ coordination mode.
- NMR experiments have demonstrated that complexes **[18a]** and **[18c]** are able to react with nucleotides through the phosphate group.
- The cytotoxic activity values of the new complexes against different cancer cell lines suggest that **[18a]**, **[18c]** (the resulting irradiated product from **[18a]**) and **[19a](BPh₄)** have promising potential as anticancer drugs.
- The cytotoxic activity depends on the counterion. Thus, BPh₄⁻ enhances the inhibitory potency of the complexes, owing to its lipophilic nature.
- Despite the high cytotoxicity of complex **[19a](BPh₄)**, its triflate counterpart **[19a](OTf)** does not interact with DNA.

3. EXPERIMENTAL SECTION

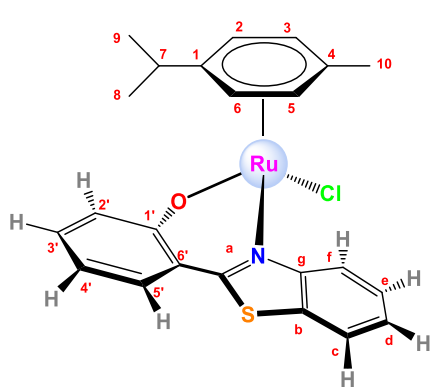
Neutral Complexes



Synthesis of $[(\eta^6\text{-}p\text{-cymene})\text{RuCl}(k^2\text{-}O,N\text{-}hpbit)]$, [16a]. In a 100 mL Schlenk flask, the ligand 2-(2'-hydroxyphenyl)benzimidazole (0.086 g, 0.409 mmol) was added to a solution of $[\text{RuCl}_2(\text{cym})]_2$ (0.1251 g, 0.204 mmol) in degassed methanol (10 mL). Et_3N (58 μL , 0.416 mmol) was then added, and the mixture was stirred at room temperature for 20 h and under a nitrogen atmosphere. The solution was concentrated and water was then added to precipitate the product and to remove Et_3NHCl . The solid was washed with cold diethyl ether (3 mL). The resulting red-brown powder was dried under vacuum. Yield: 142.8 mg (0.298 mmol, 73%). M_r ($\text{C}_{23}\text{H}_{23}\text{N}_2\text{OClRu}$) = 479.9702 g/mol. **Anal. Calc.** for $\text{C}_{23}\text{H}_{23}\text{N}_2\text{OClRu}\cdot\text{H}_2\text{O}$: C 55.47; H 5.06; N 5.63 **Found:** C 55.13; H 4.99; N 5.98. **$^1\text{H NMR}$ (400 MHz, CDCl_3 , 25 °C)** δ 10.67 (s, 1H, $\text{H}^{\text{N-H}}$), 7.43 (d, J = 8.1 Hz, 1H, H^{f}), 7.13 (d, J = 7.8 Hz, 1H, H^{c}), 7.01 (d, J = 7.6 Hz, 1H, $\text{H}^{\text{3'}}$), 6.91 – 6.81 (m, 3H, H^{e} , $\text{H}^{\text{6'}}$, $\text{H}^{\text{5'}}$), 6.63 (t, J = 7.5 Hz, 1H, H^{d}), 6.32 (t, J = 6.8 Hz, 1H, $\text{H}^{\text{4'}}$), 5.38 (d, J = 5.8 Hz, 1H, H^{3} or H^{5}), 5.35 (d, J = 5.8 Hz, 1H, H^{2} or H^{6}), 5.29 (d, J = 5.7 Hz, 1H, H^{6} or H^{2}), 5.20 (d, J = 5.7 Hz, 1H, H^{5} or H^{3}), 2.34 (d, J = 6.9 Hz, 1H, H^{7}), 2.07 (s, 3H, H^{10}), 0.91 (d, J = 6.9 Hz, 3H, H^{8} or H^{9}), 0.80 (d, J = 6.8 Hz, 3H, H^{9} or H^{8}) ppm. **$^{13}\text{C}\{^1\text{H}\} \text{NMR}$ (101 MHz, CDCl_3 , 25 °C)** δ 167.3 (s, 1C, $\text{C}^{\text{1'}}$), 148.2 (s, 1C, C^{a}), 142.0 (s, 1C, C^{g}), 133.6 (s, 1C, C^{b}), 132.0 (s, 1C, $\text{C}^{\text{5'}}$), 127.3 (s, 1C, $\text{C}^{\text{3'}}$), 122.8 (s, 1C, C^{d}), 122.7 (s, 1C, $\text{C}^{\text{5'}}$), 122.5 (s, 1C, C^{e}), 117.5 (s, 1C, C^{f}), 116.0 (s, 1C, $\text{C}^{\text{4'}}$), 115.9 (s, 1C, $\text{C}^{\text{2'}}$), 113.3 (s, 1C, C^{c}), 101.5 (s, 1C, $\text{C}^{\text{1'}}$), 97.7 (s, 1C, C^{4}), 83.0 (s, 1C, C^{2} or C^{6}), 81.8 (s, 1C, C^{3} or C^{5}), 79.9 (s, 1C, C^{5} or C^{3}), 79.8 (s, 1C, C^{6} or C^{2}), 30.5 (s, 1C, C^{7}), 22.8 (s, 1C, C^{8} or C^{9}), 21.4 (s, 1C, C^{9} or C^{8}), 18.8 (s, 1C, C^{10}) ppm. **FT-IR (KBr, cm⁻¹) selected bands:** 3053 (w, ν_{CH}), 2961 (w, ν_{CH}), 1621 (m, $\nu_{\text{C-N}}$), 1600 (s, $\nu_{\text{C=C}}$), 1532 (m), 1479 (vs, $\nu_{\text{C=N}}$), 1459 (s), 1445 (s), 1316 (m), 1261 (s, $\nu_{\text{C-O}}$), 1136 (m, $\delta_{\text{N-Hip}}$), 1035 (w), 860 (m), 743 (s, $\delta_{\text{N-Hop}}$). **MS (FAB+):** m/z (%) = 480 (5) ($[\text{M}]^+$), 445 (100) ($[\text{M}-\text{Cl}]^+$). **Molar Conductivity (CH_3CN):** 8.48 S·cm²·mol⁻¹. **Solubility:** soluble in methanol, dichloromethane, chloroform acetone and acetonitrile. Partially soluble in water.

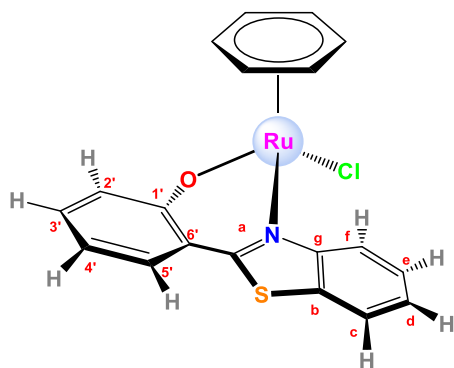


Synthesis of $[(\eta^6\text{-benzene})\text{RuCl}(\kappa^2\text{-O},\text{N-hpbim})]$, [16b]. The synthesis was performed as for [16a] in the presence of the ligand 2-(2'-hydroxyphenyl)benzimidazole (0.0843 g, 0.400 mmol), $[\text{RuCl}_2(\text{bz})]_2$ (0.0998 g, 0.200 mmol) and Et_3N (58 μL , 0.420 mmol) in methanol/acetonitrile (10:2 mL). Red-brown powder. Yield: 69.1 mg (0.163 mmol, 49%). $M_r (\text{C}_{19}\text{H}_{15}\text{NO}_2\text{ClRu}) = 423.8630$ g/mol. **Anal. Calc.** for $\text{C}_{19}\text{H}_{15}\text{NO}_2\text{ClRu}\cdot(\text{H}_2\text{O})_{1.5}$: C 50.14; H 3.61; N 6.40 **Found:** C 50.61; H 4.02; N 6.21. $^1\text{H NMR}$ (400 MHz, CDCl_3 , 25 °C) δ 10.86 (s, 1H, $\text{H}^{\text{N-H}}$), 7.56 (d, $J = 8.4$ Hz, 1H, H^{f}), 7.18 (m, 2H, H^{c} , $\text{H}^{\text{3'}}$), 7.04 – 6.98 (m, 1H, H^{e} or $\text{H}^{\text{5'}}$), 6.94 (m, 2H, $\text{H}^{\text{6'}}$, H^{e} or $\text{H}^{\text{5'}}$), 6.78 (t, $J = 7.3$ Hz, 1H, H^{d}), 6.46 (t, $J = 6.8$ Hz, 1H, $\text{H}^{\text{4'}}$), 5.56 (s, 6H, H^{b}) ppm. **FT-IR (KBr, cm⁻¹) selected bands:** 3450 (w, $\nu_{\text{N-H}}$), 3053 (w, $\nu_{=\text{CH}}$), 2961 (w, $\nu_{=\text{CH}}$), 1621 (m, $\nu_{\text{C-N}}$), 1600 (s, $\nu_{\text{C=C}}$), 1538 (m), 1479 (vs, $\nu_{\text{C=N}}$), 1460 (m), 1445 (m), 1310 (m), 1265 (s, $\nu_{\text{C-O}}$), 1139 (m, $\delta_{\text{N-Hip}}$), 1038 (w), 1006 (w), 856 (w), 765 (s, $\delta_{\text{N-Hoop}}$), 750 (s, $\delta_{\text{C-Hoop}}$). **MS (FAB+):** m/z (%) = 424 (5) ($[\text{M}]^+$), 389 (90) ($[\text{M-Cl}]^+$). **Molar Conductivity (CH₃CN):** 13 S·cm²·mol⁻¹. **Solubility:** soluble in methanol, dichloromethane, chloroform, dimethylsulfoxide and acetone. Slightly soluble in water.

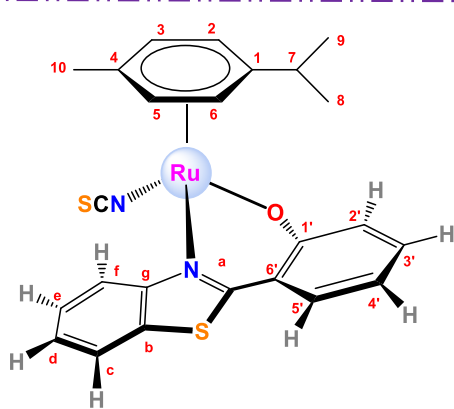


Synthesis of $[(\eta^6\text{-p-cymene})\text{RuCl}(\kappa^2\text{-O},\text{N-hpbtz})]$, [17a]. The synthesis was performed as for [16a] in the presence of the ligand 2-(2'-hydroxyphenyl)benzothiazole (0.0743 g, 0.327 mmol), $[\text{RuCl}_2(\text{cym})]_2$ (0.0999 g, 0.163 mmol) and Et_3N (48 μL , 0.347 mmol) in methanol (10 mL). Yellow-orange powder. Yield: 85 mg (0.171 mmol, 52%). $M_r (\text{C}_{23}\text{H}_{22}\text{NO}_2\text{ClRu}) = 497.0216$ g/mol. **Anal. Calc.** for $\text{C}_{23}\text{H}_{22}\text{NO}_2\text{ClRu}\cdot(\text{H}_2\text{O})_{0.5}$: C 54.59; H 4.58; N 2.77; S 6.34 **Found:** C 54.79; H 4.42; N 3.19; S 5.79. $^1\text{H NMR}$ (400 MHz, CDCl_3 , 25 °C) δ 8.47 (d, $J = 8.4$ Hz, 1H, H^{f}), 7.78 (dd, $J = 8.0, 0.6$ Hz, 1H, H^{c}), 7.54 (ddd, $J = 8.4, 7.3, 1.2$ Hz, 1H, H^{e}), 7.49 (dd, $J = 7.9, 1.7$ Hz, 1H, $\text{H}^{\text{3'}}$), 7.39 (m, 1H, H^{d}), 7.26 (m, 1H, $\text{H}^{\text{5'}}$), 7.18 (dd, $J = 8.5, 1.2$ Hz, 1H, $\text{H}^{\text{6'}}$), 6.60 (ddd, $J = 8.0, 6.9, 1.2$ Hz, 1H, $\text{H}^{\text{4'}}$), 5.49 (d, $J = 6.0$ Hz, 1H, H^{2} or H^{6}), 5.33 (d, $J = 5.9$ Hz, 1H, H^{2} or H^{6}), 5.30 (d, $J = 5.8$ Hz, 1H, H^{3} or H^{5}), 5.23 (d, $J = 5.6$ Hz, 1H, H^{3} or H^{5}), 2.68 (sept, $J = 6.9$ Hz, 1H, H^{7}), 2.04 (s, 3H, H^{10}), 1.14 (d, $J = 6.9$ Hz, 3H, H^{8} or H^{9}), 1.10 (d, $J = 6.9$ Hz, 3H, H^{8} or H^{9}) ppm. $^{13}\text{C}\{{}^1\text{H}\}$ NMR (101 MHz, CDCl_3 , 25 °C) δ 169.5 (s, 1C, $\text{C}^{\text{1'}}$), 166.9 (s, 1C, C^{a}), 153.1 (s, 1C, C^{g}), 134.0 (s, 1C, $\text{C}^{\text{5'}}$), 131.7 (s, 1C, C^{b}), 129.6 (s, 1C, $\text{C}^{\text{3'}}$), 127.1

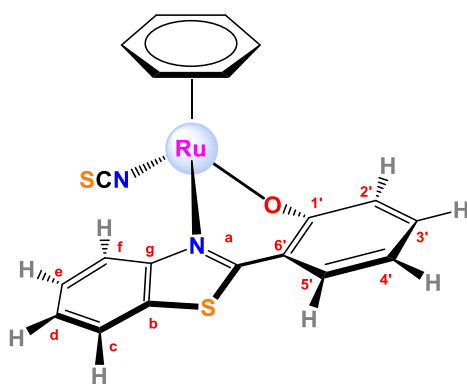
(s, 1C, C^e), 125.5 (s, 2C, C^f, C^d), 124.4 (s, 1C, C^{6'}), 121.5 (s, 1C, C^c), 121.3 (s, 1C, C^{2'}), 116.1 (s, 1C, C^{4'}), 103.3 (s, 1C, C¹ or C⁴), 97.5 (s, 1C, C¹ or C⁴), 83.0 (s), 81.24 (s), 81.1 (s), 80.60 (s), 30.9 (s, 1C, C⁷), 23.1 (s, 1C, C⁸ or C⁹), 21.6 (s, 1C, C⁸ or C⁹), 18.8 (s, 1C, C¹⁰) ppm. **FT-IR (KBr, cm⁻¹) selected bands:** 3033 (m, ν_{CH}), 2958 (w, ν_{CH}), 1597 (s, ν_{C-N}), 1540 (s, ν_{C=C}), 1491 (vs, ν_{C=N}), 1463 (s), 1441 (s), 1420 (m), 1332 (s), 1213 (s, ν_{C-O}), 1153 (s, ν_{C=S}), 1128 (w), 1033 (w), 875 (w), 832 (w), 753 (s, δ_{C-Hoop}). **MS (FAB+):** m/z (%) = 497 (14) ([M]⁺), 462 (61) ([M-Cl]⁺). **Molar Conductivity (CH₃CN):** 3.36 S·cm²·mol⁻¹. **Solubility:** soluble in acetone, dichloromethane, chloroform, methanol and acetonitrile and partially soluble in ethanol. Slightly soluble in water.



Synthesis of [(η⁶-benzene)RuCl(κ²-O,N-hpbtz)], [17b]. The synthesis was performed as for [16a] in the presence of the ligand 2-(2'-hydroxyphenyl)benzothiazole (0.0913 g, 0.402 mmol), [RuCl₂(bz)]₂ (0.1001 g, 0.200 mmol) and Et₃N (58 μL, 0.420 mmol) in methanol/acetonitrile (8:2 mL). Yellow powder. Yield: 134.6 mg (0.305 mmol, 77%). M_r (C₁₉H₁₄NOSCI₂Ru) = 440.9144 g/mol. **Anal. Calc. for C₁₉H₁₄NOSCI₂Ru·H₂O:** C 50.17; H 3.37; N 3.52; S 6.57 **Found:** C 49.73; H 3.51; N 3.05; S 6.99. **¹H NMR (400 MHz, CDCl₃, 25 °C)** δ 8.53 (d, J = 8.3 Hz, 1H, H^f), 7.80 (d, J = 8.0 Hz, 1H, H^c), 7.57 (t, J = 7.7 Hz, 1H, H^e), 7.50 (d, J = 7.8 Hz, 1H, H^{3'}), 7.42 (t, J = 7.6 Hz, 1H, H^d), 7.33 – 7.27 (m, 1H, H^{5'}), 7.24 (d, J = 8.2 Hz, 1H, H^{6'}), 6.64 (t, J = 7.2 Hz, 1H, H^{4'}), 5.63 (s, 6H, H^{bz}) ppm. **¹³C{¹H} NMR (101 MHz, CDCl₃, 25 °C)** δ 169.9 (s, 1C, C^{1'}), 167.4 (s, 1C, C^a), 152.9 (s, 1C, C^g), 134.3 (s, 1C, C^{5'}), 131.8 (s, 1C, C^b), 129.6 (s, 1C, C^{3'}), 127.4 (s, 1C, C^e), 125.6 (s, 1C, C^d), 125.2 (s, 1C, C^f), 123.7 (s, 1C, C^{6'}), 121.9 (s, 1C, C^{2'}), 121.6 (s, 1C, C^c), 116.5 (s, 1C, C^{4'}), 83.7 (s, 6C, C^{bz}) ppm. **FT-IR (KBr, cm⁻¹) selected bands:** 3056 (w), 3038 (w, ν_{CH}), 3006 (w, ν_{CH}), 1599 (s, ν_{C-N}), 1545 (m, ν_{C=C}), 1489 (vs, ν_{C=N}), 1467 (s), 1440 (s), 1420 (m), 1336 (m), 1217 (s, ν_{C-O}), 1155 (m, ν_{C=S}), 1125 (w), 1036 (w), 832 (w), 753-748 (s, δ_{C-Hoop}), 723 (m). **MS (FAB+):** m/z (%) = 406 (10) ([M-Cl]⁺). **Molar Conductivity:** It could not be measured due to their poor solubility both water and acetonitrile. **Solubility:** soluble in methanol, dichloromethane, chloroform. Partially soluble in acetone and slightly soluble in water and acetonitrile.

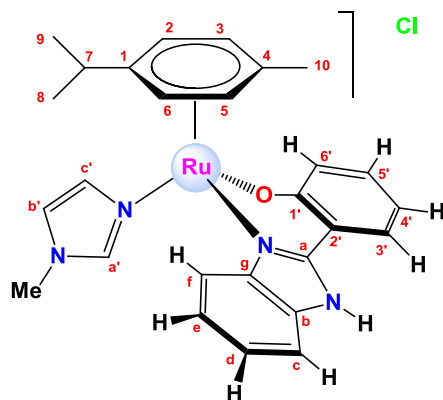


Synthesis of $[(\eta^6-p\text{-cymene})\text{Ru}(\text{NCS})(\kappa^2\text{-O},\text{N}-hpbtz)]$, [18a]. In a 100 mL Schlenk flask, The ligand 2-(2'-hydroxyphenyl)benzothiazole (0.0744 g, 0.327 mmol) was added to a solution of $[\text{RuCl}_2(\text{cym})]_2$ (0.1000 g, 0.163 mmol) in degassed methanol (8 mL). Et_3N (48 μL , 0.345 mmol) was then added, and the mixture was stirred at room temperature for 20 h and under a nitrogen atmosphere. KSCN (0.0513 g, 0.528 mmol) was added to the mixture and heated at 70°C for 4h. The precipitate was filtered and water was added to remove salts. After filter the residue was washed with diethyl ether (3mL). The resulting orange powder was dried under vacuum. Yield: 133.8 mg (0.257 mmol, 79%). **M_r** ($\text{C}_{24}\text{H}_{22}\text{N}_2\text{OS}_2\text{Ru}$) = 519.6526 g/mol. **Anal. Calc.** for $\text{C}_{24}\text{H}_{22}\text{N}_2\text{OS}_2\text{Ru}\cdot\text{H}_2\text{O}$: C 53.79; H 4.01; N 5.68; S 12.16 **Found:** C 53.61; H 4.50; N 5.21; S 11.93. ¹**H NMR** (400 MHz, CD_3CN , 25 °C) δ 8.25 (d, J = 8.4 Hz, 1H, H^f), 8.01 (dd, J = 4.3, 3.7 Hz, 1H, H^c), 7.69 (ddd, J = 8.5, 7.2, 1.3 Hz, 1H, H^e), 7.63 – 7.56 (m, 1H, H^{3'}), 7.54 (ddd, J = 8.1, 7.2, 1.1 Hz, 1H, H^d), 7.33 (ddd, J = 8.4, 7.0, 1.7 Hz, 1H, H^{5'}), 7.11 – 7.00 (m, 1H, H^{6'}), 6.67 (ddd, J = 7.9, 7.0, 1.2 Hz, 1H, H^a), 5.66 (d, J = 5.9 Hz, 1H, H² or H⁶), 5.54 (d, J = 5.3 Hz, 1H, H² or H⁶), 5.43 (d, J = 6.1 Hz, 1H, H³ or H⁵), 5.37 (d, J = 6.0 Hz, 1H, H³ or H⁵), 2.69 – 2.56 (m, 1H, H⁷), 1.85 (s, 3H, H¹⁰), 1.16 (s, 3H, H⁸ or H⁹), 1.14 (s, 3H, H⁸ or H⁹). ¹**H NMR** (400 MHz, DMSO-d_6 , 25 °C) δ 8.21 (d, J = 8.1 Hz, 1H, H^f), 8.17 (d, J = 8.0 Hz, 1H, H^c), 7.70 (t, J = 7.8 Hz, 1H, H^e), 7.58 (d, J = 6.7 Hz, 1H, H^{3'}), 7.55 (t, J = 6.3 Hz, 1H, H^d), 7.31 (t, J = 7.7 Hz, 1H, H^{5'}), 6.99 (d, J = 8.4 Hz, 1H, H^{6'}), 6.65 (t, J = 7.4 Hz, 1H, H^a), 5.80 (d, J = 5.9 Hz, 1H, H² or H⁶), 5.65 (t, J = 6.1 Hz, 2H, H⁶ or H², H³ or H⁵), 5.58 (d, J = 6.0 Hz, 1H, H⁵ or H³), 1.89 (s, 3H, H¹⁰), 1.09 (d, J = 3.5 Hz, 3H, H⁸ or H⁹), 1.07 (d, J = 3.5 Hz, 3H, H⁹ or H⁸) ppm. H⁷ is overlapped into the DMSO signal. ¹³**C{¹H} NMR** (101 MHz, CD_3CN , 25 °C) δ 147.0 (s, 1C, C¹ or C³), 145.6 (s, 1C, C¹ or C³), 141.5 (s, 1C), 140.6 (s, 1C), 135.1 (s, 1C), 130.8 (s, 1C), 128.5 (s, 1C), 126.8 (s, 1C), 125.3 (s, 1C), 124.3 (s, 1C), 123.2 (s, 1C), 117.2 (s, 1C), 105.4 (s, 1C), 99.6 (s, 1C), 84.4 (s, 1C), 83.7 (s, 1C), 83.4 (s, 1C), 82.6 (s, 1C), 31.9 (s, 1C, C⁷), 22.8 (s, 1C, C⁸ or C⁹), 21.8 (s, 1C, C⁸ or C⁹), 18.8 (s, 1C, C¹⁰). ¹³**C{¹H} NMR** (101 MHz, DMSO-d_6 , 25 °C) δ 168.4 (s, 1C, C^{1'}), 166.4 (s, 1C, C^a), 152.1 (s, 1C, C^g), 135.4 (s, 1C, C^{SCN}), 134.1 (s, 1C, C^{5'}), 131.0 (s, 1C, C^b), 129.6 (s, 1C, C^{3'}), 127.7 (s, 1C, C^e), 125.7 (s, 1C, C^d), 124.2 (s, 1C, C^f), 123.2 (s, 1C, C^{6'}), 122.5 (s, 1C, C^c), 120.6 (s, 1C, C^{2'}), 116.0 (s, 1C, C^{4'}), 103.3 (s, 1C, C^{1'}), 98.5 (s, 1C, C⁴), 83.6 (s, 1C, C² or C⁶), 82.3 (s, 1C, C⁶ or C²), 82.1 (s, 1C, C³ or C⁵), 81.5 (s, 1C, C⁵ or C³), 30.5 (s, 1C, C⁷), 22.2 (s, 1C, C⁸ or C⁹), 21.2 (s, 1C, C⁹ or C⁸), 18.1 (s, 1C, C¹⁰) ppm. **FT-IR (KBr, cm⁻¹) selected bands:** 3036 (w, ν_{CH}), 2962 (w, ν_{CH}), 2090 (vs, $\nu_{\text{C-N}(\text{SCN})}$), 1598 (s, $\nu_{\text{C-N}}$), 1543 (s, $\nu_{\text{C=C}}$), 1489 (vs, $\nu_{\text{C=N}}$), 1455 (s), 1442 (s), 1419 (m), 1336 (s), 1212 (s, $\nu_{\text{C-O}}$), 1152 (s, $\nu_{\text{C-S}}$), 1130 (w), 1032 (w), 877 (w), 836 (w), 819 (w), 751 (vs, $\nu_{\text{C-S}(\text{SCN})}$), 726 (w). **MS (FAB+):** m/z (%) = 982 (2) ([2M-NCS]⁺), 462 (100) ([M-NCS]⁺). **Molar Conductivity (CH₃CN):** 1.92 S·cm²·mol⁻¹. **Solubility:** soluble in chloroform, acetonitrile and dimethylsulfoxide. Partially soluble in methanol and insoluble in water and acetone.



Synthesis of $[(\eta^6\text{-benzene})\text{Ru}(\text{NCS})(\kappa^2\text{-O,N-hpbtz})]$, [18b]. The synthesis was performed as for [18a] in the presence of the ligand 2-(2'-hydroxyphenyl)benzothiazole (0.0911 g, 0.400 mmol), $[\text{RuCl}_2(\text{bz})]_2$ (0.1002 g, 0.200 mmol), Et_3N (59 μL , 0.424 mmol) and KSCN (0.053 g, 0.545 mmol) in methanol (8 mL). Orange powder. Yield: 113.7 mg (0.245 mmol, 62%). $\text{M}_r (\text{C}_{29}\text{H}_{35}\text{N}_5\text{OPClRu}) = 463.5454 \text{ g/mol. Anal. Calc. for } \text{C}_{20}\text{H}_{14}\text{N}_2\text{OS}_2\text{Ru}\cdot(\text{CH}_3\text{CN})_{0.25}\cdot(\text{H}_2\text{O}): \text{C } 50.06; \text{H } 3.43; \text{N } 6.41; \text{S } 13.04$ Found: C 50.20; H 3.48; N 6.08; S 12.61. $^1\text{H NMR}$ (400 MHz, CD_2Cl_2 , 25 °C) δ 8.24 (d, $J = 8.4$ Hz, 1H, H^f), 7.91 (d, $J = 8.0$ Hz, 1H, H^c), 7.68 (ddd, $J = 8.4, 7.2, 1.2$ Hz, 1H, H^e), 7.56 (dd, $J = 7.9, 1.7$ Hz, 1H, H^3'), 7.51 (ddd, $J = 8.4, 7.3, 1.1$ Hz, 1H, H^d), 7.33 (ddd, $J = 8.7, 7.0, 1.7$ Hz, 1H, $\text{H}^{5'}$), 7.17 (dd, $J = 8.4, 1.2$ Hz, 1H, H^6'), 6.69 (ddd, $J = 8.1, 7.0, 1.1$ Hz, 1H, H^4'), 5.64 (s, 6H, H^{bz}) ppm. FT-IR (KBr, cm^{-1}) selected bands: 3055 (w, $\nu_{\text{C-H}}$), 3000 (w, $\nu_{\text{C-H}}$), 2099 (vs, $\nu_{\text{C-N}(\text{SCN})}$), 1597 (s, $\nu_{\text{C-N}}$), 1543 (m, $\nu_{\text{C=C}}$), 1494 (s, $\nu_{\text{C=N}}$), 1456 (s), 1439 (s), 1420 (m), 1332 (m), 1238 (m), 1223-1210 (s, $\nu_{\text{C-O}}$), 1149 (m, $\nu_{\text{C=S}}$), 1125 (w), 1036-1016 (w), 982 (w), 834 (m), 813 (w), 750 (s, $\nu_{\text{C-S}(\text{SCN})}$), 724 (w). MS (FAB+): m/z (%) = 406 (7) ([M-NCS]⁺) Molar Conductivity: It could not be measured due to their poor solubility. Solubility: partially soluble in dichloromethane. Slightly soluble in chloroform, methanol, dimethylsulfoxide, acetonitrile, benzene and acetone. Insoluble in water.

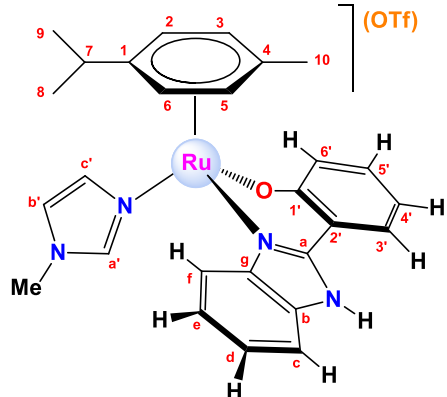
Cationic Complexes



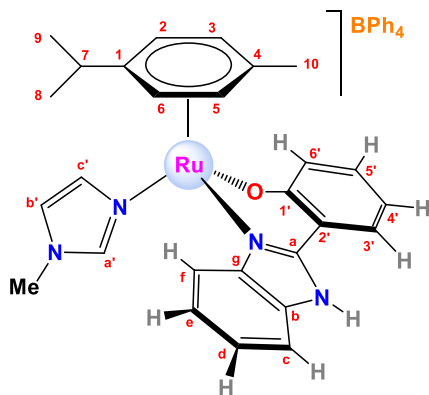
Synthesis of $[(\eta^6\text{-p-cymene})\text{Ru}(\kappa^2\text{-N,O-hpbim})(\text{MeIm})]\text{Cl}$, [19a]Cl. In a 100 mL Schlenk flask, the ligand N-methylimidazole (21.6 μL , 0.271 mmol) was added under a nitrogen atmosphere to a solution of $[\text{RuCl}(\text{cym})(\text{hpbitz})]$ ([16a]) (0.1000 g, 0.208 mmol) in degassed methanol (10 mL). Then, NaCl (0.0142 g, 0.243 mmol) was added and the mixture was stirred at 65 °C for 2 h. The solvent was evaporated to dryness and the residue was solved in dichloromethane (8 mL). The solution was filtered and the solid was precipitated with hexane (15 mL), evaporated to dryness and washed with diethyl ether (5 mL). The resulting yellow powder was dried under vacuum. Yield was not calculated since the complex was impure. $\text{M}_r (\text{C}_{27}\text{H}_{29}\text{N}_4\text{OClRu}) = 562.0750 \text{ g/mol. Anal. Calcd for } \text{C}_{27}\text{H}_{29}\text{N}_4\text{OClRu}\cdot(\text{H}_2\text{O})_{1.2}: \text{C } 55.56; \text{H } 5.42; \text{N } 9.60; \text{Found: C } 55.66; \text{H } 5.43; \text{N } 9.52.$

$^1\text{H NMR}$ (400 MHz, CDCl_3 , 25 °C) δ 14.47 (s, 1H, $\text{H}^{\text{N-H}}$), 8.36 (d, $J = 7.4$ Hz, 1H, $\text{H}^{3'}$), 7.90 (d, $J = 8.3$ Hz, 1H, H^c), 7.71 (s, 1H, $\text{H}^{a'}$), 7.30 (s, 1H, $\text{H}^{c'}$), 7.22 (dd, $J = 15.4, 7.1$ Hz, 2H), 7.11 – 7.06 (m, 2H), 7.04 (d, $J = 8.2$ Hz, 2H, H^d , $\text{H}^{6'}$), 6.81 – 6.68 (m, 2H, $\text{H}^{b'}$, $\text{H}^{4'}$), 5.75 (d, $J = 5.8$ Hz, 1H, $\text{H}^{3'}$), 5.55 (t, $J = 4.9$ Hz, 2H, H^5 , H^6), 5.42 (d, $J = 5.9$ Hz, 1H, H^2), 3.45 (s, 3H, $\text{H}^{\text{N-Me}}$), 2.50 (sept, $J = 6.9$ Hz, 1H, H^7), 1.83 (s, 3H, H^{10}), 1.03 (d, $J = 6.9$ Hz, 3H, H^8 or H^9), 0.99 (d, $J = 6.9$ Hz, 3H, H^9 or H^8) ppm. $^{13}\text{C}\{{}^1\text{H}\}$ NMR (101 MHz, CDCl_3 , 25 °C) δ 167.6 (s, 1C, C^1), 149.2 (s, 1C, C^3), 141.6 (s, 1C, C^8), 139.9 (s, 1C, C^a), 135.3 (s, 1C, C^b), 132.7 (s, 1C, $\text{C}^{5'}$), 130.9 (s, 1C, $\text{C}^{c'}$), 129.7 (s, 1C, $\text{C}^{3'}$), 123.5 (s, 1C, C^d), 123.0 (s, 1C, C^e), 121.8 (s, 1C, $\text{C}^{6'}$), 121.3 (s, 1C, $\text{C}^{4'}$), 117.4 (s, 1C, C^b), 116.6 (s, 1C, C^f), 116.4 (s, 1C, C^2),

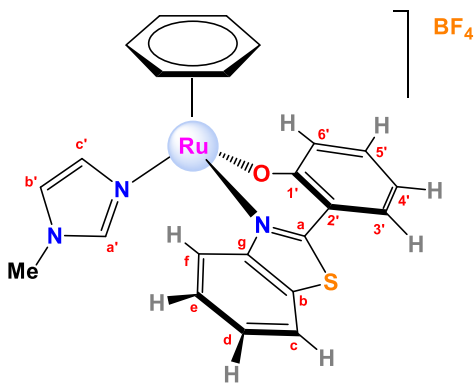
114.2 (s, 1C, C^c), 103.6 (s, 1C, C⁴), 99.5 (s, 1C, C¹), 84.7 (s, 1C, C^{p-cym}), 84.5 (s, 1C, C^{p-cym}), 81.6 (s, 1C, C^{p-cym}), 80.7 (s, 1C, C^{p-cym}), 34.8 (s, 1C, C^{N-Me}), 31.7 (s, 1C, C⁷), 30.8 (s,), 22.5 (s, 1C, C⁸ or C⁹), 22.3 (s, 1C, C⁹ or C⁸), 18.7 (s, 1C, C¹⁰) ppm. **FT-IR (KBr, cm⁻¹) selected bands:** 3362 (w), 2959 (w, ν-CH), 1620 (w), 1600 (m, ν_{C-N}), 1532 (m, ν_{C=C}), 1478 (vs, ν_{C=N}), 1458-1443 (s), 1316 (m), 1261 (s, ν_{C-O}), 1136 (m, ν_{C=S}), 1103 (s), 859-806 (m), 747 (vs), 613 (m). **MS (FAB+):** m/z (%) = 527 (3) ([M-Cl]⁺), 445 (100) ([M-Cl-MeIm]⁺). **Molar Conductivity (CH₃CN):** 67.4 S·cm²·mol⁻¹. **Solubility:** soluble in water, methanol, acetone, dichloromethane and chloroform.



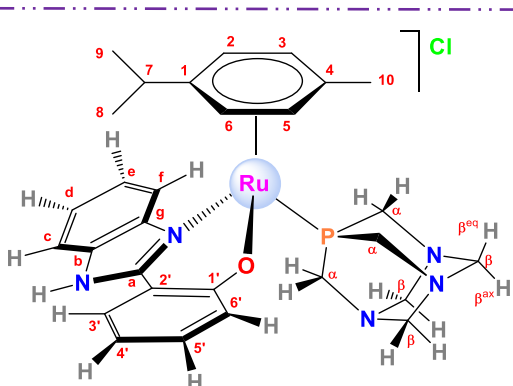
Synthesis of $[(\eta^6-p\text{-cymene})\text{Ru}(\kappa^2\text{-N},\text{O}\text{-hpbim})(\text{MeIm})](\text{OTf})$, [19a]OTf. The synthesis was performed as for [19a]Cl in the presence of the complex [RuCl(cym)(hpbim)] ([16a]) (0.0625 g, 0.130 mmol), N-methylimidazole (13.5 μL, 0.169 mmol) and NaOTf (0.0270 g, 0.157 mmol) in methanol (10 mL). Yellow powder. Yield: 73.4 mg (0.1086 mmol, 83%). M_r (C₂₈H₂₉N₄O₄F₃SRu) = 675.6898 g/mol. **Anal. Calcd for C₂₈H₂₉N₄O₄F₃SRu:** C 49.77; H 4.33; N 8.29; S 4.75; **Found:** C 50.04; H 4.67; N 8.11; S 4.62. **¹H NMR (400 MHz, CDCl₃, 25 °C)** δ 12.16 (s, 1H, H^{N-H}), 7.88 (d, J = 6.5 Hz, 1H, H^{3'}), 7.70 (d, J = 6.3 Hz, 2H, H^{a'}, H^{c'}), 7.38 (d, J = 8.2 Hz, 1H, H^f), 7.27 (s, 1H, H^{c'}), 7.24 (t, J = 7.1 Hz, 1H, H^{5'}), 7.17 (t, J = 7.7 Hz, 1H, H^e), 7.05 (dd, J = 16.2, 8.1 Hz, 2H, H^{b'}, H^d), 6.81 – 6.69 (m, 2H, H^{b'}, H^{4'}), 5.73 (d, J = 5.8 Hz, 1H, H⁵), 5.57 (d, J = 5.9 Hz, 1H, H³), 5.54 (d, J = 5.8 Hz, 1H, H²), 5.42 (d, J = 5.9 Hz, 1H, H⁶), 3.50 (s, 3H, H^{N-Me}), 2.48 (sept, J = 6.8 Hz, 1H, H⁷), 1.83 (s, 3H, H¹⁰), 1.03 (d, J = 6.9 Hz, 3H, H⁸ or H⁹), 1.00 (d, J = 6.9 Hz, 3H, H⁹ or H⁸) ppm. **¹³C{¹H} NMR (101 MHz, CDCl₃, 25 °C)** δ 167.8 (s, 1C, C^{1'}), 149.1 (s, 1C, C^a), 141.7 (s, 1C, C^g), 139.8 (s, 1C, C^{a'}), 134.6 (s, 1C, C^b), 133.0 (s, 1C, C^{5'}), 130.6 (s, 1C, C^{c'}), 128.3 (s, 1C, C^{3'}), 124.1 (s, 1C, C^d), 123.6 (s, 1C, C^e), 122.2 (s, 1C, C⁶), 121.3 (s, 1C, C^{4'}), 117.3 (s, 1C, C^{b'}), 117.0 (s, 1C, C^f), 116.0 (s, 1C, C²), 113.5 (s, 1C, C^c), 103.5 (s, 1C, C⁴), 99.8 (s, 1C, C¹), 84.9 (s, 1C, C³), 84.7 (s, 1C, C⁵), 81.4 (s, 1C, C²), 80.6 (s, 1C, C⁶), 34.8 (s, 1C, C^{N-Me}), 30.9 (s, 1C, C⁷), 22.4 (s, 1C, C⁸ or C⁹), 22.2 (s, 1C, C⁹ or C⁸), 18.7 (s, 1C, C¹⁰) ppm. **¹⁹F{¹H} NMR (376 MHz, CDCl₃, 25 °C)** δ -78.17 (s, 3F, F^{CF3}) ppm. **FT-IR (KBr, cm⁻¹) selected bands:** 3130 (w), 2964 (w, ν-CH), 1622 (w), 1601 (m, ν_{C-N}), 1536 (m, ν_{C=C}), 1478 (vs, ν_{C=N}), 1460-1445 (m), 1327 (w), 1278-1249-1223 (vs, ν_{SO₃-as}), 1159 (s, ν_{C-F}), 1028 (vs, ν_{SO₃-sym}), 858 (m), 747 (s), 559 (m). **MS (FAB+):** m/z (%) = 527 (4) ([M-OTf]⁺), 445 (100) ([M-OTf-MeIm]⁺). **Molar Conductivity (CH₃CN):** 142.5 S·cm²·mol⁻¹. **Solubility:** soluble in methanol, acetone, dichloromethane and chloroform. Partially soluble in water.



Synthesis of $[(\eta^6\text{-}p\text{-cymene})\text{Ru}(k^2\text{-}N,\text{O}\text{-}hpbit)(\text{MeIm})](\text{BPh}_4)$, [19a]BPh₄. The synthesis was performed as for [19a]Cl in the presence of the complex [RuCl(cym)(hpbit)] ([16a]) (0.100 g, 0.208 mmol), N-methylimidazole (22 μL , 0.276 mmol) and NaBPh₄ (0.0821 g, 0.240 mmol) in methanol (14 mL), and after evaporation and before solving in dichloromethane, the solid was washed with hexane (5mL), water (5 mL) and diethyl ether (5 mL). Yellow powder. Yield: 137.8 mg (0.163 mmol, 78%). **M_r** ($\text{C}_{51}\text{H}_{49}\text{N}_4\text{OBRu}$) = 845.8553 g/mol. **Anal.** **Calcd** for $\text{C}_{51}\text{H}_{49}\text{N}_4\text{OBRu}\cdot\text{H}_2\text{O}$: C 70.91; H 5.95; N 6.49; **Found**: C 70.95; H 6.16; N 6.81. **¹H NMR (400 MHz, CDCl₃, 25 °C)** δ 7.48 – 7.34 (m, 3H), 7.25 – 7.12 (m, 12H), 6.87 – 6.72 (m, 15H), 6.50 (s, 1H, H^{b'}), 5.50 (d, J = 5.9 Hz, 1H, H² or H⁶), 5.47 (d, J = 5.8 Hz, 1H, H⁶ or H²), 5.37 (d, J = 5.7 Hz, 1H, H³ or H⁵), 5.20 (d, J = 5.9 Hz, 1H, H⁵ or H³), 2.43 (sept, J = 6.9 Hz, 1H, H⁷), 2.17 (s, 3H, H^{Me}), 1.90 (s, 3H, H¹⁰), 1.01 (d, J = 6.9 Hz, 3H, H⁸ or H⁹), 0.97 (d, J = 6.9 Hz, 3H, H⁹ or H⁸) ppm. **¹H NMR (400 MHz, DMSO-d₆, 25 °C)** δ 13.36 (s, 1H, H^{N-H}), 7.82 (s, 1H, H^{a'}), 7.73 (d, J = 6.6 Hz, 1H, H^{3'}), 7.65 (d, J = 9.2 Hz, 1H, H^f), 7.51 (d, J = 9.1 Hz, 1H, H^c), 7.41 (s, 1H, H^{c'}), 7.27 (dd, J = 9.5, 5.5 Hz, 3H, H^e, H^d, H^{5'}), 7.22 (s, 1H, H^{b'}), 7.17 (bs, 8H, H^{O-Ph(BPh4)}), 7.05 (d, J = 8.5 Hz, 1H, H^{6'}), 6.92 (t, J = 7.4 Hz, 8H, H^{m-Ph(BPh4)}), 6.78 (t, J = 7.1 Hz, 4H, H^{p-Ph(BPh4)}), 6.70 (t, J = 7.5 Hz, 1H, H^{4'}), 5.95 (d, J = 6.2 Hz, 1H, H⁶), 5.76 (d, J = 6.4 Hz, 2H, H², H³), 5.67 (d, J = 6.0 Hz, 1H, H⁵), 3.57 (s, 3H, H^{N-Me}), 2.40 (sept, J = 7.0 Hz, 1H, H⁷), 1.75 (s, 3H, H¹⁰), 0.98 (d, J = 7.0 Hz, 3H, H⁸ or H⁹), 0.95 (d, J = 6.9 Hz, 3H, H⁹ or H⁸) ppm. **¹³C{¹H} NMR (101 MHz, CDCl₃, 25 °C)** δ 138.7 (s), 136.0 (s), 134.7 (s), 130.9 (s), 127.0 (s), 125.9 (s), 125.0 (s), 121.6 (s), 117.0 (s), 116.5 (s), 103.8 (s, 1C, C¹), 99.2 (s, 1C, C⁴), 84.2 (s, 1C, C² or C⁶), 83.9 (s, 1C, C⁵ or C³), 82.1 (s, 1C, C⁶ or C²), 80.7 (s, 1C, C³ or C⁵), 30.9 (s, 1C, C⁷), 22.4 (s, 1C, C⁸), 22.2 (s, 1C, C⁹), 18.8 (s, 1C, C¹⁰) ppm. Carbon NMR signals are difficult to assign because of the huge amount and complexity of signals of the BPh₄ group. **FT-IR (KBr, cm⁻¹) selected bands:** 3131 (w), 3053 (w, v_{=CH}), 2998, 2982, 2963 (w, v_{-CH}), 1622 (w), 1602 (s, v_{C=N}), 1535 (m, v_{C=C}), 1478 (vs, v_{C=N}), 1459 (s), 1445 (s), 1426 (s), 1320 (m), 1263 (s, v_{C-O}), 1136 (m, v_{C=S}), 1107 (s, $\delta_{\text{N-Hip}}$), 843 (m), 734-706 (s, v_{B-C}), 613 (m). **MS (FAB+):** m/z (%) = 527 (3) ([M-BPh₄]⁺), 445 (8) ([M-BPh₄-MeIm]⁺). **Molar Conductivity (CH₃CN):** 65 S·cm²·mol⁻¹. **Solubility:** soluble in methanol, acetone, dichloromethane and chloroform. Slightly soluble/insoluble in water.



Synthesis of $[(\eta^6\text{-benzene})\text{Ru}(\kappa^2\text{-N},\text{O}\text{-hpbtz})(\text{MeIm})](\text{BF}_4)$, [20b]BF₄. The synthesis was performed as for **[19a]Cl** in the presence of the complex [RuCl(bz)(hpbtz)] (**[17b]**) (0.0400 g, 0.091 mmol), N-methylimidazole (10 µL, 0.125 mmol) and NaBF₄ (0.0116 g, 0.101 mmol) in methanol (4 mL). Orange-yellowish powder. Yield: 43.0 mg (0.0749 mmol, 83%). M_r (**C₂₃H₂₀N₃OBF₄Ru**) = 574.3711 g/mol. **Anal. Calcd for C₂₃H₂₀N₃OBF₄Ru·(H₂O)₂(NaCl)_{0.3}:** C 43.99; H 3.85; N 6.69; S 5.11; **Found:** C 43.91; H 4.12; N 7.03; S 5.21. **¹H NMR (400 MHz, CDCl₃, 25 °C)** δ 8.97 (s, 1H, H^{a'}), 8.03 (d, J = 8.6 Hz, 1H, H^f), 7.78 (d, J = 8.0 Hz, 1H, H^{c'}), 7.70 (t, J = 7.9 Hz, 1H, H^e), 7.59 (d, J = 7.9 Hz, 1H, H^{3'}), 7.42 (t, J = 7.7 Hz, 1H, H^d), 7.39 (t, J = 7.7 Hz, 1H, H^{5'}), 7.19 (d, J = 8.4 Hz, 1H, H^{b'}), 6.78 (t, J = 7.5 Hz, 1H, H^{4'}), 6.64 (s, 1H, H^{b'}), 6.50 (s, 1H, H^{c'}), 5.90 (s, 6H, H^{bz}), 3.79 (s, 3H, H^{Me}) ppm. **¹³C{¹H} NMR (101 MHz, CDCl₃, 25 °C)** δ 168.2 (s, 1C, C^{1'}), 167.7 (s, 1C, C^a), 152.2 (s, 1C, C^g), 143.1 (s, 1C, C^{a'}), 135.2 (s, 1C, C^{5'}), 131.0 (s, 1C, C^b), 130.2 (s, 1C, C^{3'}), 129.4 (s, 1C, C^e), 127.9 (s, 1C, C^c), 126.6 (s, 1C, C^d), 123.6 (s, 1C, C^f), 123.1 (s, 1C, C^{6'}), 121.9 (s, 1C, C^c), 121.6 (s, 1C, C^{2'}), 120.9 (s, 1C, C^{b'}), 117.9 (s, 1C, C^{4'}), 85.2 (s, 1C, C^{bz}), 35.0 (s, 1C, C^{Me}) ppm. **FT-IR (KBr, cm⁻¹) selected bands:** 3447 (s), 3376 (s), 3116 (w, ν_{CH}), 2923 (w, ν_{CH}), 2852 (w), 1653 (w), 1597 (s, ν_{C=N}), 1542 (m, ν_{C=C}), 1483 (s, ν_{C=N}), 1456 (m), 1442 (m), 1419 (w), 1331 (w), 1236 (w, ν_{C-O}), 1156 (w, ν_{C=S}), 1099-1084-1035 (vs, ν_{B-F}), 837 (m), 750 (m, δ_{CHop}). **MS (FAB+):** m/z (%) = 488 (12) ([M-BF₄]⁺), 406 (9) ([M-BF₄-MeIm]⁺). **Molar Conductivity (CH₃CN):** 110 S·cm²·mol⁻¹. **Solubility:** soluble in water, acetone, dichloromethane, chloroform and methanol.



Synthesis of $[(\eta^6\text{-p-cymene})\text{Ru}(\kappa^2\text{-N},\text{O}\text{-hpbim})(\text{PTA})]\text{Cl}$, [21a]Cl. In a 100 mL Schlenk flask, the ligand PTA (1,3,5-triaza-7-phosphadamantane) (0.0127 g, 0.081 mmol) was added under a nitrogen atmosphere to a solution of [RuCl(cym)(hpbim)] (0.0336 g, 0.070 mmol) in degassed methanol (12 mL). The mixture was stirred at room temperature for 20 h. The solution was filtered and concentrated. The product was precipitated with diethyl ether (20 mL) and filtered off. The resulting yellow powder was dried under vacuum. Yield: 34.0 mg (0.0534 mmol, 76%).

M_r (C₂₉H₃₅N₅OPClRu) = 637.1249 g/mol. **Anal. Calc. for C₂₉H₃₅N₅OPClRu·H₂O:** C 53.17; H 5.69; N 10.69 **Found:** C 53.23; H 5.57; N 9.99. **¹H NMR (400 MHz, CDCl₃, 25 °C)** δ 14.79 (s, 1H, H^{N-H}), 8.43 (d, J = 7.2 Hz, 1H, H^{3'}), 8.13 – 8.05 (m, 1H, H^c), 7.32 – 7.26 (m, 2H, H^d, H^e), 7.16 (t, J = 7.5 Hz, 1H, H^{5'}), 6.96 – 6.91 (m, 1H, H^f), 6.87 (d, J = 8.4 Hz, 1H, H^{6'}), 6.76 (t, J = 7.4 Hz, 1H, H^{4'}), 5.86 (d, J = 21.3 Hz, 2H, H², H³), 5.64 (d, J = 19.2 Hz, 2H, H⁵, H⁶), 4.32 (ABq, 6H, Δδ_{AB} = 0.03, J_{AB} = 14.8 Hz, H^β), 4.02 (ABq, 6H, Δδ_{AB} = 0.07, J_{AB} = 14.4 Hz, H^α), 2.52 (sept, J = 6.8 Hz, 1H, H⁷), 2.06 (s, 3H, H¹⁰), 1.05 (d, J = 6.8 Hz, 6H, H⁸, H⁹) ppm. **³¹P{¹H} NMR (162 MHz, CDCl₃, 25 °C)** δ -30.4 (s, 1P, P^{PTA}) ppm. **¹³C{¹H} NMR (101 MHz, CDCl₃, 25°C)** δ 168.1 (s, 1C, C^{1'}), 150.0 (s, 1C, C^a), 142.3 (s, 1C, C^g), 135.4 (s, 1C, C^b), 132.6 (s, 1C, C^{5'}), 129.9 (s, 1C, C^{3'}), 124.2 (s, 1C, C^d), 123.3 (s, 1C, C^{6'}), 122.5 (s, 1C, C^e), 117.2 (s, 1C, C^f), 116.3 (s, 1C, C^{4'}), 115.8 (s, 1C, C^{2'}), 115.0 (s, 1C, C^c), 113.5 (s, 1C, C¹), 100.4 (s, 1C, C⁴), 88.8 (s, 1C, C² or C⁶), 86.9 (s, 1C, C⁵ or C³), 85.6 (s, 1C, C⁶ or C²), 84.8 (s, 1C, C³ or C⁵), 73.1 (s, 3C, C^β), 51.1 (d, ¹J_{C-P} = 13.3 Hz, 3C, C^α), 31.5 (s, 1C, C⁷), 23.2 (s, 1C, C⁸), 21.4 (s, 1C, C⁹), 19.7 (s, 1C, C¹⁰) ppm. **FT-IR (KBr, cm⁻¹) selected bands:** 3393 (m, ν_{N-H}), 3028 (w, ν_{=CH}), 2960 (w, ν_{-CH}), 1620 (m, ν_{C-N}), 1600 (s, ν_{C=C}), 1552–1530 (m), 1478 (vs, ν_{C=N}), 1458 (s), 1444 (s), 1314–1284 (m, ν_{C-N(PTA)}), 1260–1240 (s, ν_{C-O}), 1136–1097 (m), 1013 (s), 972 (s), 947 (s), 804 (m, ν_{P-C}), 744 (s), 581 (s). **MS (FAB+):** m/z (%) = 602 (6) ([M-Cl]⁺), 445 (8) ([M-Cl-PTA]⁺). **Molar Conductivity (CH₃CN):** 53.5 S·cm²·mol⁻¹. **Solubility:** soluble in water, methanol, ethanol, dichloromethane, chloroform and acetone.

4. BIBLIOGRAPHY

- (1) Yu, G.; Yin, S.; Liu, Y.; Shuai, Z.; Zhu, D. *J. Am. Chem. Soc.* **2003**, *125*, 14816–14824.
- (2) Tong, Y.-P.; Lin, Y.-W. *J. Chem. Crystallogr.* **2008**, *38*, 613–617.
- (3) Pyrz, J. W.; Pan, X.; Britton, D.; Que, L. *Inorg. Chem.* **1991**, *30*, 3461–3464.
- (4) Machura, B.; Wolff, M.; Kusz, J.; Kruszynski, R. *Polyhedron* **2009**, *28*, 2949–2964.
- (5) Krishnamurthy, N.; Shashikala, N. *J. Serbian Chem. Soc.* **2009**, *74*, 1085–1096.
- (6) Krishnamurthy, G. *Synth. React. Inorganic, Met. Nano-Metal Chem.* **2011**, *41*, 590–597.
- (7) Kärkäs, M. D.; Åkermark, T.; Johnston, E. V.; Karim, S. R.; Laine, T. M.; Lee, B. L.; Åkermark, T.; Privalov, T.; Åkermark, B. *Angew. Chemie - Int. Ed.* **2012**, *51*, 11589–11593.
- (8) Kärkäs, M. D.; Liao, R.-Z.; Laine, T. M.; Åkermark, T.; Ghanem, S.; Siegbahn, P. E. M.; Åkermark, B. *Catal. Sci. Technol.* **2016**, *6*, 1306–1319.
- (9) Rathinasamy, S.; Karki, S. S.; Bhattacharya, S.; Manikandan, L.; Prabakaran, S. G.; Gupta, M.; Mazumder, U. K. *J. Enzyme Inhib. Med. Chem.* **2006**, *21*, 501–507.
- (10) Bennett, M. A.; Smith, A. K. *J. Chem. Soc. Dalton Trans.* **1974**, 233–241.
- (11) Therrien, B. *Coord. Chem. Rev.* **2009**, *253*, 493–519.
- (12) Desiraju, G. R. *Acc. Chem. Res.* **2002**, *35*, 565–573.
- (13) Scolaro, C.; Chaplin, A. B.; Hartinger, C. G.; Bergamo, A.; Cocchietto, M.; Keppler, B. K.; Sava, G.; Dyson, P. J. *Dalton Trans.* **2007**, *2*, 5065–5072.
- (14) Daigle, D. J.; Pepperman, . B.; Jr.; Vail, S. L. *J. Heterocycl. Chem.* **1974**, *11*, 407–408.
- (15) Vock, C. a.; Renfrew, A. K.; Scopelliti, R.; Juillerat-Jeanneret, L.; Dyson, P. J. *Eur. J. Inorg. Chem.* **2008**, 1661–1671.
- (16) Angelici, R. J. In *Técnicas y Síntesis en Química Inorgánica*; Editorial Reverté, S.A., **1979**; p. 243.
- (17) Housecroft, C. E.; Sharpe, A. E. *Inorganic Chemistry*; Fourth.; Pearson, **2012**.
- (18) Vock, C. a; Scolaro, C.; Phillips, A. D.; Scopelliti, R.; Sava, G.; Dyson, P. J. *J. Med. Chem.* **2006**, *49*, 5552–5561.
- (19) Bugarcic, T.; Habtemariam, A.; Stepankova, J.; Heringova, P.; Kasparkova, J.; Deeth, R. J.; Johnstone, R. D. L.; Prescimone, A.; Parkin, A.; Parsons, S.; Brabec, V.; Sadler, P. J. *Inorg. Chem.* **2008**, *47*, 11470–11486.
- (20) Faraone, F.; Sergi, S. *J. Organometallic Chem.* **1976**, *112*, 201–207.
- (21) Jonathan W. Steed; Tocher, D. A. *J. Chem. Soc. Dalton Trans.* **1992**, 7231–7235.
- (22) Chakrabarti, P.; Bhattacharyya, R. *Prog. Biophys. Mol. Biol.* **2007**, *95*, 83–137.
- (23) Reid, K. S. .; Lindley, P. .; Thornton, J. . *FEBS Lett.* **1985**, *190*, 209–213.
- (24) Kargol, J. A.; Crecely, R. W.; Burmeister, J. L. *Inorg. Chem.* **1979**, *18*, 2532–2535.
- (25) Nakamoto, K. *Infrared and Raman Spectra of Inorganic and Coordination Compounds*; Fourth.; John Wiley and Sons, **1986**.
- (26) Campos, J.; Álvarez, E.; Carmona, E. *New J. Chem.* **2011**, *35*, 2122–2129.
- (27) Norbury, A. H. *J. Chem. Soc. Sect. A* **1971**, 1089–1091.

- (28) Norbury, A. H.; Shaw, P. E.; Sinha, A. I. P. *Chem. Commun.* **1970**, 1080.
- (29) Pearson, G. J. *Am. Chem. Soc.* **1963**, 85, 3533–3539.
- (30) Dougan, S. J.; Melchart, M.; Habtemariam, A.; Parsons, S.; Sadler, P. J. *Inorg. Chem.* **2006**, 45, 10882–10894.
- (31) Barragán, F.; López-Senín, P.; Salassa, L.; Betanzos-Lara, S.; Habtemariam, A.; Moreno, V.; Sadler, P. J.; Marchán, V. *J. Am. Chem. Soc.* **2011**, 133, 14098–14108.
- (32) Karlen, T.; Hauser, A.; Ludi, A.; Chemie, A.; Bern, U.; Bern, C. H.; November, R. *Inorg. Chem.* **1994**, 33, 2213–2218.
- (33) Martínez-Alonso, M.; Busto, N.; Jalón, F. A.; Manzano, B. R.; Leal, J. M.; Rodríguez, A. M.; García, B.; Espino, G. *Inorg. Chem.* **2014**, 53, 11274–11288.
- (34) Mendoza-Ferri, M. G.; Hartinger, C. G.; Nazarov, A. A.; Eichinger, R. E.; Jakupc, M. A.; Severin, K.; Keppler, B. K. *Organometallics* **2009**, 28, 6260–6265.
- (35) Schuecker, R.; John, R. O.; Jakupc, M. A.; Arion, V. B.; Keppler, B. K. *Organometallics* **2008**, 27, 6587–6595.
- (36) Marcus, Y. *J. Chem. Soc. Faraday Trans.* **1991**, 87, 2995–2999.
- (37) Martin, R. B. In *Cisplatin Chemistry and Biochemistry of a Leading Anticancer Drug*; Verlag Helvetica Chimica Acta: Zürich, **2006**; pp. 181–205.
- (38) Gutiérrez, A.; Cativiela, C.; Laguna, A.; Gimeno, M. C. *Dalt. Trans.* **2016**, 45, 13483–13490.
- (39) Loughrey, B. T.; Healy, P. C.; Parsons, P. G.; Williams, M. L. *Inorg. Chem.* **2008**, 47, 8589–8591.
- (40) Healy, P. C.; Loughrey, B. T.; Williams, M. L.; Parsons, P. G. *J. Inorg. Biochem.* **2010**, 104, 625–631.

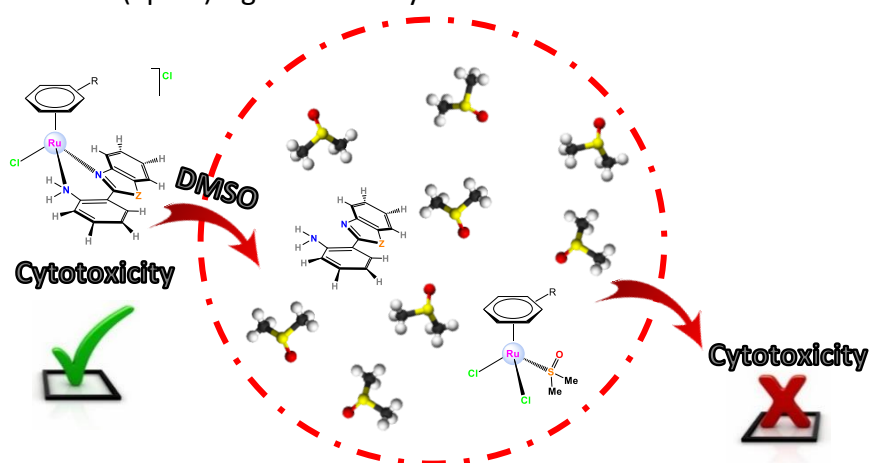
CHAPTER 4.

Ru(II) HALF-SANDWICH COMPLEXES BEARING AMINOPHENYLBENZAZOLE ANCILLARY LIGANDS: SYNTHESIS, CHARACTERIZATION AND ANTICANCER PROPERTIES



CHAPTER 4. Ru(II) HALF-SANDWICH COMPLEXES BEARING AMINOPHENYLBENZAZOLE ANCILLARY LIGANDS: SYNTHESIS, CHARACTERIZATION AND ANTICANCER PROPERTIES

ABSTRACT: In this chapter a family of 13 new complexes of general formulae $[\text{Ru}(\eta^6\text{-arene})(\kappa^2\text{-N,N-HL})\text{X}]Y$ or $[\text{Ru}(\eta^6\text{-}p\text{-cymene})(\kappa^2\text{-N,N-L})\text{X}]$ (X = leaving group; Y = counterion) bearing 2-(2'-aminophenyl)benzimidazole (apbim) and 2-(2'-aminophenyl)benzothiazole (apbtz) ligands was synthesized in order to assess their antiproliferative activity against cancer cells and to establish SARs in connection with the features of the chosen N,N-ligands. Thus, we intend to analyse the following effects:



- The size and geometry of the chelate ring (6 atoms in apbim and apbtz vs. 5 atoms in pybim and pybtz (see CHAPTER 1)).
- The hydrogen-bonding donor ability of the $-\text{NH}_2$ coordinating groups that could favour specific interactions with DNA.

Moreover, we intend to study the effects of different arenes, counterions and leaving groups on the cytotoxic potency.

CONTEXT: The search of new organometallic drugs has launched ruthenium as a promising alternative to platinum drugs, and especially, ruthenium(II) arene complexes. Among the well-known N,N-chelating ligands, bipyridine (bipy)¹ and ethylenediamine (en)^{2,3,4} have been successfully used by P. J. Sadler and co-workers in this field. However, only a few examples containing N,N-chelating ligands with both amine ($-\text{NH}_2$) and imine ($-\text{N}=\text{C}$) groups have been reported in the literature. In particular, some ruthenium arene complexes with α -amino acids (L-histidine)^{5,6} and aminooxazolines.⁷

1. RESULTS AND DISCUSSION

1.1. Synthesis

The complexes were synthesised from the ruthenium chloro-bridged dimers $[\text{Ru}(\eta^6\text{-arene})(\mu\text{-Cl})\text{Cl}]_2$ prepared by reaction of $\text{RuCl}_3 \cdot n\text{H}_2\text{O}$ with a cyclohexadiene derivative in ethanol, as shown in Chapter 1.^{8,9} The iodido derivative was synthesised from the ruthenium iodo-bridged dimer $[\text{Ru}(\eta^6\text{-}p\text{-cymene})(\mu\text{-I})\text{I}]_2$ prepared in turn, by the reaction of the ruthenium chloro-bridged dimer with potassium iodide in a mixture of water/CHCl₃ (1:1).¹⁰

All the complexes, whose schematic synthesis is shown in Fig. 1, are cationic except one neutral compound.

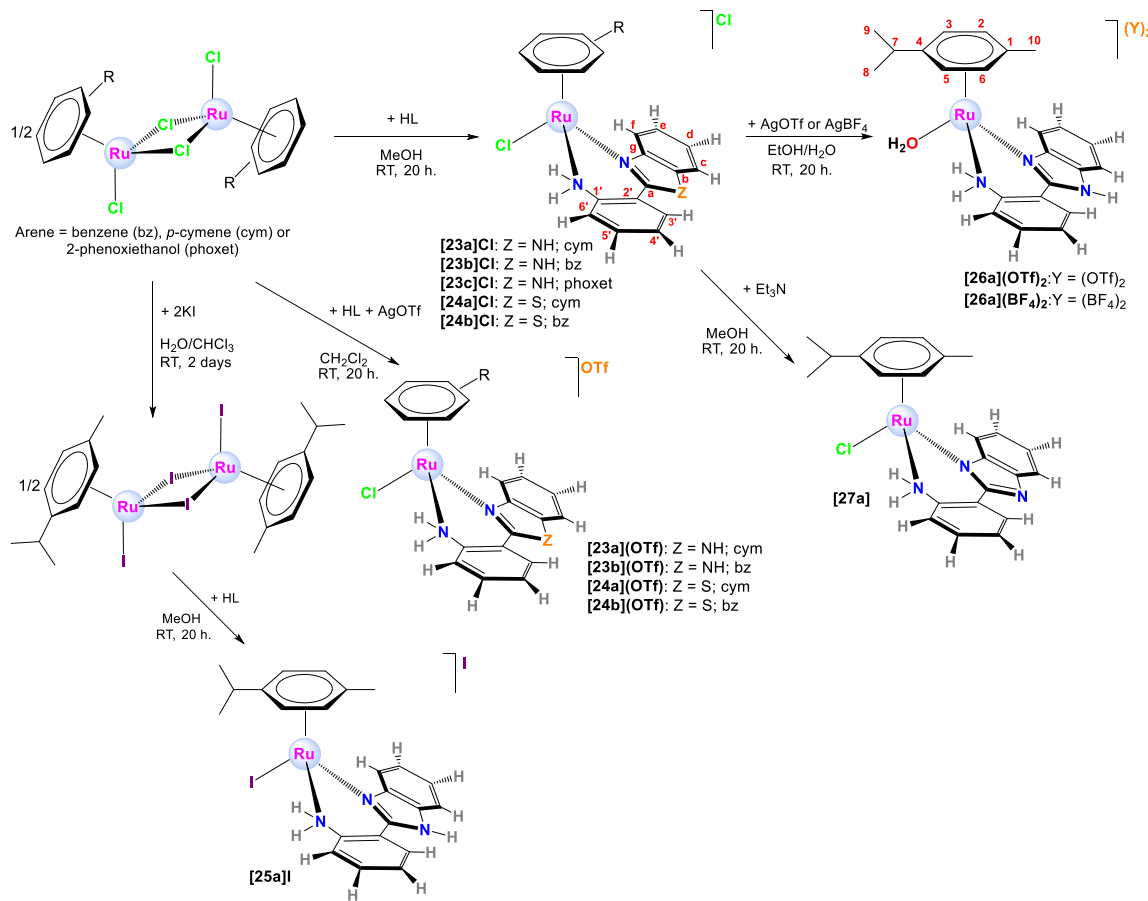


Fig. 1. Schematic synthesis of Ruthenium(II) complexes.

All the synthetic reactions were performed at room temperature and stirring overnight. In particular, the chlorido and iodido derivatives of general formula $[(\eta^6\text{-arene})\text{RuX}(\kappa^2\text{-}N,N\text{-HL})]\text{X}$ ([23a]Cl, [23b]Cl, [23c]Cl, [24a]Cl, [24b]Cl and [25a]I), where X = Cl⁻ or I⁻ and HL = apbim or apbtz, were synthesised by the reaction between the corresponding ruthenium(II) arene starting dimer and the ligands (apim and apbtz) in methanol. The respective triflate salts of the general formula $[(\eta^6\text{-arene})\text{RuCl}(\kappa^2\text{-}N,N\text{-HL})]\text{OTf}$ ([23a](OTf), [23b](OTf), [24a](OTf), [24b](OTf)) were prepared by a similar protocol in the presence of AgOTf and using dichloromethane as the solvent. Complex [23a]Cl was previously reported in the literature by J. G. Małecki, and also its crystal

structure co-crystallized with a molecule of acetone.¹¹ Recently, during the progress of this work, complexes **[23a]Cl** and **[23b]Cl** were also reported by D. S. Pandey.¹²

The aqua derivatives of general formula $[(\eta^6-p\text{-cymene})\text{Ru}(\text{H}_2\text{O})(\kappa^2\text{-}N,N\text{-apbim})](\text{Y})_2$ (**[26a](BF_4)_2**, **[26a](OTf)_2**), where $\text{Y} = \text{BF}_4^-$ or OTf^- , were prepared by the reaction of **[23a]Cl** with an excess of the corresponding silver salt (AgBF_4 and AgOTf) in a mixture of distilled water and ethanol.

The complex **[23a]Cl** was reacted with triethylamine to yield the neutral derivative **[27a]** $[(\eta^6-p\text{-cymene})\text{RuCl}(\kappa^2\text{-}N,N\text{-apbim}')]$.

It is remarkable that a little of acetonitrile was used in the synthesis of benzene derivatives, so as to enhance the solubility of the benzene dimer.

All the complexes were isolated in moderate-to-good yields (from 38% to 79%) as the corresponding racemates (R_{Ru} or S_{Ru}) in the form of yellow, brown or black powders.

1.2. Characterization

All the complexes have been fully characterised by NMR spectroscopy, IR spectroscopy, positive fast atom bombardement (FAB^+) mass spectrometry, molar conductivity and elemental analysis.

1.2.1. NMR

The ^1H NMR spectra of monocationic complexes were recorded in DMSO-d_6 , CDCl_3 or CD_3OD at 25 °C. As in previous complexes, the coordination of the ligands to the metal centres caused the inequivalence of *p*-cym and phoxet protons and hence provide an NMR pattern consistent with that of an assymmetric species (see CHAPTER 1 for more information and details). Specially, the signal for the NH group (H^{NH}) in apbim showed an enormous downfield-shift for **[23a]Cl** ($\Delta\delta = 5.31$ ppm) and for **[23b]Cl** ($\Delta\delta = 4.72$ ppm) in CDCl_3 compared to the free ligand. Furthermore, the single signal of the equivalent hydrogen atoms of the NH_2 group in the free ligands splitted into two when they bind to the metal. Thus, both hydrogen atoms become inequivalent, with different chemical environments (see below). This behaviour is observed both in CDCl_3 and DMSO-d_6 , although the increment in δ was more pronounced in CDCl_3 and bigger for the apbtz ligand. However, the spectra of complexes **[24a]Cl** and **[24b]Cl** (with the ligand apbtz) in DMSO-d_6 showed three sets of signals both in the aromatic and in the aliphatic areas (see Fig. 2). The most downfield-shifted set in the aromatic area corresponds to the original complex, whereas the other set corresponds to the free ligand. Furthermore, apart from the expected signals of the *p*-cym in **[24a]Cl**, there was another set with symmetry, assigned to the species $[(\eta^6\text{-arene})\text{Ru}(\text{DMSO-d}_6)\text{Cl}_2]$, well known since it forms when the dimer is dissolved in DMSO-d_6 .^{13,14,15} The comparison of these spectra (see Fig. 4) illustrates the solvolysis of these compounds and demonstrates the lability of the ligand apbtz (see Fig. 3). The same effect occurs for complexes with the apbim ligand and with both chloride and triflate anions, although it is less marked.

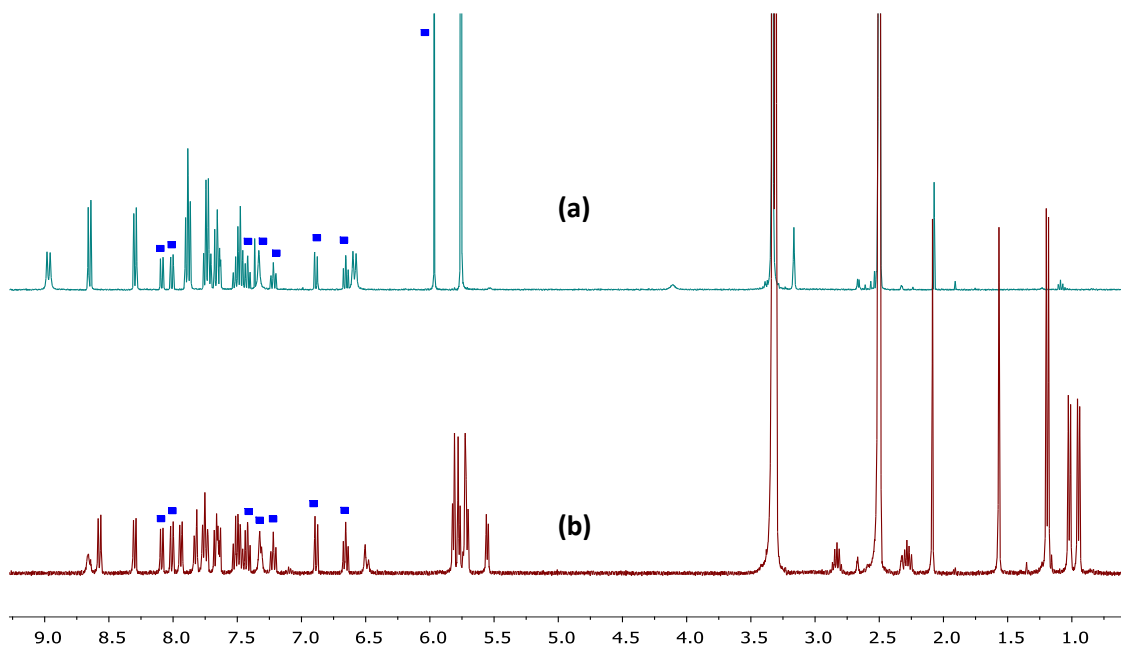


Fig. 2. Comparison between the ^1H -NMR spectra of: (a) [24a]Cl and (b) [24b]Cl in DMSO-d_6 at 25°C . Blue squares correspond to the free ligand.

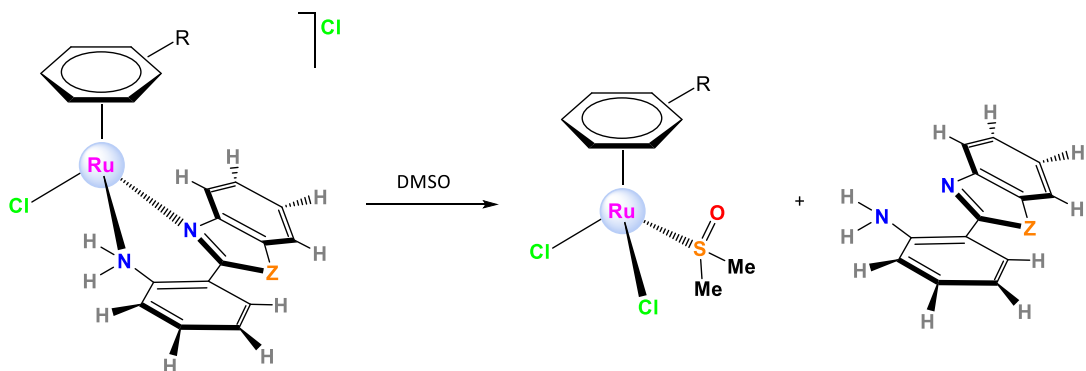


Fig. 3. Graphical illustration of the solvolysis process in the presence of DMSO.

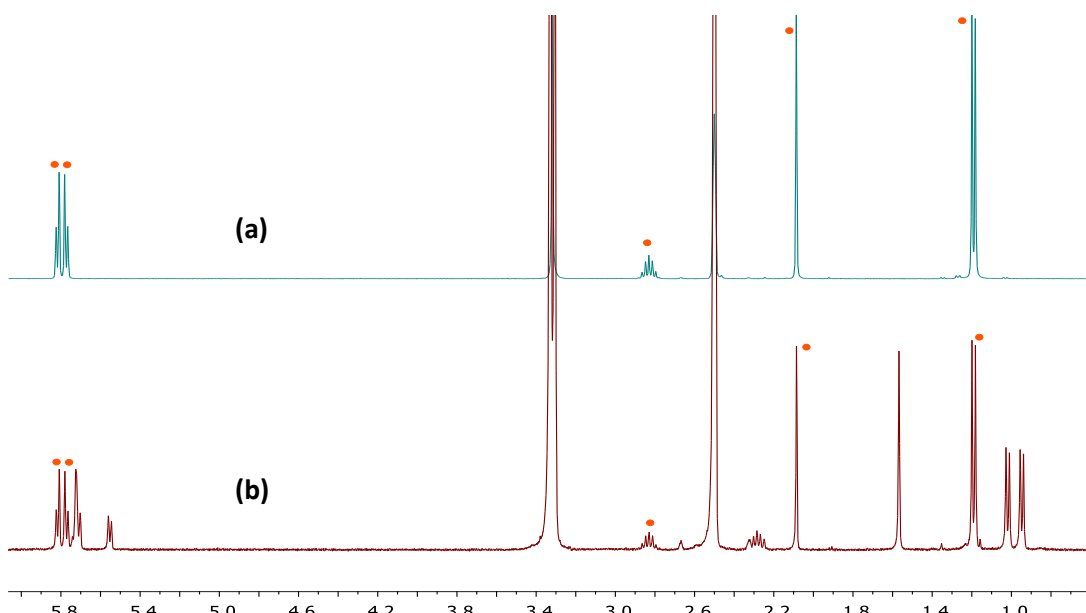


Fig. 4. Comparison of the *p*-cymene area of ^1H -NMR spectra between (a) $[\text{RuCl}_2(\text{p-cym})(\text{DMSO-d}_6)]$ and (b) [24a]Cl in DMSO-d_6 at 25°C .

Inequivalent hydrogens in NH₂ group.

As said before, hydrogen atoms in the NH₂ group became inequivalent once the metal is coordinated (see Fig. 5).

The ¹H-¹H COSY spectra confirmed the coupling between both NH₂ protons that formed an AX spin system (two doublets H^A and H^X with geminal coupling constants ²J_{AX} ≈ 8.6 -11 Hz). Furthermore, the ¹H-¹H NOESY spectra showed some interesting NOE cross peaks and chemical exchange peaks (see Fig. 6):

- NOE interactions between H^A and H^X.
- Some intramolecular NOE interactions: H^A with H^{6'} and H^{cym}, so that H^A was assigned to the equatorial hydrogen, since it is in the plane of the chelate ring. Therefore, it is the only one which could interact with H^{6'} and H^{cym}.
- An intermolecular NOE interaction of H^A with the residual water peak as impurity.
- Chemical exchange peaks between H^X with the residual water peak.

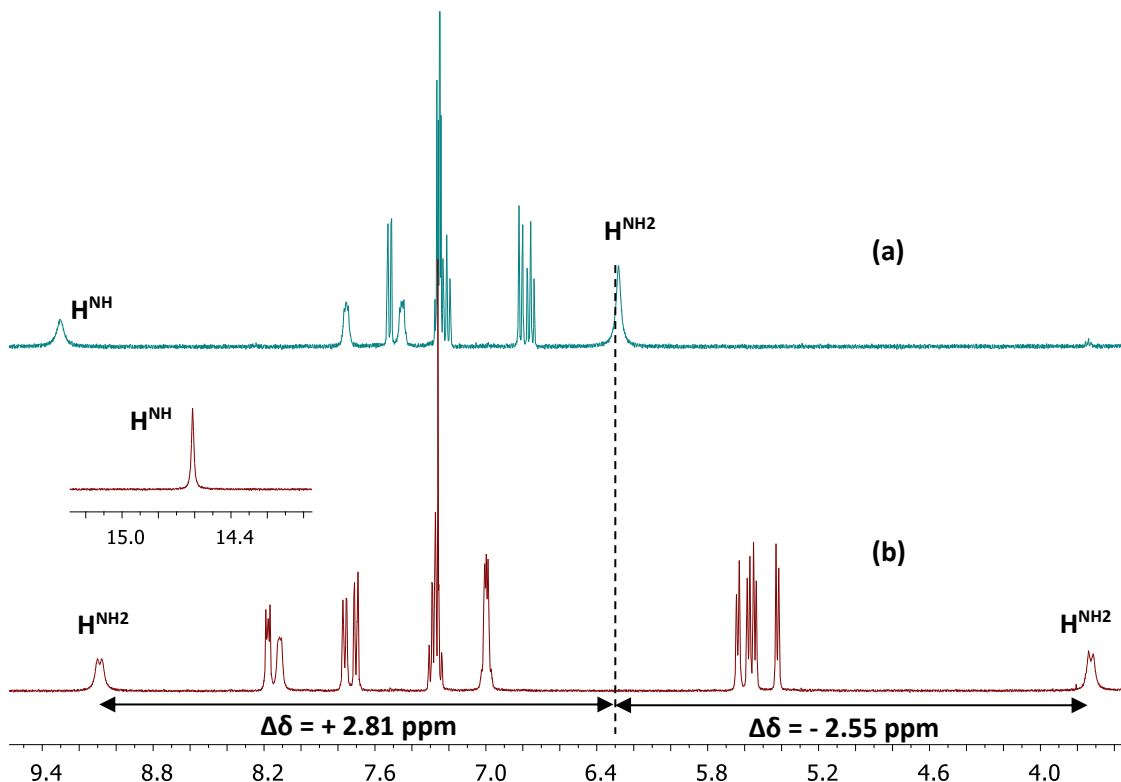


Fig. 5. Comparison between the ¹H-NMR spectra of the ligand apim (a) and [23a]Cl (b) in CDCl₃ at 25 °C.

Regarding H^A, the lack of chemical exchange with water and the strongly deshielded signal in relation to the NH₂ for the free ligand suggest that H^A is taking part in hydrogen bonding that stabilizes it against chemical exchange processes. In CDCl₃, this interaction might involve the chloride anion, therefore giving rise to ion pairing entities, whereas in DMSO-d₆ a molecule of solvent could be the hydrogen bond acceptor. This fact could explain the differences of chemical shift in both solvents. Some X-ray structures actually illustrate the hydrogen bonding between the chloride anion and the complex through H^A (vide infra).

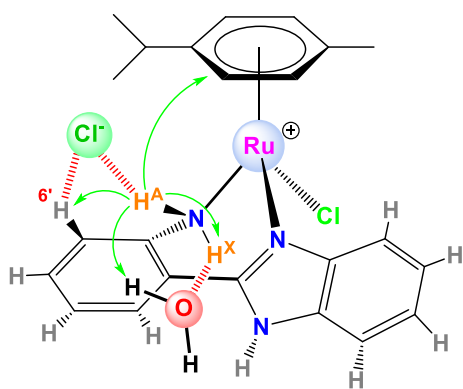


Fig. 6. Graphical illustration of NOE cross peaks with chloride and the water molecule.

As far as H^X is concerned, it participates in a chemical exchange process by proton transfer with the water molecule (water is more basic than chloride or DMSO). As a consequence, the signal is strongly shielded because it tends to coalesce with the water resonance. H^X is more upfield shifted in CDCl_3 than in DMSO-d_6 as the chemical shift of water in the former is lower (1.56 ppm) than in the latter (3.33 ppm). Furthermore, this water molecule placed in the second coordination sphere, interacts with H^A (see Fig. 6). This signal splitting was observed as well for [25a]I.

The ^1H NMR spectra of the aqua derivatives were registered in D_2O at 25 °C and were similar to those of the monocationic derivatives. Regarding the ^1H - ^1H NOESY spectra, the aqua derivative $[\mathbf{26a}](\text{BF}_4)_2$ shows exchange peaks between H^2 and H^6 and H^3 and H^5 , implying an interconversion process between the two enantiomers (R_{Ru} or S_{Ru}), in which the water molecule is presumably involved, as in previous aquo derivatives (see discussion in CHAPTER 1). In addition, some signals of *p*-cym in $[\mathbf{26a}](\text{OTf})_2$ are broadened, in agreement with this fact. To prove this hypothesis $[\mathbf{26a}](\text{BF}_4)_2$ was reacted with NaHCO_3 in D_2O and the evolution of the mixture was monitored by ^1H NMR at 25 °C. Consequently, all the signals shifted upfield as a result of deprotonation which produces $[\mathbf{26a}']^+$. The N atom becomes anionic and therefore, the peaks are shielded (see Fig. 7).

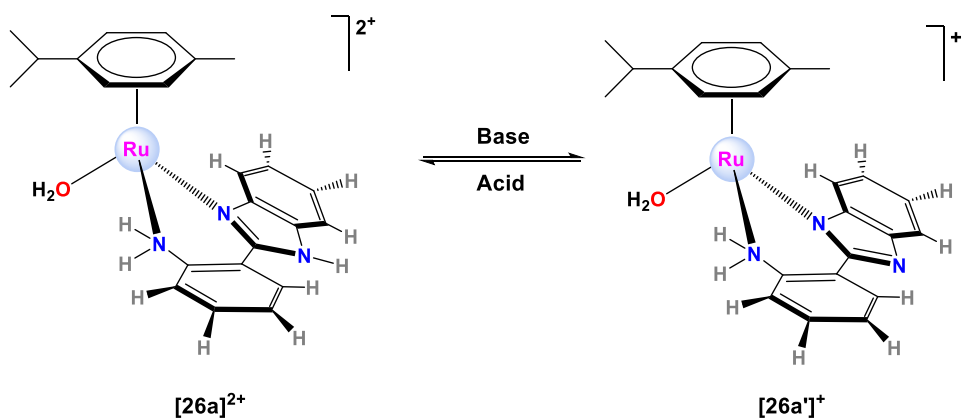


Fig. 7. Acid-base reaction of complex $[\mathbf{26a}]^{2+}$.

The ^1H NMR spectrum of the neutral complex **[27a]** in CDCl_3 did not show the H^NH signal, as expected.

The $^{13}\text{C}\{\text{H}\}$ NMR spectra of the complexes showed a common pattern in all the solvents. The most downfield-shifted peaks were those of the quaternary carbons, with C^a as the most deshielded signal (around 147 ppm for complexes with apbim and around 166 ppm for those with apbtz), in contrast to those of the complexes bearing hydroxyphenylbenzazole as the ancillary ligand (see CHAPTER 3), in which the most deshielded peak was C^l' . In the case of the hydroxy-derivatives, the O atom is more electronegative than the N atom in the amino-derivatives, causing a higher deshielding of the contiguous C atom (C^l'). However, the shifts of the rest of the quaternary carbons are observed at similar chemical shifts in both cases, since they are far from the O atom.

The $^{19}\text{F}\{\text{H}\}$ NMR spectra were recorded for all complexes with BF_4^- and OTf^- as counterions. A singlet was detected for triflate and two singlets were observed for tetrafluoroborate, due to isotopic effect for ^{10}B and ^{11}B . The latter underwent slow hydrolysis in D_2O (see CHAPTER 1).

Deprotonation of the secondary amine (-NH₂)

In order to study the behaviour in solution of some of the complexes, the deprotonation of the secondary amine was studied by the addition of a base (Et_3N) in CD_3OD . The deprotonation of the secondary amine of **[23a]Cl** was unsuccessful, as only the NH group of the benzimidazole moiety was deprotonated, leading to the formation of **[27a]**. On the other hand, the deprotonation was apparently successful for the complex **[24a]Cl**, yet the spectrum displayed too many products: the deprotonation of the NH_2 , the loss of the ligand and even methanol substitution.

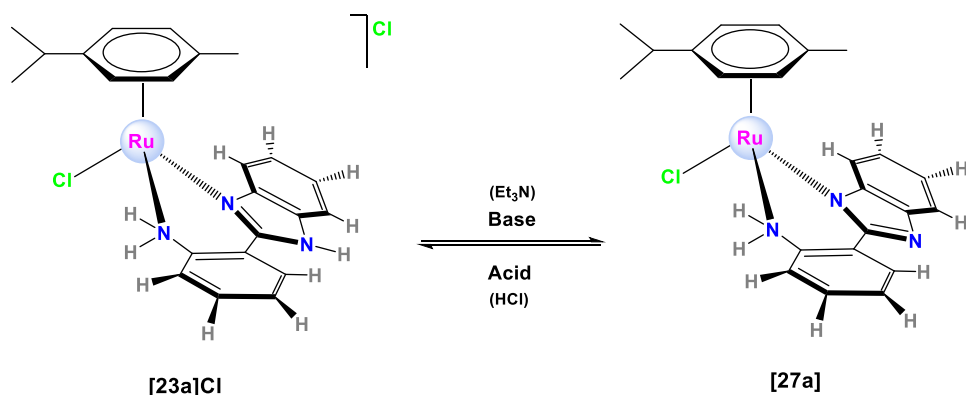


Fig. 8. Acid-base reaction of complex **[23a]Cl** in MeOD-d_4 with Et_3N .

In order to check the reversibility of the deprotonation reaction for **[23a]Cl**, HCl was added to a sample of **[27a]** in CDCl_3 . The deshielded signal of the NH group appeared and the resultant spectrum was compared with that of its precursor **[23a]Cl** to verify their resemblance (see Fig. 8).

1.2.2. Mass Spectra

The FAB⁺ mass spectra of the complexes exhibit characteristic sets of peaks according to isotopic distribution patterns. [M-Y]⁺ fragments were detected for monocationic complexes, where Y is the counterion; fragments with a water molecule for the aqua derivatives and [M]⁺ fragment for the neutral complex **[27a]**.

1.2.3. IR Spectra

Infrared spectra show characteristic peaks for the normal vibrational modes of $\nu_{C=N}$, $\nu_{C=C}$, $\delta_{CH\text{oop}}$, the ν_{NH} and ν_{NH_2} bands¹⁶ and very strong peaks (see Table 1) for the TfO⁻ and BF₄⁻ counterions. For BF₄⁻, the characteristic peak ν_{B-F} appears at 1084-1037 cm⁻¹. For the triflate anion there are three characteristic bands, ν_{C-F} , $\nu_{SO_3-\text{as}}$, $\nu_{SO_3-\text{sym}}$ at 1287-1224, 1168-1157 and 1031-1028 cm⁻¹ respectively.^{17,18,19}

Table 1. IR characteristic peaks for the NH and NH₂ groups.

Ref.	IR (cm ⁻¹)		
	$\nu_{N\text{-Hassociated}}$	ν_{NH_2}	$\nu_{NH_2+\text{hydrogen bonds}}$
[23a]Cl	3227	3047	2963
[23b]Cl	3123	3054	-
[23c]Cl	-	3060	-
[23a](OTf)	3129	3067	2966-2927
[23b](OTf)	3229-3136	-	-
[24a]Cl	3226	-	2963
[24b]Cl	3227	3048	-
[24a](OTf)	3202	-	2966
[24b](OTf)	3207-3132	-	-
[25a]I	-	3056	2964
[26a](BF ₄) ₂	3284	3076	2973
[26a](OTf) ₂	3203	-	2969
[27a]	3243	3054	2970

1.2.4. Molar Conductivity

Molar conductivity (Λ_M) for the complexes (see Table 2) was measured in aqueous solutions (10⁻³ M). The values reflect the 1:1 electrolyte nature of monocationic complexes, although the conductivities were a bit higher than expected²⁰, owing to the aquation processes. The values for the aqua complexes were also higher, as expected for the electrolytes 2:1. No relevant differences were detected when changing the ligand or the counterion, except for the iodido derivative **[25a]I**. The conductivity value of this complex is below the normal range. The comparison of the iodide complex **[25a]I** with the analogous chlorido derivative **[23a]Cl**, shows a clear effect attributed to the counterion. This fact is explained by means of the hydration energy, widely explained in CHAPTER 5. In particular, we propose that aquation takes place in a higher extent for Ru-Cl than for Ru-I.

Table 2. Molar conductivity values for complexes measured in water.

Complex	Solvent	Λ_m ($\text{S}\cdot\text{cm}^2\cdot\text{mol}^{-1}$)
[23a]Cl	H ₂ O	174.4
[23b]Cl	H ₂ O	152.1
[23c]Cl	H ₂ O	126.6
[23a](OTf)	H ₂ O	140.1
[23b](OTf)	H ₂ O	163.6
[24a]Cl	H ₂ O	132.7
[24b]Cl	H ₂ O	147.3
[24a](OTf)	H ₂ O	119.2
[24b](OTf)	insoluble	-
[25a]I	H ₂ O	91.2
[26a](BF ₄) ₂	H ₂ O	201.2
[26a](OTf) ₂	H ₂ O	192.3

1.2.5. Elemental Analysis

The aqua derivative [26a](BF₄)₂ showed possible contamination with AgBF₄. Thus, it was ruled out for cytotoxicity studies. Traces of unknown impurities were detected in [27a].

1.2.6. X Ray Diffraction

Single crystals suitable for X-ray diffraction analysis were obtained for [23a]Cl, [23b]Cl·3H₂O, [23b](OTf), [24b](OTf) and [25a]I·CH₃OH, by slow evaporation of the corresponding solvent: CH₂Cl₂/MeOH; water; water/acetone; water/MeOH and MeOH, respectively. As commented before, the crystal structure of [23a]Cl was reported by J. G. Małecki with acetone in the asymmetric unit.¹¹ However, we have resolved the structure without any co-crystallization solvent. Thus, the crystal data are different.

The ORTEP diagrams for all the complexes are represented in Fig. 9. The unit cells show the expected two enantiomers (R_{Ru} and S_{Ru}) with the pseudooctahedral three-legged piano-stool geometry and the ruthenium π-bonded to a n⁶-arene. Selected bond lengths and angles with estimated standard deviations are collected in Table 3, and crystallographic refinement parameters are given in Table 4.

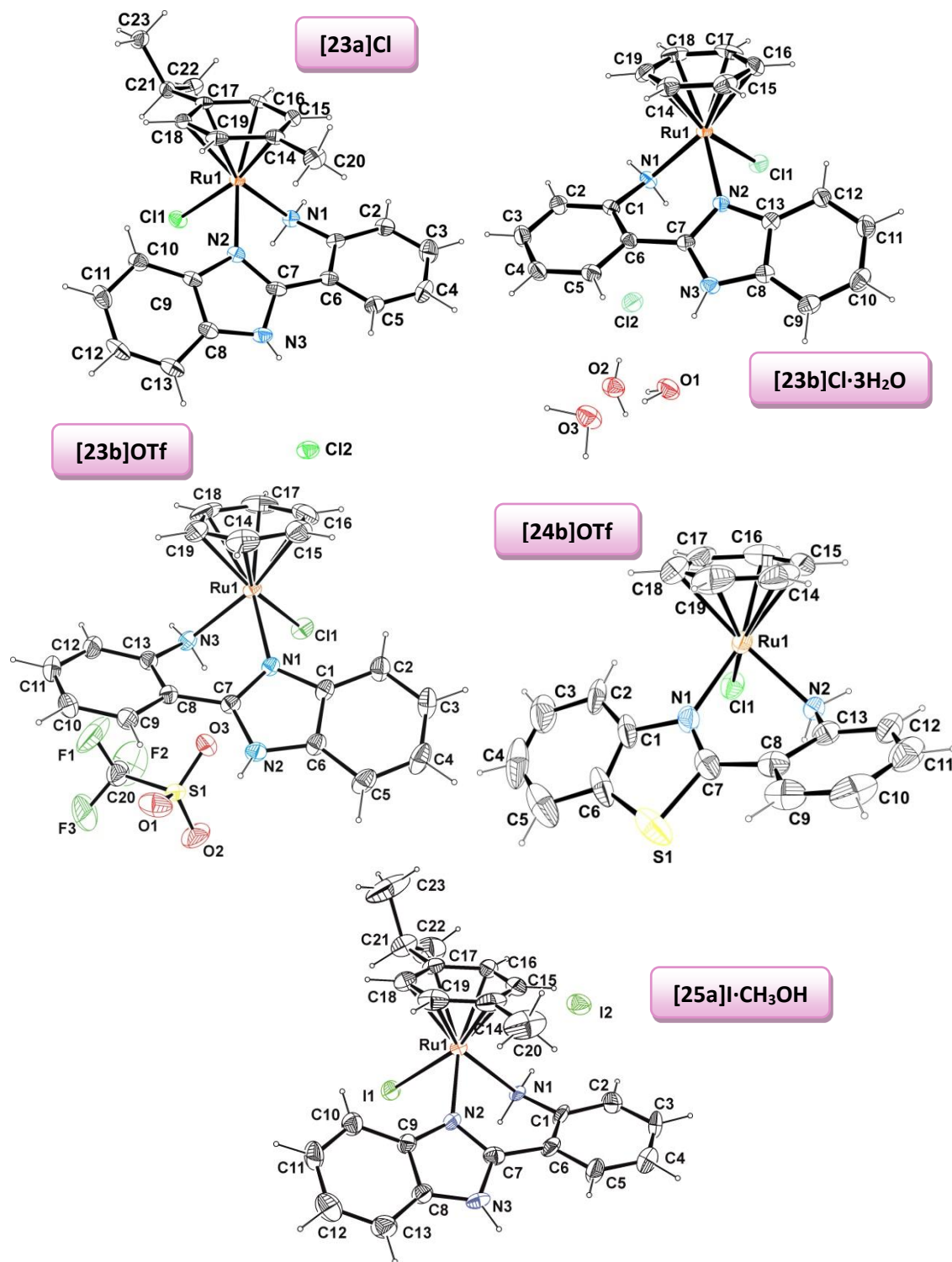


Fig. 9. ORTEP diagrams for complexes [23a]Cl, [23b]Cl·3H₂O, [23b](OTf), [24b](OTf) and [25a]I·CH₃OH. Ellipsoids are shown at 30% probability.

The Ru-centroid distances fall in a narrow interval (1.656-1.683 Å). The Ru-Cl bond distances (2.3945-2.4079 Å) are in the usual range. However, the Ru-I bond distance (2.7395 Å) is far longer than those for the chlorido derivatives, owing to the bigger size of the iodine van der Waals atomic radii. The Ru-N distances are shorter for

the benzazole heterocycle ($\text{Ru-N} = 2.087\text{-}2.101 \text{\AA}$) than for the aminophenyl moiety ($\text{Ru-N} = 2.111\text{-}2.169 \text{\AA}$), with the longest distance for the complex **[25a]I**.

The N-Ru-N angles of the chelate rings ($79.60^\circ\text{-}81.0^\circ$) are determined by the features of the corresponding free bidentate ligands. These angles are very similar for all the complexes, although they are higher than those of other N,N-chelating ligands (see CHAPTER 1), as the chelate ring include one more atom than in complexes with pybim (see CHAPTER 1).

Table 3. Selected bond lengths (\AA) and angles ($^\circ$) for complexes **[23a]Cl**, **[23b]Cl·3H₂O**, **[23b](OTf)**, **[24b](OTf)** and **[25a]I·CH₃OH**.

<i>Distance/angle</i>	[23a]Cl	[23b]Cl·3H₂O	[23b](OTf)	[24b](OTf) (R)	[24b](OTf) (S)	[25a]I·CH₃OH
<i>Ru1-C1/I1</i>	2.3945(9)	2.4079(7)	2.4065(7)	2.399(2)	2.407(2)	2.7295(10)
<i>Ru1-N1/N3^a/N2^b(NH2)</i>	2.111(3)	2.1321(18)	2.118(2)	2.113(7)	2.122(5)	2.169(6)
<i>Ru1-N2/N1^{a,b}(bim/btz)</i>	2.087(3)	2.0938(17)	2.101(2)	2.128(5)	2.121(5)	2.087(6)
<i>N1/N3^a/N2^b-C1/C13^{a,b}</i>	1.441(4)	1.446(3)	1.436(3)	1.437(9)	1.449(6)	1.454(11)
<i>N2/N1^{a,b}-C7</i>	1.327(4)	1.333(3)	1.337(3)	1.325(11)	1.319(8)	1.341(11)
<i>N3/N2^a-C7</i>	1.350(5)	1.346(3)	1.344(4)	-	-	1.362(10)
<i>S1-C7</i>	-	-	-	1.701(9)	1.713(7)	-
<i>N1/N3^a/N2^b-Ru1-N2/N1^{a,b}</i>	80.99(13)	80.65(7)	76.60(9)	80.5(2)	80.7(2)	81.0(3)
<i>N1/N3^a/N2^b-Ru1-C1/I1</i>	82.51(9)	83.38(5)	84.50(7)	82.96(17)	83.4(1)	85.12(18)
<i>N2/N1^{a,b}-Ru1-C1/I1</i>	83.65(8)	85.39(5)	85.69(6)	86.30(19)	87.8(2)	86.35(19)

^a Atom numbering for **[23b](OTf)**.

^b Atom numbering for **[24b](OTf)**.

Table 4. Selected geometric parameters^[a] for the metal complexes of **[23a]Cl**, **[23b]Cl·3H₂O**, **[23b](OTf)**, **[24b](OTf)** and **[25a]I·CH₃OH**.

<i>Distance/angle</i>	[23a]Cl	[23b]Cl·3H₂O	[23b]OTf	[24b]OTf (R)	[24b]OTf (S)	[25a]I·CH₃OH
<i>Range of Ru-C distances</i>	2.148(4)-2.199(3)	2.163(3)-2.182(2)	2.140(3)-2.182(4)	2.139(9)-2.173(9)	2.135(4)-2.210(4)	2.154(10)-2.224(9)
<i>Ru-centroid</i>	1.656	1.669	1.670	1.661	1.670	1.683
α	24.55	23.36	28.83	30.40	22.48	24.96
ϑ (<i>N-C-C-C</i>)	-24.84	24.76	28.94	-29.50	22.42	-26.41
β (<i>chelate-arene</i>)	20.17	19.76	12.55	14.81	12.58	14.48
γ (<i>Cx-C_{ipso}-Ru-Y</i>)	114.84	-	-	-	-	115.14
λ	39.03	38.98	44.79	44.70	44.20	41.92

[a]Calculated with Mercury, version 3.8.

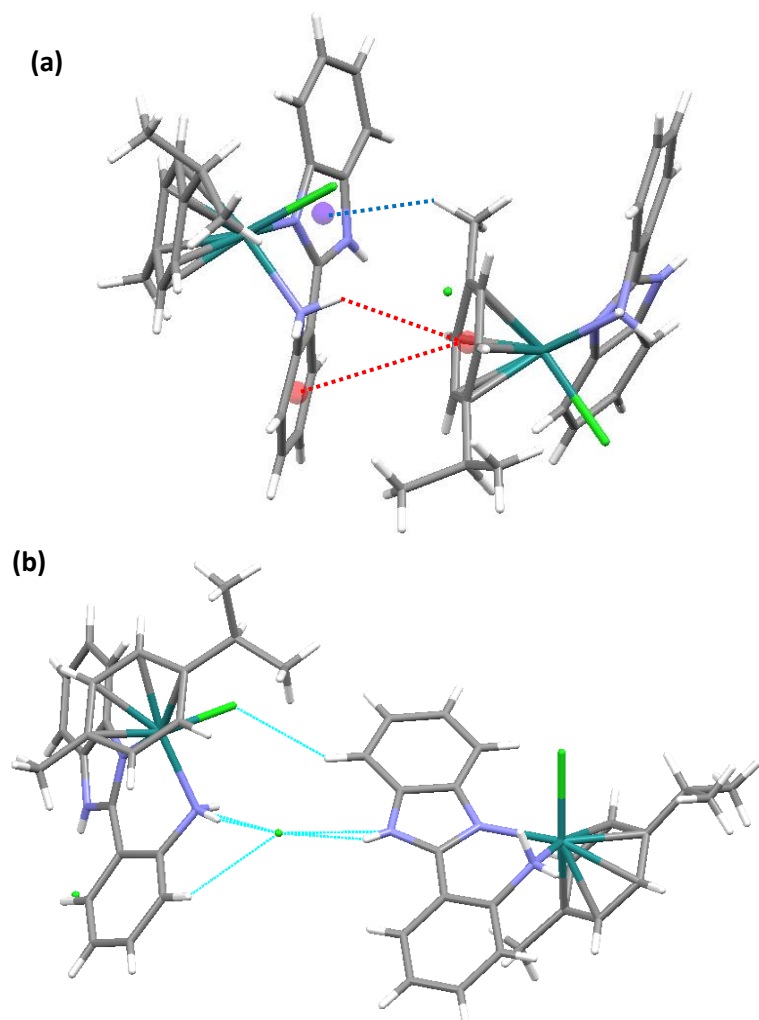


Fig. 10. (a) Short contact interactions between the arene and the apbim moiety in the crystal structure of [23a]Cl: $\pi\text{-}\pi$ stacking reinforced by a $\text{N-H}\cdots\pi$ interaction (red) and $\text{C-H}\cdots\pi$ interaction (blue). (b) Hydrogen bonding involving chloride and amino groups in [23a]Cl.

Regarding complex **[23a]Cl**. Its 3D architecture shows both $\pi\text{-}\pi$ stacking and H-bonding interactions. Fig. 10a displays $\pi\text{-}\pi$ and $\pi\text{-}\sigma$ contacts ($\text{N-H}\cdots\pi$ and $\text{C-H}\cdots\pi$) between the *p*-cymene ring and the bidentate chelating ligand, whereas Fig. 10b represents the hydrogen bonding involving chloride counterions and both amino groups (NH_2 and NH). Moreover, the parameters of the $\pi\text{-}\pi$ interactions are gathered in Table 5 and those for the $\pi\text{-}\pi$ interaction in Table 6.

Table 5. Parameters of X-H···π interactions for complex [23a]Cl.

Compound	$d_{X\text{-cent}}$ (Å)	$d_{H\text{-cent}}$ (Å)	$d_{X\text{-H}}$ (Å)	$\angle X\text{-H-cent}$ (°)	$\angle H\text{-cent-normal}$ (°)
[23a]Cl (N-H···π)	3.691	2.978	0.900	137.34	174.02
[23a]Cl (C-H···π)	3.470	2.759	0.960	131.50	168.19

Complex **[23b](OTf)** features a dimeric association between the enantiomers R_{Ru} and S_{Ru} , where the O atoms of triflate molecules are connected to the NH groups (both

NH and NH₂) of the coordinated ligands (apbim) belonging to neighbouring complexes (N-H···O). In addition, the H atom in the NH₂ group, which does not participate in the hydrogen bond with the triflate, is involved in a hydrogen bond with the chloride ligand of a neighbour complex (N-H···Cl). Moreover, a weak C-H···Cl interaction is observed (see Fig. 11). Furthermore, the triflate molecule adopts a staggered conformation (torsion angle $\theta = 59.17^\circ$ - see Fig. 11a).

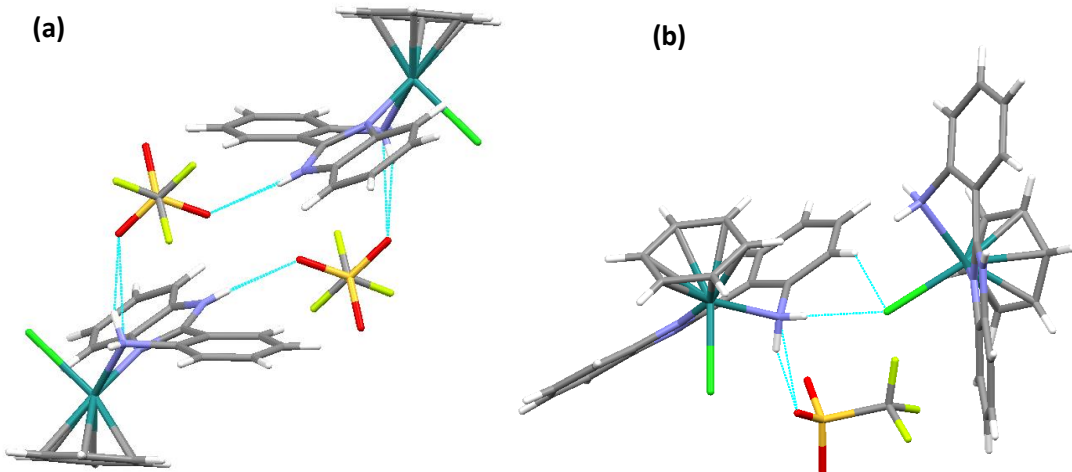


Fig. 11. 3D architecture motifs for the complex [23b]OTf. (a) Dimeric association between enantiomers. (b) Hydrogen bonding involving the NH₂ group.

As for the complex **[24b](OTf)**, the asymmetric unit presents both enantiomers, R_{Ru} and S_{Ru}, and contains two triflate molecules in the staggered conformation (torsion angles: $\theta = 60.72^\circ$ and $\theta = 61.22^\circ$, respectively). Both of them are connected to the R enantiomer through hydrogen bonding, one to the NH₂ group (S=O···H-N) and the other to the benzene and the aminophenyl rings (S=O···H-C). Furthermore, the R enantiomer contain an intramolecular hydrogen bond between the chloride ligand and the nearest hydrogen of the benzothiazolyl ring (Cl···H-C). Fig. 12 depicts both enantiomers with the above-mentioned hydrogen bonding contacts.

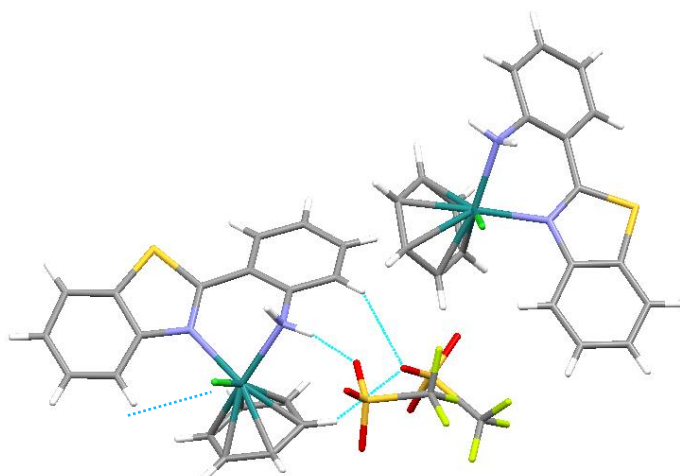


Fig. 12. Hydrogen bonding between enantiomers in the asymmetric unit of [24b](OTf). The enantiomer S presents disorder.

Complexes **[23b]Cl·3H₂O** and **[25a]I·CH₃OH** contain solvent molecules in their second coordination spheres. In the former, three water molecules act as connectors among metal entities through hydrogen bonding. Each water molecule takes part in a hydrogen bond with different groups of three neighbouring metal complexes: H₂O···H-N(bim); H₂O···H-N(aph) and H₂O···Cl (see Fig. 13a). This structure also shows π-π stacking interactions between the *p*-cymene ring and the benzene ring of the benzimidazole moiety, reinforced by a hydrogen bond (C-H···Cl) (see Fig. 13b). The parameters of the offset face-to-face π-π stacking are in the usual range (see Table 6).²¹

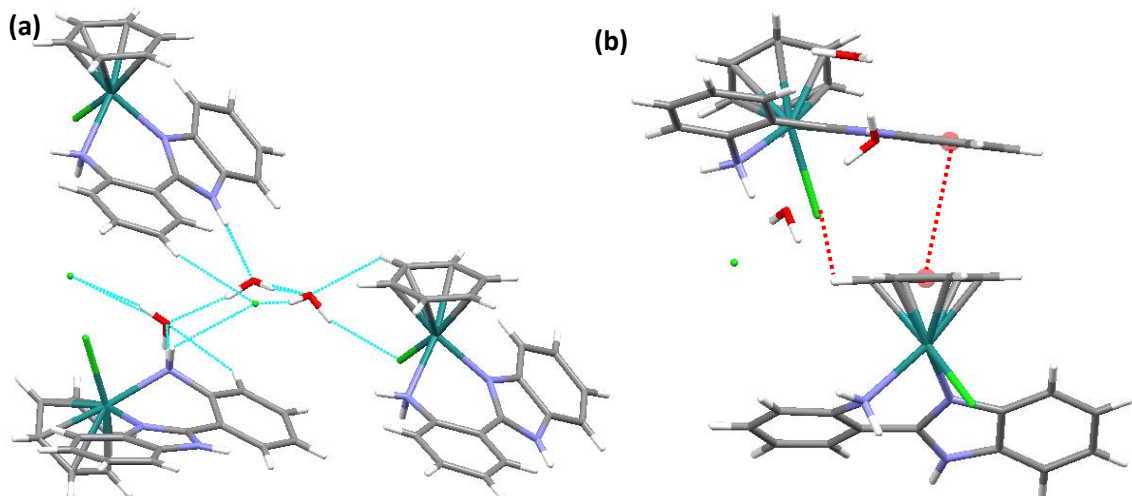


Fig. 13. Hydrogen bonding (a) and π-π stacking interactions in the crystal structure of (b) for complex **[23b]Cl·3H₂O**.

Regarding the complex **[25a]I·CH₃OH**, the methanol molecule connects four metallic entities through hydrogen bonding and weak interactions of the type C-H···π (see Fig. 14).

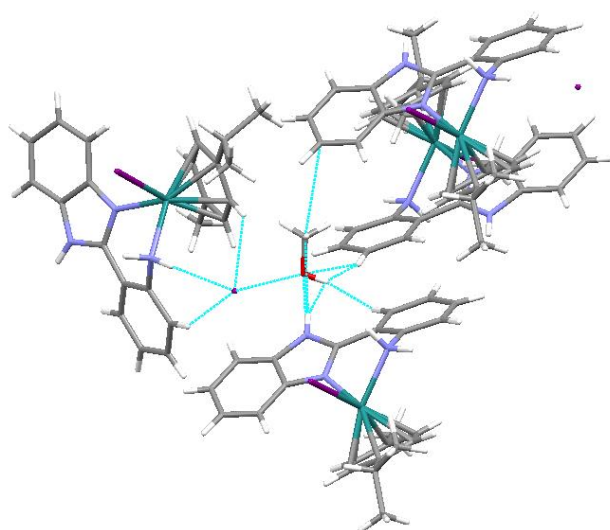


Fig. 14. Motifs in the crystal architecture of complex **[25a]I·CH₃OH**, showing hydrogen bonding and weak interactions.

Table 6. π - π offset stacking parameters for complexes [23a]Cl and [23b]Cl·3H₂O.

Compound	$d_{\text{cent-cent}}$ (Å)	α (°)	$d_{\text{cent-pl}}$ (Å)	β (°)	d_{offset} (Å)
[23a]Cl	4.278	21.23	3.148	42.62	2.897
			3.680	30.66	2.181
[23b]Cl·3H ₂ O	3.688	7.99	3.414	22.23	1.394
			3.468	19.89	1.255

1.3. Aqueous Solubility

The aqueous solubility of selected complexes (see Table 7) was determined at room temperature (19 – 21 °C). All the complexes are water-soluble, whereas the free ligands are not, presumably due to strong self-association by hydrogen bonding and π - π stacking interactions (see CHAPTER 1). Likewise, the solubility depends on the counterion, the overall charge of the complex and the arene identity. As in previous studies, the chloride salts are much more soluble in water than their OTf⁻ derivatives, owing to the high hydration energy attributed to the Cl⁻ anion.^{22,23} The solubility decreases drastically when the Cl⁻ is changed by triflate as the counterion. The same effect also explains the lower solubility of the iodide salt [25a]I. Regarding the arene, *p*-cymene derivatives give better solubilities than the benzene and phenoxyethanol derivatives. Regarding the ligands, the most soluble complexes are those with apbtz, approximately twice the solubility of complexes with apbim. These differences could be explained owing to the possibility of the NH group to form hydrogen bonding, and as a consequence, molecular self-association, which could decrease solubility.

Table 7. Solubility data in water (mM) and the aquation-anation ratio (%) at different NaCl concentrations for selected compounds.

Ref.	Compound	Solubility (mM)	% aquation		
			0 mM NaCl	5 mM NaCl	100 mM NaCl
[23a]Cl	[(<i>p</i> -cym)RuCl(apbim)]Cl	22.2	25.4	20.7	0
[23b]Cl	[(bz)RuCl(apbim)]Cl	20.7	29.0	22.0	0
[24a]Cl	[(<i>p</i> -cym)RuCl(apbtz)]Cl	49.8	15.8	10.7	0
[24b]Cl	[(bz)RuCl(apbtz)]Cl	42.0	22.4	16.3	0
[23a]OTf	[(<i>p</i> -cym)RuCl(apbim)]OTf	6.2	46.7	25.6	0
[23b]OTf	[(bz)RuCl(apbim)]OTf	2.8	59.5	34.6	0
[24a]OTf	[(<i>p</i> -cym)RuCl(apbtz)]OTf	5.9	41.2	17.8	0
[24b]OTf	[(bz)RuCl(apbtz)]OTf	5.2	39.6	21.5	0
[25a]I	[(<i>p</i> -cym)RuI(apbim)]I	0.8	-	-	-

1.4. Aquation-Anation Equilibria

The aquation-anation equilibria were studied for selected complexes under pseudopharmacological conditions by recording the corresponding ¹H NMR spectra of 5 mM solutions in D₂O at 25 °C, in the absence of NaCl and then in the presence of NaCl (5 mM or 100 mM as model concentrations for the intracellular and blood plasma conditions, respectively). Two sets of signals were observed, remaining constant after half an hour, which implies a fast equilibration. The arene signals were selected for the

integration, H^{10} for the *p*-cym derivatives and H^{benzene} for those with benzene. In the absence of NaCl, all the monocationic complexes undergo aquation to a notable extent, from 16 to 60 %, with some differences depending on the counterion, the arene, or the benzazole unit. As far as the latter is concerned, the complexes with the apbim ligand present the highest aquation values, probably due to the higher electron-donor capacity of the imidazole ring, compared to that of the thiazole ring. Thus, the highest aquation percentage correspond to the complex **[23b]OTf**. In the presence of NaCl, the equilibria are shifted to the chlorido side with complete suppression of the aqua-derivatives in 100 mM NaCl (see Table 7).

1.5. Cytotoxic Activity

The cytotoxicity of selected complexes was evaluated in a comparative in vitro MTT cell viability assay after incubation times of 24 h at 37 °C in human lung carcinoma cells (A549). This cell line is less sensitive to chemotherapeutic drugs, so that IC₅₀ values, even for cisplatin, are higher than in other cell lines. The values, gathered in Table 8, show moderate values with the best result for the monocationic complex **[24a]Cl** (IC₅₀ = 90 µM), followed by **[24b]Cl** (IC₅₀ = 120 µM) and **[26a](OTf)₂** (IC₅₀ = 120 µM). Complexes **[23a]Cl** and **[25a]I** were unstable and their values could not be determined properly. The same behaviour was detected for the iridium complex (see complex **[39a]Cl** in CHAPTER 6).

Table 8. IC₅₀ (mM, 24 h, 37 °C) values for selected compounds in the A549 cell line.

Ref.	Compound	Solvents	IC ₅₀ (µM)
	cisplatin		114.2 ^a
[23a]Cl	$[(p\text{-cym})\text{RuCl}(\text{apbim})]\text{Cl}$	H ₂ O/DMSO	unstable
[23b]Cl	$[(bz)\text{RuCl}(\text{apbim})]\text{Cl}$	H ₂ O	150
[24a]Cl	$[(p\text{-cym})\text{RuCl}(\text{apbtz})]\text{Cl}$	H ₂ O	90
[24b]Cl	$[(bz)\text{RuCl}(\text{apbtz})]\text{Cl}$	H ₂ O	120
[23a]OTf	$[(p\text{-cym})\text{RuCl}(\text{apbim})]\text{OTf}$	DMSO	250
[23b]OTf	$[(bz)\text{RuCl}(\text{apbim})]\text{OTf}$	DMSO	220
[24a]OTf	$[(p\text{-cym})\text{RuCl}(\text{apbtz})]\text{OTf}$	H ₂ O/DMSO	140
[24b]OTf	$[(bz)\text{RuCl}(\text{apbtz})]\text{OTf}$	MeOH	200
[25a]I	$[(p\text{-cym})\text{Rul}(\text{apbim})]\text{I}$	H ₂ O/DMSO	unstable
[26a](OTf)₂	$[(p\text{-cym})\text{Ru}(\text{H}_2\text{O})(\text{apbim})](\text{OTf})_2$	H ₂ O	120

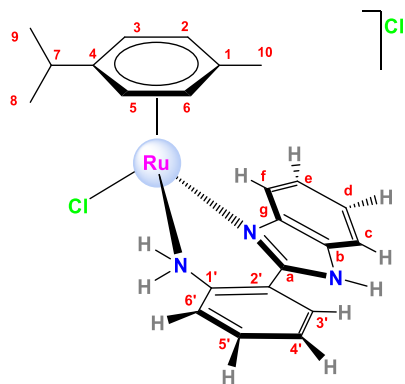
^a Bibliographic data.²⁴

As some of the cytotoxic tests have been performed in DMSO, the results could be distorted, owing to the solvolysis of the complexes in DMSO (see Fig. 3). However, some interesting tendencies can be observed. Complexes with chloride as the counterion show better cytotoxicities than their analogues with triflate. In addition, the antiproliferative activity of compounds with the ligand apbtz is higher than that for the derivatives with apbim. Curiously, the solubility and aquation-anation studies show a possible correlation, that is, the complex with the best result of cytotoxic activity **[24a]Cl** is also the most water-soluble complex and the one that undergo less aquation, suggesting that aquation leads to deactivation.

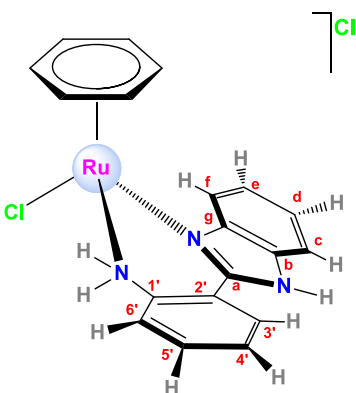
2. CONCLUDING REMARKS

- A family of 13 new complexes has been synthesised and thoroughly characterised, both in solution and some of them in solid state.
- All the complexes are water soluble, though those complexes bearing triflate as the counterion show a dramatic decrease in their solubility compared to those that bear chloride. Moreover, the complexes with apbtz are more soluble in water than those with apbim.
- All the complexes undergo aquation, which is completely suppressed in 100 mM NaCl, the blood plasma salt concentration.
- The NH₂ protons of the ancillary ligand become inequivalent when they coordinate to the metal centre and modify their reactivity.
- The complexes undergo solvolysis in DMSO, releasing the ancillary ligand.
- The cytotoxicity data point out that the complex [24a]Cl (IC₅₀ = 90 µM) is the most active in the cell line A549, showing a direct relationship between activity and both the solubility and the aquation degree. The same is true for all the derivatives.

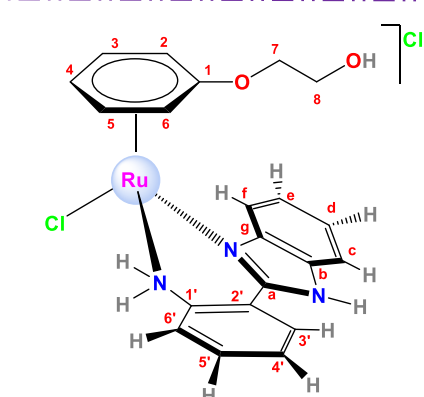
3. EXPERIMENTAL SECTION



Synthesis of $[(\eta^6\text{-}p\text{-cymene})\text{RuCl}(\text{apbim})]\text{Cl}$, [23a]Cl. In a 100 mL Schlenk flask, the ligand 2-(2'aminophenyl)benzimidazole (0.0682 g, 0.326 mmol) was added to a solution of $[\text{RuCl}_2(\text{cym})]_2$ (0.0998 g, 0.163 mmol) in degassed methanol (8 mL), and the mixture was stirred at room temperature for 20 h and under a nitrogen atmosphere. The solvent was evaporated to dryness and the residue was washed with hexane (5 mL). The resulting yellow powder was dried under vacuum. Yield: 133.2 mg (0.26 mmol, 79%). **M_r** ($\text{C}_{23}\text{H}_{25}\text{N}_3\text{Cl}_2\text{Ru}$) = 515.446 g/mol. **Anal. Calcd for** $\text{C}_{23}\text{H}_{25}\text{N}_3\text{Cl}_2\text{Ru}\cdot(\text{H}_2\text{O})_{0.2}$: C 53.22; H 4.93; N 8.10; **Found:** C 53.22; H 4.98; N 8.21. **¹H NMR (400 MHz, CDCl₃, 25 °C)** δ 14.61 (s, 1H, H^{N-H}), 9.09 (d, *J* = 9.4 Hz, 1H, H^{N-H(NH₂)}), 8.28 – 8.15 (m, 1H, H^{3'}), 8.14 – 8.09 (m, 1H, H^{6'}), 7.76 (d, *J* = 7.1 Hz, 1H, H^c), 7.70 (d, *J* = 7.4 Hz, 1H, H^f), 7.33 – 7.21 (m, 2H, H^{e,d}), 7.03 – 6.97 (m, 2H, H^{5',4'}), 5.64 (d, *J* = 5.9 Hz, 1H, H³), 5.58 (d, *J* = 5.9 Hz, 1H, H²), 5.54 (d, *J* = 5.9 Hz, 1H, H⁶), 5.42 (d, *J* = 5.9 Hz, 1H, H⁵), 3.73 (d, *J* = 10.0 Hz, 1H, H^{N-H(NH₂)}), 2.18 (sept, *J* = 6.9 Hz, 1H, H⁷), 1.69 (s, 3H, H¹⁰), 0.90 (d, *J* = 6.9 Hz, 3H, H^{8 o H⁹}), 0.82 (d, *J* = 6.9 Hz, 3H, H^{9 o H⁸}) ppm. **¹H NMR (400 MHz, DMSO-d₆, 25 °C)** δ 14.39 (s, 1H, H^{N-H}), 8.62 (d, *J* = 10.5 Hz, 1H, H^{N-H(NH₂)}), 7.99 (dd, *J* = 7.8, 1.2 Hz, 1H, H^{3'}), 7.92 (dd, *J* = 6.3, 3.0 Hz, 1H, H^f), 7.82 (d, *J* = 7.7 Hz, 1H, H^{6'}), 7.76 – 7.66 (m, 1H, H^c), 7.63 (t, *J* = 7.8 Hz, 1H, H^{5'}), 7.46 (s, *J* = 7.5 Hz, 1H, H^{4'}), 7.43 – 7.40 (m, 2H, H^{d,e}), 6.08 (d, *J* = 9.9 Hz, 1H, H^{N-H(NH₂)}), 5.65 (dd, *J* = 13.5, 6.2 Hz, 3H, H^{2,6,3}), 5.53 (d, *J* = 6.0 Hz, 1H, H⁵), 2.21 (sept, *J* = 6.9 Hz, 1H, H⁷), 1.62 (s, 1H, H¹⁰), 0.96 (d, *J* = 6.9 Hz, 3H, H^{8 o H⁹}), 0.88 (d, *J* = 6.8 Hz, 3H, H^{9 o H⁸}) ppm. **¹³C{¹H} NMR (101 MHz, CDCl₃, 25 °C)** δ 147.2 (s, 1C, C^a), 142.6 (s, 1C, C^g), 140.7 (s, 1C, C^{1'}), 134.5 (s, 1C, C^b), 132.2 (s, 1C, C^{5'}), 130.1 (s, 1C, C^{3'}), 127.0 (s, 1C, C^{4'}), 125.0 (s, 1C, C^d), 124.1 (s, 1C, C^e), 122.4 (s, 1C, C^{6'}), 121.0 (s, 1C, C^{2'}), 119.5 (s, 1C, C^f), 113.7 (s, 1C, C^c), 106.1 (s, 1C, C¹), 97.6 (s, 1C, C⁴), 83.7 (s, 1C, C³), 83.5 (s, 1C, C⁵), 81.0 (s, 1C, C²), 79.9 (s, 1C, C⁶), 30.7 (s, 1C, C⁷), 22.9 (s, 1C, C^{8 o C⁹}), 21.2 (s, C^{9 o C⁸}), 18.1 (s, 1C, C¹⁰) ppm. **FT-IR (KBr, cm⁻¹) selected bands:** 3403 (m, v_{O-H}), 3227 (m, v_{N-H}associated), 3047 (w, v_{=CH}, v_{NH₂}), 2963 (vs, v_{NH₂+hydrogen bonds}), 1619–1597–1582 (w, v_{C=C+C-N}), 1485 (m), 1463–1447 (vs, v_{C=N}), 1418 (m), 1387 (w, δ_{CH₃}), 1323 (w), 1145–1112 (w), 762–750 (s, δ_{CH_{loop}}), 533 (w), 450 (w). **MS (FAB+):** m/z (%) = 480 (9) ([M-Cl]⁺), 444 (8) ([M-2Cl-H]⁺). **Molar Conductivity (H₂O):** 174.4 S·cm²·mol⁻¹. **Solubility:** soluble in water, methanol, ethanol, dichloromethane, chloroform, dimethyl sulfoxide and acetone.

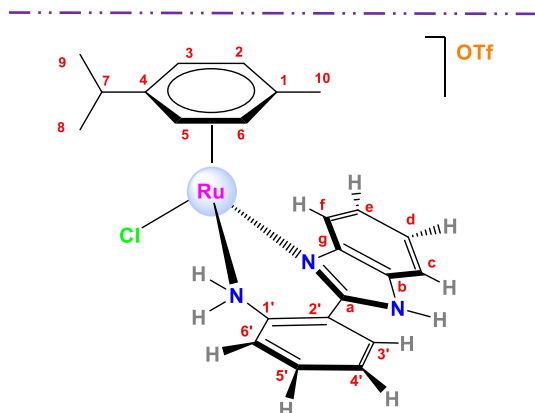


Synthesis of $[(\eta^6\text{-benzene})\text{RuCl}(\text{apbim})]\text{Cl}$, [23b]Cl. In a 100 mL Schlenk flask, the ligand apbim (0.0842 g, 0.4 mmol) was added to a solution of $[\text{RuCl}_2(\text{bz})]_2$ (0.1004 g, 0.201 mmol) in a mixture of degassed methanol/acetonitrile (10:1, 11 mL), and the mixture was stirred at room temperature for 20 h and under a nitrogen atmosphere. The solution was concentrated, the solid was filtered and washed with diethyl ether (5 mL). The resulting yellow powder was dried under vacuum. Yield: 70.7 mg (0.154 mmol, 38%). $M_r (\text{C}_{19}\text{H}_{17}\text{N}_3\text{Cl}_2\text{Ru}) = 459.3388 \text{ g/mol}$. **Anal. Calcd for $\text{C}_{22}\text{H}_{25}\text{N}_3\text{OB}_2\text{F}_8\text{Ru}\cdot(\text{H}_2\text{O})_{1.15}(\text{CH}_3\text{OH})_{0.4}$:** C 47.28; H 4.27; N 8.53; **Found:** C 47.28; H 4.30; N 8.74. **$^1\text{H NMR}$ (400 MHz, DMSO-d₆, 25 °C)** δ 14.46 (s, 1H, $\text{H}^{\text{N-H}}$), 8.87 (d, $J = 10.1$ Hz, 1H, $\text{H}^{\text{N-H(NH}_2\text{)}}$), 8.05 – 7.96 (m, 2H, $\text{H}^{3',f}$), 7.83 (d, $J = 7.9$ Hz, 1H, H^{c}), 7.72 – 7.65 (m, 1H, H^{c}), 7.62 (t, $J = 7.7$ Hz, 1H, $\text{H}^{5'}$), 7.46 (t, $J = 7.6$ Hz, 1H, $\text{H}^{\text{d'}}$), 7.44 – 7.38 (m, 2H, $\text{H}^{\text{d,e}}$), 6.21 (d, $J = 10.0$ Hz, 1H, $\text{H}^{\text{N-H(NH}_2\text{)}}$), 5.70 (s, 6H, $\text{H}^{\text{benzene}}$) ppm. **$^{13}\text{C}\{{}^1\text{H}\}$ NMR (101 MHz, DMSO-d₆, 25 °C)** δ 148.6 (s, 1C, C^{a}), 143.6 (s, 1C, C^{l}), 142.4 (s, 1C, C^{g}), 134.1 (s, 1C, C^{b}), 132.0 (s, 1C, $\text{C}^{5'}$), 129.0 (s, 1C, $\text{C}^{3'}$), 125.8 (s, 1C, $\text{C}^{4'}$), 124.2 (s, 1C, C^{d}), 123.3 (s, 1C, C^{e}), 121.8 (s, 1C, $\text{C}^{2'}$), 120.8 (s, 1C, C^{f}), 120.3 (s, 1C, C^{l}), 112.3 (s, 1C, C^{c}), 84.1 (s, 6C, $\text{C}^{\text{benzene}}$) ppm. **FT-IR (KBr, cm⁻¹) selected bands:** 3345 (m, $\nu_{\text{O-H}}$), 3123 (m, $\nu_{\text{N-H associated}}$), 3054 (s, $\nu_{\text{C-H}}$), 1620–1597 (w, $\nu_{\text{C=C+C-N}}$), 1490 (m), 1464–1449 (s, $\nu_{\text{C=N}}$), 1393–1382 (w, δ_{CH_3}), 1323 (w), 1282–1229 (w), 1146 (s), 1032 (s), 842 (m), 776 (w, $\delta_{\text{C-C}}$), 764–752 (vs, $\delta_{\text{CH}_2\text{O}}$), 691 (w), 451 (w). **MS (FAB+):** m/z (%) = 577 (4), 424 (100) ($[\text{M-Cl}]^+$), 404 (5) ($[\text{M-2Cl-H+NH}_2]^+$), 388 (75) ($[\text{M-2Cl-H}]^+$), 345 (6) ($[\text{M-Cl-H-C}_6\text{H}_6]^+$), 309 (12) ($[\text{M-2Cl-2H-C}_6\text{H}_6]^+$). **Molar Conductivity (H₂O):** 152.1 S·cm²·mol⁻¹. **Solubility:** soluble in water, THF and DMSO. Insoluble in chloroform, dichloromethane and methanol.



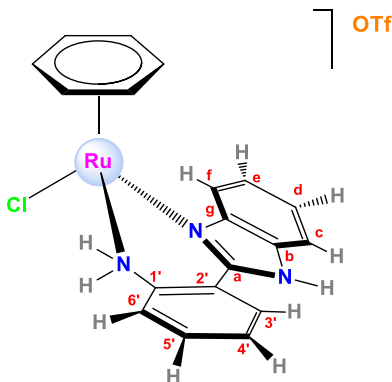
Synthesis of $[(\eta^6\text{-phenoxyethanol})\text{RuCl}(\text{apbim})]\text{Cl}$, [23c]Cl. The synthesis was performed as for [23a]Cl in the presence of the ligand 2-(2'-hydroxyphenyl)benzimidazole (0.2056 g, 0.983 mmol) and $[\text{RuCl}_2(\text{phoxet})]_2$ (0.2999 g, 0.483 mmol) in degassed methanol (14 mL). Brown-green powder. Yield is not calculated due to the great ability of oxidation of the Ru(II) centre. $M_r (\text{C}_{21}\text{H}_{21}\text{N}_3\text{O}_2\text{Cl}_2\text{Ru}) = 521.3721 \text{ g/mol}$. **Anal. Calcd for $\text{C}_{21}\text{H}_{21}\text{N}_3\text{O}_2\text{Cl}_2\text{Ru}\cdot(\text{H}_2\text{O})_{0.1}$:** C 48.4; H 4.10; N

8.06; Found: C 48.37; H 4.29; N 8.36. **¹H NMR (400 MHz, CD₃OD, 25 °C)** δ 8.12 – 8.05 (m, 1H, H^f), 7.95 (d, J = 7.5 Hz, 1H, H^{3'}), 7.73 (d, J = 7.8 Hz, 1H, H^{6'}), 7.69 – 7.63 (m, 2H, H^{5'}, H^d), 7.51 (t, J = 7.5 Hz, 1H, H^{4'}), 7.48 – 7.41 (m, 2H, H^d, H^e), 5.93 (t, J = 5.6 Hz, 1H, H³ o H⁵), 5.85 (t, J = 5.5 Hz, 1H, H⁵ o H³), 5.45 (d, J = 5.9 Hz, 1H, H² o H⁶), 5.34 (d, J = 5.4 Hz, 1H, H⁶ o H²), 5.03 (t, J = 5.2 Hz, 1H, H⁴), 3.93 (t, J = 4.6 Hz, 2H, H⁷), 3.68 – 3.62 (m, 2H, H⁸) ppm. **¹³C{¹H} NMR (101 MHz, CD₃OD, 25 °C)** δ 150.0 (s, 1C, C^a), 144.1 (s, 1C, C^g), 143.9 (s, 1C, C^{1'}), 137.3 (s, 1C, C¹), 135.7 (s, 1C, C^b), 133.5 (s, 1C, C^{5'}), 129.9 (s, 1C, C^{3'}), 127.9 (s, 1C, C^{4'}), 126.0 (s, 1C, C^d), 124.9 (s, 1C, C^e), 123.3 (s, 1C, C^{2'}), 122.3 (s, 1C, C^{6'}), 121.5 (s, 1C, C^c), 113.4 (s, 1C, C^f), 91.9 (s, 1C, C³ o C⁵), 91.6 (s, 1C, C⁵ o C³), 74.1 (s, 1C, C⁴), 72.4 (s, 1C, C⁷), 64.8 (s, 2C, C², C⁶), 60.7 (s, 1C, C⁸) ppm. **FT-IR (KBr, cm⁻¹) selected bands:** 3393 (s, ν_{O-H}), 3060 (vs, ν_{=CH}, ν_{NH2}, ν_{NH2+(hydrogen bonds)}), 1618–1597 (w, ν_{C=C + C-N}), 1521 (s,), 1488 (m), 1463–1448 (vs, ν_{C=N}), 1418 (m), 1323 (w), 1263 (s, ν_{C-O-Cas}), 1145 (w), 1080 (w, ν_{C-Osym}), 762–751 (s, δ_{CHOop}), 662 (m, δ_{O-Hoop}), 533 (w), 450 (w). **MS (FAB+):** m/z (%) = 519 (25) ([M]⁺), 485 (38) ([M-Cl+H]⁺), 448 (100) ([M-2Cl+H]⁺), 418 (25) ([M-2Cl-CH₂OH]⁺), 404 (12) ([M-2Cl-CH₂CH₂OH]⁺), 388 (14) ([M-2Cl-OCH₂CH₂OH]⁺), 309 (30) ([M-2Cl-phoxet+2H]⁺). **Molar Conductivity (H₂O):** 126.6 S·cm²·mol⁻¹. **Solubility:** soluble in methanol. Insoluble in acetone, dichloromethane and chloroform.

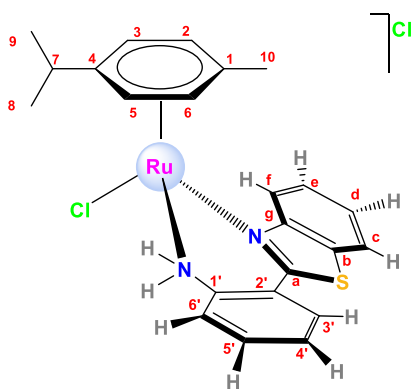


Synthesis of [(\eta⁶-p-cymene)RuCl(apbim)]OTf, [23a]OTf. In a 100 mL Schlenk flask protected from light, AgOTf (0.0927 g, 0.361 mmol, 6% exc.) was added under a nitrogen atmosphere to a solution of [RuCl₂(cym)]₂ (0.0999 g, 0.163 mmol) in degassed dichloromethane (12 mL). The suspension was stirred for 30 minutes at room temperature. The ligand apbim (0.0732 g, 0.350 mmol) was then added and the mixture stirred for 24 additional hours at room temperature. The AgCl was filtered off. The solvent was removed under vacuum and the solid residue was washed with diethyl ether (8 mL) and dried under vacuum, to produce a yellow solid. Yield: 123.9 mg (0.197 mmol, 60%). **M_r (C₂₄H₂₅N₃O₃F₃SClRu) = 629.0637 g/mol. Anal. Calcd for C₂₄H₂₅N₃O₃F₃SClRu·(CH₂Cl₂)_{0.4}(C₁₀H₁₄O)_{0.6}:** C 45.50; H 4.53; N 5.94; S 4.53; **Found:** C 45.55; H 4.52; N 6.31; S 4.15. **¹H NMR (400 MHz, CDCl₃, 25 °C)** δ 13.02 (s, 1H, H^{N-H}), 7.90 (d, J = 6.7 Hz, 1H, H^{3'}), 7.78 (d, J = 10.8 Hz, 1H, H^{N-H(NH₂)}), 7.73 – 7.67 (m, 2H, H^{f,c}), 7.58 (d, J = 7.9 Hz, 1H, H^{6'}), 7.37 – 7.26 (m, 2H, H^{e,d}), 7.15 (t, J = 7.5 Hz, 1H, H^{4'}), 7.02 (t, J = 7.2 Hz, 1H, H^{5'}), 5.52 (t, J = 5.4 Hz, 2H, H^{3,2}), 5.41 (d, J = 6.2 Hz, 1H, H⁶), 5.37 (d, J = 6.1 Hz, 1H, H⁵), 3.59 (d, J = 11.0 Hz, 1H, H^{N-H(NH₂)}), 2.23 – 2.07 (sept, J = 6.9 Hz, 1H, H⁷), 1.69 (s, 3H, H¹⁰), 0.88 (d, J = 7.0 Hz, 3H, H⁹ o H⁸), 0.84 (d, J = 6.9 Hz, 3H, H⁸ o H⁹) ppm. **¹H NMR (400 MHz, DMSO-d₆, 25 °C)** δ 14.10 (s, 1H, H^{N-H}), 8.70 – 8.36 (m, 1H, H^{N-H(NH₂)}), 7.97 – 7.89 (m, 2H, H^{f,3'}), 7.74 (d, J = 7.6 Hz, 1H, H^{6'}), 7.68–7.63 (m, 2H, H^{5,c}), 7.48 (t, J = 7.6 Hz, 1H, H^{4'}), 7.45 – 7.41 (m, 2H, H^{d,e}), 6.10 (d, J = 9.7 Hz, 1H, H^{N-H(NH₂)}), 5.65 (d, J = 7.1 Hz, 3H, H^{2,6,3}), 5.52 (d, J = 6.0 Hz, 1H, H⁵), 2.22 (sept, J = 6.9 Hz, 1H, H⁷), 1.61 (s, 3H, H¹⁰), 0.97 (d, J = 6.9

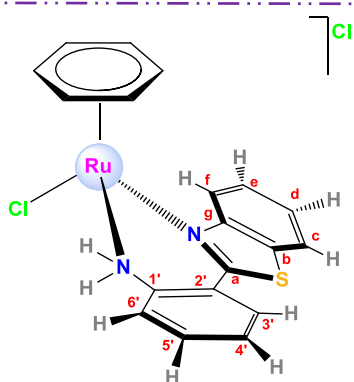
Hz, 3H, H⁸ o H⁹), 0.89 (d, *J* = 6.9 Hz, 3H, H⁹ o H⁸) ppm. ¹³C{¹H} NMR (101 MHz, CDCl₃, 25 °C) δ 146.8 (s, 1C, C^a), 142.6 (s, 1C, C^g), 140.3 (s, 1C, C^{1'}), 134.2 (s, 1C, C^b), 132.7 (s, 1C, C^{5'}), 129.5 (s, 1C, C^{3'}), 127.8 (s, 1C, C^{4'}), 125.4 (s, 1C, C^d), 124.5 (s, 1C, C^e), 121.6 (s, 1C, C^{6'}), 120.7 (s, 1C, C^{2'}), 120.6 (q, *J*_{C-F} = 319.0 Hz, 1C, COTf), 119.7 (s, 1C, C^f), 113.7 (s, 1C, C^g), 106.5 (s, 1C, C¹), 97.6 (s, 1C, C⁴), 83.6 (s, 2C, C^{3,5}), 80.8 (s, 1C, C⁶ o C²), 79.5 (s, 1C, C² o C⁶), 30.8 (s, 1C, C⁷), 22.8 (s, 1C, C⁹ o C⁸), 21.0 (s, 1C, C⁸ o C⁹), 18.0 (s, 1C, C¹⁰) ppm. FT-IR (KBr, cm⁻¹) selected bands: 3394 (m, ν_{O-H} or ν_{NH2}), 3129 (m, ν_{N-H}associated), 3067 (m, ν_{=CH}, ν_{NH2}), 2966-2927 (m, ν_{NH2+(hydrogen bonds)}), 1684-1601 (w, ν_{C=C+C-N}), 1490 (m), 1465-1448 (m, ν_{C=N}), 1284-1246 (vs, ν_{C-F}), 1168 (vs, ν_{SO3^-as}), 1029 (vs, ν_{SO3^-sym}), 762-749 (s, δ_{CHoop}), 638 (s, δ_{CF3}), 516 (w). MS (FAB+): m/z (%) = 480 (5) ([M-TfO]⁺), 444 (8) ([M-TfO-Cl]⁺). Molar Conductivity (H₂O): 140.1 S·cm²·mol⁻¹. Solubility: soluble in water, methanol, ethanol, dichloromethane, chloroform, dimethyl sulfoxide and acetone.



Synthesis of [(*η*⁶-benzene)RuCl(apbim)]OTf, [23b]OTf. The synthesis was performed as for [23a]OTf in the presence of AgOTf (0.1108 g, 0.431 mmol, 8% exc.), [RuCl₂(bz)]₂ (0.1004 g, 0.201 mmol) and the ligand 2-(2'-hydroxyphenyl)benzimidazole (0.2056 g, 0.983 mmol) in dichloromethane (10 mL). Yellow-greenish powder. Yield 152.5 mg (0.266 mmol, 66%). M_r (C₂₀H₁₇N₃O₃SF₃ClRu) = 572.9565 g/mol. Anal. Calcd for C₂₀H₁₇N₃O₃SF₃ClRu·(H₂O)_{0.25}: C 41.60; H 3.05; N 7.28; S 5.55; Found: C 41.60; H 3.44; N 7.33; S 5.54. ¹H NMR (400 MHz, DMSO-d₆, 25 °C) δ 14.02 (s, 1H, H^{N-H}), 8.72 (d, *J* = 10.2 Hz, 1H, H^{N-H(NH2)}), 8.03 – 7.99 (m, 1H, H^f), 7.88 (d, *J* = 7.7 Hz, 1H, H^{3'}), 7.70 (t, *J* = 7.1 Hz, 1H, H^{6'}), 7.67 (dd, *J* = 4.8, 1.6 Hz, 1H, H^c), 7.64 (t, *J* = 7.6 Hz, 1H, H^{5'}), 7.48 (t, *J* = 8.0 Hz, 1H, H^{4'}), 7.46 – 7.41 (m, 2H, H^{d,e}), 6.23 (d, *J* = 9.7 Hz, 1H, H^{N-H(NH2)}), 5.69 (s, 6H, H^{benzene}) ppm. ¹³C{¹H} NMR (101 MHz, DMSO-d₆, 25 °C) δ 148.7 (s, 1C, C^a), 143.6 (s, 1C, C^{1'}), 142.3 (s, 1C, C^g), 134.0 (s, 1C, C^b), 132.2 (s, 1C, C^{5'}), 128.8 (s, 1C, C^{3'}), 125.9 (s, 1C, C^{4'}), 124.4 (s, 1C, C^d), 123.4 (s, 1C, C^e), 121.7 (s, 1C, C^{2'}), 120.7 (q, *J*_{C-F} = 322.4 Hz, 1C, C^{CF3}), 120.6 (s, 1C, C^{6'}), 120.4 (s, 1C, C^f), 112.3 (s, 1C, C^c), 84.1 (s, 6C, C^{benzene}) ppm. ¹⁹F{¹H} NMR (376 MHz, DMSO-d₆, 25 °C) δ -78.1 (s, 3F, F^{CF3}) ppm. FT-IR (KBr, cm⁻¹) selected bands: 3229 (m, ν_{N-H}associated), 3136 (m, ν_{=CH}, ν_{NH2}), 1622-1598 (w, ν_{C=C+C-N}), 1489 (m), 1465-1450-1439 (m, ν_{C=N}), 1287-1227 (vs, ν_{C-F}), 1180-1164 (s, ν_{SO3^-as}), 1028 (vs, ν_{SO3^-sym}), 849 (w), 761-752 (s, δ_{CHoop}), 642 (s, δ_{CF3}), 517 (w). MS (FAB+): m/z (%) = 441 (28) ([M-OTf]⁺), 388 (15) ([M-OTf-Cl-H]⁺), 210 (5) ([apbim+H]⁺). Molar Conductivity (H₂O): 163.6 S·cm²·mol⁻¹. Solubility: soluble in methanol and dimethyl sulfoxide. Slightly soluble in acetone, dichloromethane and chloroform.

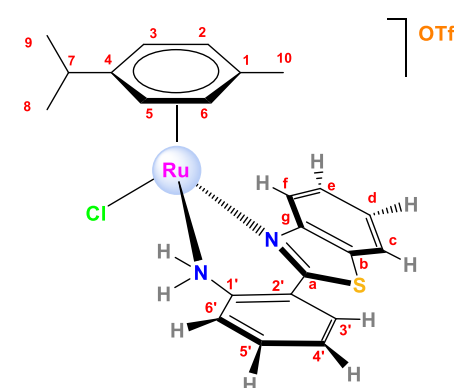


Synthesis of $[(\eta^6\text{-}p\text{-cymene})\text{RuCl}(\text{apbtz})]\text{Cl}$, [24a]Cl. The synthesis was performed as for [23a]Cl in the presence of the ligand 2-(2'-hydroxyphenyl)benzothiazole (0.0596 g, 0.263 mmol) and $[\text{RuCl}_2(\text{cym})]_2$ (0.0802 g, 0.131 mmol) in degassed methanol (8 mL). Yellow powder. Yield: 108 mg (0.20 mmol, 77%). $\mathbf{M_r}$ ($\mathbf{C_{23}H_{24}N_2SCl_2Ru \cdot (H_2O)_{1.1}}$) = 532.4974 g/mol. **Anal. Calcd for $C_{23}H_{24}N_2SCl_2Ru \cdot (H_2O)_{1.1}$:** C 50.02; H 4.78; N 5.07; S 5.81; **Found:** C 50.02; H 4.73; N 5.35; S 5.73. $^1\text{H NMR}$ (400 MHz, CDCl_3 , 25 °C) δ 10.75 (d, J = 8.8 Hz, 1H, $H^{N\text{-}H(NH^2)}$), 9.15 (d, J = 7.9 Hz, 1H, H^6'), 8.59 (d, J = 8.4 Hz, 1H, H^f), 7.95 (d, J = 8.1 Hz, 1H, H^c), 7.77 (d, J = 7.8 Hz, 1H, $H^{3'}$), 7.70 (t, J = 7.9 Hz, 2H, $H^{d,5'}$), 7.59 (t, J = 7.6 Hz, 1H, H^e), 7.41 (t, J = 7.7 Hz, 1H, H^4'), 6.09 (d, J = 5.8 Hz, 1H, H^3), 5.99 (d, J = 6.0 Hz, 1H, H^6), 5.80 (d, J = 5.6 Hz, 1H, H^2), 5.77 (d, J = 6.0 Hz, 1H, H^5), 4.32 (d, J = 10.4 Hz, 1H, $H^{N\text{-}H(NH^2)}$), 2.33 (sept, J = 6.9 Hz, 1H, H^7), 1.87 (s, 3H, H^{10}), 1.00 (dd, J = 8.7, 7.0 Hz, 6H, $H^{8,9}$) ppm. $^{13}\text{C}\{^1\text{H}\}$ NMR (101 MHz, CDCl_3 , 25 °C) δ 166.2 (s, 1C, C^a), 153.0 (s, 1C, C^g), 141.1 (s, 1C, $C^{1'}$), 134.8 (s, 1C, $C^{5'}$), 132.0 (s, 1C, C^b), 130.9 (s, 1C, $C^{3'}$), 128.3 (s, 1C, C^e), 127.6 (s, 1C, C^4'), 127.6 (s, 1C, C^d), 126.4 (s, 1C, C^f), 125.3 (s, 1C, C^2), 124.9 (s, 1C, C^6'), 122.5 (s, 1C, C^c), 107.2 (s, 1C, C^1), 97.9 (s, 1C, C^4), 85.3 (s, 1C, C^3), 84.0 (s, 1C, C^5), 82.3 (s, 1C, C^2), 79.9 (s, 1C, C^6), 31.0 (s, 1C, C^7), 23.3 (s, 1C, C^8 o C^9), 21.2 (s, 1C, C^9 o C^8), 18.3 (s, 1C, C^{10}) ppm. FT-IR (KBr, cm^{-1}) selected bands: 3381 (m, $\nu_{\text{O-H}}$), 3226 (m, $\nu_{\text{N-H associated}}$), 2963 (vs, $\nu_{\text{NH}_2\text{(hydrogen bonds)}}$), 1611 (m, $\nu_{\text{C=C + C-N}}$), 1499 (w), 1478 (vs, $\nu_{\text{C=N}}$), 1456-1426 (s), 1387 (w, δ_{CH_3}), 1323 (w), 1248 (m), 1122-1088 (m, $\nu_{\text{C=S}}$), 993 (m), 880 (w), 759 (vs, $\delta_{\text{CH}_\text{loop}}$), 463 (w). MS (FAB+): m/z (%) = 497 (42) ($[\text{M-Cl}]^+$), 461 (25) ($[\text{M-2Cl-H}]^+$). Molar Conductivity (H_2O): 132.7 $\text{S}\cdot\text{cm}^2\cdot\text{mol}^{-1}$. Solubility: soluble in water, methanol, ethanol, chloroform and acetone.

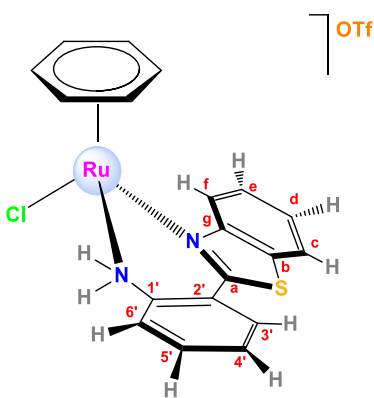


Synthesis of $[(\eta^6\text{-benzene})\text{RuCl}(\text{apbtz})]\text{Cl}$, [24b]Cl. The synthesis was performed as for [23a]Cl in the presence of the ligand 2-(2'-hydroxyphenyl)benzothiazole (0.0914 g, 0.404 mmol) and $[\text{RuCl}_2(\text{bz})]_2$ (0.0999 g, 0.200 mmol) in a mixture of degassed methanol/acetonitrile (10:1.5, 11.5 mL), and washing with diethyl ether. Yellow-greenish powder. Yield: 127.2 mg (0.267 mmol, 67%). $\mathbf{M_r}$ ($\mathbf{C_{19}H_{16}N_2SCl_2Ru \cdot (H_2O)_{1.85}}$) = 476.3902 g/mol. **Anal. Calcd for $C_{19}H_{16}N_2SCl_2Ru \cdot (H_2O)_{1.85}$:** C 44.77;

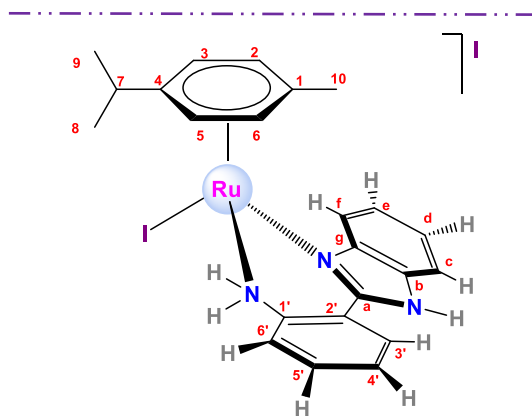
H 3.90; N 5.50; S 6.29; **Found:** C 44.77; H 3.99; N 5.67; S 6.12. **^1H NMR (400 MHz, CDCl_3 , 25 °C)** δ 10.63 (d, J = 8.6 Hz, 1H, $\text{H}^{\text{N}-\text{H}(\text{NH}_2)}$), 8.87 (d, J = 7.4 Hz, 1H, H^{f}), 8.61 (d, J = 8.0 Hz, 1H, H^{f}), 7.95 (d, J = 7.6 Hz, 1H, H^{c}), 7.75 (d, J = 7.5 Hz, 1H, $\text{H}^{\text{3'}}$), 7.66 (dd, J = 17.1, 7.9 Hz, 2H, $\text{H}^{\text{e},\text{5'}}$), 7.54 (t, J = 7.2 Hz, 1H, H^{d}), 7.40 (t, J = 7.2 Hz, 1H, $\text{H}^{\text{4'}}$), 5.88 (s, 6H, $\text{H}^{\text{benzene}}$), 4.44 (d, J = 9.5 Hz, 1H, $\text{H}^{\text{N}-\text{H}(\text{NH}_2)}$) ppm. **$^{13}\text{C}\{^1\text{H}\}$ NMR (101 MHz, CDCl_3 , 25 °C)** δ 166.9 (s, 1C, C^{a}), 152.4 (s, 1C, C^{g}), 141.5 (s, 1C, $\text{C}^{\text{1'}}$), 134.6 (s, 1C, $\text{C}^{\text{5'}}$), 132.2 (s, 1C, C^{b}), 131.0 (s, 1C, $\text{C}^{\text{3'}}$), 128.4 (s, 1C, C^{e}), 127.7 (s, 1C, $\text{C}^{\text{4'}}$), 127.5 (s, 1C, C^{d}), 126.2 (s, 1C, C^{f}), 125.5 (s, 1C, $\text{C}^{\text{2'}}$), 123.7 (s, 1C, $\text{C}^{\text{6'}}$), 122.6 (s, 1C, C^{c}), 85.2 (s, 6C, $\text{C}^{\text{benzene}}$) ppm. **FT-IR (KBr, cm⁻¹) selected bands:** 3393 (m, $\nu_{\text{O}-\text{H}}$), 3227 (m, $\nu_{\text{N-Hassociated}}$), 3048 (w, $\nu_{=\text{CH}}$, ν_{NH_2}), 1611 (m, $\nu_{\text{C=C+C-N}}$), 1499 (w), 1479 (vs, $\nu_{\text{C=N}}$), 1455-1427 (s), 1323 (w, δ_{CH_3}), 1249 (m), 1127 (m, $\nu_{\text{C-S}}$), 995 (m), 842 (m), 759 (vs, δ_{CHoop}). **MS (FAB+):** m/z (%) = 441 (32) ([M-Cl]⁺), 405 (21) ([M-2Cl-H]⁺), 327 (3) ([M-2Cl-H-bz]⁺), 227 (5) ([apbtz+H]⁺). **Molar Conductivity (H_2O):** 147.3 S·cm²·mol⁻¹. **Solubility:** soluble in water, methanol, chloroform, dimethylsulfoxide and acetone.



Synthesis of $[(\eta^6-p\text{-cymene})\text{RuCl}(\text{apbtz})]\text{OTf}$, [24a]OTf. The synthesis was performed as for [23a]OTf in the presence of AgOTf (0.0895 g, 0.348 mmol, 6% exc.), $[\text{RuCl}_2(\text{cym})]_2$ (0.1004 g, 0.164 mmol) and the ligand 2-(2'-hydroxyphenyl)benzothiazole (0.0745 g, 0.329 mmol) in dichloromethane (10 mL). Yellow-orange powder. Yield: 138.1 mg (0.214 mmol, 65%). **M_r** ($\text{C}_{24}\text{H}_{24}\text{N}_2\text{S}_2\text{F}_3\text{O}_3\text{ClRu}$) = 646.1151 g/mol. **Anal. Calcd for** $\text{C}_{24}\text{H}_{24}\text{N}_2\text{S}_2\text{F}_3\text{O}_3\text{ClRu} \cdot (\text{H}_2\text{O})_{0.2}$: C 44.37; H 3.79; N 4.31; S 9.87; **Found:** C 44.36; H 4.07; N 4.47; S 9.44. **^1H NMR (400 MHz, CDCl_3 , 25 °C)** δ 8.69 (d, J = 10.7 Hz, 1H, $\text{H}^{\text{N}-\text{H}(\text{NH}_2)}$), 8.52 (d, J = 8.4 Hz, 1H, H^{f}), 8.35 (d, J = 8.0 Hz, 1H, $\text{H}^{\text{6'}}$), 7.95 (d, J = 8.0 Hz, 1H, H^{c}), 7.81 (dd, J = 7.8, 1.2 Hz, 1H, $\text{H}^{\text{3'}}$), 7.74 (t, J = 6.6 Hz, 1H, $\text{H}^{\text{5'}}$), 7.70 (t, J = 6.5 Hz, 1H, H^{e}), 7.60 (t, J = 7.7 Hz, 1H, H^{d}), 7.45 (t, J = 7.6 Hz, 1H, $\text{H}^{\text{4'}}$), 5.78 (d, J = 6.0 Hz, 1H, $\text{H}^{\text{2'}}$), 5.74 (d, J = 6.1 Hz, 1H, $\text{H}^{\text{3'}}$), 5.66 (d, J = 6.4 Hz, 2H, $\text{H}^{\text{6',5'}}$), 4.41 (d, J = 11.0 Hz, 1H, $\text{H}^{\text{N}-\text{H}(\text{NH}_2)}$), 2.32 (hept, J = 6.9 Hz, 1H, $\text{H}^{\text{7'}}$), 1.76 (s, 3H, $\text{H}^{\text{10'}}$), 1.02 (d, J = 7.0 Hz, 3H, $\text{H}^{\text{8' or } \text{9'}}$), 0.98 (d, J = 6.9 Hz, 3H, $\text{H}^{\text{9' or } \text{8'}}$) ppm. **$^{13}\text{C}\{^1\text{H}\}$ NMR (101 MHz, CDCl_3 , 25 °C)** δ 166.1 (s, 1C, C^{a}), 152.7 (s, 1C, C^{g}), 140.1 (s, 1C, $\text{C}^{\text{1'}}$), 135.0 (s, 1C, $\text{C}^{\text{5'}}$), 132.0 (s, 1C, C^{b}), 131.2 (s, 1C, $\text{C}^{\text{3'}}$), 128.4 (s, 1C, C^{e}), 127.9 (s, 1C, $\text{C}^{\text{4'}}$), 127.7 (s, 1C, C^{d}), 126.2 (s, 1C, C^{f}), 125.0 (s, 1C, $\text{C}^{\text{2'}}$), 123.4 (s, 1C, $\text{C}^{\text{6'}}$), 122.5 (s, 1C, C^{c}), 120.8 (q, $J_{\text{C-F}} = 319.8$ Hz, 1C, C^{CF_3}), 107.9 (s, 1C, $\text{C}^{\text{1'}}$), 97.9 (s, 1C, $\text{C}^{\text{4'}}$), 85.2 (s, 1C, $\text{C}^{\text{5' or } \text{3'}}$), 83.8 (s, 1C, $\text{C}^{\text{3' or } \text{5'}}$), 81.8 (s, 1C, $\text{C}^{\text{6' or } \text{2'}}$), 79.2 (s, 1C, $\text{C}^{\text{2' or } \text{6'}}$), 31.0 (s, 1C, $\text{C}^{\text{7'}}$), 23.2 (s, 1C, $\text{C}^{\text{8' or } \text{9'}}$), 20.7 (s, $\text{C}^{\text{8' or } \text{9'}}$), 18.1 (s, 1C, $\text{C}^{\text{10'}}$) ppm. **$^{19}\text{F}\{^1\text{H}\}$ NMR (376 MHz, CDCl_3 , 25 °C)** δ -78.5 (s, 3F, F^{CF_3}), -79.0 (s), -90.7 (s) ppm. **FT-IR (KBr, cm⁻¹) selected bands:** 3503 (m, $\nu_{\text{O-H}}$), 3202 (m, $\nu_{\text{N-Hassociated}}$), 2966 (m, $\nu_{\text{NH}_2+(\text{hydrogen bonds})}$), 1616 (w, $\nu_{\text{C=C+C-N}}$), 1504 (w), 1479 (s, $\nu_{\text{C=N}}$), 1457-1427 (m), 1388 (w, δ_{CH_3}), 1323 (w), 1278-1250-1224 (vs, $\nu_{\text{C-F}}$), 1157 (s, $\nu_{\text{SO}_3^- \text{as}}$), 1030 (vs, $\nu_{\text{SO}_3^- \text{sym}}$), 758 (s, δ_{CHoop}), 637 (s, δ_{CF_3}), 517 (w). **MS (FAB+):** m/z (%) = 1143 (6) ([2M-OTf]⁺), 497 (96) ([M-OTf]⁺), 461 (100) ([M-OTf-Cl-H]⁺), 327 (12) ([M-OTf-Cl-H-bz]⁺), 227 (13) ([apbtz+H]⁺). **Molar Conductivity (H_2O):** 119.2 S·cm²·mol⁻¹. **Solubility:** soluble in methanol, acetone, water, dichloromethane and chloroform.

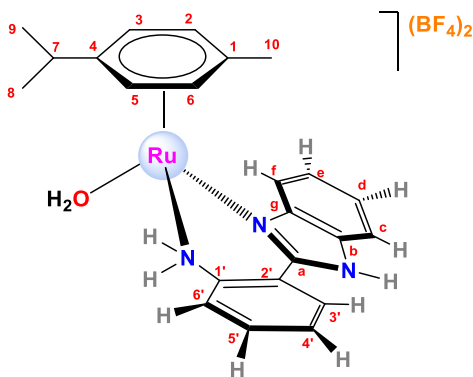


Synthesis of $[(\eta^6\text{-}p\text{-cymene})\text{RuCl}(\text{apbtz})]\text{OTf}$, [24b]OTf. The synthesis was performed as for **[23a]OTf** in the presence of AgOTf (0.1092 g, 0.348 mmol, 6.5% exc.), $[\text{RuCl}_2(\text{bz})]_2$ (0.0998 g, 0.200 mmol) and the ligand 2-(2'-hydroxyphenyl)benzothiazole (0.0905 g, 0.400 mmol) in dichloromethane (10 mL). Yellow powder. Yield: 117.1 mg (0.198 mmol, 50%). M_r ($\text{C}_{20}\text{H}_{16}\text{N}_2\text{O}_3\text{S}_2\text{F}_3\text{ClRu}$) = 590.0079 g/mol. **Anal. Calcd for** $\text{C}_{20}\text{H}_{16}\text{N}_2\text{O}_3\text{S}_2\text{ClRu}(\text{H}_2\text{O})_{0.5}(\text{C}_{10}\text{H}_{14}\text{O})_{0.1}$: C 40.41; H 2.99; N 4.62; S 10.57; **Found:** C 40.39; H 3.30; N 4.78; S 10.66. **¹H NMR (400 MHz, CDCl₃, 25 °C)** δ 8.74 (d, J = 10.8 Hz, 1H, H^{N-H(NH₂)}), 8.62 (d, J = 8.2 Hz, 1H, H^f), 8.28 (d, J = 8.1 Hz, 1H, H^{6'}), 7.98 (d, J = 7.9 Hz, 1H, H^c), 7.79 (d, J = 7.7 Hz, 1H, H^{3'}), 7.72 (t, J = 7.6 Hz, 2H, H^{5',e}), 7.62 (t, J = 7.7 Hz, 1H, H^d), 7.46 (t, J = 7.7 Hz, 1H, H^{4'}), 5.79 (s, 6H, H^{benzene}), 4.42 (d, J = 10.6 Hz, 1H, H^{N-H(NH₂)} ppm. **¹³C{¹H} NMR (101 MHz, CDCl₃, 25 °C)** δ 166.8 (s, 1C, C^a), 152.4 (s, 1C, C^b), 140.7 (s, 1C, C^{1'}), 135.1 (s, 1C, C^{5'}), 132.2 (s, 1C, C^b), 131.1 (s, 1C, C^{3'}), 128.6 (s, 1C, C^e), 128.1 (s, 1C, C^{4'}), 127.8 (s, 1C, C^d), 126.1 (s, 1C, C^f), 125.2 (s, 1C, C^{2'}), 122.9 (s, 1C, C^{6'}), 122.6 (s, 1C, C^c), 85.1 (s, 1C, C^{benzene}) ppm. **¹⁹F{¹H} NMR (376 MHz, CDCl₃, 25 °C)** δ -78.6 (s, 3F, FCF₃), -108.9 (s) ppm. **FT-IR (KBr, cm⁻¹) selected bands:** 3503 (w, v_{O-H}), 3207 (m, v_{N-H} associated), 3132 (m, v_{NH2+(hydrogen bonds)}), 1611-1597 (w, v_{C=C+C-N}), 1479 (m, v_{C=N}), 1458-1437 (m), 1324 (w), 1268-1247-1225 (vs, v_{C-F}), 1157 (s, v_{SO3^-as}), 1031 (vs, v_{SO3^-sym}), 774-758 (m, δ_{CHoop}), 638 (vs, δ_{CF₃}), 518 (w). **MS (FAB+):** m/z (%) = 1031 (4) ([2M-OTf]⁺), 441 (75) ([M-OTf]⁺), 405 (55) ([M-OTf-Cl-H]⁺), 327 (9) ([M-OTf-Cl-H-bz]⁺), 227 (10) ([apbtz+H]⁺). **Molar Conductivity (H₂O):** Insoluble. **Solubility:** soluble in methanol and acetone and slightly soluble in dichloromethane, chloroform and water.



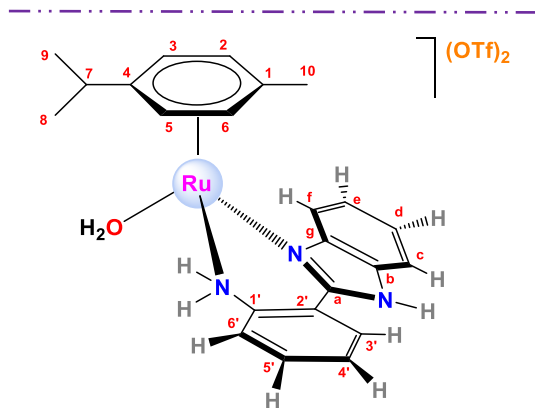
Synthesis of $[(\eta^6\text{-}p\text{-cymene})\text{RuI}(\text{apbim})]\text{I}$, [25a]I. The synthesis was performed as for **[23a]Cl** in the presence of the ligand 2-(2'-hydroxyphenyl)benzimidazole (0.0173 g, 0.0827 mmol) and $[\text{RuI}_2(\text{cym})]_2$ (0.0405 g, 0.0414 mmol) in degassed methanol (18 mL). Orange powder. Yield: 23.9 mg (0.0342 mmol, 41%). M_r ($\text{C}_{23}\text{H}_{25}\text{N}_3\text{I}_2\text{Ru}$) = 698.3496 g/mol. **Anal. Calcd for** $\text{C}_{23}\text{H}_{25}\text{N}_3\text{I}_2\text{Ru}\cdot(\text{CH}_3\text{OH})_{0.7}$: C 39.49; H 3.89; N 5.83; **Found:** C 39.63; H 3.94; N 5.5. **¹H NMR (400**

MHz, CDCl₃, 25 °C) δ 13.64 (s, 1H, H^{N-H}), 8.23 (d, J = 7.8 Hz, 1H, H^{6'}), 8.16 (d, J = 7.4 Hz, 1H, H^{3'}), 7.96 (d, J = 7.0 Hz, 1H, H^c), 7.89 (s, 1H, H^{N-H(NH2)}), 7.79 (d, J = 7.4 Hz, 1H, H^f), 7.47 – 7.36 (m, 2H, H^e, H^d), 7.20 (t, J = 7.6 Hz, 1H, H^{4'}), 7.03 (t, J = 7.3 Hz, 1H, H^{5'}), 5.64 (d, J = 5.9 Hz, 1H, H³), 5.51 (d, J = 6.2 Hz, 1H, H²), 5.36 (d, J = 6.0 Hz, 2H, H⁶, H⁵), 3.39 (s, 1H, H^{N-H(NH2)}), 2.39 (sept, J = 6.8 Hz, 1H, H⁷), 1.93 (s, 3H, H¹⁰), 0.93 (d, J = 6.9 Hz, 3H, H⁸ o H⁹), 0.86 (d, J = 6.9 Hz, 3H, H⁹ o H⁸) ppm. **¹³C NMR (101 MHz, CDCl₃, 25 °C)** δ 146.4 (s, 1C, C^a), 143.8 (s, 1C, C^g), 141.6 (s, 1C, C^{1'}), 133.9 (s, 1C, C^b), 133.0 (s, 1C, C^{5'}), 130.9 (s, 1C, C^{3'}), 128.3 (s, 1C, C^{4'}), 125.6 (s, 1C, C^d), 124.0 (s, 1C, C^e), 121.8 (s, 1C, C^f), 120.8 (s, 1C, C^{2'}), 120.7 (s, 1C, C^{5'}), 113.7 (s, 1C, C^c), 108.4 (s, 1C, C¹), 97.4 (s, 1C, C⁴), 84.6 (s, 1C, C⁵), 82.8 (s, 1C, C³), 81.1 (s, 1C, C⁶), 78.4 (s, 1C, C²), 31.7 (s, 1C, C⁷), 23.0 (s, 1C, C⁸ o C⁹), 21.7 (s, 1C, C⁹ o C⁸), 19.8 (s, 1C, C¹⁰) ppm. **FT-IR (KBr, cm⁻¹) selected bands:** 3426 (s, ν_{O-H}), 3056 (vs, ν=CH, ν_{NH2}), 2964 (s, ν_{NH2+(hydrogen bonds)}), 1619-1597-1577 (m, ν_{C=C + C-N}), 1487 (m), 1462-1447 (vs, ν_{C=N}), 1418(m), 1387 (w, δ_{CH3}), 1322 (w), 1144-1103 (m), 761-750 (s, δ_{CHoop}), 531 (w). **MS (FAB+):** m/z (%) = 573 (12) ([M-I+H]⁺), 445 (10) ([M-2I]⁺). **Molar Conductivity (H₂O):** 91.2 S·cm²·mol⁻¹. **Solubility:** soluble in methanol, dichloromethane, chloroform and acetone.

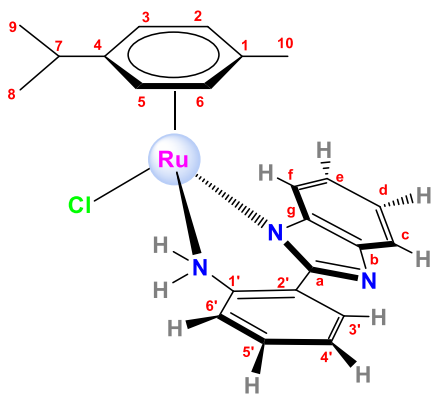


Synthesis of [(η⁶-p-cymene)Ru(OH₂)(apbim)(BF₄)₂, [26a](BF₄)₂. In a 100 mL Schlenk flask, AgBF₄ (0.0629 g, 3.23 mmol, 67% exc.) was added to a solution of [23a]Cl (0.0499 g, 0.097 mmol) in a mixture water/ethanol (1:1, 10 mL). The mixture was stirred at room temperature for 20 h, under a nitrogen atmosphere and preserved from light. The AgCl was filtered and the solvent was evaporated to dryness. The residue was washed with diethylether (5 mL) and hexane (5 mL). The resulting black-brownish powder was dried under vacuum. **M_r (C₂₃H₂₇N₃OB₂F₈Ru) = 636.165 g/mol. Anal. Calcd for C₂₃H₂₇N₃OB₂F₈Ru·(AgBF₄)_{0.3}:** C 39.77; H 3.92; N 6.05; **Found:** C 39.52; H 3.92; N 6.23. **¹H NMR (400 MHz, D₂O, 25 °C)** δ 7.98 (dd, J = 7.8, 1.4 Hz, 1H, H^{3'}), 7.95 – 7.92 (m, 1H, H^f), 7.79 (dt, J = 7.0, 2.4 Hz, 2H, H^c, H^{6'}), 7.72 (td, J = 7.7, 1.5 Hz, 1H, H^{5'}), 7.62 – 7.53 (m, 3H, H^e, H^d, H^{4'}), 6.03 (d, J = 6.1 Hz, 1H, H²), 5.99 (d, J = 5.9 Hz, 1H, H³), 5.83 (d, J = 5.9 Hz, 1H, H⁶), 5.78 (d, J = 6.2 Hz, 1H, H⁵), 2.08 – 2.00 (m, J = 6.9 Hz, 1H, H⁷), 1.83 (s, 3H, H¹⁰), 0.93 (d, J = 6.9 Hz, 3H, H⁸ o H⁹), 0.84 (d, J = 6.9 Hz, 3H, H⁹ o H⁸) ppm. **¹³C{¹H} NMR (101 MHz, D₂O, 25 °C)** δ 149.0 (s, 1C, C^a), 142.2 (s, 1C, C^g), 141.0 (s, 1C, C^{1'}), 134.7 (s, 1C, C^b), 133.7 (s, 1C, C^{5'}), 130.0 (s, 1C, C^{3'}), 128.1 (s, 1C, C^{4'}), 126.1 (s, 1C, C^d), 125.3 (s, 1C, C^e), 122.1 (s, 1C, C^{6'}), 121.3 (s, 1C, C^{2'}), 118.7 (s, 1C, C^f), 113.9 (s, 1C, C^c), 103.3 (s, 1C, C¹), 99.2 (s, 1C, C⁴), 83.6 (s, 1C, C³), 82.5 (s, 1C, C⁵), 82.4 (s, 1C, C²), 82.1 (s, 1C, C⁶), 30.8 (s, 1C, C⁷), 22.6 (s, 1C, C⁸ o C⁹), 20.5 (s, 1C, C⁹ o C⁸), 17.7 (s, 1C, C¹⁰) ppm. **¹⁹F{¹H} NMR (376 MHz, D₂O, 25 °C)** δ -130.4 (s), -144.2 (dd, J = 29.4, 14.5 Hz), -150.91 (s, ¹⁰B-F, BF₄⁻), -150.96 (s, ¹¹B-F, BF₄⁻) ppm. Integration ratio (1:4) in agreement with the isotopic distribution for ¹⁰B/¹¹B. **FT-IR (KBr, cm⁻¹) selected bands:** 3381 (m, ν_{O-H}), 3284 (m, ν_{N-Hassociated}), 3076 (w, ν=CH, ν_{NH2}), 2973 (vs, ν_{NH2+(hydrogen bonds)}), 1620-1599 (vw, ν_{C=C + C-N}), 1488 (m), 1466-1448

(m, $\nu_{C=N}$), 1420 (w), 1084-1060-1037 (vs, ν_{B-F}), 741 (m, $\delta_{CH_{oop}}$), 533-523 (w). **MS (FAB+):** m/z (%) = 565 (5), 463 (7) ($[M-2BF_4]^+$), 446 (92) ($[M-2BF_4-H_2O+H]^+$), 445 (96) ($[M-2BF_4-H_2O]^+$), 310 (24) ($[M-2BF_4-H_2O-C_{10}H_{14}-H]^+$). **Molar Conductivity (H₂O):** 201.2 S·cm²·mol⁻¹. **Solubility:** soluble in water.



Synthesis of $[(\eta^6\text{-}p\text{-cymene})Ru(OH_2)(apbim)(OTf)_2, [26a](OTf)_2]$. The synthesis was performed as for $[26a](BF_4)_2$ in the presence of AgOTf (0.0532 g, 0.207 mmol, 5.7% exc.) and $[23a]Cl$ (0.0505 g, 0.098 mmol) in a mixture water/ethanol (1:1, 6 mL), and washing with diethyl ether (5 mL). Yellow powder. **M_r** ($C_{25}H_{27}N_3O_7S_2F_6Ru$) = 760,6966 g/mol. **Anal. Calcd for** $C_{22}H_{25}N_3OB_2F_8Ru \cdot (C_4H_{10}O)_{0.3}$: C 40.19; H 3.86; N 5.37; S 8.19; **Found:** C 40.37; H 3.48; N 5.85; S 8.07. **¹H NMR (400 MHz, D₂O, 25 °C)** δ 7.98 (d, $J = 7.7$ Hz, 1H, H^{3'}), 7.95 – 7.91 (m, 1H, H^f), 7.79 (dd, $J = 6.9, 3.0$ Hz, 2H, H^c, H^{6'}), 7.72 (t, $J = 7.7$ Hz, 1H, H^{5'}), 7.61 – 7.52 (m, 3H, H^e, H^d, H^{4'}), 5.90 (bd, $J = 14.8$ Hz, 4H, H², H³, H⁵, H⁶), 2.04 (hept, $J = 7.0$ Hz, 1H, H⁷), 1.83 (s, 3H, H¹⁰), 0.88 (bd, $J = 6.7$ Hz, 6H, H⁸, H⁹) ppm. **¹H NMR (400 MHz, DMSO-d₆, 25 °C)** δ 14.35 (s, 1H, H^{N-H}), 8.98 – 8.88 (m, 1H, H^{N-H(NH₂)}), 8.11 (d, $J = 7.5$ Hz, 1H, H^f), 7.98 (d, $J = 7.5$ Hz, 1H, H^c), 7.81 (d, $J = 8.0$ Hz, 1H, H^{3'}), 7.78 – 7.71 (m, 2H, H^{4'}, H^{5'}), 7.60 – 7.52 (m, 3H, H^{6'}, H^d, H^e), 6.06 (d, $J = 10.1$ Hz, 1H, H^{N-H(NH₂)}), 6.00 (d, $J = 5.8$ Hz, 1H, H³ o H⁵), 5.96 (d, $J = 6.1$ Hz, 1H, H² o H⁶), 5.92 (d, $J = 5.7$ Hz, 1H, H⁵ o H³), 5.83 (d, $J = 5.8$ Hz, 1H, H⁶ o H²), 2.05 (sept, $J = 6.9$ Hz, 1H, H⁷), 1.74 (s, 3H, H¹⁰), 0.85 (dd, $J = 6.8, 3.0$ Hz, 6H, H⁸, H⁹) ppm. **¹⁹F{¹H} NMR (376 MHz, D₂O, 25°C)** δ -79.24 (s, 6F, F^{CF₃}) ppm. **¹⁹F{¹H} NMR (376 MHz, DMSO-d₆, 25°C)** δ -78.13 (s, 6F, F^{CF₃}) ppm. **FT-IR (KBr, cm⁻¹) selected bands:** 3203 (m, $\nu_{N\text{-Hassociated}}$), 2969 (w, $\nu_{NH_2\text{+}(hydrogen bonds)}$), 1623 (w, $\nu_{C=C + C-N}$), 1491 (m), 1466-1450 (m, $\nu_{C=N}$), 1255 (vs, ν_{C-F}), 1165 (s, $\nu_{SO_3^-as}$), 1031 (vs, $\nu_{SO_3^-sym}$), 745 (m, $\delta_{CH_{oop}}$), 640 (s, δ_{CF_3}), 517 (m). **MS (FAB+):** m/z (%) = 444 (100) ($[M-2(OTf)-H_2O-H]^+$). **Molar Conductivity (H₂O):** 192.3 S·cm²·mol⁻¹. **Solubility:** soluble in water, acetone, dimethyl sulfoxide.



Synthesis of $[(\eta^6\text{-}p\text{-cymene})\text{RuCl}(\text{apbim}')]$, [27a]. In a 100 mL Schlenk flask, Et_3N (12 μl , 0.086 mmol) was added to a solution [23a]Cl (0.0215 g, 0.042 mmol) in degassed methanol (6 mL), and the mixture was stirred at room temperature for 20 h and under a nitrogen atmosphere. The solid was filtered and washed with diethyl ether (5 mL). The resulting yellow solid was dried under vacuum. **M_r** ($\text{C}_{23}\text{H}_{24}\text{N}_3\text{ClRu}$) = 478.9854 g/mol. **$^1\text{H NMR}$ (400 MHz, CDCl_3 , 25 °C)** δ 8.24 (d, J = 7.5 Hz, 1H), 7.86 – 7.78 (m, 1H), 7.70 – 7.59 (m, 1H), 7.25 – 7.13 (m, 4H), 6.63 (bs, 1H), 6.31 (bs, 1H), 5.40 – 4.93 (bm, 4H, H^2 , H^3 , H^5 , H^6), 2.04 (sept, J = 7.1 Hz, 1H, H^7), 1.43 (s, 3H, H^{10}), 0.82 (bd, J = 48.3 Hz, 6H, H^8 , H^9) ppm. **FT-IR (KBr, cm⁻¹) selected bands:** 3243 (s, $\nu_{\text{N-H}}$), 3054 (s, $\nu_{=\text{CH}}$, ν_{NH_2}), 2970 (s, $\nu_{\text{NH}_2\text{+(hydrogen bonds)}}$), 1625–1604 (w, $\nu_{\text{C=C+C-N}}$), 1465 (vs, $\nu_{\text{C=N}}$), 1423 (s), 1369 (vs, δ_{CH_3}), 1338 (w), 1284 (m), 1107 (s), 1039 (vs), 863 (m), 739 (vs, $\delta_{\text{CH}_\text{loop}}$), 546 (w). **MS (FAB+):** m/z (%) = 480 (30) ([M+H]⁺), 444 (8) ([M-Cl]⁺).

4. BIBLIOGRAPHY

- (1) Bugarcic, T.; Habtemariam, A.; Stepankova, J.; Heringova, P.; Kasparkova, J.; Deeth, R. J.; Johnstone, R. D. L.; Prescimone, A.; Parkin, A.; Parsons, S.; Brabec, V.; Sadler, P. J. *Inorg. Chem.* **2008**, *47*, 11470–11486.
- (2) Peacock, A. F. A.; Sadler, P. J. *Chem. An Asian J.* **2008**, *3*, 1890–1899.
- (3) Wang, F.; Xu, J.; Habtemariam, A.; Bella, J.; Sadler, P. J. *J. Am. Chem. Soc.* **2005**, *127*, 17734–17743.
- (4) Wang, F.; Habtemariam, A.; van der Geer, E. P. L.; Deeth, R. J.; Gould, R.; Parsons, S.; Sadler, P. J. *JBIC J. Biol. Inorg. Chem.* **2009**, *14*, 1065–1076.
- (5) Sheldrick, W. S.; Heeb, S. *J. Organomet. Chem.* **1989**, *377*, 357–366.
- (6) Kramer, R.; Polbornz, K.; Wanjek, H.; Zahn, I. **1990**, *123*, 767–778.
- (7) Cabeza, J. A.; da Silva, I.; del Río, I.; Gossage, R. A.; Martínez-Méndez, L.; Miguel, D. *J. Organomet. Chem.* **2007**, *692*, 4346–4352.
- (8) Bennett, M. A.; Smith, A. K. *J. Chem. Soc. Dalton Trans.* **1974**, 233–241.
- (9) Therrien, B. *Coord. Chem. Rev.* **2009**, *253*, 493–519.
- (10) Mendoza-Ferri, M. G.; Hartinger, C. G.; Nazarov, A. A.; Eichinger, R. E.; Jakupc, M. A.; Severin, K.; Keppler, B. K. *Organometallics* **2009**, *28*, 6260–6265.
- (11) Małecki, J. G. *Struct. Chem.* **2011**, *23*, 461–472.
- (12) Kumar, A.; Kumar, A.; Gupta, R. K.; Paitandi, R. P.; Singh, K. B.; Trigun, S. K.; Hundal, M. S.; Pandey, D. S. *J. Organomet. Chem.* **2016**, *801*, 68–79.
- (13) Gopal, Y. N. V.; Jayaraju, D.; Kondapi, A. K. *Biochemistry* **1999**, *38*, 4382–4388.
- (14) Zelonka, R. a.; Baird, M. C. *Can. J. Chem.* **1972**, *50*, 3063–3072.
- (15) Patra, M.; Joshi, T.; Pierroz, V.; Ingram, K.; Kaiser, M.; Ferrari, S.; Spingler, B.; Keiser, J.; Gasser, G. *Chem. - A Eur. J.* **2013**, *19*, 14768–14772.
- (16) Taylor, P.; Roopashree, B.; Gayathri, V. *J. Coord. Chem.* **2012**, *65*, 1354–1370.
- (17) Pretsch, E.; Bühlmann, P.; Affolter, C.; Herrera, A.; Martínez, R. *Determinación estructural de compuestos orgánicos*; **2005**. Orig.; MASSON, S.A.: Barcelona, **2005**.
- (18) Nakamoto, K. *Infrared and Raman Spectra of Inorganic and Coordination Compounds*; Fourth Edition; John Wiley and Sons, **1986**.
- (19) Heyns, A. M. *Spectrochímica Acta A* **1977**, *33*, 315–322.
- (20) Angelici, R. J. In *Técnicas y Síntesis en Química Inorgánica*; Editorial Reverté, S.A., **1979**; p. 243.
- (21) Janiak, C. *Dalt. Trans.* **2000**, 3885–3896.
- (22) Schuecker, R.; John, R. O.; Jakupc, M. A.; Arion, V. B.; Keppler, B. K. *Organometallics* **2008**, *27*, 6587–6595.
- (23) Marcus, Y. *J. Chem. Soc. Faraday Trans.* **1991**, *87*, 2995–2999.
- (24) Gutiérrez, A.; Cativiela, C.; Laguna, A.; Gimeno, M. C. *Dalt. Trans.* **2016**, *45*, 13483–13490.

CHAPTER 5.

Ru(II) HALF-SANDWICH COMPLEXES BEARING PYRIDYLBENZOXAZOLE AND THIABENDAZOLE: SYNTHESIS, CHARACTERIZATION AND ANTICANCER PROPERTIES



CHAPTER 5. Ru(II) HALF-SANDWICH COMPLEXES BEARING PYRIDYLBENZOXAZOLE AND THIABENDAZOLE: SYNTHESIS, CHARACTERIZATION AND ANTICANCER PROPERTIES

ABSTRACT: In this chapter a family of 6 new complexes of general formula $[\text{Ru}(\eta^6-p\text{-cymene})(\kappa^2-N,N\text{-HL})X]Y$ ($X =$ leaving group; $Y =$ counterion) bearing 2-(2'-pyridyl)benzoxazole (pybox) and 2-(4'-thiazolyl)benzimidazole (thiabendazole, tbz) as bidentate ligands was prepared in order to assess their cytotoxic potency and establish some structure-activity relationships as a result of comparative analysis of the IC_{50} values. The specific objectives of this chapter are to study the effect on the anticancer properties of the following features:

- The replacement of the NH unit in pybim type ligands with an O atom (pybox).
- The substitution of the pyridine ring in pybim by the electron-rich thiazolyl ring.
- The replacement of Cl^- with I^- as the leaving group, which strongly affects the solubility and aquation properties.

CONETXT: Likewise 2-(2'-pyridyl)benzimidazole ligands in CHAPTER 1, 2-(2'-pyridyl)benzoxazoles have been used in platinum,¹ rhenium² and octahedral ruthenium complexes,^{3,4} as catalysts and owing to their good luminescent properties. Only one Ru(II) half-sandwich complex bearing 2-phenoxyethanol as the arene has been reported during the development of this work and used in the hydrogenation of alkenes and alkynes.⁵ Regarding the thiabendazole, it has been widely used as antifungal, as previously seen (see GENERAL INTRODUCTION), yet it has been scarcely used in the preparation of metal complexes as anticancer drugs^{6,7}. In addition, no ruthenium complexes have been reported in the literature so far.



1. RESULTS AND DISCUSSION

1.1. Synthesis

The chlorido-complexes were synthesised from the ruthenium chloro-bridged dimer $[\text{Ru}(\eta^6\text{-}p\text{-cymene})(\mu\text{-Cl})\text{Cl}]_2$ (see CHAPTER 1).^{8,9} The iodide-derivatives were synthesised from the ruthenium iodo-bridged dimer $[\text{Ru}(\eta^6\text{-}p\text{-cymene})(\mu\text{-I})\text{I}]_2$ prepared by the reaction of the ruthenium chloro-bridged dimer with potassium iodide in a mixture of water/CHCl₃ (1:1).¹⁰

All the complexes, whose schematic synthesis is shown in Fig. 1, are cationic. The chlorido and iodido derivatives of general formula $[(\eta^6\text{-}p\text{-cymene})\text{RuX}(\kappa^2\text{-}N,N\text{-HL})]\text{X}$ (**[28]Cl**, **[29]I**, **[31]Cl** and **[32]I**), where X = Cl⁻ or I⁻ and HL=ligand, were synthesised by the reaction between the arene ruthenium(II) starting dimer and the ligands (pybox and tbz) in methanol at room temperature and stirring overnight. The respective aqua derivatives of general formula $[(\eta^6\text{-}p\text{-cymene})\text{Ru}(\text{H}_2\text{O})(\kappa^2\text{-}N,N\text{-HL})](\text{OTf})_2$ (**[30](OTf)₂**, **[33](OTf)₂**), were prepared by the reaction of **[28]Cl** and **[31]Cl** respectively, with an excess of the AgOTf salt in a mixture of distilled water and ethanol. The ¹H NMR showed some impurities in the complexes, so they could not be used in biological tests.

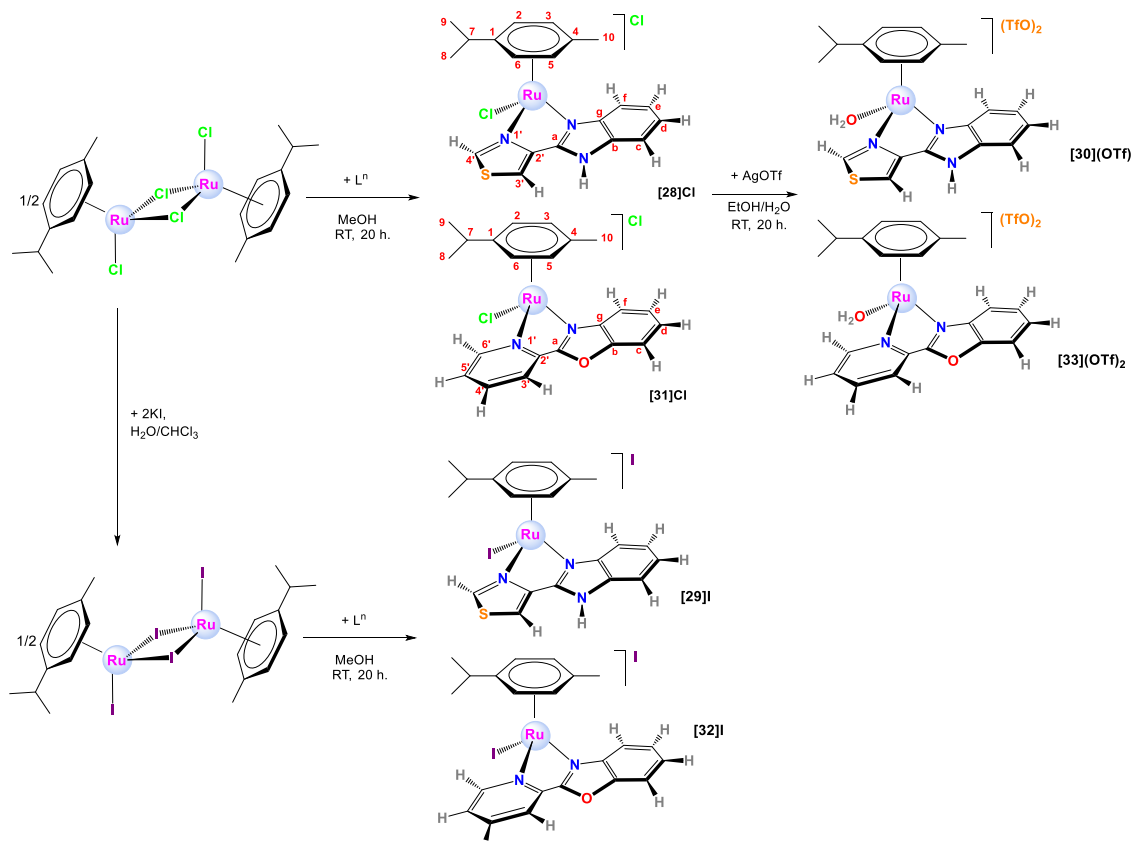


Fig. 1. Schematic synthesis of the new Ruthenium(II) complexes.

All the complexes were isolated in moderate-to-good yields (from 59% to 88%) as the corresponding racemates (R_{Ru} or S_{Ru}) in the form of yellow, orange, red-brown or green powders.

1.2. CHARACTERIZATION

All the complexes have been fully characterised by NMR spectroscopy, IR spectroscopy, positive fast atom bombardment (FAB^+) mass spectrometry, molar conductivity and elemental analysis.

1.2.1. NMR

The ^1H NMR spectra of monocationic complexes ([28]Cl, [29]I, [31]Cl and [32]I) were recorded in CDCl_3 or CD_3OD at 25 °C. As in previous complexes, a down-field shift for the signals of the N,N-ligands was observed when they coordinate to the metal ion. Complexes with tbz also showed a broad resonance at 15 ppm corresponding to the N-H group. The *p*-cym evidenced an ABCD spin system and two doublets for the diastereotopic methyls of *iPr*. When the spectra of the chlorido and iodido derivatives are compared, a remarkable shift of the signals is detected. Aromatic resonances for the iodido derivatives are shielded with regard to those of the chlorido derivatives, whereas aliphatic *p*-cymene signals are deshielded.

The ^1H NMR spectra of the aqua derivatives ([30](OTf)₂, [33](OTf)₂) were recorded in D_2O at 25 °C. The ^1H - ^1H NOESY for [30](OTf)₂ (see Fig. 2) showed an interconversion between enantiomers, since exchange peaks are observed in the spectrum, as for other aqua derivatives (see CHAPTER 1). Curiously, the complex [33](OTf)₂ did not show similar evidences.

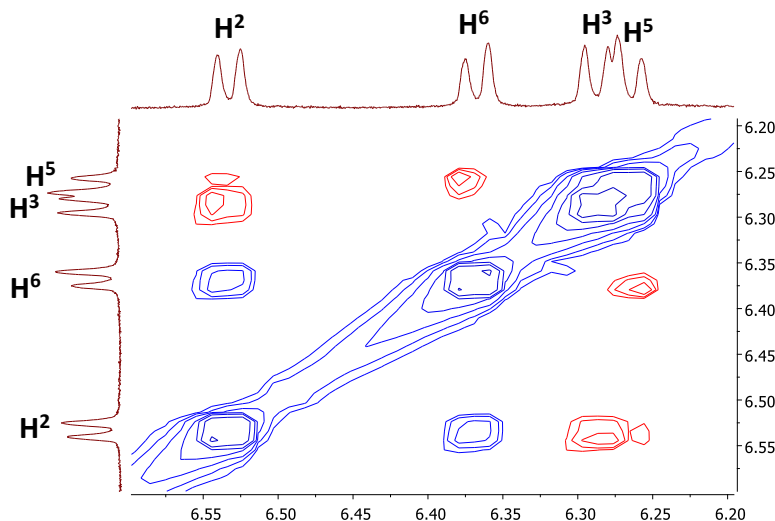


Fig. 2. *p*-cym aromatic protons area in the NOESY spectra of complex [30](OTf)₂ (D_2O at 25 °C).

Regarding $^{13}\text{C}\{^1\text{H}\}$ NMR, it evidences the different areas specified in previous chapters. The spectra of the aquo derivatives did not show the resonances of the triflate anion, due to the low solubility of the complexes in deuterated water.

1.2.2. Mass Spectra

The FAB^+ mass spectra of the complexes exhibit characteristic sets of peaks according to isotopic distribution patterns: $[\text{M}-\text{Y}]^+$ fragments for monocationic

complexes, where Y is the counterion Cl^- or I^- and fragments with a water molecule for the aquo derivatives.

1.2.3. IR Spectra

Infrared spectra show characteristic peaks for the normal vibrational modes of the corresponding rings ($\nu_{\text{C}=\text{N}}$, $\nu_{\text{C}=\text{C}}$ and $\delta_{\text{CH}_{\text{loop}}}$, and $\nu_{\text{C}-\text{S}}$, $\nu_{\text{C}=\text{S}}$ specifically for tbz). The aquo complexes show very strong and diagnostic peaks for triflate, $\nu_{\text{C}-\text{F}}$, $\nu_{\text{SO}_3-\text{as}}$, $\nu_{\text{SO}_3-\text{sym}}$ at 1288-1225, 1167-1158 and 1030-1029 cm^{-1} , respectively.

1.2.4. Molar Conductivity

Molar conductivity (Λ_m) for the complexes (see Table 1) was measured in aqueous solutions (10^{-3} M). The values do not correctly reflect either the 1:1 electrolyte nature of monocationic complexes or the 2:1 for dicationic derivatives.¹¹ The values for the complexes with pybox are lower than expected, whereas those with tbz fit better and are higher than the formers. Moreover, the conductivity is slightly higher for the complex with chloride, [31]Cl (79.4 $\text{S}\cdot\text{cm}^2\cdot\text{mol}^{-1}$), than for the complex with iodide, [32]I (65.7 $\text{S}\cdot\text{cm}^2\cdot\text{mol}^{-1}$). These subtle differences are explained as a result of the higher hydration energy of Cl^- relative to I^- (see page 241). Molar conductivity of the aqua complexes is also lower than those in other aqua derivatives studied before (see CHAPTER 1). These results can be interpreted taking into account the aquation processes that undergo the monocationic complexes. This implies a change in the global charge of the complex and therefore, an increase in the molar conductivity. All in all, all of the complexes show values under the usual range, probably due to ion-pairing.

Table 1. Molar conductivity values for complexes measured in water.

Complex	Solvent	Λ_m ($\text{S}\cdot\text{cm}^2\cdot\text{mol}^{-1}$)
[28]Cl	H_2O	164.4
[29]I	insoluble	-
[31]Cl	H_2O	79.4
[32]I	H_2O	65.7
[30](OTf) ₂	H_2O	115.6
[33](OTf) ₂	H_2O	139.2

1.2.5. Elemental Analysis

The aqua derivatives showed possible contamination with AgBF_4 . Thus, they were ruled out for cytotoxicity studies. Moreover, [33](OTf)₂ exhibited impurities as shown by ¹H NMR. Likewise, the ¹H NMR spectrum of [31]Cl showed traces of the starting dimeric product.

1.2.6. X Ray Diffraction

Single crystals suitable for X-ray diffraction analysis were obtained for [28]Cl (unsuitable to publish) from a solution in CH_2Cl_2 and [33](OTf)₂· H_2O from a solution in

water by slow evaporation of the corresponding solvents. Bond lengths, angles and other relevant features of the structures are gathered in Table 2 and Table 3.

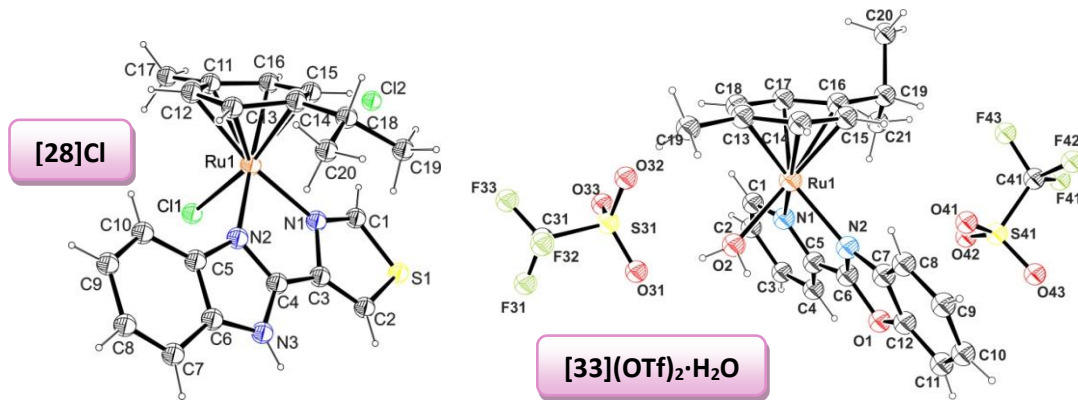


Fig. 3. ORTEP diagrams for complexes [28]Cl and [33](OTf)₂·H₂O. Ellipsoids are shown at 30% probability.

The corresponding unit cells of both complexes show the two possible enantiomers (R_{Ru} and S_{Ru}) resulting from the stereogenic nature of the metal centre. The complexes adopt the expected half-sandwich pseudo-octahedral three-legged piano-stool geometry, and the arene ring displays a π -bounded η^6 -coordination mode, whereas the pyridylbenzoxazole or thiabendazole ligands assume a bidentate-chelate coordination mode ($\kappa^2\text{-N,N}$). The third position is occupied by a chloride or a water molecule. Regarding the complex [33](OTf)₂·H₂O, the Ru-centroid distance (1.672 Å) falls in the same interval as for other Ru-N,N complexes, for instance, those in CHAPTER 1. Among the Ru-N distances, the Ru-N(py) is the shorter one (2.088 Å), whereas the Ru-N(box) is the longer one (2.167 Å). The N-Ru-N angle of the chelate ring is 76.8(3) $^\circ$ and the chelate ring exhibits planarity in itself and coplanarity for the two aromatic rings of the ligand (3.32 $^\circ$). The structure presents disorder in the benzene ring and in the triflate molecules. This disorder in the triflate is bound to be caused by an **isotropic oscillation** around the centre of gravity of the anion¹². In addition, the group CF₃ rotates faster than the SO₃ group at the acquisition temperature (RT), which would explain the disorder of only the CF₃ group in one of the molecules.

Table 2. Selected bond lengths (Å) and angles (°) for complex [33](OTf)₂·H₂O.

<i>Distance/angle</i>	[33](OTf) ₂ ·H ₂ O
Ru1-O2	2.106(5)
Ru1-N1	2.167(8)
Ru1-N2	2.088(7)
N2-C6	1.313(10)
O1-C6	1.360(10)
N2-Ru1-N1	76.8(3)
N2-Ru1-O2	80.5(2)
O2-Ru1-N1	82.6(2)

Table 3. Selected geometric parameters^[a] for the metal complex of [33](OTf)₂·H₂O.

<i>Distance/angle</i>	[33](OTf) ₂ ·H ₂ O
<i>Range of Ru-C distances</i>	2.156(9)-2.232(8)
<i>Ru-centroid</i>	1.672
α	3.32
ϑ (<i>N-C-C-N</i>)	1.73
β (<i>chelate-arene</i>)	62.83
γ (<i>Cx-C_{ipso}-Ru-O</i>)	0.34
λ	2.95

[a]Calculated with Mercury, version 3.8.

The triflate molecules are connected to the ruthenium complex through intramolecular hydrogen bonding interactions involving the coordinated water molecule and the *p*-cymene ring (see Table 5). The stereochemistry of both triflate molecules is different (see Fig. 4). Thus, the former shows an eclipsed conformation (torsion angle, $\theta = 7.80^\circ$), whereas the latter acquires a staggered configuration (torsion angle, $\theta = 38.57^\circ$).^{12,13}

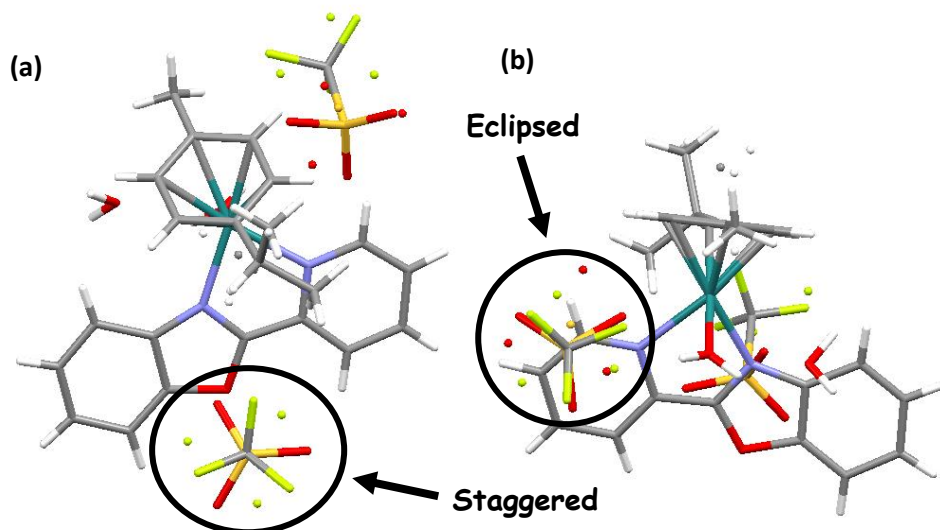


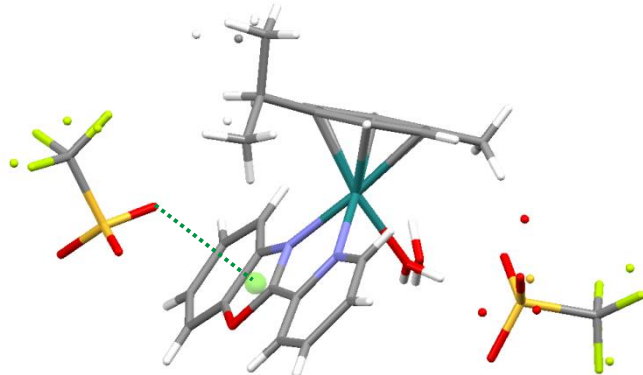
Fig. 4. Staggered (a) and eclipsed (b) conformations for triflate molecules in the crystal structure of [33](OTf)₂·H₂O.

It is worth mentioning that an unusual non-covalent interaction called anion- π or $l\pi-\pi$ ($l\pi$ = lone pair) interaction is observed in the 3D-structure (see Fig. 5). This kind of interactions generally occurs when the aromatic ring exhibits heterogeneous electron distribution in the π -cloud and they are extremely common in supramolecular chemistry (e.g. nucleic acids). These contacts were first detected in hexafluorobenzene and those arenes that possess electron deficient areas, with heteroatoms or withdrawing groups. Thus, electron-rich moieties locate above them.^{14,15,16} The oxazole entity has got electron-deficient zones in the π -cloud of its aromatic ring^{17,18}, since the heteroatoms (O and N) withdraw electronic density from the ring. Table 4 gathers the characteristic parameters of $l\pi-\pi$ interaction between the O atom of triflate and the oxazole ring.

Table 4. Geometric parameters of $\text{Ip}\cdots\pi$ interactions ($\text{S}=\text{O}\cdots\pi$) for the complex $[\text{33}](\text{OTf})_2\cdot\text{H}_2\text{O}$.

Compound	$d_{\text{O-cent}}$ (Å)	$d_{\text{O-plane}}$ (Å)	d_{offset} (Å)	$\alpha_{\text{S-O-cent}}$ (°)	θ (°)
$[\text{33}](\text{OTf})_2\cdot\text{H}_2\text{O}$	3.100	3.098	0.111	128.17	87.94

* d_{offset} has been calculated as $(d_{\text{centroid}}^2 - d_{\text{plane}}^2)^{1/2}$.¹⁴

**Fig. 5.** $\text{Ip}\cdots\pi$ interaction in the crystal structure of $[\text{33}](\text{OTf})_2\cdot\text{H}_2\text{O}$.

The structure of $[\text{33}](\text{OTf})_2\cdot\text{H}_2\text{O}$ presents a water molecule in the second coordination sphere linked through intermolecular hydrogen bonding to the coordinated water molecule and two triflate entities. Thus, three different complex cations are connected (see Table 5).

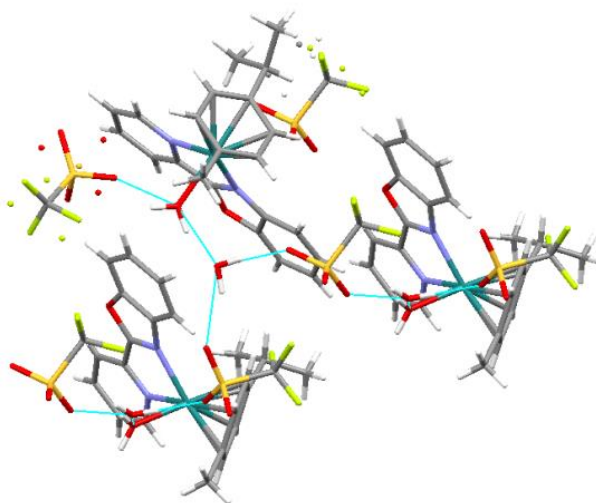
**Fig. 6.** Intermolecular hydrogen bonding showing the connection among ruthenium complexes in the crystal structure of $[\text{33}](\text{OTf})_2\cdot\text{H}_2\text{O}$.

Table 5. Intra and intermolecular hydrogen bonding parameters for [33](OTf)₂·H₂O.

	H-bonding	D···A (Å)	X···A (Å)	D···X (Å)	α (°)
Intramolecular H-bonding	O(2)-H(2B)···O(3)	2.572	1.881	0.854	136.93
	O(2)-H(2A)···O(32)	2.658	1.926	0.865	141.58
	C(21)-H(21B)···F(43)	3.326	2.607	0.961	131.89
	C(41)-F(43)···H(21B)	3.548	2.607	1.330	125.41
	C(19)-H(19B)···O(32)	3.349	2.466	0.959	152.93
Intermolecular H-bonding	O(3)-H(3A)···O(43)	2.744	1.949	0.866	152.04
	O(3)-H(3B)···O(42)	2.785	1.876	0.912	174.14
	C(14)-H(14)···O(42)	3.388	2.521	0.929	155.49
	C(41)-F(42)···O(43)	4.056	2.781	1.311	163.66

1.3. Aqueous Solubility

The aqueous solubility of some complexes (see Table 6) was measured at room temperature (19 – 21 °C). Only the chlorido and aquo complexes are water-soluble, whereas the iodido analogues are slightly soluble, due to the lower [hydration energy](#) of I⁻ compared to that of Cl⁻ (see next page). In this family, the solubility also depends on the bidentate chelating ligand (tbz or pybox). Complexes with the ligand pybox are more water-soluble than those with tbz.

Comparing the complexes [1a]Cl (pybim, in CHAPTER 1) and [31]Cl (pybox), solubility is higher for the former, since the NH group is able to form hydrogen bonds, improving dramatically its solubility in water.

1.4. Aquation-Anation Equilibria

The aquation-anation equilibria of complexes ([28]Cl, [29]I, [31]Cl, [32]I,[30](OTf)₂, [33](OTf)₂) were studied under pseudopharmacological conditions by recording the corresponding ¹H NMR spectra of 3 mM solutions in D₂O at 25 °C, in the absence of NaCl and then in the presence of NaCl (5 or 100 mM as model concentrations for the intracellular and blood plasma conditions, respectively)¹⁹ (see Table 6). Two sets of signals were observed, remaining constant after one hour, which implies a fast equilibration. The more deshielded doublets were assigned to H^{6'} protons of the aqua derivatives (10.20-9.7 ppm) and its chlorido precursor (10.01-9.55 ppm). In the case of the iodo-complexes, only one doublet appeared at 9.49 for [32]I, suggesting that the aquation process is non-existent or extremely slow. In the absence of NaCl only the cloro-complexes undergo aquation, with big differences depending on the ligand. The aquation for complex [28]Cl is approximately 2.3 times higher than for [31]Cl. In the presence of NaCl, the equilibria are shifted to [Ru-Cl]⁺ with very similar aquation values for all the complexes, between moderate (in 5 mM NaCl) and low (in 100 mM NaCl), being completely suppressed for [33](OTf)₂. When analogous complexes with different chelating ligands are compared, for instance [28]Cl and [31]Cl, the aquation extent [Ru-Cl]⁺→[Ru- OH₂]²⁺ are 49.5% and 19.3% for 5 mM NaCl and 14.6% and 8.3% for 100 mM.

Table 6. Solubility Data in water and the aquation-anation ratio at different NaCl concentrations for selected compounds, expressed as a percentage of the aqua derivative in the respective equilibrium mixture of Ru-OH₂ and Ru-Cl complexes in D₂O (3 mM).

Ref.	Compound	Solubility (mM)	% aquation		
			0 mM NaCl	5 mM NaCl	100 mM NaCl
[28]Cl	[(<i>p</i> -cym)RuCl(tbz)]Cl	15.9	69.9	49.5	14.6
[29]I	[(<i>p</i> -cym)RuI(tbz)]I	0.8	0*	0*	0*
[30](OTf) ₂	[(<i>p</i> -cym)Ru(OH ₂)(tbz)](OTf) ₂	12.7	100	60.6	12.5
[31]Cl	[(<i>p</i> -cym)RuCl(pybox)]Cl	27.7	29.7	19.3	8.3
[32]I	[(<i>p</i> -cym)RuI(pybox)]I	1.1	0	0	0
[33](OTf) ₂	[(<i>p</i> -cym)Ru(OH ₂)(pybox)](OTf) ₂	16.6	97.1	36.8	0

* Aquation could not be measured correctly due to its insolubility.

1.5. Hydration Energy

According to the previous results, both the solubility and aquation of the iodido derivatives are almost nonexistent. However, the analogues with chloride are more soluble and dissociate more easily. This curious behaviour could be explained as a consequence of the hydration energy for the halides. When a salt is dissolved in a solvent, the ions are dissociated and then solvated or hydrated (if the solvent is water). For cations the hydration could be described as an ion-dipole interaction, whereas for anions it is also an ion-dipole interaction, but established on the basis of hydrogen bonds.²⁰ The hydration energy is lower for I⁻ than for Cl⁻, following the next decreasing sequence: F⁻>Cl⁻>Br⁻>I⁻ (see Table 7). This parameter is in agreement with the size of the radii. The bigger the radii, the lower the hydration energy. As chloride hydration energy is higher in protic solvents, dissociation of the Ru-Cl bond is more favoured. In this case, the aquation process is favoured with regard to the iodido derivative, and consequently its solubility increases.^{20,21,22}

Table 7. Absolute values of $\Delta_{\text{hyd}}H^\circ$, $\Delta_{\text{hyd}}S^\circ$, $\Delta_{\text{hyd}}G^\circ$ (at 298 K), and ionic radii for selected ions. (Figure adapted from Housecroft, C. E.; Sharpe, A. G. *Inorganic Chemistry*; Second Edition; Pearson Education Limited: Edinburgh, 2005.)²⁰

Ion	$\Delta_{\text{hyd}}H^\circ$ / kJ mol ⁻¹	$\Delta_{\text{hyd}}S^\circ$ / J K ⁻¹ mol ⁻¹	$T\Delta_{\text{hyd}}S^\circ$ / kJ mol ⁻¹ (for T = 298 K)	$\Delta_{\text{hyd}}G^\circ$ / kJ mol ⁻¹	r_{ion} / pm [†]
F ⁻	-504	-150	-45	-459	133
Cl ⁻	-361	-90	-27	-334	181
Br ⁻	-330	-70	-21	-309	196
I ⁻	-285	-50	-15	-270	220

[†]Values of r_{ion} refer to a coordination number of 6 in the solid state.

1.6. Cytotoxic Activity

The cytotoxic activity of some selected complexes has been evaluated in a comparative in vitro MTT cell viability assay after incubation times of 24 h at 37 °C with human lung carcinoma cells (A549). The values (see Table 8) are expressed as the inhibitory potency (IC₅₀) and cisplatin was used as the positive control. The cytotoxicity of free ligands is very low (IC₅₀ > 100 µM). Likewise, the dimeric starting material is inactive in these cell lines according to literature. The complexes tested in the cell line A549 show very low activities. However, the comparison of complexes [28]Cl and [29]I

show that the chloride derivative is more cytotoxic than its iodide analogue, probably owing to the fact that complex **[28]Cl** undergoes aquation, leaving a free position for a possible coordination with DNA or with another target.

Table 8. IC₅₀ (μM, 24 h, 37 °C) values for selected compounds in the cell line A549.

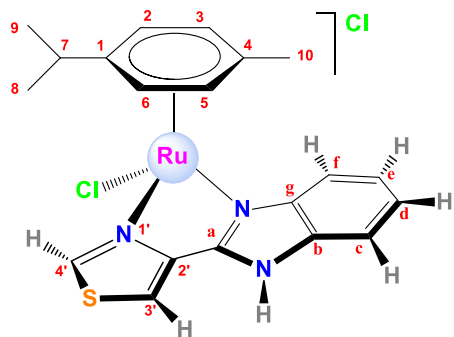
Ref.	Compound	A549
	cisplatin	114.2 ^a
[28]Cl	$[(p\text{-cym})\text{RuCl}(\text{tbz})]\text{Cl}$	>150
[29]I	$[(p\text{-cym})\text{RuI}(\text{tbz})]\text{I}$	440
[32]I	$[(p\text{-cym})\text{RuI}(\text{pybox})]\text{I}$	Unstable

^a. Bibliographic data.²⁴

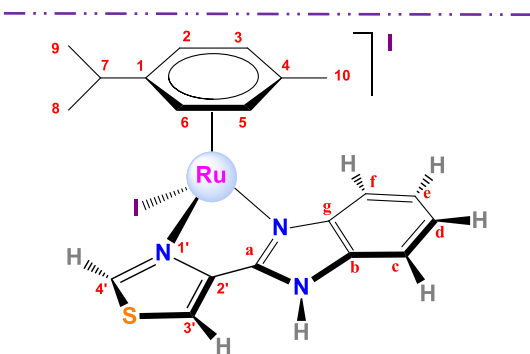
2. CONCLUDING REMARKS

- A new family of 6 new complexes has been synthesised and completely characterised, both in solution and some of them in solid state.
- All the complexes are water-soluble, and follow the next trend: $[\text{Ru-Cl}]^+ > [\text{Ru-OH}_2]^{2+} > [\text{Ru-I}]^+$.
- The chlorido derivatives undergo aquation, whereas the respective iodido complexes are inert against aquation.
- The cytotoxic activity is better for the chlorido derivative **[28]Cl** in comparison to the iodido analogue **[29]I**, though the IC₅₀ values are high in both cases.

3. EXPERIMENTAL SECTION

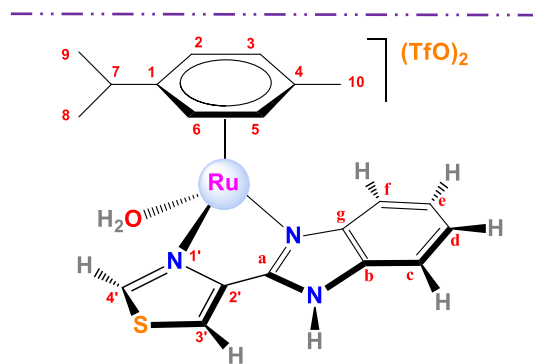


Synthesis of $[(\eta^6\text{-}p\text{-cymene})\text{RuCl}(\kappa^2\text{-}N,N\text{-}tbz)]\text{Cl}$, [28]Cl. In a 100 mL Schlenk flask, the ligand tbz (0.0664 g, 0.330 mmol) was added to a solution of $[\text{RuCl}_2(\text{cym})]_2$ (0.1008 g, 0.165 mmol) in degassed methanol (18 mL), and the mixture was stirred at room temperature for 20 h and under a nitrogen atmosphere. The solution was filtered and concentrated. The product was precipitated with diethyl ether (15 mL) and filtered off. The resulting yellow powder was dried under vacuum. Yield: 114.0 mg (0.225 mmol, 68%). **M_r** ($\text{C}_{20}\text{H}_{21}\text{N}_3\text{SCl}_2\text{Ru}$) = 507.4474 g/mol. **Anal. Calcd for** $\text{C}_{20}\text{H}_{21}\text{N}_3\text{SCl}_2\text{Ru} (\text{H}_2\text{O})_2$: C 44.20; H 4.64; N 7.73; S 5.90; **Found:** C 44.11; H 4.10; N 7.30; S 5.94. **¹H NMR (400 MHz, CDCl₃, 25 °C)** δ 15.29 (s, 1H, H^{N-H}), 10.34 (s, 1H, H^{5'}), 9.41 (s, 1H, H^{3'}), 7.89 – 7.79 (m, 1H, H^c), 7.77 – 7.65 (m, 1H, H^f), 7.50 – 7.38 (m, 2H, H^d, H^e), 6.13 (d, *J* = 4.9 Hz, 1H, H² or H⁶), 6.03 (d, *J* = 5.4 Hz, 1H, H³ or H⁵), 6.00 (d, *J* = 5.7 Hz, 1H, H⁶ or H²), 5.84 (d, *J* = 5.9 Hz, 1H, H⁵ or H³), 2.61 – 2.50 (sept, *J* = 7.0 Hz, 1H, H⁷), 2.23 (s, 3H, H¹⁰), 1.00 (d, *J* = 6.8 Hz, 3H, H⁸ or H⁹), 0.95 (d, *J* = 6.9 Hz, 3H, H⁹ or H⁸) ppm. **¹³C{¹H} NMR (101 MHz, CDCl₃, 25 °C)** δ 160.9 (s, 1C, C^a), 146.2 (s, 1C, C^{2'}), 144.1 (s, 1C, C^{5'}), 140.8 (s, 1C, C^g), 135.0 (s, 1C, C^b), 125.7 (s, 1C, C^d), 124.8 (s, 1C, C^e), 123.5 (s, 1C, C^{3'}), 116.4 (s, 1C, C^f), 115.0 (s, 1C, C^c), 104.0 (s, 1C, C¹), 103.0 (s, 1C, C⁴), 84.7 (s, 1C, C² or C⁶), 82.6 (s, 1C, C³ or C⁵), 82.3 (s, 1C, C⁶ or C²), 80.0 (s, 1C, C⁵ or C³), 31.3 (s, 1C, C⁷), 22.4 (s, 1C, C⁸ or C⁹), 22.3 (s, 1C, C⁹ or C⁸), 19.3 (s, 1C, C¹⁰) ppm. **FT-IR (KBr, cm⁻¹) selected bands:** 3387 (vs, v_{N-H}), 3049-3000-2969 (vs, v_{=CH}, v_{-CH}), 2620 (s), 1624-1609 (m, v_{C=N(imid)}), 1515 (m, v_{C=C}), 1480 (s, v_{C=N(thiaz)}), 1431 (vs), 1329 (vs), 1227 (w, v_{C-S}), 1018 (s, v_{C=S}), 875-842 (s), 765 (vs, δ_{NHoop}), 755 (vs, δ_{CHOop}), 637 (w). **MS (FAB+):** m/z (%) = 472 (56) ([M-Cl]⁺), 436 (22) ([M-2Cl-H]⁺). **Molar Conductivity (H₂O):** 164 S·cm²·mol⁻¹. **Solubility:** soluble in water, methanol, ethanol, dichloromethane, chloroform and acetone.

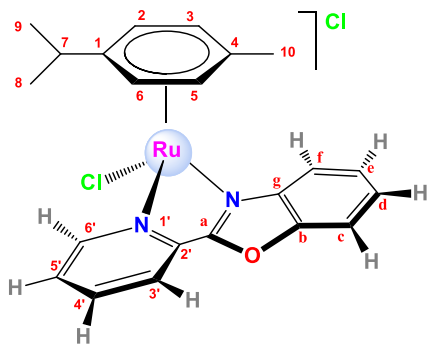


Synthesis of $[(\eta^6\text{-}p\text{-cymene})\text{RuI}(\kappa^2\text{-}N,N\text{-}tbz)]\text{I}$, [29]I. The synthesis was performed as for [28]Cl in the presence of the ligand thiabendazole (0.0340 g, 0.169 mmol) and $[\text{RuI}_2(\text{cym})]_2$ (0.0801 g, 0.082 mmol) in methanol (17 mL). Orange powder. Yield: 98.8 mg (0.143 mmol, 88%). **M_r**

$(C_{20}H_{20}N_3Si_2Ru) = 689.3431$ g/mol. **Anal. Calcd for** $C_{20}H_{20}N_3Si_2Ru \cdot (CH_3OH)_2(H_2O)$: C 34.21; H 4.05; N 5.44; S 4.15; **Found:** C 34.26; H 4.47; N 5.48; S 4.14. **1H NMR (400 MHz, CD₃OD, 25 °C)** δ 10.03 (d, $J = 1.7$ Hz, 1H, H^{5'}), 8.53 (d, $J = 1.8$ Hz, 1H, H^{3'}), 7.93 (dd, $J = 6.7, 2.2$ Hz, 1H, H^f), 7.71 (dd, $J = 6.3, 1.9$ Hz, 1H, H^c), 7.62 – 7.48 (m, 2H, H^d, H^e), 6.15 (d, $J = 5.9$ Hz, 1H, H² or H⁶), 6.09 (d, $J = 6.3$ Hz, 1H, H⁶ or H²), 6.04 – 5.96 (m, 2H, H³, H⁵), 2.75 (sept, $J = 7.0$ Hz, 1H, H⁷), 2.49 (s, 3H, H¹⁰), 1.08 (d, $J = 7.0$ Hz, 3H, H⁸ or H⁹), 1.06 (d, $J = 7.0$ Hz, 3H, H⁹ or H⁸) ppm. **$^{13}C\{^1H\}$ NMR (101 MHz, CD₃OD, 25 °C)** δ 163.1 (s, 1C, C^{5'}), 146.6 (s, 1C, C^{2'}), 144.9 (s, 1C, C³), 142.9 (s, 1C, C^b or C^g), 136.2 (s, 1C, C^g or C^b), 127.0 (s, 1C, C^d), 126.0 (s, 1C, C^e), 122.3 (s, 1C, C^{3'}), 119.0 (s, 1C, C^c), 114.6 (s, 1C, C^f), 108.0 (s, 1C, C⁴), 102.3 (s, 1C, C¹), 85.2 (s, 1C, C⁶ or C²), 83.8 (s, 1C, C³ or C⁵), 83.4 (s, 1C, C² or C⁶), 83.2 (s, 1C, C⁵ or C³), 33.1 (s, 1C, C⁷), 22.6 (s, 1C, C⁸ or C⁹), 22.1 (s, 1C, C⁹ or C⁸), 21.1 (s, 1C, C¹⁰) ppm. **FT-IR (KBr, cm⁻¹) selected bands:** 3435 (s, v_{N-H}), 3052-2963 (vs, v_{=CH}, v_{-CH}), 1607-1591 (w, v_{C=N(imid)}), 1508 (m, v_{C=C}), 1478-1461 (s, v_{C=N(thiaz)}), 1430 (vs), 1322 (vs), 1279 (w, v_{C-S}), 1017 (s, v_{C=S}), 873 (s), 768 (vs, δ_{NHoop}), 755 (s, δ_{CHoop}), 673 (w). **MS (FAB+):** m/z (%) = 564 (15) ([M-I]⁺), 436 (5) ([M-2I]⁺). **Molar Conductivity (H₂O):** N/A, water insoluble. **Solubility:** soluble in methanol, chloroform and acetone. Partially soluble in dichloromethane. Slightly soluble in water.

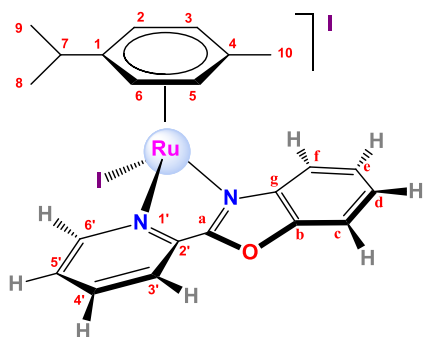


Synthesis of $[(\eta^6-p\text{-cymene})Ru(OH_2)(\kappa^2\text{-}N,N\text{-}tbz)](OTf)_2$, [30](OTf)₂. In a 100 mL Schlenk flask, AgOTf (0.0624 g, 0.243 mmol) was added to a solution of [28]Cl (0.0499 g, 0.098 mmol) in a mixture of water/ethanol (1:1, 6 mL). The slurry was stirred at room temperature for 20 h, under a nitrogen atmosphere and preserved from light. The AgCl was filtered after centrifugation and the solvent was evaporated to dryness. The residue was washed twice with diethylether (10 mL). The resulting yellow powder was dried under vacuum. Yield: not calculated. **M_r** ($C_{22}H_{22}N_3O_7S_3F_6Ru$) = 751.6901 g/mol. **Anal. Calcd for** $C_{22}H_{22}N_3O_7S_3F_6Ru \cdot (AgOTf)_{0.15}(H_2O)_{1.5}$: C 32.51; H 3.20; N 5.14; S 12.34; **Found:** C 32.58; H 3.22; N 5.41; S 12.65. **1H NMR (400 MHz, D₂O, 25 °C)** δ 10.23 (d, $J = 1.9$ Hz, 1H, H^{5'}), 8.55 (d, $J = 1.9$ Hz, 1H, H^{3'}), 8.13 (d, $J = 7.5$ Hz, 1H, H^f), 7.80 (d, $J = 8.2$ Hz, 1H, H^c), 7.66 (td, $J = 8.2, 1.3$ Hz, 1H, H^e), 7.62 (td, $J = 7.5, 1.3$ Hz, 1H, H^d), 6.53 (d, $J = 6.2$ Hz, 1H, H² or H⁶), 6.37 (d, $J = 6.2$ Hz, 1H, H⁶ or H²), 6.29 (d, $J = 6.2$ Hz, 1H, H³ or H⁵), 6.27 (d, $J = 6.5$ Hz, 1H, H⁵ or H³), 2.40 (sept, $J = 6.9$ Hz, 1H, H⁷), 2.21 (s, 3H, H¹⁰), 0.91 (d, $J = 6.9$ Hz, 3H, H⁸ or H⁹), 0.87 (d, $J = 6.9$ Hz, 3H, H⁹ or H⁸) ppm. **$^{19}F\{^1H\}$ NMR (376 MHz, D₂O, 25 °C)** δ -79.40 (s, 6F, FCF₃) ppm. **FT-IR (KBr, cm⁻¹) selected bands:** 3475 (m, v_{N-H}), 3098-2973 (s, v_{=CH}, v_{-CH}), 1629-1598 (w, v_{C=N(imid)}), 1522 (w, v_{C=C}), 1466 (m, v_{C=N(thiaz)}), 1436 (m), 1330 (s), 1284-1249-1226 (vs, v_{C-S}), 1167 (vs, v_{SO₃⁻as}), 1029 (s, v_{SO₃⁻sym}, v_{C=S}), 879-846 (w), 761 (m, δ_{NHoop}), 748 (m, δ_{CHoop}), 638 (vs, δ_{CF_3}), 575 (m), 517 (s). **MS (FAB+):** m/z (%) = 586 (28) ([M-OTf-H₂O]⁺), 452 (5) ([M-2(OTf)-2H]⁺), 436 (100) ([M-2(OTf)-H₂O-H]⁺). **Molar Conductivity (H₂O):** 116 S·cm²·mol⁻¹. **Solubility:** soluble in methanol, ethanol and acetone. Slightly soluble in dichloromethane, chloroform and water.

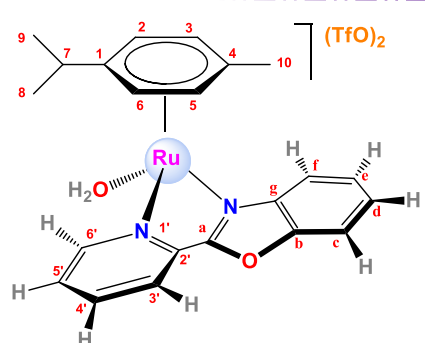


*Synthesis of the ligand 2-(2'-pyridyl)benzoxazole, **pybox**.* In a 100 mL Schlenk flask, 2-pyridylcarboxaldehyde (0.4287 g, 4.00 mmol) was added to a solution of 2-aminophenol (0.4409 g, 4.04 mmol) and molecular sieve (4 g) in ethyl acetate (10 mL). The mixture was stirred at 80 °C for 1 h under a nitrogen atmosphere and then, at 45 °C for 12 h. IBX (2.24 g, 3.60 mmol) was added and the resulting mixture was stirred at 80 °C for 6 h and then, at room temperature for 2 days. The solid was filtered and the product separated by column chromatography using ethyl acetate/hexane (1:1) as the eluent. The product was recrystallized from water/acetone to afford red crystals. The crystals were washed with water and the resulting orange solid was dried under vacuum. Yield: 0.1232 g (0.628 mmol, 16 %).

*Synthesis of $[(\eta^6\text{-}p\text{-cymene})\text{RuCl}(\kappa^2\text{-N,N-pybox})]\text{Cl}$, **[31]Cl**.* The synthesis was performed as for **[28]Cl** in the presence of the ligand pybox (0.0389 g, 0.1983 mmol) and $[\text{RuCl}_2(\text{cym})]_2$ (0.0405 g, 0.0414 mmol) in methanol (12 mL). Green powder. Yield: 57.4 mg (0.1143 mmol, 59%). **M_r** ($\text{C}_{22}\text{H}_{22}\text{N}_2\text{OCl}_2\text{Ru}$) = 502.404 g/mol. **Anal. Calcd for** $\text{C}_{22}\text{H}_{22}\text{N}_2\text{OCl}_2\text{Ru}\cdot(\text{H}_2\text{O})$: C 50.77; H 4.65; N 5.38; **Found:** C 50.80; H 4.50; N 4.98. **¹H NMR** (400 MHz, CDCl_3 , 25 °C) δ 10.45 (s, 1H, $\text{H}^{3'}$), 8.17 (q, J = 7.8 Hz, 2H, H^6 , $\text{H}^{5'}$), 8.10 (d, J = 7.9 Hz, 1H, H^c), 7.99 (s, 1H, H^4'), 7.79 (d, J = 8.1 Hz, 1H, H^f), 7.74 (t, J = 7.5 Hz, 1H, H^d), 7.68 (t, J = 7.8 Hz, 1H, H^e), 6.70 (d, J = 3.9 Hz, 1H, H^2 or H^6), 6.46 (d, J = 3.9 Hz, 1H, H^3 or H^5), 6.36 (d, J = 5.1 Hz, 1H, H^6 or H^2), 6.29 (d, J = 5.0 Hz, 1H, H^5 or H^3), 2.73 (sept, J = 6.8 Hz, 1H, H^7), 2.29 (s, 3H, H^{10}), 1.06 (dd, J = 6.8, 3.9 Hz, 6H, H^8 , H^9) ppm. **¹³C{¹H} NMR** (101 MHz, CDCl_3 , 25 °C) δ 162.1 (s, 1C, C^2'), 160.4 (s, 1C, C^3), 151.0 (s, 1C, C^g), 142.9 (s, 1C, C^3'), 139.8 (s, 1C, C^6), 138.3 (s, 1C, C^b), 130.7 (s, 1C, C^4), 129.3 (s, 1C, C^e), 128.2 (s, 1C, C^d), 124.8 (s, 1C, C^5'), 118.9 (s, 1C, C^c), 113.1 (s, 1C, C^f), 105.9 (s, 1C, C^1), 104.3 (s, 1C, C^4), 86.5 (s, 1C, C^2 or C^6), 83.7 (s, 1C, C^6 or C^2), 83.2 (s, 1C, C^3 or C^5), 81.8 (s, 1C, C^5 or C^3), 31.5 (s, 1C, C^7), 22.49 (s, 1C, C^8 or C^9), 22.47 (s, 1C, C^9 or C^8), 19.5 (s, 1C, C^{10}) ppm. **FT-IR (KBr, cm⁻¹) selected bands:** 3418 (m, $\nu_{\text{O-H}}$), 3047 (m, $\nu_{\text{C-H}}$), 2952 (m, $\nu_{\text{C-H}}$), 1596 (w, $\nu_{\text{C-N}}$), 1565-1552 (m, $\nu_{\text{C=C}}$), 1477-1453 (s, $\nu_{\text{C=N}}$), 1402 (vs), 1263-1253 (w), 1160-1109 (m, $\nu_{\text{C-O-C}}$), 1057-1020 (w, δ_{CHip}), 816-801 (m, $\delta_{\text{C-C}}$), 757 (vs, δ_{CHOop}), 690 (m). **MS (FAB+):** m/z (%) = 467 (57) ($[\text{M-Cl}]^+$), 432 (7) ($[\text{M-2Cl}]^+$). **Molar Conductivity (H₂O):** 79 S·cm²·mol⁻¹. **Solubility:** soluble in methanol, dichloromethane, chloroform and acetone. Partially soluble in water.



Synthesis of $[(\eta^6\text{-}p\text{-cymene})\text{Ru}(\kappa^2\text{-N,N-pybox})]\text{I}$, [32]I. The synthesis was performed as for [28]Cl in the presence of the ligand pybzOx (0.0283 g, 0.1442 mmol) and $[\text{RuI}_2(\text{cym})]_2$ (0.0702 g, 0.0718 mmol) in methanol (2 mL). Red-brown powder. Yield: 72.7 mg (0.1061 mmol, 74%). **M_r** ($\text{C}_{22}\text{H}_{22}\text{N}_2\text{O}\text{I}_2\text{Ru}$) = 685.3076 g/mol. **Anal. Calcd for** $\text{C}_{22}\text{H}_{22}\text{N}_2\text{O}\text{I}_2\text{Ru}\cdot(\text{H}_2\text{O})_{0.7}$: C 37.86; H 3.38; N 4.01; **Found:** C 37.93; H 3.57; N 3.68. **¹H NMR (400 MHz, CDCl₃, 25 °C)** δ 10.04 (d, J = 5.6 Hz, 1H, H^{6'}), 8.25 (d, J = 7.9 Hz, 1H, H^{3'}), 8.16 (td, J = 7.7, 1.0 Hz, 1H, H^{4'}), 7.97 (ddd, J = 7.5, 5.7, 1.5 Hz, 1H, H^{5'}), 7.93 – 7.86 (m, 1H, H^f), 7.86 – 7.79 (m, 1H, H^c), 7.77 – 7.67 (m, 2H, H^d, H^e), 6.50 (d, J = 5.8 Hz, 1H, H² or H⁶), 6.29 (d, J = 6.2 Hz, 2H, H³, H⁵), 6.23 (d, J = 6.8 Hz, 1H, H⁶ or H²), 3.01 (sept, J = 6.9 Hz, 1H, H⁷), 2.50 (s, 3H, H¹⁰), 1.20 (d, J = 6.9 Hz, 3H, H⁸ or H⁹), 1.17 (d, J = 6.9 Hz, 3H, H⁹ or H⁸) ppm. **¹³C{¹H} NMR (101 MHz, CDCl₃, 25 °C)** δ 160.9 (s, 1C, C^{6'}), 160.7 (s, 1C, C^a), 151.0 (s, 1C, C^b), 142.0 (s, 1C, C^{2'}), 139.4 (s, 1C, C^{4'}), 139.1 (s, 1C, C^g), 130.2 (s, 1C, C^{5'}), 129.4 (s, 1C, C^d), 128.0 (s, 1C, C^e), 125.3 (s, 1C, C^{3'}), 118.7 (s, 1C, C^f), 113.4 (s, 1C, C^c), 108.2 (s, 1C, C¹), 102.4 (s, 1C, C⁴), 85.7 (s, 1C, C² or C⁶), 83.7 (s, 1C, C³ or C⁵), 83.6 (s, 1C, C⁵ or C³), 83.4 (s, 1C, C⁶ or C²), 32.5 (s, 1C, C⁷), 22.9 (s, 1C, C⁸ or C⁹), 22.5 (s, 1C, C⁹ or C⁸), 21.1 (s, 1C, C¹⁰) ppm. **FT-IR (KBr, cm⁻¹) selected bands:** 3434 (m, $\nu_{\text{O-H}}$), 3048 (m, $\nu_{\text{C-H}}$), 2958 (m, $\nu_{\text{C-H}}$), 1595 (w, $\nu_{\text{C-N}}$), 1564–1549 (m, $\nu_{\text{C=C}}$), 1475–1448 (s, $\nu_{\text{C=N}}$), 1407 (vs), 1261–1250 (w), 1156–1093 (m, $\nu_{\text{C-O-C}}$), 1054–1021 (w, δ_{CHip}), 815–788 (m, $\delta_{\text{C-C}}$), 752 (vs, δ_{CHoop}), 683 (m). **MS (FAB+):** m/z (%) = 686 (5) ([M]⁺), 559 (48) ([M-I]⁺), 432 (14) ([M-2I]⁺). **Molar Conductivity (H₂O):** 66 S·cm²·mol⁻¹. **Solubility:** soluble in methanol, dichloromethane, chloroform and acetone. Slightly soluble in water.



Synthesis of $[(\eta^6\text{-}p\text{-cymene})\text{Ru}(\text{OH}_2)(\kappa^2\text{-N,N-pybox})]\text{(OTf)}_2$, [33](OTf)₂. In a 100 mL Schlenk flask, AgOTf (0.0669 g, 0.260 mmol) was added to a solution of $[\text{RuCl}_2(\text{cym})]_2$ (0.0284 g, 0.046 mmol) in a mixture water/ethanol (1:1, 16 mL). After stirring 30 min, the ligand 2-(2'-pyridyl)benzoxazole (0.0181 g, 0.092 mmol) was added. The mixture was stirred at room temperature for 20 h, under a nitrogen atmosphere and preserved from light. The AgCl was filtered and the solvent was evaporated to dryness. The residue was washed twice with diethylether (10 mL). The resulting brown-yellow powder was dried under vacuum. Yield: not

calculated. **M_r** (**C₂₄H₂₄N₂O₈S₂F₆Ru**) = 474.6546 g/mol. **Anal.** Calcd for **C₂₄H₂₄N₂O₈S₂F₆Ru·(AgOTf)_{0.2}(H₂O)_{0.5}**: C 35.97; H 3.12; N 3.47; S 8.73; **Found:** C 36.19; H 3.36; N 3.32; S 9.02. **¹H NMR (400 MHz, D₂O, 25 °C)** δ 9.73 (d, *J* = 5.6 Hz, 1H, H^f), 8.52 – 8.39 (m, 2H, H^{4'}, H^{3'}), 8.30 – 8.25 (m, 1H, H^f), 8.04 – 7.96 (m, 2H, H^{5'}, H^d), 7.87 – 7.82 (m, 2H, H^e, H^c), 6.59 (d, *J* = 6.0 Hz, 1H, H² or H⁶), 6.50 (d, *J* = 6.1 Hz, 1H, H⁶ or H²), 6.32 (t, *J* = 6.0 Hz, 2H, H³, H⁵), 2.57 (sept, *J* = 6.9 Hz, 1H, H⁷), 2.20 (s, 3H, H¹⁰), 1.03 (dd, *J* = 6.9, 2.5 Hz, 6H, H⁸, H⁹) ppm. **¹⁹F{¹H} NMR (376 MHz, D₂O, 25 °C)** δ -78.9 (s, 6F, F^{CF₃}) ppm. **¹³C{¹H} NMR (101 MHz, D₂O, 25°C)** δ 157.4 (s, 1C), 157.1 (s, 1C), 143.8 (s, 1C), 142.6 (s, 1C), 142.4 (s, 1C), 141.5 (s, 1C), 140.3 (s, 1C), 138.2 (s, 1C), 130.9 (s, 1C), 130.2 (s, 1C), 128.6 (s, 1C), 126.7 (s, 1C), 124.2 (s, 1C), 118.9 (s, 1C), 113.8 (s, 1C), 104.2 (s, 1C, C⁴), 102.8 (s, 1C, C¹), 86.5 (s, 1C, C² or C⁶), 84.7 (s, 1C, C⁶ or C²), 83.0 (s, 1C, C³ or C⁵), 81.4 (s, 1C, C⁵ or C³), 31.3 (s, 1C, C⁷), 21.8 (s, 1C, C⁸ or C⁹), 21.7 (s, 1C, C⁹ or C⁸), 18.4 (s, 1C, C¹⁰) ppm. **FT-IR (KBr, cm⁻¹) selected bands:** 3447 (m, ν_{O-H}), 3077 (m, ν_{=CH}), 2954-2924 (s, ν_{-CH}), 1637 (m, ν_{H-O-H}), 1600 (w, ν_{C-N}), 1569-1551 (m, ν_{C=C}), 1479-1466-1451 (m, ν_{C=N}), 1418 (s), 1288-1245-1225 (vs, ν_{C-F}), 1158 (vs, ν_{SO₃⁻as}), 1058 (w, δ_{CHip}), 1030 (vs, ν_{SO₃⁻sym}), 817-793 (m, δ_{C-C}), 758-745 (s, δ_{CHOop}), 637 (vs, δ_{CF₃}), 515 (m). **MS (FAB+):** m/z (%) = 432 (5) ([M-(OTf)₂-H₂O]⁺). **Molar Conductivity (H₂O):** 139 S·cm²·mol⁻¹. **Solubility:** soluble in water.

4. BIBLIOGRAPHY

- (1) He, X.-F.; Vogels, C. M.; Decken, A.; Westcott, S. A. *Polyhedron* **2004**, *23*, 155–160.
- (2) Czerwieniec, R.; Kapturkiewicz, A.; Lipkowski, J.; Nowacki, J. *Inorganica Chim. Acta* **2005**, *358*, 2701–2710.
- (3) Ogweno, A. O.; Ojwach, S. O.; Akerman, M. P. *Dalt. Trans.* **2014**, *43*, 1228–1237.
- (4) Chanda, N.; Paul, D.; Kar, S.; Mobin, S. M.; Datta, A.; Puranik, V. G.; Rao, K. K.; Lahiri, G. K. *Inorg. Chem.* **2005**, *44*, 3499–3511.
- (5) Ogweno, A. O.; Ojwach, S. O.; Akerman, M. P. *Appl. Catal. A Gen.* **2014**, *486*, 250–258.
- (6) Devereux, M.; O Shea, D.; Kellett, A.; McCann, M.; Walsh, M.; Egan, D.; Deegan, C.; Kędziora, K.; Rosair, G.; Müller-Bunz, H. *J. Inorg. Biochem.* **2007**, *101*, 881–892.
- (7) Wisniewski, M. Z.; Glowiāk, T.; Opolski, A.; Wietrzyk, J. *Met. drugs* **2001**, *8*, 189–194.
- (8) Bennett, M. A.; Smith, A. K. *J. Chem. Soc. Dalt. Trans.* **1974**, 233–241.
- (9) Therrien, B. *Coord. Chem. Rev.* **2009**, *253*, 493–519.
- (10) Mendoza-Ferri, M. G.; Hartinger, C. G.; Nazarov, A. A.; Eichinger, R. E.; Jakupcic, M. A.; Severin, K.; Keppler, B. K. *Organometallics* **2009**, *28*, 6260–6265.
- (11) Angelici, R. J. In *Técnicas y Síntesis en Química Inorgánica*; Editorial Reverté, S.A., **1979**; p. 243.
- (12) Dinnebier, R.; Sofina, N.; Jansen, M. *Zeitschrift für Anorg. und Allg. Chemie* **2004**, *630*, 1613–1616.
- (13) Clayden, J.; Greeves, N.; Warren, S.; Wothers, P. *Organic Chemistry*; First.; OXFORD University Press: New York, **2001**.
- (14) Hay, B. P.; Custelcean, R. *Cryst. Growth Des.* **2009**, *9*, 2539–2545.
- (15) Schottel, B. L.; Chifotides, H. T.; Dunbar, K. R. *Chem. Soc. Rev.* **2008**, *37*, 68–83.
- (16) Egli, M.; Sarkhel, S. *Acc. Chem. Res.* **2007**, *40*, 197–205.
- (17) Suárez-Moreno, G. V.; González-Zamora, E.; Méndez, F. *Org. Lett.* **2011**, *13*, 6358–6361.
- (18) Boger, D. L. *Chem. Rev.* **1986**, *86*, 781–793.
- (19) Martin, R. B. In *Cisplatin Chemistry and Biochemistry of a Leading Anticancer Drug*; Verlag Helvetica Chimica Acta: Zürich, **2006**; pp. 181–205.
- (20) Housecroft, C. E.; Sharpe, A. G. *Inorganic Chemistry*; Second.; Pearson Education Limited: Edinburgh, **2005**.
- (21) Marcus, Y. *J. Chem. Soc. Faraday Trans.* **1991**, *87*, 2995–2999.
- (22) Romero-Canelón, I.; Salassa, L.; Sadler, P. J. *J. Med. Chem.* **2013**, *56*, 1291–1300.
- (23) Khang, G. N.; Sai, C. L. *Singapore J. Educ.* **1980**, *3*, 27–31.
- (24) Gutiérrez, A.; Cativiela, C.; Laguna, A.; Gimeno, M. C. *Dalt. Trans.* **2016**, *45*, 13483–13490.

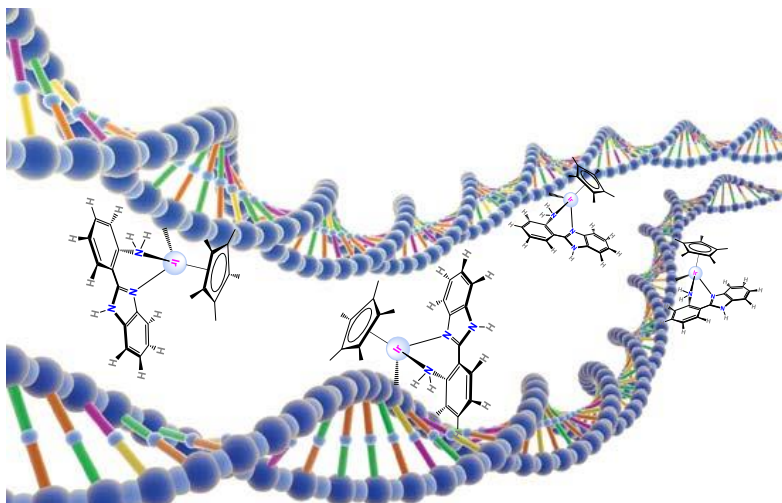
CHAPTER 6.

Ir(III) HALF-SANDWICH COMPLEXES BEARING ARYLBENZAZOLE ANCILLARY LIGANDS: SYNTHESIS, CHARACTERIZATION AND ANTICANCER PROPERTIES



CHAPTER 6. Ir(III) HALF-SANDWICH COMPLEXES BEARING ARYLBENZAZOLE ANCILLARY LIGANDS: SYNTHESIS, CHARACTERIZATION AND ANTICANCER PROPERTIES

ABSTRACT: In this chapter a family of 12 new Ir(III) half-sandwich complexes of general formula $[\text{Ir}(\eta^5\text{-Cp}^*)(\kappa^2\text{-N,N-HL})\text{X}]\text{Y}$ or $[\text{Ir}(\eta^5\text{-Cp}^*)(\kappa^2\text{-O,N-L})\text{X}]\text{Y}$ (X = leaving group; Y = counterion) bearing the different N,N- and N,O-ligands (pybim, pyim, pyMebim, pybox, tbz, apbim, apbtz, hpbim and hpbtz) was prepared in order to compare their cytotoxicity with that of the corresponding ruthenium derivatives. That is, to check the effect of changing the metal fragment on the anticancer properties.



CONTEXT: Iridium(III) complexes have been much less explored as anticancer drugs than their ruthenium(II) congeners, probably because in general, Ir(III) derivatives are commonly too inert. Nonetheless, the negatively charged pentamethylcyclopentadienyl ligand turns half-sandwich complexes of the type $[\text{Ir}(\eta^5\text{-Cp}^*)(\text{N}^{\text{N}})\text{Cl}]^+$ into much more reactive species regarding substitution process.^{1,2} Thus, they offer promising alternatives to half-sandwich ruthenium drugs. Furthermore, the benzimidazole-derivative ligands have been slightly used in this kind of complexes: only some aqua derivatives with pybim and pyim have been tested as catalysts³ and some substituted pybim ligands have been employed to prepare anticancer metallo-drugs by J. Ruiz⁴.

1. RESULTS AND DISCUSSION

1.1. Synthesis

The complexes were synthesised from the iridium chlorido-bridged dimer $[\text{Ir}(\eta^5\text{-Cp}^*)(\mu\text{-Cl})\text{Cl}]_2$, prepared in turn by reaction of the iridium chloride salt ($\text{IrCl}_3\cdot n\text{H}_2\text{O}$) with 1,2,3,4,5-pentamethylcyclopentadiene (see CHAPTER 2).

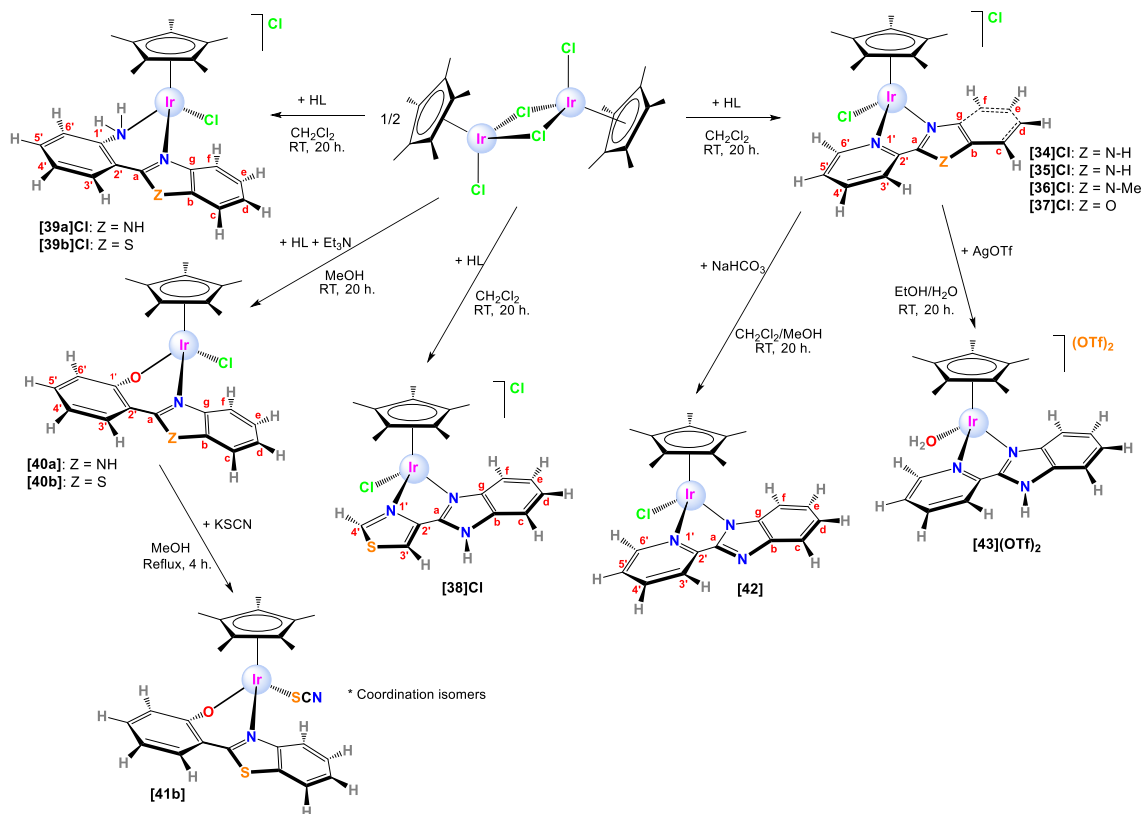


Fig. 1. Schematic synthesis of the half-sandwich iridium(III) complexes

Most complexes, whose schematic synthesis is shown in Fig. 1, are cationic except four of them which are neutral, and a dicationic aquo complex.

Monocationic complexes

The chlorido derivatives of general formula $[(\eta^5\text{-Cp}^*)\text{IrCl}(\kappa^2\text{-N,N-HL})]\text{Cl}$ ($[\text{34}]\text{Cl}$, $[\text{35}]\text{Cl}$, $[\text{36}]\text{Cl}$, $[\text{37}]\text{Cl}$, $[\text{38}]\text{Cl}$, $[\text{39a}]\text{Cl}$ and $[\text{39b}]\text{Cl}$), where HL=ligand, were synthesised by the reaction between the corresponding iridium(III) chlorido-bridged dimer and the ligands (pybim, pim, pybox, tbz, apim and apbtz) in dichloromethane at room temperature and stirring overnight. Derivatives of complexes $[\text{34}]^+$ and $[\text{35}]^+$ bearing PF_6^- as the counterion were reported by Kollipara.⁵ Recently, during the progress of this work, complex $[\text{39a}]\text{Cl}$ was reported by D. S. Pandey.⁶

Dicationic complex

The aquo complex of formula $[(\eta^5\text{-Cp}^*)\text{Ir}(\kappa^2\text{-N,N-}\text{HL})(\text{OH}_2)](\text{OTf})_2$ (**[43](OTf)₂**), was synthesised by the reaction of the neutral complex **[34]Cl** with an excess of AgOTf in a mixture of distilled water and ethanol. This aquo complex was reported in the literature as the disulphate salt by Himeda.³

Neutral complexes

The neutral complexes of general formula $[(\eta^5\text{-Cp}^*)\text{IrCl}(\kappa^2\text{-O,N-L})]$ (**[40a]** and **[40b]**), where L is the deprotonated ligand (hpbitm or hpbtz), were prepared by a similar protocol in the presence of Et₃N and using methanol as the solvent. The thiocyanate derivative of formula $[(\eta^5\text{-Cp}^*)\text{Ir}(\kappa^2\text{-O,N-L})(\text{SCN})]$ (**[41b]**) was synthesized by a metathesis reaction of **[40b]** with an excess of KSCN at 70 °C. The reaction of **[34]Cl** with a weak base (Na₂CO₃) at room temperature in a dichloromethane/methanol mixture yielded the neutral complex **[42]** of formula $[(\eta^5\text{-Cp}^*)\text{IrCl}(\kappa^2\text{-N,N-L})]$, where L is the deprotonated pybim ligand.

All the complexes were isolated in moderate-to-good yields (from 38% to 98%) as the corresponding racemates (R_{Ir} or S_{Ir}) in the form of yellow, orange or brown powders.

1.2. Characterization

All complexes have been fully characterised by NMR spectroscopy, IR spectroscopy, positive fast atom bombardment (FAB⁺) mass spectrometry, molar conductivity and elemental analysis.

1.2.1. NMR

The ¹H NMR spectra of the complexes were recorded in CDCl₃, DMSO-d₆ or D₂O at 25 °C. The coordination of the corresponding ligands to the metal centre was proved taking into account that some signals were deshielded with respect to those of the free ligands. The spectra showed the same characteristic areas as those found for the analogous Ru complexes, except for an intense singlet (15 H) at around 1.4–1.8 ppm, attributed to the methyl groups of the Cp^{*} (all the -Me groups are equivalent in solution by rotation). Furthermore, the compounds had *a priori* the same peculiarities as their Ru analogues: the hydrogen of the NH group of the benzimidazole moiety was very downfield-shifted; the hydrogens of the NH₂ group of aminophenylbenzazoles were also inequivalent; and there was no resonance for the OH group of hydroxyphenylbenzazole ligands, all of which evidenced the metal-ligand coordination. In addition, complexes **[39b]Cl**, **[40a]** and **[40b]** underwent substitution of the chloride, when dissolved in DMSO (see CHAPTER 4).

The ¹H NMR spectrum of the neutral complex **[41b]** in CDCl₃ (see Fig. 2) showed the two possible coordination isomers (thiocyanate and isothiocyanate). Though most of the signals were coincident or appeared very close one to another, only those of the

methyls of the Cp* were completely separated, which allowed us to measure the percentage of each of the species (56.7% - 43.3%). For instance, H^f appeared as a triplet when it was actually a mixture of the two doublets corresponding to the two isomers.

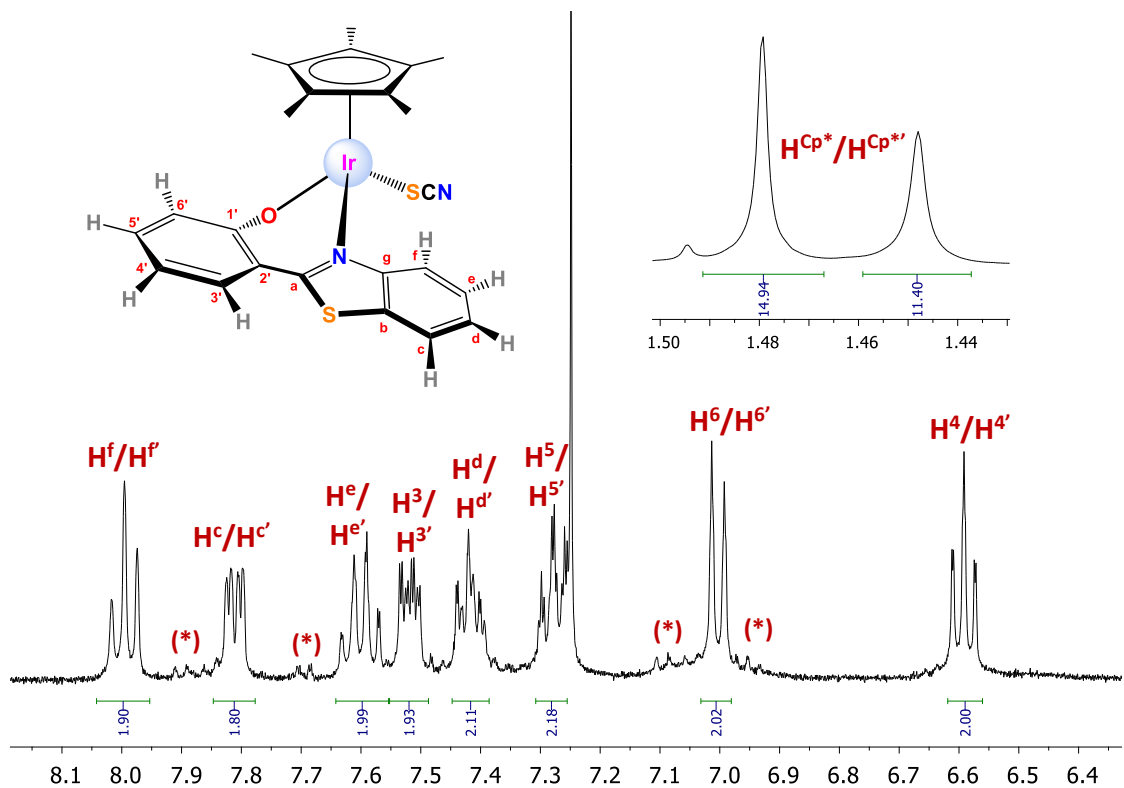


Fig. 2. ¹H-NMR spectrum of [41b] in CDCl₃ at 25 °C showing the signals of the two coordination isomers (-NCS/-SCN), and the integration of the signals. (*) Unknown impurity.

The ¹H-¹H NOESY spectra of the complexes displayed some NOE cross peaks between the methyl groups of the Cp* and the hydrogen atoms of the ancillary ligand, which are near in the space. Chemical exchange peaks were only detected for those complexes involving NH or NH₂ and H₂O.

Regarding ¹³C{¹H} NMR, it showed the characteristic areas of the Cp*. The quaternary carbons appeared at 84–93 ppm, whereas the primary ones were closed to 10 ppm. Table 1 gathers the carbon resonances for all the complexes. All of them are very similar with the exception of those for complexes [39a]Cl (with an unusually low value for C^{Cp(Me)}), [40a] (with a very high value for C^{CpC}) and [40b] (with an uncommon low value for C^{CpC}). In addition, the spectrum of the thiocyanato-complex [41b] did not show the quaternary carbon resonance for the SCN⁻, due to its poor quality.

Table 1. Chemical shifts in ppm of the carbon atoms of Cp* for the different complexes in divergent solvents.

Comp.	[34]Cl	[35]Cl	[36]Cl	[37]Cl	[38]Cl	[39a]Cl	[39b]Cl	[40a]	[40b]	[42]	[43] (OTf) ₂
C ^{CpC}	88.3	88.9	87.9	89.8	87.9	86.0	87.8	93.1	84.6	87.9	89.4
C ^{Cp(Me)}	9.7	9.8	9.9	10.2	9.9	8.1	9.3	8.5	9.2	9.2	9.3

A ¹⁹F{¹H} NMR spectrum was recorded for the dicationic complex [43](OTf)₂, with OTF⁻ as the counterion. As in previous complexes, a singlet was observed at -79.3 ppm.

1.2.2. Mass Spectra

The FAB⁺ mass spectra of the complexes exhibit characteristic sets of peaks according to isotopic distribution patterns. [M]⁺ fragments were detected for neutral complexes and [M-Y]⁺ fragments for the monocationic ones, where Y is the counterion and a fragment with a water molecule for the aquo derivative.

1.2.3. IR Spectra

Infrared spectra confirm characteristic peaks for the normal vibrational modes of the corresponding rings $\nu_{C=N}$, $\nu_{C=C}$ and δ_{CHoop} , besides ν_{C-S} , $\nu_{C=S}$ for thiabendazole, ν_{NH} and ν_{NH_2} for aminophenylbenzazoles and ν_{C-O} for hydroxyphenylbenzazole ligands. The thiocyanate derivative shows characteristic peaks at 2098 cm⁻¹ (ν_{C-N}) and 750 cm⁻¹ (ν_{C-S}). The aquo complex shows very strong and diagnostic peaks for triflate, ν_{C-F} , ν_{SO_3-as} , ν_{SO_3-sym} at 1286-1235-1221, 1178-1156 and 1029 cm⁻¹ respectively (see experimental section for further details).

1.2.4. Molar Conductivity

Molar conductivity (Λ_M) for the complexes was measured in acetonitrile (10⁻³ M), since some of them were insoluble in water. The values, gathered in Table 2, do not correctly reflect the 1:1 electrolyte nature of monocationic complexes,⁷ being all of the conductivities below the normal range with the exception of that for **[36]Cl**. However, some tendencies and conclusions can be established. Among the cationic complexes, all those with the benzimidazole moiety present extremely lower values (27.1 – 50.6 S·cm²·mol⁻¹) than those with benzothiazole or benzoxazole. The NH group is prone to participating in hydrogen bonding interactions, promoting the formation of ion-pairing with chloride, which is favoured in apolar solvents of low dielectric constant or in a protic solvent. Dielectric constants are key parameters to determine ion-pairing. The complexes with benzoxazole and benzothiazole moieties (79.6 – 89.4 S·cm²·mol⁻¹) have intermediate values, as they are also able to form ion pairing; **[37]Cl** through the O atom, and **[39b]Cl** through the NH₂ group. Nonetheless, in complex **[36]Cl** (140.9 S·cm²·mol⁻¹) the N-Me unit prevents the N atom from taking part in hydrogen bonding interactions. Therefore, its molar conductivity value is in the normal range. Regarding the neutral complexes and just as expected, they have the lowest conductivities (10.5 – 19.0 S·cm²·mol⁻¹), with the exception of **[41b]** (28.1 S·cm²·mol⁻¹), whose value is slightly elevated for a non-electrolyte.

Table 2. Molar conductivity values for complexes measured in acetonitrile.

Complex	Solvent	Λ_m (S·cm ² ·mol ⁻¹)
[34]Cl	acetonitrile	27.1
[35]Cl	acetonitrile	34.6
[36]Cl	acetonitrile	140.9
[37]Cl	acetonitrile	89.4
[38]Cl	acetonitrile	35.4
[39a]Cl	acetonitrile	50.6
[39b]Cl	acetonitrile	79.6
[40a]	acetonitrile	insoluble
[40b]	acetonitrile	10.5
[41b]	acetonitrile	28.1
[42]	acetonitrile	19.0

1.2.5. Elemental Analysis

Elemental analysis was performed for all complexes.

1.2.6. X Ray Diffraction

Single crystals suitable for X-ray diffraction analysis were obtained for [34]Cl·2H₂O, [39a]Cl·H₂O and [40b], by slow evaporation of solvents: methanol/acetone, methanol/water and methanol/dichloromethane, respectively. The structure of [39a]Cl was reported by A. Kumar et al. in 2016⁶, during the realization of this work.

The ORTEP diagrams for all the complexes are represented in Fig. 3 and the unit cells show the expected two possible enantiomers (R_{Ir} and S_{Ir}) with the pseudooctahedral three-legged piano-stool geometry and the iridium π-bonded to a η⁵-Cp*. The Ir-centroid distances are in a similar range (1.790-1.766 Å) with the shortest distance for the neutral complex [40b] (1.766 Å). They are even shorter than other similar complexes reported in the literature.^{8,9} The Ir-Cl distances (2.385-2.405 Å) are as well in a similar range as those in the literature.^{8,9} The Ir-N(bim or btz) distances fall in a narrow interval (2.088-2.098 Å), whereas the Ir-N/O(pyridyl, aminophenyl or hydroxyphenyl) distances are longer (2.110-2.140 Å).

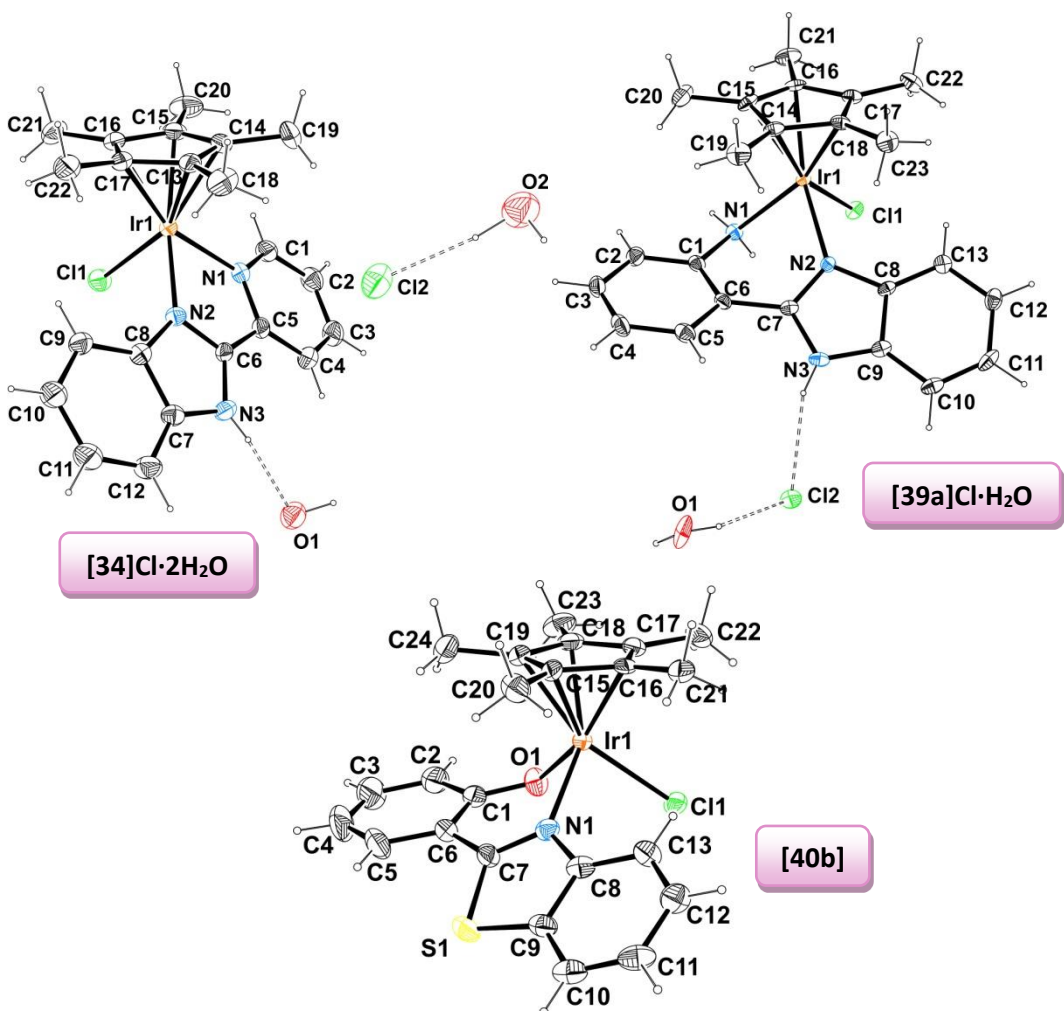


Fig. 3. ORTEP diagrams for complexes $[34]\text{Cl}\cdot 2\text{H}_2\text{O}$, $[39\text{a}]\text{Cl}\cdot \text{H}_2\text{O}$ and $[40\text{b}]$. Ellipsoids are shown at 30% probability.

The N-Ir-X ($\text{X} = \text{N}$ or O) angles ($78\text{--}80^\circ$) of the chelate rings are determined by the features of the corresponding free bidentate ligands. Although this angle is different for each compound, they tend to be bigger than those of the Ru(II) congeners ($76\text{--}77^\circ$).^{10,11}

Table 3. Selected bond lengths (\AA) and angles ($^\circ$) for complexes $[34]\text{Cl}\cdot 2\text{H}_2\text{O}$, $[39\text{a}]\text{Cl}\cdot \text{H}_2\text{O}$ and $[40\text{b}]$.

<i>Distance/ angle</i>	$[34]\text{Cl}\cdot 2\text{H}_2\text{O}$	<i>Distance/ angle</i>	$[39\text{a}]\text{Cl}\cdot \text{H}_2\text{O}$	<i>Distance/ angle</i>	$[40\text{b}]$
Ir1-Cl1	2.3914(12)	Ir1-Cl1	2.4048(12)	Ir1-Cl1	2.3847(11)
Ir1-N2	2.088(3)	Ir1-N2	2.090(4)	Ir1-N1	2.098(4)
Ir1-N1	2.136(4)	Ir1-N1	2.140(4)	Ir1-O1	2.110(3)
-	-	N1-C1	1.456(6)	O1-C1	1.312(6)
N2-C6	1.345(5)	N2-C7	1.331(6)	N1-C7	1.311(6)
N3-C6	1.336(6)	N3-C7	1.348(6)	S1-C7	1.741(5)
N1-Ir1-N2	78.28(14)	N1-Ir1-N2	80.34(15)	O1-Ir1-N1	81.77(14)
N1-Ir1-Cl1	87.41(10)	N1-Ir1-Cl1	83.14(12)	O1-Ir1-Cl1	85.20(10)
N2-Ir1-Cl1	84.29(10)	N2-Ir1-Cl1	84.35(11)	N1-Ir1-Cl1	86.62(11)

Table 4. Selected geometric parameters^[a] for the metal complexes of [34]Cl·2H₂O, [39a]Cl·H₂O and [40b].

<i>Distance/angle</i>	[34]Cl·2H ₂ O	[39a]Cl·H ₂ O	[40b]
<i>Range of Ir-C distances</i>	2.153(4)-2.179(4)	2.132(4)-2.167(5)	2.137(4)-2.154(4)
<i>Ir-centroid</i>	1.790	1.774	1.766
α	11.75	30.95	27.27
ϑ (<i>N-C-C-X</i>) (<i>X=N,C</i>)	-2.33	30.47	25.08
β (<i>chelate-Cp*</i>)	49.39	14.73	15.81
λ	6.74	44.79	42.87

[a]Calculated with Mercury, version 3.8.

The complex **[34]Cl·2H₂O** exhibits two water molecules in the second coordination sphere, connected through hydrogen bonding to the NH group of the benzimidazole unit (N-H···O), and the chloride counterion (O-H···Cl). It is remarkable that the chelate ligands present a light curvature. Moreover, the coordinated chloride links both enantiomers through a weak hydrogen bond (C-H···Cl). Fig. 4 displays both interactions.

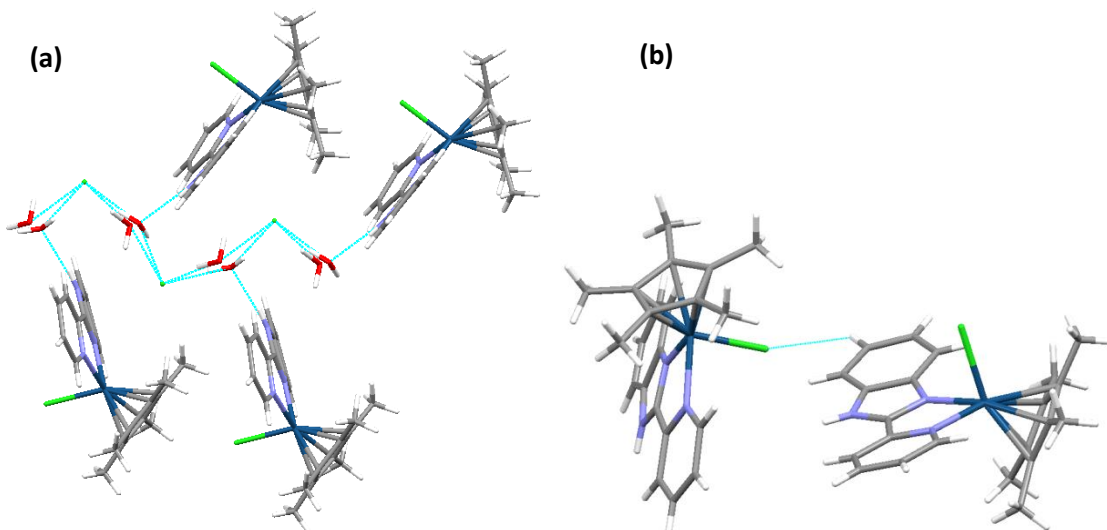


Fig. 4. (a) Motifs in the 3D architecture of [34]Cl·2H₂O showing the aquo-chloro bridges through hydrogen bonding and (b) C-H···Cl interaction between enantiomers.

The complex **[39a]Cl·H₂O** displays a water molecule in the second coordination sphere, which connects the chloride counterion and a second water molecule. Furthermore, the water molecules link the complexes through weak hydrogen bonds. The chloride counterion acts as a bridge between the NH group of a molecule and one H of the NH₂ groups. The other hydrogen stays unlinked. The architecture of the crystal is based on hydrogen bonding (see Fig. 5a) and C-H···π interactions (see Table 7). The latter are built among some methyl hydrogens and the aromatic rings of the benzimidazole (see Fig. 5b).

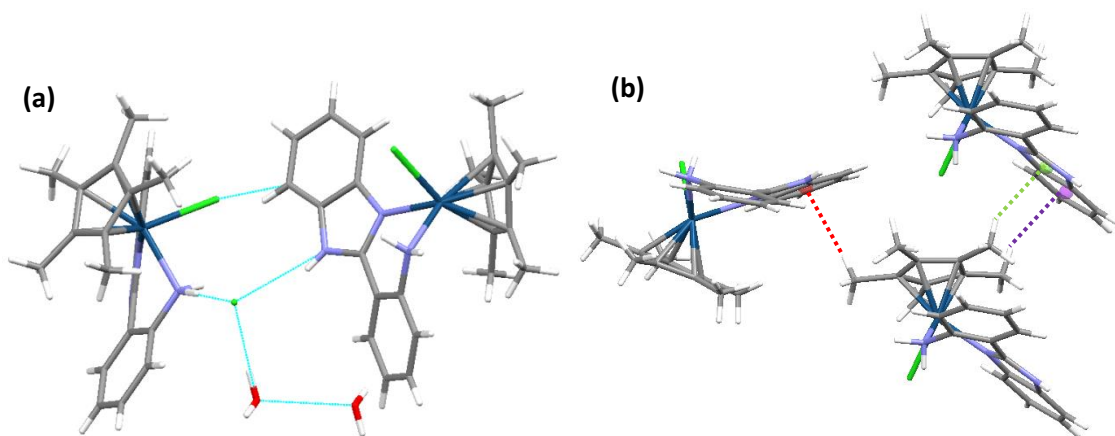


Fig. 5. Motifs in the crystal structure of [39a]Cl·H₂O: (a) Hydrogen bonding among the polar groups, the counterion and the water molecule and (b) C-H···π interactions between the Cp* ring and the benzimidazole moieties.

The 3D structure of complex **[40b]** is built on the basis of strong hydrogen bonding and weak (C-H···π and π-π stacking) interactions (see Fig. 6a). In addition, the nature of the hydrogen bonds is both intramolecular and intermolecular (see Table 5). The π-π stacking between the Cp* and the phenyl ring of benzothiazole moiety (see Fig. 6b) is reinforced by the C-H···π interactions of the methyl groups of Cp* (see Table 6 and Table 7). Although these interactions are unusual and weak, some examples involving Cp* in complexes with other metal ions have been reported in the literature.^{12,13,14,15}

Table 5. Intra- and intermolecular hydrogen bonding for complex [40b].

	H-bonding	D···A (Å)	X···A (Å)	D···X (Å)	α (°)
Intramolecular H-bonding	C(13)-H(13)···Cl(1)	2.797	3.311	0.930	115.92
Intermolecular H-bonding	C(10)-H(10)···O(1)	2.476	3.385	0.931	165.62
	C(11)-H(11)···Cl(1)	2.731	3.450	0.929	134.85
	C(21)-H(21C)···Cl(1)	2.817	3.490	0.960	127.89
	C(20)-H(20A)···Cl(1)	2.941	3.553	0.960	122.76

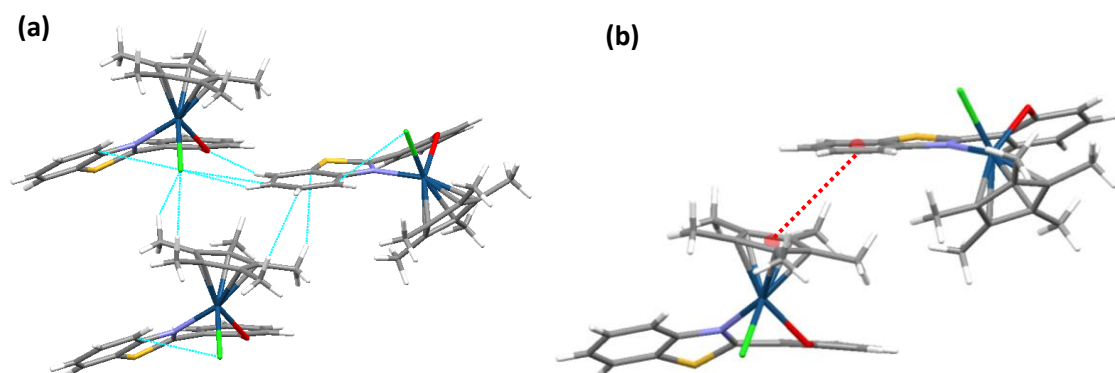


Fig. 6. (a) Hydrogen bonding and weak interactions in the 3D architecture of [40b] and (b) π-π stacking between Cp* and the benzothiazole moiety.

Table 6. π - π offset stacking parameters for complex [40b].

Compound	$d_{\text{cent-cent}}$ (Å)	α (°)	$d_{\text{cent-pl}}$ (Å)	β (°)	d_{offset} (Å)
[40b]	4.428	12.11	3.063	46.23	3.198
			3.661	34.23	2.491

Table 7. Parameters of C-H \cdots π interactions for complexes [39a]Cl and [40b].

Compound	$d_{\text{C-cent}}$ (Å)	$d_{\text{H-cent}}$ (Å)	$d_{\text{C-H}}$ (Å)	$\angle \text{C-H-cent}$ (°)	$\angle \text{H-cent-normal}$ (°)
[39a]Cl \cdot H ₂ O C(21)-H(21A) \cdots π	3.839	2.887	0.961	171.12	163.28
[39a]Cl \cdot H ₂ O C(23)-H(23A) \cdots π	3.647	2.768	0.960	152.53	170.37
[39a]Cl \cdot H ₂ O C(19)-H(19A) \cdots π	3.715	2.863	0.960	148.36	160.39
[40b] C(23)-H(23A) \cdots π	3.842	3.220	0.959	124.20	152.30

1.3. Aquation-Anation Equilibria

The aquation-anation equilibria were studied for complexes [34]Cl and [36]Cl under pseudopharmacological conditions by recording the corresponding ¹H NMR spectra of a 5 mM solution in D₂O at 25 °C, in the absence of NaCl and then in the presence of NaCl (100 mM as model concentrations for blood plasma conditions and only for [34]Cl).

When the complexes were dissolved in water (see Fig. 7), the signals did not shift, so only two interpretations are possible: either the aquation process is extremely fast or the aquation reaction does not occur. The addition of NaCl to [34]Cl (see Fig. 7a) did not shift the signals either, which *a priori* confirmed the last hypothesis, although some solid precipitated due to the common-ion effect.

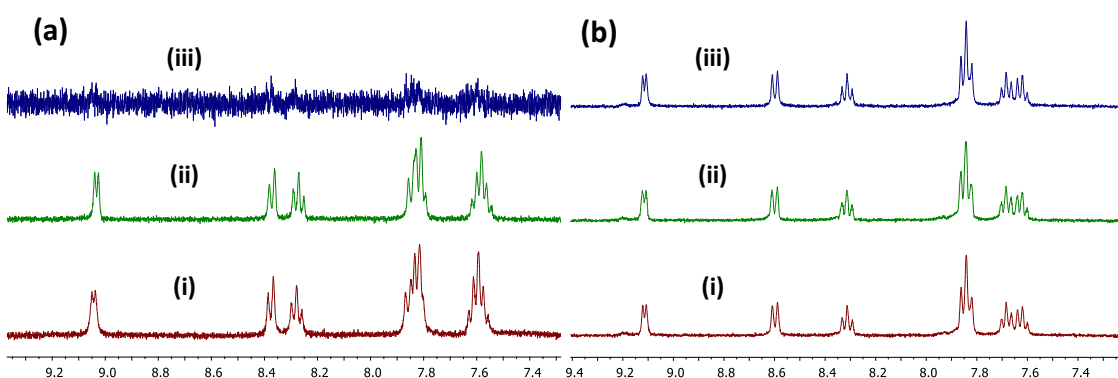


Fig. 7. (a) Aquation-anation equilibrium for [34]Cl: (i) spectrum of [34]Cl in D₂O after 30 min, (ii) spectrum after addition of NaCl 100 mM and (iii) after 23 h. (b) Aquation process for [36]Cl after (i) 5 min, (ii) 15 min and (iii) 30 min.

In order to support one of these theories, extra experiments were performed. Over 5 mM solutions of the complexes ([34]Cl and [36]Cl), 2.5 μ L DCl (1M) was added,

confirming again that aquation was not taken place (see Fig. 8). Then, increasing amounts (step 2.5 μ L) of NaOH (0.5 M in D₂O) were added to check the reversibility of the process.

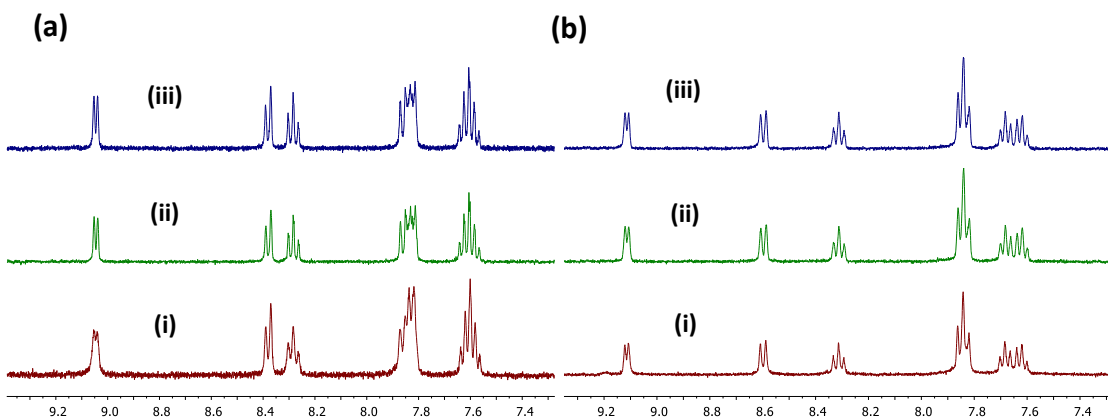


Fig. 8. (a) Addition of DCI to a solution of [34]Cl (i) at t=0, (ii) t=5 min and (iii) t=20 min. (b) Addition of DCI to a solution of [36]Cl (i) at t=0, (ii) t=5 min and (iii) t=10 min.

As far as the complex [34]Cl is concerned, the evolution of the sample when adding NaOH (see Fig. 9) followed different steps. After the first 5 μ L, no changes were observed, since the base is initially consumed in the neutralization of the excess acid content. Afterwards, the peaks decreased and shifted upfield, and a precipitate appeared. When 12.5 μ L were added, a new set of shielded signals began to grow and the addition of extra NaOH did not show more changes (see Fig. 11a).

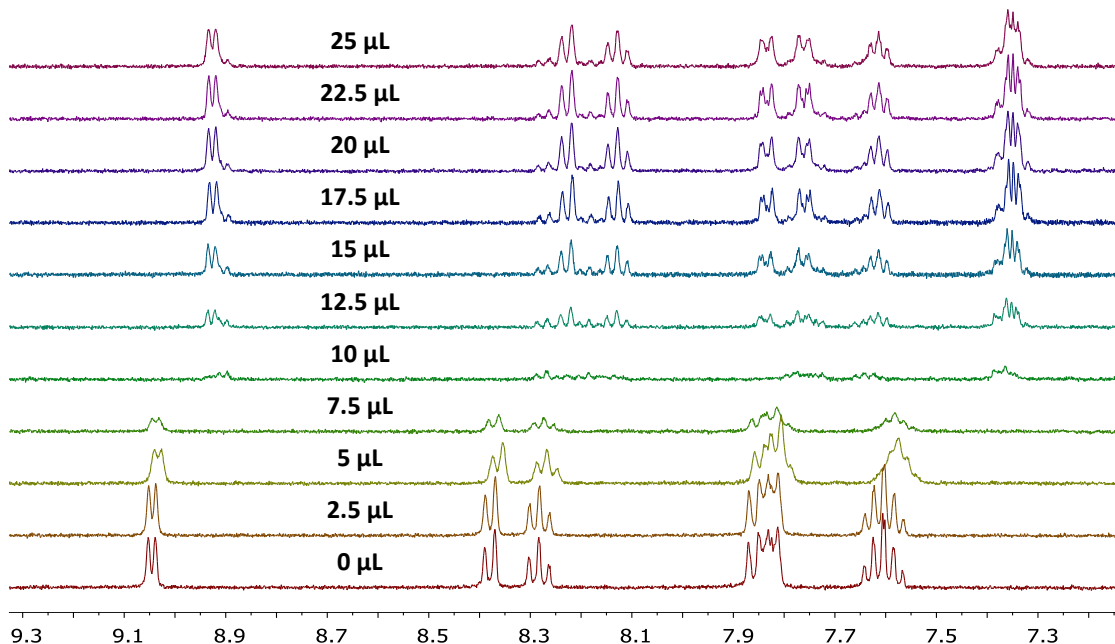


Fig. 9. Evolution of a sample of [34]Cl in D₂O after adding increasing amounts (2.5 μ L) of NaOH from 0 to 25 μ L.

As for the complex [36]Cl, the evolution of the sample after adding NaOH (see Fig. 10) also followed different steps. The first 2.5 μ L were used to neutralize the acid. When

an additional fraction ($5 \mu\text{L}$) of NaOH was added a new set of deshielded signals began to grow and the addition of extra NaOH led to a unique complex (see Fig. 11b).

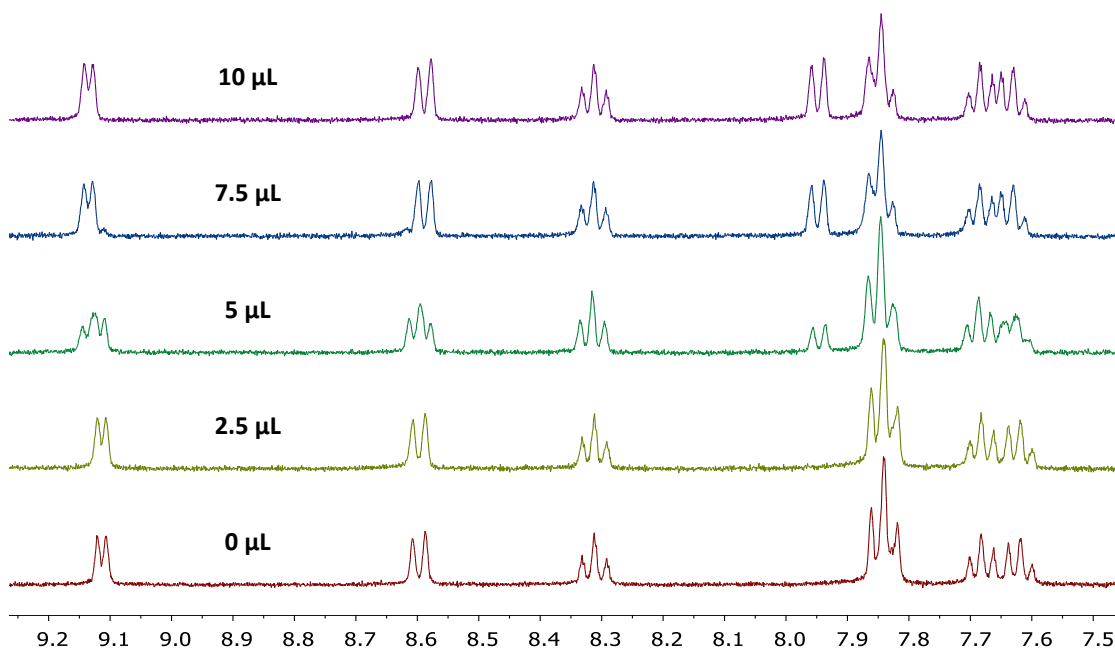


Fig. 10. Evolution of a sample of $[36]\text{Cl}$ in D_2O after adding increasing amounts ($2.5 \mu\text{L}$) of NaOH from 0 to $10 \mu\text{L}$.

To sum up, there is no aquation, but an equilibrium process concerning the deprotonation of the ligand takes place at basic pH, as depicts Fig. 11.

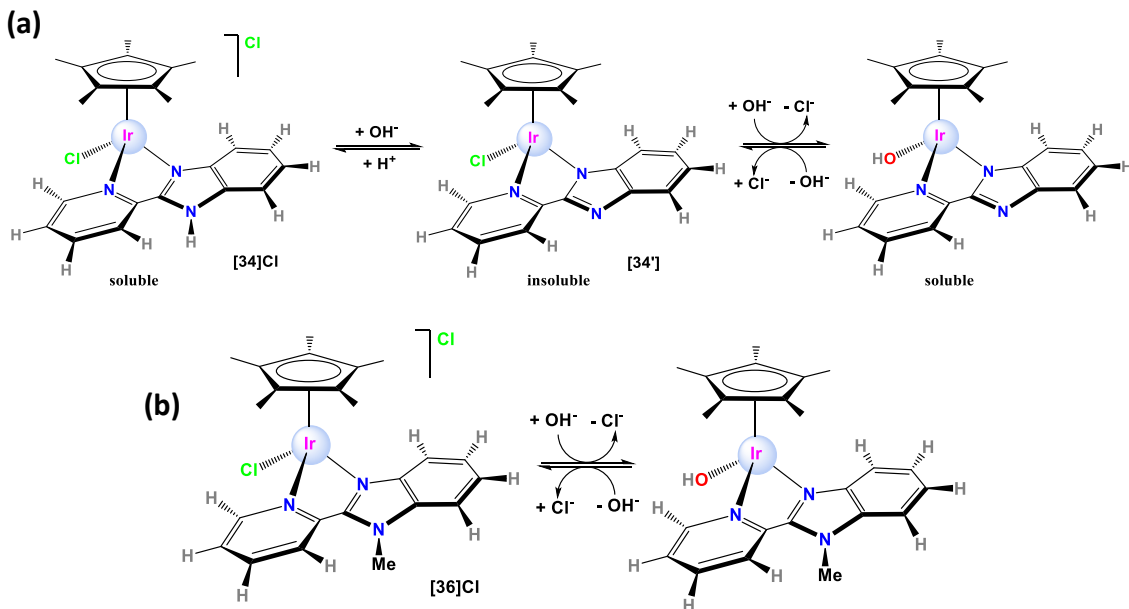


Fig. 11. Proposed equilibria for complexes $[34]\text{Cl}$ (a) and $[36]\text{Cl}$ (b) at different pH values.

1.4. Reactivity against Nucleobases, Nucleotides and DNA: A Deep ^1H NMR Study

The reactivity of selected complexes versus nucleobases, nucleotides and DNA was studied by ^1H NMR. In particular, the reaction between complexes $[34]\text{Cl}$, $[39\text{a}]\text{Cl}$ and

[43](OTf)₂ and 9MeG, GMP or DNA was monitored at 25 °C and pH 7 or pH 5, in case of precipitation.

Reactivity against the nucleobase

The reaction between 9MeG and **[34]Cl** or **[43](OTf)₂** was studied by ¹H NMR in D₂O at 25 °C. A solution 10 mM of **[34]Cl** (250 µL) was prepared in D₂O and the pH adjusted to 5, as a solid precipitated at pH 7. A spectrum was recorded and then, a 10 mM solution of 9MeG (250 µL) at pH 7 was added. The sample contained a final concentration 5 mM of both the complex and the nucleobase (1:1). Various spectra were recorded during 30 minutes.

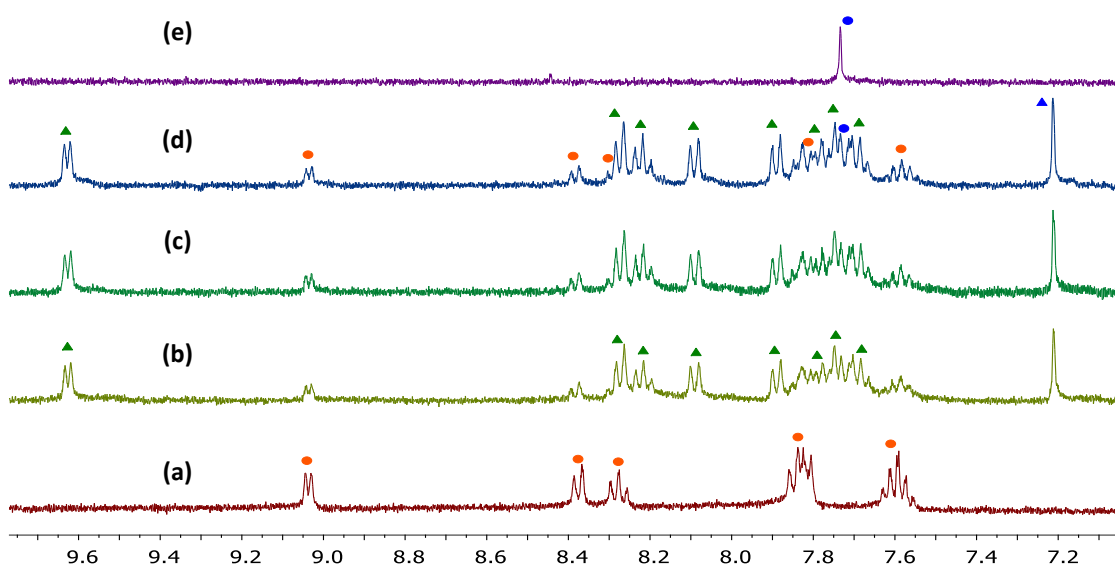


Fig. 12. Evolution of the aromatic region in the ¹H NMR spectrum of **[34]Cl** with 9MeG in D₂O at 25 °C. The orange spots refer to the complex **[34]Cl**, the blue ones to the free 9MeG, the green triangles refer to the new product **[34'-G]⁺** and the blue triangle to the coordinated 9MeG. (a) Spectrum of the complex at t=0, (b) at t=5 min, (c) at t=10 min, (d) at t=30 min and (e) spectrum of free 9MeG at pH 7.

Since the signal H8 of the 9MeG shifts strongly upfield ($\Delta\delta = 0.52$ ppm) and a set of new peaks for the ligand appear (see Fig. 12), the coordination of 9MeG to **[34]Cl** clearly occurs and probably through N7. As above-mentioned **[34]Cl** do not undergo aquation and is in equilibrium with the neutral species resulting from NH deprotonation at pH 7. Therefore, we propose that the Cl ligand is directly replaced with 9MeG on either **[34]⁺** or **[34']** to give **[34-G]²⁺** or **[34'-G]⁺**.

A solution of **[43](OTf)₂** was prepared in the manner of **[34]Cl** without adjusting the pH and its spectrum registered before and after the addition of 9MeG. The reaction between **[43](OTf)₂** and 9MeG seems to follow the same pattern as that for **[34]Cl**. The signal H8 of the 9MeG also shifts strongly upfield ($\Delta\delta = 0.50$ ppm) and a new set of resonances for the coordinated pybim ligand appear (see Fig. 13). In addition, a new intense peak in the aliphatic area grows, corresponding to the Cp* of the new complex. Unlike the previous case, in this new complex the guanine displaces straightaway the water molecule, implying a faster process, which is completely finished in 20 minutes.

The adduct formed, however, could be $[43\text{-G}]^{2+}$ or $[43'\text{-G}]^+$, as the NH group could have also lost its proton.

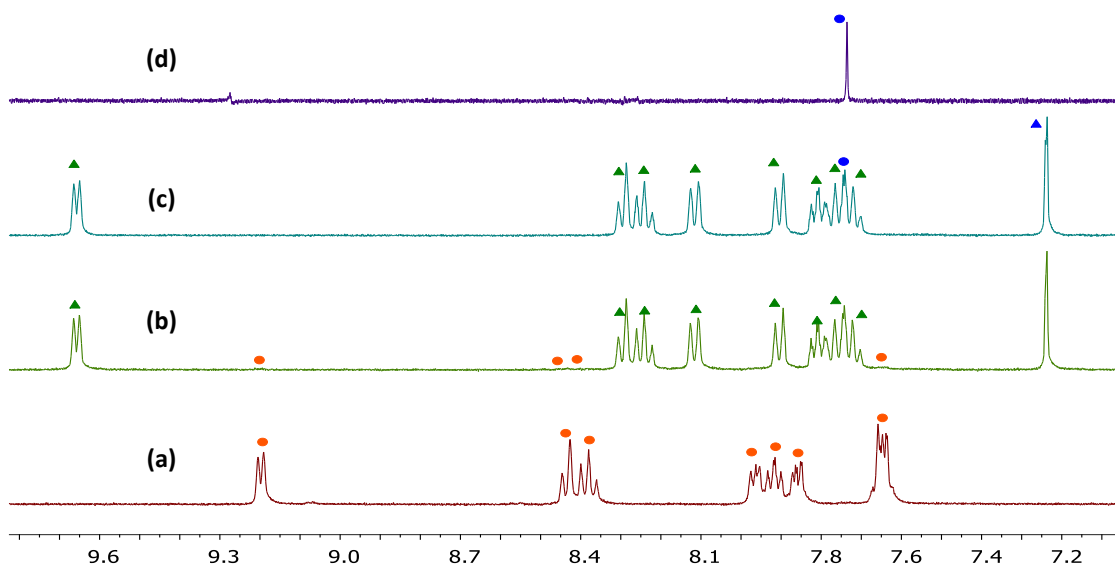


Fig. 13. Evolution of the aromatic region of $[43](\text{OTf})_2$ with 9MeG in D_2O at 25°C . The orange spots correspond to the complex $[43](\text{OTf})_2$, the blue ones to the free 9MeG, the green triangles refer to the new product and the blue triangle to the coordinated 9MeG. (a) Spectrum of the complex at $t=0$, (b) at $t=5$ min, (c) at $t=10$ min, and (d) spectrum of free 9MeG at pH 7.

Comparing the resulting spectra of both complexes, we notice the same product. Therefore, $[34\text{-G}]^{2+}$ and $[43\text{-G}]^{2+}$ are the same adduct, although we cannot confirm whether the NH group of the benzimidazole moiety is deprotonated or not.

Reactivity against the nucleotide

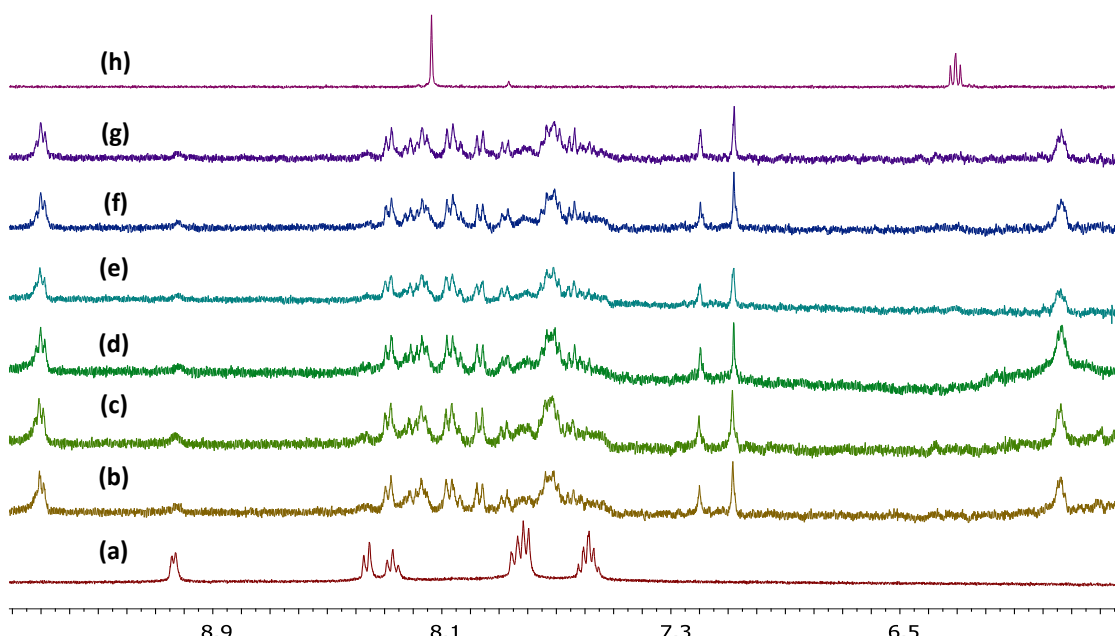


Fig. 14. Evolution of the aromatic region of $[34]\text{Cl}$ with 5'-GMP in D_2O at 25°C . (a) Spectrum at $t=0$, (b) at $t=5$ min, (c) at $t=25$ min, (d) at $t=1$ h, (e) at $t=4$ h, (f) at $t=22$ h and (g) at $t=48$ h. (h) Spectrum of 5'-GMP.

The reaction between 5'-GMP and [34]Cl or [39a]Cl was studied by ^1H NMR in D_2O at 25 °C. Two solutions 10 Mm of [34]Cl and [39a]Cl (250 μL) were prepared in D_2O and adjusted to pH 5 for [34]Cl (as a solid precipitated at pH 7) and to pH 6.5 for [39a]Cl. After recording spectra for the complexes, a 10 mM solution of 5'-GMP (250 μL) at pH 7 for [34]Cl and pH 6.5 for [39a]Cl was added. The samples contained a final concentration 5 mM of both the complex and the nucleotide (1:1).

The reaction evolved really fast for [34]Cl and it was almost finished in 5 minutes. The spectra showed two different sets of signals, since two singlets appeared for the H8 proton of the 5'-GMP (see Fig. 14), as well as two singlets for the Cp*.

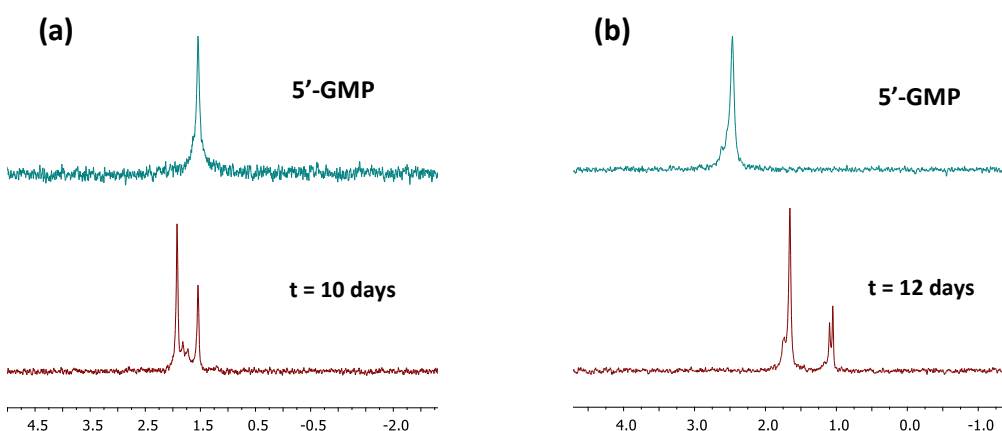


Fig. 15. $^{31}\text{P}\{{}^1\text{H}\}$ NMR spectra for the reaction of 5'-GMP with complexes [34]Cl (a) and [39a]Cl (b) recorded after 10 and 12 days, respectively. The upper spectra show the free 5'-GMP, and the lower the coordinated adducts.

The $^{31}\text{P}\{{}^1\text{H}\}$ NMR showed two intense peaks and two weaker signals among them (see Fig. 15a), being the most shielded the free 5'-GMP. In light of the previous results with 9MeG, and both the ^1H and the ^{31}P NMR experiments, we can conclude that the coordination of 5'-GMP to the metallic fragment of [34]Cl occurs initially through the phosphate and then, through the N7 of the nucleobases.

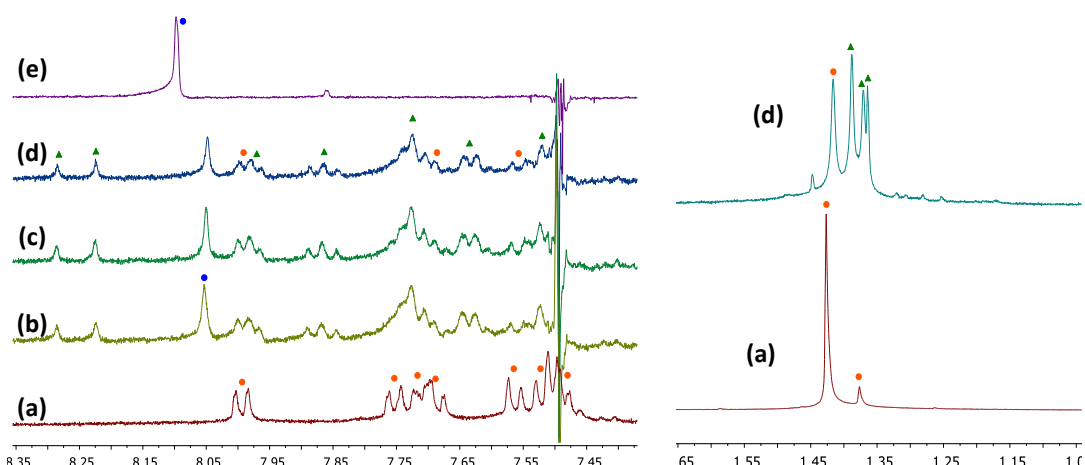


Fig. 16. Evolution of the aromatic and aliphatic regions of [39a]Cl with 5'-GMP in D_2O at 25 °C. The orange spots illustrate the complex $[39\text{a}-\text{H}_2\text{O}]^{2+}$, the blue ones the free 5'-GMP and the green triangles refer to the new product $[39\text{a}-\text{GMP}]^{2+}$. (a) Spectrum at $t = 0$, (b) at $t = 5$ min, (c) at $t = 20$ min, (d) at $t = 1$ h. (e) Spectrum of 5'-GMP.

Regarding the reaction with **[39a]Cl**, the evolution of the spectra displayed apparently two sets of peaks (apart from those for the initial compound), although the aliphatic region showed a complex signal related to even four different products. However, one of them likely corresponds to the initial complex (see Fig. 16).

The $^{31}\text{P}\{\text{H}\}$ NMR showed three peaks (see Fig. 15b), suggesting the formation of different products through different binding sites, and even their diastereoisomers.¹⁶ These facts, along with the FAB⁺ mass spectrum, which supports the link with the phosphate ($[\text{M-Cl}+\text{PO}_4^{3-}]^+$), demonstrate the substitution of the water molecule of **[39a]Cl** by 5'-GMP, at least through two different sites (see Fig. 17).

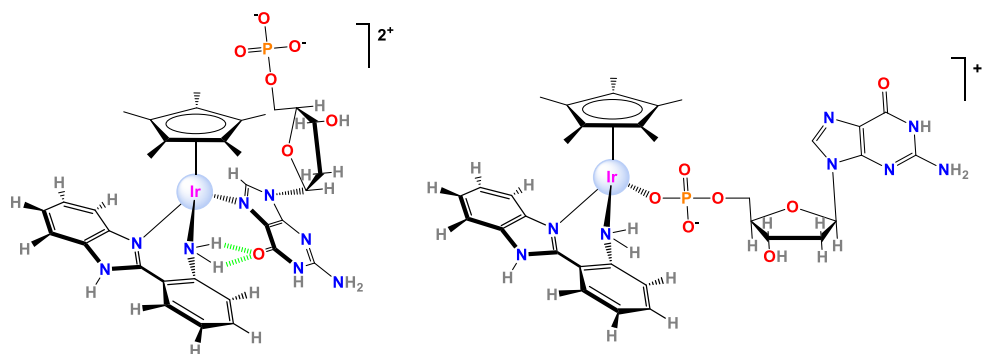


Fig. 17. Products formed after reaction of **[39a]Cl** with 5'-GMP.

Reactivity against DNA

The interaction of **[39a]Cl** with an oligonucleotide of 12 nitrogenous bases, consisting of the sequence 5'-GGATGTGGATGT-3' was studied by 1D (^1H –with and without water presaturation– and ^{31}P) and 2D (gCOSY, NOESY, TOCSY and HETCOR) NMR experiments, comparing the free oligonucleotide with the oligonucleotide plus the complex. An aliquot (450 μL) of a stock solution of free oligonucleotide 1 mM in 10 mM buffer Tris, 50 mM NaCl, 1 mM EDTA and pH 7.5 in H_2O was added to 50 μL of D_2O . The ionic strength (I) was adjusted to 27 mM with NaClO_4 and the final pH was fixed to 7. Thus, the final sample contained 0.9 mM of DNA in 90 % H_2O and 10 % D_2O . For the sample with the complex, 0.32 mg of **[39a]Cl** were added, and the sample was incubated for 1 h at 37°C.

The comparison of the ^1H NMR and the $^{31}\text{P}\{\text{H}\}$ NMR spectra of both the free oligonucleotide and the oligonucleotide with the complex, showed some differences, pointing out an interaction of the complex with the DNA, specially through the phosphate backbone. However, the bidimensional experiments did not have quality enough to determine the coordination mode of the DNA.

1.5. Cytotoxic Activity

Cytotoxicity of some of the complexes was measured in a MTT cell viability assay after 24h incubation at 37 °C with human lung carcinoma cells (A549). The values, gathered in Table 8, show complexes **[39a]Cl**, **[39b]Cl** and **[40a]** as promising cytotoxic

drugs. Curiously, a remarkable difference is found between some Ir(III) complexes, which are moderately active in the cell line A549, whereas their Ru(II) congeners are inactive. For instance, the neutral complex **[40a]** is cytotoxic, whereas their Ru(II) congeners **[16a]** and **[16b]** are innocuous. The same occurs with the derivative of apbim **[39a]Cl**, with its respective Ru(II) analogues **[23a]Cl** and **[23b]Cl**. On the contrary, the inhibitory potency of both the Ir(III) (IC_{50} **[39b]Cl** = 91 μ M) and Ru(II) (IC_{50} **[24a]Cl** = 90 μ M) complexes is the same. To sum up, the change in the metal centre clearly modifies the inhibitory potency of the drugs.

Table 8. IC_{50} (μ M, 24 h, 37 °C) values for selected compounds in the cell line A549.

Ref.	Compound	Solvent	IC_{50} (μ M)
	cisplatin		114.2 ^b
[34]Cl	$[(Cp^*)IrCl(pybim)]Cl$	H ₂ O	166
[35]Cl	$[(Cp^*)IrCl(pyim)]Cl$	H ₂ O	306
[36]Cl	$[(Cp^*)IrCl(pyMebim)]Cl$	H ₂ O	271.6
[38]Cl	$[(Cp^*)IrCl(tbz)]Cl$	H ₂ O	285 ^a
[39a]Cl	$[(Cp^*)IrCl(apbim)]Cl$	H ₂ O/DMSO	52.7 ^a
[39b]Cl	$[(Cp^*)IrCl(apbtz)]Cl$	DMSO	91
[40a]	$[(Cp^*)IrCl(hpbim)]$	DMSO/MeOH	66
[40b]	$[(Cp^*)IrCl(hpbtz)]$	DMSO	371.5

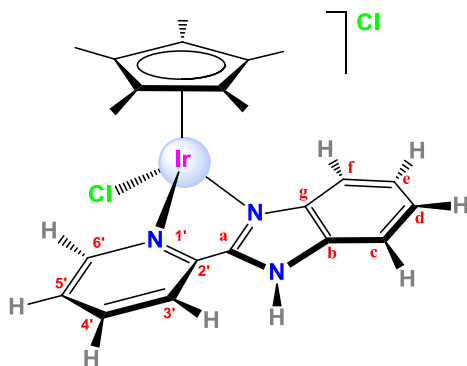
^aThe results are ambiguous.

^bBibliographic data.¹⁷

2. CONCLUDING REMARKS

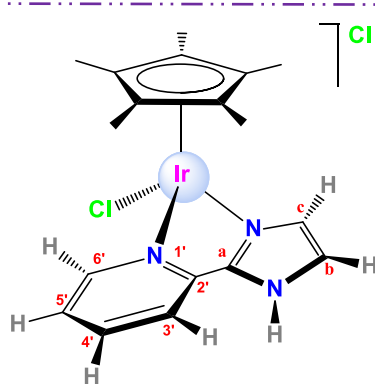
- A family of 12 new complexes has been prepared and fully characterised, both in solution and some of them in solid state.
- NMR experiments have demonstrated that complexes **[34]Cl** and **[43](OTf)₂** react with 9MeG. In addition, **[34]Cl** and **[39a]Cl** react also with 5'-GMP. Complex **[39a]Cl** react with DNA.
- The cytotoxic activity assays allowed us to conclude that complexes **[39a]Cl**, **[39b]Cl** and **[40a]** are the most promising cytotoxic drugs in this family.
- The substitution of Ir(III) by Ru(II) modifies the cytotoxic activity of the complexes.

3. EXPERIMENTAL SECTION



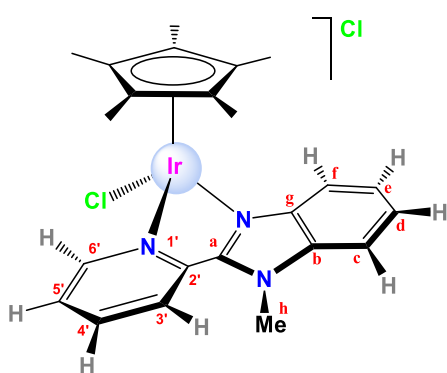
Synthesis of $[(\eta^5\text{-Cp}^)\text{IrCl}(\kappa^2\text{-N,N-pybim})]\text{Cl}$, [34]Cl.* In a 100 mL Schlenk flask, the ligand pybim (0.0505 g, 0.259 mmol) was added to a solution of $[\text{IrCl}_2(\text{Cp}^*)]_2$ (0.1002 g, 0.126 mmol) in dichloromethane (14 mL), and the mixture was stirred at room temperature for 20 h and under a nitrogen atmosphere. The solution was concentrated and the product was precipitated with hexane and filtered off. The resulting yellow powder was dried under vacuum. Yield: 147.7 mg (0.249 mmol, 98%). $M_r (\text{C}_{22}\text{H}_{24}\text{N}_3\text{Cl}_2\text{Ir}) = 593.5771 \text{ g/mol}$. **Anal. Calcd for $\text{C}_{22}\text{H}_{24}\text{N}_3\text{Cl}_2\text{Ir} \cdot (\text{CH}_2\text{Cl}_2)_{1.1}$:** C 40.50; H 3.78 N 5.45; **Found:** C 40.39; H 3.84; N 6.12. $^1\text{H NMR}$ (400 MHz, CDCl_3 , 25 °C) δ 16.21 (s, 1H, $\text{H}^{\text{N-H}}$), 9.67 (d, $J = 8.2 \text{ Hz}$, 1H, $\text{H}^{\text{3'}}$), 8.76 (d, $J = 5.7 \text{ Hz}$, 1H, $\text{H}^{\text{6'}}$), 8.15 (t, $J = 7.8 \text{ Hz}$, 1H, $\text{H}^{\text{4'}}$), 8.01 (d, $J = 8.2 \text{ Hz}$, 1H, H^{c}), 7.65 (d, $J = 8.1 \text{ Hz}$, 1H, H^{f}), 7.61 – 7.53 (m, 1H, $\text{H}^{\text{5'}}$), 7.53 – 7.45 (m, 1H, H^{d}), 7.42 (t, $J = 7.7 \text{ Hz}$, 1H, H^{e}), 1.75 (s, 15H, $\text{H}^{\text{Cp(Me)}}$) ppm. $^{13}\text{C}\{^1\text{H}\}$ NMR (101 MHz, CDCl_3 , 25 °C) δ 152.3 (s, 1C, C^{a}), 150.64 (s, 1C, $\text{C}^{\text{6'}}$), 148.2 (s, 1C, $\text{C}^{\text{2'}}$), 140.8 (s, 1C, $\text{C}^{\text{4'}}$), 138.7 (s, 1C, C^{g}), 135.5 (s, 1C, C^{b}), 127.4 (s, 1C, $\text{C}^{\text{5'}}$), 126.5 (s, 1C, $\text{C}^{\text{3'}}$), 126.2 (s, 1C, C^{d}), 125.1 (s, 1C, C^{e}), 116.2 (s, 1C, C^{d}), 115.8 (s, 1C, C^{f}), 88.3 (s, 1C, C^{CpC}), 9.7 (s, 1C, $\text{C}^{\text{Cp(Me)}}$) ppm. **FT-IR (ATR, cm⁻¹) selected bands:** 3389 (vs, $\nu_{\text{N-H}}$), 3029 (w, $\nu_{\text{C=CH}}$), 2963–2915 (w, ν_{CH}), 1612–1594 (m, $\nu_{\text{C=C-N}}$), 1484–1457–1447 (vs, $\nu_{\text{C=N}}$), 1382 (m, δ_{CH_3}), 1325 (m), 1261 (m), 1028 (s), 795 (m, $\delta_{\text{C-C}}$), 760 (s, δ_{CHoop}). **MS (FAB+):** m/z (%) = 648 (4), 559 (12) ($[\text{M-Cl}+\text{H}]^+$), 522 (5) ($[\text{M}-2\text{Cl}-\text{H}]^+$). **Molar Conductivity (CH₃CN):** 27.1 S·cm²·mol⁻¹.

1. Solubility: soluble in water, dichloromethane, chloroform, acetonitrile and acetone.

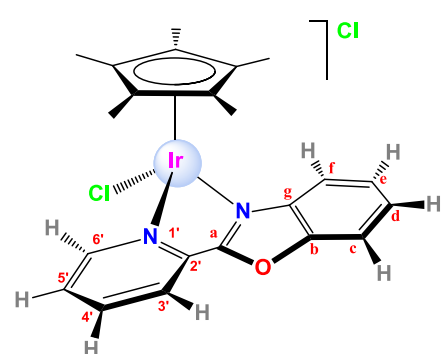


Synthesis of $[(\eta^5\text{-Cp}^)\text{IrCl}(\kappa^2\text{-N,N-pyim})]\text{Cl}$, [35]Cl.* The synthesis was performed as for [34]Cl in the presence of the ligand 2-(2'-pyridyl)imidazole (0.0414 g, 0.257 mmol, 90% pure) and $[\text{IrCl}_2(\text{Cp}^*)]_2$ (0.1001 g, 0.129 mmol) dichloromethane (11 mL). Yellow powder. Yield: 118.9 mg (0.219 mmol, 85%). $M_r (\text{C}_{18}\text{H}_{22}\text{N}_3\text{Cl}_2\text{Ir}) = 543.5173 \text{ g/mol}$. **Anal. Calcd for $\text{C}_{18}\text{H}_{22}\text{N}_3\text{Cl}_2\text{Ir} \cdot (\text{H}_2\text{O})_{0.5}$:** C 39.13; H 4.20; N 7.61; **Found:** C 39.15; H 4.32; N 7.08. $^1\text{H NMR}$ (400 MHz, CDCl_3 , 25 °C) δ 16.21 (s, 1H, $\text{H}^{\text{N-H}}$), 9.39 (d, $J = 8.0 \text{ Hz}$, 1H, $\text{H}^{\text{3'}}$), 8.60 (d, $J = 4.9 \text{ Hz}$, 1H, $\text{H}^{\text{6'}}$), 8.05 (t, $J = 7.8 \text{ Hz}$, 1H, $\text{H}^{\text{4'}}$), 7.49 (d, $J = 1.4 \text{ Hz}$, 1H, H^{b}), 7.45 (t, $J = 6.9 \text{ Hz}$, 1H, $\text{H}^{\text{5'}}$), 7.23 (d, $J = 1.2 \text{ Hz}$, 1H, H^{c}), 1.73 (s, 15H,

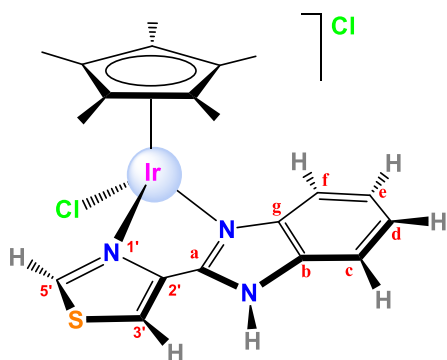
$\text{H}^{\text{Cp(Me)}}$) ppm. $^{13}\text{C}\{\text{H}\}$ NMR (101 MHz, CDCl_3 , 25 °C) δ 150.4 (s, 1C, C^{6'}), 148.7 (s, 1C, C^a), 147.9 (s, 1C, C^{2'}), 140.6 (s, 1C, C^{4'}), 126.3 (s, 1C, C^{5'}), 126.1 (s, 1C, C^c), 124.5 (s, 1C, C^{3'}), 123.0 (s, 1C, C^b), 87.9 (s, 1C, C^{CpC}), 9.2 (s, 1C, C^{Cp(Me)}) ppm. FT-IR (ATR, cm⁻¹) selected bands: 3105-3049 (w, $\nu_{\text{C}=\text{CH}}$), 2990-2962-2912 (w, ν_{CH}), 2437 (m, br), 1614 (m, $\nu_{\text{C}=\text{C} + \text{C}_\text{N}}$), 1497-1468 (vs, $\nu_{\text{C}=\text{N}}$), 1377 (m, δ_{CH_3}), 1193 (m), 1158 (m), 1127 (m), 1028 (s), 930-915 (s), 783-769 (vs, $\delta_{\text{C}-\text{C}}$), 755 (s, δ_{CHOop}) 702 (s). MS (FAB+): m/z (%) = 508 (100) ([M-Cl]⁺), 472 (30) ([M-2Cl-H]⁺), 363 (15) ([M-Cl-pyIm]⁺). Molar Conductivity (CH_3CN): 34.6 S·cm²·mol⁻¹. Solubility: soluble methanol, dichloromethane, chloroform, acetonitrile and acetone.



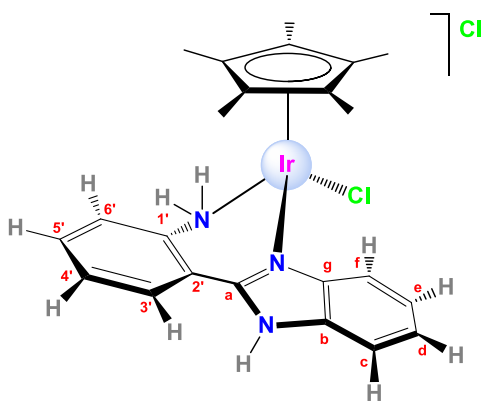
Synthesis of $[(\eta^5-\text{Cp}^*)\text{IrCl}(\kappa^2-\text{N},\text{N}-\text{pyMebim})]\text{Cl}$, [36]Cl. The synthesis was performed as for [34]Cl in the presence of the ligand 2-(2'-pyridyl)-N-Methylbenzimidazole (0.0344 g, 0.164 mmol) and $[\text{IrCl}_2(\text{Cp}^*)]_2$ (0.0574 g, 0.074 mmol) dichloromethane (6 mL). The product was precipitated with diethyl ether. Yellow powder. Yield: 81.8 mg (0.135 mmol, 91%). M_r ($\text{C}_{23}\text{H}_{26}\text{N}_3\text{Cl}_2\text{Ir}$) = 607.6039 g/mol. Anal. Calcd for $\text{C}_{23}\text{H}_{26}\text{N}_3\text{Cl}_2\text{Ir} \cdot (\text{CH}_2\text{Cl}_2)_{0.5}(\text{H}_2\text{O})_{0.4}$: C 42.95; H 4.26; N 6.39; Found: C 42.99; H 4.47; N 5.96. ^1H NMR (400 MHz, CDCl_3 , 25 °C) δ 9.29 (d, J = 8.0 Hz, 1H, H^{3'}), 8.89 (d, J = 5.6 Hz, 1H, H^{6'}), 8.41 (t, J = 8.0 Hz, 1H, H^{4'}), 7.74 – 7.63 (m, 3H, H^f, H^{5'}, H^c), 7.62 – 7.55 (m, 1H, H^d), 7.53 – 7.48 (m, 1H, H^e), 4.70 (s, 3H, H^{Me}), 1.78 (s, 15H, H^{Cp(Me)}) ppm. $^{13}\text{C}\{\text{H}\}$ NMR (101 MHz, CDCl_3 , 25 °C) δ 152.0 (s, 1C, C^{6'}), 151.8 (s, 1C, C^a), 146.9 (s, 1C, C^{2'}), 141.6 (s, 1C, C^{4'}), 138.1 (s, 1C, C^g), 136.9 (s, 1C, C^b), 128.1 (s, 1C, C^{5'}), 127.1 (s, 1C, C^{3'}), 126.6 (s, 1C, C^d), 125.7 (s, 1C, C^e), 116.9 (s, 1C, C^f), 112.7 (s, 1C, C^c), 88.9 (s, 1C, C^{CpC}), 9.8 (s, 1C, C^{Cp(Me)}) ppm. FT-IR (ATR, cm⁻¹) selected bands: 3444-3379 (m, $\nu_{\text{N}-\text{H}}$), 3069 (w, $\nu_{\text{C}=\text{CH}}$), 1606 (m, $\nu_{\text{C}=\text{C} + \text{C}_\text{N}}$), 1524 (m), 1490-1468-1441 (vs, $\nu_{\text{C}=\text{N}}$), 1354-1334 (w, δ_{CH_3}), 1153 (m), 1030 (s), 832 (w), 792 (m, $\delta_{\text{C}-\text{C}}$), 756-742 (vs, δ_{CHOop}), 582 (m), 545 (m), 507 (w). MS (FAB+): m/z (%) = 572 (33) ([M-Cl]⁺), 536 (4) ([M-2Cl-H]⁺), 363 (5) ([M-Cl-NMePybzIm-H]⁺). Molar Conductivity (CH_3CN): 140.9 S·cm²·mol⁻¹. Solubility: soluble in water, methanol, dichloromethane and chloroform.



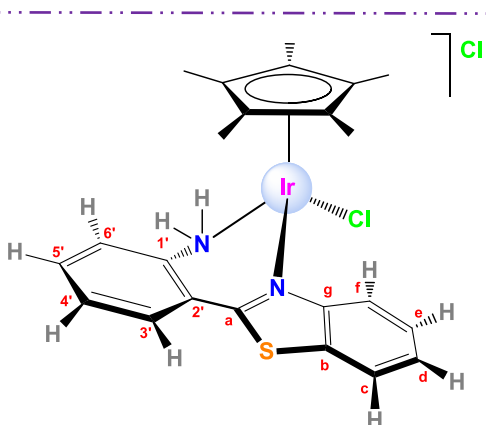
Synthesis of $[(\eta^5\text{-Cp}^)\text{IrCl}(\kappa^2\text{-N,N-pybox})]\text{Cl}$, [37]Cl.* In a 100 mL Schlenk flask, the ligand 2-(2'-pyridyl)benzoxazole (0.0388 g, 0.198 mmol) was added to a solution of $[\text{IrCl}_2(\text{Cp}^*)]_2$ (0.0602 g, 0.078 mmol) in dichloromethane (12 mL), and the mixture was stirred at room temperature for 20 h and under a nitrogen atmosphere. The solution was concentrated and the product was precipitated with diethyl ether and filtered off. The resulting orange powder was dried under vacuum. Yield: It was not calculated M_r ($\text{C}_{22}\text{H}_{23}\text{N}_2\text{OCl}_2\text{Ir}$) = 594.5619 g/mol. **Anal. Calcd for** $\text{C}_{22}\text{H}_{23}\text{N}_2\text{OCl}_2\text{Ir} (\text{CH}_2\text{Cl}_2)_{1.6}$: C 38.81; H 3.62 N 3.84; **Found:** C 38.85 H 3.70; N 3.49. **$^1\text{H NMR}$ (400 MHz, CDCl₃, 25 °C)** δ 9.18 (d, J = 5.0 Hz, 1H, H^{5'}), 8.49 (d, J = 7.8 Hz, 1H, H^{3'}), 8.37 (t, J = 7.2 Hz, 1H, H^{4'}), 8.24 (t, J = 6.7 Hz, 1H, H^{5'}), 7.86 (d, J = 7.7 Hz, 1H, H^c), 7.83 (dd, J = 7.9, 1.1 Hz, 1H, H^f), 7.68 (td, J = 7.9, 1.5 Hz, 1H, H^d), 7.63 (td, J = 7.8, 1.1 Hz, 1H, H^e), 1.93 (s, 15H, H^{Cp(Me)}) ppm. **$^{13}\text{C}\{{}^1\text{H}\}$ NMR (101 MHz, CDCl₃, 25 °C)** δ 153.1 (s, 1C, C^{6'}), 151.7 (s, 1C, C^b), 141.2 (s, 1C, C^{4'}), 136.8 (s, 1C, C^g), 132.1 (s, 1C, C^{5'}), 129.0 (s, 1C, C^d), 127.6 (s, 1C, C^e), 126.3 (s, 1C, C^{3'}), 117.3 (s, 1C, C^f), 113.7 (s, 1C, C^c), 89.8 (s, 1C, C^{CpC}), 10.2 (s, 1C, C^{Cp(Me)}) ppm. The peaks of C^{2'} and C^a do not appear. **FT-IR (KBr, cm⁻¹) selected bands:** 3048 (w, v_{C=CH}), 2965-2915 (w, v_{-CH}), 1626 (m, v_{C=C + C-N}), 1547 (m, v_{C=C}), 1476-1448-1412 (s, v_{C=N}), 1382 (m, δ_{CH3}), 1293 (m), 1161 (m, v_{C-O-C}), 1032 (s, δ_{CHip}), 819-804 (s, δ_{C-C}), 765 (vs, δ_{CHoop}). **MS (FAB+):** m/z (%) = 560 (11) ([M-Cl+H]⁺). **Molar Conductivity (CH₃CN):** 89.4 S·cm²·mol⁻¹. **Solubility:** soluble in acetonitrile, dichloromethane, chloroform and acetone.



Synthesis of $[(\eta^5\text{-Cp}^)\text{IrCl}(\kappa^2\text{-N,N-tbz})]\text{Cl}$, [38]Cl.* The synthesis was performed as for [36]Cl in the presence of the ligand thiabendazole (0.0521 g, 0.259 mmol) and $[\text{IrCl}_2(\text{Cp}^*)]_2$ (0.1002 g, 0.129 mmol) dichloromethane (11 mL). Yellow powder. Yield: 145.2 mg (0.242 mmol, 94%). M_r ($\text{C}_{20}\text{H}_{22}\text{N}_3\text{S}\text{Cl}_2\text{Ir}$) = 599.6053 g/mol. **Anal. Calcd for** $\text{C}_{20}\text{H}_{22}\text{N}_3\text{S}\text{Cl}_2\text{Ir} (\text{CH}_2\text{Cl}_2)_{1.1}$: C 36.57; H 3.52; N 6.06; S 4.63; **Found:** C 36.56; H 3.68; N 5.67; S 4.73. **$^1\text{H NMR}$ (400 MHz, CDCl₃, 25 °C)** δ 15.91 (s, 1H, H^{N-H}), 9.99 (s, J = 1.7 Hz, 1H, H^{3'}), 9.14 (d, J = 2.1 Hz, 1H, H^{5'}), 7.87 (d, J = 8.1 Hz, 1H, H^c), 7.58 (d, J = 7.7 Hz, 1H, H^f), 7.50 – 7.35 (m, 2H, H^d, H^e), 1.79 (s, 15H, H^{Cp(Me)}) ppm. **$^{13}\text{C}\{{}^1\text{H}\}$ NMR (101 MHz, CDCl₃, 25 °C)** δ 154.1 (s, 1C, C^{5'}), 147.5 (s, 1C, C^a), 145.9 (s, 1C, C^{2'}), 138.3 (s, 1C, C^g), 135.4 (s, 1C, C^b), 125.7 (s, 1C, C^d), 124.7 (s, 1C, C^e), 124.6 (s, 1C, C^{3'}), 115.9 (s, 1C, C^f), 115.6 (s, 1C, C^c), 87.9 (s, 1C, C^{CpC}), 9.9 (s, 1C, C^{Cp(Me)}) ppm. **FT-IR (ATR, cm⁻¹) selected bands:** 3466 (m, v_{N-H}), 3095-2910-2822-2739 (m, v_{=CH}, v_{-CH}), 1614 (m, v_{C=N(imid)}), 1517 (m, v_{C=C}), 1481-1462-1428 (s, v_{C=N(thiaz)}), 1378 (m, δ_{CH3}), 1328 (m), 1226 (w, v_{C-S}), 1029-1015 (s, v_{C=S}), 879-846 (m), 763 (vs, δ_{NHoop}), 747 (vs, δ_{CHoop}), 638 (w). **MS (FAB+):** m/z (%) = 564 (15) ([M-Cl]⁺), 528 (4) ([M-2Cl-H]⁺), 363 (6) ([M-Cl-thbzol]⁺). **Molar Conductivity (CH₃CN):** 35.4 S·cm²·mol⁻¹. **Solubility:** soluble in water, dichloromethane, chloroform, acetonitrile and acetone. Partially soluble in methanol.

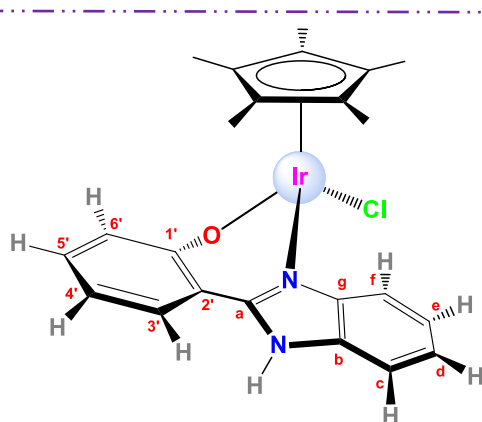


Synthesis of $[(\eta^5\text{-Cp}^*)\text{IrCl}(\kappa^2\text{-N,N-apbim})]\text{Cl}$, [39a]Cl. The synthesis was performed as for [36]Cl in the presence of the ligand 2-(2'-aminophenyl)benzimidazole (0.0546 g, 0.261 mmol) and $[\text{IrCl}_2(\text{Cp}^*)]_2$ (0.1000 g, 0.126 mmol) dichloromethane (14 mL). Yellow powder. Yield: 122.0 mg (0.201 mmol, 80%). $M_r (\text{C}_{23}\text{H}_{26}\text{N}_3\text{Cl}_2\text{Ir}) = 607.6039 \text{ g/mol}$. **Anal. Calcd for** $\text{C}_{23}\text{H}_{26}\text{N}_3\text{Cl}_2\text{Ir} \cdot (\text{CH}_2\text{Cl}_2)_{0.3}$: C 44.25; H 4.18; N 6.13; **Found:** C 44.21; H 4.24; N 6.62. **¹H NMR (400 MHz, DMSO-d₆, 25 °C)** δ 14.61 (s, 1H, H^{N-H}), 8.23 (d, *J* = 9.7 Hz, 1H, H^{NH₂}), 8.08 (d, *J* = 7.6 Hz, 1H, H^{3'}), 7.85 (d, *J* = 11.0 Hz, 1H, H^{NH₂}), 7.75 – 7.70 (m, 1H, H^c), 7.67 (dd, *J* = 5.6, 3.7 Hz, 1H, H^f), 7.63 (t, *J* = 7.7 Hz, 1H, H^{5'}), 7.52 (d, *J* = 7.8 Hz, 1H, H^{6'}), 7.47 – 7.36 (m, 3H, H^a, H^b, H^d, H^e), 1.46 (d, *J* = 63.7 Hz, 1H, H^{Cp(Me)}) ppm. **¹³C{¹H} NMR (101 MHz, DMSO-d₆, 25 °C)** δ 147.2 (s, 1C, C^a), 141.9 (s, 1C, C^{1'}), 139.4 (s, 1C, C^g), 134.0 (s, 1C, C^b), 131.5 (s, 1C, C^{5'}), 129.0 (s, 1C, C^{3'}), 126.0 (s, 1C, C^{4'}), 124.5 (s, 1C, C^d), 123.4 (s, 1C, C^e), 121.6 (s, 1C, C^{2'}), 121.0 (s, 1C, C^f), 118.8 (s, 1C, C^c or C^f), 112.6 (s, 1C, C^f or C^{5'}), 86.0 (s, 1C, C^{CpC}), 8.1 (s, 1C, C^{Cp(Me)}) ppm. **FT-IR (ATR, cm⁻¹) selected bands:** 3425 (w, v_{O-H}), 3025 (vs, v_{=CH}, v_{NH₂}), 2962-2900 (vs, v_{NH₂(hydrogen bonds)}), 1620-1598 (w, v_{C=C + C-N}), 1541 (m), 1485 (s), 1463-1450 (vs, v_{C=N}), 1417 (s), 1382 (m, δ_{CH₃}), 1325 (m), 1161 (m), 1032 (m), 799 (m, δ_{C-C}), 762-747 (s, δ_{CH_{loop}}). **MS (FAB+):** m/z (%) = 573 (25) ([M-Cl+H]⁺), 537 (21) ([M-2Cl]⁺). **Molar Conductivity (CH₃CN):** 50.6 S·cm²·mol⁻¹. **Solubility:** soluble in water, methanol, dimethylsulfoxide and acetonitrile. Insoluble in dichloromethane and acetone.

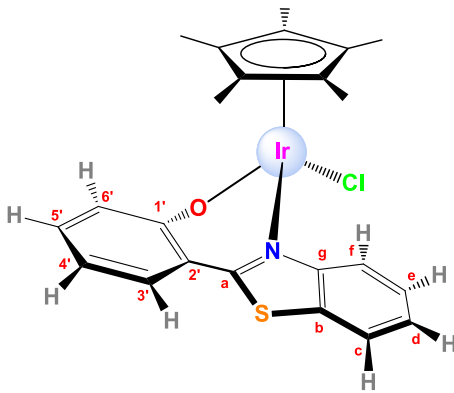


Synthesis of $[(\eta^5\text{-Cp}^*)\text{IrCl}(\kappa^2\text{-N,N-apbtz})]\text{Cl}$, [39b]Cl. The synthesis was performed as for [36]Cl in the presence of the ligand 2-(2'-aminophenyl)benzothiazole (0.0546 g, 0.258 mmol) and $[\text{IrCl}_2(\text{Cp}^*)]_2$ (0.0999 g, 0.125 mmol) dichloromethane (14 mL). Yellow powder. Yield: 114.9 mg (0.184 mmol, 73%). $M_r (\text{C}_{23}\text{H}_{25}\text{N}_2\text{S}\text{Cl}_2\text{Ir}) = 624.6553 \text{ g/mol}$. **Anal. Calcd for** $\text{C}_{23}\text{H}_{25}\text{N}_2\text{S}\text{Cl}_2\text{Ir} \cdot (\text{CH}_2\text{Cl}_2)_{1.1}$: C 40.31; H 3.82; N 3.90; S 4.47; **Found:** C 40.19; H 3.92; N 3.55; S 4.47. **¹H NMR (400 MHz, CDCl₃, 25 °C)** δ 10.58 (d, *J* = 10.9 Hz, 1H, H^{NH₂}), 8.77 (d, *J* = 7.8 Hz, 1H, H^{6'}),

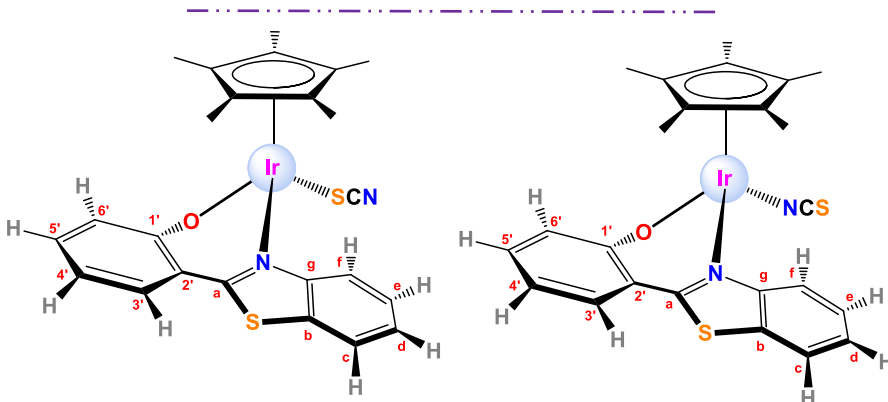
8.34 (d, $J = 8.3$ Hz, 1H, H^f), 7.97 (d, $J = 7.9$ Hz, 1H, H^c), 7.82 (d, $J = 7.7$ Hz, 1H, H^{3'}), 7.68 (t, $J = 7.8$ Hz, 1H, H^{5'}), 7.62 (t, $J = 7.1$ Hz, 1H, H^e), 7.56 (t, $J = 7.4$ Hz, 1H, H^d), 7.38 (t, $J = 7.5$ Hz, 1H, H^{4'}), 5.87 (d, $J = 10.5$ Hz, 1H, H^{NH2}), 1.54 (s, 15H, H^{Cp(Me)}) ppm. ¹³C{¹H} NMR (101 MHz, CDCl₃, 25 °C) δ 165.4 (s, 1C, C^a), 150.3 (s, 1C, C^g), 140.4 (s, 1C, C^{1'}), 134.0 (s, 1C, C^{5'}), 132.5 (s, 1C, C^b), 130.3 (s, 1C, C^{3'}), 128.1 (s, 1C, C^e), 127.8 (s, 1C, C^{4'}), 127.7 (s, 1C, C^d), 125.7 (s, 1C, C^f), 125.4 (s, 1C, C^{2'}), 124.8 (s, 1C, C^{6'}), 122.6 (s, 1C, C^c), 87.8 (s, 1C, C^{CpC}), 9.3 (s, 1C, C^{Cp(Me)}) ppm. FT-IR (ATR, cm⁻¹) selected bands: 3408 (w, ν_{O-H}), 3024 (m, ν_{=CH}, ν_{NH2}), 2963-2922 (s, ν_{NH2+(hydrogen bonds)}), 1607 (w, ν_{C=C + C-N}), 1574 (w), 1477-1449 (vs, ν_{C=N}), 1430 (s), 1380 (m, δ_{CH3}), 1322 (w), 1254 (m), 1176 (m), 1078 (m, ν_{C=S}), 1031-997 (s), 789 (vs, δ_{C-C}), 755 (vs, δ_{CHOop}), 718 (s), 689 (m). MS (FAB+): m/z (%) = 590 (16) ([M-Cl+H]⁺), 554 (9) ([M-2Cl]⁺). Molar Conductivity (CH₃CN): 79.6 S·cm²·mol⁻¹. Solubility: soluble in dichloromethane, chloroform, acetonitrile and dimethylsulfoxide.



Synthesis of [(η⁵-Cp)IrCl(κ²-O,N-hpbim)], [40a].* In a 100 mL Schlenk flask, the ligand 2-(2'-hidroxyphenyl)benzimidazole (0.0541 g, 0.257 mmol) was added to a solution of [IrCl₂(Cp*)]₂ (0.0999 g, 0.125 mmol) and Et₃N (37 μL, 0.266 mmol) in dichloromethane (15 mL), and the mixture was stirred at room temperature for 20 h and under a nitrogen atmosphere. The product was filtered and washed with water and diethyl ether. The resulting yellow powder was dried under vacuum. Yield: 116.8 mg (0.204 mmol, 81%). M_r (C₂₃H₂₄N₂OClIr) = 572.1281 g/mol. Anal. Calcd for C₂₃H₂₄N₂OClIr·(CH₂Cl₂)_{0.3}: C 46.83; H 4.15; N 4.69; Found: C 46.89; H 4.13; N 4.28. ¹H NMR (400 MHz, DMSO-d₆/MeOD-d₄, 25 °C) δ 7.78 (dd, $J = 7.9, 1.7$ Hz, 1H, H^{3'}), 7.66 (dd, $J = 7.0, 1.0$ Hz, 1H, H^c), 7.46 (td, $J = 7.5, 1.2$ Hz, 1H, H^e), 7.41 (td, $J = 7.5, 1.2$ Hz, 1H, H^d), 7.34 (dd, $J = 7.2, 1.0$ Hz, 1H, H^f), 7.28 (t, $J = 7.6, 1.0$ Hz, 1H, H^{5'}), 6.92 (dd, $J = 8.4, 1.1$ Hz, 1H, H^{6'}), 6.75 (td, $J = 7.6, 1.0$ Hz, 1H, H^{4'}), 1.47 (s, 15H, H^{Cp(Me)}) ppm. ¹³C{¹H} NMR (101 MHz, DMSO-d₆/MeOD-d₄, 25 °C) δ 166.0 (s, 1C, C^{1'}), 148.6 (s, 1C, C^a), 140.3 (s, 1C, C^g), 135.1 (s, 1C, C^b), 133.4 (s, 1C, C^{5'}), 128.3 (s, 1C, C^{3'}), 125.8 (s, 1C, C^d), 124.8 (s, 1C, C^e), 123.9 (s, 1C, C^f), 118.5 (s, 1C, C^{4'}), 117.6 (s, 1C, C^c), 116.1 (s, 1C, C^{2'}), 113.6 (s, 1C, C^b), 93.1 (s, 1C, C^{CpC}), 8.5 (s, 1C, C^{Cp(Me)}) ppm. FT-IR (ATR, cm⁻¹) selected bands: 3165-3141 (m), 3044 (w, ν_{=CH}), 2983 (w, ν_{-CH}), 1620 (m, ν_{C=N}), 1600 (s, ν_{C=C}), 1552-1532 (m), 1476-1444 (vs, ν_{C=N}), 1315 (s), 1259 (s, ν_{C-O}), 1137 (m), 1033 (m), 858 (m), 771-749 (s, δ_{CHOop}), 689 (w). MS (FAB+): Of the substitution complex with DMSO: m/z (%) = 616 (10) ([M-Cl+DMSO+H]⁺), 538 (72) ([M-DMSO+H]⁺). Solubility: soluble in a mixture of dimethylsulfoxide/methanol (3:2). Slightly soluble in methanol. Insoluble in water, dimethylsulfoxide, dichloromethane, acetonitrile and acetone.

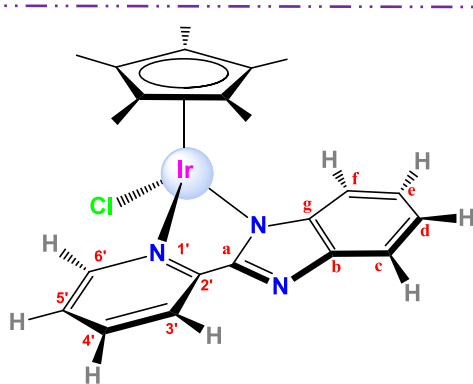


Synthesis of $[(\eta^5\text{-Cp}^*)\text{IrCl}(\kappa^2\text{-O},\text{N-}hpbtz)]$, [40b]. The synthesis was performed as for [40a] in the presence of the ligand 2-(2'-hydroxyphenyl)benzothiazole (0.0541 g, 0.259 mmol), $[\text{IrCl}_2(\text{Cp}^*)]_2$ (0.0999 g, 0.125 mmol) and Et_3N (37 μL , 0.266 mmol) in dichloromethane (12 mL). Yellow powder. Yield: 81.4 mg (0.138 mmol, 55%). **M_r** ($\text{C}_{23}\text{H}_{23}\text{NOClIr}$) = 589.1795 g/mol. **Anal. Calcd for** $\text{C}_{23}\text{H}_{23}\text{NOClIr} \cdot (\text{CH}_2\text{Cl}_2)_{0.3}$: C 45.53; H 3.87; N 2.28; S 5.22; **Found:** C 45.51; H 4.00; N 2.01; S 5.06. **¹H NMR** (400 MHz, CDCl_3 , 25 °C) δ 8.28 (dd, J = 8.4, 0.6 Hz, 1H, H^f), 7.77 (dd, J = 8.0, 0.6 Hz, 1H, H^c), 7.54 – 7.49 (m, 2H, $\text{H}^{3',e}$), 7.37 (td, J = 7.3, 1.1 Hz, 1H, H^d), 7.31 – 7.23 (m, 1H, H^5'), 7.06 – 7.01 (m, 1H, H^6'), 6.56 (ddt, J = 8.1, 7.0, 1.1 Hz, 1H, H^4'), 1.43 (s, 15H, $\text{H}^{\text{Cp(Me)}}$) ppm. **¹³C{¹H} NMR** (101 MHz, CDCl_3 , 25 °C) δ 167.7 (s, 1C, $\text{C}^{1'}$), 165.4 (s, 1C, C^a), 151.2 (s, 1C, C^g), 133.6 (s, 1C, $\text{C}^{5'}$), 131.9 (s, 1C, C^b), 129.2 (s, 1C, $\text{C}^{3'}$), 126.9 (s, 1C, C^e), 125.7 (s, 1C, C^d), 125.3 (s, 1C, C^f), 124.4 (s, 1C, $\text{C}^{6'}$), 121.7 (s, 1C, $\text{C}^{2'}$), 121.4 (s, 1C, C^c), 116.5 (s, 1C, $\text{C}^{4'}$), 84.6 (s, 1C, C^{CpC}), 9.2 (s, 1C, $\text{C}^{\text{Cp(Me)}}$) ppm. **FT-IR (ATR, cm⁻¹) selected bands:** 3408 (w, $\nu_{\text{O-H}}$), 3050 (w, $\nu_{\text{C-H}}$), 2964 (w, $\nu_{\text{C-H}}$), 1599 (s, $\nu_{\text{C=C+C-N}}$), 1543 (m), 1492-1453 (vs, $\nu_{\text{C=N}}$), 1377 (m, δ_{CH_3}), 1325 (s), 1240-1223-1209 (s, $\nu_{\text{C-O}}$), 1147 (m), 1077 (w, $\nu_{\text{C-S}}$), 1032 (m), 771-733 (s, δ_{CHop}), 689 (w). **MS (FAB+):** m/z (%) = 590 (23) ([M]⁺), 555 (100) ([M-Cl+H]⁺). **Molar Conductivity (CH₃CN):** 10.5 $\text{S}\cdot\text{cm}^2\cdot\text{mol}^{-1}$. **Solubility:** soluble in dichloromethane, chloroform, acetonitrile and acetone. Slightly soluble in methanol and insoluble in water.

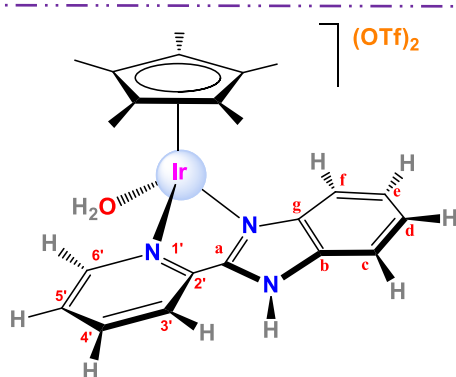


Synthesis of $[(\eta^5\text{-Cp}^*)\text{Ir}(\kappa^2\text{-O},\text{N-}hpbtz)(\text{SCN})]$, [41b]. In a 100 mL Schlenk flask, the salt KSCN (0.0199 g, 0.205 mmol) was added under a nitrogen atmosphere to a solution of [40b] (0.0500 g, 0.085 mmol) in degassed methanol (14 mL) and the mixture was stirred at 70 °C for 4h. The solvent was evaporated to dryness and the residue was washed with hexane. Water was added to remove salts and the solid was washed with diethyl ether. The resulting orange powder was dried under vacuum. Yield: 24.1 mg (0.039 mmol, 46%). **M_r** ($\text{C}_{24}\text{H}_{23}\text{N}_2\text{OS}_2\text{Ir}$) = 611.8105 g/mol. **Anal. Calcd for** $\text{C}_{24}\text{H}_{23}\text{N}_2\text{OS}_2\text{Ir}$ $\text{C}_{24}\text{H}_{23}\text{N}_2\text{OS}_2\text{Ir} \cdot (\text{KCl})_{1.2}$: C 41.11; H 3.31; N 3.99; S 9.14; **Found:** C

41.02; H 3.52; N 3.55; S 9.59. **¹H NMR (400 MHz, CDCl₃, 25 °C)** δ 8.00 (t, *J* = 8.7 Hz, 2H, H^f, H^g), 7.81 (dd, *J* = 7.7, 2.9 Hz, 2H, H^c, H^{c'}), 7.60 (dd, *J* = 16.5, 8.0 Hz, 2H, H^e, H^{e'}), 7.56 – 7.48 (m, 2H, H³, H^{3'}), 7.46 – 7.38 (m, 2H, H^d, H^{d'}), 7.32 – 7.25 (m, 2H, H⁵, H^{5'}), 7.00 (d, *J* = 8.5 Hz, 2H, H⁶, H^{6'}), 6.62 – 6.56 (m, 2H, H⁴, H^{4'}), 1.48 (s, 15H, H^{Cp(Me)} or H^{Cp(Me)'}), 1.45 (s, 15H, H^{Cp(Me)'} or H^{Cp(Me)}) ppm. **FT-IR (KBr, cm⁻¹) selected bands:** 3403 (w, v_{O-H}), 2963-2915 (w, v_{-CH}), 2098 (vs, v_{N=C=S}), 1597 (s, v_{C-N}), 1542 (m, v_{C=C}), 1488 (vs, v_{C=N}), 1454-1443-1420 (vs), 1378 (s, δ_{CH3}), 1330 (m), 1218 (s, v_{C-O}), 1152 (m, v_{C=S}), 1125 (w), 1028 (vs), 834 (m), 750 (vs, v_{C-S(SCN)}), 726 (m), 571 (w), 463 (w), 432 (w). **MS (ESI+):** m/z (%) = 1166 (4) ([2M-SCN]⁺), 635 (9) ([M+Na]⁺), 554 (100) ([M-SCN]⁺). **Molar Conductivity (CH₃CN):** 28.1 S·cm²·mol⁻¹. **Solubility:** soluble in acetonitrile, methanol, acetone, dichloromethane and chloroform.



Synthesis of [(η⁵-Cp)IrCl(κ²-N,N-pybim')], [42].* In a 100 mL Schlenk flask, NaHCO₃ (0.0113 g, 0.135 mmol) was added to a solution of [34]Cl (0.0501 g, 0.084 mmol) in dichloromethane (10 mL) and methanol (2 mL), and the mixture was stirred at room temperature for 20 h and under a nitrogen atmosphere. The solution was filtered and concentrated to dryness. The product was dissolved in dichloromethane, precipitated with diethyl ether and washed again with diethyl ether. The resulting yellow powder was dried under vacuum. Yield: 17.9 mg (0.032 mmol, 38%). **M_r (C₂₂H₂₃N₃ClIr) = 557.1165 g/mol. Anal. Calcd for C₂₂H₂₃N₃ClIr·(CH₂Cl₂)_{1.1}: C 42.65; H 3.90; N 6.46; Found: C 42.63; H 4.18; N 5.97.** **¹H NMR (400 MHz, CDCl₃, 25 °C)** δ 8.98 (s, 1H, H^{3'}), 8.71 (d, *J* = 5.7 Hz, 1H, H^{6'}), 8.00 (t, *J* = 7.6 Hz, 1H, H^{4'}), 7.90 (d, *J* = 7.9 Hz, 1H, H^c), 7.61 (d, *J* = 7.7 Hz, 1H, H^f), 7.43 (t, *J* = 6.4 Hz, 1H, H^{5'}), 7.36 – 7.27 (m, 2H, H^d, H^e), 1.74 (s, 15H, H^{Cp(Me)}) ppm. **FT-IR (KBr, cm⁻¹) selected bands:** 3429 (w, v_{O-H}), 2962-2916 (w, v_{-CH}), 1612 (s, v_{C=C+C-N}), 1481-1445 (vs, v_{C=N}), 1380 (m, δ_{CH3}), 1333 (m), 1260 (m), 1100 (m), 1028 (s), 797 (m, δ_{C-C}), 752 (s, δ_{CHOOP}). **MS (FAB+):** m/z (%) = 558 (25) ([M+H]⁺), 522 (16) ([M-Cl]⁺). **Molar Conductivity (CH₃CN):** 19.0 S·cm²·mol⁻¹. **Solubility:** soluble in acetonitrile, dichloromethane, chloroform and acetone.



Synthesis of $[(\eta^5-Cp^)Ir(\kappa^2-N,N\text{-}pybim})(OH_2)](OTf)_2$, [43](OTf)₂.* In a 100 mL Schlenk flask, AgOTf (0.0348 g, 0.135 mmol) was added to a solution of [34]Cl (0.0306 g, 0.052 mmol) in a mixture water/ethanol (1:1, 10 mL). The mixture was stirred at room temperature for 20 h, under a nitrogen atmosphere and preserved from light. The AgCl was filtered and the solvent was evaporated to dryness. The residue was washed twice with diethyl ether (10 mL). The resulting yellow powder was dried under vacuum. **M_r** (**C₂₄H₂₆N₃O₇S₂F₆Ir**) = 838.8277 g/mol. **Anal. Calcd for C₂₄H₂₆N₃O₇S₂F₆Ir (CF₃SO₃Ag)_{0.05}:** C 33.92; H 3.08; N 4.93; S 7.72; **Found:** C 33.98; H 3.26; N 5.28; S 8.16. **¹H NMR (400 MHz, D₂O, 25 °C)** δ 9.20 (d, *J* = 5.6 Hz, 1H, H^{6'}), 8.43 (d, *J* = 7.3 Hz, 1H, H^{3'}), 8.38 (t, *J* = 7.8 Hz, 1H, H^{4'}), 8.00 – 7.94 (m, 1H, H^f), 7.91 (t, *J* = 6.7 Hz, 1H, H^{5'}), 7.88 – 7.83 (m, 1H, H^c), 7.69 – 7.59 (m, 2H, H^e, H^d), 1.75 (s, *J* = 15.5 Hz, 15H, H^{Cp(Me)}) ppm. **¹³C{¹H} NMR (101 MHz, D₂O, 25 °C)** δ 154.7 (s, 1C, C^a), 152.8 (s, 1C, C^{6'}), 147.8 (s, 1C, C^{2'}), 142.5 (s, 1C, C^{4'}), 139.0 (s, 1C, C^g), 135.2 (s, 1C, C^b), 129.9 (s, 1C, C^{5'}), 127.3 (s, 1C, C^d), 126.3 (s, 1C, C^e), 124.4 (s, 1C, C^{3'}), 120.3 (q, *J* = 317.7 Hz, 2C, C^{OTf}), 117.1 (s, 1C, C^f), 115.0 (s, 1C, C^c), 89.4 (s, 1C, C^{CpC}), 9.3 (s, 1C, C^{Cp(Me)}) ppm. **¹⁹F{¹H} NMR (376 MHz, D₂O, 25 °C)** δ -79.3 (s, 6F, F^{CF₃}) ppm. **FT-IR (KBr, cm⁻¹) selected bands:** 3104-3004 (w, v_{C=CH+V-CH}), 1617-1602 (w, v_{C=C + C-N}), 1488-1459-1450 (m, v_{C=N}), 1389 (m, δ_{CH₃}), 1329 (w), 1286-1235-1221 (vs, v_{C-F}), 1178-1156 (vs, v_{SO₃^{-as}}), 1065 (w, δ_{CHip}), 1029 (vs, v_{SO₃^{-sym}}), 791 (s, δ_{C-C}), 756-738 (s, δ_{CHoop}), 634 (vs, δ_{CF₃}), 511 (s). **MS (FAB+):** m/z (%) = 672 (10) ([M-(OTf)-H₂O]⁺), 522 (58) ([M-(OTf)₂-H₂O-H]⁺). **Solubility:** soluble in water, ethanol and acetone.

4. BIBLIOGRAPHY

- (1) Liu, Z.; Habtemariam, A.; Pizarro, A. M.; Fletcher, S. A.; Kisova, A.; Vrana, O.; Salassa, L.; Bruijnincx, P. C. A.; Clarkson, G. J.; Brabec, V.; Sadler, P. J. *J. Med. Chem.* **2011**, *54*, 3011–3026.
- (2) Liu, Z.; Habtemariam, A.; Pizarro, A. M.; Clarkson, G. J.; Sadler, P. J. *Organometallics* **2011**, *30*, 4702–4710.
- (3) Manaka, Y.; Wang, W.-H.; Suna, Y.; Kambayashi, H.; Muckerman, J. T.; Fujita, E.; Himeda, Y. *Catal. Sci. Technol.* **2014**, *4*, 34–37.
- (4) Yellol, G. S.; Yellol, J. G.; Kenche, V. B.; Liu, X. M.; Barnham, K. J.; Donaire, A.; Janiak, C.; Ruiz, J. *Inorg. Chem.* **2015**, *54*, 470–475.
- (5) Pachhunga, K.; Therrien, B.; Kreisel, K. A.; Yap, G. P. A.; Kollipara, M. R. *Polyhedron* **2007**, *26*, 3638–3644.
- (6) Kumar, A.; Kumar, A.; Gupta, R. K.; Paitandi, R. P.; Singh, K. B.; Trigun, S. K.; Hundal, M. S.; Pandey, D. S. *J. Organomet. Chem.* **2016**, *801*, 68–79.
- (7) Angelici, R. J. In *Técnicas y Síntesis en Química Inorgánica*; Editorial Reverté, S.A., 1979; p. 243.
- (8) Liu, Z.; Salassa, L.; Habtemariam, A.; Pizarro, A. M.; Clarkson, G. J.; Sadler, P. J. *Inorg. Chem.* **2011**, *50*, 5777–5783.
- (9) Gupta, R. K.; Pandey, R.; Sharma, G.; Prasad, R.; Koch, B.; Srikrishna, S.; Li, P.-Z.; Xu, Q.; Pandey, D. S. *Inorg. Chem.* **2013**, *52*, 3687–3698.
- (10) Chanda, N.; Paul, D.; Kar, S.; Mobin, S. M.; Datta, A.; Puranik, V. G.; Rao, K. K.; Lahiri, G. K. *Inorg. Chem.* **2005**, *44*, 3499–3511.
- (11) Martínez-Alonso, M.; Busto, N.; Jalón, F. A.; Manzano, B. R.; Leal, J. M.; Rodríguez, A. M.; García, B.; Espino, G. *Inorg. Chem.* **2014**, *53*, 11274–11288.
- (12) Smith, D. P.; Chen, H.; Ogo, S.; Elduque, A. I.; Eisenstein, M.; Olmstead, M. M.; Fish, R. H. *Organometallics* **2014**, *33*, 2389–2404.
- (13) Nomura, M.; Tsukano, E.; Fujita-Takayama, C.; Sugiyama, T.; Kajitani, M. J. *Organomet. Chem.* **2009**, *694*, 3116–3124.
- (14) Nomura, M.; Fourmigué, M. *Inorg. Chem.* **2008**, *47*, 1301–1312.
- (15) Eichhorn, D. M.; Telser, J.; Stern, C. L.; Hoffman, B. M. *Inorg. Chem.* **1994**, *33*, 3533–3537.
- (16) Busto, N.; Valladolid, J.; Martínez-Alonso, M.; Lozano, H. J.; Jalón, F. A.; Manzano, B. R.; Rodríguez, A. M.; Carrión, M. C.; Biver, T.; Leal, J. M.; Espino, G.; García, B. *Inorg. Chem.* **2013**, *52*, 9962–9974.
- (17) Gutiérrez, A.; Cativiela, C.; Laguna, A.; Gimeno, M. C. *Dalt. Trans.* **2016**, *45*, 13483–13490.

ANNEX i

Table 1. Crystal data and structure refinement for [1a](BF₄)·H₂O, [1b](BF₄)·2H₂O, [1c]Cl·2H₂O and [2a]Cl.

	[1a](BF ₄)·H ₂ O	[1b](BF ₄)·2H ₂ O	[1c]Cl·2H ₂ O	[2a]Cl
Empirical formula	C ₂₂ H ₂₅ BClF ₄ N ₃ ORu	C ₁₈ H ₁₈ BClF ₄ N ₃ O _{1.50} Ru	C ₂₀ H ₁₉ Cl ₂ N ₃ O ₂ Ru·2(H ₂ O)	C ₂₃ H ₂₅ Cl ₂ N ₃ Ru
Formula weight	570.78	523.68	541.38	515.43
Temperature (K)	100(2)	290(2)	100(2)	293(2)
Wavelength (Å)	0.71073	0.71073	0.71073	0.71073
Crystal system	Triclinic	Monoclinic	Monoclinic	Monoclinic
Space group	P <bar{1}< td=""><td>P₂₁/c</td><td>P₂₁/c</td><td>P₂₁/c</td></bar{1}<>	P ₂ ₁ /c	P ₂ ₁ /c	P ₂ ₁ /c
a (Å)	8.340(2)	8.5135(7)	7.1156(13)	18.343(4)
b (Å)	10.076(3)	19.5527(15)	25.881(5)	8.0292(16)
c (Å)	14.514(4)	12.8900(10)	11.671(2)	16.932(3)
α (°)	98.068(4)	90	90	90
β (°)	100.090(4)	94.0600(10)	103.311(3)	111.272(4)
γ (°)	107.928(4)	90	90	90
Volume (Å³)	1117.7(5)	2140.3(3)	2091.5(7)	2323.8(8)
Z	2	4	4	4
Density (calculated) (g/cm³)	1.696	1.625	1.719	1.473
Absorption coefficient (mm⁻¹)	0.875	0.908	1.038	0.918
F(000)	576	1044	1096	1048
Crystal size (mm³)	0.21 x 0.12 x 0.05	0.31 x 0.11 x 0.11	0.55 x 0.32 x 0.28	0.12 x 0.11 x 0.11
Theta range for data collection (°)	1.46 to 25.00	1.90 to 25.00	1.57 to 27.00	2.38 to 25.00
Index ranges	-9≤h≤9, -11≤k≤11, -17≤l≤17	-10≤h≤10, -23≤k≤23, -15≤l≤15	-8≤h≤9, -32≤k≤33, -14≤l≤14	-21≤h≤21, -9≤k≤9, -20≤l≤20
Reflections collected	7705	20862	23509	22215
Independent reflections	3866 [R(int) = 0.1191]	3769 [R(int) = 0.0475]	4537 [R(int) = 0.0734]	4089 [R(int) = 0.0859]
Completeness to theta = 25.00°	98.6 %	99.9 %	99.7 %	99.9 %
Absorption correction	Semi-empirical from equivalents	Semi-empirical from equivalents	Semi-empirical from equivalents	Semi-empirical from equivalents
Max. and min. transmission	0.9576 and 0.8376	0.9068 and 0.7662	0.7598 and 0.5990	0.9057 and 0.8978
Refinement method	Full-matrix least-squares on F ²	Full-matrix least-squares on F ²	Full-matrix least-squares on F ²	Full-matrix least-squares on F ²
Data / restraints / parameters	3866 / 0 / 305	3769 / 0 / 253	4537 / 0 / 276	4089 / 0 / 266
Goodness-of-fit on F²	1.013	1.100	1.103	0.974
Final R indices [I>2sigma(I)]	R1 = 0.0437, wR2 = 0.1140	R1 = 0.0554, wR2 = 0.1665	R1 = 0.0317, wR2 = 0.0833	R1 = 0.0381, wR2 = 0.0825
R indices (all data)	R1 = 0.0497, wR2 = 0.1173	R1 = 0.0630, wR2 = 0.1726	R1 = 0.0339, wR2 = 0.0868	R1 = 0.0526, wR2 = 0.0868
Largest diff. peak and hole, e·Å⁻³	1.093 and -1.006	1.429 and -0.658	0.984 and -0.573	0.408 and -0.377

Table 2. Crystal data and structure refinement for [4a'](BF₄), [4a](OTf)₂·H₂O, {[4b](BF₄)(SiF₆)_{0.5}}·2H₂O and [6a](PF₆)₂·H₂O

	[4a'](BF ₄)	[4a](OTf) ₂ ·H ₂ O	{[4b](BF ₄)(SiF ₆) _{0.5} }·2H ₂ O	[6a](PF ₆) ₂ ·H ₂ O
Empirical formula	C ₂₂ H ₂₅ BClF ₄ N ₃ ORu	C ₂₄ H ₂₇ F ₆ N ₃ O ₈ RuS ₂	C ₃₆ H ₄₀ B ₂ F ₁₄ N ₆ O ₅ Ru ₂ Si	C ₂₈ H ₃₁ F ₁₂ N ₈ O _{1.5} P ₂ Ru
Formula weight	570.78	764.68	1154.59	894.62
Temperature (K)	100(2)	290(2)	100(2)	290(2)
Wavelength (Å)	0.71073	0.71073	0.71073	0.71073
Crystal system	Triclinic	Monoclinic	Triclinic	Triclinic
Space group	P <bar{1}< td=""><td>P2₁/c</td><td>P-1</td><td>P<bar{1}< td=""></bar{1}<></td></bar{1}<>	P2 ₁ /c	P-1	P <bar{1}< td=""></bar{1}<>
a (Å)	8.340(2)	9.4783(11)	8.020(4)	9.2531(8)
b (Å)	10.076(3)	32.077(4)	10.144(5)	10.9702(10)
c (Å)	14.514(4)	10.0286(12)	14.527(7)	18.7620(16)
α (°)	98.068(4)	90	78.741(7)	83.3600(10)
β (°)	100.090(4)	94.168(2)	82.356(7)	78.1130(10)
γ (°)	107.928(4)	90	69.764(7)	71.2350(10)
Volume (Å³)	1117.7(5)	3041.0(6)	1084.8(8)	1762.1(3)
Z	2	4	1	2
Density (calculated) (g/cm³)	1.696	1.670	1.767	1.686
Absorption coefficient (mm⁻¹)	0.875	0.740	0.834	0.638
F(000)	576	1544	576	898
Crystal size (mm³)	0.21 x 0.12 x 0.05	0.29 x 0.11 x 0.10	0.31 x 0.22 x 0.09	0.30 x 0.30 x 0.30
Theta range for data collection (°)	1.46 to 25.00	2.13 to 25.00	1.43 to 25.00	1.11 to 25.00
Index ranges	-9≤h≤9, -11≤k≤11, -17≤l≤17	-11≤h≤11, -38≤k≤38, -11≤l≤11	-9≤h≤9, -12≤k≤12, -17≤l≤17	-10≤h≤10, -13≤k≤13, -22≤l≤22
Reflections collected	7705	29186	10329	17459
Independent reflections	3866 [R(int) = 0.1191]	5336 [R(int) = 0.0768]	3816 [R(int) = 0.1375]	6168 [R(int) = 0.0278]
Completeness to theta = 25.00°	98.6 %	99.9 %	99.6 %	99.8 %
Absorption correction	Semi-empirical from equivalents	Semi-empirical from equivalents	Semi-empirical from equivalents	Semi-empirical from equivalents
Max. and min. transmission	0.9576 and 0.8376	0.9297 and 0.8141	0.9287 and 0.7821	0.8315 and 0.8315
Refinement method	Full-matrix least-squares on F ²	Full-matrix least-squares on F ²	Full-matrix least-squares on F ²	Full-matrix least-squares on F ²
Data / restraints / parameters	3866 / 0 / 305	5336 / 55 / 392	3816 / 38 / 341	6168 / 0 / 488
Goodness-of-fit on F²	1.013	1.062	1.083	1.065
Final R indices [I>2sigma(I)]	R1 = 0.0437, wR2 = 0.1140	R1 = 0.0728, wR2 = 0.1951	R1 = 0.0573, wR2 = 0.1301	R1 = 0.0488, wR2 = 0.1447
R indices (all data)	R1 = 0.0497, wR2 = 0.1173	R1 = 0.1059, wR2 = 0.2106	R1 = 0.0712, wR2 = 0.1394	R1 = 0.0528, wR2 = 0.1499
Largest diff. peak and hole, e·Å⁻³	1.093 and -1.006	0.693 and -0.990	1.105 and -0.659	1.141 and -0.615

Table 3. Crystal data and structure refinement for [8] and [11](PF₆).

	[8]	[11](PF ₆)
Empirical formula	C ₂₃ H ₂₃ ClN ₂ Ru	C ₂₉ H ₃₅ F ₆ N ₅ P ₂ Ru
Formula weight	463.95	730.63
Temperature (K)	298(2)	293(2)
Wavelength (Å)	0.71073	0.71073
Crystal system	Monoclinic	Monoclinic
Space group	P2 ₁ /n	P 2 ₁ /n
a (Å)	10.328(3)	9.6667(11)
b (Å)	15.186(4)	17.602(2)
c (Å)	12.167(3)	18.098(2)
α (°)	90	90
β (°)	92.557(4)	101.311(2)
γ (°)	90	90
Volume (Å³)	1906.4(8)	3019.5(6)
Z	4	4
Density (calculated) (g/cm³)	1.616	1.607
Absorption coefficient (mm⁻¹)	0.973	0.692
F(000)	944	1488
Crystal size (mm³)	0.11 x 0.11 x 0.10	0.31 x 0.22 x 0.13
Theta range for data collection (°)	2.15 to 26.99	1.629 to 24.999
Index ranges	-13 ≤ h ≤ 13, 0 ≤ k ≤ 19, 0 ≤ l ≤ 15	-11 ≤ h ≤ 11, -20 ≤ k ≤ 20, -21 ≤ l ≤ 21
Reflections collected	4141	29271
Independent reflections	4141 [R(int) = 0.0000]	5322 [R(int) = 0.0455]
Completeness to theta = 25.00°	99.5 %	97.2 %
Absorption correction	Semi-empirical from equivalents	Semi-empirical from equivalents
Max. and min. transmission	0.9090 and 0.9005	1.000 and 0.834
Refinement method	Full-matrix least-squares on F2	Full-matrix least-squares on F2
Data / restraints / parameters	4141 / 0 / 247	5322 / 0 / 391
Goodness-of-fit on F2	1.077	1.083
Final R indices [I>2sigma(I)]	R1 = 0.0256, wR2 = 0.0636	R1 = 0.0802, wR2 = 0.1885
R indices (all data)	R1 = 0.0294, wR2 = 0.0649	R1 = 0.0940, wR2 = 0.1979
Largest diff. peak and hole, e·Å⁻³	0.921 and -0.582	1.823 and -1.426

Table 4. Crystal data and structure refinement for [16a], [16b]·CH₃OH, [17a] and [18d].

	[16a]	[16b]·CH ₃ OH	[17a]	[18d]
Empirical formula	C ₂₃ H ₂₃ CIN ₂ ORu	C ₁₉ H ₁₉ CIN ₂ O ₂ Ru	C ₂₃ H ₂₂ CINORuS	C ₃₆ H ₄₀ N ₄ O ₆ Ru ₂ S ₈
Formula weight	479.95	443.88	497.00	1083.34
Temperature (K)	173(2)	293(2)	173(2)	173(2)
Wavelength (Å)	0.71073	0.71073	0.71073	0.71073
Crystal system	Triclinic	Orthorhombic	Monoclinic	Monoclinic
Space group	P $\bar{1}$	P2 ₁ 2 ₁ 2 ₁	P2 ₁ /c	P 2 ₁ /n
a (Å)	10.3197(15)	9.6699(15)	22.673(3)	13.5514(14)
b (Å)	10.6722(16)	9.7690(15)	10.0510(12)	8.8594(9)
c (Å)	11.1748(16)	19.355(3)	18.302(2)	17.9189(18)
α (°)	108.293(2)	90	90	90
β (°)	104.331(2)	90	92.331(2)	105.152(2)
γ (°)	110.299(2)	90	90	90
Volume (Å³)	1004.3(3)	1828.4(5)	4167.3(8)	2076.5(4)
Z	2	4	8	2
Density (calculated) (g/cm³)	1.587	1.613	1.584	1.733
Absorption coefficient (mm⁻¹)	0.930	1.018	0.994	1.180
F(000)	488	896	2016	1096
Crystal size (mm³)	9.00 × 0.12 × 0.10	0.11 × 0.10 × 0.10	0.20 × 0.10 × 0.05	0.210 × 0.200 × 0.050
Theta range for data collection (°)	2.095 to 28.036	2.10 to 28.05	0.90 to 25.00	1.689 to 27.966
Index ranges	-13 ≤ h ≤ 13, -14 ≤ k ≤ 13, -14 ≤ l ≤ 14	-12 ≤ h ≤ 12, -12 ≤ k ≤ 12, -25 ≤ l ≤ 25	-26 ≤ h ≤ 26, -11 ≤ k ≤ 11, -21 ≤ l ≤ 21	-17 ≤ h ≤ 16, -11 ≤ k ≤ 11, -23 ≤ l ≤ 23
Reflections collected	11470	21161	40293	22463
Independent reflections	4432 [R(int) = 0.0419]	4209 [R(int) = 0.0544]	7331 [R(int) = 0.0644]	4692 [R(int) = 0.0364]
Completeness to theta = 25.00°	99.5 %	97.1 %	100.0 %	99.9 %
Absorption correction	Semi-empirical from equivalents	Semi-empirical from equivalents	Semi-empirical from equivalents	Semi-empirical from equivalents
Max. and min. transmission	1.000 and 0.817	0.9051 and 0.8963	0.9520 and 0.8259	1.000 and 0.788
Refinement method	Full-matrix least-squares on F ²	Full-matrix least-squares on F ²	Full-matrix least-squares on F ²	Full-matrix least-squares on F ²
Data / restraints / parameters	4432 / 0 / 260	4209 / 240 / 290	7331 / 0 / 511	4692 / 0 / 253
Goodness-of-fit on F²	0.991	0.870	0.920	1.223
Final R indices [I > 2sigma(I)]	R1 = 0.0371, wR2 = 0.0670	R1 = 0.0296, wR2 = 0.0563	R1 = 0.0375, wR2 = 0.0736	R1 = 0.0485, wR2 = 0.1039
R indices (all data)	R1 = 0.0490, wR2 = 0.0698	R1 = 0.0332, wR2 = 0.0575	R1 = 0.0594, wR2 = 0.0791	R1 = 0.0563, wR2 = 0.1068
Largest diff. peak and hole, e·Å⁻³	0.739 and -0.645	0.874 and -0.428	0.590 and -0.338	0.812 and -0.721

Table 5. Crystal data and structure refinement for [20b](BF₄)·H₂O and [21a]Cl·CDCl₃·H₂O.

	[20b](BF ₄)·H ₂ O	[21a]Cl·CDCl ₃ ·H ₂ O
Empirical formula	C ₂₃ H ₂₂ BF ₄ N ₃ O ₂ RuS	C ₃₀ H ₃₇ Cl ₄ N ₅ O _{1.50} PRu
Formula weight	592.38	765.48
Temperature (K)	173(2)	293(2)
Wavelength (Å)	0.71073	0.71073
Crystal system	Monoclinic	Monoclinic
Space group	P2 ₁ /n	P 2 ₁ /c
a (Å)	10.6443(15)	14.322(2)
b (Å)	8.1103(12)	12.0795(18)
c (Å)	26.129(4)	18.949(3)
α (°)	90	90
β (°)	92.674(2)	97.666(3)
γ (°)	90	90
Volume (Å³)	2253.2(6)	3248.8(8)
Z	4	4
Density (calculated) (g/cm³)	1.746	1.565
Absorption coefficient (mm⁻¹)	0.850	0.896
F(000)	1192	1564
Crystal size (mm³)	0.19 x 0.11 x 0.08	0.210 x 0.200 x 0.180
Theta range for data collection (°)	1.56 to 25.00	1.435 to 24.998
Index ranges	-12≤h≤12, -9≤k≤9, -31≤l≤31	-16≤h≤17, -14≤k≤14, -22≤l≤22
Reflections collected	21485	31535
Independent reflections	3971 [R(int) = 0.0551]	5724 [R(int) = 0.0568]
Completeness to theta = 25.00°	100.0 %	97.2 %
Absorption correction	Semi-empirical from equivalents	Semi-empirical from equivalents
Max. and min. transmission	0.9351 and 0.8552	1.000 and 0.744
Refinement method	Full-matrix least-squares on F2	Full-matrix least-squares on F2
Data / restraints / parameters	3971 / 0 / 317	5724 / 0 / 395
Goodness-of-fit on F2	1.107	0.927
Final R indices [I>2sigma(I)]	R1 = 0.0278, wR2 = 0.0698	R1 = 0.0378, wR2 = 0.0804
R indices (all data)	R1 = 0.0307, wR2 = 0.0755	R1 = 0.0527, wR2 = 0.0841
Largest diff. peak and hole, e·Å⁻³	0.576 and -0.315	0.919 and -0.730

Table 6. Crystal data and structure refinement for [23a]Cl, [23b]Cl·3H₂O and [23b](OTf).

	[23a]Cl	[23b]Cl·3H ₂ O	[23b](OTf)
Empirical formula	C ₂₃ H ₂₅ Cl ₂ N ₃ Ru	C ₁₉ H ₂₃ Cl ₂ N ₃ O ₃ Ru	C ₂₀ H ₁₇ ClF ₃ N ₃ O ₃ RuS
Formula weight	515.45	513.37	572.95
Temperature (K)	170(2)	290(2)	290(2)
Wavelength (Å)	0.71073	0.71073	0.71073
Crystal system	Orthorhombic	Monoclinic	Monoclinic
Space group	Aba2	P2 ₁ /c	P2 ₁ /n
a (Å)	13.608(3)	13.005(2)	14.3937(16)
b (Å)	18.051(4)	12.5510(19)	7.8999(9)
c (Å)	17.118(4)	14.079(2)	19.195(2)
α (°)	90	90	90
β (°)	90	117.381(2)	101.489(2)
γ (°)	90	90	90
Volume (Å³)	4204.8(15)	2040.7(5)	2138.9(4)
Z	8	4	4
Density (calculated) (g/cm³)	1.628	1.671	1.779
Absorption coefficient (mm⁻¹)	1.015	1.056	1.010
F(000)	2096	1040	1144
Crystal size (mm³)	0.20 × 0.10 × 0.10	0.31 × 0.11 × 0.11	0.29 × 0.27 × 0.26
Theta range for data collection (°)	2.22 to 25.00	2.30 to 24.99	2.17 to 24.99
Index ranges	-16 ≤ h ≤ 16, -21 ≤ k ≤ 21, -20 ≤ l ≤ 20	-15 ≤ h ≤ 15, -14 ≤ k ≤ 14, -16 ≤ l ≤ 16	-17 ≤ h ≤ 17, -9 ≤ k ≤ 9, -22 ≤ l ≤ 22
Reflections collected	20082	19831	20436
Independent reflections	3705 [R(int) = 0.0630]	3599 [R(int) = 0.0526]	3771 [R(int) = 0.0736]
Completeness to theta = 25.00°	99.9 %	100.0 %	99.9 %
Absorption correction	Semi-empirical from equivalents	Semi-empirical from equivalents	Semi-empirical from equivalents
Max. and min. transmission	0.9053 and 0.8228	0.8927 and 0.7356	0.7792 and 0.7583
Refinement method	Full-matrix least-squares on F ²	Full-matrix least-squares on F ²	Full-matrix least-squares on F ²
Data / restraints / parameters	3705 / 1 / 277	3599 / 0 / 241	3771 / 0 / 301
Goodness-of-fit on F²	1.023	0.927	1.083
Final R indices [I>2sigma(I)]	R1 = 0.0262, wR2 = 0.0524	R1 = 0.0236, wR2 = 0.0604	R1 = 0.0283, wR2 = 0.0777
R indices (all data)	R1 = 0.0277, wR2 = 0.0529	R1 = 0.0271, wR2 = 0.0618	R1 = 0.0314, wR2 = 0.0791
Largest diff. peak and hole, e·Å⁻³	0.545 and -0.531	0.439 and -0.331	0.575 and -0.326

Table 7. Crystal data and structure refinement for [24b](OTf) and [25a]I·CH₃OH.

	[24b](OTf)	[25a]I·CH ₃ OH
Empirical formula	C ₂₀ H ₁₆ ClF ₃ N ₂ O ₃ RuS ₂	C ₂₄ H ₂₉ I ₂ N ₃ ORu
Formula weight	589.99	730.37
Temperature (K)	298(2)	290(2)
Wavelength (Å)	0.71073	0.71073
Crystal system	Monoclinic	Monoclinic
Space group	P 2 ₁ /n	P 2 ₁ /n
a (Å)	10.5043(8)	12.597(2)
b (Å)	24.9337(19)	9.7730(18)
c (Å)	17.1279(13)	21.637(4)
α (°)	90	90
β (°)	95.721(2)	91.462(3)
γ (°)	90	90
Volume (Å³)	4463.6(6)	2662.9(9)
Z	8	4
Density (calculated) (g/cm³)	1.756	1.822
Absorption coefficient (mm⁻¹)	1.060	2.927
F(000)	2352	1408
Crystal size (mm³)	0.27 x 0.22 x 0.15	0.210 x 0.100 x 0.090
Theta range for data collection (°)	1.633 to 24.997	1.850 to 24.999
Index ranges	-12≤h≤12, -29≤k≤29, -20≤l≤20	-14≤h≤14, -10≤k≤11, -25≤l≤25
Reflections collected	43935	13165
Independent reflections	7857 [R(int) = 0.0854]	4522 [R(int) = 0.1157]
Completeness to theta = 25.00°	97.3 %	94.0 %
Absorption correction		
Max. and min. transmission		
Refinement method	Full-matrix least-squares on F ²	Full-matrix least-squares on F ²
Data / restraints / parameters	7857 / 24 / 536	4522 / 0 / 275
Goodness-of-fit on F²	0.864	0.984
Final R indices [I>2sigma(I)]	R1 = 0.0578, wR2 = 0.1420	R1 = 0.0552, wR2 = 0.1260
R indices (all data)	R1 = 0.0989, wR2 = 0.1574	R1 = 0.0875, wR2 = 0.1389
Largest diff. peak and hole, e·Å⁻³	1.260 and -0.683	1.580 and -0.993

Table 8. Crystal data and structure refinement for [33](OTf)₂·H₂O.

[33](OTf) ₂ ·H ₂ O	
Empirical formula	C ₂₄ H ₂₆ F ₆ N ₂ O ₉ RuS ₂
Formula weight	765.66
Temperature (K)	293(2)
Wavelength (Å)	0.71073
Crystal system	Monoclinic
Space group	P 2 ₁ /c
a (Å)	9.4370(7)
b (Å)	31.838(2)
c (Å)	10.1220(7)
α (°)	90
β (°)	95.3160(10)
γ (°)	g = 90
Volume (Å³)	3028.1(4)
Z	4
Density (calculated) (g/cm³)	1.679
Absorption coefficient (mm⁻¹)	0.745
F(000)	1544
Crystal size (mm³)	0.290 x 0.120 x 0.100
Theta range for data collection (°)	1.279 to 24.997
Index ranges	-11≤h≤11, -37≤k≤37, -12≤l≤12
Reflections collected	29581
Independent reflections	5319 [R(int) = 0.0633]
Completeness to theta = 25.00°	97.1 %
Refinement method	Full-matrix least-squares on F ₂
Data / restraints / parameters	5319 / 37 / 372
Goodness-of-fit on F₂	1.017
Final R indices [I>2sigma(I)]	R1 = 0.0803, wR2 = 0.2319
R indices (all data)	R1 = 0.1122, wR2 = 0.2522
Largest diff. peak and hole, e·Å⁻³	0.881 and -0.904

Table 9. Crystal data and structure refinement for [34]Cl·H₂O, [39]Cl·H₂O and [40b].

	[34]Cl·H ₂ O	[39]Cl·H ₂ O	[40b]
Empirical formula	C ₂₂ H ₂₈ Cl ₂ IrN ₃ O ₂	C ₂₃ H ₂₇ Cl ₂ IrN ₃ O _{0.50}	C ₂₃ H ₂₃ ClIrNOS
Formula weight	629.57	616.57	589.13
Temperature (K)	290(2)	290(2)	293(2)
Wavelength (Å)	0.71073	0.71073	0.71073
Crystal system	Monoclinic	Monoclinic	Monoclinic
Space group	P 2 ₁ /c	C 2/c	P 2 ₁ /c
a (Å)	17.356(4)	a = 39.176(5)	17.492(2)
b (Å)	7.4700(17)	b = 7.2131(8)	7.1040(10)
c (Å)	18.290(5)	c = 17.803(2)	17.238(2)
α (°)	90	a= 90	90
β (°)	93.749(4)	b= 115.546(2)	103.360(2)
γ (°)	90	g = 90	90
Volume (Å³)	2366.2(10)	4539.0(9)	2084.1(5)
Z	4	8	4
Density (calculated) (g/cm³)	1.767	1.805	1.878
Absorption coefficient (mm⁻¹)	5.891	6.136	6.649
F(000)	1232	2408	1144
Crystal size (mm³)	0.29 x 0.11 x 0.10	0.390 x 0.210 x 0.180	0.300 x 0.110 x 0.100
Theta range for data collection (°)	2.232 to 24.999	2.289 to 24.999	2.393 to 24.999
Index ranges	-20≤h≤20, -8≤k≤8, -21≤l≤21	-46≤h≤46, -8≤k≤8, -21≤l≤21	-20≤h≤20, -8≤k≤8, -20≤l≤20
Reflections collected	21956	21497	19814
Independent reflections	4073 [R(int) = 0.0326]	4009 [R(int) = 0.0409]	3684 [R(int) = 0.0302]
Completeness to theta = 25.00°	95.3 %	97.6 %	97.5 %
Absorption correction	Semi-empirical from equivalents	Semi-empirical from equivalents	
Max. and min. transmission	1.000 and 0.346	1.000 and 0.512	
Refinement method	Full-matrix least-squares on F2	Full-matrix least-squares on F2	Full-matrix least-squares on F2
Data / restraints / parameters	4073 / 0 / 280	4009 / 2 / 288	3684 / 0 / 258
Goodness-of-fit on F2	1.051	0.993	1.023
Final R indices [I>2sigma(I)]	R1 = 0.0258, wR2 = 0.0593	R1 = 0.0253, wR2 = 0.0632	R1 = 0.0257, wR2 = 0.0608
R indices (all data)	R1 = 0.0285, wR2 = 0.0604	R1 = 0.0296, wR2 = 0.0652	R1 = 0.0267, wR2 = 0.0614
Largest diff. peak and hole, e·Å⁻³	2.385 and -0.610	1.450 and -0.873	3.283 and -0.846

PART II. Ir(III) BISCYCLOMETALATED COMPLEXES WITH LUMINESCENT PROPERTIES



LUMINESCENCE IN ORGANOMETALLIC COMPOUNDS: A BRIEF REVIEW OF PROCESSES, FEATURES, PROPERTIES AND APPLICATIONS



1. LUMINESCENCE

The interest for luminescent organometallic complexes aroused from ancient times. The word "luminescence", which comes from the Latin root *lumen* = light, was first used in 1888 by a German physicist, Eilhardt Wiedemann, who divided luminescence into six different types: photoluminescence, thermoluminescence, electroluminescence, crystalloluminescence, triboluminescence and chemiluminescence. Nonetheless, Francis Bacon reported the first recorded discovery of mechanoluminescence in 1605. In 1663, Robert Boyle began some luminescent studies with diamond, describing phosphorescence, thermoluminescence, electroluminescence and triboluminescence in a single substance, a diamond. In any case, the year 1603 marked the beginning of modern luminescent materials, when the Italian shoemaker and alchemist Vicenzo Cascariolo tried to turn the mineral barite (BaSO_4) into gold, obtaining a luminescent material. Consequently, by the end of the 1700s, a number of minerals with mechanoluminescence were known. Afterwards, in the 19th and 20th centuries, the German Philip E.A. Lenard used rare earth and heavy metal ions as luminescent materials.^{1,2}

Photoluminescence, the emission of light arising from direct photoexcitation of the emitting species, is divided into fluorescence and phosphorescence. These kinds of luminescence are also called *cold light*, since they do not either require high temperatures or produce noticeable heat, unlike incandescence.² Fluorescence and phosphorescence were traditionally thought to differ in the lifetime, being longer *a priori* for phosphorescence. Nevertheless, this is a mistaken criterion, because there are long-lived fluorescences as well as short-lived phosphorescences. The correct term has to do with the spin multiplicity of the excited state from which the emission of light is produced. Thus, the spin multiplicity is retained in fluorescence processes, whereas phosphorescence involves a change in spin multiplicity in the emission or radiative process, from a triplet state to a singlet one. Thus, phosphorescence typically takes more time than fluorescence² (see spin multiplicity in Fig. 1).

1.1. Process of Luminescence

The emission of light in the phenomenon of photoluminescence occurs when a **fluorophore** absorbs energy from light of a specific wavelength and then re-emits energy at a different but also specific wavelength.³ The Jablonski diagram⁴ in Fig. 1 depicts the electronic levels and the transitions between singlet and triplet states. Firstly, a photon is absorbed by a molecule, reaching an excited state of high energy. This energy is too large to be reached by thermal activation, so that light is necessary.⁵ Absorptions for organometallic complexes can arise from different types of transitions:

- Transitions between metal-centred orbitals possessing d-character (d-d transitions).

- Transitions between metal- and ligand-centred molecular orbitals (MOs) with transfer charge from the metal to the ligand (MLCT) or from the ligand to the metal (LMCT).

Intense absorptions correspond to charge transfer (CT) processes and often occur at higher energies, whereas d-d bands are usually weaker and fall at lower energies. Absorption bands in electronic spectra are usually broad, since the absorption of a photon of light occurs in $\approx 10^{-18}$ s and molecular vibrations and rotations are slower. Regarding these transitions, they can be allowed or forbidden, according to the selection rules.⁶

- **Spin selection rule: $\Delta S = 0$**

Transitions are only allowed between states with the same spin multiplicity (singlet to singlet or triplet to triplet), and forbidden between states with different spin multiplicity.

- **Laporte selection rule: $\Delta l = \pm 1$**

This selection rule only applies to centrosymmetric molecules (those with an inversion centre). It states that electronic transitions that conserve parity are forbidden, whereas electronic transitions that involve a change in parity are allowed. Thus, allowed transitions are those between different orbitals involving $\Delta l = \pm 1$, that is $s \rightarrow p$, $p \rightarrow d$, $d \rightarrow f$, whereas those implying $\Delta l = 0$ ($s \rightarrow s$, $p \rightarrow p$, $d \rightarrow d$, $f \rightarrow f$) or $\Delta l = \pm 2$ ($s \rightarrow d$, $p \rightarrow f$) are forbidden.

Nonetheless, there are some mechanisms capable of mixing singlet and triplet states, on the one hand, and p and d orbitals, on the other hand, which turns some forbidden transitions into allowed ones.⁶

- **Spin-orbit coupling:** This kind of coupling allows spin-forbidden transitions by mixing states with different spin multiplicity. In particular, the transitions between states of different spin multiplicity give rise to the so-called intersystem crossing processes. For first row metals the degree of mixing is small and the intensity of absorption bands is very weak.⁶
- **Vibronic coupling:** Spin-allowed d-d transitions still remain Laporte-forbidden. However, an octahedral complex with a centre of symmetry can momentarily lose this symmetry due to molecular vibrations. In this moment a mixing between d and p orbitals can occur. Since the lifetime of vibration ($\approx 10^{-13}$ s) is longer than that of an electronic transition ($\approx 10^{-18}$ s), a d-d transition involving an orbital of mixed p-d character can occur although the absorption is still relatively weak. In non-centrosymmetric molecules, for instance, tetrahedral, p-d mixing can occur to a greater extent and the probability of d-d transitions is greater than in a centrosymmetric complex. Therefore, tetrahedral complexes are more coloured than the octahedral ones.⁶

The absorption spectra of d-block metals show some important features⁶:

- d^1 , d^4 , d^6 and d^9 complexes provide one absorption spectra;
- d^2 , d^3 , d^7 and d^8 complexes provide three absorptions spectra;
- d^5 complexes provide a series of very weak, relatively sharp absorptions in their spectra.

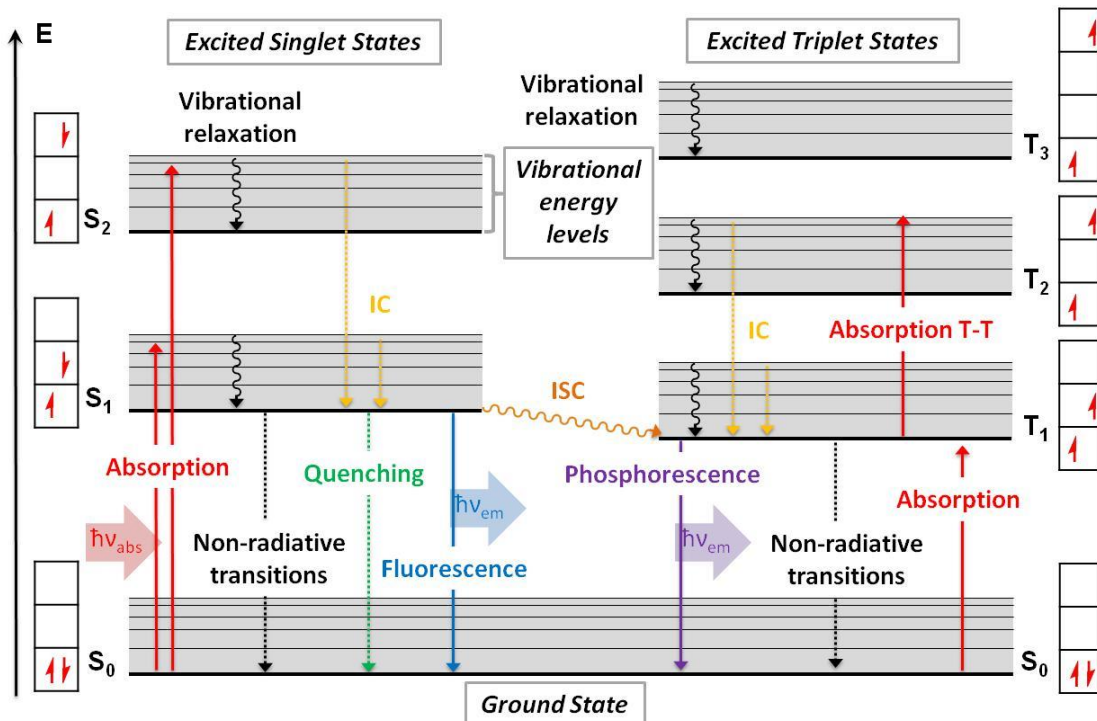


Fig. 1. Jablonski energy diagram illustrating electronic levels and possible transitions between different singlet and triplet states. IC means internal conversion and ISC intersystem crossing. Timescale of processes: absorption ($\sim 10^{-15}$ s); vibrational relaxation and internal conversion ($\sim 10^{-14} - 10^{-10}$ s); non-radiative transitions and quenching ($\sim 10^{-7} - 10^{-5}$ s); fluorescence ($\sim 10^{-9} - 10^{-7}$ s); phosphorescence ($\sim 10^{-3} - 100$ s); intersystem crossing ($\sim 10^{-10} - 10^{-8}$ s). Self-creation based on traditional Jablonski diagram.

Once the molecule is in an unstable excited state, the molecule must undergo some type of deactivation or relaxation in different ways (see Fig. 1)^{7,8}:

- From singlet states:
 - **Internal Conversion:** from a singlet state S_n ($n > 1$) to the lowest excited singlet state S_1 .
 - From S_1 to the ground state S_0 via:
 - **Fluorescence:** direct emission of a photon between singlet states.
 - **Non-radiative transitions:** dissipation of part of the absorbed energy as heat.
 - **Quenching:** transfer of energy to another molecule at distance (energy transfer at distance) or by collision (collisional quenching).
 - **Intersystem crossing:** relaxation from a singlet state S_1 to a triplet state T_1 , with lower energy than that of S_1 .

- From triplet states:
 - o **Internal Conversion:** from a triplet T_n to the lowest triplet excited state T_1 .
 - o **Phosphorescence:** emission of a photon from T_1 to the ground state S_0 .
 - o **Non-radiative transitions:** dissipation of non-radiative energy in form of heat.
 - o **Quenching:** transfer of energy to another molecule at distance or by collision.

Fluorescence and internal conversion are spin-allowed processes, whereas phosphorescence and intersystem crossing are spin-forbidden phenomena (triplet/singlet). They need spin reorientation and therefore, their lifetimes tend to be much longer than those for spin-allowed processes.⁸ Each intramolecular decay process is characterized by its own rate constant and each excited state is characterized by its **lifetime (τ)**.⁷ The most important features defining a fluorophore are lifetime as well as **quantum yield (PLQY, ϕ)**. Quantum yield reflects the number of emitted photons relative to the number of absorbed photons, being the unit the maximum value. Lifetime, however, depicts the average time the molecule spends in the excited state prior to return to the ground state.⁵ All these processes and transitions are gathered in the Jablonski diagram in Fig. 1.

1.2. d-Block Metal Complexes

Organometallic complexes of transition elements belonging to d- and f-blocks are on top of phosphorescent compounds. Lanthanides(III) have excellent luminescent properties, since the excited state can be populated easily and the non-radiative deactivation paths are minimized.⁹ Regarding the d-block, the most studied systems are the d⁶ complexes of rhenium, ruthenium and iridium, although some d⁸ and d¹⁰ platinum and gold complexes have been also used.¹⁰ All of them share some common features:

- **Photophysics:** the emission mainly involves metal-to-ligand charge transfer (MLCT) processes from electron-rich low oxidation state mid- to late-transition metals to conjugated aromatic heterocycles capable of accepting electrons, although they usually are mixed with intra- or inter-ligand (IL) electron transfer transitions. Polypyridyl N⁺N ligands (Ru, Rh) and cyclometalating C⁺N ligands (Ir, Rh), along with alkyl and thiolate ligands (Pt, Au) belong to the most common systems used.¹⁰ Furthermore, they present excitation in the visible region of the spectrum, large Stockes' shifts and long lifetimes.¹¹
- **Photostability:** They show reduced **photobleaching** in comparison with other organic fluorophores.¹¹
- **Kinetic stability toward ligand exchange:** They possess low rates of ligand exchange, reducing the toxicity of the complexes.¹¹

A search of the published papers from 1980 to 2015, with the term “metal luminescent” (*e.g.* ruthenium luminescent or rhenium luminescent) in the Web of Science can get an idea of the quick increase of publications of some metal complexes with luminescent properties. Some of them, such as gold, ruthenium and iridium, have experienced a quasi-exponential tendency, whereas some other metal complexes, such as palladium or rhenium, have grown more slowly, following a linear tendency (see Fig. 2). Moreover, despite the huge amount of iridium cyclometalated complexes already studied, iridium is still behind other metal complexes, being the number of publications half of those for ruthenium complexes (see Fig. 2).

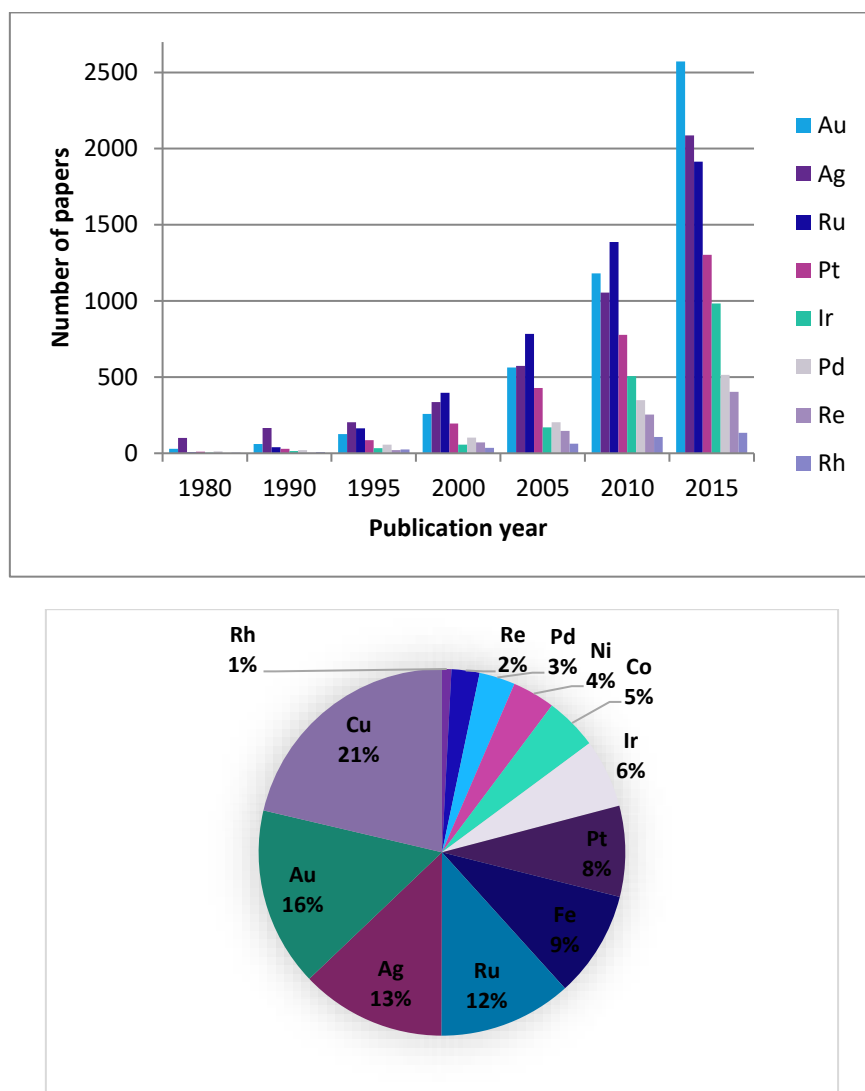


Fig. 2. Bar codes and pie chart for published papers from 1980 to 2015 about luminescent metal complexes. (a) Evolution of different transition metals and (b) relative abundance of papers for different metal complexes.

Hence, we will focus on the cyclometalated Ir(III) and Rh(III) d-block metals.

1.3. Cyclometalated Ir(III) and Rh(III) complexes

Cyclometalated Ir(III) and Rh(III) complexes are octahedral complexes, consisting of three bidentate chelating ligands. When the three ligands are cyclometalated and equal

in nature, the complexes are called *homoleptic* ($[\text{Ir}(\text{C}^{\wedge}\text{N})_3]$), whereas when the ligands are different (*i.e.* only two of them are identical), they are called *heteroleptic* or biscyclocmetalated ($[\text{Ir}(\text{C}^{\wedge}\text{N})_2(\text{N}^{\wedge}\text{N})]$).¹²

1.3.1. Synthesis

The synthetic methodology for cyclometalated Ir(III) complexes is simple and effective and basically consists in two steps:

- Synthesis of dinuclear starting products.** Previous studies of the reaction of 2,2'-bipyridine (bpy) with Ir(III) indicated that the carbo-metalation occurred sometimes spontaneously through the C-3 position of a pyridine, adjacent to a second N-coordinated pyridine.^{13,14} Thus, Nonoyama¹⁵ and then, Sprouse¹⁴ reported a method to synthesize neutral dinuclear chloride-bridged Ir(III) complexes. In this protocol iridium trichloride ($\text{IrCl}_3 \cdot n\text{H}_2\text{O}$) is reacted with the cyclometalating pro-ligand ($\text{HC}^{\wedge}\text{N}$, *e.g.* 2-phenylpyridine) in a mixture of 2-ethoxyethanol and water (3:1 v/v) and refluxed for 24 h under inert atmosphere, yielding the air-stable starting material (see Fig. 3).¹⁴

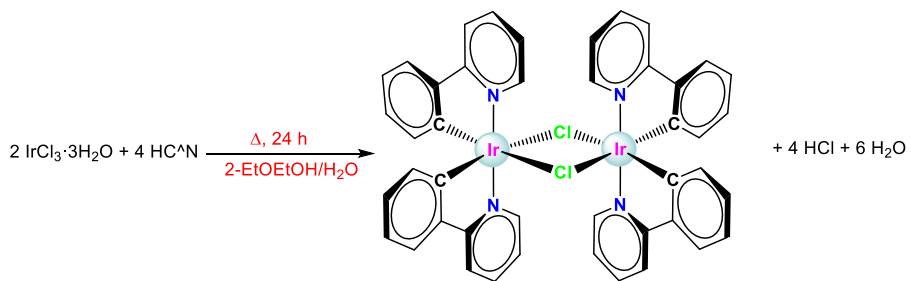


Fig. 3. Synthesis of the dinuclear chlorido-bridged Ir(III) complex $[\text{Ir}(\text{ppy})_2\text{Cl}]_2$.

- Synthesis of mononuclear complexes.** Depending on the nature of the complexes, we can divide the synthesis in two different sections: homoleptic complexes and heteroleptic complexes.

- Synthesis of homoleptic neutral complexes.** The dinuclear starting product $[\text{Ir}(\text{ppy})_2\text{Cl}]_2$ is reacted with a cyclometalating proligand (*e.g.* 2-phenylpyridine) in 2-ethoxyethanol and heated under an inert atmosphere to 100 °C for 18 h (see Fig. 4).¹⁶ The resulting product $[\text{Ir}(\text{ppy})_3]$ was first isolated as a by-product in the synthesis of the dimeric Ir(III) complex. In addition, some other methods have been described, starting from $\text{Ir}(\text{acac})_3$.¹⁷

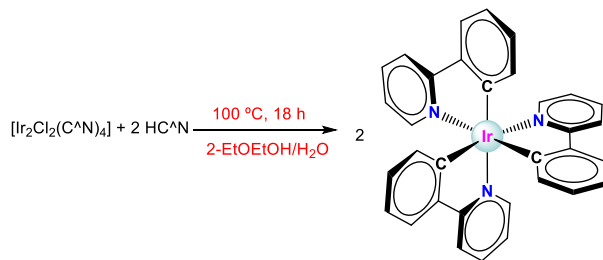


Fig. 4. Synthesis of the homoleptic tris-cyclometalated Ir(III) complex $[\text{Ir}(\text{ppy})_3]$.

b. Synthesis of heteroleptic biscyclometalated cationic and neutral complexes. The synthesis of *heteroleptic biscyclometalated diimine* complexes was first reported by Watts,¹⁸ by reacting the starting dimer $[\text{Ir}(\text{ppy})_2\text{Cl}]_2$ with the chosen diimine N^N ligand (*e.g.* bipyridine, bpy; or phenanthroline, phen) in dichloromethane under inert atmosphere at room temperature for 12 h.¹⁸ However, another more effective synthetic strategy was followed, involving the reaction of the Ir(III) dimer with the diimine ligand in a $\text{CH}_2\text{Cl}_2/\text{MeOH}$ (5:4 v/v) mixture at refluxing temperature for 24 h under inert atmosphere (see Fig. 5).¹⁹ The synthesis of *heteroleptic neutral* complexes with N^O ligands was performed under harsher conditions. The starting dimer was reacted with the desired ligand, in the presence of a base (*e.g.* Na_2CO_3) in refluxing 2-ethoxyethanol or 2-ethoxyethanol/water mixtures (high-boiling alcohols are required) under inert atmosphere for 24 h (see Fig. 5).^{17,20}

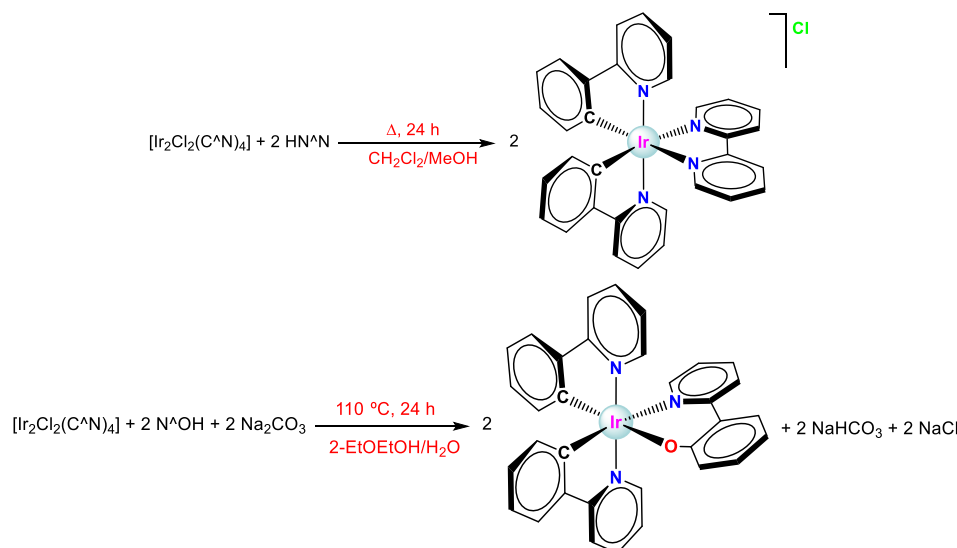


Fig. 5. Synthesis of the heteroleptic bis-cyclometalated Ir(III) complexes $[\text{Ir}(\text{ppy})_2(\text{N}^{\text{N}})]^+$ (up) and $[\text{Ir}(\text{ppy})_2(\text{N}^{\text{O}})]$ (down).

1.4. Stereoisomerism

All the products described before can present different configurations, depending on the mutual disposition of the ligands, and so they possess stereoisomerism. In particular, they exhibit two types of **stereoisomerism**: (a) Diastereoisomerism: *cis*- and *trans*-isomers or *mer*- and *fac*-isomers (b) Enantiomerism or optical isomerism derived from helical chirality.⁶

1.4.1. Diastereoisomerism: *cis*- and *trans*- and *fac*- and *mer*- isomers

With regard to the *cis* and *trans* isomerism,²¹ it is widely established that owing to the strong *trans* effect exerted by the M-C atoms, the cyclometalating carbons generally adopt a *cis* disposition one to another, whereas the N atoms adopt a *trans*

disposition in most of the biscyclometalated compounds.^{13,14} Thus, in both the heteroleptic biscyclometalated complexes and the dinuclear chlorido bridged dimers, the *trans*-N,N *cis*-C,C configuration is favoured over the two other possible stereoisomers or diastereoisomers (see Fig. 6).¹³

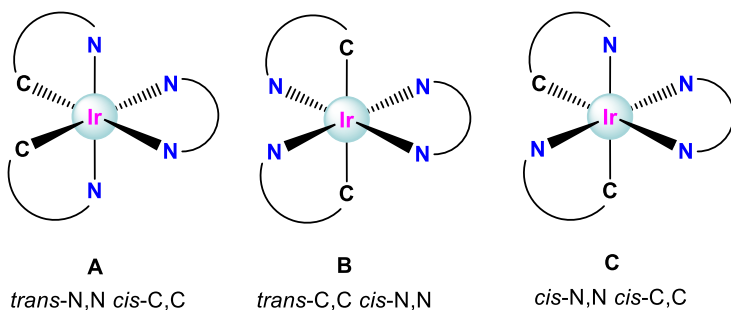


Fig. 6. Geometrical isomers for heteroleptic Ir(III) complexes.

As for homoleptic complexes, there are two possible diastereoisomers: *fac* (facial) and *mer* (meridional) (see Fig. 7).²¹ The *fac* isomer is the thermodynamically favoured isomer (more stable), whereas the *mer* isomer is the kinetic product.¹² Furthermore, there are some differences regarding the structural properties. In a *fac* isomer the Ir-C and Ir-N bonds have nearly identical lengths. For the *mer* isomer, the bonds *trans* to the Ir-C bond are slightly longer than those *trans* to the Ir-N bonds.¹³ In addition, the *mer* isomer can be converted into the *fac* isomer by thermal or photochemical conversion.¹²

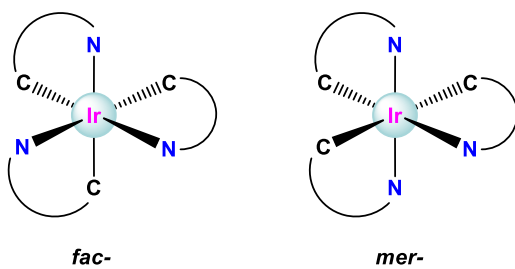


Fig. 7. Optical isomers for homoleptic Ir(III) complexes.

1.4.2. Enantiomerism derived from helicoidal chirality

On the other hand, hexacoordinated octahedral complexes with either two bidentate chelate ligands in a *cis* disposition (*cis*-bis-chelate complexes) or three bidentate chelate ligands (*tris*-chelate complexes) display helicoidal or helical chirality. The chiral element in these molecules arises from the geometry of a helix, which is by nature chiral. The resulting enantiomers are distinguished by using the labels (descriptors) Λ and Δ to specify their absolute configuration. To assign the labels, the octahedron must be viewed down a 3-fold axis, so that the chelates define then either a right- or a left-handed helix. The enantiomer with righthandedness (clockwise motion) is labelled Δ , and that with left-handedness (anticlockwise motion) is labelled Λ (see Fig. 8).^{6,21}

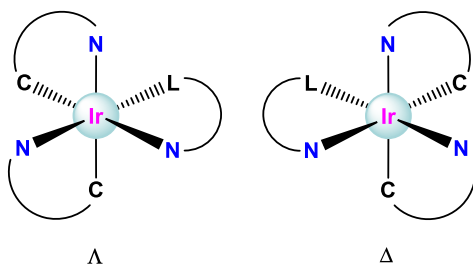


Fig. 8. Λ, Δ -isomers for octahedral Ir(III) complexes.

In particular, regarding the dimeric starting products, there are two helices in every molecule and hence two stereogenic or chiral elements. As a result, three possible stereoisomers or diastereoisomers result in theory (see Fig. 9)²¹:

- the *racemate*, which consists of an equimolar mixture of the two enantiomers (Λ, Λ) and (Δ, Δ).
- And the *meso* form, which is labelled as (Λ, Δ) = (Δ, Λ), and is achiral. The two possible configurations of the *meso* form are equivalent and therefore they are the same compound. Besides, the *meso* compound and each of the enantiomers in the racemate are diastereoisomers.

Nevertheless, x-ray structures and structural models have determined that the racemate is favoured, since there is high steric hindrance in the *meso* form.¹⁴

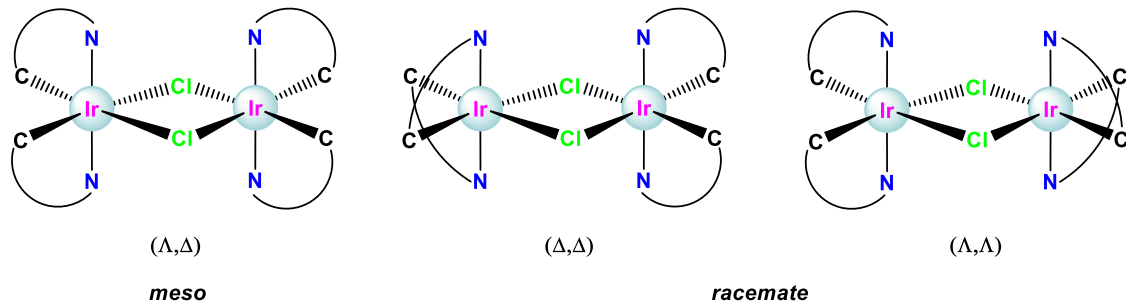


Fig. 9. Stereoisomerism for the dimeric bis-cyclometalated Ir(III) complexes.

1.5. Intrinsic Properties

Rh(III) and Ir(III) possess $4d^6$ and $5d^6$ configurations, respectively.¹³ In an octahedral environment, the d orbitals split into two sets of degenerate orbitals, t_{2g} and e_g , separated by an energy gap (Δ_{oct}), so that the t_{2g} orbitals are fully occupied and the e_g fully unoccupied (see Fig. 10). The magnitude of Δ_{oct} depends on (i) the oxidation state of the metal, (ii) the size of the orbitals and (iii) the field strength of the ligands.²²

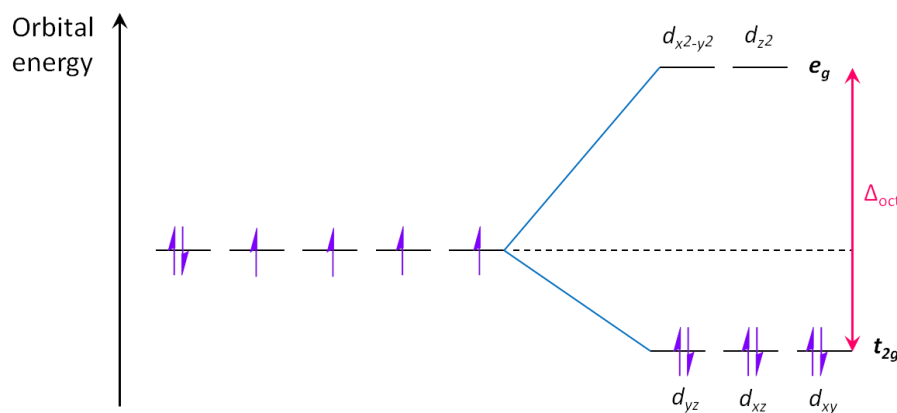


Fig. 10. Crystal field splitting diagram (LFSE) and d^6 electronic configuration for the free metal M(III) in gas phase (left) and for the octahedral complexes (right).

The value of the Δ_{oct} follows an experimental spectrochemical series for metals (independent of the ligands) and shows the next sequence⁶:



As we can see, the crystal field strength for Ir(III) is higher than for Rh(III), due to the higher size of the 5d orbitals compared to the 4d.²² In addition, and considering the spectrochemical series for ligands (see below)⁶, we can conclude that the LFSE (Ligand-Field Splitting Energy) for polypyridyl complexes shows a very high magnitude.



Strong-field N^{^4}N ligands, such as bpy and phen, stabilize the electronic configuration, the same as the C^{^4}N ligands do, owing to their strong σ -donor and π -acceptor properties.²² Thus, this kind of compounds possess special features, making them truly relevant as luminescent complexes, specially the bis-cyclometalated Ir(III) complexes. The properties of these complexes are gathered below:

- **High thermal and chemical stability** and very low ligand exchange rates,^{11,22,23} due to the strong σ -donor and covalent character of the Ir-C(C^{^4}N) bond. Most of these complexes remain stable even after photoirradiation or repeating electrochemical cycling.²²
- **Intrinsic photophysical properties.**
 - o *High spin-orbit coupling (SOC).* Indeed, Ir(III) presents the largest spin-orbit coupling constant of any metal in the d-block. $\xi_{\text{Ir}} = 3909 \text{ cm}^{-1}$, compared to $\xi_{\text{Fe}} = 431 \text{ cm}^{-1}$, $\xi_{\text{Ru}} = 1042 \text{ cm}^{-1}$, $\xi_{\text{Os}} = 3381 \text{ cm}^{-1}$ ²² and $\xi_{\text{Rh}} = 1425 \text{ cm}^{-1}$.²⁴ This leads to highly mixed spin character of the emitting excited states,²⁵ making in turn the ISC so fast as to be considered unitary.^{22,26}
 - o *Large Stokes' shifts.* The Stokes' shift is the difference in energy between the lowest-energy absorption band and the emitting band.²⁷ In other

words, in phosphorescent compounds, it is the energy lost in the conversion process from the singlet to a triplet state and its subsequent geometrical reorganisation.¹⁰ Organic fluorophores usually have small Stokes' shifts, since the excited state is the same (normally S_1). Furthermore, self-absorption of light (self-quenching) occurs when there is overlapping of the emission and absorption spectra. On the contrary, phosphorescence in metal complexes emerges from different states (energy absorption from a singlet state to a excited singlet state and emission from a triplet state), so that overlapping is almost impossible.²⁷

- *Large Δ_{oct} .* The high oxidation state of Ir(III) along with the size of the 5d orbitals,²² make the energy-gap for Ir-polyimine complexes increase, reaching energies in the range 2.1 to 3 eV.¹³ In addition, the strong σ -donor of C^N ligands increases the Δ_{oct} gap, making the CT transitions (MLCT and LLCT or LC) accessible, and avoiding the non-emissive MC transitions involved in phosphorescence quenching.^{22,24,28}
- **Long luminescence lifetimes.** Lifetimes of excited states in Ir(III) complexes fall in the scale ns- μ s to even ms.^{23,29} This is the consequence of the forbidden nature of the $^3\text{MLCT}$ transitions (triplet to singlet transition along with the following spin reorganization).^{10,30} In addition, typical radiative constants of the $^3\text{MLCT}$ transitions are higher, than those of the ^3LC transitions, leading to shorter lifetimes for the former.¹³ Nonetheless, long lifetimes run the risk of increasing the excited state quenching processes,³⁰ for instance, by triplet quenchers as $^3\text{O}_2$.²³
- **High Quantum Yields (QY).** The QY of the Ir(III)-cyclometalated family is defined as a mixture of luminescence efficiencies of the $^3\text{MLCT}$ and ^3LC levels. High QY of Ir(III) complexes, approaching 100% have been reported.^{12,22,31}
- **Colour tuning.** The emission colour of cyclometalated Ir(III) and Rh(III) complexes can be easily tuned, varying the energy gap difference. This is the difference between the HOMO (usually located on the metal and C^N ligands in heteroleptic biscyclometalated complexes) and LUMO (usually located on the ancillary N,N ligands in heteroleptic biscyclometalated complexes).¹³ Thus, independent chemical modifications on both the cyclometalating and the ancillary ligands can lead to efficient colour tuning as well as variations in quantum yields and lifetimes.³⁰ To begin with, we ought to analyse the transitions that define the absorption and emission spectra.
 - *Absorption spectra.*^{12,22,32,33} The UV-vis spectra shows two main types of transitions and another weaker one:
 - LC (ligand centered) or IL (intraligand, $\pi-\pi^*$) transitions in the same bidentate ligand (< 350 nm).
 - CT (350 – 450 nm). There are two possibilities:
 - MLCT ($d-\pi^*$) transitions (300 – 380 nm).

- LLCT (π - π^*) transitions in different bidentate ligands (only in heteroleptic complexes) (> 380 nm).
- d-d transitions. These transitions are usually overlapped with more intense LC and MLCT transitions, so that they are not commonly observed.

On the whole, the transitions follow the next energy order: ${}^1\text{LC} > {}^1\text{MLCT} > {}^3\text{MLCT} > {}^3\text{LC}$.²⁴ The singlet ${}^1\text{LC}$ and ${}^1\text{MLCT}$ transitions are spin-allowed, whereas the triplet ${}^3\text{MLCT}$ and ${}^3\text{LC}$ are spin-forbidden, and therefore, less intense.

- *Emission spectra.* The shape of the emission spectra depends on the transitions nature. Although there is usually a mixture of ${}^3\text{MLCT}$ and ${}^3\text{LC}$ transitions, each of them shows typical features.³⁴
 - ${}^3\text{MLCT}$ transitions present broad and structureless bands, independent of the excitation wavelength (λ_{exc}).²⁵ They usually exhibit large Stokes' shifts and solvent dependence.³⁴ Moreover, they tend to be lower in energy (red-shifted),²⁹ and are associated to the ancillary ligand.³¹
 - ${}^3\text{LC}$ transitions show vibrationally structured bands with small Stokes' shifts,³⁴ which are usually blue-shifted.²⁹ They also are less sensitive to environmental changes,³⁴ and associated to the cyclometalated ligands.³¹

The HOMO and LUMO levels in Ir(III) complexes are located in different parts, depending on their nature:

- *Homoleptic complexes.* The HOMO is localized on the phenyl ring of the cyclometalated ligand (π orbital) and in the Ir(III) centre, while the LUMO is distributed on the pyridine ring of the same ligand (π^* orbital).^{24,28}
- *Heteroleptic complexes.* The HOMO is also located on the phenyl ring of the cyclometalated ligand and in the Ir(III) centre, yet the LUMO is placed on the ancillary ligand.^{24,25}

Thus, there are three main strategies to tune the emission colour by adding electron-withdrawing or electron-donating groups to (i) the pyridine rings of the ppy ligand (LUMO), (ii) the phenyl rings of the ppy ligands (HOMO) or (iii) the ancillary ligand (LUMO). Fig. 11 shows an example of colour tuning for homoleptic and heteroleptic cyclometalated Ir(III) complexes, changing the three possible moieties.

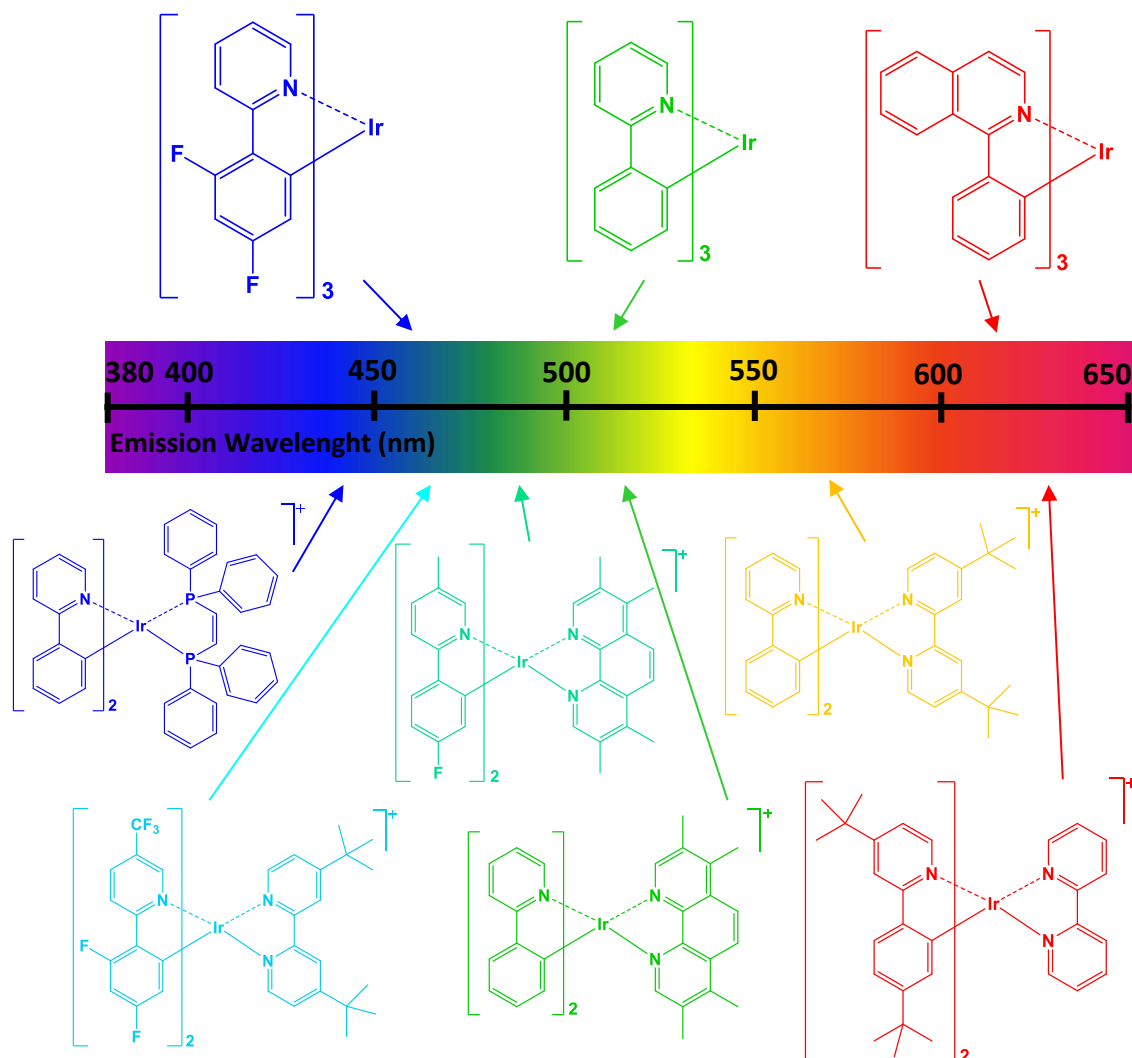


Fig. 11. The visible emission spectrum and versatility of typical homoleptic (up) and heteroleptic (down) cyclometalated Ir(III) complexes. Diagram based on Fan, C.; Yang, C. *Chem. Soc. Rev.* 2014, **43**, 6439–6469 and Lowry, M. S.; Bernhard, S. *Chem. - A Eur. J.* 2006, **12**, 7970–7977.^{28,31}

The electronic delocalization of π -extended systems in the pyridyl ring of C^N ligands or in the ancillary ligand N^N causes the stabilization of the LUMO in homoleptic and heteroleptic complexes respectively.^{13,31} As a consequence, the energy gap diminishes, leading to red-shifted colours (see Fig. 11). When the pyridyl moiety is changed, however, by a pyrazole in homoleptic complexes, a blue-shift is produced.¹⁷

Electron-withdrawing substituents ($-F$, $-CF_3$) at the phenyl-cyclometalating ring tends to stabilize the HOMO by removing electron density from the metal,^{13,31} leading to larger energy gaps and blue-shifted colours (see Fig. 11). Nevertheless, when these groups are attached to the pyridyl moiety or to the ancillary ligand in homoleptic and heteroleptic complexes respectively, the LUMO stabilizes, shifting to the red.³⁵ On the other hand, electron-donating substituents ($-C(CH_3)_3$, $-OCH_3$) have just the opposite effect.³⁶ In addition, these effects depend on the position of the groups with respect to the cyclometalating carbon atom.¹⁷ That

is, electron-withdrawing groups in *meta*- have the same effect as electron-donating substituents in *ortho*- or *para*-, and vice versa.³¹

Altering the size of the ligands, localizing electron density in discrete regions of the molecule or destroying ligand aromaticity are other well-established strategies to tune the colour emission. However, non-radiative decay can occur, when, for instance, bulky pendant groups are used to distort a ligand from planarity with the consequent destabilization of its π orbitals.³¹

1.6. Properties according to External Features

Furthermore, these complexes show other properties related to phosphorescence, according to external stimuli:

- *Mechanochromism.* These materials present changes in the emission colour in the presence of mechanical stimuli (e.g. shearing, grinding and rubbing) due to the interruption of intermolecular interactions, such as π - π stacking or hydrogen bonding.³⁷
- *Piezochromism* (piezochromic luminescence, PCL). PCL is a specific kind of mechanochromism, when the external condition is pressure. A bathochromic effect occurs upon grinding and the initial colour is usually recovered with heating or fuming.^{22,24,38} In fact, this colour change has been attributed to crystalline-amorphous phase transformations.³⁹ Modifications in the length of the N-alkyl chain in the ancillary ligands easily cause emission colour changes.^{38,39}
- *Vapochromism.* A change on the emission colour occurs as a response to volatile organic compounds.³⁷
- *Solvatochromism.* The emission colour changes, depending on the solvent in which the complex is dissolved.³⁷ Solvatochromism is characteristic of CT transitions⁴⁰ and polar solvents induce high-energy shifts (hypsochromic shift).⁴¹
- *Rigidochromism.* When a solution of a complex is cooled to 77 K, it becomes a solid matrix, the surrounding medium dipoles are unable to reorient to change its dipole character between excited and ground states.²⁵ This lead to divergent situations, regarding the emission spectra:
 - o The spectrum becomes structured. In this case LC transitions are predominant.⁴²
 - o The spectrum red-shifts. LC transitions cause slightly red-shifts or they are unaffected by the cooling.¹³
 - o The spectrum blue-shifts. CT transitions undergo large blue-shifts^{13,43}
 - o An increase in the bandwidth implies a major extent of CT transitions and a decrease, an increment in the LC transitions.²⁵
- *Electrochromism.* This property illustrates the capability of a material to alter its optical properties under electrical stimuli.⁴⁴ An applied voltage causes a change of colour. However, this effect does not originate from redox reactions, since the

complexes remain unchanged. It is the result of the non-homogeneous distribution of the ions, leading to a strong electric field.³⁷

- *pH-chromism.* Small changes in the pH of a solution of an iridium(III) cyclometalated complex can lead to large changes in the emission colour. Some groups or substituents are prone to protonating or deprotonating, modifying its electron-donating or electron-withdrawing ability and consequently, the colour of the emission spectrum.⁴⁵

1.7. Applications

Taking into account all these features, bis-cyclometalated Ir(III) complexes can be postulated as the most suitable compounds for almost any luminescent use among all of the d-block metal complexes, whereas Rh(III) have limited properties. Thus, the applicability of this kind of complexes is really wide.

- *Sensors.*

- *Analytes detection: cations, anions (chemosensors).* Cation sensors are based on the incorporation of a cation-receptor such as a Lewis base or a crown ether into the polypyridine complexes. The inclusion of sulphur atoms, for example, causes soft-soft interactions with Hg²⁺.^{46,20} Other Ir(III) complexes also work as Zn(II), Cr(III) or Cu(II) sensors.³² Binding of anions to functional polypyridine ligands can affect the emission properties of the complexes, due to electronic effects or chemical reactions between the ion and the complex. In addition, it is important to take into account the molecular geometry and the basicity of the anions.⁴⁶
 - *pH probes.* Ir(III) polypyridine complexes with basic or acidic groups can be used as pH sensors. Many complexes with this property have been reported to date.^{45,46,47,48}
 - *Oxygen detection.* Oxygen is a potent quencher of biscyclometalated Ir(III) polypyridine complexes, based on the energy transfer from the triplet state of the Ir(III) complex to triplet oxygen (ground state oxygen)⁴⁹. Thus, emission is quenched. A sensor for oxygen should accomplish some important requirements: high emission quantum yields, long emission lifetimes, high sensitivity, high reversibility and fast response time.^{46,50}
 - *Biomolecules detection.* Some biomolecules such as DNA,¹⁰ proteins⁴⁶ or amino acids, especially those with thiol groups,⁴⁸ are common targets prone to quenching phosphorescence.
 - *Explosive detection.* There are not many sensors based on heavy-metal complexes able to detect nitroaromatic explosives. Nonetheless, some examples of Ir(III) bis-cyclometalated complexes, whose phosphorescence is quenched by some explosives, like PA (2,4,6-

trinitrophenol) or TNT (2,4,6-trinitrotoluene), have been reported recently.^{39,51}

- *Photodynamic therapy (PDT).* PDT is an alternative for cancer treatment due to its high therapeutic efficacy and lower side effects, allowing targeting the tumour cells with precision.^{52,53} The methodology consists on the irradiation at a specific wavelength of a photosensitizer (PS), an ideally non-toxic molecule with affinity for cancer cells over healthy cells, which is able to reach a singlet excited state ($^1\text{PS}^*$). The PS, then, undergo ISC to reach a triplet state ($^3\text{PS}^*$). At this point, the PS can react with a substrate or solvent molecules (type I reaction), through a proton or an electron transfer process, generating radicals. The PS can also transfer energy to molecular oxygen (type II reaction), forming singlet oxygen ($^1\text{O}_2$) and other reactive oxygen species (ROS) (see Fig. 12).^{52,53,54,55} Singlet oxygen is an oxidizing agent able to cause, ultimately, cell death in a biological environment.⁴⁹

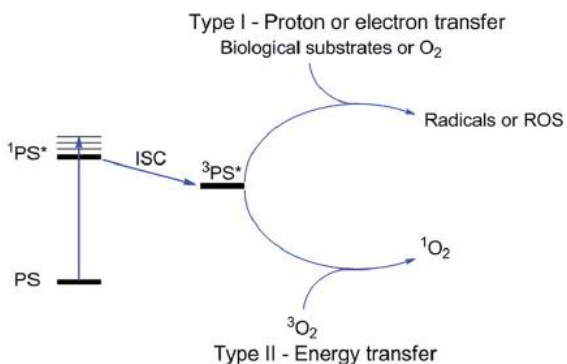


Fig. 12. Mechanisms of action of PDT. Figure extracted from Mari, C.; Pierroz, V.; Ferrari, S.; Gasser, G. *Chem. Sci.* 2015, 6, 2660–2686.⁵⁴

- *Bioimaging.* The properties of this kind of complexes are excellent for biolabel and staining applications.^{24,48} Phosphorescence bioimaging have some advantages over fluorescence techniques because of its properties: (i) large Stokes' shifts, that prevent from self-absorption of light (self-quenching), (ii) high luminescent efficiency (the brighter the emission, less excitation intensity is needed), (iii) facile colour tuning and (iv) long lifetimes, which allow discriminating the signal from the background noise.^{27,32,56}
- *Photoredox catalysis.* As cyclometalated Ir(III) and Rh(III) octahedral complexes possess fully saturated coordination spheres around their Ir or Rh cores, direct interactions with Ir/Rh centres are scarce. Nevertheless, many oxidation states are photoinductively available.²⁴ Thus, there are numerous redox reactions, that cyclometalated Ir(III) or Rh(III) complexes can catalyse, such as CO_2 reduction⁵⁷ or hydrogen production,¹⁷ either from water reduction^{31,58} or proton reduction.⁵⁹
- *Solid-state lightning (SSL).* Semiconductor materials produce visible light under the action of an electrical field in special devices where the transport of charge

occurs unidirectionally. These devices are divided into three groups: light-emitting diodes (LEDs), organic light-emitting diodes (OLEDs) and light-emitting electrochemical cells (LECs). Ir(III) bis-cyclometalated complexes take part in OLEDs when the complexes are neutral, and in LECs when they are cationic.^{17,60} In the recent years, many examples of this kind of complexes have been reported by E. Ortí and H. Bolink,^{61,62} and Y. Choe.^{63,64}

- *Data recording and storage.* In the last years, this field of research have developed much interest, since it is widely used in our daily life as well as in economic and military fields. Thus, the Ir(III) bis-cyclometalated complexes are a promising alternative to organic devices, owing to its great tunable capacity.^{37,44,65}
- *Organic photovoltaic (OPV) cells.* The OPV cells based on cyclometalated Ir(III) complexes have some advantages over silicon-based photovoltaic cells, such as flexibility, easy fabrication, low manufacturing costs and synthetic tunability.^{24,66}

2. BIBLIOGRAPHY

- (1) Virk, H. S. *Defect Diffus. Forum* **2015**, *361*, 1–13.
- (2) Valeur, B.; Berberan-Santos, M. N. *J. Chem. Educ.* **2011**, *88*, 731–738.
- (3) Sauer, M.; Hofkens, J.; Enderlein, J. In *Handbook of Fluorescence Spectroscopy and Imaging*; WILEY-VCH Verlag GmbH: Weinheim, **2011**; pp. 1–29.
- (4) Jabłoński, A. *Zeitschrift für Phys.* **1935**, *94*, 38–46.
- (5) Lakowitz, J. R. *Principles of Fluorescence Spectroscopy*; Third Edition; Springer: Baltimore, Maryland, USA, **2006**.
- (6) Housecroft, C. E.; Sharpe, A. E. *Inorganic Chemistry*; Fourth Edition; Pearson, 2012.
- (7) Juris, A.; Balzani, V.; Barigelli, F.; Campagna, S.; Belser, P.; von Zelewsky, A. *Coord. Chem. Rev.* **1988**, *84*, 85–277.
- (8) Albani, J. R. *Principles and Applications of Fluorescence Spectroscopy*; Blackwell, **2007**.
- (9) Bünzli, J.-C. G.; Piguet, C. *Chem. Soc. Rev.* **2005**, *34*, 1048–1077.
- (10) Coogan, M. P.; Fernández-Moreira, V. *Chem. Commun.* **2014**, *50*, 384–399.
- (11) Coogan, M. P.; Pope, S. J. A. In *The Chemistry of Molecular Imaging*; John Wiley & Sons, Inc: Hoboken, NJ, **2014**; pp. 275–298.
- (12) Zanoni, K. P. S.; Coppo, R. L.; Amaral, R. C.; Murakami Iha, N. Y. *Dalt. Trans.* **2015**, *44*, 14559–14573.
- (13) Balzani, V.; Credi, A.; Venturi, M. *Coord. Chem. Rev.* **1998**, *171*, 3–16.
- (14) Sprouse, S.; King, K. A.; Spellane, P. J.; Watts, R. J. *J. Am. Chem. Soc.* **1984**, *106*, 6647–6653.
- (15) Nonoyama, M. *Bull. od Chem. Soc. Japan* **1974**, *47*, 767–768.
- (16) Sun, J.; Wu, W.; Zhao, J. *Chem. - A Eur. J.* **2012**, *18*, 8100–8112.
- (17) Ulbricht, C.; Beyer, B.; Friebel, C.; Winter, A.; Schubert, U. S. *Adv. Mater.* **2009**, *21*, 4418–4441.
- (18) Ohsawa, Y.; Sprouse, S.; King, K. A.; DeArmond, M. K.; Hanck, K. W.; Watts, R. J. *J. Phys. Chem.* **1988**, *91*, 1047–1054.
- (19) Murphy, L.; Congreve, A.; Pålsson, L.-O.; Williams, J. A. G. *Chem. Commun.* **2010**, *46*, 8743–8745.
- (20) Liu, Y.; Li, M.; Zhao, Q.; Wu, H.; Huang, K.; Li, F. *Inorg. Chem.* **2011**, *50*, 5969–5977.
- (21) Amouri, H.; Gruselle, M. *Chirality in Transition Metal Chemistry: Molecules, Supramolecular Assemblies and Materials*; John Wiley & Sons, Ltd., **2008**.
- (22) Ladouceur, S.; Zysman-Colman, E. *Eur. J. Inorg. Chem.* **2013**, *2013*, 2985–3007.
- (23) Fernández-Moreira, V.; Thorp-Greenwood, F. L.; Coogan, M. P. *Chem. Commun. (Camb.)* **2010**, *46*, 186–202.
- (24) You, Y.; Nam, W. *Chem. Soc. Rev.* **2012**, *41*, 7061–7084.
- (25) Zanoni, K. P. S.; Kariyazaki, B. K.; Ito, A.; Brenneman, M. K.; Meyer, T. J.; Murakami Iha, N. Y. *Inorg. Chem.* **2014**, *53*, 4089–4099.
- (26) Smith, A. R. G.; Burn, P. L.; Powell, B. J. *ChemPhysChem* **2011**, *12*, 2429–2438.
- (27) Baggaley, E.; Weinstein, J. a.; Williams, J. a G. *Coord. Chem. Rev.* **2012**, *256*, 1762–1785.
- (28) Fan, C.; Yang, C. *Chem. Soc. Rev.* **2014**, *43*, 6439–6469.
- (29) Lowry, M. S.; Hudson, W. R.; Pascal, R. A.; Bernhard, S. J. *J. Am. Chem. Soc.* **2004**, *126*, 14129–14135.
- (30) Kappaun, S.; Slugovc, C.; List, E. J. W. *Int. J. Mol. Sci.* **2008**, *9*, 1527–1547.

- (31) Lowry, M. S.; Bernhard, S. *Chem. - A Eur. J.* **2006**, *12*, 7970–7977.
- (32) You, Y.; Cho, S.; Nam, W. *Inorg. Chem.* **2014**, *53*, 1804–1815.
- (33) Darmawan, N.; Yang, C.-H.; Mauro, M.; Fröhlich, R.; De Cola, L.; Chang, C.-H.; Wu, Z.-J.; Tai, C.-W. *J. Mater. Chem. C* **2014**, *2*, 1–15.
- (34) Colombo, M. G.; Güdel, H. U. *Inorg. Chem.* **1993**, *32*, 3081–3087.
- (35) Chang, C.-J.; Yang, C.-H.; Chen, K.; Chi, Y.; Shu, C.-F.; Ho, M.-L.; Yeh, Y.-S.; Chou, P.-T. *Dalt. Trans.* **2007**, *2*, 1881–1890.
- (36) Hasan, K.; Bansal, A. K.; Samuel, I. D. W.; Roldán-Carmona, C.; Bolink, H. J.; Zysman-Colman, E. *Sci. Rep.* **2015**, *5*, 12325.
- (37) Sun, H.; Liu, S.; Lin, W.; Zhang, K. Y.; Lv, W.; Huang, X.; Huo, F.; Yang, H.; Jenkins, G.; Zhao, Q.; Huang, W. *Nat. Commun.* **2014**, *5*, 3601.
- (38) Han, Y.; Cao, H.-T.; Sun, H.-Z.; Wu, Y.; Shan, G.-G.; Su, Z.-M.; Hou, X.-G.; Liao, Y. *J. Mater. Chem. C* **2014**, *2*, 7648–7655.
- (39) Shan, G.-G.; Li, H.-B.; Sun, H.-Z.; Zhu, D.-X.; Cao, H.-T.; Su, Z.-M. *J. Mater. Chem. C* **2013**, *1*, 1440–1449.
- (40) Dedeian, K.; Shi, J.; Forsythe, E.; Morton, D. C.; Zavalij, P. Y. *Inorg. Chem.* **2007**, *46*, 1603–1611.
- (41) Liu, Q. De; Jia, W. L.; Wang, S. *Inorg. Chem.* **2005**, *44*, 1332–1343.
- (42) Baranoff, E.; Curchod, B. F. E.; Frey, J.; Scopelliti, R.; Kessler, F.; Tavernelli, I.; Rothlisberger, U.; Grätzel, M.; Nazeeruddin, M. K. *Inorg. Chem.* **2012**, *51*, 215–224.
- (43) Tamayo, A. B.; Garon, S.; Sajoto, T.; Djurovich, P. I.; Tsyba, I. M.; Bau, R.; Thompson, M. E. *Inorg. Chem.* **2005**, *44*, 8723–8732.
- (44) Lin, W.; Zhao, Q.; Sun, H.; Zhang, K. Y.; Yang, H.; Yu, Q.; Zhou, X.; Guo, S.; Liu, S.; Huang, W. *Adv. Opt. Mater.* **2015**, *3*, 368–375.
- (45) Nakagawa, A.; Hisamatsu, Y.; Moromizato, S.; Kohno, M.; Aoki, S. *Inorg. Chem.* **2014**, *53*, 409–422.
- (46) Lo, K. K.-W.; Li, S. P.-Y.; Zhang, K. Y. *New J. Chem.* **2011**, *35*, 265–287.
- (47) Aoki, S.; Matsuo, Y.; Ogura, S.; Ohwada, H.; Hisamatsu, Y.; Moromizato, S.; Shiro, M.; Kitamura, M. *Inorg. Chem.* **2011**, *50*, 806–818.
- (48) *Luminescent and Photoactive Transition Metal Complexes as Biomolecular Probes and Cellular Reagents*; Kam, K.; Lo, W., Eds.; Structure and Bonding; Springer Berlin Heidelberg: Berlin, Heidelberg, **2015**; Vol. 165.
- (49) Kuimova, M. K.; Yahioglu, G.; Ogilby, P. R. *J. Am. Chem. Soc.* **2009**, *131*, 332–340.
- (50) Jiang, X.; Peng, J.; Wang, J.; Guo, X.; Zhao, D.; Ma, Y. *ACS Appl. Mater. Interfaces* **2016**, *8*, 3591–3600.
- (51) Bejoymohandas, K. S.; George, T. M.; Bhattacharya, S.; Natarajan, S.; Reddy, M. L. *P. J. Mater. Chem. C* **2014**, *2*, 515–523.
- (52) Ye, R.-R.; Tan, C.-P.; He, L.; Chen, M.-H.; Ji, L.-N.; Mao, Z.-W. *Chem. Commun.* **2014**, *50*, 10945–10948.
- (53) Li, S. P.-Y.; Lau, C. T.-S.; Louie, M.-W.; Lam, Y.-W.; Cheng, S. H.; Lo, K. K.-W. *Biomaterials* **2013**, *34*, 7519–7532.
- (54) Mari, C.; Pierroz, V.; Ferrari, S.; Gasser, G. *Chem. Sci.* **2015**, *6*, 2660–2686.
- (55) Frei, A.; Rubbiani, R.; Tubafard, S.; Blacque, O.; Anstaett, P.; Felgenträger, A.; Maisch, T.; Spiccia, L.; Gasser, G. *J. Med. Chem.* **2014**, *57*, 7280–7292.
- (56) Zhao, Q.; Huang, C.; Li, F. *Chem. Soc. Rev.* **2011**, *40*, 2508–2524.
- (57) Kuramochi, Y.; Ishitani, O. *Inorg. Chem.* **2016**, *55*, 5702–5709.

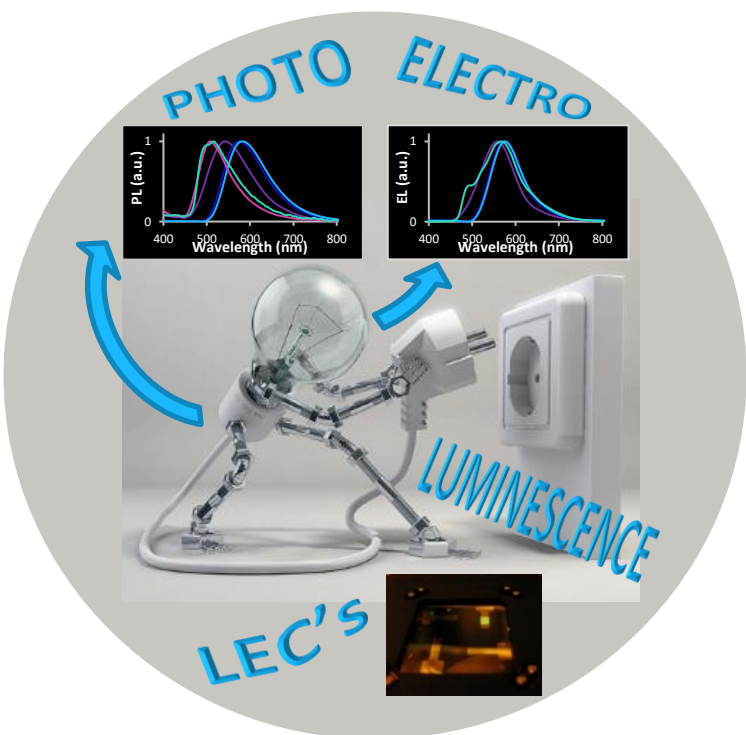
- (58) Whang, D. R.; Sakai, K.; Park, S. Y. *Angew. Chemie Int. Ed.* **2013**, *52*, 11612–11615.
- (59) Stoll, T.; Castillo, C. E.; Kayanuma, M.; Sandroni, M.; Daniel, C.; Odobel, F.; Fortage, J.; Collomb, M.-N. *Coord. Chem. Rev.* **2015**, *304–305*, 20–37.
- (60) Holder, E.; Langeveld, B. M. W.; Schubert, U. S. *Adv. Mater.* **2005**, *17*, 1109–1121.
- (61) Meier, S. B.; Tordera, D.; Pertegás, A.; Roldán-Carmona, C.; Ortí, E.; Bolink, H. J. *Mater. Today* **2014**, *17*, 217–223.
- (62) Monti, F.; Baschieri, A.; Gualandi, I.; Serrano-Pérez, J. J.; Junquera-Hernández, J. M.; Tonelli, D.; Mazzanti, A.; Muzzioli, S.; Stagni, S.; Roldan-Carmona, C.; Pertegás, A.; Bolink, H. J.; Ortí, E.; Sambri, L.; Armaroli, N. *Inorg. Chem.* **2014**, *53*, 7709–7721.
- (63) Jeon, Y.; Sunesh, C. D.; Chitumalla, R. K.; Jang, J.; Choe, Y. *Electrochim. Acta* **2016**, *195*, 112–123.
- (64) Kwon, Y.; Sunesh, C. D.; Choe, Y. *Opt. Mater. (Amst.)* **2015**, *39*, 40–45.
- (65) Akamatsu, M.; Mori, T.; Okamoto, K.; Sakai, H.; Abe, M.; Hill, J. P.; Ariga, K. *Chem. - A Eur. J.* **2014**, *20*, 16293–16300.
- (66) Xu, H.; Chen, R.; Sun, Q.; Lai, W.; Su, Q.; Huang, W.; Liu, X. *Chem. Soc. Rev.* **2014**, *43*, 3259–3302.

CHAPTER 7.

Ir(III) BISCYCLOMETALATED COMPLEXES BEARING ARYLAZOLE ANCILLARY LIGANDS: SYNTHESIS, CHARACTERIZATION AND LUMINESCENT PROPERTIES. APPLICATION IN LEC DEVICES

CHAPTER 7. Ir(III) BISCYCLOMETALATED COMPLEXES BEARING ARYLIAZOLE ANCILLARY LIGANDS: SYNTHESIS, CHARACTERIZATION AND LUMINESCENT PROPERTIES. APPLICATION IN LEC DEVICES

ABSTRACT: In this chapter a family of 11 new bis-cyclometalated heteroleptic iridium(III) complexes of general formula $[\text{Ir}(\kappa^2-\text{C},\text{N}-\text{ppy})_2(\kappa^2-\text{N},\text{N}-\text{HL})]\text{X}$ (X = counterion) bearing 2-phenylpyridinate (ppy') (as cyclometalating ligands) and five derivatives of arylimidazole and arylbenzimidazole (as ancillary ligands) was prepared. The complexes were completely characterized and tested in LEC devices in collaboration with the groups of H. Ortí and H. Bolink.



CONTEXT: Light Emitting Electrochemical Cells (LECs) are solid state lighting devices that typically incorporate a charged phosphorescent Ionic Transition Metal Complex (iTMC) as the luminophore. These devices are energy-saving and have higher quality than the widely-used OLEDs. LECs are composed of a single active layer of an ionic organic or organometallic semiconductor placed between two electrodes. Iridium(III) cyclometalating complexes have been selected, due to their efficient spin-orbit coupling. In addition, the electroluminescence properties of Ir-iTMCs bearing arylazole units as cyclometalating ligands have been widely investigated in LECs.^{1,2,3,4} In contrast, few examples of Ir-iTMCs with arylazole-based ancillary ligands have been tested in LECs. Only Choe and coworkers have reported and characterized LECs based on arylimidazole ancillary ligands exhibiting high brightness and color tunability, although without description of the time-response characteristics.^{5,6,7}

1. RESULTS AND DISCUSSION

1.1. Synthesis

The complexes were synthesised from the iridium chloro-bridged dimer $[\text{Ir}(\text{ppy})_2(\mu\text{-Cl})]_2$ prepared by the Nonoyama protocol by reaction of $\text{IrCl}_3 \cdot n\text{H}_2\text{O}$ with phenylpyridine (Hppy) in a 2-ethoxyethanol/water mixture (3:1, v/v), as shown in Fig. 1.^{8,9}

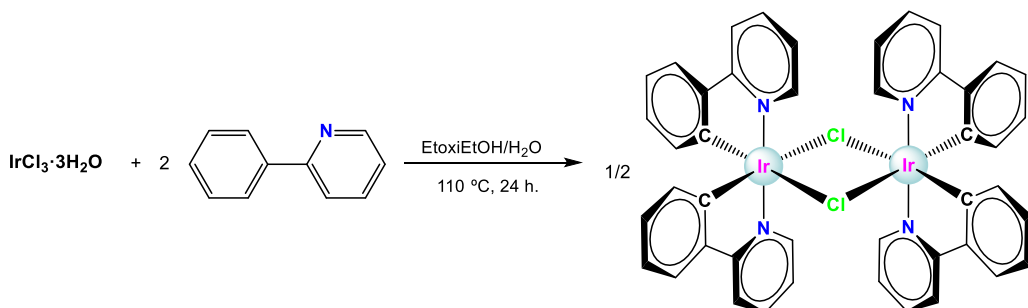


Fig. 1. Synthesis of the dinuclear bis-cyclometalated Ir(III) complexes.

The ligands used in this chapter are 2-(2'-pyridyl)imidazole (pyim), 2-(2'-pyridyl)benzimidazole (pybim), 2-(2'-pyridyl)-N-methylbenzimidazole (pyMebim), thiabendazole (tbz) and N-methylthiabendazole (Metbz), gathered in Fig. 2 and all the resulting complexes are cationic.

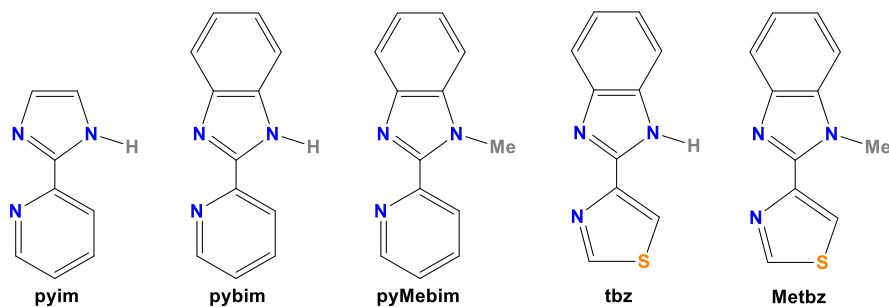


Fig. 2. Ancillary ligands derived from imidazole and benzimidazole.

The reaction between the dinuclear Ir(III) starting material and the above-mentioned ligands were carried out in dichloromethane/methanol at the refluxing temperature of the mixture for 24 h. The complexes have the general formula $[\text{Ir}(\text{ppy})_2(\text{HL})]\text{Cl}$ ([43]Cl, [44]Cl, [45]Cl and [46]Cl), where HL is the ligand and ppy⁻ phenylpyridinate. The respective PF_6^- , BPh_4^- and OTs^- salts of the general formula $[\text{Ir}(\text{ppy})_2(\text{HL})]\text{X}$ ([43]PF₆, [44]PF₆, [45]PF₆, [45]BPh₄, [45]OTs, [46]PF₆, [47]PF₆), where HL is the ligand and X the counterion, were synthesised by a related protocol in the presence of the corresponding salts (NH_4PF_6 , NaBPh_4 and AgOTs) in the same solvent mixture (see Fig. 3).

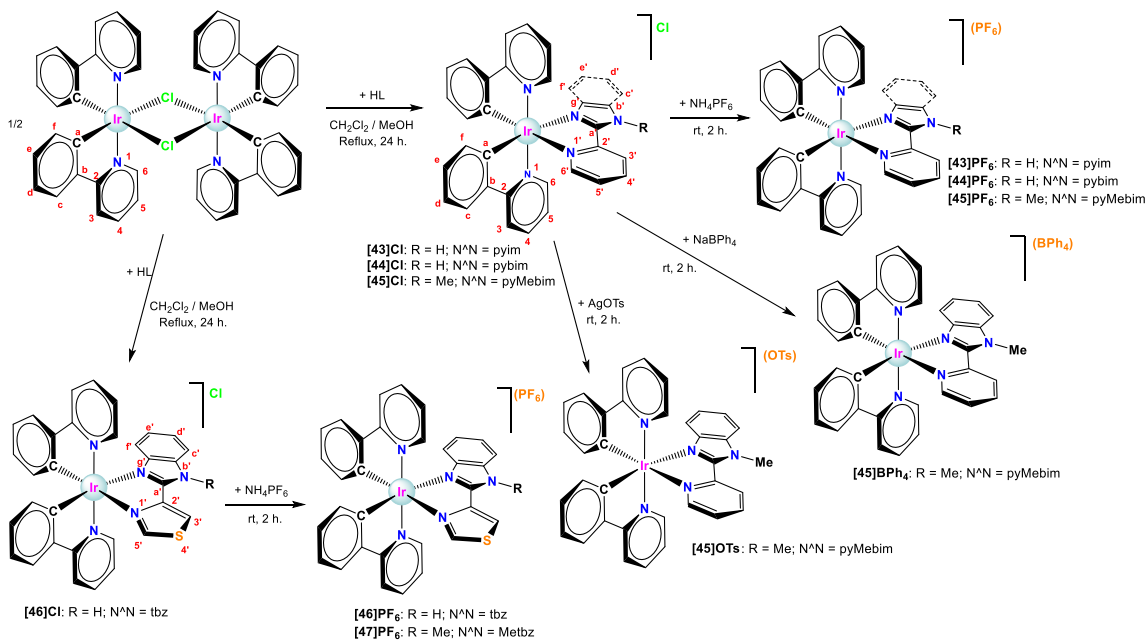


Fig. 3. Schematic synthesis of biscyclometalated Ir(III) complexes.

Complexes **[44]Cl** and **[44]PF₆** were known before the beginning of this work,^{10,11} although they had not been used in LEC devices yet, while the complex **[45]PF₆** and its use in LECs was reported during the course of this study,⁶ but no studies on its lifetime or turn-on times have been published to date.

All the complexes were isolated in moderate-to-very good yields (from 41% to 97%, being higher for the chlorido derivatives), as the corresponding racemates (Δ_{Ir} or Λ_{Ir}) in the form of yellow or orange powders.

1.2. Characterization

All the complexes have been fully characterised by NMR spectroscopy, IR spectroscopy, positive fast atom bombardment (FAB⁺) or electrospray ionization mass spectrometry, molar conductivity and elemental analysis. In addition, fluorescence spectroscopy was used to characterize the luminescent properties of the complexes.

1.2.1. NMR

The asymmetric nature of the synthesized compounds (C1-symmetry) renders the two phenylpyridinate ligands in every complex inequivalent and thus the corresponding ¹H and ¹³C{¹H} NMR spectra show two different sets of signals for the C^N donors. The ¹H NMR spectra of the complexes were recorded in CDCl₃, DMSO-d₆ and THF-d₈ at 25 °C. All the complexes exhibit a similar pattern of signals, with a broad downfield-shifted peak (δ = 12–16 ppm) detected for the H^{NH} in those complexes with the imidazole unit in the ancillary ligand (**[43]**⁺, **[44]**⁺ and **[46]**⁺) and a sharp singlet around 4.5 ppm related to the H^{NMe} for those complexes with the methyl N-Me group (**[45]**⁺ and **[47]**⁺). In the series **[43]**⁺, **[44]**⁺ and **[45]**⁺, the peaks of the phenyl protons of phenylpyridinate in **[43]**⁺ and **[45]**⁺ are upfield shifted compared to those of **[44]**⁺ as a

consequence of the higher donor abilities of pyim and pyMebim versus pybim. These electronic effects are due to the higher electron-releasing character of N-Me compared to N-H in the first case and the lower conjugation on pyim in the second case compared to pybim. The counterion plays an important role in the chemical shift of the resonances, as a result of the strength of the N-H···X hydrogen bonds and to a lesser extent, owing to the strength of the weak interactions involving the N-Me group. The effect is more pronounced in solvents with low dielectric constant, like CDCl_3 , able to favour ion-pairing. Thus, the effect is hardly appreciable in DMSO-d_6 . The chloride ion impact has been well studied by means of ^1H NMR by E. C. Constable and C. E. Housecroft.¹²

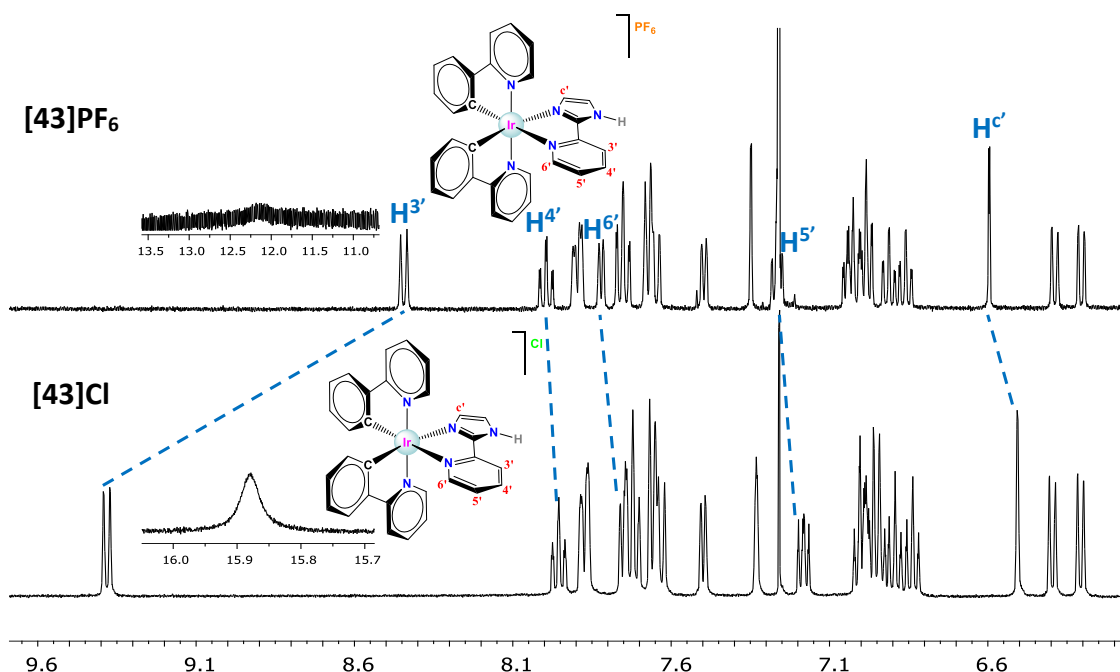


Fig. 4. Comparative ^1H NMR spectra of $[43]\text{Cl}$ and $[43]\text{PF}_6$ in CDCl_3 at 25°C , highlighting the most shifted signals.

Fig. 4 shows the comparison of the spectra of $[43]\text{Cl}$ and $[43]\text{PF}_6$ in CDCl_3 at 25°C . The chemical shifts of the NH and the $\text{H}^{3'}$ protons are downfield shifted when counterion is changed from PF_6^- to Cl^- , which is in agreement with the hydrogen bonding capability of the anions in solution ($\text{PF}_6^- < \text{Cl}^-$).^{13,14} The increase in the strength of a hydrogen bond causes the decrease in the electron density of the hydrogen atom, but an increase in the electron density on the donor nitrogen, resulting in a downfield shift of the proton chemical shift.¹¹

Fig. 5 shows the comparison of the spectra of $[45]\text{Cl}$ and $[45]\text{PF}_6$ in CDCl_3 at 25°C . It is remarkable that only the signals closed to the N-Me group deshielded, specially $\text{H}^{3'}$ and $\text{H}^{4'}$, when the counterion is changed from PF_6^- to Cl^- . The effect is the same as in the previous comparison, although in this case the signals are downfield shifted and the interaction must be a weak contact, probably C-H···Cl or C-H···F. On the contrary, this effect is not observed in DMSO-d_6 solutions (see Fig. 6).

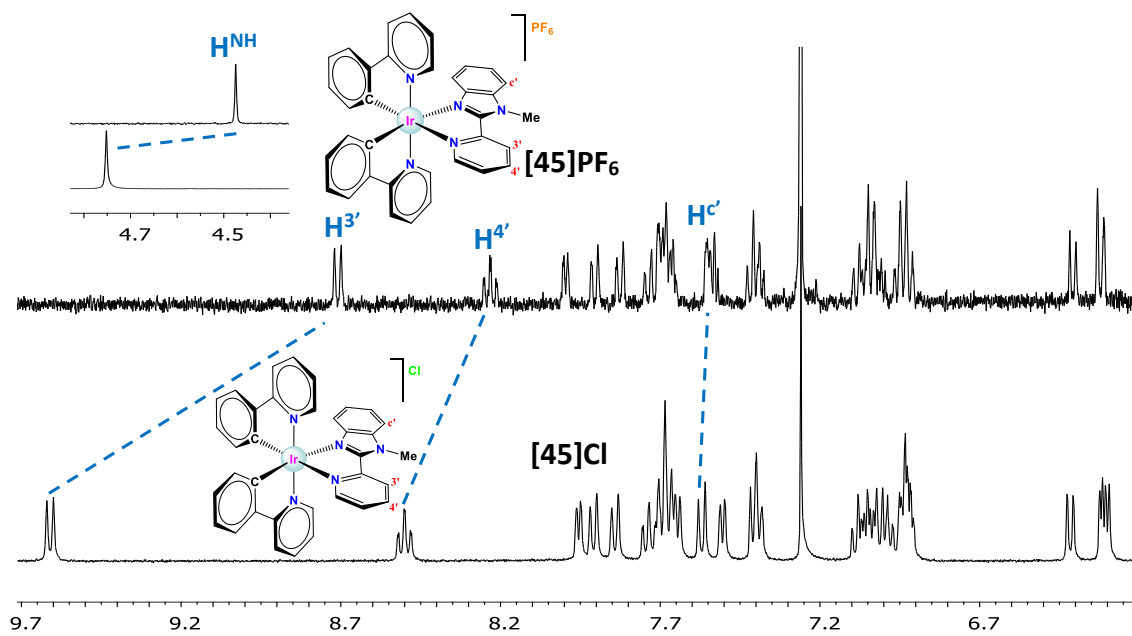


Fig. 5. Comparative spectra of $[45]\text{Cl}$ and $[45]\text{PF}_6$ in CDCl_3 at 25°C , with the highlight of most shifted signals.

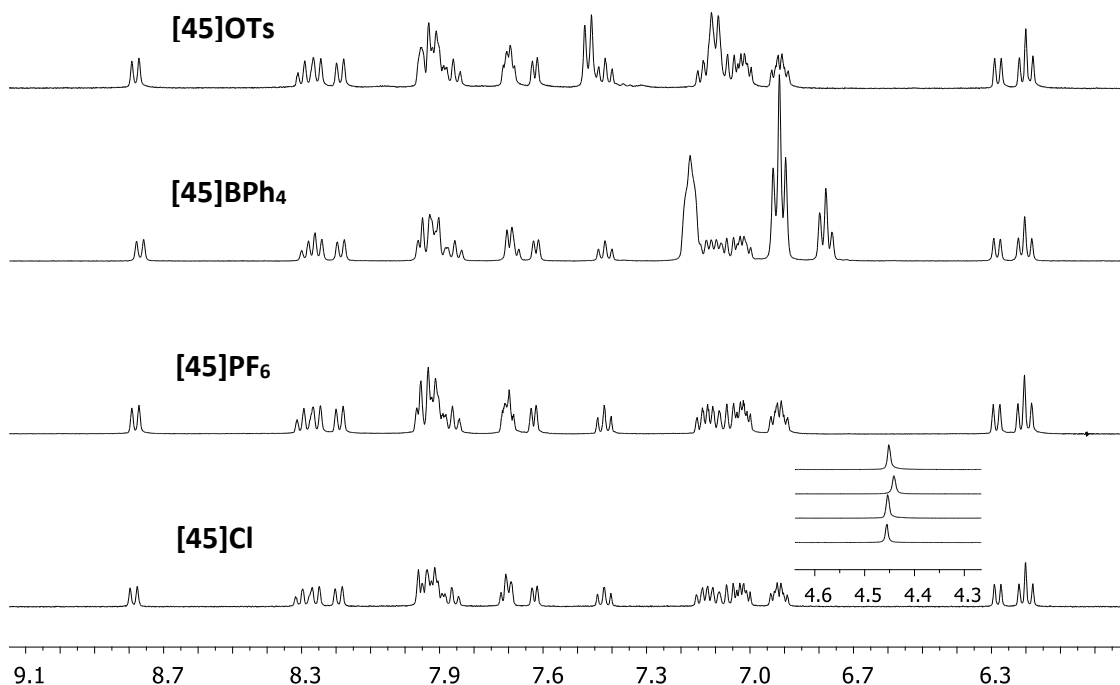


Fig. 6. Comparative spectra of $[43]\text{Cl}$, $[43]\text{PF}_6$, $[43]\text{BPh}_4$ and $[43]\text{OTs}$ in DMSO-d_6 at 25°C .

The signals have been completely assigned on the basis of triangular inter-ligand and through inter-ring NOE cross peaks in the 2D NOESY spectra. The spectrum of complex $[43]\text{Cl}$, for instance, clearly exhibits all the triangular interactions (see Fig. 7), with the exception of $\text{H}^{\text{f}} \leftrightarrow \text{H}^{\text{c}'}$ (dashed arrow). Moreover, the spectrum shows the inter-ring NOE cross peaks among the NH proton and $\text{H}^{3'}$ and $\text{H}^{\text{b}'}$, as well as the exchange peak of the NH proton with a water molecule (see Fig. 8).

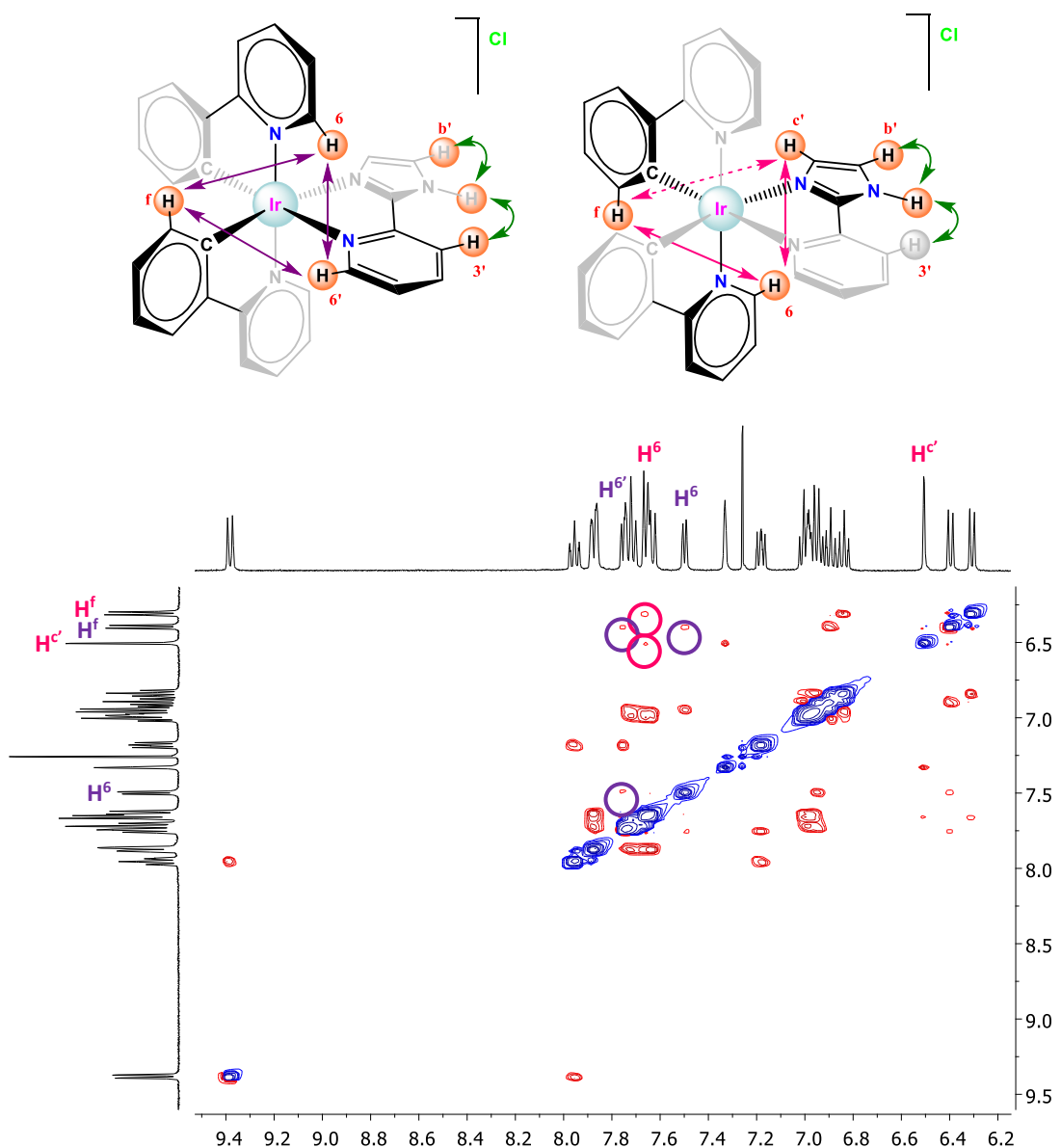


Fig. 7. Representation of inter-ligand NOE cross peaks in the structure of **[43]Cl** in CDCl_3 , showing the triangular interactions.

The spectra of complexes **[45]BPh₄** and **[45]OTs** show characteristic signals of the corresponding counterions. For BPh_4^- , three peaks were detected: a broad singlet at 7.17 ppm ($\text{H}^{\text{o-Ph(BPh}_4^-)}$), an intense triplet at 6.91 ppm ($\text{H}^{\text{m-Ph(BPh}_4^-)}$) and a triplet at 6.78 ppm ($\text{H}^{\text{p-Ph(BPh}_4^-)}$). For OTs^- , two doublets appeared at 7.47 ppm ($\text{H}^{\text{o-(OTs}}^-)$) and 7.10 ppm ($\text{H}^{\text{m-(OTs}}^-)$) (see Fig. 6).

The $^{13}\text{C}\{^1\text{H}\}$ NMR spectra showed the expected signals for the C^N and N^N ligands and are fully consistent with the structural features ascertained by ^1H NMR. The signals were completely assigned with the help of bidimensional experiments HSQC and HMBC. In addition, complexes **[45]BPh₄** and **[45]OTs** show characteristic signals for the corresponding counterions.

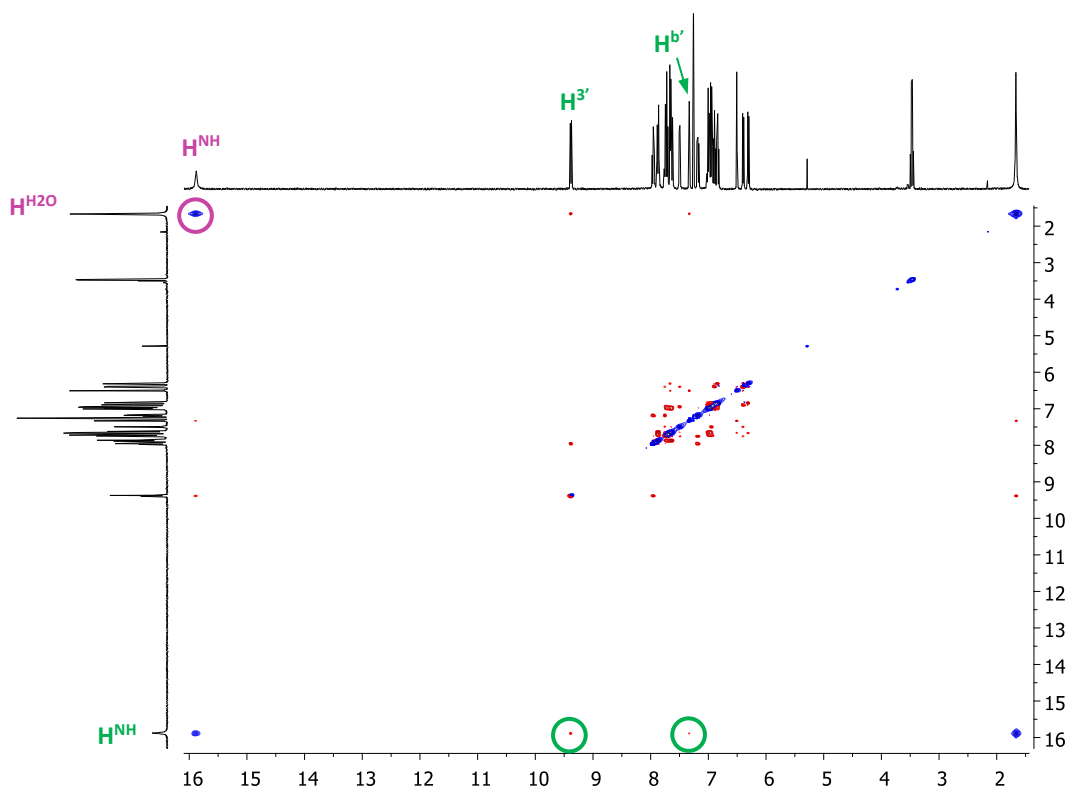


Fig. 8. Representation of inter-ring NOE cross peaks (green) and exchange peak (orange) in the structure of [43]Cl.

The $^{19}\text{F}\{\text{H}\}$ NMR and $^{31}\text{P}\{\text{H}\}$ NMR spectra were recorded in DMSO-d₆ for the PF₆⁻ derivatives. The coupling ^{19}F - ^{31}P showed a doublet in the ^{19}F NMR spectrum and a septuplet in the ^{31}P NMR spectrum.

1.2.2. Mass Spectra

The FAB⁺ mass spectra of the complexes exhibit characteristic sets of peaks according to isotopic distribution patterns, among which stand out two peaks: the molecular ion [M-X] (where X is the counterion) and the [M-X-ancillary ligand]⁺ fragment. This last peak is always identical for Ir(III) complexes of this chapter, bearing the same biscyclometalated fragment: for the compounds with phenylpyridinate [M-X-ancillary ligand]⁺ = 501.

1.2.3. IR Spectra

The infrared spectra show the characteristic peaks for the normal vibrational modes of the corresponding rings $\nu_{\text{C}=\text{N}}$, $\nu_{\text{C}=\text{C}}$, $\delta_{\text{CH}_{\text{ip}}}$ and $\delta_{\text{CHO}_{\text{op}}}$, besides $\nu_{\text{C-S}}$ for thiabendazole ligands, and the characteristic peaks of the counterions: $\nu_{\text{P-F}_{\text{sym}}}$ and $\nu_{\text{P-F}_{\text{as}}}$ for PF₆⁻, $\nu_{\text{B-C}}$ for BPh₄⁻ and $\nu_{\text{SO}_3^{-\text{as}}}$, $\nu_{\text{SO}_3^{-\text{sym}}}$ and $\nu_{\text{S-O}}$ for OTs⁻.

1.2.4. Molar Conductivity

Molar conductivity (Λ_M) values were measured in acetonitrile (10⁻³ M). The values reflect the 1:1 electrolyte nature, with the exception of some conductivities unusually below the normal range¹⁵ ([43]Cl, [44]Cl, [46]Cl and [45]BPh₄). The reason dwells in the NH group (for the first three complexes), which is prone to participating in

hydrogen bonding interactions to form ion-pairing with chloride. Thus, the conductivity of complex **[45]Cl** with N-Me, is in the normal range. Regarding the complex **[45]BPh₄**, π-π stacking interactions are thought to be responsible for the ion-pairing.

Table 1. Molar conductivity values for complexes measured in acetonitrile.

Complex	Solvent	Λ_m (S·cm ² ·mol ⁻¹)
[43]Cl	acetonitrile	28.4
[44]Cl	acetonitrile	24.7
[45]Cl	acetonitrile	129.0
[46]Cl	acetonitrile	21.0
[43](PF₆)	acetonitrile	136.5
[44](PF₆)	acetonitrile	132.1
[45](PF₆)	acetonitrile	139.2
[46](PF₆)	acetonitrile	132.6
[47](PF₆)	acetonitrile	137.7
[45](OTs)	acetonitrile	134.7
[45](BPh₄)	acetonitrile	91.1

1.2.5. Elemental Analysis

Elemental analysis was performed for all complexes. Intriguingly, complexes bearing PF₆⁻ as the counterion tend to enclose some water in their structures. The rest also retain other solvent molecules.

1.2.6. X-Ray Diffraction

Single crystals suitable for X-ray diffraction analysis were obtained for **[46]PF₆** and **[47]PF₆** by the diffusion of hexane into a solution of the former in CH₂Cl₂/CH₃CN and by the slow evaporation of a solution of the latter in CH₂Cl₂, respectively.

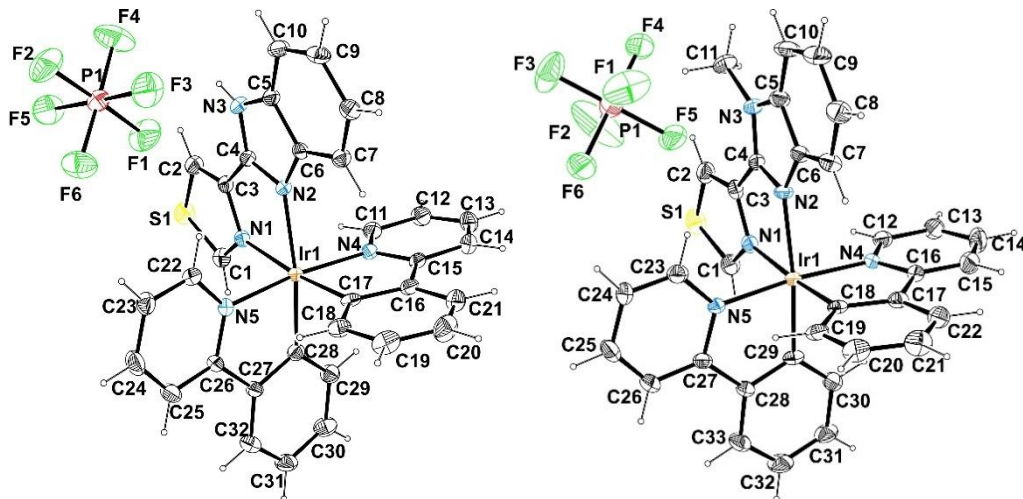


Fig. 9. ORTEP diagrams for complexes Λ -[46]PF₆ and Λ -[47]PF₆.

The ORTEP diagrams for the asymmetric units are presented in Fig. 9, whereas selected bond lengths and angles with estimated standard deviations are gathered in

Table 2. The corresponding unit cells of both complexes show two pairs of enantiomers (Λ and Δ , the racemate), owing to the helicoidal chirality inherent to trischelate octahedral metal complexes.

Table 2. Selected bond lengths (Å) and angles (°) for complexes [46]PF₆ and [47]PF₆.

<i>Distance/angle</i>	[46]PF ₆	[47]PF ₆
<i>Ir1-N1</i>	2.153(3)	2.154(3)
<i>Ir1-N2</i>	2.143(3)	2.153(3)
<i>Ir1-C17/C18</i>	2.010(4)	1.999(4)
<i>Ir1-C28/C29</i>	2.004(4)	2.020(4)
<i>Ir1-N4</i>	2.050(3)	2.046(3)
<i>Ir1-N5</i>	2.040(3)	2.045(3)
<i>C17/C18-Ir1-C28/C29</i>	89.35(15)	89.03(16)
<i>C17/C18-Ir1-N4</i>	80.95(14)	80.26(16)
<i>C28/C29-Ir1-N4</i>	95.09(13)	95.47(15)
<i>C17/C18-Ir1-N5</i>	92.38(14)	94.83(16)
<i>C28/C29-Ir1-N5</i>	80.43(13)	80.59(15)
<i>C17/C18-Ir1-N2</i>	97.41(13)	98.58(14)
<i>N4-Ir1-N2</i>	89.76(11)	88.34(12)
<i>N5-Ir1-N2</i>	95.42(11)	96.17(13)
<i>C28/C29-Ir1-N1</i>	97.29(14)	96.50(15)
<i>N4-Ir1-N1</i>	97.03(12)	98.44(13)
<i>N5-Ir1-N1</i>	90.09(11)	86.81(13)
<i>N2-Ir1-N1</i>	76.06(12)	75.93(13)

The iridium centre displays a slightly distorted octahedral coordination geometry with the expected *cis*-C,C and *trans*-N,N mutual disposition for the ppy ligands. The Ir-C_{ppy} and Ir-N_{ppy} distances are very similar and close to 2 Å, with the Ir-N_{ppy} distances a bit longer than those for Ir-C_{ppy}. In addition, the Ir-N distances for the ancillary ligand are slightly longer due to the so-called *trans effect* attributed to the C-donors, inducing preferential labilization of the bonds located *trans* to them.¹⁶ The bite angles for tbz and Metbz, N(2)-Ir(1)-N(1) = 76.06(12) and 75.93(13)°, respectively, are in agreement with 5-membered iridacycles reported in the literature.^{17,18} The bite angles for the cyclometalated C^N ligands, C(17/18)-Ir(1)-N(4) = 80.95(14) and 80.26(16)°; and C(28/29)-Ir(1)-N(5)° = 80.43(13) and 80.59(15)°, are standard.^{19,20}

The 3D crystal packing of both complexes is built on the basis of hydrogen bonding contacts (see Table 3) and anion-π interactions, in which the PF₆⁻ anions occupy a central position, as well as π-π stacking and C-H⋯π interactions. The PF₆⁻ anion participates in an anion-π interaction, between a fluoride atom and the imidazole ring of the benzimidazole moiety and connects up to 5 metal units (see Fig. 10 and Table 4).

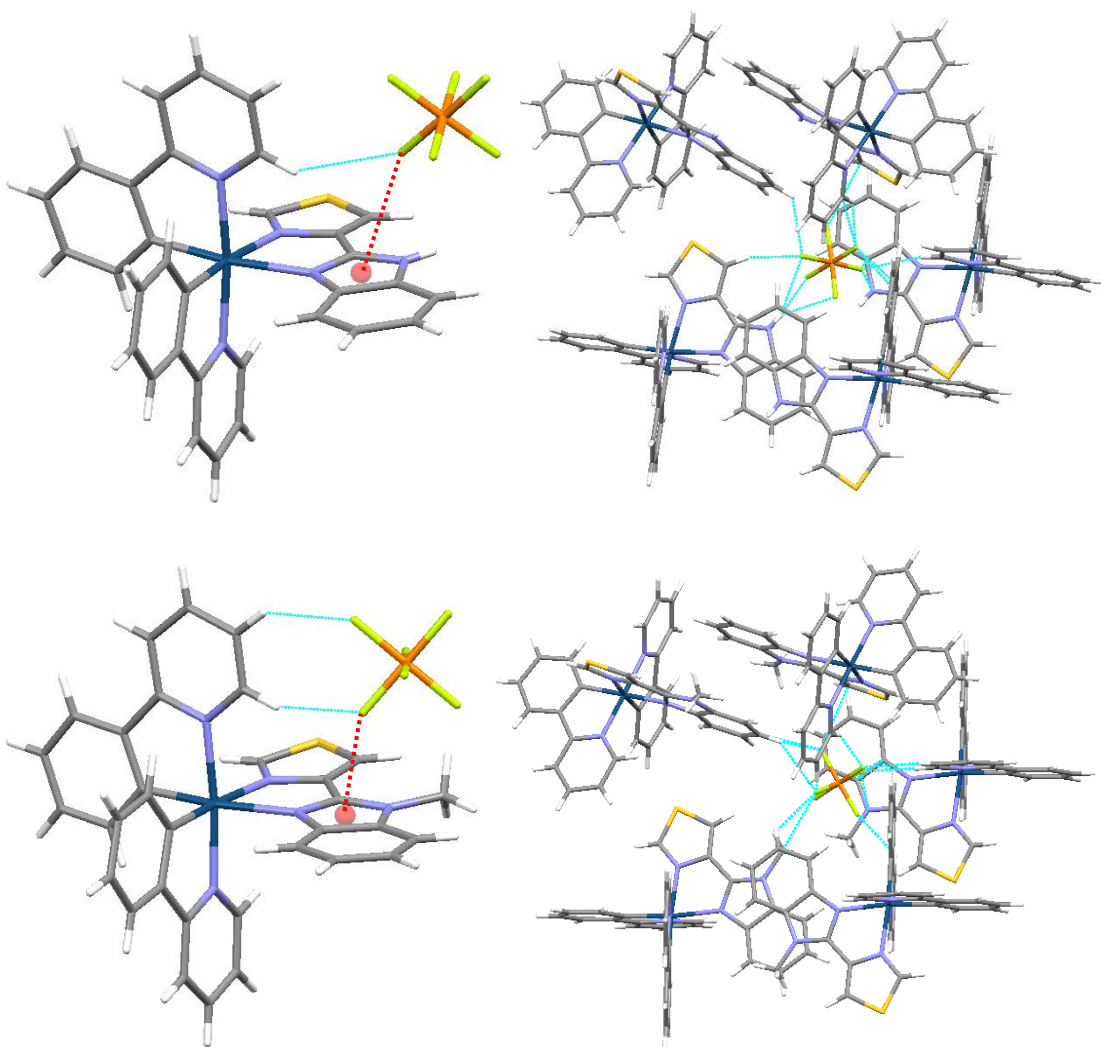


Fig. 10. Assemblies in the crystal structure of complexes $[46]\text{PF}_6$ (up) and $[47]\text{PF}_6$ (down), showing (a) the anion- π interaction and (b) the connection among cationic fragments through one PF_6^- .

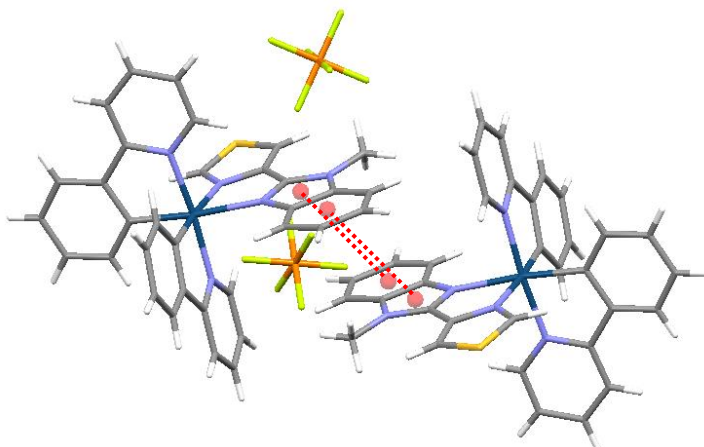
Table 3. Features and parameters of intramolecular hydrogen bonding interactions of complexes $[46]\text{PF}_6$ and $[47]\text{PF}_6$.

	H-bonding	D···A (Å)	X···A (Å)	D···X (Å)	α (°)
$[46]\text{PF}_6$	N(3)-H(3)···F(2)	3.340	2.641	0.755	154.70
	N(3)-H(3)···F(5)	3.102	2.422	0.755	150.64
	N(3)-H(3)···F(4)	3.283	2.640	0.755	144.16
	C(23)-H(23)···F(6)	3.397	2.616	0.929	142.08
	C(22)-H(22)···F(1)	3.649	2.822	0.930	148.77
$[47]\text{PF}_6$	C(23)-H(23)···F(5)	3.245	2.350	0.950	156.78
	C(24)-H(24)···F(6)	3.241	2.434	0.950	142.80
	C(11)-H(11C)···F(4)	3.297	2.862	0.980	107.77
	C(11)-H(11C)···F(2)	3.743	2.957	0.980	137.89

Table 4. Geometric parameters of anion- π interactions ($P\text{-F}\cdots\pi$) for complexes $[46]\text{PF}_6$ and $[47]\text{PF}_6$.

Compound	$d_{\text{F-cent}}$ (Å)	$d_{\text{F-plane}}$ (Å)	d_{offset} (Å)	$\alpha_{\text{P-F-cent}}$ (°)	θ (°)
$[46]\text{PF}_6$ ($P\text{-F}\cdots\pi$)	3.197	2.965	1.196	149.57	21.96
$[47]\text{PF}_6$ ($P\text{-F}\cdots\pi$)	2.856	2.771	0.692	142.97	14.01

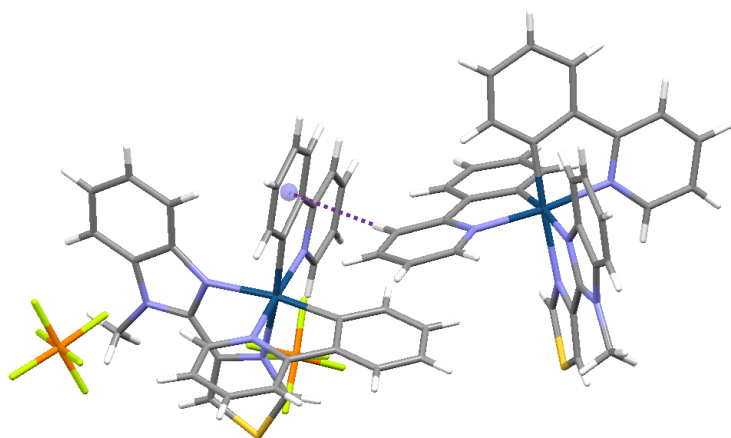
* d_{offset} has been calculated as $(d_{\text{centroid}}^2 - d_{\text{plane}}^2)^{1/2}$.²¹

**Fig. 11.** $\pi\text{-}\pi$ stacking interactions in the crystal structure of complex $[47]\text{PF}_6$.

The benzimidazole entities of the ancillary ligands are involved in the $\pi\text{-}\pi$ stacking interactions (see Fig. 11 and Table 5), which form dimeric structures between the Λ and Δ enantiomers. However, these interactions are weakened in $[47]\text{PF}_6$, owing to the N-Me group. Thus, the centroid-centroid distance is longer than that for $[46]\text{PF}_6$ (3.87 vs. 3.58 Å). On the other hand, the cyclometalated ligands participate in the C-H $\cdots\pi$ interactions also connecting the enantiomers Λ and Δ (see Fig. 12 and Table 6).

Table 5. Offset $\pi\text{-}\pi$ stacking interactions of complexes $[46]\text{PF}_6$ and $[47]\text{PF}_6$.

Compound	$d_{\text{cent-cent}}$ (Å)	α (°)	$d_{\text{cent-pl}}$ (Å)	β (°)	d_{offset} (Å)
$[46]\text{PF}_6$ (ph/im)	3.579	1.28	3.341	21.01	1.283
			3.346	20.79	1.270
$[47]\text{PF}_6$ (ph/im)	3.871	1.71	3.423	27.84	1.808
			3.384	29.05	1.943

Fig. 12. C-H···π interactions between enantiomers for complex [47]PF₆.Table 6. Parameters of the C-H···π interaction in complexes [46]PF₆ and [47]PF₆.

Compound	d _{C-cent} (Å)	d _{H-cent} (Å)	d _{C-H} (Å)	<C-H-cent (°)	<H-cent-normal (°)
[46]PF ₆ (C-H···π)	3.462	2.653	0.931	145.61	140.02
[47]PF ₆ (C-H···π)	3.454	2.663	0.949	141.32	140.44

Complex [46]PF₆ shows another kind of weak interaction between the S atom of the thiazole ring and the π-electron cloud of the phenyl ring of the benzimidazole entity of an adjacent complex (see Fig. 13). This contact is called S-π, S-aromatic or even Ip-π interaction.^{22,23} Complex [47]PF₆ also displays this interaction, although it is much weaker. The parameters of these interactions are gathered in Table 7.

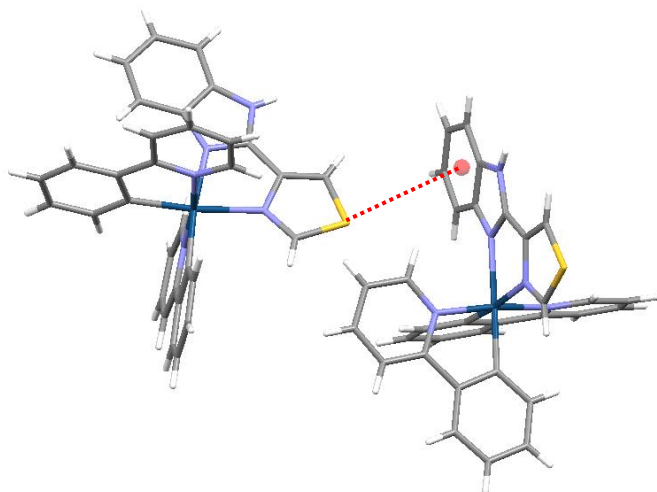
Fig. 13. S-aromatic interaction in the crystal network of [46]PF₆.

Table 7. Geometric parameters of $\text{Ip}\cdots\pi$ interactions ($\text{S}\cdots\pi$) for complexes **[46]PF₆** and **[47]PF₆**.

Compound	$d_{\text{S-cent}}$ (Å)	$d_{\text{S-plane}}$ (Å)	d_{offset} (Å)	ϕ_1 (°)
[46]PF₆ C(14)-S(2)…π	3.867	3.416	1.812	27.95
[47]PF₆ C(14)-S(2)…π	4.346	3.696	2.286	31.74

* d_{offset} has been calculated as $(d_{\text{S-centroid}}^2 - d_{\text{S-plane}}^2)^{1/2}$.

The H-H interligand distances for **[47]PF₆**, $\text{H}^6\leftrightarrow\text{H}^{\text{f}}\leftrightarrow\text{H}^{\text{f'}}$ and $\text{H}^6\leftrightarrow\text{H}^{\text{f}}\leftrightarrow\text{H}^5\leftrightarrow\text{H}^6$, are lower than 3.75 Å, whereas the distance $\text{H}^{\text{f'}}\leftrightarrow\text{H}^6$ is a bit longer (3.952 Å). Despite this fact, all of them appear in the 2D NOESY spectrum of **[47]PF₆**. The NOE interactions $\text{H}^{3'}\leftrightarrow\text{H}^{\text{NMe}}\leftrightarrow\text{H}^{\text{c}}$ are also detected, owing to the short distances (2.3 – 2.5 Å).

1.3. Photophysical Properties

Emission spectroscopy

The emission spectra of complexes **[43]PF₆-[47]PF₆** were recorded in deoxygenated acetonitrile at room temperature (25 °C) with the collaboration of the group of E. Ortí and H. Bolink (ICMol, Universidad de Valencia). The spectra of complexes **[44]PF₆** and **[45]PF₆** show broad and structureless bands (only a shoulder), indicating higher contribution of the ³MLCT transitions on the excited state. Complexes **[43]PF₆**, **[46]PF₆** and **[47]PF₆** exhibit vibronically structured spectra, showing higher contribution of ³LC transitions. The emission maxima ranged from 508-594 nm, yielding colours from blue to orange (see Fig. 14 and Table 8).

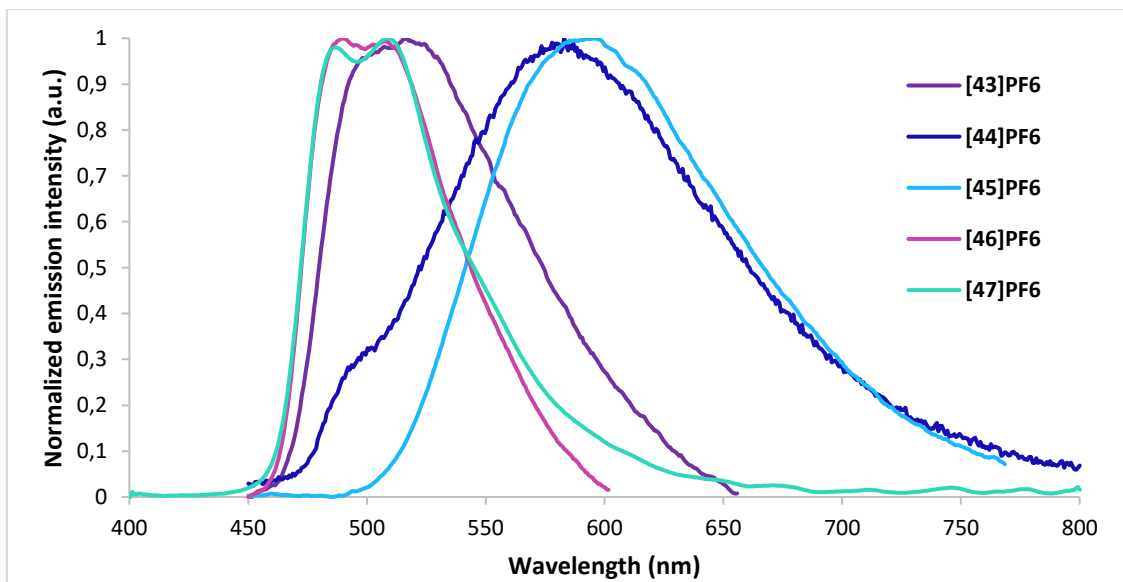


Fig. 14. Emission spectra of complexes **[43](PF₆)**, **[44](PF₆)**, **[45](PF₆)**, **[46](PF₆)** and **[47](PF₆)** ($\lambda_{\text{exc}} = 360$ nm) in deoxygenated acetonitrile (10^{-5} M) at 25 °C.

The variety of emission colours in this family of Ir(III) derivatives depends on the ancillary ligand. Thus, complex **[45]PF₆** with pyMebim, is the most red-shifted, whereas

complexes **[46]PF₆** and **[47]PF₆** with tbz and Metbz are the most blue-shifted ($\Delta\lambda_{\text{em}} = 86$ nm). The change in the ancillary ligand from pyim (**[43]PF₆**) to pybim (**[44]PF₆**) causes a red shift (52 nm). In addition, the substitution of the pyridyl (6-membered) ring for a thiazolyl (5-membered) ring in **[46]PF₆** (tbz as ancillary ligand) or **[47]PF₆** (Metbz as ancillary ligand) causes a noticeable blue shift (74–93 nm), this is, an increment in the energy gap. When the hydrogen of the amino group in **[44]PF₆** is substituted by a methyl (an electron-donor group) in **[45]PF₆** (pyMebim as the ancillary ligand), produces a small red shift (13 nm).

Cooling the samples to 77 K with liquid N₂, the shape of the emission spectra changes from structureless or slightly structured (at room temperature) to vibronically structured, yet all of them with the same outline: two peaks and a shoulder (see Fig. 15 and Table 8). This effect is called rigidochromism (see page 304, LUMINESCENCE IN ORGANOMETALLIC COMPOUNDS: A BRIEF REVIEW OF PROCESSES, FEATURES, PROPERTIES AND APPLICATIONS). The shift in the emission maxima still keeps the same tendency. Nonetheless, spectra of complexes **[44]PF₆** and **[45]PF₆** blue shift with regard to those recorded at room temperature, whereas spectra of complexes **[43]PF₆**, **[46]PF₆** and **[47]PF₆** do not. The explanation to this fact results from the composition of the emissive excited states. The structured spectra arise from LC transitions²⁴, which do not cause any shift,¹⁶ whereas the large blue shifts arise from CT transitions.^{16,2} Thus, only **[44]PF₆** and **[45]PF₆** have MLCT transitions as predominant, although LC are also important. In the rest, the transitions are mainly LC.

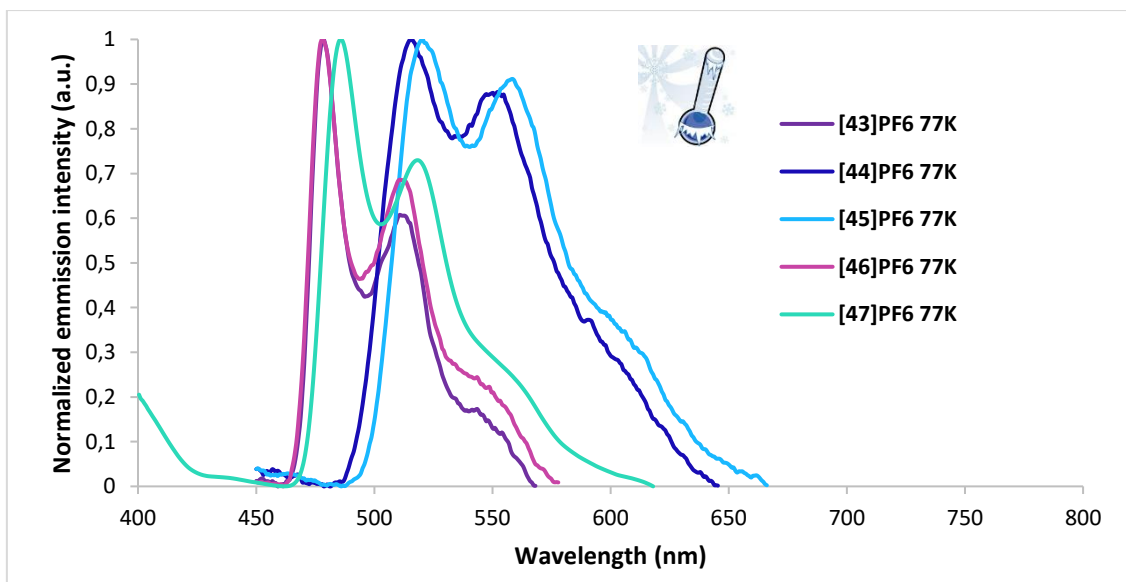


Fig. 15. Emission spectra of complexes **[43](PF₆)**, **[44](PF₆)**, **[45](PF₆)**, **[46](PF₆)** and **[47](PF₆)** ($\lambda_{\text{exc}} = 360$ nm) in deoxygenated acetonitrile (10^{-5} M) at 77 K.

Complexes **[46]PF₆** and **[47]PF₆** show weak emission (PLQY = 9% and 4%, respectively), in good agreement with the ³LC character predicted for the emissive state in these complexes. In comparison, complexes **[44]PF₆** and **[45]PF₆** feature significantly higher PLQYs (38% and 39%, respectively). In this case, the ³MLCT character of the

emissive state favours the intersystem crossing, making the $S_1 \rightarrow T_1$ and the $T_1 \rightarrow S_0$ transitions allowed. The value of complex **[44]PF₆** (20.4%) is in the middle, since the emissive states are composed by a mixture of ³LC and ³MLCT states. Furthermore, the change of the counterion causes the decrease of the PLQY (see Table 8)

Table 8. Photophysical properties of complexes [43](PF₆)-[46](PF₆) and [45]⁺ in deoxygenated acetonitrile (10⁻⁵ M) at 25 °C and 77 K.

Compound	λ_{exc} (nm)	λ_{em} (nm)	$\lambda_{\text{em 77K}}$ (nm)	Φ
[43](PF ₆)	360	516 (cyan)	479/511 (blue-cyan)	0.20
[44](PF ₆)	360	582 (yellow)	516/551 (cyan-green)	0.39
[45](PF ₆)	360	594 (orange)	521/557 (green)	0.39
[46](PF ₆)	360	489/508 (blue-cyan)	479/511 (blue-cyan)	0.09
[47](PF ₆)	360	487/508 (blue-cyan)	486/518 (blue-cyan)	0.04
[45](BPh ₄)	360	591 (orange)	526/559 (green)	0.15
[45](OTs)	360	591 (orange)	521/556 (green)	0.13

1.4. Electrochemistry

The electrochemical measurements were performed in collaboration with the group of A. Colina and A. Heras, from the Universidad de Burgos. The voltammograms were recorded in acetonitrile solution (10⁻³ M) by cyclic voltammetry using TBAPF₆ as supporting electrolyte and a glassy carbon as working electrode. All potentials were defined respect to the ferrocene/ferrocenium (Fc/Fc⁺) couple, whose cyclic voltammogram has been monitored at 0.15 V s⁻¹ in 10⁻³ M of ferrocene and 0.1 M (nBu₄N)(PF₆) acetonitrile solution. All the electrochemical experiments were performed under argon atmosphere. The cyclic voltammogram of every PF₆⁻ salt only shows a unique quasi-reversible oxidation peak in the anodic potential region between +0.74 and +0.79 V, which is ascribed to the oxidation of the ppy-Ir environment as discussed below.

The analysis of the cathodic region allowed us to establish the following trends: (a) all the complexes with N-H groups in the ancillary ligand ([43]PF₆, [44]PF₆, and [46]PF₆) show totally irreversible peaks at -2.20, -1.95, and -2.14 V, respectively, indicating the instability of the reduced species; (b) complex [45]PF₆, where the reactive N-H group of pybim has been replaced with a methyl group, displays a quasi-reversible reduction peak at -1.91 V, which supports the higher stability of [45]PF₆ versus [44]PF₆; (c) complex [47]PF₆, also with a N-Me group, shows a reduction peak at -2.27 V, giving rise to the largest electrochemical gap (3.04 V), and its irreversible nature suggests that the

reduction mechanism is different to that of **[45]PF₆**. These results anticipate a very good stability for complex **[45]PF₆** under the operation conditions used in LEC devices owing to the reversible nature of the oxidation/reduction processes in which the complex is involved in those devices. The final values are shown in Table 9.

Tentatively, we propose that the irreversible reduction of the complexes with N-H groups (**[43]PF₆**, **[44]PF₆** and **[46]PF₆**), involves the formation of H₂, and the neutral derivatives of general formula [Ir(ppy)₂(N⁺N)]. This is a direct result of the acidic character of the N-H group in the coordinated N⁺N ligands.

Table 9. Cyclic Voltammetric Data Referred to Fc⁺/Fc in Acetonitrile Solution (10⁻³ M).^a

Compound	$E^{\text{ox}}_{1/2}$ (V)	$E^{\text{red}}_{1/2}$ (V)	$\Delta E_{1/2}$ (V)
[43]PF₆	+0,74 (qr)	-2.20 (ir)	2.94
[44]PF₆	+0,77 (qr)	-1.95 (ir)	2.72
[45]PF₆	+0,79 (qr)	-1.91 (qr)	2.70
[46]PF₆	+0,76 (qr)	-2.14 (ir)	2.90
[47]PF₆	+0,77 (qr)	-2.27 (ir)	3.04

^a Measured using 0.1 M [ⁿBu₄N][PF₆] as supporting electrolyte and a scan rate of 0.15 V·s⁻¹ (qr = quasi-reversible, ir = irreversible).

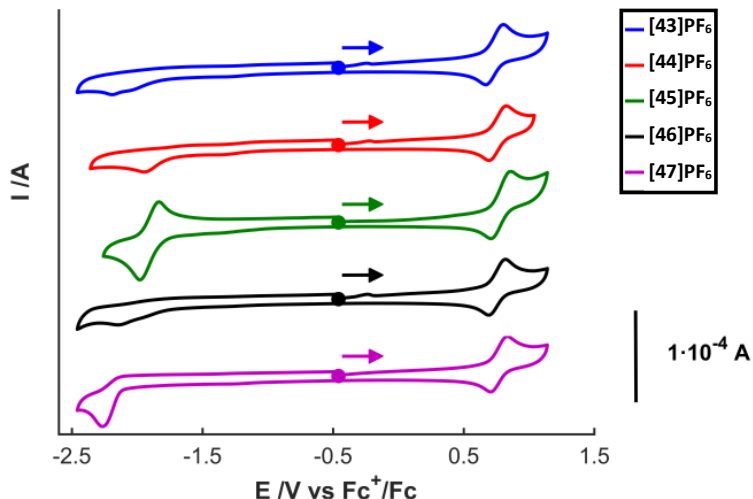


Fig. 16. Cyclic voltammograms of complexes [43]PF₆ - [47]PF₆ in acetonitrile solution (10⁻³ M), using 0.1 M [ⁿBu₄N][PF₆] as supporting electrolyte. Scan rate of 0.15 V·s⁻¹. (•) Indicates the starting (E_i) and final potential (E_f), E_i = E_f = -0.46 V (vs. Fc/Fc⁺), clockwise scan.

1.5. Theoretical Calculations

Density functional theory (DFT) and time-dependent DFT (TD-DFT) calculations were performed by the group of Pr. Enrique Ortí on the cations of complexes **[43]PF₆-[47]PF₆** to get a better understanding of their electrochemical and photophysical properties, as well as the influence of the substituted ancillary ligands on the LEC devices. Calculations were carried out at the B3LYP//(6-31G**+LANL2DZ) level including solvent effects.

Calculations predict a near-octahedral structure for cations **[43]⁺-[47]⁺** in their ground electronic state (S₀), in good agreement with the results observed for similar

complexes in previous studies^{4,25,26,27,28} and the X-Ray structures reported above for complexes **[46]PF₆** and **[47]PF₆** (see Fig. 9). Both the cyclometalating and the ancillary ligands display co-planarity for their constituting rings, as it is usually found for iTMC complexes possessing five-atoms chelate rings and without bulky substituents in their molecular structure.²⁹ The largest deviation from co-planarity is indeed found for the pyMebim N⁺N ligand (7.3°) in **[45]PF₆**, due to the methyl group introduced in the interannular region. The values predicted for the bite angles C–Ir–N (~80.°) and N–Ir–N (~74.5° for **[43]⁺**, **[44]⁺**, and **[46]⁺**, and ~74.0° for **[45]⁺** and **[47]⁺**) are very close to those obtained from the X-Ray structures of **[46]PF₆** and **[47]PF₆**.

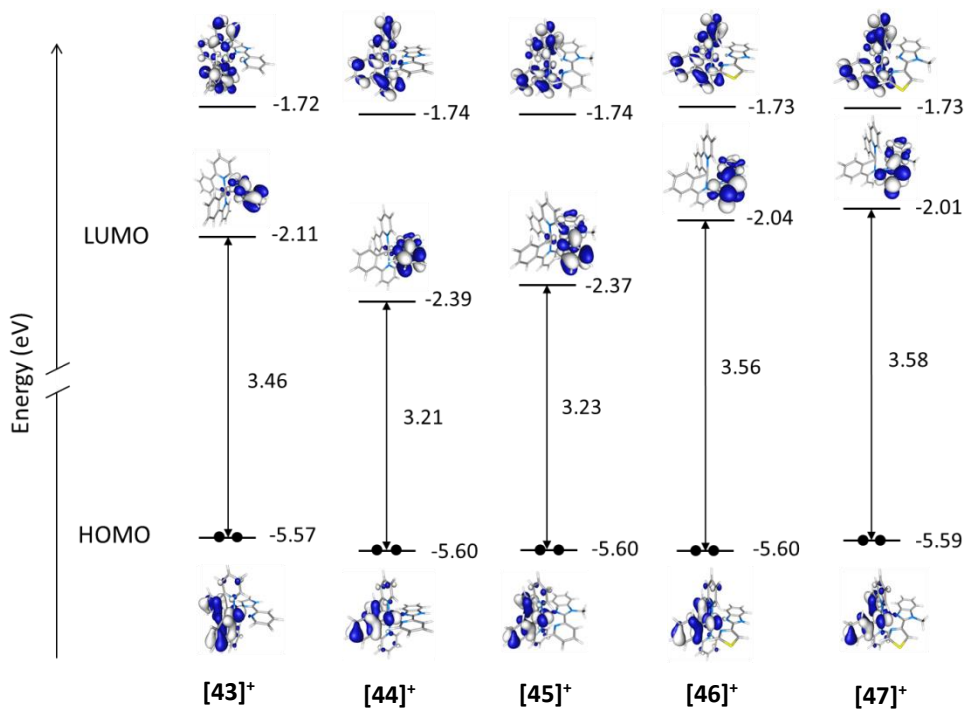


Fig. 17. Energy diagram showing the isovalue contours (± 0.03 au) and the energy values calculated for the HOMO, LUMO, and LUMO+1 of complexes **[43]⁺** to **[47]⁺**.

Fig. 17 displays the isovalue contours calculated for the HOMO and LUMO orbitals of all the **[43]⁺** to **[47]⁺** cations. The LUMO+1 is also displayed because it plays a relevant role in the photophysical properties. As it is usually found for ppy-based cyclometalated Ir-iTMCs,^{30,26,31} the HOMO of cations **[43]⁺**–**[47]⁺** results from a mixture of d_x orbitals of Ir(III) and phenyl π orbitals, with some contribution from the pyridine rings of the cyclometalating ligands. As the five complexes share the same C^N ligand, the HOMO has almost identical energies for all of them. This is in good agreement with the experimental $E^{\text{ox}}_{1/2}$ values, which remain almost constant (see Table 9) and imply the oxidation of the Ir(ppy)₂⁺ environment. The same trend is found for the LUMO+1, which is centred on the cyclometalating ligands and presents almost the same energy for all the complexes (see Fig. 17).

In contrast to the HOMO, the LUMO is fully located over the ancillary N⁺N ligand, and its energy varies upon modifying the identity of the ligand. The condensation of a benzene ring to the imidazole ring to produce a benzimidazole unit leads to the stabilization of the LUMO by ~0.3 eV due to the extended conjugation. On the contrary, the exchange of the pyridine ring by a thiazole ring in [46]⁺ and [47]⁺ compensates the effect of the benzene condensation and leads to a strong destabilization of the LUMO (~0.35 eV) compared to [44]⁺ and [45]⁺. This destabilization is due to the strong electron-donating character of the thiazole ring resulting from the presence of the S atom, which contributes with a lone electron pair to the aromatic π -system of the five-membered ring. Methylation of the imidazole ring has a very small effect, destabilizing the LUMO by around 0.02 eV. The changes predicted for the energy of the LUMO justify the less negative reduction potentials measured for [44]PF₆ (-1.95 V) and [45]PF₆ (-1.91 V) compared with [43]PF₆ (-2.20 V), and the increase of the potential in passing from [44]PF₆ and [45]PF₆ to [46]PF₆ (-2.14 V) and [47]PF₆ (-2.27 V), respectively. Upon reduction, the extra electron fully enters in the N⁺N ligand as illustrated by the unpaired-electron spin densities shown in Fig. 18 for the radical species [45][•] and [47][•]. It is to be noted that for [47][•] a high spin density of 0.47e is located on the C2 atom of the thiazole ring. The highly localized nature of the unpaired electron could explain the instability of the reduced species of [47]PF₆ despite the N-H group of the pybim unit is protected with a methyl group as in [45]PF₆.

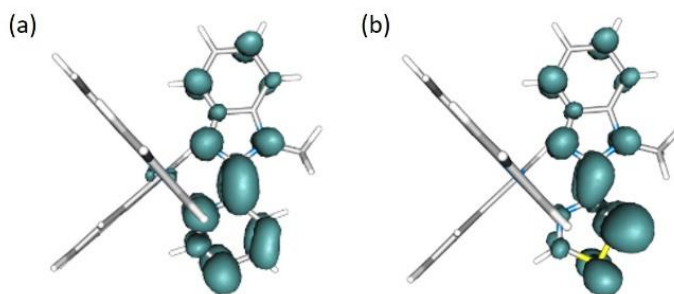


Fig. 18. Unpaired-electron spin-density contours (0.002 a.u.) calculated for fully relaxed doublet (D_0) states of the radical neutral species [45][•] and [47][•] resulting from the reduction of [45]⁺ and [47]⁺.

The size of the HOMO–LUMO energy gap is therefore mainly determined by the position of the LUMO and increases along the series [44]⁺ ≈ [45]⁺ < [43]⁺ < [46]⁺ ≈ [47]⁺. Obviously, if a direct correlation is established between the HOMO–LUMO gap and the emission energy, bluer emissions have to be expected along this series, which is indeed in agreement with the experimental trend observed for the emission maxima (see Table 8). However, the picture is not as simple since experimental evidences point to a different electronic nature of the emitting triplet state. Therefore, we cannot directly presume that emission originates from the HOMO → LUMO transition for all the complexes.

TD-DFT calculations determined the energy of the triplet states as well as the character of these states (see Fig. 19 and Table 10). Thus, the emission could occur from

different triplet states when they are close in energy. The calculated emission energies, estimated as the vertical energy difference between T_1 and S_0 at the optimized minimum-energy geometry of T_1 , follow closely the experimental values of the emission maxima. The values predicted for **[44]⁺** (590 nm) and **[45]⁺** (593 nm) are in good accord with the experimental values (583 and 596 nm, respectively), whereas those obtained for **[43]⁺** (534 nm), **[46]⁺** (527 nm), and **[47]⁺** (528 nm) slightly overestimate the experimental values (516, 489-508, 486-508 nm, respectively).

Table 10. Lowest triplet excited states calculated at the TD-DFT B3LYP/(6-31G+LANL2DZ) level for complexes [1]⁺ to [5]⁺ in acetonitrile solution. Vertical excitation energies (E), dominant monoexcitations with contributions (within parentheses) greater than 30%, nature of the electronic transition and description of the excited state are summarized. H and L denote HOMO and LUMO, respectively.**

Complex	State	E (eV)	Monoexcitations	Nature	Description ^a
[43]⁺	T_1	2.73	$H \rightarrow L$ (72)	$d_{\pi}(Ir) + \pi_{C^N} \rightarrow \pi_{N^N}^*$	${}^3MLCT/{}^3LLCT$
	T_2	2.75	$H \rightarrow L+1$ (54)	$d_{\pi}(Ir) + \pi_{C^N} \rightarrow \pi_{C^N}^*$	${}^3LC(C^N)$
	T_3	2.79	$H \rightarrow L+2$ (58)	$d_{\pi}(Ir) + \pi_{C^N} \rightarrow \pi_{C^N}^*$	${}^3LC(C^N)$
	T_4	2.93	$H-2 \rightarrow L$ (35)	$d_{\pi}(Ir) + \pi_{C^N} + \pi_{N^N} \rightarrow \pi_{N^N}^*$	${}^3LC(N^N)/{}^3MLCT/{}^3LLCT$
			$H-6 \rightarrow L$ (30)	$\pi_{N^N} \rightarrow \pi_{N^N}^*$	${}^3LC(N^N)$
[44]⁺	T_1	2.51	$H \rightarrow L$ (95)	$d_{\pi}(Ir) + \pi_{C^N} \rightarrow \pi_{N^N}^*$	${}^3MLCT/{}^3LLCT$
	T_2	2.70	$H-1 \rightarrow L$ (39)	$d_{\pi}(Ir) + \pi_{C^N} + \pi_{N^N} \rightarrow \pi_{N^N}^*$	${}^3LC(N^N)/{}^3MLCT/{}^3LLCT$
	T_3	2.75	$H \rightarrow L+1$ (67)	$d_{\pi}(Ir) + \pi_{C^N} \rightarrow \pi_{C^N}^*$	${}^3LC(C^N)$
	T_4	2.80	$H \rightarrow L+2$ (56)	$d_{\pi}(Ir) + \pi_{C^N} \rightarrow \pi_{C^N}^*$	${}^3LC(C^N)$
[45]⁺	T_1	2.51	$H \rightarrow L$ (92)	$d_{\pi}(Ir) + \pi_{C^N} \rightarrow \pi_{N^N}^*$	${}^3MLCT/{}^3LLCT$
	T_2	2.69	$H-1 \rightarrow L$ (52)	$d_{\pi}(Ir) + \pi_{C^N} + \pi_{N^N} \rightarrow \pi_{N^N}^*$	${}^3LC(N^N)/{}^3MLCT/{}^3LLCT$
	T_3	2.75	$H \rightarrow L+1$ (70)	$d_{\pi}(Ir) + \pi_{C^N} \rightarrow \pi_{C^N}^*$	${}^3LC(C^N)$
	T_4	2.80	$H \rightarrow L+2$ (67)	$d_{\pi}(Ir) + \pi_{C^N} \rightarrow \pi_{C^N}^*$	${}^3LC(C^N)$
[46]⁺	T_1	2.75	$H \rightarrow L+1$ (67)	$d_{\pi}(Ir) + \pi_{C^N} \rightarrow \pi_{C^N}^*$	${}^3LC(C^N)$
	T_2	2.79	$H \rightarrow L+2$ (56)	$d_{\pi}(Ir) + \pi_{C^N} \rightarrow \pi_{C^N}^*$	${}^3LC(C^N)$
	T_3	2.84	$H-1 \rightarrow L$ (37)	$d_{\pi}(Ir) + \pi_{C^N} + \pi_{N^N} \rightarrow \pi_{N^N}^*$	${}^3LC(N^N)/{}^3MLCT/{}^3LLCT$
	T_4	2.95	$H \rightarrow L$ (87)	$d_{\pi}(Ir) + \pi_{C^N} \rightarrow \pi_{N^N}^*$	${}^3MLCT/{}^3LLCT$
[47]⁺	T_1	2.75	$H \rightarrow L+1$ (67)	$d_{\pi}(Ir) + \pi_{C^N} \rightarrow \pi_{C^N}^*$	${}^3LC(C^N)$
	T_2	2.79	$H \rightarrow L+2$ (56)	$d_{\pi}(Ir) + \pi_{C^N} \rightarrow \pi_{C^N}^*$	${}^3LC(C^N)$
	T_3	2.85	$H-1 \rightarrow L$ (46)	$d_{\pi}(Ir) + \pi_{C^N} + \pi_{N^N} \rightarrow \pi_{N^N}^*$	${}^3LC(N^N)/{}^3MLCT/{}^3LLCT$
	T_4	2.97	$H \rightarrow L$ (90)	$d_{\pi}(Ir) + \pi_{C^N} \rightarrow \pi_{N^N}^*$	${}^3MLCT/{}^3LLCT$

^a Triplets ${}^3LC(C^N)$ due to the $HOMO \rightarrow LUMO+1$ and $LUMO+2$ excitations show some contribution of MLCT character (~15%).

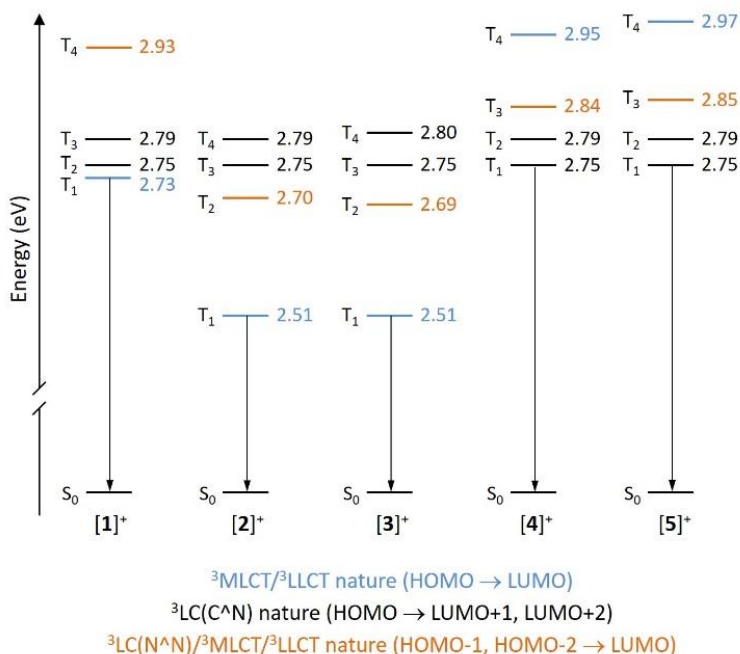


Fig. 19. Energy diagram showing the energy values calculated for the lowest-energy triplet excited states (T_n) of complexes [43]⁺ to [47]⁺. The different electronic nature of the T_n states is denoted by using different colours.

2. APPLICATIONS: LEC DEVICES

The concept of lighting has changed in the last two decades. In fact, solid-state lighting (SSL) is a new concept for illumination. It involves an organic semiconductor material sandwiched between two metal electrodes, which are stimulated to produce visible light under the application of external electrical field. The SSL is divided into two main families of devices: light-emitting diodes (LEDs) and organic light-emitting diodes (OLEDs). Nowadays, OLEDs are gaining great attention in display applications. However, they have some limitations, such as their complex and costly manufacturing procedures, which have prevented this technology from being completely accepted in the market. These drawbacks have encouraged the need for new concepts for flat electroluminescent (EL) lighting devices. Among these, light-emitting electrochemical cells (LECs) are the most popular. Furthermore, LECs have some advantages over OLEDs, as they have a much simple architecture and packing. Depending on the light-emitting material, there are two kind of devices: when it is a polymer, they are known as polymer LECs (PLECs); and when it is an ionic transition-metal complex (with small molecular weight), they are called iTMC-LECs.^{7,30,32} The operation of LECs is simple, although two models have been proposed, the electrodynamic (ED) and the electrochemical doping (ECD). The former assumes that after application of an electric field, the charged species in the active layer move towards the electrodes, accumulating at the interfaces and causing a sharp drop of the potential near the electrode interfaces with the subsequent formation of doped zones. In this situation, emission of light takes place at the intrinsic region.³³ The latter, on the other hand, assumes that the accumulation of ions at the anode and cathode leads to the formation of highly conductive p- and n-doped regions.

The doped regions widen over time, until a p-i-n junction (*i* = intrinsic, undoped) between them is formed. In this region, the applied potential drops substantially and favours charge recombination and light emission (see Fig. 20).³⁰

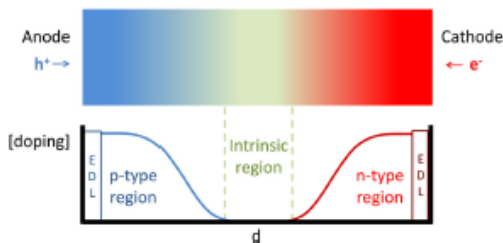


Fig. 20. Schematic representation of the operation mechanism of LECs at sufficient high voltages after formation of the electric double layers (EDLs) and the p- and n-type doped zones. Figure extracted from Meier, S. B.; Tordera, D.; Pertegás, A.; Roldán-Carmona, C.; Ortí, E.; Bolink, H. J. *Mater. Today* 2014, 17, 217–223.³²

2.1. Fabrication of LEC devices

LECs were prepared by the group of Henk Bolink (ICMol, Universidad de Valencia) in a cleanroom. The devices were prepared over a patterned indium tin oxide (ITO) coated glass substrate. This coated glass was previously cleaned, following four steps: a) sonication with soap, b) deionized water, c) *i*-propanol and d) UV-O₃ lamp for 20 min. Then, a thin layer (80 nm) of a suspension PEDOT:PSS [poly(3,4-ethylenedioxythiophene):poly(styrenesulfonate)] was deposited by spin-coating. The emitting layer (100 nm) was also prepared by spin-coating of an acetonitrile solution of the iTMC (the Ir(III) complex) with the addition of the ionic liquid (IL) [Bmim][PF₆] (1-butyl-3-methylimidazolium hexafluorophosphate) in a 4:1 molar ratio (iTMC-IL). The devices were then transferred to an inert atmosphere glovebox, where a layer (70 nm) of aluminum was thermally evaporated and deposited onto the devices. Thus, the structure of the device was: Glass/ITO/PEDOT:PSS/Ir complexes:[Bmim][PF₆] 4:1 molar ratio/Al, with a final area of 6.5 mm². Fig. 21 shows the fabrication process and the composition of a device as well as the equipment required to deposit the thin films.

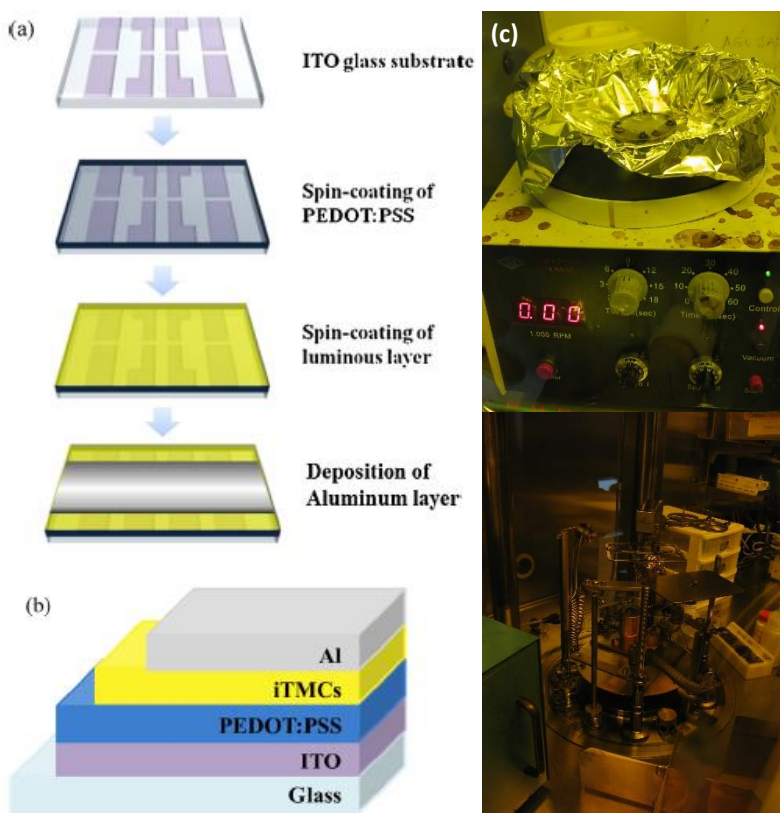


Fig. 21. (a) Configuration of the device fabrication process by spin-coating and **(b)** structure of the bi-layered LECs (figure extracted from Jeon, Y.; Sunesh, C. D.; Chitumalla, R. K.; Jang, J.; Choe, Y. *Electrochim. Acta* 2016, **195**, 112–123.)⁷. Equipment of coating: **(c)** spin-coater and **(d)** evaporator (the heat is supplied by electric current between two electrodes).

2.2. PL in thin films

Besides the features measured for the devices, the photoluminescence and the quantum yield were measured in thin films with an integrating sphere. The thin film consisted in the deposition of a solution of the Ir(III) complex by spin-coating on a quartz glass, mimicking the conditions of devices. Fig. 22 displays the emission spectra of the complexes in thin films, this is, in solid state. The tendency of the emission maxima is similar to that observed in the spectra of the complexes in solution. Nonetheless, the emission maxima are shifted. Regarding the PLQY, the values are quite similar. Table 11 shows the PL emission wavelength and PLQY for selected complexes.

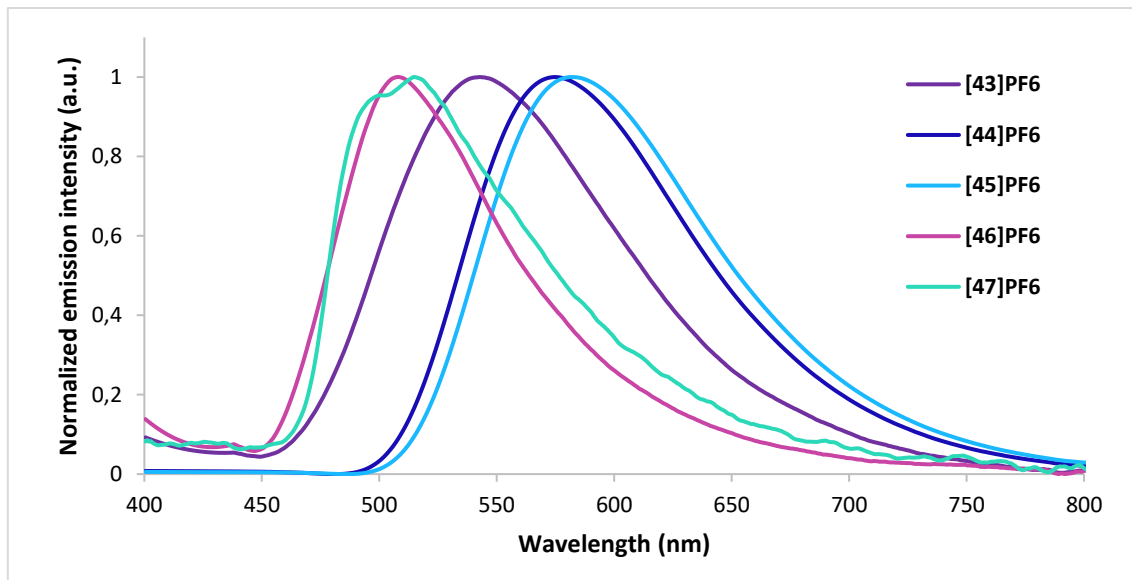


Fig. 22. Emission spectra of complexes $[43](\text{PF}_6)$, $[44](\text{PF}_6)$, $[45](\text{PF}_6)$, $[46](\text{PF}_6)$ and $[47](\text{PF}_6)$ in a thin film ($\lambda_{\text{exc}} = 320 \text{ nm}$) at 25°C .

2.3. Electroluminescent properties of the LECs

The devices **lifetime** was measured applying a pulsed current and monitoring the voltage and the **luminance** versus time. The average **current density** was determined multiplying the peak current density by the **turn-on time** and dividing by the total cycle time. The average luminance was directly obtained correlating the average of the photodiode luminance to the value of a luminance meter. The **current efficiency** was obtained dividing the average luminance by the average current density (see Fig. 23).

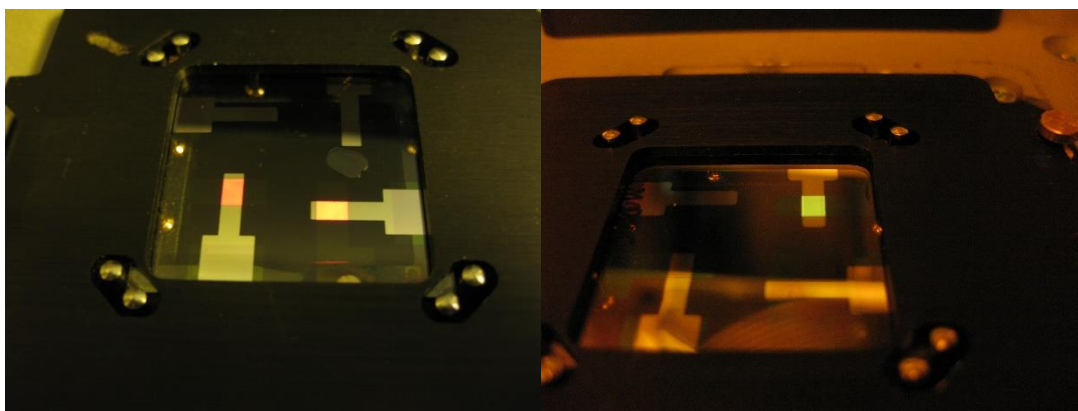


Fig. 23. Assembly of the device into the BoTEST (Botest OLT OLED Lifetime-Test System), able to measure the parameters of the LEC. The equipment is located inside a glovebox.

The LEC devices were operated under inert conditions applying pulsed current methods and driven at an average current density of $100 \text{ A}\cdot\text{m}^{-2}$ using duty cycle of 50%. Fig. 24 exhibits the colour modulation on electroluminescence of selected LECs.

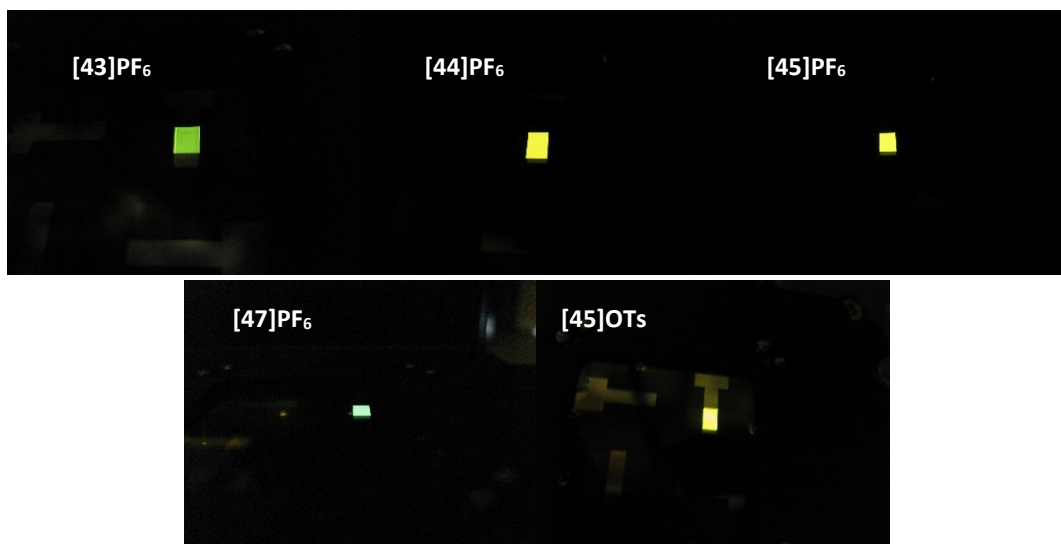


Fig. 24. Switched-on of LEC devices for selected complexes.

The electroluminescent spectra were recorded during the device lifetime measurement (see Fig. 25). The emission maxima were immobile or slightly bathochromic-shifted with regard to the PL spectra in thin films, except for the complex **[47]PF₆**, which shifts 49 nm. In addition, the spectra were structureless. Table 11 gathers the comparison of the PL emission maxima of the complexes in solution and in thin film with the EL emission maxima. Likewise, the PLQY are also gathered in solution and in thin film.

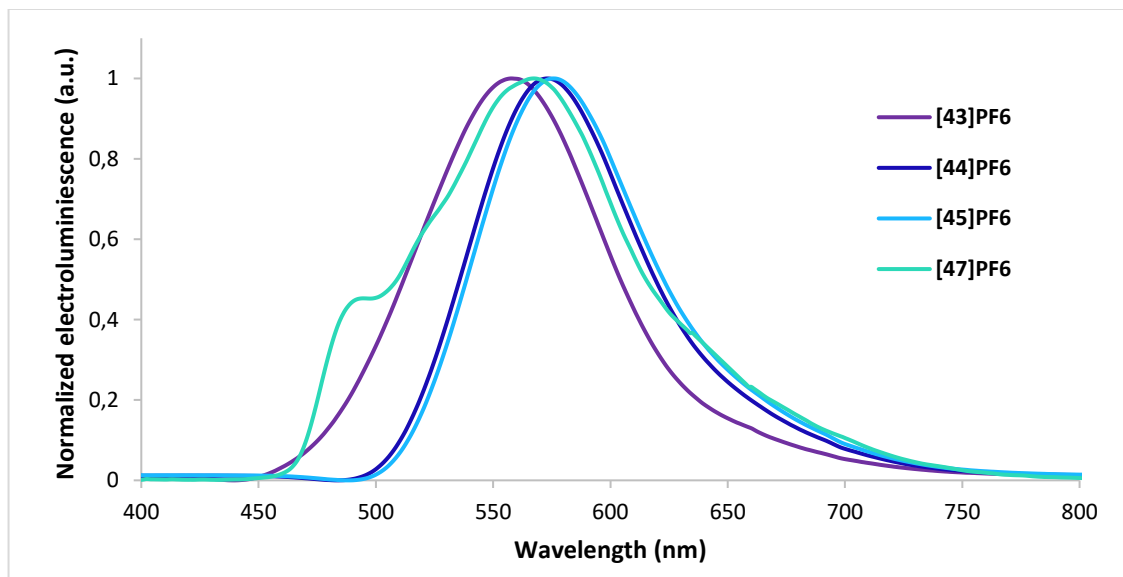


Fig. 25. Electroluminescence spectra of complexes **[43](PF₆)**, **[44](PF₆)**, **[45](PF₆)** and **[47](PF₆)** in the LEC devices at 25 °C and recorded under N₂ atmosphere (inside a glovebox).

Table 11. Photoluminescence in solution and in thin film, and electroluminescence. of Ir(III) complexes.

Compound	$\lambda_{\text{em sol.}} (\text{nm})$	$\Phi_{\text{sol.}}$	$\lambda_{\text{em film}} (\text{nm})$	Φ_{film}	$\lambda_{\text{em EL}} (\text{nm})$
[43](PF ₆)	516 (cyan)	0.20	542 (green)	0.06	558 (green)
[44](PF ₆)	582 (yellow)	0.39	574 (yellow)	0.32	573 (yellow)
[45](PF ₆)	594 (orange)	0.39	581 (yellow)	0.45	576 (yellow)
[46](PF ₆)	489/508 (blue-cyan)	0.09	507 (cyan)	0.03	-
[47](PF ₆)	487/508 (blue-cyan)	0.04	499(sh)/518 (blue-cyan)	0.06	493(sh)/567 (blue-yellow)
[45](BPh ₄)	591 (orange)	0.15	583 (yellow)	0.23	-
[45](OTs)	591 (orange)	0.13	567 (yellow)	0.26	570 (yellow)

The device parameters are gathered in Table 12 and Fig. 26 and Fig. 27 display the graphs illustrating the luminance, average voltage and PCE vs. time. All the devices present a fast initial decrease of the voltage until a minimum stable value (2.3–2.7 V) is reached. This behavior is typical under the pulsed current driving applied due to the operation mechanism of LECs. The fact that the voltage remains in all cases close to the minimum along the device operation time reveals that there are no signs of charge transport issues or chemical degradation. Except for devices with [46]PF₆, that does not emit any light. The t_{on} for some devices was not established because these LECs did not achieve the threshold of 100 cd m⁻². The absence of light emission for [46]PF₆ and the low luminance observed for [43]PF₆ and [47]PF₆ can be related with the nature of the emitting state, and, in the case of [46]PF₆, with the observed formation of dimeric entities in the crystal that favor self-quenching processes. The emitting state of these complexes has a predominant ³LC character with small participation of the iridium center. This limits the intersystem crossing and, as a consequence, low PLQY values are obtained for [43]PF₆ (5.5%), [46]PF₆ (3.3%), and [47]PF₆ (6.0%) in thin film (see Table 11). In contrast, [44]PF₆ and [45]PF₆ have emitting states of ³MLCT/³LLCT nature with higher PLQY values (32.1 and 44.6%, respectively), and their LECs feature much higher luminances ($\text{Lum}_{\text{max}} = 460$ and 906 cd·m⁻², respectively). The higher luminance registered for the [45]PF₆ device combines with a top efficiency (efficacy of 9.2 cd·A⁻¹ and external quantum efficiency of 3.0%), and is in good agreement with the higher PLQY recorded for this complex in thin film. In addition, the LECs built with [44]PF₆ and [45]PF₆ show a fast response, the longest t_{on} (7 s) being found for the LEC with [45]PF₆.

Table 12. Performance of LEC devices for complexes [43]⁺-[47]⁺.

iTMC	Lum ₀ (cd·m ⁻²)	Lum _{max} (cd·m ⁻²)	t _{on} (s)	t _{max} (min)	t _{1/2} (h)	Efficacy (cd·A ⁻¹)	EQE (%)	PCE (lm·W ⁻¹)
[43]PF ₆	18	25	-	15	2.25	0.3	0.1	1.3
[44]PF ₆	143	460	< 2	18	0.30	4.6	1.4	2.5
[45]PF ₆	44	904	6.9	1680	>2000	9.2	3.0	5.7
[46]PF ₆	-	0	-	-	-	-	-	-
[47]PF ₆	51	61	-	1	200	0.6	0.2	0.3

The stability of the devices was estimated as the decay time required for reaching one-half of the maximum luminance ($t_{1/2}$) after the t_{max} is attained. The values obtained for $t_{1/2}$ (see Table 12) indicate that the condensation of a benzene ring to the imidazole heterocycle on going from [43]PF₆ to [44]PF₆, although produces a huge increase of the light emitted, it does not assure a high stability and device lifetime. In fact, the device made with the pybim-containing complex [44]PF₆ features a short $t_{1/2}$ of only 0.30 h, shorter than that of the pyim-containing [43]PF₆ (2.25h). However, when the imidazole N–H group is substituted with a N-Me group, the LEC stability improves dramatically, and $t_{1/2}$ grows up to 200 h in [47]PF₆ and above 2000 h in [45]PF₆. The luminance of the [45]PF₆ device indeed decreases only by 12% after 650 h (27 days) of continuous operation, and the linear extrapolation of the time dependence of luminance provides the value of $t_{1/2} = 2700$ h, which is a remarkable result for a LEC (see Fig. 26). The unprotection of the N-H bond of some species could be the reason of the limited device stability of [43]PF₆, [44]PF₆ and [46]PF₆. The value of $t_{1/2}$ extrapolated for [45]PF₆ is within the best values available in the bibliography for LECs. In a recent review,³⁴ Henwood and Zysman-Colman concluded that the most stable emitter reported to date under the same pulsed current operation of 100 A m⁻² was presented by Tordera et al.,³⁵ who described a LEC device based on an imidazole-including complex ([Ir(ppy)₂(imp)]⁺ (imp = 1H-imidazo[4,5-f][1,10]phenanthroline)) that featured high lifetime and luminescence and low turn-on times. The results obtained here for the device manufactured with complex [45]PF₆ are even better than those of the device with [Ir(ppy)₂(imp)]⁺. While the stability is comparable for both devices ($t_{1/2} \approx 2000$ h), the turn-on time obtained when using [45]PF₆ is shorter (6.9 vs. 45 s), the maximum luminance is higher (904 vs. 684 cd·m⁻²), and the maximum current efficiency is also higher (9.2 vs. 6.5 cd·A⁻¹). This is certainly above to the most stable ($t_{1/2} \approx 4000$ h) yellow-orange emitting LEC (3.6 cd·A⁻¹), that was operated under different pulsed current conditions (30% of duty cycle),³⁶ and competitive to the top peak efficiencies (18.6 cd·A⁻¹) obtained by He et al. under constant voltage operation that usually leads to higher peak values.³⁷ Interestingly, the exceptional efficiency found for the [45]PF₆ LEC (9.2 cd·A⁻¹) overcomes the efficiency previously obtained for this complex under voltage scan (1.5 cd·A⁻¹).⁶

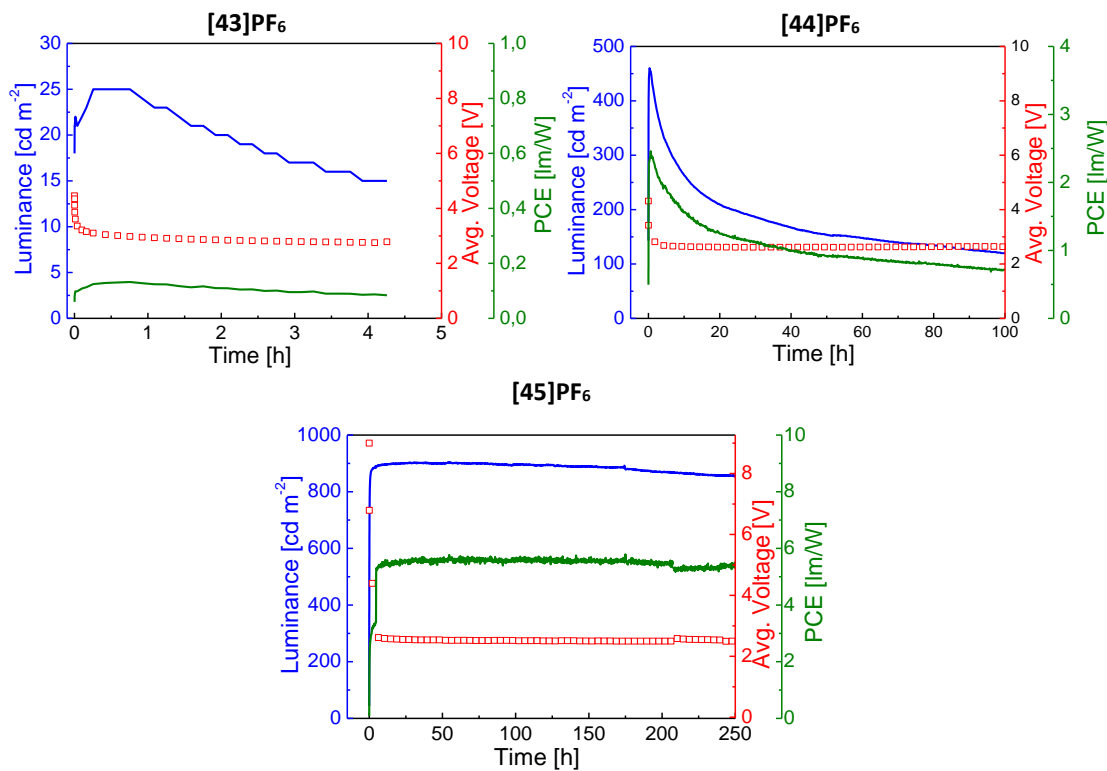


Fig. 26. Luminescence (blue), average voltage (red) and PCE (green) vs. time (black) for complexes **[43]PF₆**-**[45]PF₆**.

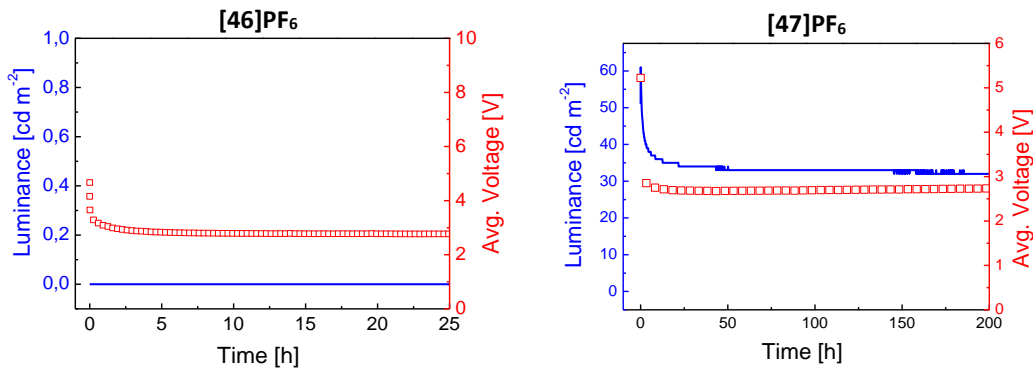


Fig. 27. Luminescence (blue) and average voltage (red) vs. time (black) for complexes **[46]PF₆**-**[45]PF₆**.

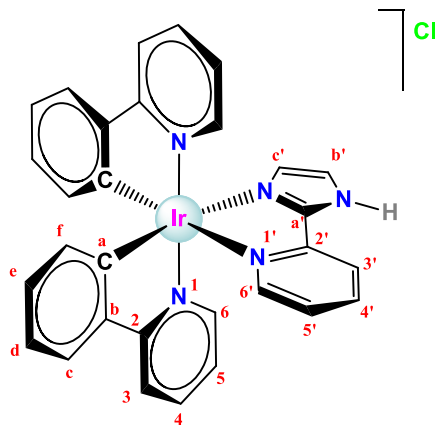
3. CONCLUDING REMARKS

- A family of 11 new complexes has been synthesised and fully characterised, both in solution and some of them in solid state.
- The photoluminescent properties of the complexes in solution change depending on the identity of the ancillary ligand. Complexes **[44]⁺** and **[45]⁺** show high PLQY and broad and unstructured bands in the emission spectra, whereas **[43]⁺**, **[46]⁺** and **[47]⁺** present lower PLQY and a vibrationally-structured spectrum.
- Theoretical calculations have supported the photophysical behaviour of complexes **[43]PF₆** to **[47]PF₆**. The benzimidazole unit in **[44]PF₆** and **[45]PF₆** stabilizes the LUMO (located on the ancillary ligand) and determined a

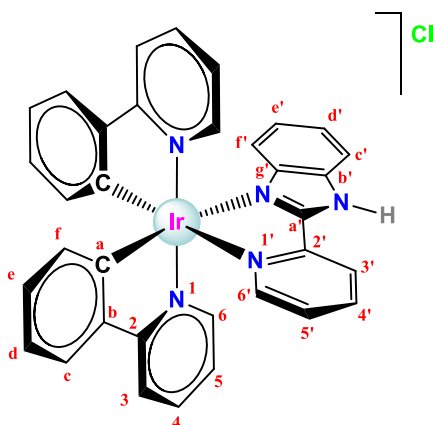
$^3\text{MLCT}/^3\text{LLCT}$ character for the lowest-energy emitting triplet state. On the other hand, the thiazolyl ring destabilizes the LUMO, and thereby the $\text{HOMO} \rightarrow \text{LUMO}$ $^3\text{MLCT}/^3\text{LLCT}$ state, and the emitting triplet has a predominant ^3LC nature in **[46]PF₆** and **[47]PF₆**. Complex **[43]PF₆** displays an intermediate behaviour due to close energy of the $^3\text{MLCT}/^3\text{LLCT}$ and ^3LC states.

- 5 LEC devices have been fabricated, obtaining different features and emission colours. The best result has been obtained for the device prepared with **[45]PF₆**, whose stability ($t_{1/2} \approx 2000\text{h}$), short turn-on time (6.9 s) and maximum luminance (904 cd m⁻²) make it one of the top LEC devices reported to date.

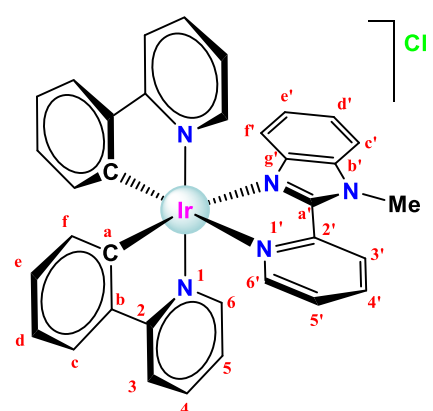
4. EXPERIMENTAL SECTION



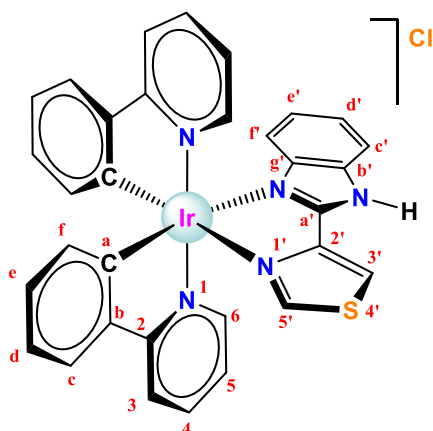
Synthesis of $[Ir(ppy)_2(pyim)]Cl$, [43]Cl. In a 100 mL Schlenk flask, the ligand pyim (0.0312 g, 0.193 mmol) was added to a solution of $[Ir(ppy)_2Cl]_2$ (0.1002 g, 0.093 mmol) in a mixture of dichloromethane/methanol (4:5 13.5 mL), and the mixture was stirred at 60 °C for 24 h and under a nitrogen atmosphere. The solution was filtered and the solid precipitated with diethyl ether. The product was washed again with diethyl ether. The resulting yellow powder was dried under vacuum. Yield: 102.1 mg (0.150 mmol, 80%). **M_r** ($C_{30}H_{23}N_5ClIr$) = 681.2179 g/mol. **Anal. Calcd for** $C_{30}H_{23}N_5ClIr \cdot (CH_3OH)_{1.2}(CH_2Cl_2)_{0.2}$: C 51.20; H 3.86; N 9.51; **Found:** C 51.13; H 3.79; N 9.05. **¹H NMR (400 MHz, CDCl₃, 25 °C)** δ 15.88 (s, 1H, H^{N-H}), 9.38 (dd, *J* = 8.1, 0.8 Hz, 1H, H^{3'}), 7.95 (t, *J* = 7.8 Hz, 1H, H^{4'}), 7.87 (dd, *J* = 8.1, 1.3 Hz, 2H, H³, H³), 7.79 – 7.69 (m, 3H, H^{6'}, H⁴, H⁴), 7.66 (d, *J* = 7.1 Hz, 2H, H^c, H⁶), 7.63 (d, *J* = 7.7 Hz, 1H, H^c), 7.50 (dd, *J* = 5.8, 0.7 Hz, 1H, H⁶), 7.33 (s, 1H, H^{b'}), 7.21 – 7.16 (m, 1H, H^{5'}), 7.03 – 6.92 (m, 4H, H^d, H^d, H⁵, H⁵), 6.89 (t, *J* = 7.4 Hz, 1H, H^e), 6.84 (t, *J* = 7.4 Hz, 1H, H^e), 6.51 (s, 1H, H^{c'}), 6.40 (d, *J* = 7.6 Hz, 1H, H^f), 6.31 (d, *J* = 7.6 Hz, 1H, H^f) ppm. **¹³C{¹H} NMR (101 MHz, CDCl₃, 25 °C)** δ 168.31 (s, 1C, C²), 168.28 (s, 1C, C²), 152.2 (s, 1C, C^a), 149.9 (s, 1C, C⁶), 149.1 (s, 1C, C⁶), 148.8 (s, 1C, C^{2'}), 148.6 (s, 1C, C⁶), 148.4 (s, 1C, C^{a'}), 147.6 (s, 1C, C^a), 144.2 (s, 1C, C^b), 143.8 (s, 1C, C^b), 139.5 (s, 1C, C^{4'}), 137.7 (s, 1C, C⁴), 137.6 (s, 1C, C⁴), 132.2 (s, 1C, C^f), 132.0 (s, 1C, C^f), 130.7 (s, 1C, C^e), 130.2 (s, 1C, C^e), 127.2 (s, 1C, C^{c'}), 125.8 (s, 1C, C^{5'}), 124.8 (s, 1C, C^c), 124.40 (s, 1C, C^c), 124.36 (s, 1C, C^{3'}), 123.0 (s, 1C, C⁵), 122.8 (s, 1C, C⁵), 122.29 (s, 1C, C^d), 122.25 (s, 1C, C^{b'}), 122.1 (s, 1C, C^d), 119.3 (s, 2C, C³, C³) ppm. **FT-IR (ATR, cm⁻¹) selected bands:** 3418 (w, v_{N-H}asociado), 3032 (w, v_{C=CH}), 2965-2850-2739-2638-2508 (w, v_{-CH}), 1608-1583 (s, v_{C=C + C-N}), 1478 (s), 1468 (s, v_{C=N}), 1439-1419 (m), 1301 (m), 1267 (m), 1157 (m, v_{C-C}), 1118 (m), 1065-1032 (m, δ_{C-Hip}), 928 (m), 790 (m, δ_{C-C}), 770-753 (vs, δ_{C-Hoop}), 707 (s), 670 (m), 630 (w). **MS (FAB+):** m/z (%) = 647 (100) ([M-Cl+H]⁺), 501 (48) ([M-Cl-pyim]⁺). **Molar Conductivity (CH₃CN):** 28 S·cm²·mol⁻¹. **Solubility:** soluble in dichloromethane, chloroform, acetonitrile, DMSO.



Synthesis of $[Ir(ppy)_2(pybim)]Cl$, [44]Cl.¹⁰ The synthesis was performed as for [43]Cl in the presence of the ligand pybim (0.0390 g, 0.199 mmol) and $[Ir(ppy)_2Cl]_2$ (0.1000 g, 0.093 mmol). Yield: 131.8 mg (0.180 mmol, 92%). **M_r** ($C_{34}H_{25}N_5ClIr \cdot (CH_3OH)(CH_2Cl_2)_{0.3}$) = 731.2777 g/mol. **Anal. Calcd for** $C_{34}H_{25}N_5ClIr \cdot (CH_3OH)(CH_2Cl_2)_{0.3}$: C 53.75; H 3.78; N 8.88; **Found:** C 53.68; H 3.79; N 8.64. **¹H NMR (400 MHz, CDCl₃, 25 °C)** δ 16.22 (s, 1H, H^{N-H}), 9.72 (d, *J* = 8.1 Hz, 1H, H^{3'}), 8.06 (t, *J* = 7.8 Hz, 1H, H^{4'}), 7.93 (d, *J* = 8.4 Hz, 1H, H^{c'}), 7.89 (d, *J* = 8.2 Hz, 1H, H³), 7.88 – 7.82 (m, 2H, H³, H^{6'}), 7.76 – 7.62 (m, 5H, H⁴, H⁴, H^c, H^c, H⁶), 7.48 (d, *J* = 5.4 Hz, 1H, H⁶), 7.35 – 7.27 (m, 2H, H^{5'}, H^{d'}), 7.09 (t, *J* = 7.3 Hz, 1H, H^d), 7.03 (t, *J* = 7.6 Hz, 1H, H^d), 6.98 – 6.88 (m, 5H, H^{e'}, H⁵, H⁵, H^e, H^e), 6.43 (d, *J* = 7.6 Hz, 1H, H^f), 6.38 (d, *J* = 7.6 Hz, 1H, H^f), 6.19 (d, *J* = 8.2 Hz, 1H, H^{f'}) ppm. **¹³C{¹H} NMR (101 MHz, CDCl₃, 25 °C)** δ 168.4 (s, 1C, C²), 168.1 (s, 1C, C²), 153.0 (s, 1C, C^{a'}), 151.7 (s, 1C, C^a), 150.3 (s, 1C, C^{6'}), 149.7 (s, 1C, C⁶), 148.9 (s, 1C, C^{2'}), 148.5 (s, 1C, C⁶), 147.2 (s, 1C, C^a), 144.22 (s, 1C, C^b), 144.16 (s, 1C, C^b), 140.2 (s, 1C, C^{g'}), 139.6 (s, 1C, C^{4'}), 137.8 (s, 1C, C⁴), 137.6 (s, 1C, C⁴), 135.3 (s, 1C, C^{b'}), 132.5 (s, 1C, C^f), 132.0 (s, 1C, C^f), 130.8 (s, 1C, C^e), 130.2 (s, 1C, C^e), 127.2 (s, 1C, C^{5'}), 126.6 (s, 1C, C^{3'}), 125.6 (s, 1C, C^{d'}), 124.8 (s, 1C, C^c), 124.7 (s, 1C, C^c), 124.6 (s, 1C, C^{e'}), 123.2 (s, 1C, C⁵), 122.9 (s, 1C, C⁵), 122.5 (s, 1C, C^d), 122.4 (s, 1C, C^d), 119.39 (s, 1C, C³), 119.37 (s, 1C, C³), 117.2 (s, 1C, C^{f'}), 115.0 (s, 1C, C^{c'}) ppm. **FT-IR (ATR, cm⁻¹) selected bands:** 3373 (w, v_{N-H}asociado), 3034 (w, v_{C=CH}), 2964 (w, v_{CH}), 1604–1581 (m, v_{C=C + C-N}), 1475 (s), 1455 (m, v_{C=N}), 1438–1416 (m), 1304 (m), 1267 (m), 1157 (m, v_{C-C}), 1062–1031–1007–979 (m, δ_{C-Hip}), 794 (w, δ_{C-C}), 753–739 (vs, δ_{C-Hoop}), 630 (m). **MS (FAB+):** m/z (%) = 697 (50) ([M-Cl+H]⁺), 501 (18) ([M-Cl-pybim]⁺). **Molar Conductivity (CH₃CN):** 25 S·cm²·mol⁻¹. **Solubility:** soluble in water, methanol, dichloromethane, chloroform and acetone.

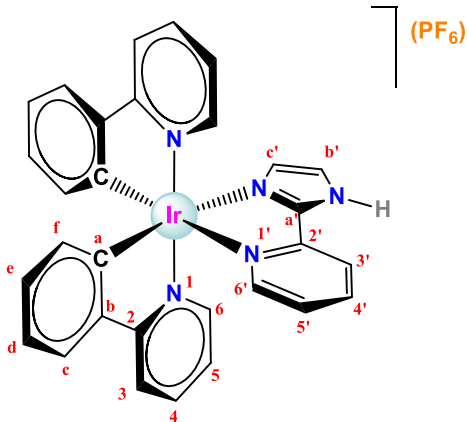


Synthesis of $[Ir(ppy)_2(pyMebim)]Cl$, [45]Cl. The synthesis was performed as for [43]Cl in the presence of the ligand pyMebim (0.0101 g, 0.048 mmol) and $[Ir(ppy)_2Cl]_2$ (0.0260 g, 0.024 mmol). Yield: 35.0 mg (0.047 mmol, 97%). M_r ($C_{35}H_{27}N_5ClIr$) = 745.3045 g/mol. **Anal. Calcd for** $C_{35}H_{27}N_5ClIr \cdot (CH_2Cl_2)_{0.45}(H_2O)_{0.5}$: C 53.73; H 3.68; N 8.84; **Found:** C 53.76; H 3.65; N 8.88. **1H NMR (400 MHz, CDCl₃, 25 °C)** δ 9.61 (d, J = 8.2 Hz, 1H, H^{3'}), 8.50 (t, J = 7.2 Hz, 1H, H^{4'}), 7.96 (d, J = 4.6 Hz, 1H, H^{6'}), 7.91 (d, J = 8.0 Hz, 1H, H³), 7.84 (d, J = 8.3 Hz, 1H, H³), 7.73 (t, J = 8.0 Hz, 1H, H⁴), 7.68 (t, J = 8.0 Hz, 3H, H⁴, H^c, H^c), 7.65 (d, J = 5.8 Hz, 1H, H⁶), 7.57 (d, J = 8.4 Hz, 1H, H^c), 7.51 (d, J = 5.2 Hz, 1H, H⁶), 7.40 (t, J = 7.3 Hz, 2H, H^{5'}, H^{d'}), 7.08 (t, J = 5.8 Hz, 1H, H^d), 7.07 – 6.96 (m, 3H, H^d, H^e, H⁵), 6.96 – 6.90 (m, 3H, H⁵, H^e, H^e), 6.42 (d, J = 7.5 Hz, 1H, H^f), 6.32 (d, J = 4.1 Hz, 1H, H^f), 6.30 (d, J = 4.8 Hz, 1H, H^f), 4.75 (s, 3H, H^{Me}) ppm. **$^{13}C\{^1H\}$ NMR (101 MHz, CDCl₃, 25 °C)** δ 168.3 (s, 1C, C²), 168.0 (s, 1C, C²), 152.8 (s, 1C, C^a), 151.6 (s, 1C, C^a), 151.4 (s, 1C, C⁶'), 149.6 (s, 1C, C⁶), 148.7 (s, 1C, C⁶), 147.4 (s, 1C, C^{2'}), 147.0 (s, 1C, C^a), 144.2 (s, 1C, C^b), 143.9 (s, 1C, C^b), 141.3 (s, 1C, C^{g'}), 139.5 (s, 1C, C^{4'}), 137.9 (s, 1C, C⁴), 137.7 (s, 1C, C⁴), 136.8 (s, 1C, C^b'), 132.5 (s, 1C, C^f), 131.8 (s, 1C, C^f), 131.0 (s, 1C, C^e), 130.3 (s, 1C, C^e), 128.1 (s, 1C, C^{5'}), 128.0 (s, 1C, C^{3'}), 126.1 (s, 1C, C^{d'}), 125.4 (s, 1C, C^c), 125.0 (s, 1C, C^c), 124.7 (s, 1C, C^{e'}), 123.4 (s, 1C, C⁵), 123.2 (s, 1C, C⁵), 122.7 (s, 1C, C^d), 122.5 (s, 1C, C^d), 119.6 (s, 1C, C³), 119.4 (s, 1C, C³), 118.3 (s, 1C, C^f), 111.7 (s, 1C, C^{c'}), 34.9 (s, 1C, C^{NMe}) ppm. **FT-IR (ATR, cm⁻¹) selected bands:** 3345 (w), 3029 (w, ν_{C=CH}), 1604–1582 (m, ν_{C=C+C-N}), 1474 (s), 1456 (m, ν_{C=N}), 1438–1418 (m), 1333 (w, δ_{CH3}), 1267 (m), 1156 (m, ν_{C-C}), 1063–1032–1011 (m, δ_{C-Hip}), 792 (m, δ_{C-C}), 765–755–741 (vs, δ_{C-Hoop}), 630 (m), 415 (m). **MS (FAB+):** m/z (%) = 711 (15) ([M-Cl+H]⁺), 501 (5) ([M-Cl-pyMebim]⁺). **Molar Conductivity (CH₃CN):** 129 S·cm²·mol⁻¹. **Solubility:** soluble in acetone and dichloromethane, chloroform and acetonitrile.



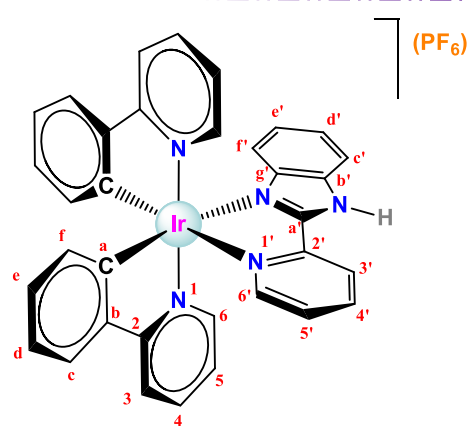
Synthesis of $[Ir(ppy)_2(tbz)]Cl$, [46]Cl. The synthesis was performed as for [43]Cl in the presence of the ligand tbz (0.0375 g, 0.186 mmol) and $[Ir(ppy)_2Cl]_2$ (0.1001 g, 0.093 mmol). Yield: 110.5 mg (0.153 mmol, 82%). M_r ($C_{32}H_{23}N_5SClIr$) = 737.3069 g/mol. **Anal. Calcd for** $C_{32}H_{23}N_5SClIr \cdot (CH_2Cl_2)_{0.7}(H_2O)_{0.8}$: C 49.27; H 3.29; N 7.03; S 4.02; **Found:** C 49.32; H 3.33; N 9.11; S 4.19. **1H NMR (400 MHz, CDCl₃, 25 °C)** δ 15.73 (s, 1H, H^{N-H}), 10.09 (d, J = 1.3 Hz, 1H, H^{3'}), 8.13 (d, J = 2.1 Hz, 1H, H^{5'}), 7.89 (d, J = 8.7 Hz, 1H, H³), 7.85 (d, J = 7.8 Hz, 1H, H³), 7.78 (d, J = 8.2 Hz, 1H, H^c), 7.76 – 7.70 (m, 2H, H⁴, H⁶), 7.70 – 7.62 (m, 3H, H⁴, H^c, H^c), 7.52 (d, J = 5.8 Hz, 1H, H⁶), 7.25 (t, J = 8.2 Hz, 1H, H^{d'}), 7.07 (t, J = 7.5 Hz, 1H, H^d), 7.00 (t, J = 7.5 Hz, 1H, H^d), 6.98 – 6.85 (m, 5H, H^e, H⁵, H⁵, H^e, H^e), 6.45 (d, J = 7.9 Hz, 1H, H^f), 6.40 (d, J = 7.3 Hz, 1H, H^f), 6.16 (d, J = 8.3 Hz, 1H, H^f) ppm. **$^{13}C\{^1H\}$ NMR (101 MHz, CDCl₃, 25 °C)** δ 168.4 (s, 1C, C²), 168.1 (s, 1C, C²), 155.1 (s,

1C, C^{5'}), 149.8 (s, 1C, C⁶), 148.6 (s, 1C, C^a), 148.29 (s, 1C, C⁶), 148.25 (s, 1C, C^{2'}), 146.73 (s, 1C, C^a), 146.65 (s, 1C, C^{a'}), 144.5 (s, 1C, C^b), 144.3 (s, 1C, C^b), 139.8 (s, 1C, C^{g'}), 137.9 (s, 1C, C⁴), 137.7 (s, 1C, C⁴), 134.9 (s, 1C, C^{b'}), 132.5 (s, 1C, C^f), 132.3 (s, 1C, C^f), 130.5 (s, 1C, C^e), 130.1 (s, 1C, C^e), 125.6 (s, 1C, C^{3'}), 125.1 (s, 1C, C^{d'}), 124.59 (s, 1C, C^c), 124.56 (s, 1C, C^c), 124.2 (s, 1C, C^{e'}), 123.2 (s, 1C, C⁵), 122.9 (s, 1C, C⁵), 122.5 (s, 1C, C^d), 122.4 (s, 1C, C^d), 119.3 (s, 2C, C³, C^{3'}), 117.1 (s, 1C, C^{f'}), 114.4 (s, 1C, C^{c'}) ppm. **FT-IR (ATR, cm⁻¹) selected bands:** 3372 (w, v_{N-H}asociado), 3034 (w, v_{C=CH}), 2618 (w, v_{-CH}), 1606-1579 (m, v_{C=C + C-N}), 1476 (s), 1455 (w, v_{C=N}), 1416 (s), 1267 (m), 1227 (m) 1161 (m, v_{C-C}), 1060-1030-1011-994 (m, δ_{C-Hip}), 830 (m), 795 (w, δ_{C-C}), 751 (vs, δ_{C-Hoop}), 630 (m), 560 (m), 436-421 (m). **MS (FAB+):** m/z (%) = 1404 (3) ([2M-2Cl]⁺), 703 (100) ([M-Cl+H]⁺), 501 (58) ([M-Cl-tbz]⁺). **Molar Conductivity (CH₃CN):** 21 S·cm²·mol⁻¹. **Solubility:** soluble in dichloromethane, chloroform and acetone. Partially soluble in methanol and insoluble in water.

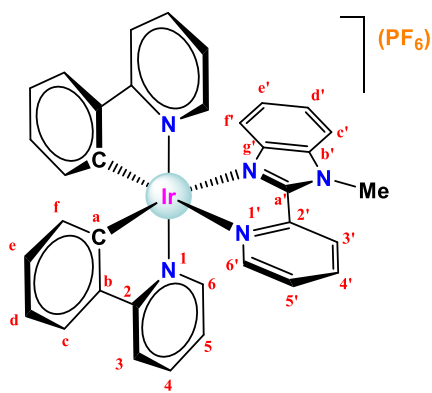


Synthesis of [Ir(ppy)₂(pyim)](PF₆), [43]PF₆. In a 100 mL Schlenk flask, the ligand pyim (0.0310 g, 0.214 mmol) was added to a solution of [Ir(ppy)₂Cl]₂ (0.1002 g, 0.093 mmol) in a mixture of dichloromethane/methanol (4:5 18 mL), and the suspension was stirred at 60 °C for 24 h and under a nitrogen atmosphere. An excess of NH₄PF₆ (0.3053 g, 1.87 mmol) was added, the mixture was stirred for 2 h at room temperature and then filtered. The metallic product was precipitated with diethyl ether and filtered. The yellow solid crude was dissolved in dichloromethane (10 mL), filtered and precipitated again with diethyl ether (15 mL). The resulting yellow powder was dried under vacuum. Yield: 79.5 mg (0.101 mmol, 54%). M_r (C₃₀H₂₃N₅PF₆Ir) = 790.7294 g/mol. **Anal. Calcd for C₃₀H₂₃N₅PF₆Ir·(H₂O)_{0.7}:** C 44.87; H 2.97; N 8.73; **Found:** C 44.86; H 3.06; N 8.72. **¹H NMR (400 MHz, DMSO-d₆, 25 °C)** δ 14.40 (s, 1H, H^{N-H}), 8.35 (d, J = 8.0 Hz, 1H, H^{3'}), 8.26 – 8.14 (m, 3H, H³, H³, H^{4'}), 7.96 – 7.88 (m, 3H, H⁴, H⁴, H^c), 7.86 (d, J = 7.7 Hz, 1H, H^c), 7.74 (d, J = 5.5 Hz, 1H, H^{6'}), 7.71 (d, J = 1.4 Hz, 1H, H^{b'}), 7.65 (t, J = 6.7 Hz, 2H, H⁶, H⁶), 7.54 (t, J = 6.9, 6.2 Hz, 1H, H^{5'}), 7.21 (t, J = 6.6 Hz, 1H, H⁵), 7.17 (t, J = 6.7 Hz, 1H, H⁵), 7.00 (t, J = 7.4 Hz, 1H, H^d), 6.96 (t, J = 7.7 Hz, 1H, H^d), 6.89 (t, J = 7.4 Hz, 1H, H^e), 6.83 (t, J = 7.4 Hz, 1H, H^e), 6.52 (d, J = 1.4 Hz, 1H, H^{c'}), 6.26 (d, J = 7.6 Hz, 1H, H^f), 6.20 (d, J = 7.7 Hz, 1H, H^f) ppm. **¹⁹F{¹H} NMR (376 MHz, DMSO-d₆, 25 °C)** δ -70.5 (d, J_{F-P} = 712.5 Hz, 6F, F^{PF6}) ppm. **³¹P{¹H} NMR (162 MHz, DMSO-d₆, 25 °C)** δ -143.3 (hept, J_{P-F} = 712.0 Hz, 1P, P^{PF6}) ppm. **¹³C{¹H} NMR (101 MHz, DMSO-d₆, 25 °C)** δ 167.2 (s, 1C, C²), 167.0 (s, 1C, C²), 151.6 (s, 1C, C^a), 149.9 (s, 1C, C^{6'}), 149.0 (s, 1C, C⁶), 148.7 (s, 1C, C⁶), 148.0 (s, 1C, C^{a'}), 147.28 (s, 1C, C^{2'} or C^a), 147.25 (s, 1C, C^a or C^{2'}), 144.3 (s, 1C, C^b), 144.0 (s, 1C, C^b), 139.8 (s, 1C, C^{a'}), 138.5 (s, 1C, C⁴), 138.3 (s, 1C, C⁴), 131.3 (s, 1C, C^f), 131.2 (s, 1C, C^f), 130.0 (s, 1C, C^e), 129.5 (s, 1C, C^e), 127.3 (s, 1C, C^{c'}), 126.9 (s, 1C, C^{5'}), 125.0 (s, 1C, C^c), 124.5 (s, 1C, C^c), 123.7 (s, 2C, C⁵, C⁵), 122.8 (s, 1C, C^{b'}), 121.9 (s, 1C, C^{3'} or C^d), 121.71 (s, 1C, C^d

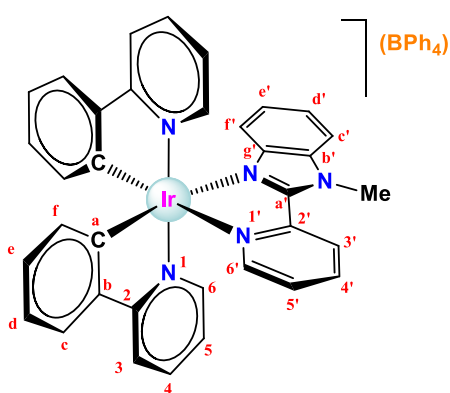
or C^{3'}), 121.68 (s, 1C, C^d), 119.8 (s, 1C, C³), 119.5 (s, 1C, C³) ppm. **FT-IR (ATR, cm⁻¹) selected bands:** 3448 (w, v_{N-H}asociado), 3039 (w, v_{C=CH}), 1608-1582 (m, v_{C=C + C-N}), 1476 (s), 1439-1421 (m), 1268 (m), 1163 (m, v_{C-C}), 1100 (m), 1065-1031 (m, δ_{C-Hip}), 837 (vs, v_{P-Fsym}), 794 (m, δ_{C-C}), 763-753 (vs, δ_{C-Hoop}), 738-729 (s), 669 (m), 630 (w), 552 (vs, v_{P-Fas}). **MS (FAB+):** m/z (%) = 646 (72) ([M-PF₆]⁺), 501 (23) ([M-PF₆-pyim]⁺). **Molar Conductivity (CH₃CN):** 137 S·cm²·mol⁻¹. **Solubility:** soluble in dichloromethane, chloroform, methanol, acetone and dimethylsulfoxide. Insoluble in water.



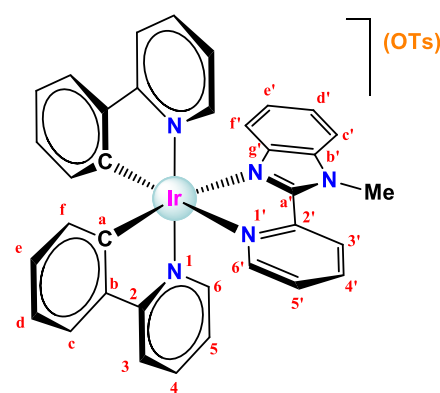
Synthesis of [Ir(ppy)₂(pybim)](PF₆), [44]PF₆. The synthesis was performed as for [43]PF₆ in the presence of the ligand pybim (0.0367 g, 0.188 mmol) and [Ir(ppy)₂Cl]₂ (0.1003 g, 0.094 mmol) followed by the addition of NH₄PF₆ (0.367 g, 2.25 mmol) to force anion exchange from Cl⁻ to PF₆⁻. Yield: 64.6 mg (0.077 mmol, 41%). **M_r (C₃₄H₂₅N₅PF₆Ir)** = 840.7892 g/mol. **Anal. Calcd for C₃₄H₂₅N₅PF₆Ir·(H₂O)_{0.1}:** C 48.47; H 3.01; N 8.31; **Found:** C 48.46; H 3.10; N 8.28. **¹H NMR (400 MHz, DMSO-d₆, 25 °C)** δ 14.76 (s, 1H, H^{N-H}), 8.61 (d, J = 8.0 Hz, 1H, H^{3'}), 8.34 (t, J = 7.9 Hz, 1H, H^{4'}), 8.25 (d, J = 8.2 Hz, 1H, H³), 8.19 (d, J = 7.9 Hz, 1H, H³), 7.96 – 7.82 (m, 5H, H⁴, H⁴, H^c, H^c, H^{6'}), 7.76 (d, J = 8.3 Hz, 1H, H^c), 7.68 (m, 3H, H^{5'}, H⁶, H⁶), 7.37 (t, J = 7.7 Hz, 1H, H^{d'}), 7.13 (dd, J = 13.3, 6.5 Hz, 2H, H⁵, H⁵), 7.07 (t, J = 7.5 Hz, 1H, H^d), 7.02 (m, 2H, H^d, H^{e'}), 6.92 (m, 2H, H^e, H^e), 6.32 (d, J = 7.6 Hz, 1H, H^f), 6.25 (d, J = 7.6 Hz, 1H, H^f), 6.16 (d, J = 8.3 Hz, 1H, H^{f'}) ppm. **¹⁹F{¹H} NMR (376 MHz, DMSO-d₆, 25 °C)** δ -70.5 (d, J_{F-P} = 712.5 Hz, 6F, F^{PF6}) ppm. **³¹P{¹H} NMR (162 MHz, DMSO-d₆, 25 °C)** δ -143.4 (hept, J_{P-F} = 712.6 Hz, 1P, P^{PF6}) ppm. **¹³C{¹H} NMR (101 MHz, DMSO-d₆, 25 °C)** δ 167.1 (s, 1C, C²), 167.0 (s, 1C, C²), 153.4 (s, 1C, C^{a'}), 151.0 (s, 1C, C^a), 150.3 (s, 1C, C^{b'}), 149.4 (s, 1C, C^b), 149.1 (s, 1C, C⁶), 147.3 (s, 1C, C²), 147.0 (s, 1C, C^a), 144.5 (s, 1C, C^b), 144.2 (s, 1C, C^b), 140.0 (s, 1C, C^{g'}), 139.9 (s, 1C, C^{4'}), 138.5 (s, 1C, C⁴), 138.3 (s, 1C, C⁴), 134.5 (s, 1C, C^{b'}), 131.7 (s, 1C, C^f), 131.0 (s, 1C, C^f), 130.2 (s, 1C, C^e), 129.5 (s, 1C, C^e), 128.6 (s, 1C, C^{5'}), 125.5 (s, 1C, C^{a'}), 125.0 (s, 1C, C^c), 124.7 (s, 1C, C^c), 124.4 (s, 1C, C^{e'}), 124.2 (s, 1C, C^{3'}), 123.8 (s, 1C, C⁵), 123.7 (s, 1C, C⁵), 122.1 (s, 1C, C^d), 122.0 (s, 1C, C^d), 119.8 (s, 1C, C³), 119.5 (s, 1C, C³), 116.5 (s, 1C, C^{f'}), 113.9 (s, 1C, C^{c'}) ppm. **FT-IR (ATR, cm⁻¹) selected bands:** 3353 (w, v_{N-H}asociated), 3038 (w, v_{C=CH}), 1608-1581 (m, v_{C=C + C-N}), 1478 (s), 1457 (m, v_{C=N}), 1444-1417 (s), 1267 (m), 1163 (m, v_{C-C}), 1064-1031-1011 (m, δ_{C-Hip}), 843-829 (vs, v_{P-Fsym}), 788 (w, δ_{C-C}), 758-751-741-730 (vs, δ_{C-Hoop}), 669 (m), 630 (m), 555 (vs, v_{P-Fas}), 434-413 (m). **MS (FAB+):** m/z (%) = 696 (59) ([M-PF₆]⁺), 501 (22) ([M-PF₆-pybim]⁺). **Molar Conductivity (CH₃CN):** 132 S·cm²·mol⁻¹. **Solubility:** soluble in water, methanol, dichloromethane, chloroform and acetone.



Synthesis of $[Ir(ppy)_2(pyMebim)](PF_6)$, [45]PF₆. The synthesis was performed as for **[43]PF₆** in the presence of the ligand pyMebim (0.0395 g, 0.189 mmol) and $[Ir(ppy)_2Cl]_2$ (0.1001 g, 0.093 mmol) followed by the addition of NH₄PF₆ (0.3050 g, 1.87 mmol) to force anion exchange from Cl⁻ to PF₆⁻. Yield: 132.0 mg (0.154 mmol, 89%). **M_r (C₃₅H₂₉N₅PF₆Ir) = 854.8160 g/mol.** **Anal. Calcd for C₃₅H₂₉N₅PF₆Ir·(H₂O)_{0.4}:** C 48.77; H 3.25; N 8.12; **Found:** C 48.73; H 3.12; N 8.10. **¹H NMR (400 MHz, DMSO-d₆, 25 °C)** δ 8.78 (d, *J* = 8.3 Hz, 1H, H^{3'}), 8.30 (t, *J* = 7.7 Hz, 1H, H^{4'}), 8.26 (d, *J* = 8.4 Hz, 1H, H³), 8.19 (d, *J* = 8.3 Hz, 1H, H³), 7.98 – 7.89 (m, 5H, H^c, H^c, H^{6'}, H^c, H⁴), 7.86 (t, *J* = 7.8 Hz, 1H, H⁴), 7.74 – 7.66 (m, 2H, H^{5'}, H⁶), 7.63 (d, *J* = 5.8 Hz, 1H, H⁶), 7.42 (t, *J* = 7.8 Hz, 1H, H^{d'}), 7.17 – 7.08 (m, 2H, H⁵, H⁵), 7.08 – 6.98 (m, 3H, H^d, H^d, H^e), 6.95 – 6.88 (m, 2H, H^e, H^e), 6.29 (d, *J* = 7.7 Hz, 1H, H^f), 6.20 (t, *J* = 7.9 Hz, 2H, H^f, H^f), 4.45 (s, 3H, H^{NMe}) ppm. **¹⁹F{¹H} NMR (376 MHz, DMSO-d₆, 25 °C)** δ -70.5 (d, *J*_{F-P} = 712.6 Hz, 6F, F^{PF6}) ppm. **³¹P{¹H} NMR (162 MHz, DMSO-d₆, 25 °C)** δ -143.1 (hept, *J*_{P-F} = 711.3 Hz, 1P, P^{PF6}) ppm. **¹³C{¹H} NMR (101 MHz, DMSO-d₆, 25 °C)** δ 167.0 (s, 1C, C²), 166.9 (s, 1C, C²), 152.8 (s, 1C, C^{a'}), 151.6 (s, 1C, C^a), 150.9 (s, 1C, C^{6'}), 149.6 (s, 1C, C⁶), 149.1 (s, 1C, C⁶), 147.5 (s, 1C, C^a), 147.0 (s, 1C, C²), 144.4 (s, 1C, C^b), 144.1 (s, 1C, C^b), 139.5 (s, 1C, C^{4'}), 138.7 (s, 1C, C^{g'}), 138.5 (s, 1C, C⁴), 138.3 (s, 1C, C⁴), 136.5 (s, 1C, C^{b'}), 131.7 (s, 1C, C^f), 130.9 (s, 1C, C^f), 130.2 (s, 1C, C^e), 129.5 (s, 1C, C^e), 128.4 (s, 1C, C^{5'}), 126.1 (s, 1C, C^{3'}), 125.4 (s, 1C, C^{d'}), 125.1 (s, 1C, C^c), 124.8 (s, 1C, C^c), 124.6 (s, 1C, C^{e'}), 123.7 (s, 1C, C⁵), 123.6 (s, 1C, C⁵), 122.2 (s, 1C, C^d), 122.0 (s, 1C, C^d), 119.8 (s, 1C, C³), 119.5 (s, 1C, C³), 116.8 (s, 1C, C^f), 112.5 (s, 1C, C^{c'}), 33.4 (s, 1C, C^{NMe}) ppm. **FT-IR (ATR, cm⁻¹) selected bands:** 3037 (w, v_{C=CH}), 1605-1581 (m, v_{C=C} + _{C-N}), 1476 (s), 1457 (m, v_{C=N}), 1438-1417 (m), 1351-1341 (w, δ_{CH3}), 1267 (m), 1164 (m, v_{C-C}), 1063-1030-1012 (m, δ_{C-Hip}), 834 (vs, v_{P-Fsym}), 748-730 (vs, δ_{C-Hoop}), 556 (vs, v_{P-Fas}), 416 (m). **MS (FAB+):** m/z (%) = 710 (100) ([M-PF₆]⁺), 501 (25) ([M-PF₆-pyMebim]⁺). **Molar Conductivity (CH₃CN):** 139 S·cm²·mol⁻¹. **Solubility:** soluble in acetone, dichloromethane, chloroform, methanol, acetonitrile and DMSO.

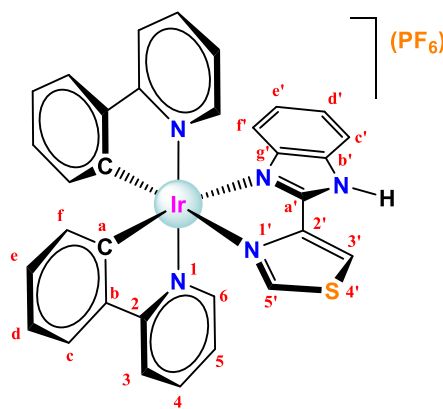


Synthesis of $[Ir(ppy)_2(pyMebim)](BPh_4)$, [45]BPh₄. In a 100 mL Schlenk flask, the ligand pyMebim (0.0395 g, 0.189 mmol) was added to a solution of $[Ir(ppy)_2Cl_2$] (0.1001 g, 0.093 mmol) in a mixture of dichloromethane/methanol (4:5 18 mL), and the suspension was stirred at 60 °C for 24 h and under a nitrogen atmosphere. NaBPh₄ (0.6384 g, 1.87 mmol) was added along with additional dichloromethane until complete dissolution of the solid. Then the solution was filtered twice and the product was precipitated with diethyl ether and filtered. The yellow solid was dissolved in dichloromethane (10 mL), the solution was filtered and the product was precipitated again with diethyl ether (15 mL). The resulting orange powder was washed with water and diethyl ether and dried under vacuum. Yield: 142.0 mg (0.138 mmol, 74%). **M_r** ($C_{59}H_{47}N_5BIr$) = 1029.0848 g/mol. **Anal. Calcd for $C_{59}H_{47}N_5BIr$ (CH_2Cl_2)_{0.24}:** C 67.80; H 4.56; N 6.67; **Found:** C 67.83; H 4.62; N 6.64. **¹H NMR (400 MHz, DMSO-d₆, 25 °C)** δ 8.77 (d, *J* = 8.2 Hz, 1H, H^{3'}), 8.32 – 8.21 (m, 2H, H^{4'}, H³), 8.19 (d, *J* = 8.2 Hz, 1H, H³), 7.99 – 7.88 (m, 5H, H^{c'}, H^c, H^c, H^{b'}, H^b), 7.86 (t, *J* = 8.7 Hz, 1H, H^d), 7.74 – 7.66 (m, 2H, H⁶, H^{5'}), 7.62 (d, *J* = 5.6 Hz, 1H, H⁶), 7.42 (t, *J* = 8.0 Hz, 1H, H^{d'}), 7.17 (s, 8H, H^{o-Ph(BPh_4)4}), 7.14 – 7.04 (m, 3H, H⁵, H⁵, H^d), 7.04 – 6.98 (m, 2H, H^d, H^e), 6.91 (t, *J* = 7.3 Hz, 10H, H^e, H^e, H^{m-Ph(BPh_4)4}), 6.78 (t, *J* = 7.1 Hz, 4H, H^{p-Ph(BPh_4)4}), 6.28 (d, *J* = 7.5 Hz, 1H, H^f), 6.20 (t, *J* = 7.8 Hz, 2H, H^f, H^{f'}), 4.44 (s, 3H, H^{NMe}) ppm. **¹³C{¹H} NMR (101 MHz, DMSO-d₆, 25 °C)** δ 167.0 (s, 1C, C²), 166.9 (s, 1C, C²), 164.1 (s, 1C, C^{ipso-Ph(BPh_4)4}), 163.6 (s, 1C, C^{ipso-Ph(BPh_4)4}), 163.1 (s, 1C, C^{ipso-Ph(BPh_4)4}), 162.6 (s, 1C, C^{ipso-Ph(BPh_4)4}), 152.8 (s, 1C, C^{a'}), 151.6 (s, 1C, C^a), 150.9 (s, 1C, C^{e'}), 149.5 (s, 1C, C⁶), 149.1 (s, 1C, C⁶), 147.5 (s, 1C, C^a), 147.0 (s, 1C, C²), 144.4 (s, 1C, C^b), 144.1 (s, 1C, C^b), 139.5 (s, 1C, C^{4'}), 138.7 (s, 1C, C^{g'}), 138.5 (s, 1C, C⁴), 138.3 (s, 1C, C⁴), 136.5 (s, 1C, C^{b'}), 135.5 (d, *J* = 1.4 Hz, 1C, C^{o-Ph(BPh_4)4}), 131.7 (s, 1C, C^f), 130.9 (s, 1C, C^f), 130.2 (s, 1C, C^e), 129.5 (s, 1C, C^e), 128.4 (s, 1C, C^{5'}), 126.1 (s, 1C, C^{3'}), 125.3 (dd, *J* = 5.5, 2.8 Hz, 1C, C^{m-Ph(BPh_4)4}), 125.1 (s, 1C, C^{d'}), 124.8 (s, 1C, C^c), 124.6 (s, 1C, C^c), 123.7 (s, 1C, C⁵), 123.6 (s, 1C, C⁵), 122.2 (s, 1C, C^d), 122.0 (s, 1C, C^d), 121.5 (s, 1C, C^{p-Ph(BPh_4)4}), 119.9 (s, 1C, C³), 119.5 (s, 1C, C³), 116.8 (s, 1C, C^{f'}), 112.5 (s, 1C, C^{c'}), 54.9 (s), 33.4 (s, 1C, C^{NMe}) ppm. **FT-IR (ATR, cm⁻¹) selected bands:** 3052 (w, v_{C=CH}), 1604–1581 (m, v_{C=C + C-N}), 1476 (s), 1455 (m, v_{C=N}), 1438–1417 (m), 1347–1334 (w, δ_{CH₃}), 1267 (m), 1162 (m, v_{C-C}), 1063–1031–1010 (m, δ_{C-Hip}), 847 (w), 731–703 (vs, δ_{C-Hoop}), 607 (s, v_{B-C}), 549 (w), 418 (w). **MS (FAB+):** m/z (%) = 710 (100) ([M-BPh₄]⁺), 501 (75) ([M-BPh₄-pyMebim]⁺). **Molar Conductivity (CH₃CN):** 91 S·cm²·mol⁻¹. **Solubility:** soluble in acetone, dichloromethane, chloroform, acetonitrile and DMSO. Insoluble in methanol and water.



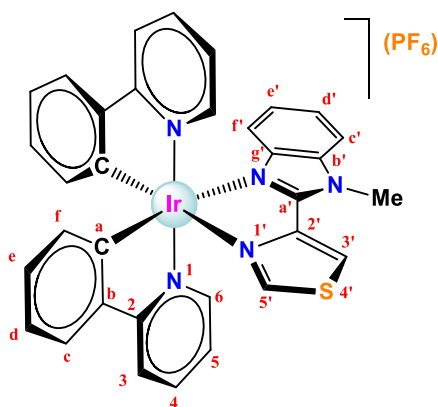
Synthesis of $[Ir(ppy)_2(pyMebim)](OTs)$, [45]OTs. In a 100 mL Schlenk flask, the salt AgOTs (0.1252 g, 0.45 mmol) was added to a solution of $[Ir(ppy)_2Cl_2$] (0.1000 g, 0.093 mmol) in methanol (11

mL) and the mixture was stirred at room temperature for 4 h under a nitrogen atmosphere. The solution was filtered and the ligand pyMebim (0.0395 g, 0.189 mmol) was added. The mixture was stirred at 60 °C for 20 h. Then it was filtered and the solvent evaporated to dryness. The orange residue was dissolved in dichloromethane, the solution was filtered twice and the product precipitated with hexane/diethyl ether. The solid was filtered and washed with hexane, water, hexane/diethyl ether and hexane. The orange powder was dried under vacuum. Yield: 133.3 mg (0.130 mmol, 81%). **M_r** (**C₄₂H₃₄N₅SO₃Ir**) = 881.0483 g/mol. **Anal. Calcd for C₄₂H₃₄N₅SO₃Ir (CH₂Cl₂)_{0.3}(H₂O)₂: C 53.90; H 4.13; N 7.43; S 3.40; **Found:** C 53.95; H 4.13; N 7.81; S 3.22.** **¹H NMR (400 MHz, DMSO-d₆, 25 °C)** δ 8.78 (d, *J* = 8.2 Hz, 1H, H^{3'}), 8.33 – 8.22 (m, 2H, H^{4'}, H³), 8.19 (d, *J* = 8.3 Hz, 1H, H³), 7.99 – 7.88 (m, 5H, H^c, H^c, H^b, H^d), 7.86 (t, *J* = 7.9 Hz, 1H, H⁴), 7.73 – 7.68 (m, 2H, H^{5'}, H⁶), 7.62 (d, *J* = 5.8 Hz, 1H, H⁶), 7.47 (d, *J* = 7.8 Hz, 2H, H^{o-(OTs)}), 7.42 (t, *J* = 7.8 Hz, 1H, H^q), 7.14 (t, *J* = 6.1 Hz, 1H, H⁵), 7.10 (d, *J* = 7.9 Hz, 3H, H⁵, H^{m-(OTs)}), 7.08 – 7.04 (m, 1H, H^d), 7.04 – 6.98 (m, 2H, H^d, H^e), 6.95 – 6.88 (m, 2H, H^e, H^e), 6.28 (d, *J* = 7.5 Hz, 1H, H^f), 6.20 (t, *J* = 7.8 Hz, 2H, H^f, H^f), 4.45 (s, 3H, H^{NMe}), 2.28 (s, 3H, H^{Me(OTs)}) ppm. **¹³C{¹H} NMR (101 MHz, DMSO-d₆, 25 °C)** δ 167.0 (s, 1C, C²), 166.9 (s, 1C, C²), 152.8 (s, 1C, C^{a'}), 151.6 (s, 1C, C^a), 150.9 (s, 1C, C^{6'}), 149.6 (s, 1C, C⁶), 149.1 (s, 1C, C⁶), 147.5 (s, 1C, C^a), 147.0 (s, 1C, C²), 145.8 (s, 1C, C^{ipso-(OTs)}), 144.4 (s, 1C, C^b), 144.2 (s, 1C, C^b), 139.5 (s, 1C, C^{4'}), 138.7 (s, 1C, C^{g'}), 138.5 (s, 1C, C⁴), 138.3 (s, 1C, C⁴), 137.5 (s, 1C, C^{p-(OTs)}), 136.5 (s, 1C, C^{b'}), 132.0 (s, 1C, C^f), 130.9 (s, 1C, C^f), 130.2 (s, 1C, C^e), 129.5 (s, 1C, C^e), 128.4 (s, 1C, C^{5'}), 128.0 (s, 1C, C^{m-(OTs)}), 126.2 (s, 1C, C^{3'}), 125.5 (s, 1C, C^{o-(OTs)}), 125.4 (s, 1C, C^d), 125.1 (s, 1C, C^c), 124.7 (s, 1C, C^c), 124.6 (s, 1C, C^e), 123.71 (s, 1C, C⁵), 123.65 (s, 1C, C⁵), 122.2 (s, 1C, C^d), 122.0 (s, 1C, C^d), 119.9 (s, 1C, C³), 119.5 (s, 1C, C³), 116.8 (s, 1C, C^f), 112.6 (s, 1C, C^c), 33.4 (s, 1C, C^{NMe}), 20.8 (s, 1C, C^{Me(OTs)}) ppm. **FT-IR (ATR, cm⁻¹) selected bands:** 3038 (w, v_{C=CH}), 1605-1582 (m, v_{C=C + C-N}), 1477 (s), 1456 (m, v_{C=N}), 1439-1418 (m), 1335 (w, δ_{CH3}), 1268 (m), 1214-1187-1160-1120 (s, v_{SO3-_{as}}), 1120 (m, v_{C-C}), 1063-1032-1010 (s, v_{SO3-_{sym}}), 740 (vs, b, δ_{C-Hoop}), 679 (vs, v_{S-O}), 563 (vs, v_{S-O}), 416 (m). **MS (FAB+):** m/z (%) = 710 (100) ([M-OTs]⁺), 501 (45) ([M-OTs-pyMebim]⁺). **Molar Conductivity (CH₃CN):** 135 S·cm²·mol⁻¹. **Solubility:** soluble in acetone, dichloromethane, chloroform, methanol, acetonitrile and DMSO. Slightly soluble in diethyl ether. Insoluble in water.



Synthesis of [Ir(ppy)₂(tbz)](PF₆), [46]PF₆. The synthesis was performed as for [43]PF₆ in the presence of the ligand tbz (0.0377 g, 0.186 mmol) and [Ir(ppy)₂Cl]₂ (0.1000 g, 0.093 mmol) followed by the addition of NH₄PF₆ (0.3044 g, 1.87 mmol) to force anion exchange from Cl⁻ to PF₆⁻. Yield: 108 mg (0.128 mmol, 68%). **M_r** (**C₃₂H₂₃N₅SPF₆Ir**) = 846.8174 g/mol. **Anal. Calcd for**

C₃₂H₂₃N₅SPF₆Ir·(H₂O)_{0.3}: C 45.14; H 2.92; N 8.07; S 3.68; **Found:** C 45.10; H 2.79; N 8.22; S 3.76. **¹H NMR (400 MHz, DMSO-d₆, 25 °C)** δ 14.53 (s, 1H, H^{N-H}), 8.81 (s, 1H, H^{3'}), 8.49 (s, 1H, H^{5'}), 8.26 (d, J = 8.4 Hz, 1H, H³), 8.18 (d, J = 8.2 Hz, 1H, H³), 7.94 – 7.84 (m, 4H, H⁴, H⁴, H^c, H^c), 7.78 – 7.74 (m, 2H, H⁶, H^{c'}), 7.72 (d, J = 8.3 Hz, 1H, H⁶), 7.30 (t, J = 7.7 Hz, 1H, H^{d'}), 7.21 – 7.10 (m, 2H, H⁵, H⁵), 7.06 (t, J = 7.5 Hz, 1H, H^d), 7.03 – 6.94 (m, 2H, H^d, H^{e'}), 6.94 – 6.84 (m, 2H, H^e, H^e), 6.34 (d, J = 7.7 Hz, 1H, H^f), 6.28 (d, J = 7.5 Hz, 1H, H^f), 6.10 (d, J = 8.3 Hz, 1H, H^f) ppm. **¹⁹F{¹H} NMR (376 MHz, DMSO-d₆, 25 °C)** δ -70.5 (d, J_{F-P} = 712.6 Hz, 6F, F^{PF6}) ppm. **³¹P{¹H} NMR (162 MHz, DMSO-d₆, 25 °C)** δ -143.4 (hept, J_{P-F} = 712.5 Hz, 1P, P^{PF6}) ppm. **¹³C{¹H} NMR (101 MHz, DMSO-d₆, 25 °C)** δ 167.1 (s, 1C, C²), 167.0 (s, 1C, C²), 159.2 (s, 1C, C^{5'}), 149.4 (s, 1C, C⁶), 148.9 (s, 1C, C⁶), 148.5 (s, 1C, C^{2'}), 148.3 (s, 1C, C^a), 146.9 (s, 1C, C^a), 144.6 (s, 1C, C^b), 144.5 (s, 1C, C^b), 144.4 (s, 1C, C^{a'}), 139.5 (s, 1C, C^{e'}), 138.5 (s, 1C, C⁴), 138.3 (s, 1C, C⁴), 134.4 (s, 1C, C^{b'}), 131.7 (s, 1C, C^f), 131.4 (s, 1C, C^f), 129.8 (s, 1C, C^e), 129.4 (s, 1C, C^e), 125.2 (s, 1C, C^{3'}), 124.82 (s, 1C, C^c), 124.77 (s, 1C, C^c), 124.7 (s, 1C, C^{d'}), 123.9 (s, 1C, C⁵), 123.8 (s, 1C, C^{e'}), 123.7 (s, 1C, C⁵), 122.0 (s, 1C, C^d), 121.9 (s, 1C, C^d), 119.8 (s, 1C, C³), 119.4 (s, 1C, C³), 116.3 (s, 1C, C^f), 113.6 (s, 1C, C^c) ppm. **FT-IR (ATR, cm⁻¹)** selected bands: 3362 (w, v_{N-H}asociado), 3110-3034 (w, v_{C=CH}), 1607-1581 (m, v_{C=C + C-N}), 1477 (s), 1460 (w, v_{C=N}), 1413 (s), 1268 (m), 1228 (m) 1160 (m, v_{C-C}), 1064-1031-1014 (m, δ_{C-Hip}), 828 (vs, v_{P-Fsym}), 750-730 (vs, δ_{C-Hoop}), 630 (m), 553 (vs, v_{P-Fas}), 435-418 (m). **MS (FAB+):** m/z (%) = 702 (48) ([M-PF₆]⁺), 501 (22) ([M-PF₆-thbzol]⁺). **Molar Conductivity (CH₃CN):** 133 S·cm²·mol⁻¹. **Solubility:** soluble in DMSO and acetone. Partially soluble in dichloromethane, chloroform, methanol and water.



Synthesis of the ligand N-methyl-thiabendazole, Metbz. In a 100 mL Schlenk flask, Cs₂CO₃ (4.8607 g, 14.92 mmol) was added to a solution of thiabendazole (1.500 g, 7.45 mmol) in DMSO (50 mL). The mixture was stirred at 80 °C for 90 min under a nitrogen atmosphere. Then methyl iodide (696 µL, 11.18 mmol) was added and the resulting mixture was stirred for 20 h at room temperature. The crude product was precipitated with water as a white solid. This solid was filtered, washed with water (2x10 mL) and dried in a desiccator until constant weight. Yield: 1.142 g (5.30 mmol, 71%).

Synthesis of [Ir(ppy)₂(Metbz)](PF₆), [47]PF₆. The synthesis was performed as for [43]PF₆ in the presence of the ligand Metbz (0.0409 g, 0.190 mmol) and [Ir(ppy)₂Cl]₂ (0.1002 g, 0.093 mmol) followed by the addition of NH₄PF₆ (0.3049 g, 1.87 mmol) to force anion exchange from Cl⁻ to PF₆⁻. Yield: 114.1 mg (0.133 mmol, 71%). **M_r** (**C₃₃H₂₅N₅SPF₆Ir**) = 860.8442 g/mol. **Anal. Calcd for**

C₃₃H₂₅N₅SPF₆Ir (H₂O)_{0.4}: C 45.66; H 3.00; N 8.07; S 3.69; **Found:** C 45.70; H 3.03; N 7.99; S 3.31. **¹H NMR (400 MHz, DMSO-d₆, 25 °C)** δ 9.10 (d, *J* = 1.8 Hz, 1H, H^{3'}), 8.53 (d, *J* = 1.7 Hz, 1H, H^{5'}), 8.26 (d, *J* = 8.0 Hz, 1H, H^{3'}), 8.18 (d, *J* = 7.9 Hz, 1H, H^{3'}), 7.97 – 7.83 (m, 5H, H⁴, H⁴, H^c, H^c, H^{c'}), 7.77 (d, *J* = 5.8 Hz, 1H, H⁶), 7.71 (d, *J* = 5.8 Hz, 1H, H⁶), 7.37 (t, *J* = 7.8 Hz, 1H, H^d), 7.17 (t, *J* = 6.6 Hz, 1H, H⁵), 7.13 (t, *J* = 6.6 Hz, 1H, H⁵), 7.06 (t, *J* = 7.0 Hz, 1H, H^d), 7.03 – 6.97 (m, 2H, H^d, H^e), 6.94 – 6.86 (m, 2H, H^e, H^e), 6.32 (d, *J* = 7.6 Hz, 1H, H^f), 6.26 (d, *J* = 7.6 Hz, 1H, H^f), 6.12 (d, *J* = 8.3 Hz, 1H, H^f), 4.31 (s, 3H, H^{NMe}) ppm. **¹⁹F{¹H} NMR (376 MHz, DMSO-d₆, 25 °C)** δ -70.2 (d, *J*_{F-P} = 711.3 Hz, 6F, F^{PF6}) ppm. **³¹P NMR (162 MHz, DMSO-d₆, 25 °C)** δ 105.7 ((hept, *J*_{P-F} = 711.3 Hz, 1P, P^{PF6}) ppm. **¹³C{¹H} NMR (101 MHz, DMSO-d₆, 25 °C)** δ 167.5 (s, 1C, C²), 167.4 (s, 1C, C²), 159.0 (s, 1C, C^{5'}), 150.0 (s, 1C, C⁶), 149.4 (s, 1C, C⁶), 149.1 (s, 1C, C^{2'}), 148.9 (s, 1C, C^a), 147.7 (s, 1C, C^a), 145.0 (s, 1C, C^b), 144.9 (s, 1C, C^b), 144.0 (s, 1C, C^{a'}), 139.1 (s, 1C, C^{b'}), 138.9 (s, 1C, C⁴), 138.8 (s, 1C, C⁴), 136.5 (s, 1C, C^{b'}), 132.1 (s, 1C, C^f), 131.7 (s, 1C, C^f), 130.3 (s, 1C, C^e), 129.9 (s, 1C, C^e), 126.6 (s, 1C, C^{3'}), 125.2 (s, 1C, C^c), 125.1 (s, 2C, C^c, C^{d'}), 124.6 (s, 1C, C^{e'}), 124.12 (s, 1C, C⁵), 124.06 (s, 1C, C⁵), 122.5 (s, 1C, C^d), 122.4 (s, 1C, C^d), 120.2 (s, 1C, C³), 119.9 (s, 1C, C³), 116.9 (s, 1C, C^f), 112.7 (s, 1C, C^{c'}), 32.6 (s, 1C, C^{NMe}) ppm. **FT-IR (ATR, cm⁻¹) selected bands:** 3036 (w, ν_{C=CH}), 1606-1580 (m, ν_{C=C} + C-N), 1476 (s), 1437 (m, ν_{C=N}), 1413 (m), 1267 (m), 1225 (m) 1160 (m, ν_{C-C}), 1063-1030-1011 (m, δ_{C-Hip}), 833 (vs, ν_{P-Fsym}), 755-729 (vs, δ_{C-Hoop}), 630 (m), 553 (vs, ν_{P-Fas}), 418 (m). **MS (FAB+):** m/z (%) = 716 (100) ([M-PF₆]⁺), 501 (60) ([M-PF₆-NMethbzol]⁺). **Molar Conductivity (CH₃CN):** 138 S·cm²·mol⁻¹. **Solubility:** soluble in DMSO, acetonitrile and acetone. Partially soluble in dichloromethane, chloroform, methanol and water.

5. BIBLIOGRAPHY

- (1) Ladouceur, S.; Fortin, D.; Zysman-Colman, E. *Inorg. Chem.* **2011**, *50*, 11514–11526.
- (2) Tamayo, A. B.; Garon, S.; Sajoto, T.; Djurovich, P. I.; Tsyba, I. M.; Bau, R.; Thompson, M. E. *Inorg. Chem.* **2005**, *44*, 8723–8732.
- (3) Fernández-Hernández, J. M.; Yang, C. H.; Beltrán, J. I.; Lemaire, V.; Polo, F.; Fröhlich, R.; Cornil, J.; De Cola, L. *J. Am. Chem. Soc.* **2011**, *133*, 10543–10558.
- (4) Monti, F.; Baschieri, A.; Gualandi, I.; Serrano-Pérez, J. J.; Junquera-Hernández, J. M.; Tonelli, D.; Mazzanti, A.; Muzzioli, S.; Stagni, S.; Roldan-Carmona, C.; Pertegás, A.; Bolink, H. J.; Ortí, E.; Sambri, L.; Armaroli, N. *Inorg. Chem.* **2014**, *53*, 7709–7721.
- (5) Sunesh, C. D.; Choe, Y. *Mater. Chem. Phys.* **2015**, *156*, 206–213.
- (6) Sunesh, C. D.; Mathai, G.; Choe, Y. *ACS Appl. Mater. Interfaces* **2014**, *6*, 17416–17425.
- (7) Jeon, Y.; Sunesh, C. D.; Chitumalla, R. K.; Jang, J.; Choe, Y. *Electrochim. Acta* **2016**, *195*, 112–123.
- (8) Sprouse, S.; King, K. A.; Spellane, P. J.; Watts, R. J. *J. Am. Chem. Soc.* **1984**, *106*, 6647–6653.
- (9) Nonoyama, M. *Bull. od Chem. Soc. Japan* **1974**, *47*, 767–768.
- (10) Murphy, L.; Congreve, A.; Pålsson, L.-O.; Williams, J. A. G. *Chem. Commun.* **2010**, *46*, 8743–8745.
- (11) Sun, H.; Liu, S.; Lin, W.; Zhang, K. Y.; Lv, W.; Huang, X.; Huo, F.; Yang, H.; Jenkins, G.; Zhao, Q.; Huang, W. *Nat. Commun.* **2014**, *5*, 3601.
- (12) Schneider, G. E.; Bolink, H. J.; Constable, E. C.; Ertl, C. D.; Housecroft, C. E.; Pertegas, A.; Zampese, J. A.; Kanitz, A.; Kessler, F.; Meier, S. B. *Dalt. Trans.* **2014**, *43*, 1961–1964.
- (13) Lungwitz, R.; Spange, S. *New J. Chem.* **2008**, *32*, 392–394.
- (14) Marcus, Y. *J. Chem. Soc. Faraday Trans.* **1991**, *87*, 2995–2999.
- (15) Angelici, R. J. In *Técnicas y Síntesis en Química Inorgánica*; Editorial Reverté, S.A., **1979**; p. 243.
- (16) Balzani, V.; Credi, A.; Venturi, M. *Coord. Chem. Rev.* **1998**, *171*, 3–16.
- (17) Shan, G.-G.; Li, H.-B.; Mu, Z.-C.; Zhu, D.-X.; Su, Z.-M.; Liao, Y. *J. Organomet. Chem.* **2012**, *702*, 27–35.
- (18) Ladouceur, S.; Zysman-Colman, E. *Eur. J. Inorg. Chem.* **2013**, *2013*, 2985–3007.
- (19) Liu, Y.; Li, M.; Zhao, Q.; Wu, H.; Huang, K.; Li, F. *Inorg. Chem.* **2011**, *50*, 5969–5977.
- (20) Neve, F.; Crispini, A.; Campagna, S.; Serroni, S. *Inorg. Chem.* **1999**, *38*, 2250–2258.
- (21) Hay, B. P.; Custelcean, R. *Cryst. Growth Des.* **2009**, *9*, 2539–2545.
- (22) Chakrabarti, P.; Bhattacharyya, R. *Prog. Biophys. Mol. Biol.* **2007**, *95*, 83–137.
- (23) Reid, K. S.; Lindley, P.; Thornton, J. *FEBS Lett.* **1985**, *190*, 209–213.
- (24) Baranoff, E.; Curchod, B. F. E.; Frey, J.; Scopelliti, R.; Kessler, F.; Tavernelli, I.; Rothlisberger, U.; Grätzel, M.; Nazeeruddin, M. K. *Inorg. Chem.* **2012**, *51*, 215–224.

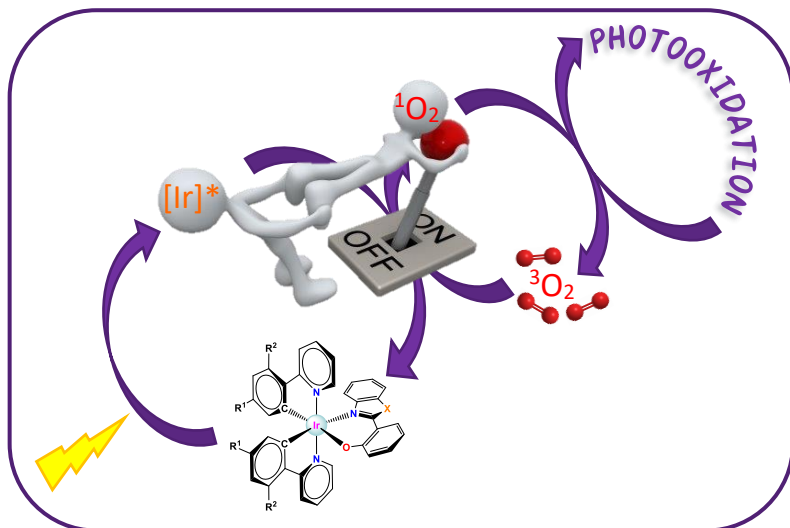
- (25) Costa, R. D.; Ortí, E.; Bolink, H. J.; Graber, S.; Schaffner, S.; Neuburger, M.; Housecroft, C. E.; Constable, E. C. *Adv. Funct. Mater.* **2009**, *19*, 3456–3463.
- (26) Baranoff, E.; Bolink, H. J.; Constable, E. C.; Delgado, M.; Häussinger, D.; Housecroft, C. E.; Nazeeruddin, M. K.; Neuburger, M.; Ortí, E.; Schneider, G. E.; Tordera, D.; Walliser, R. M.; Zampese, J. a *Dalt. Trans.* **2013**, *42*, 1073–1087.
- (27) Meier, S. B.; Sarfert, W.; Junquera-Hernández, J. M.; Delgado, M.; Tordera, D.; Ortí, E.; Bolink, H. J.; Kessler, F.; Scopelliti, R.; Grätzel, M.; Nazeeruddin, M. K.; Baranoff, E. *J. Mater. Chem. C* **2013**, *1*, 58–68.
- (28) De Angelis, F.; Fantacci, S.; Evans, N.; Klein, C.; Zakeeruddin, S. M.; Moser, J.-E.; Kalyanasundaram, K.; Bolink, H. J.; Grätzel, M.; Nazeeruddin, M. K. *Inorg. Chem.* **2007**, *46*, 5989–6001.
- (29) Pla, P.; Junquera-Hernández, J. M.; Bolink, H. J.; Ortí, E. *Dalt. Trans.* **2015**, *44*, 8497–8505.
- (30) Costa, R. D.; Ortí, E.; Bolink, H. J.; Monti, F.; Accorsi, G.; Armaroli, N. *Angew. Chemie Int. Ed.* **2012**, *51*, 8178–8211.
- (31) Tordera, D.; Bünzli, A. M.; Pertegás, A.; Junquera-Hernández, J. M.; Constable, E. C.; Zampese, J. A.; Housecroft, C. E.; Ortí, E.; Bolink, H. J. *Chem. - A Eur. J.* **2013**, *19*, 8597–8609.
- (32) Meier, S. B.; Tordera, D.; Pertegás, A.; Roldán-Carmona, C.; Ortí, E.; Bolink, H. J. *Mater. Today* **2014**, *17*, 217–223.
- (33) Bünzli, A. M.; Constable, E. C.; Housecroft, C. E.; Prescimone, A.; Zampese, J. a.; Longo, G.; Gil-Escrig, L.; Pertegás, A.; Ortí, E.; Bolink, H. J. *Chem. Sci.* **2015**, *6*, 2843–2852.
- (34) Henwood, A. F.; Zysman-Colman, E. *Top. Curr. Chem.* **2016**, *374*, 36.
- (35) Tordera, D.; Pertegás, A.; Shavaleev, N. M.; Scopelliti, R.; Ortí, E.; Bolink, H. J.; Baranoff, E.; Grätzel, M.; Nazeeruddin, M. K. *J. Mater. Chem.* **2012**, *22*, 19264–19268.
- (36) Tordera, D.; Meier, S.; Lenes, M.; Costa, R. D.; Ortí, E.; Sarfert, W.; Bolink, H. J. *Adv. Mater.* **2012**, *24*, 897–900.
- (37) He, L.; Qiao, J.; Duan, L.; Dong, G.; Zhang, D.; Wang, L.; Qiu, Y. *Adv. Funct. Mater.* **2009**, *19*, 2950–2960.

CHAPTER 8.

Ir(III) BIS-CYCLOMETALATED COMPLEXES BEARING HYDROXYPHENYLBENZAZOLE ANCILLARY LIGANDS: SYNTHESIS, CHARACTERIZATION AND LUMINESCENT PROPERTIES. PHOTOCATALYSIS

CHAPTER 8. Ir(III) BIS-CYCLOMETALATED COMPLEXES BEARING HYDROXYPHENYLBENZAZOLE ANCILLARY LIGANDS: SYNTHESIS, CHARACTERIZATION AND LUMINESCENT PROPERTIES. PHOTOCATALYSIS

ABSTRACT: In this chapter a family of 2 new biscyclometalated heteroleptic iridium(III) complexes of general formula $[\text{Ir}(\kappa^2\text{-C},\text{N-ppy})(\kappa^2\text{-N,O-L})]$ ($\text{L} = \text{hpbitm, hpbtz}$) bearing 2-phenylpyridinate (as the cyclometalating ligand) and hydroxyphenylbenzazolate derivatives (as the ancillary ligands) were prepared. The described complexes were completely characterized and tested as photocatalysts in the oxidation of thioanisole with oxygen.



CONTEXT: As we have already mentioned in the previous chapter, phosphorescent biscyclometalated iridium(III) complexes display very interesting photophysical properties, e.g., high quantum yields, large Stoke's shifts, long-lived phosphorescence, modular color-tuning possibilities and good photo-stability. They also work as efficient photosensitizers in singlet oxygen production. Previous reports have shown that biscyclometalated Ir(III) complexes with 2-(2-hydroxyphenyl)oxazole-based ancillary ligands exhibit highly efficient phosphorescence.¹

On the other hand, organo-sulfoxides are key intermediates in the preparation of pharmaceuticals and other strategic chemicals, and the selective oxidation of organo-sulfides to organo-sulfoxides is a fundamental step in the corresponding synthetic processes.² Thus, hydroxyphenylbenzazolate derivatives are promising candidates to photocatalyse these reactions through the activation of triplet oxygen.

1. RESULTS AND DISCUSSION

1.1. Synthesis

The new complexes used in this chapter were synthesised from the iridium chloro-bridged dimers $[\text{Ir}(\text{C}^{\text{N}}\text{N})_2(\mu\text{-Cl})]_2$ prepared by reaction of $\text{IrCl}_3\cdot\text{nH}_2\text{O}$ with 2-phenylpyridine (ppy), difluorophenylpyridine (dfppy) or *p*-tolylpyridine (tpy) in a 2-ethoxyethanol/water mixture (3:1, v/v), as shown in CHAPTER 7.^{3,4}

In the next step, the pro-ligands 2-(2'-hydroxiphenyl)benzimidazole (hpbitm-H) and 2-(2'-hydroxiphenyl)benzothiazole (hpbtz-H), gathered in Fig. 1, were refluxed in a mixture of 2-ethoxyethanol/water for 24 h with the dinuclear Ir(III) starting material in the presence of Na_2CO_3 to produce the neutral compounds of general formula $[\text{Ir}(\text{ppy})_2(\text{O}^{\text{N}})]$ (**[48a]** and **[48b]**), where O^{N} are the ancillary ligands hpbitm or hpbtz in their anionic forms, and ppy is 2-phenylpyridinate (see Fig. 2).⁵

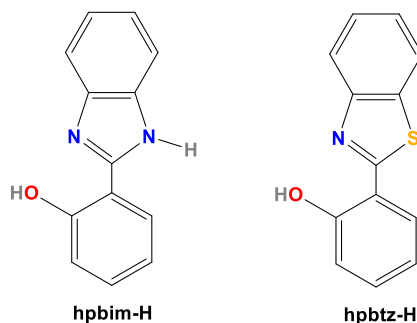


Fig. 1. Ancillary pro-ligands used in this chapter.

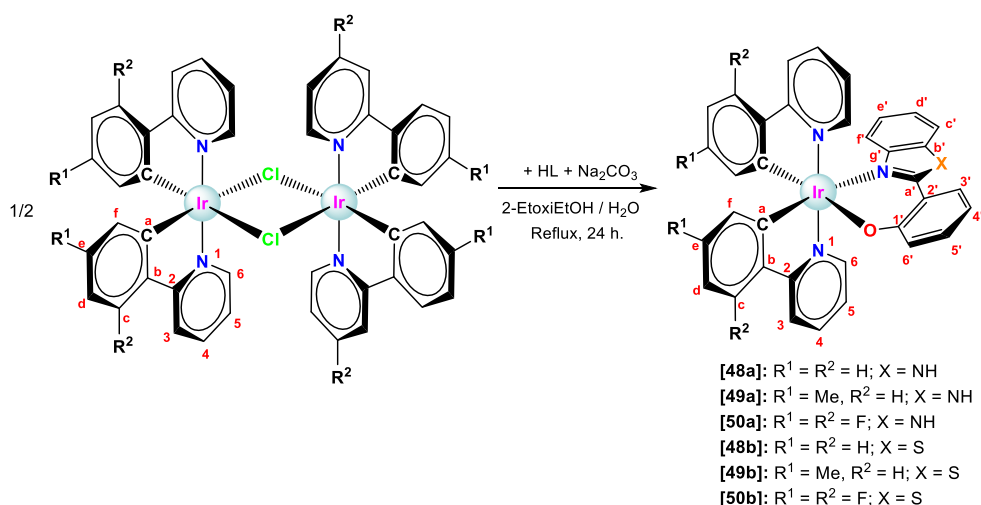


Fig. 2. Schematic synthesis of neutral biscyclometalated Ir(III) complexes.

Moreover, four additional compounds with general formulae $[\text{Ir}(\text{dfppy})_2(\text{O}^{\text{N}})]$ (**[49a]** and **[49b]**, dfppy = 2,4-difluorophenylpyridinate, O^{N} = hpbitm or hpbtz), and $[\text{Ir}(\text{tpy})_2(\text{O}^{\text{N}})]$ (**[50a]** and **[50b]**, tpy = *p*-tolylpyridinate, O^{N} = hpbitm or hpbtz), where prepared by other members of our group using a similar protocol (see Fig. 2) and have been used in this thesis to perform a wider catalysts screening in the photooxidation of thioanisole (*vide infra*). Hence, the preparation of complexes **[49x]** and **[50x]** is not

reported in this chapter of the thesis but elsewhere (TFM by Larry Danilo Aguirre and TFG by Leticia Berlanga).

Complex **[48b]** had already been reported in the literature as a Hg^{2+} and histidine sensor.^{5,6,7}

All the complexes were isolated in moderate yields (63% to 68%) as the corresponding racemates (Δ_{Ir} or Λ_{Ir}) in the form of green, yellow or orange powders.

1.2. Characterization

All the complexes have been fully characterised by NMR spectroscopy, IR spectroscopy, positive fast atom bombardment (FAB⁺) mass spectrometry, molar conductivity and elemental analysis. In addition, fluorescence spectroscopy was used to characterize the luminescent properties of the complexes.

1.2.1. NMR

The ^1H NMR spectra of complexes **[48a]** and **[48b]** were recorded in DMSO-d₆ and THF-d₈ at 25 °C. THF-d₈ was selected to avoid either decomposition of the complex or a feasible solvent substitution. It is well established by ^1H NMR, that HCl traces from CDCl₃ (or other acid traces) break this kind of complexes, releasing the ancillary ligand and regenerating the dimeric product.⁸ Both complexes, **[48a]** and **[48b]**, show a similar pattern of signals with two sets of resonances for the inequivalent ppy⁻ ligands (C_1 symmetry), and with the exception of a downfield-shifted broad singlet detected at 12.90 ppm in DMSO-d₆ and at 11.84 ppm in THF-d₈ for complex **[48a]**, undoubtedly attributed to the NH group. In addition, the signals have been completely assigned on the basis of triangular interactions through inter-ligand and inter-ring NOE cross peaks in the NOESY spectra (see Fig. 3).

Regarding the $^{13}\text{C}\{^1\text{H}\}$ NMR spectra, only a quality spectrum was obtained for complex **[48b]** in THF-d₈. The signals were completely assigned with the support of the 2D experiments HSQC and HMBC. The most deshielded peak, at 170 ppm, was attributed to the quaternary carbons C^{a'} and C^{g'}, immediately followed by C² and C², appearing at 169.9 and 169.4 ppm. Curiously, the carbon atoms directly attached to the iridium centre (C^a) appeared at 152.5 and 150.1 ppm.

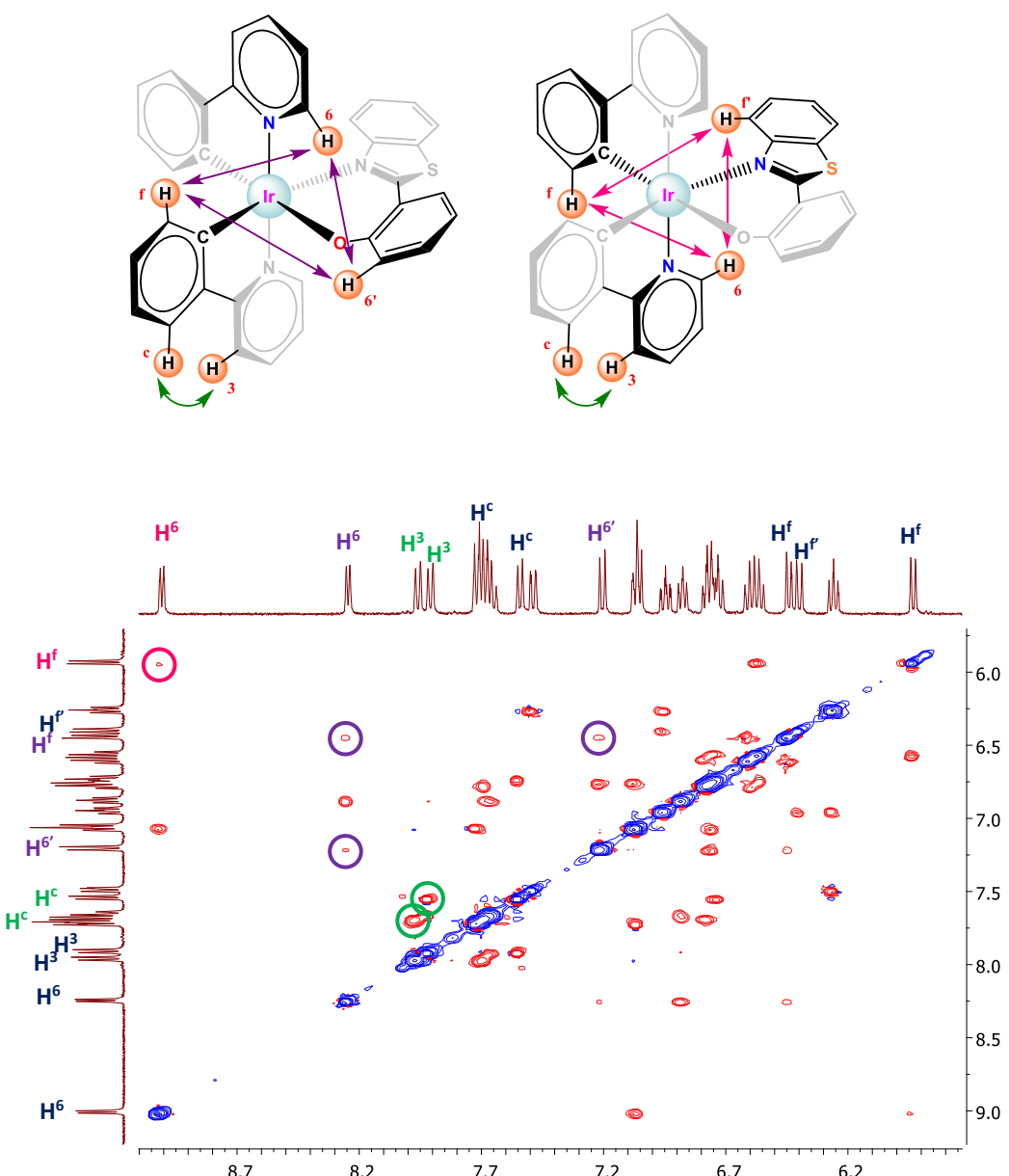
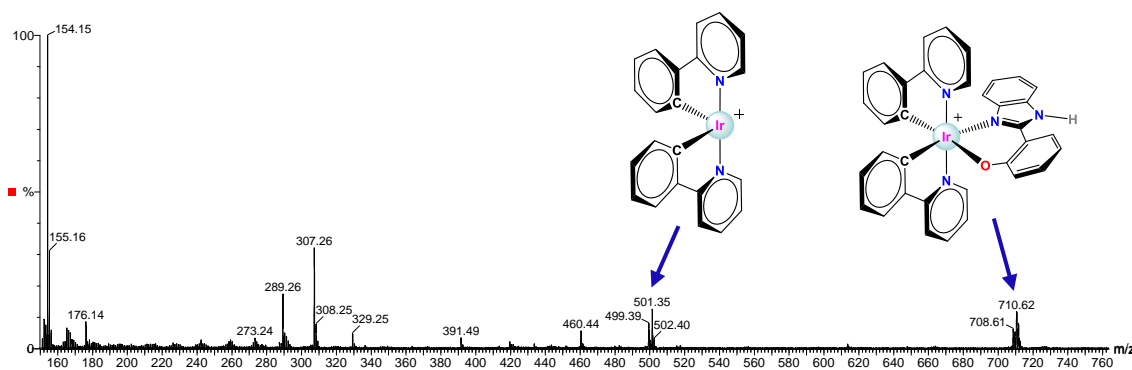


Fig. 3. Representation of inter-ligand and inter-ring NOE cross peaks in the structure of [48b], showing the triangular interactions (up).

1.2.2. Mass Spectra

The FAB⁺ and ESI-MS mass spectra of the complexes exhibit characteristic sets of peaks in agreement with the isotopic distribution patterns expected for Ir fragments, among which stand out two peaks: the molecular ion $[M]^+$ and the $[M-(O^N)]^+$ fragment. The latter peak is identical for both Ir(III) complexes, since both bear the same biscyclometalated ligand. In particular, $m/z [M-(O^N)]^+ = 501$ (see Fig. 4).

Fig. 4. FAB⁺ mass spectra of complex [48a].

1.2.3. IR Spectra

Infrared spectra confirm the presence of characteristic peaks for the normal vibrational modes of the corresponding rings $\nu_{C=N}$, $\nu_{C=C}$, δ_{CHip} and δ_{CHoop} , besides ν_{C-O} for hydroxyphenylbenzazolate ligands and $\nu_{C=S}$ for the benzothiazole moiety (see Table 1).

Table 1. Characteristic IR bands for complexes [48a] and [48b].

	[48a]	[48b]
$\nu_{C=CH}$	3054	3039
$\nu_{C=C + C-N}$	1604-1583	1603-1580
$\nu_{C=N}$	1480	1475
ν_{C-O}	1139	1148
δ_{CHip}	1059-1030	1056-1029-970
δ_{C-C}	806-791	791
δ_{CHoop}	752-737-729	750-738-728

1.2.4. Molar Conductivity

Molar conductivity (Λ_M) values were measured in acetonitrile (10^{-3} M). The low conductivity values ($3.9 \text{ S}\cdot\text{cm}^2\cdot\text{mol}^{-1}$ for [48a] and $6.2 \text{ S}\cdot\text{cm}^2\cdot\text{mol}^{-1}$ for [48b]) illustrate the non-electrolyte nature of the complexes.⁹

1.2.5. Elemental Analysis

Elemental analyses were performed for all complexes. As previously commented, this kind of complexes tend to enclose some water in their structures.

1.3. Photophysical Properties

The photophysical properties of these derivatives were determined by M^a del Carmen Carrión Núñez from the group of Félix A. Jalón and Blanca R. Manzano (University of Castilla La Mancha, Ciudad Real).

UV-Visible absorption spectroscopy

The electronic absorption spectra of complexes [48a], [48b], [49a], [49b], [50a] and [50b] were recorded in deoxygenated acetonitrile (10^{-5} M) at 25 °C. All complexes exhibit intense high-energy bands below 300 nm, assigned to the spin-allowed singlet

ligand centered transitions (^1LC) ($^1\pi \rightarrow \pi^*$) in the cyclometalated ligand (C^N) and the ancillary ligand (N^O). Lower intensity bands and shoulders above 350 nm are assigned to spin-allowed singlet-to-singlet metal to ligand charge transfer transitions ($^1\text{MLCT}$). The less intense absorption bands (≈ 450 nm) are attributed to spin-forbidden singlet-to-triplet metal to ligand charge transfer transitions ($^3\text{MLCT}$) ($d_\pi(\text{Ir}) \rightarrow \pi^*(\text{C}^\text{N} \text{ and } \text{N}^\text{O})$), spin forbidden ligand-to-ligand charge transfer transitions ($^3\text{LLCT}$) ($^3\pi_{\text{ligand}\text{C}^\text{N}} \rightarrow \pi^*_{\text{ligand}\text{C}^\text{N}}$ or vice versa) and triplet ligand centered transitions (^3LC) ($^3\pi-\pi^*$). d-d transitions are usually not observed because of the overlapping with the far more intense MLCT or LLCT transitions.^{10,11}

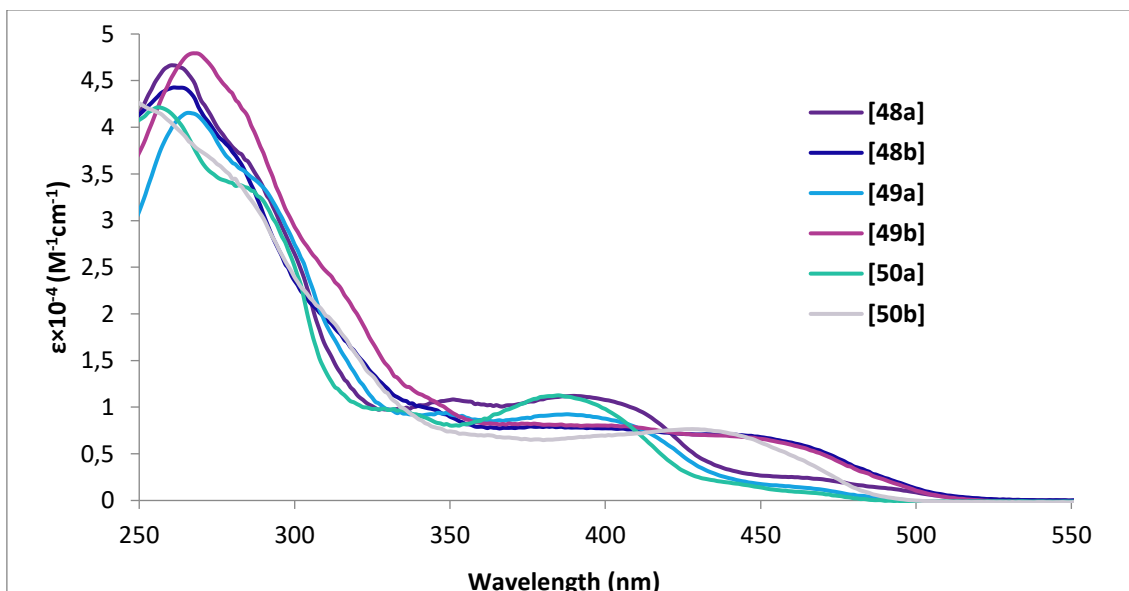


Fig. 5. Overlaid UV-vis absorption spectra of complexes [48a]-[50a] and [48b]-[50b] in deoxygenated acetonitrile (10^{-5} M) at 25 °C.

Apart from the above-mentioned features common to all the complexes, some differences are found in the absorption spectra of these derivatives depending on the ancillary ligand. In particular, complexes with hpbim, **[48a]**, **[49a]** and **[50a]**, exhibit relative maxima between 350-390 nm ($9240 < \epsilon < 11270 \text{ M}^{-1}\cdot\text{cm}^{-1}$) and then a pronounced drop in the absorption, whereas complexes with hpbtz, **[48b]**, **[49b]** and **[50b]**, lack relative maxima in this range but display a more extended absorption that introduces itself well into the visible range ($\lambda > 450$ nm with $\epsilon > 6000 \text{ M}^{-1}\cdot\text{cm}^{-1}$) (see Fig. 5).

Emission spectroscopy

The emission spectra were recorded in deoxygenated acetonitrile at room temperature (25 °C). The emission spectra of the above-mentioned complexes (see Fig. 6) show broad and unstructured bands, indicating an important contribution of the $^3\text{MLCT}$ transitions to the emitting triplet (T_1). The emission maxima ranged from 512 to 607 nm for complexes bearing hpbim **[48a]-[50a]**, which show light colours from cyan

to green (512-533 nm), and from 580 to 607 nm for complexes with hpbtz, [48b]-[50b], which exhibit light colors from yellow to orange.

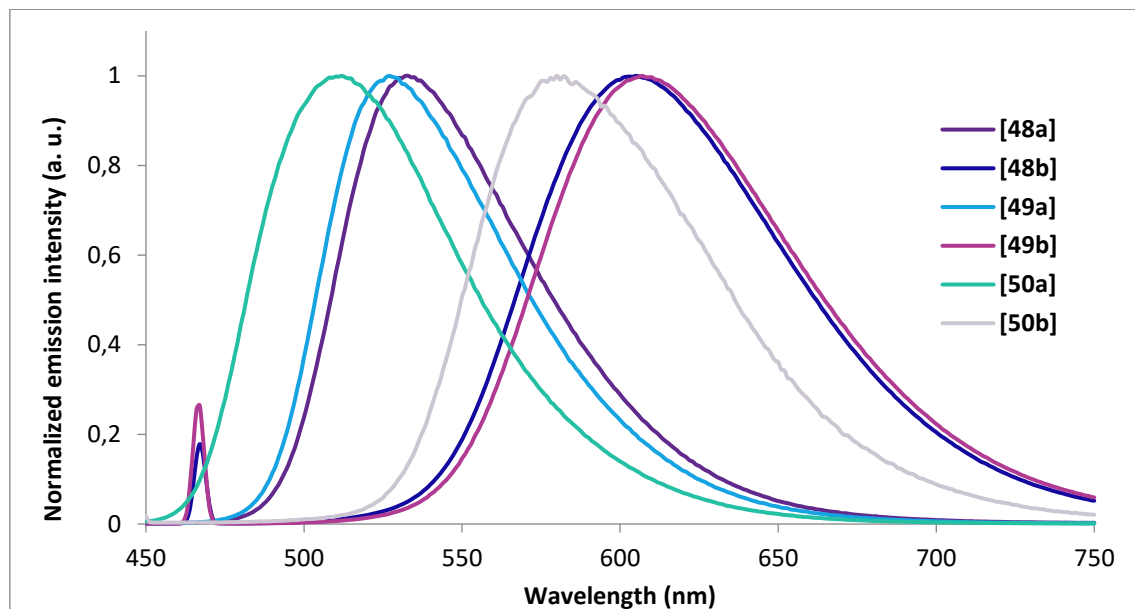


Fig. 6. Overlaid emission spectra of complexes [48a] ($\lambda_{\text{exc}} = 420 \text{ nm}$), [48b] ($\lambda_{\text{exc}} = 469 \text{ nm}$), [49a] ($\lambda_{\text{exc}} = 399 \text{ nm}$), [49b] ($\lambda_{\text{exc}} = 469 \text{ nm}$), [50a] ($\lambda_{\text{exc}} = 399 \text{ nm}$) and [50b] ($\lambda_{\text{exc}} = 451 \text{ nm}$) in deoxygenated acetonitrile (10^{-4} M) at 25°C .

Table 2. Photophysical properties of complexes [48a]-[50a] and [48b]-[50b] and the ancillary ligands (hpbitm and hpbtz) in deoxygenated acetonitrile (10^{-4} M) at 25°C .

Compound	λ_{exc} (nm)	λ_{em} (nm)	$\Delta\lambda$ (nm) ^a	Φ	τ (ns)
hpbitm	338	457 (blue)	119	0.63	-
hpbtz	311	363 (UV)	52	0.002	-
[48a]	420	533 (green)	113	0.95	1134
[48b]	469	605 (orange)	136	0.11	-
[49a]	399	527 (green)	128	0.75	-
[49b]	469	607 (orange)	138	0.09	-
[50a]	399	512 (cyan)	113	0.85	-
[50b]	451	580 (yellow)	129	0.30	-

^a $\Delta\lambda$ = Stokes shift.

Table 2 gathers the photophysical properties of the complexes. Thus, complexes with hpbtz undergo a red-shift ($\Delta\lambda_{\text{em}} = 68-80 \text{ nm}$) with regard to those bearing hpbitm. Furthermore, changes in the C^N ligand also affect, although to a lesser extent, to the emission colour. The methyl group on the tpy ligand hardly affects the emission (5 nm blue-shift comparing [48a] and [49a], and 2 nm red-shift comparing [48b] and [49b]).

However, the F atoms on the dfppy ligand shifts the emission to the blue (20 nm comparing **[48a]** with **[50a]** and 25 nm comparing **[48b]** with **[50b]**). The photoluminescent quantum yields (PLQY) of complexes **[48a]-[50a]** are very high (0.75-0.95), while those of complexes **[48b]-[50b]** are considerably lower (0.09-0.30). Low luminescence of red-shifted complexes has been previously reported in some papers by H. Bolink and coworkers.^{12,13}

1.4. Theoretical Calculations

The DFT calculations were performed by Pr. José Vicente Cuevas Vicario, in order to better understand the nature of the optoelectronic properties, in relation with both the C^N and O^N ligands. These calculations were performed at the B3LYP/(6-31G*/LANL2DZ)^{14,15,16} level on the [Ir(C^N)₂(N^O)] complexes including solvent effects (CH₃CN).

Fig. 7 displays the molecular orbital representation calculated for the highest-occupied and lowest-unoccupied molecular orbitals of **[48a]** and **[48b]**. In these complexes the HOMO is composed of a mixture of Ir(III) d_π orbitals (t_{2g}) and π orbitals of the phenoxy fragment of the (N^O) ligand¹⁷ which is in contrast with the calculated composition for the HOMO of the well-known bis-cyclometalated iridium complexes with diimine or bpy type ligands. In the latter case, the HOMO is composed of a mixture of Ir(III) d_π orbitals (t_{2g}) and π orbitals of the cyclometalating ligands.^{18,19,20,21} Moreover, significant differences were found in the LUMOs of **[48a]** and **[48b]**. While in complex **[48a]** the LUMO is composed by π* orbitals of the cyclometalating ligands, in complex **[48b]** the LUMO is composed by π* orbitals of the ancillary ligand (the topology of this molecular orbital is almost the same as that for the LUMO in the free ligand). The topology of both the LUMO and the LUMO +1 in compound **[48a]** are very similar to the LUMO+1 and the LUMO+2 in compound **[48b]** (all of them mainly located in the cyclometalating ligands). In addition, the topology of the LUMO of complex **[48b]** is analogous to the LUMO+2 of complex **[48a]** (in both cases these molecular orbitals correspond to the π* LUMO of the ancillary ligands). This change in order of the energy levels of the unoccupied molecular orbitals is due to the strong stabilization (0.5 eV) of the ancillary ligand π* MO as we move from **[48a]** (LUMO+2) to **[48b]** (LUMO) and could be explained as a result of the poorer overlapping ability of the 3p orbital in the S atom (hpbtz) compared to the 2p orbital of N in hpbim. Consequently, the energy gap is smaller for **[48b]** (3.36 eV) than for **[48a]** (3.48 eV).

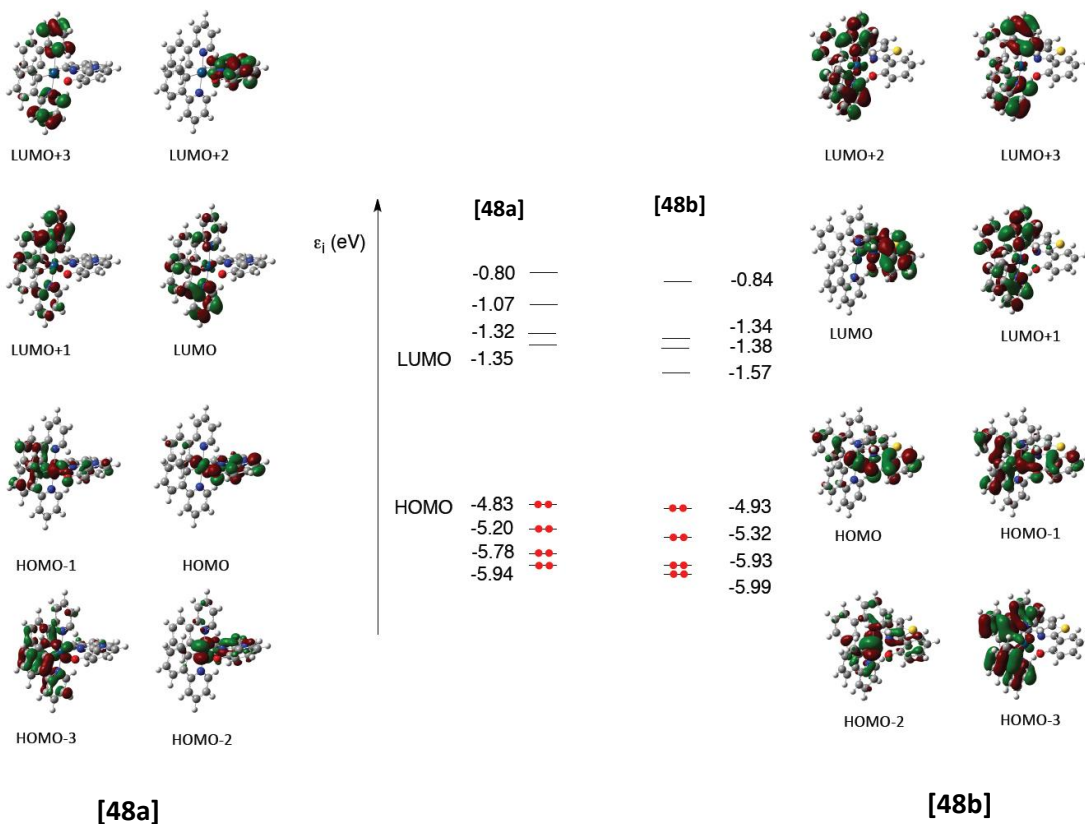


Fig. 7. Schematic representation showing the frontier molecular orbitals for [48a] and [48b] and their calculated energies.

Usually, it is not possible to establish a direct correlation between the HOMO-LUMO gap and the emission energy. Thus, to investigate the nature of the emitting excited state, the low-lying singlet and triplet states of the complexes **[48x]**, **[49x]** and **[50x]** were calculated at the optimized geometries of the ground state (S_0) using the time-dependent DFT (TD-DFT) approach. Table 3 summarizes the vertical excitation energies calculated for the first two singlets and three triplets, together with their molecular orbital description and electronic nature. For complex **[48a]**, TD-DFT calculations predict that the two first singlet states are transitions $\text{HOMO} \rightarrow \text{LUMO}$ and $\text{HOMO} \rightarrow \text{LUMO+1}$ with oscillator strength values of 0.0080 and 0.0194 respectively. On the basis of these values, it will be logical to conclude that the transition from the ground state (S_0) to the second singlet excited state (S_2) (i.e., $S_0 \rightarrow S_2$) is the most dominant, since the calculated energy of this transition (2.82 eV, 439.4 nm) is in good agreement with the experimental value (420 nm). TD-DFT calculations predict the three first triplet states at close energies for complexes **[48a]** and **[49a]** (separated by 0.05 eV and 0.07 eV respectively). In complex **[48a]**, these triplet states are mainly defined by transitions from the HOMO to the LUMO, LUMO+1 and LUMO+2 and are described as triplet metal-to-ligand charge transfer (${}^3\text{MLCT}$) as well as triplet ligand-to-ligand charge transfer (${}^3\text{LLCT}$) and ligand centered (${}^3\text{LC}$), since both HOMO and LUMO+2 involve the (N^\bulletO) ligand with participation of the Ir core, while LUMO and LUMO+1 involve the (C^\bulletN) ligands (see Fig. 7). For complex **[49a]**, the triplet states are mainly defined by a combination of

transitions from the HOMO or HOMO-1 to the LUMO, LUMO+1 and LUMO+2, and can be described in a similar way to the triplet states of [48a] but taking into account that the HOMO-1 has participation of the (O^N) ligand, the (C^N) ligands and the iridium core. For complex [50a], TD-DFT calculations predict a bigger separation between the triplet states and the one with smaller energy is defined by a transition from the HOMO to the LUMO+2 and described as a ligand centered (3LC), since both the HOMO and the LUMO+2 involve the (O^N) with some metal-to-ligand charge transfer (3MLTC) because of the participation of the iridium core in the HOMO. For complexes bearing hpbtz as the ancillary ligand TD-DFT calculations predict a bigger separation between the first triplet state and the next triplet states (about 0.4 eV), for this reason we only consider the first triplet state in complexes [48b], [49b] and [50b]. For complexes [48b] and [50b], the triplet state is mainly defined by a transition from the HOMO to the LUMO and has a 3LC nature with some 3MLCT character. Finally, for complex [49b] the triplet state is mainly a transition from the HOMO to the LUMO with a little contribution of a transition from the HOMO-1 to the LUMO that has a 3LC nature with some 3MLCT and 3LLCT character.

Table 3. Lowest singlet and triplet excited states calculated at the TD-DFT B3LYP/(6-31G*+LANL2DZ) level for complexes [48x]-[50x] in acetonitrile solution^a.

State	E(eV)	Monoexcitations	Nature	Description
[48a]				
S ₁	2.77	H→L (90)	d _π (Ir) + π _{hpbtz} → π* _{ppy}	${}^1MLCT/{}^1LLCT$
S ₂	2.82	H→L+1 (93)	d _π (Ir) + π _{hpbtz} → π* _{ppy}	${}^1MLCT/{}^1LLCT$
T ₁	2.58	H→L (45) H→L+2 (40)	d _π (Ir) + π _{hpbtz} → π* _{ppy} d _π (Ir) + π _{hpbtz} → π* _{hpbtz}	${}^3MLCT/{}^3LLCT$ ${}^3LC/{}^3MLCT$
T ₂	2.60	H→L+1 (42) H→L+2 (19)	d _π (Ir) + π _{hpbtz} → π* _{ppy} d _π (Ir) + π _{hpbtz} → π* _{hpbtz}	${}^3MLCT/{}^3LLCT$ ${}^3MLCT/{}^3LC$
T ₃	2.63	H→L+1 (27) H→L+2 (31)	d _π (Ir) + π _{hpbtz} → π* _{ppy} d _π (Ir) + π _{hpbtz} → π* _{hpbtz}	${}^3MLCT/{}^3LLCT$ ${}^3MLCT/{}^3LC$
[48b]				
S ₁	2.72	H→L (92)	d _π (Ir) + π _{hpbtz} → π* _{hpbtz}	${}^1LC/{}^1MLCT$
S ₂	2.86	H→L+1 (76)	d _π (Ir) + π _{hpbtz} → π* _{ppy}	${}^1MLCT/{}^1LLCT$
T ₁	2.24	H→L (89)	d _π (Ir) + π _{hpbtz} → π* _{hpbtz}	${}^3LC/{}^3MLCT$
T ₂	2.63	H-1→L+1 (16) H→L+1 (70)	d _π (Ir) + π _{ppy} + π _{hpbtz} → π* _{ppy} d _π (Ir) + π _{hpbtz} → π* _{ppy}	${}^3LC/{}^3MLCT/{}^3LLCT$ ${}^3LC/{}^3MLCT$
T ₃	2.67	H-1→L+2 (17) H→L+2 (69)	d _π (Ir) + π _{ppy} + π _{hpbtz} → π* _{ppy} d _π (Ir) + π _{hpbtz} → π* _{ppy}	${}^3LC/{}^3MLCT/{}^3LLCT$ ${}^3LC/{}^3MLCT$
[49a]				
S ₁	2.81	H→L (91)	d _π (Ir) + π _{hpbtz} → π* _{ppy}	${}^1MLCT/{}^1LLCT$
S ₂	2.88	H→L+1 (94)	d _π (Ir) + π _{hpbtz} → π* _{ppy}	${}^1MLCT/{}^1LLCT$
T ₁	2.59	H→L (29) H→L+2 (56)	d _π (Ir) + π _{hpbtz} → π* _{ppy} d _π (Ir) + π _{hpbtz} → π* _{ppy}	${}^3MLCT/{}^3LLCT$ ${}^3MLCT/{}^3LLCT$
T ₂	2.63	H-1→L (18) H→L (36)	d _π (Ir) + π _{hpbtz} + π* _{ppy} → π* _{ppy} d _π (Ir) + π _{hpbtz} → π* _{ppy}	${}^3MLCT/{}^3LLCT$ ${}^3MLCT/{}^3LLCT$

		H→L+2 (19)	$d_{\pi}(\text{Ir}) + \pi_{\text{hpbim}} \rightarrow \pi^*_{\text{hpbim}}$	${}^3\text{LC}/{}^3\text{MLCT}$
T ₃	2.66	H-1→L+1 (22) H→L+1 (47)	$d_{\pi}(\text{Ir}) + \pi_{\text{hpbim}} + \pi^*_{\text{ppy}} \rightarrow \pi^*_{\text{ppy}}$ $d_{\pi}(\text{Ir}) + \pi_{\text{hpbim}} \rightarrow \pi^*_{\text{ppy}}$	${}^3\text{MLCT}/{}^3\text{LLCT}$ ${}^3\text{MLCT}/{}^3\text{LLCT}$
[49b]				
S ₁	2.69	H→L (95)	$d_{\pi}(\text{Ir}) + \pi_{\text{hpbtz}} \rightarrow \pi^*_{\text{hpbtz}}$	${}^1\text{LC}/{}^1\text{MLCT}$
S ₂	2.87	H→L+1 (83)	$d_{\pi}(\text{Ir}) + \pi_{\text{hpbtz}} \rightarrow \pi^*_{\text{ppy}}$	${}^1\text{MLCT}/{}^1\text{LLCT}$
T ₁	2.23	H-1→L (15) H→L (85)	$d_{\pi}(\text{Ir}) + \pi_{\text{hpbtz}} + \pi^*_{\text{ppy}} \rightarrow \pi^*_{\text{hpbtz}}$ $d_{\pi}(\text{Ir}) + \pi_{\text{hpbtz}} \rightarrow \pi^*_{\text{hpbtz}}$	${}^3\text{LC}/{}^3\text{MLCT}/{}^3\text{LLCT}$ ${}^3\text{LC}/{}^3\text{MLCT}$
T ₂	2.62	H-1→L+1 (15) H→L+1 (70)	$d_{\pi}(\text{Ir}) + \pi_{\text{ppy}} + \pi_{\text{hpbtz}} \rightarrow \pi^*_{\text{ppy}}$ $d_{\pi}(\text{Ir}) + \pi_{\text{hpbtz}} \rightarrow \pi^*_{\text{ppy}}$	${}^3\text{LC}/{}^3\text{MLCT}/{}^3\text{LLCT}$ ${}^3\text{LC}/{}^3\text{MLCT}$
T ₃	2.66	H-2→L+1 (15) H-1→L+2 (16) H→L+2 (69)	$d_{\pi}(\text{Ir}) + \pi_{\text{ppy}} \rightarrow \pi^*_{\text{ppy}}$ $d_{\pi}(\text{Ir}) + \pi_{\text{ppy}} + \pi_{\text{hpbtz}} \rightarrow \pi^*_{\text{ppy}}$ $d_{\pi}(\text{Ir}) + \pi_{\text{hpbtz}} \rightarrow \pi^*_{\text{ppy}}$	${}^3\text{LC}$ ${}^3\text{LC}/{}^3\text{MLCT}/{}^3\text{LLCT}$ ${}^3\text{LC}/{}^3\text{MLCT}$
[50a]				
S ₁	2.85	H→L (93)	$d_{\pi}(\text{Ir}) + \pi_{\text{hpbim}} \rightarrow \pi^*_{\text{ppy}}$	${}^1\text{MLCT}/{}^1\text{LLCT}$
S ₂	2.90	H→L+1 (96)	$d_{\pi}(\text{Ir}) + \pi_{\text{hpbim}} \rightarrow \pi^*_{\text{ppy}}$	${}^1\text{MLCT}/{}^1\text{LLCT}$
T ₁	2.62	H→L+2 (89)	$d_{\pi}(\text{Ir}) + \pi_{\text{hpbim}} \rightarrow \pi^*_{\text{hpbim}}$	${}^3\text{LC}/{}^3\text{MLCT}$
T ₂	2.74	H→L (69)	$d_{\pi}(\text{Ir}) + \pi_{\text{hpbim}} \rightarrow \pi^*_{\text{ppy}}$	${}^3\text{MLCT}/{}^3\text{LLCT}$
T ₃	2.77	H-1→L+1 (21) H→L+1 (71)	$d_{\pi}(\text{Ir}) + \pi_{\text{ppy}} \rightarrow \pi^*_{\text{ppy}}$ $d_{\pi}(\text{Ir}) + \pi_{\text{hpbim}} \rightarrow \pi^*_{\text{ppy}}$	${}^3\text{MLCT}/{}^3\text{LLCT}$ ${}^3\text{MLCT}/{}^3\text{LLCT}$
[50b]				
S ₁	2.78	H→L (85) H→L+1 (15)	$d_{\pi}(\text{Ir}) + \pi_{\text{hpbtz}} \rightarrow \pi^*_{\text{hpbtz}}$ $d_{\pi}(\text{Ir}) + \pi_{\text{hpbtz}} \rightarrow \pi^*_{\text{ppy}}$	${}^1\text{LC}/{}^1\text{MLCT}$ ${}^1\text{MLCT}/{}^1\text{LLCT}$
S ₂	2.88	H→L+1 (28) H→L+2 (72)	$d_{\pi}(\text{Ir}) + \pi_{\text{hpbtz}} \rightarrow \pi^*_{\text{ppy}}$ $d_{\pi}(\text{Ir}) + \pi_{\text{hpbtz}} \rightarrow \pi^*_{\text{ppy}}$	${}^1\text{MLCT}/{}^1\text{LLCT}$ ${}^1\text{MLCT}/{}^1\text{LLCT}$
T ₁	2.34	H→L (90)	$d_{\pi}(\text{Ir}) + \pi_{\text{hpbtz}} \rightarrow \pi^*_{\text{hpbtz}}$	${}^3\text{LC}/{}^3\text{MLCT}$
T ₂	2.71	H→L+1 (76) H-1→L+1 (15)	$d_{\pi}(\text{Ir}) + \pi_{\text{hpbtz}} \rightarrow \pi^*_{\text{ppy}}$ $d_{\pi}(\text{Ir}) + \pi^*_{\text{hpbtz}} + \pi_{\text{ppy}} \rightarrow \pi^*_{\text{ppy}}$	${}^3\text{MLCT}/{}^3\text{LLCT}$ ${}^3\text{MLCT}/{}^3\text{LLCT}$
T ₃	2.75	H→L+2 (75)	$d_{\pi}(\text{Ir}) + \pi_{\text{hpbtz}} \rightarrow \pi^*_{\text{ppy}}$	${}^3\text{MLCT}/{}^3\text{LLCT}$

^aVertical excitation energies (E), dominant monoexcitations with contributions (within parentheses) of >15%, the nature of the electronic transition, and the description of the excited state are summarized.

The theoretically calculated emission energy values were not in good agreement with the experimental values in the photophysical experiments, although they follow the same tendency. Compounds with hpbim as the ancillary ligand have higher energetic triplet states than the homologous complexes with hpbtz (see energy of triplet states of complexes **a** and **b** in Table 3), and experimentally, complexes with the ancillary ligand hpbim have the emission at lower wavelength than complexes with hpbtz. In order to obtain more information about the system, the lowest triplet states of these complexes were located by optimizing their geometries using the spin-unrestricted DFT approach. After full-geometry relaxation the estimated emission energy was calculated as the vertical energy difference between these triplet states and the singlet states, obtaining closer values to those measured experimentally (see Table 4).

Table 4. Difference of energy between the optimized triplet state (T_{opt}) and the singlet ground state (S_0) and comparison with the experimental emission values.

Compound	Theoretical emission	Experimental emission
	Dif. $T_{opt}-S_0$ (eV; nm)	(nm)
[48a]	2.46; 504.4	533
[48b]	2.09; 594.4	605
[49a]	2.48; 499.5	527
[49b]	2.07; 597.9	607
[50a]	2.48; 499.8	512
[50b]	2.12; 585.0	580

1.5. Oxygen-Sensitive Photoluminescence

The O_2 -sensitive photoluminescence of bis-cyclometalated iridium(III) complexes has been widely described in the literature.^{22,23,24} Triplet oxygen (3O_2) is a potent quencher of phosphorescent Ir(III) complexes, which undergo a deactivation of their excited state through an energy transfer process. This process simultaneously turns molecular oxygen into singlet oxygen (1O_2), an extremely reactive species, able to oxidize other molecules. This ability was visually probed for complexes [48a], [49a] and [50a], taking photographs of the deoxygenated solutions in acetonitrile (10^{-4} M) under UV light ($\lambda_{exc} = 365$ nm). When oxygen (air) was left to diffuse into a solution of [48a], [49a] or [50a] prepared in acetonitrile under nitrogen atmosphere (see Fig. 8-a), a light quenching was observed after a minute (see Fig. 8-b). After one additional minute of air-bubbling, a fast switch off in the emission was detected (see Fig. 8-c). Then, the photoluminescence was switched on again after deoxygenating the solutions by bubbling N_2 during a minute (see Fig. 8-d). This fact illustrates the reversibility of the process. Fig. 10 displays the complete process of the photoluminescence decay for [49a] as a result of O_2 diffusion during a period of 2 minutes. Moreover, the comparison of the photoluminescence emission spectra of complex [49a] in deoxygenated and oxygenated acetonitrile (10^{-4} M) at 25 °C shows a dramatic drop in the intensity of the emission band for the latter (Fig. 9).

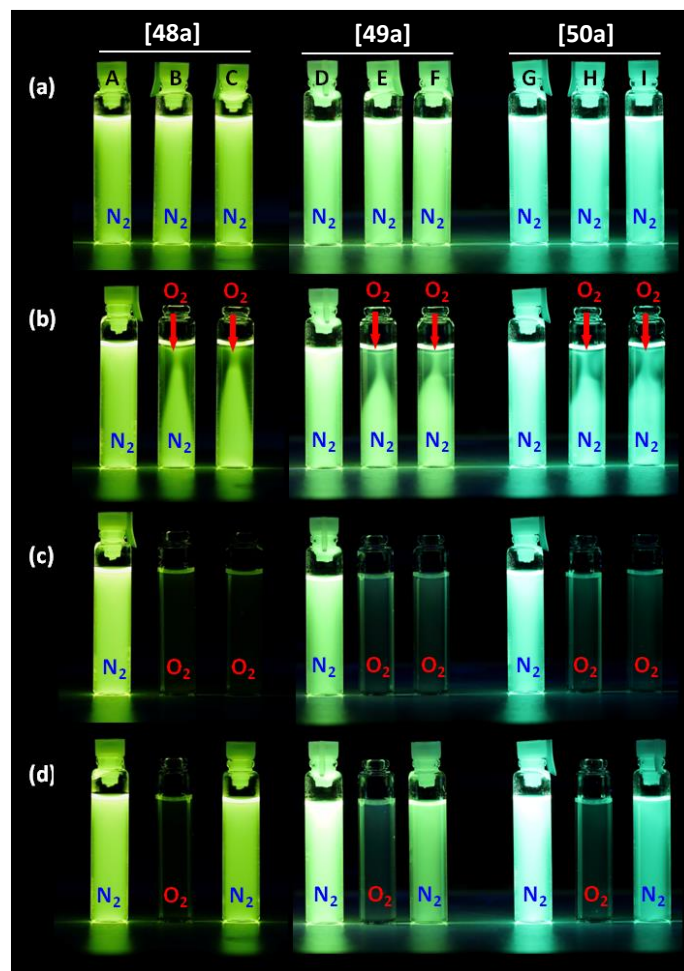


Fig. 8. (a) Photoluminescence under UV light (365 nm) at room temperature of complexes [48a] (samples A, B and C), [49a] (samples D, E and F) and [50a] (samples G, H and I) in acetonitrile solutions (10^{-4} M), prepared under N_2 atmosphere in glove box. (b) Effect of O_2 diffusion (1 min) on samples B, C, E, F and H, I. (c) Total quenching of luminescence upon O_2 bubbling with Pasteur pipette (1 min) on samples B, C, E, F and H, I. (d) Effect of N_2 bubbling with Pasteur pipette in glove box (1 min) over samples C, F and I.

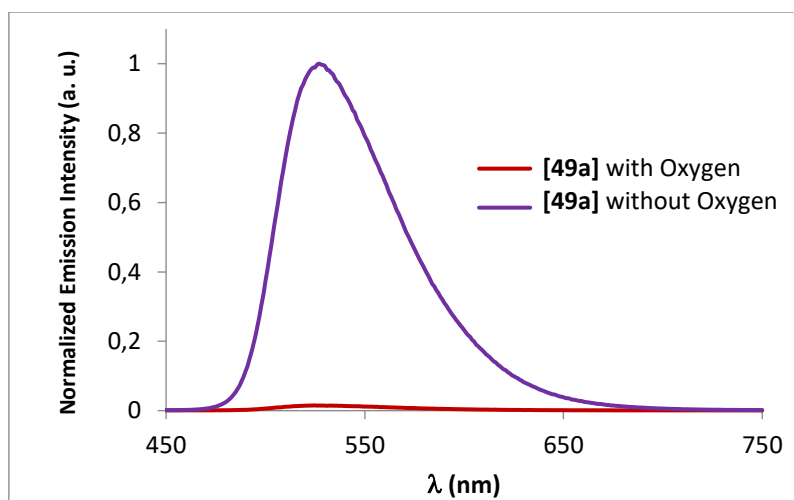


Fig. 9. Emission spectra of complex [49a] ($\lambda_{\text{exc}} = 399$ nm) in deoxygenated acetonitrile (10^{-4} M) at 25°C and after 5 min of O_2 diffusion.

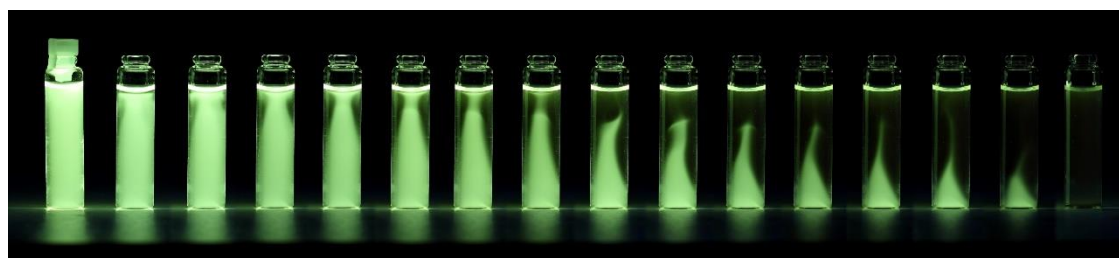


Fig. 10. Sequence of photographs illustrating the quenching of photoluminescence under UV light (365 nm) for complex [49a] as a result of O_2 diffusion during a period of 2 min.

1.6. Photocatalysis

1.6.1. Oxidation of thioanisole

In order to check the ability of complexes [48a-b], [49a-b] and [50a-b] as photosensitizers in the formation of singlet oxygen (1O_2), we analyzed experimentally the catalytic activity of these derivatives in the photooxidation of thioanisole. The substrate, thioanisole, has been selected, since it has been already used in the literature with other catalysts², but also with some Ir(III) complexes.²⁴ All the experiments were performed in quartz tubes, bubbling 500 mL of air before the irradiation and then proceeding to seal the tubes. The reaction was followed by 1H NMR before irradiation and 4h, 8h and 12h after irradiation with an UV lamp (VL-215.BL 2x15W Lamp, $\lambda_{exc} = 365$ nm), and the conversion percentage was calculated from the integration peaks of both the aromatic protons and the methyl group (see Fig. 11).

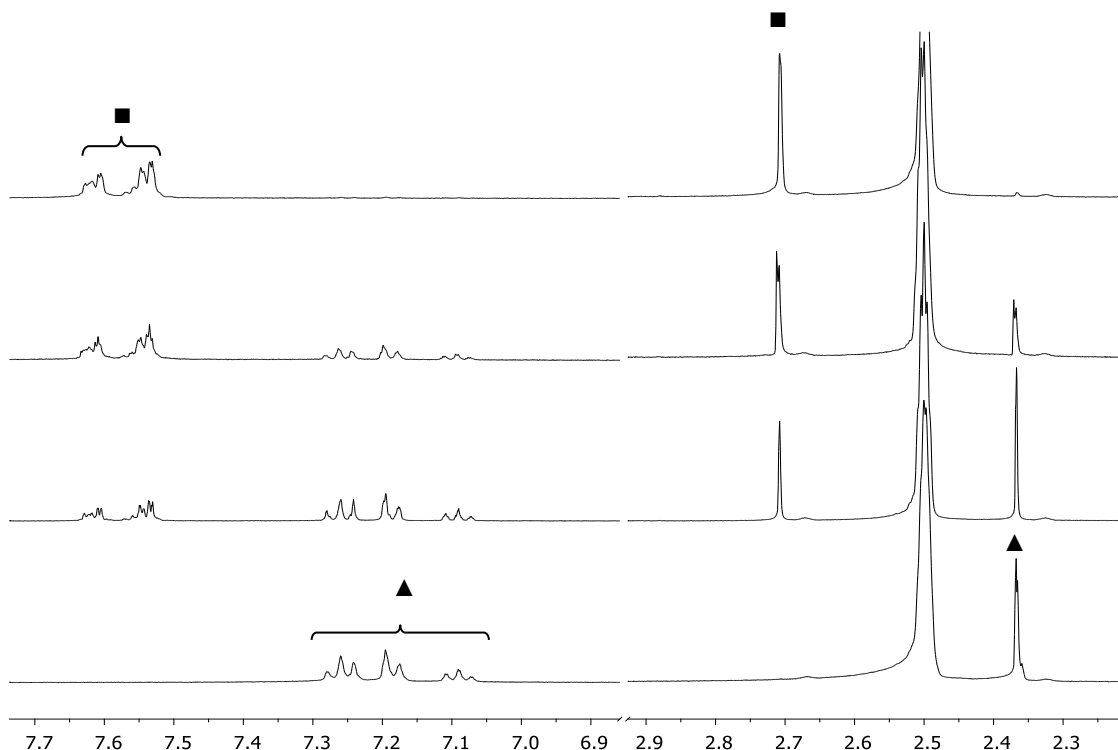


Fig. 11. Evolution with time of the 1H NMR spectra in $D_2O/DMSO-d_6$ (2:3) at 25 °C of thioanisole (10 mM) in the presence of [50b] (0.1 % mol) under light irradiation (UV lamp). Signal of thioanisole are labelled as (▲) and those of methyl phenyl sulfoxide are labelled as (■).

The conversion percentages are gathered in Fig. 12 and Table 5. The bar graphic shows a conversion of 96.11 % for complex **[50b]** after 12 h. Regarding the catalysts screening, two main effects are observed: (a) *ancillary ligand effect*, since the conversion percentages for the photo-oxidation reaction with complexes bearing benzothiazole (**[48b]**, **[49b]** and **[50b]**) are higher than those bearing the benzimidazole (**[48a]**, **[49a]** and **[50a]**); (b) *cyclometalating ligand effect*, since complexes with dfppy work better than those bearing ppy, and the latter better in turn than those with ptpy. Furthermore, three control experiments were performed in order to clarify the nature of the photo-oxidation process:

- **Control experiment 1** was performed in the presence of NaN_3 , a singlet oxygen quencher,^{25,26} and in the presence of **[48b]** providing a very low conversion (< 3.7 % after 12 h.). This result suggests that the photo-oxidation of thioanisole in the presence of dioxygen is necessarily mediated by $^1\text{O}_2$.
- **Control experiment 2** was performed without light and in the presence of **[48b]**. In this case, no conversion was detected at all, insinuating that the formation of $^1\text{O}_2$ is not possible in the absence of light.
- **Control experiment 3** was carried out without catalyst but in the presence of UV light. In these conditions, unexpectedly the reaction proceeded to some degree (58 % after 12 h.), which proves that the formation of $^1\text{O}_2$ is promoted by UV light (365 nm) even in the absence of metal catalysts, though some of the Ir(III) photo-sensitizers cooperate in the activation of $^3\text{O}_2$ to $^1\text{O}_2$.⁽¹⁾

Table 5. Percentage of conversion of thioanisole. Control 1 is the experiment performed with sodium azide and a catalyst, control 2 the experiment performed in the absence of light and control 3 is the experiment carried out without catalyst.

	0h	4h	8h	12h
[48a]	0	27,13	54,13	81,68
[48b]	0	27,87	48,60	80,00
[49a]	0	20,70	38,63	59,07
[49b]	0	23,86	42,50	73,97
[50a]	0	21,75	42,92	77,62
[50b]	0	41,06	66,16	96,11
Control 1 ([48b]+NaN_3)	0	0,78	1,56	3,66
Control 2 (no light)	0	0,00	0,00	0,00
Control 3 (no cat.)	0	4,83	22,32	55,10

⁽¹⁾ The literature results states that no conversion is obtained in the absence of catalyst.²⁴

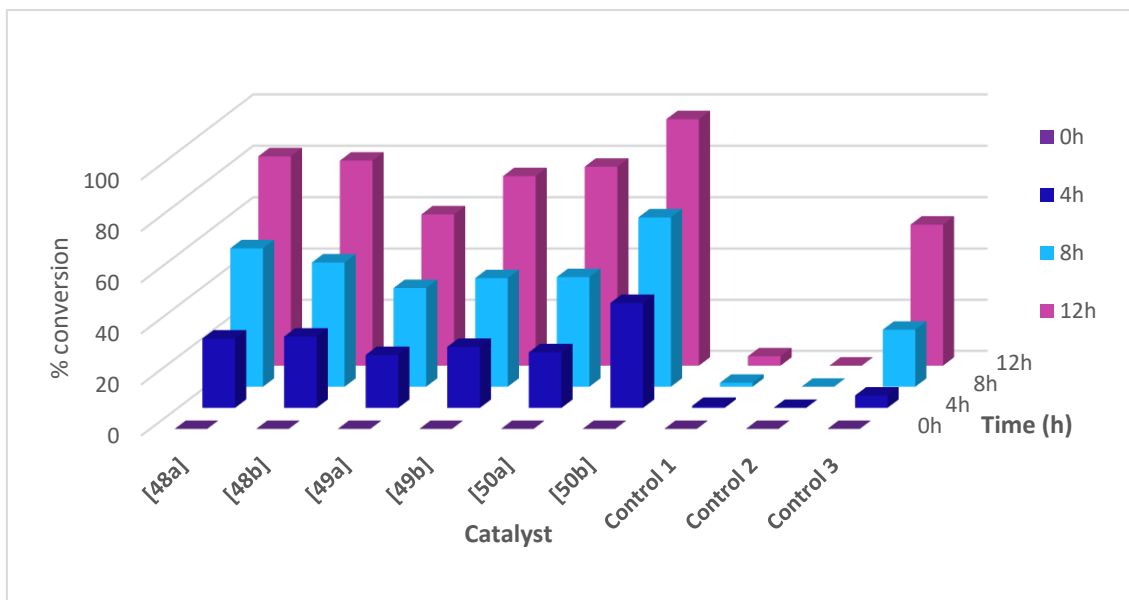


Fig. 12. Percentage of conversion of thioanisole. The bars present the amount of methylphenyl sulfoxide measured by ^1H NMR at different irradiation times.

Mechanism of the photooxidation reaction

According to the literature, we tentatively propose the following mechanism for the photooxidation of thioanisole with O_2 in the presence of the Ir(III) complexes as photo-sensitizers: upon irradiation with a UV light lamp (VL-215.BL 2x15W Lamp, $\lambda_{\text{exc}} = 365 \text{ nm}$), the Ir(III) photosensitizer (Ir-PS) in the ground state (S_0) is excited to higher energy singlet states (S_n) and then decays to the lowest energy excited singlet state (S_1). Next, the (Ir-PS) may undergo intersystem crossing from the S_1 state to the lowest energy excited triplet state (T_1). Finally, $^3\text{O}_2$ quenches the T_1 of the sensitizer via an energy transfer process to produce $^1\text{O}_2$, which is the actual oxidant species taking part in the oxidation of thioanisole (see Fig. 13).

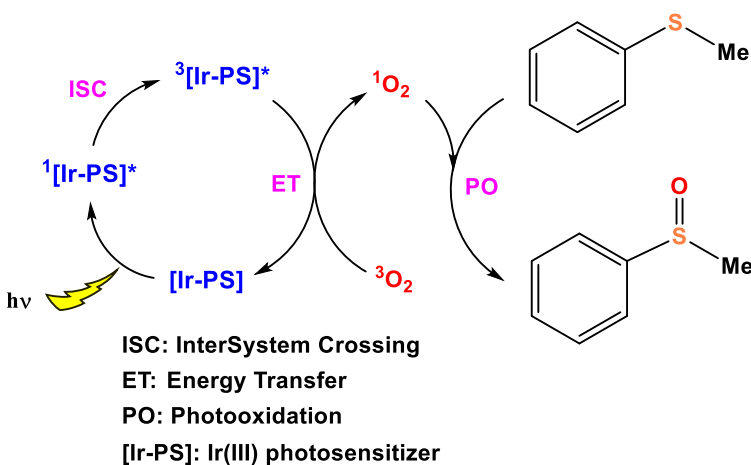


Fig. 13. Mechanism for the [48a]-catalyzed photooxidation of thioanisole with $^1\text{O}_2$

1.7. pH-dependent Photoluminescence and Reactivity of [48a]

Some papers have reported the ability of polypiridine complexes to be sensitive to pH changes.^{27,28} Since the ancillary ligand of complex **[48a]** possesses a N-H group, the behaviour of this moiety was explored against pH changes visually and by ¹H NMR. When NaOH (3 µL 0.5 M in D₂O) was added to a solution of **[48a]** in water (5·10⁻⁵ M), the colour of the emission under UV irradiation (365 nm) changed from green to orange. On the other hand, when a solution of **[48a]** in water (5·10⁻⁵ M) was acidified with HCl (1 M in D₂O, 3 µL) the colour of the emission changed from green to blue (see Fig. 14).



Fig. 14. Pictures of aqueous solutions of **[48a]** (5·10⁻⁵ M) (a) under visible light and (b) irradiated with UV light ($\lambda = 365\text{ nm}$). Photos taken by José García Calvo (Organic Chemistry, UBU).

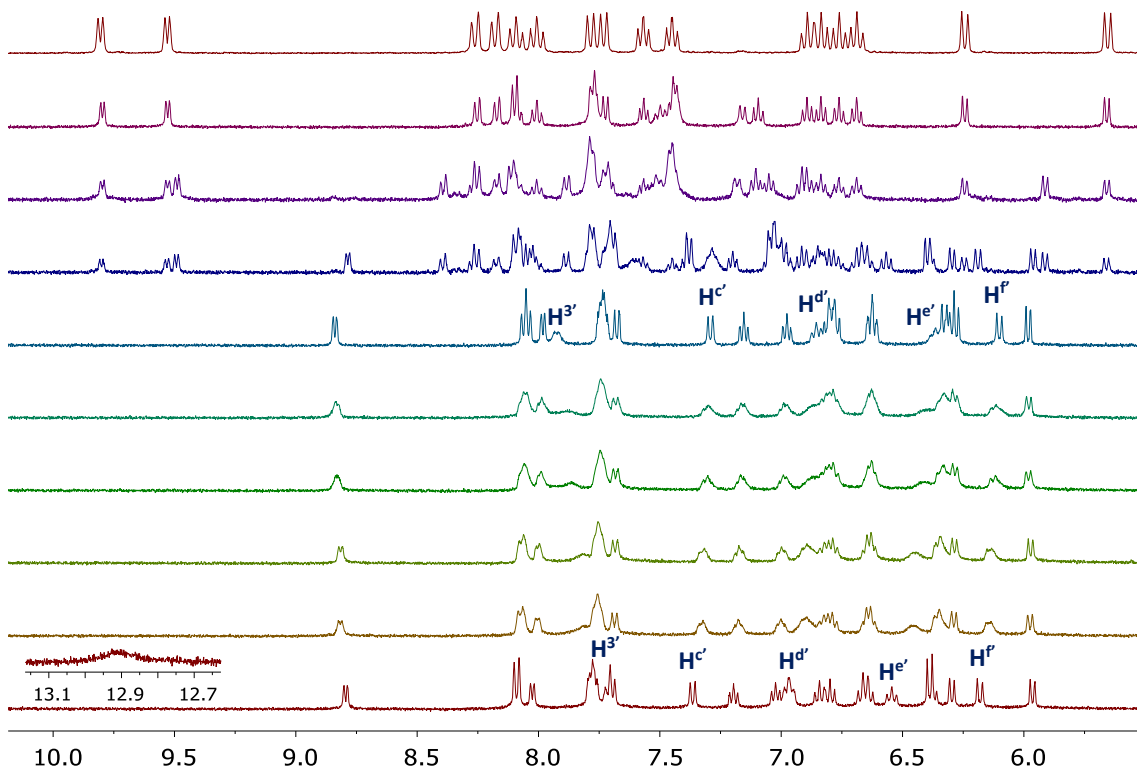


Fig. 15. Aromatic region of the ¹H NMR spectrum: (a) for **[48a]** in DMSO-d₆ (4 mM) at 25 °C, (b-f) for the evolution over time after the addition of NaOH (0.5 M in D₂O, 3 µL), (g-i) after addition of HCl (1 M in D₂O, 3 µL), (j) for **[Ir(ppy)₂Cl(DMSO-d₆)]** in DMSO-d₆ at 25 °C.

The acid-base equilibrium was monitored by ¹H NMR in DMSO-d₆ at 25 °C. Thus, aliquots of a solution of NaOH (0.5 M in D₂O) were added to a solution of **[48a]** (4 mM, 0.5 mL) in DMSO-d₆. After the addition of 1.4 µL, the evolution was monitored during 30 min. The downfield-shifted signal of the NH group disappeared and most of the peaks

slightly shifted, with the broadening of some of the signals, suggesting a fast equilibrium between two species, **[48a]** and its conjugated base **[48a']⁻**. A new spectrum was recorded after the addition of an excess of NaOH (0.5 M, final volume = 3 μ L) and after 24 h. The resulting spectrum showed one set of narrow signals assigned to the deprotonated complex **[48a']⁻** (see Fig. 16), whose emission colour is orange. Furthermore, the shift and broadening of the resonances was more accused for those hydrogen atoms closed to the NH such as H^{3'} and H^{c'}, in agreement with the above-mentioned deprotonation process (see Fig. 15 a-f).

Then, DCl (1 M in D₂O, 3 μ L) was added in two portions and several spectra were recorded. They finally showed a mixture between the non-emissive complex **[Ir(ppy)₂Cl(DMSO-d₆)]** and the blue-emissive free pro-ligand hpbim-H (see Fig. 15 g-i). Thus, the following acid-base equilibria were proposed to explain the latter observations (see Fig. 16).

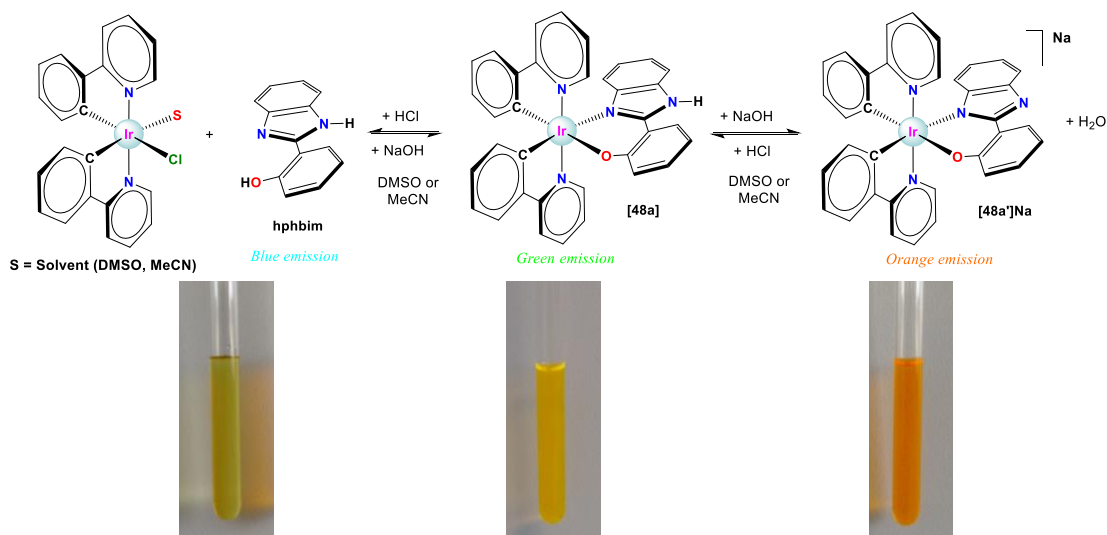
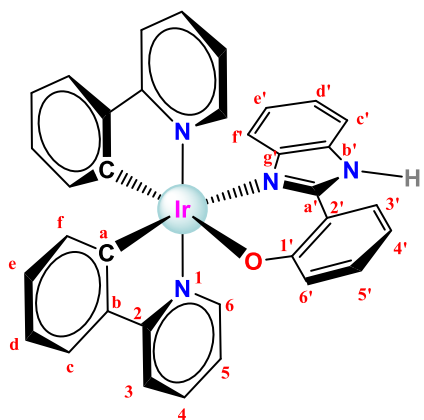


Fig. 16. (a) Acid-base equilibrium for complex **[48a]** and (b) pictures of the different complexes and molecules as a function of the pH under visible light.

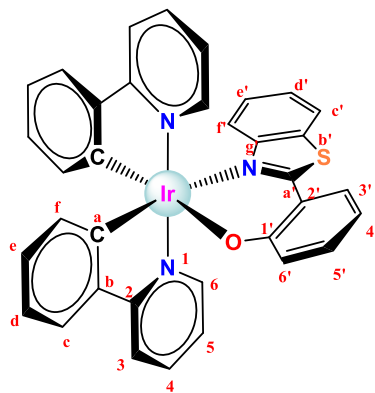
2. CONCLUSIONS/CONCLUDING REMARKS

- A family of 6 new complexes have been synthesised and completely characterised (4 of them by colleagues in the group).
- The luminescent properties of the new derivatives have been experimentally determined.
- All the complexes show oxygen-sensitive phosphorescence.
- The complexes have been tested as photocatalysts in the oxidation of thioanisole by $^1\text{O}_2$ with good conversion values.
- Structure-luminescence-photocatalytic activity relationships have been established.
- Theoretical calculations have successfully confirmed the tendency of the emission wavelength for the complexes.

3. EXPERIMENTAL SECTION



Synthesis of $[Ir(ppy)_2(hpbim)]$, [48a]. In a 100 mL Schlenk flask, the pro-ligand hpbim (0.0488 g, 0.232 mmol) was added to a solution of $[Ir(ppy)_2Cl]_2$ (0.0999 g, 0.093 mmol) in a mixture of 2-ethoxyethanol/water (1:1 14 mL). Na_2CO_3 (0.0410 g, 0.387 mmol) was added as the base, and the mixture was stirred at 110 °C for 24 h and under a nitrogen atmosphere. The solid was filtered and washed with diethyl ether and acetone. The resulting yellow powder was dried under vacuum. Yield: 90.0 mg (0.117 mmol, 68%). **M_r** ($C_{35}H_{25}N_4OIr$) = 709.8287 g/mol. **Anal. Calcd for $C_{35}H_{25}N_4OIr \cdot (H_2O)_{1.3}$:** C 57.33; H 3.79; N 7.64; **Found:** C 57.30; H 3.65; N 7.88. **¹H NMR (400 MHz, DMSO-d₆, 25 °C)** δ 12.90 (s, 1H, H^{N-H}), 8.80 (d, *J* = 5.0 Hz, 1H, H⁶), 8.09 (d, *J* = 7.9 Hz, 2H, H³, H^{3'}), 8.02 (d, *J* = 5.9 Hz, 1H, H⁶), 7.83 – 7.72 (m, 4H, H⁴, H⁴, H^c, H^{3'}), 7.69 (d, *J* = 7.6 Hz, 1H, H^c), 7.36 (d, *J* = 7.8 Hz, 1H, H^{c'}), 7.19 (t, *J* = 6.5 Hz, 1H, H⁵), 7.02 (t, *J* = 6.5 Hz, 1H, H⁵), 6.96 (t, *J* = 7.4 Hz, 2H, H^{5'}, H^d), 6.84 (d, *J* = 7.3 Hz, 1H, H^d), 6.80 (t, *J* = 7.1 Hz, 1H, H^d), 6.65 (q, *J* = 7.7 Hz, 2H, H^e, H^e), 6.53 (t, *J* = 8.2 Hz, 1H, H^{e'}), 6.45 – 6.34 (m, 2H, H^{6'}, H^{4'}), 6.30 (d, *J* = 7.3 Hz, 1H, H^f), 6.18 (d, *J* = 8.4 Hz, 1H, H^f), 5.97 (d, *J* = 7.5 Hz, 1H, H^f) ppm. **¹H NMR (400 MHz, THF-d₈, 25 °C)** δ 11.84 (s, 1H, H^{N-H}), 8.98 (d, *J* = 6.6 Hz, 1H), 8.13 (d, *J* = 6.0 Hz, 1H), 7.90 (d, *J* = 7.9 Hz, 1H), 7.89 (d, *J* = 8.2 Hz, 1H), 7.69 – 7.58 (m, 3H), 7.55 (dd, *J* = 7.7, 1.3 Hz, 1H), 7.48 (dd, *J* = 8.0, 1.9 Hz, 1H), 7.26 (d, *J* = 7.8 Hz, 1H), 7.01 (ddd, *J* = 7.1, 5.7, 1.4 Hz, 1H), 6.95 – 6.86 (m, 2H), 6.82 – 6.76 (m, 2H), 6.75 – 6.69 (m, 1H), 6.63 – 6.53 (m, 3H), 6.47 (d, *J* = 7.4 Hz, 2H), 6.37 (d, *J* = 7.8 Hz, 1H), 6.28 (ddd, *J* = 8.0, 6.8, 1.2 Hz, 1H), 6.06 (dd, *J* = 7.5, 1.1 Hz, 1H) ppm. **FT-IR (ATR, cm⁻¹) selected bands:** 3054 (w, v_{C=CH}), 1604-1583 (s, v_{C=C+N}), 1551 (m), 1480 (s, v_{C=N}), 1440 (m), 1422 (m), 1310 (s), 1254 (s), 1161 (w, v_{C-C}), 1139 (s, v_{C-O}), 1059-1030 (m, δ_{C-Hip}), 864 (m), 806-791 (w, δ_{C-C}), 752-737-729 (vs, δ_{C-Hoop}), 630 (m), 519 (s). **MS (FAB+):** m/z (%) = 711 (12) ([M+H]⁺), 501 (11) ([M-hpbim]⁺). **Molar Conductivity (CH₃CN):** 3.9 S·cm²·mol⁻¹. **Solubility:** soluble in dimethylsulfoxide, methanol and acetone. Partially soluble in dichloromethane and tetrahydrofuran.



Synthesis of $[Ir(ppy)_2(hpbtz)]$, **48b.** The synthesis was performed as for **48a** in the presence of the ligand hpbtz (0.0530 g, 0.233 mmol) and $[Ir(ppy)_2Cl]_2$ (0.1001 g, 0.093 mmol), followed by the addition of Na_2CO_3 (0.0498 g, 0.470 mmol). Red powder. Yield: 85.0 mg (0.117 mmol, 63%). **M_r** ($C_{35}H_{24}N_3OSIr$) = 726.8801 g/mol. **Anal. Calcd for** $C_{35}H_{24}N_3OSIr \cdot (H_2O)_{0.9}$: C 56.57; H 3.50; N 5.65; S 4.32; **Found:** C 56.58; H 3.41; N 5.30; S 4.34. **¹H NMR (400 MHz, DMSO-d₆, 25 °C)** δ 8.83 (d, *J* = 5.8 Hz, 1H, H⁶), 8.21 (d, *J* = 5.4 Hz, 1H, H⁶), 8.16 (d, *J* = 8.0 Hz, 1H, H³), 8.10 (d, *J* = 8.3 Hz, 1H, H³), 7.93 (d, *J* = 8.0 Hz, 1H, H^{3'}), 7.90 – 7.77 (m, 3H, H⁴, H⁴, H^c), 7.69 (d, *J* = 7.4 Hz, 1H, H^c), 7.53 (dd, *J* = 8.0, 1.7 Hz, 1H, H^{c'}), 7.24 (t, *J* = 7.1 Hz, 1H, H⁵), 7.16 (t, *J* = 7.6 Hz, 1H, H^{4'}), 7.08 (t, *J* = 6.9 Hz, 1H, H⁵), 7.06 – 6.99 (m, 2H, H^e, H^{6'}), 6.86 – 6.75 (m, 3H, H^d, H^d, H^{5'}), 6.65 (q, *J* = 7.7 Hz, 2H, H^e, H^e), 6.37 (t, *J* = 7.4 Hz, 1H, H^{d'}), 6.33 (d, *J* = 8.4 Hz, 1H, H^{f'}), 6.29 (d, *J* = 7.7 Hz, 1H, H^f), 5.83 (d, *J* = 7.4 Hz, 1H, H^f) ppm. **¹H NMR (400 MHz, THF-d₈, 25 °C)** δ 9.01 (dd, *J* = 5.8, 0.8 Hz, 1H, H⁶), 8.25 (dd, *J* = 5.8, 0.8 Hz, 1H, H⁶), 7.96 (d, *J* = 8.3 Hz, 1H, H³), 7.91 (d, *J* = 8.0 Hz, 1H, H³), 7.75 – 7.62 (m, 4H, H⁴, H⁴, H^c, H^{3'}), 7.54 (d, *J* = 7.6 Hz, 1H, H^c), 7.49 (dd, *J* = 8.1, 1.6 Hz, 1H, H^{c'}), 7.21 (d, *J* = 8.6 Hz, 1H, H^{6'}), 7.06 (t, *J* = 7.3 Hz, 2H, H^{4'}, H⁵), 6.95 (td, *J* = 7.9, 1.1 Hz, 1H, H^{e'}), 6.88 (t, *J* = 6.6 Hz, 1H, H⁵), 6.75 (ddt, *J* = 11.1, 10.3, 6.7 Hz, 3H, H^d, H^d, H^{5'}), 6.58 (dt, *J* = 15.5, 7.4 Hz, 2H, H^e, H^e), 6.44 (d, *J* = 7.7 Hz, 1H, H^f), 6.40 (d, *J* = 8.5 Hz, 1H, H^f), 6.26 (td, *J* = 7.5, 0.6 Hz, 1H, H^{d'}), 5.93 (d, *J* = 7.7 Hz, 1H, H^f) ppm. **¹³C{¹H} NMR (101 MHz, THF-d₈, 25 °C)** δ 170.0 (s, 2C, C^a, C^{g'}), 169.6 (s, 1C, C²), 169.4 (s, 1C, C²), 155.4 (s, 1C, C^{1'}), 152.5 (s, 1C, C^a), 151.2 (s, 1C, C⁶), 150.2 (s, 1C, C⁶), 150.1 (s, 1C, C^a), 146.1 (s, 1C, C^b), 145.4 (s, 1C, C^b), 138.0 (s, 1C, C⁴), 137.7 (s, 1C, C⁴), 134.7 (s, 1C, C^f), 133.9 (s, 1C, C^{e'}), 133.1 (s, 1C, C^{2'}), 131.9 (s, 1C, C^f), 131.3 (s, 1C, C^{c'}), 129.9 (s, 1C, C^e), 129.4 (s, 1C, C^e), 126.7 (s, 1C, C^{5'}), 125.9 (s, 1C, C^{b'}), 125.7 (s, 1C, C^c), 125.2 (s, 1C, C^{4'}), 124.3 (s, 1C, C^c), 123.9 (s, 1C, C^{6'}), 122.5 (s, 1C, C⁵), 122.1 (s, 1C, C⁵), 121.8 (s, 1C, C^{3'}), 121.7 (s, 1C, C^d), 121.1 (s, 1C, C^{f'}), 120.8 (s, 1C, C^d), 119.5 (s, 1C, C³), 119.3 (s, 1C, C³), 114.5 (s, 1C, C^{d'}) ppm. **FT-IR (ATR, cm⁻¹) selected bands:** 3039 (w, $\nu_{C=CH}$), 1603–1580 (m, $\nu_{C=C + C-N}$), 1475 (s, $\nu_{C=N}$), 1454 (m), 1413 (s), 1346 (m), 1194 (s, $\nu_{C=S}$), 1148 (s, ν_{C-O}), 1056–1029–970 (m, δ_{C-Hip}), 831 (m), 791 (w, δ_{C-C}), 750–738–728 (vs, δ_{C-Hoop}), 629 (m), 563–545 (m), 420 (m). **MS (FAB+):** m/z (%) = 728 (25) ([M+H]⁺), 501 (36) ([M-hpbtz]⁺). **Molar Conductivity (CH₃CN):** 6.2 S·cm²·mol⁻¹. **Solubility:** soluble in dichloromethane, chloroform, dimethylsulfoxide and tetrahydrofuran. Partially soluble in methanol, acetone and water.

4. BIBLIOGRAPHY

- (1) You, Y.; Seo, J.; Kim, S. H.; Kim, K. S.; Ahn, T. K.; Kim, D.; Park, S. Y. *Inorg. Chem.* **2008**, *47*, 1476–1487.
- (2) Li, W.; Xie, Z.; Jing, X. *Catal. Commun.* **2011**, *16*, 94–97.
- (3) Sprouse, S.; King, K. A.; Spellane, P. J.; Watts, R. J. *J. Am. Chem. Soc.* **1984**, *106*, 6647–6653.
- (4) Nonoyama, M. *Bull. od Chem. Soc. Japan* **1974**, *47*, 767–768.
- (5) Liu, Y.; Li, M.; Zhao, Q.; Wu, H.; Huang, K.; Li, F. *Inorg. Chem.* **2011**, *50*, 5969–5977.
- (6) Hao, Y.; Guo, X.; Lei, L.; Yu, J.; Xu, H.; Xu, B. *Synth. Met.* **2010**, *160*, 1210–1215.
- (7) Whang, D. R.; You, Y.; Chae, W.-S.; Heo, J.; Kim, S.; Park, S. Y. *Langmuir* **2012**, *28*, 15433–15437.
- (8) Ramlot, D.; Rebarz, M.; Volker, L.; Ovaere, M.; Beljonne, D.; Dehaen, W.; Van Meervelt, L.; Moucheron, C.; Kirsch-De Mesmaeker, A. *Eur. J. Inorg. Chem.* **2013**, 2031–2040.
- (9) Angelici, R. J. In *Técnicas y Síntesis en Química Inorgánica*; Editorial Reverté, S.A., **1979**; p. 243.
- (10) Sunesh, C. D.; Choe, Y. *Mater. Chem. Phys.* **2015**, *156*, 206–213.
- (11) Zanoni, K. P. S.; Coppo, R. L.; Amaral, R. C.; Murakami Iha, N. Y. *Dalt. Trans.* **2015**, *44*, 14559–14573.
- (12) Rodríguez-Redondo, J. L.; Costa, R. D.; Ortí, E.; Sastre-Santos, A.; Bolink, H. J.; Fernández-Lázaro, F. *Dalton Trans.* **2009**, 9787–9793.
- (13) Hasan, K.; Bansal, A. K.; Samuel, I. D. W.; Roldán-Carmona, C.; Bolink, H. J.; Zysman-Colman, E. *Sci. Rep.* **2015**, *5*, 12325.
- (14) Becke, A. D. *J. Chem. Phys.* **1993**, *98*, 5648–5652.
- (15) Lee, C. T.; Yang, W. T.; Parr, R. G. *Phys. Rev. B* **1988**, *37*, 785–789.
- (16) Hay, P. J.; Wadt, W. R. *J. Chem. Phys.* **1985**, *82*, 299.
- (17) Liu, Z.; Bian, Z.; Huang, C. Bozec, H.; Guerchais, V., Eds.; Springer Berlin Heidelberg: Berlin, Heidelberg, **2010**; pp. 113–142.
- (18) Costa, R. D.; Ortí-, E.; Bolink, H. J.; Gruber, S.; Schaffner, S.; Neuburger, M.; Housecroft, C. E.; Constable, E. C. *Adv. Funct. Mater.* **2009**, *19*, 3456–3463.
- (19) De Angelis, F.; Fantacci, S.; Evans, N.; Klein, C.; Zakeeruddin, S. M.; Moser, J.-E.; Kalyanasundaram, K.; Bolink, H. J.; Grätzel, M.; Nazeeruddin, M. K. *Inorg. Chem.* **2007**, *46*, 5989–6001.
- (20) Tordera, D.; Delgado, M.; Ortí, E.; Bolink, H. J.; Frey, J.; Nazeeruddin, M. K.; Baranoff, E. *Chem. Mater.* **2012**, *24*, 1896–1903.
- (21) Tamayo, A. B.; Garon, S.; Sajoto, T.; Djurovich, P. I.; Tsypa, I. M.; Bau, R.; Thompson, M. E. *Inorg. Chem.* **2005**, *44*, 8723–8732.
- (22) Jiang, X.; Peng, J.; Wang, J.; Guo, X.; Zhao, D.; Ma, Y. *ACS Appl. Mater. Interfaces* **2016**, *8*, 3591–3600.
- (23) You, Y.; Nam, W. *Chem. Soc. Rev.* **2012**, *41*, 7061–7084.
- (24) Nakagawa, A.; Hisamatsu, Y.; Moromizato, S.; Kohno, M.; Aoki, S. *Inorg. Chem.*

- 2014**, **53**, 409–422.
- (25) Wefers, H.; Sies, H. *Eur. J. Biochem.* **1983**, *137*, 29–36.
- (26) Mari, C.; Pierroz, V.; Ferrari, S.; Gasser, G. *Chem. Sci.* **2015**, *6*, 2660–2686.
- (27) Lo, K. K.-W.; Li, S. P.-Y.; Zhang, K. Y. *New J. Chem.* **2011**, *35*, 265–287.
- (28) Aoki, S.; Matsuo, Y.; Ogura, S.; Ohwada, H.; Hisamatsu, Y.; Moromizato, S.; Shiro, M.; Kitamura, M. *Inorg. Chem.* **2011**, *50*, 806–818.

ANNEX ii

Table 1. Crystal data and structure refinement for [46](PF₆)·and [47](PF₆).

	[46]PF ₆	[47]PF ₆
Empirical formula	C ₃₂ H ₂₃ F ₆ IrN ₅ PS	C ₃₃ H ₂₅ F ₆ IrN ₅ PS
Formula weight	846.78	860.81
Temperature (K)	290(2)	173(2)
Wavelength (Å)	0.71073	0.71073
Crystal system	Orthorhombic	Orthorhombic
Space group	P b c a	P b c a
a (Å)	10.4654(12)	10.9995(14)
b (Å)	17.1582(19)	16.694(2)
c (Å)	32.605(4)	33.686(4)
α (°)	90	90
β (°)	90	90
γ (°)	90	90
Volume (Å³)	5854.8(11)	6185.5(13)
Z	8	8
Density (calculated) (g/cm³)	1.921	1.849
Absorption coefficient (mm⁻¹)	4.759	4.507
F(000)	3296	3360
Crystal size (mm³)	0.510 x 0.220 x 0.110	0.12 x 0.11 x 0.08
Theta range for data collection (°)	2.313 to 28.219	2.211 to 28.051
Index ranges	-13≤h≤13, -22≤k≤21, -41≤l≤43	-14≤h≤14, -21≤k≤21, -42≤l≤43
Reflections collected	64069	67392
Independent reflections	6974 [R(int) = 0.1226]	7273 [R(int) = 0.1159]
Completeness to theta = 25.00°	100.0 %	100.0 %
Absorption correction	Semi-empirical from equivalents	
Max. and min. transmission	0.7457 and 0.4133	
Refinement method	Full-matrix least-squares on F2	Full-matrix least-squares on F2
Data / restraints / parameters	6974 / 0 / 419	7273 / 0 / 425
Goodness-of-fit on F2	0.944	0.814
Final R indices [I>2sigma(I)]	R1 = 0.0334, wR2 = 0.0705	R1 = 0.0333, wR2 = 0.0694
R indices (all data)	R1 = 0.0485, wR2 = 0.0737	R1 = 0.0547, wR2 = 0.0731
Largest diff. peak and hole, e·Å⁻³	2.174 and -1.696	2.220 and -1.362

GLOSSARY

Pharmacophore	A special arrangement of particular functionalities that are common to more than one drug and form the basis of the biological activity. The pharmacophore is responsible for the target binding. ¹
Anthelmintic	Anthelmintics are drugs that are used to treat infections with parasitic worms. ²
Antineoplastic	Acting to prevent, inhibit or halt the development of a neoplasm (a tumor). ³
Apoptosis	Programmed cell death. ¹ A cell that undergoes apoptosis dies neatly, without damaging its neighbors. The cell shrinks and condenses. The cytoskeleton collapses, the nuclear envelope disassembles, and the nuclear DNA breaks up into fragments. Most importantly, the cell surface is altered, displaying properties that cause the dying cell to be rapidly phagocytosed, either by a neighboring cell or by a macrophage, before any leakage of its contents occurs. This not only avoids the damaging consequences of cell necrosis but also allows the organic components of the dead cell to be recycled by the cell that ingests it. ⁴
Necrosis	Cell death in response to an acute insult such as trauma or a lack of blood supply. Necrotic cells swell and burst, spilling their contents over the neighbours and eliciting an inflammatory response. ⁴
Carcinostatic	Pertaining to slowing or stopping the growth of cancer. ⁵
Homeostatic balance	Biological systems maintain relatively constant conditions in the internal environment while continuously interacting with and adjusting to changes originating within or outside the system. There are thousands of homeostatic control systems within the body; some of these systems operate within the cell and others operate within an aggregate of cells (organs) to control the complex interrelationships among the various organs. ⁶
Oligonucleotide	Short segment of DNA, with only a little number of nucleotides. The nucleotides are the building blocks of the DNA and RNA.
Diastereotopic groups	Two identical atoms or groups attached to the same atom in a chiral molecule, which upon replacement of one of them with a different group create a new molecule that possess diastereomers. The reason is that the addition of another atom creates a second stereogenic centre. They appear at different chemical shifts in the NMR spectrum. ^{7,8}

Isotropic oscillation	The oscillation method is the most straightforward technique where the crystal is simply rotated around an axis (the oscillation axis) that is perpendicular to the X-ray beam. ⁹ Thus, the isotropic oscillation occurs, when the crystal equally rotates in every direction.
Tumour suppressor p53	The tumour suppressor p53 protects the cell against cancer by inducing cell cycle arrest and apoptosis in response to oncogenic stress. Some human cancers have point mutations in the gene for p53 that inactivate its transcriptional activity. ¹⁰
Fluorophore	The part or moiety of a molecule responsible for the emission of light. They were historically called chromophores, although it implies the absorption of light, whereas a fluorophore also implies emission of light. ¹¹
Stereoisomerism	Stereoisomers possess the same connectivity of atoms, but differ in the spatial arrangement of atoms or groups. Examples include <i>trans</i> - and <i>cis</i> -isomers, and <i>mer</i> - and <i>fac</i> -isomers. If the stereoisomers are not mirror images of one another, they are called diastereoisomers. Stereoisomers that are mirror images of one another are called enantiomers
Photobleaching	Photochemical alteration of a dye or a fluorophore molecule such that it permanently is unable to fluoresce. ¹²
Spin-orbit coupling (SOC)	Interaction of a particle's spin with its motion. ¹³
Luminance (<i>L</i>)	Flux of light emitted by the device, measured in candela per surface unit ($\text{cd}\cdot\text{m}^{-2}$). ¹⁴
Current density (<i>J</i>)	Flux of current through the device, measured in ampere per surface unit ($\text{A}\cdot\text{m}^{-2}$). ¹⁴
Lifetime ($t_{1/2}$)	Time to reach half of the maximum luminance. ¹⁴
Turn-on time (t_{on})	Time needed to reach the maximum luminance. It is also used t_{100} , this is, the time to reach $L = 100 \text{ cd}\cdot\text{m}^{-2}$. ¹⁴
Total emitted energy (E_{tot})	It is calculated by integrating the radiant flux of the device vs. time from $t = 0$ to $t = t_{1/5}$. This value is divided by the electrode area to yield the total emitted energy density (U_{tot}), which allows devices to have electrodes of different shapes. ¹⁴
Current efficiency or efficacy	Emitted light per electric flux, measured in candela per ampere ($\text{cd}\cdot\text{A}^{-1}$). ¹⁴
Power efficiency (PCE)	Flux of light per electric input, measured in lumens per watt ($\text{lm}\cdot\text{W}^{-1}$). ¹⁴

External Quantum Efficiency (EQE)	The ratio of photons emerging from the device per injected electrons. EQE is also defined through the equation $\text{EQE} = b\Phi/2n^2$, where b is the recombination efficiency (equal to unit for two ohmic contacts), Φ is the fraction of excitons that decay radiatively, and n is the refractive index of the glass substrate and is equal to 1.5. ¹⁴
--	---

In the text, the words will appear in bold.

BIBLIOGRAPHY

- (1) Klebe, G. *Drug Design*; Klebe, G., Ed.; Springer Berlin Heidelberg: Berlin, Heidelberg, **2013**.
- (2) Holden-Dye, L. *WormBook* **2007**, 44, 1–13.
- (3) Antineoplastic
<http://www.medicinenet.com/script/main/art.asp?articlekey=22631>.
(03/10/2016)
- (4) Alberts, B.; Johnson, A.; Lewis, J.; Raff, M.; Roberts, K.; Walter, P. *Molecular Biology of the Cell*; 4th Edition; New York: Garland Science: New York, 2002.
- (5) Carcinogenic
<https://www.cancer.gov/publications/dictionaries/cancer-terms?cdrid=44273>.
(30/11/2016)
- (6) Miller-Keane; O'Toole, M. T. *Encyclopedia and Dictionary of Medicine, Nursing, and Allied Health*; Seventh Edition; **2003**.
- (7) Clayden, J.; Greeves, N.; Warren, S.; Wothers, P. *Organic Chemistry*; First Edition; OXFORD University Press: New York, **2001**.
- (8) Smith, M. B. *March's Advanced Organic Chemistry*; Sixth Edition; John Wiley & Sons, Inc.: Hoboken, New Jersey, **2007**.
- (9) Oscillation method
http://hazeslab.med.ualberta.ca/tutorials/data_collection/oscillation.html.
(21/11/2016)
- (10) Issaeva, N.; Friedler, A.; Bozko, P.; Wiman, K. G.; Fersht, A. R.; Selivanova, G. *Proc. Natl. Acad. Sci.* **2003**, 100, 13303–13307.
- (11) Sauer, M.; Hofkens, J.; Enderlein, J. In *Handbook of Fluorescence Spectroscopy and Imaging*; WILEY-VCH Verlag GmbH: Weinheim, **2011**; pp. 1–29.
- (12) Photobleaching <https://en.wikipedia.org/wiki/Photobleaching>. (03/10/2016)
- (13) Spin-Orbit Coupling
https://en.wikipedia.org/wiki/Spin%25E2%2580%2593orbit_interaction.
(03/10/2016)
- (14) Costa, R. D.; Ortí, E.; Bolink, H. J.; Monti, F.; Accorsi, G.; Armaroli, N. *Angew. Chemie Int. Ed.* **2012**, 51, 8178–8211.